# The Magmatic Evolution of Krafla, NE Iceland.

Hugh Nicholson

Thesis submitted for the degree of Doctor of Philosophy

University of Edinburgh

1990

# DECLARATION

I declare that this thesis is my own work except where otherwise stated.

Hugh Nicholson

# ABSTRACT

Krafla is an active central volcano in the NE axial rift zone of Iceland associated with a fissure swarm which trends NNE-SSW. Lava/hyaloclastite samples were collected from the volcanic system, covering the last 4 interglacial and 3 glacial periods. A stratigraphic framework for the volcanic system has been established by use of the Hekla tephra layers and the distinctive volcanic products of glacial and interglacial periods. Recent volcanic activity has shown that there is a shallow magma reservoir beneath the central volcano, which supplies magma laterally to the fissure swarms forming dykes and to the surface directly for eruption.

The Krafla rocks contain the following phenocryst assemblages: ol + plag, ol + plag + cpx, plag + cpx ± ol, plag + cpx + opx + FeTi oxides, plag + FeTi oxides ± cpx ± fayalitic ol. These distinct assemblages suggest that the Krafla suite evolves predominantly by fractional crystallisation. They are also similar to the assemblages found in other mid-ocean ridge basalt (MORB) suites. Most samples, excluding rhyolites, contain plagioclase xenocrysts, implying that there has been at least 2 stages of magma mixing prior to eruption. The absence of plagioclase xenocrysts in the rhyolites suggests that they formed in isolation from the most primitive magmas, with or without crustal assimilation.

Fractional crystallisation using the observed phenocryst assemblage explains many aspects of the major-element compositions of the suite. Least-squares modelling confirms this observation, although it also suggests that the rhyolites contain higher concentrations of $K_2O$ than would be predicted by closed-system fractional crystallisation. This discrepancy may be explained by open system fractionation and/or by crustal assimilation. Numerical modelling of phase equilibria suggests that fractional crystallisation occurs over a range of pressures from 1-3.5 kbar. As was suspected, magma mixing also appears to be a significant process in the Krafla system and may explain some of the scatter on major-element variation diagrams. The Krafla suite is more differentiated than the majority of MORB suites, consistent with the development of long-lived magma reservoirs. The suite also has higher average values of total iron oxide and lower average values of $Na_2O$ (for a given MgO content), which are explicable by larger degrees of melting at higher than average pressures than for the majority of MORBs.

Trace-element compositions also confirm the role of fractional crystallisation. Although the trace-element data also show that the highly incompatible trace elements (e.g. Th,U,Rb) show have high concentrations in the rhyolites like $K_2O$. As mentioned above, this enrichment in the most incompatible elements may be explained by either open system effects and/or by crustal assimilation. However, the temporal variation in rock composition shows no evidence for enrichment in the more incompatible elements when compared with the less incompatible elements, effectively reducing the role of open system fractionation. This suggests that the enrichment in incompatible elements occurs through crustal assimilation of possibly basaltic wall-rock which has undergone relatively small degrees of melting. Ratios of incompatible trace elements also suggest that the Krafla basalts are distinctive from most MORBs in that they appear to be derived from a less incompatible element enriched mantle source.

The major- and the trace-element compositions of the most primitive Krafla basalts show evidence for variable degrees of melting of mantle or possibly variations of the source. In particular, the major-element concentrations, when compared with data from experimental studies, suggest that the basalts derived from the smallest degrees of melting are also produced at the highest pressures. The variation in the incompatible trace elements appears to be "coupled" to that seen in the major elements. The least-differentiated Krafla compositions are also compared with melt compositions predicted from the parameterisation of melting experiments (McKenzie & Bickle 1988). After correcting for the effects of fractional crystallisation, the Krafla melts are most consistent with model compositions produced by a value of 1480°C for the mantle potential temperature. Discrepancies between model compositions and the Krafla compositions may possibly be explained by the dynamic effects of a mantle plume on the melting processes.

The Krafla lavas show anomalously low $\delta^{18}O$ values compared with the majority of MORBs. The $\delta^{18}O$ values of the lavas correlate positively with the MgO content. This correlation is consistent with crustal assimilation of low-$^{18}O$ hydrothermally-altered country-rock. The assimilation process appears to be coupled to fractional crystallisation, although the linearity of the $\delta^{18}O$ *vs* MgO plot appears to confirm that magma mixing is also operating. The ($^{230}Th/^{232}Th$) values of postglacial rocks also correlate positively with MgO content, consistent with their origin by the same crustal assimilation process. The O- and Th-isotope ratios may be modelled by an assimilation with fractional crystallisation (AFC) model, providing the $\delta^{18}O$ value

of the assimilant is assumed. An assimilant produced at the top of the magma reservoir is likely to have a $\delta^{18}O$ value of about -10‰. If this value of $\delta^{18}O$ is used for the assimilant, then a single-stage AFC model requires that the assimilant has to contain between 3-5 ppm Th and r=0.15-0.20. A 2-stage model, however, gives a better fit with the O-Th isotopic data, with an assimilant containing about 1 ppm Th in the first stage of differentiation and 7 ppm in the second stage. Both models can generate the high values of the most incompatible trace elements in the rhyolites.

# ACKNOWLEDGEMENTS

Firstly I would like to thank my supervisors Godfrey Fitton and Brian Upton for supervision and friendly guidance during the last three years. Assistance in the field proved vital to the project and particular thanks must go to Karl Grönvold and Kristjan Saemundsson who patiently put up with my requests for yet more samples. Kristjan is particularly thanked for his help in establishing the stratigraphy of the volcanic system. I am grateful to Karl for many things; notably for my introduction to Icelandic petrology and geochemistry and to Icelandic life in general. The trip to Kverkfjöll with Karl, Konni and Ritva will remain in my memory for a long time. The support of the Nordic Volcanological Institute in the form of 4WD-transport and accommodation is gratefully acknowledged. Brian Upton is also thanked for his "surprise visit" to Myvatn; for his help in planning the collection of samples and teaching me, amongst other things, a good hammering technique.

There are many people whose help proved invaluable in the laboratory. In semi-chronological order they are: Godfrey Fitton and Dodie James for XRF; Pete Hill and Stuart Kearns for the microprobe; Adrian Boyce, Terry Donnelly, Julie Gerc, Alison McDonald and Graeme Rogers for isotope work at East Kilbride; Michel Condomines, Catherine Daniel, Jean Sérange and Olgeir Sigmarsson for U-series disequilibrium work at Clermont-Ferrand, whilst not forgetting my introduction to this technique by Frances Lindsay and Graham Shimmield in Edinburgh; and finally to all the people at the Geochemistry Lab. at Royal Holloway and Bedford New College (London), especially Jan Barker, Nick Walsh, Alison Warren, Anne, Claire and Nigel.

Invaluable discussion has been had with many people over the last 3 years (of course not forgetting Godfrey and Brian), especially with Paul Beattie, Michel Condomines, John Dixon, Tony Fallick, Martin Fisk, Karl Grönvold, Björn Hardarsson, Dodie James, Gawen Jenkins, Dave Latin, Dave McGarvie, Sue Mingard, Graeme Rogers, Olgeir Sigmarsson, John Valley, Sue Wallis and Martin Wilding.

Others not mentioned above have been vital in making these 3 years enjoyable ones in the Grant Institute. I must thank my fellow rats in the Genome building; especially my office-mates Björn, Dave, Mike, Sue, and Martin (especially for his performance at the 1989 Christmas Party!) and for many others in the Department.

Especial thanks go to Dave Latin for introducing me to the "Dan Clan", for unravelling McKenzie's FORTRAN programs and for critically reading several chapters. Sue Mingard is also thanked for wading through several chapters.

Additionally my sanity was preserved (!) by support from my flatmates and friends; in particular Dave, Susan and Ingrid (who supplied much valuable literature not in the reference list) and not forgetting Pete and the Hairies (see Dymoke 1988) and my home group at St. Paul's & St. George's.

Finally my family is thanked for love and support. My father is especially thanked for enthusiastically reading much of the first-draft of the script and my mother for proof-reading at the end of the write-up. I gratefully acknowledge receipt of a NERC research studentship.

# TABLE OF CONTENTS

*He looks at the earth and it trembles;*
*He touches the mountains and they smoke.*

**Psalm 104:32**

# Chapter 1

# Introduction

## 1.1 Regional Setting

Krafla is an active central volcano in the NE axial rift zone of Iceland associated with a NNE-SSW trending fissure swarm (Fig. 1.1). This NE axial rift zone is the landward extension of the Mid-Atlantic Ridge, which is offset by the Tjörnes fracture zone just north of Iceland. It consists of several volcanic systems (central volcanoes and their fissure swarms) which are arranged in an en echelon manner (cf. the overlapping spreading centres of the East Pacific Rise; Macdonald, 1982). The NE axial zone began operating about 3-4 Ma ago, when spreading stopped on a zone (Skagi) now to the west of Krafla and a new rift zone was formed in older crust (Saemundsson, 1974). The Krafla central volcano is the second most northerly of the NE volcanic centres and, although its age is not known precisely, it is probably in excess of 400 ka. South of this active spreading area, the NE axial zone the neovolcanic area of Iceland splits into two, with one branch proceeding to the west to join up with the Reykjanes Ridge whilst the other (SE zone) forms what is thought to be a newly propagating rift zone (Saemundsson, 1977). This SE zone terminates with the off-shore volcanism of Surtsey.

The age of the crust increases away from the neovolcanic zone and reaches a maximum of about 16 Ma in the extreme eastern and western parts of Iceland (Moorbath & Walker, 1963). The mechanism of crustal formation in Iceland has been modelled by Pálmason (1981) and the vectors for crustal motion are shown in Fig. 1.2.

The eroded older areas in east and west Iceland expose Tertiary central volcanoes and fissure swarms, showing their internal structure and revealing their evolution with time (e.g. Walker, 1958, 1963). A typical central volcano is built up from a fissure swarm (Jakobsson, 1979) and develops a longer-lived central magma reservoir than is found in the original fissure swarm. This reservoir allows the formation of magmas which are more differentiated than those typical of simple fissure swarms and is surrounded by a zone of intense hydrothermal activity. Additionally, a mature central volcano may undergo caldera collapse (Gudmundsson, 1988). In some cases this produces a well-defined ring structure (e.g. Askja and Kverkfjöll). In Krafla such a structure is poorly defined whereas in other central volcanoes (e.g. Theistareykir to the north of Krafla) it may be absent altogether.

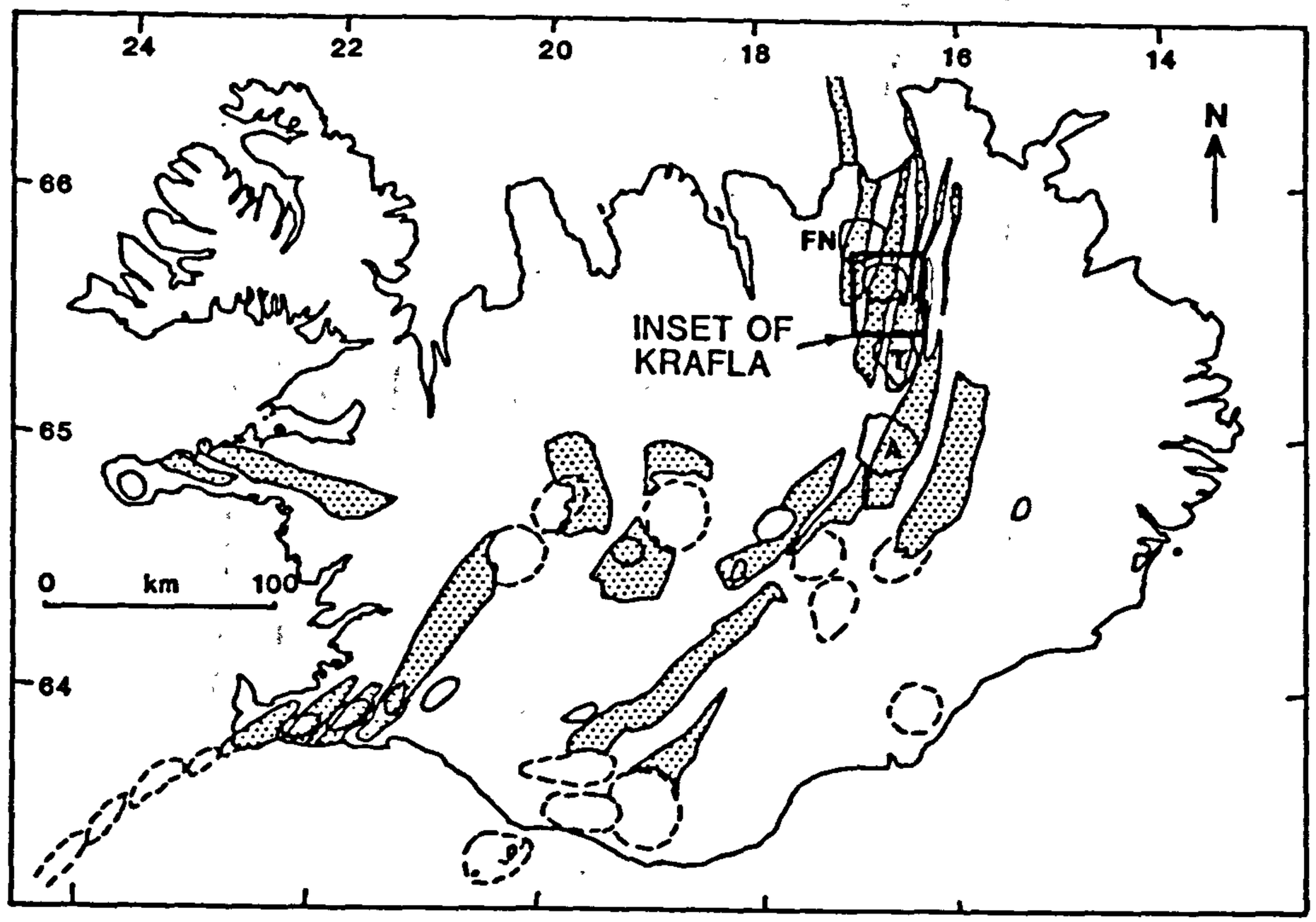


**Fig. 1.1** Map of Iceland, showing the fissure swarms (stippled) and the central volcanoes or volcanic complexes (solid or dashed lines). Krafla is in NE Iceland (inset - for other maps), A=Askja, FN=Fremri-Námur, T=Theistareykir. Adapted from Saemundsson (1977).

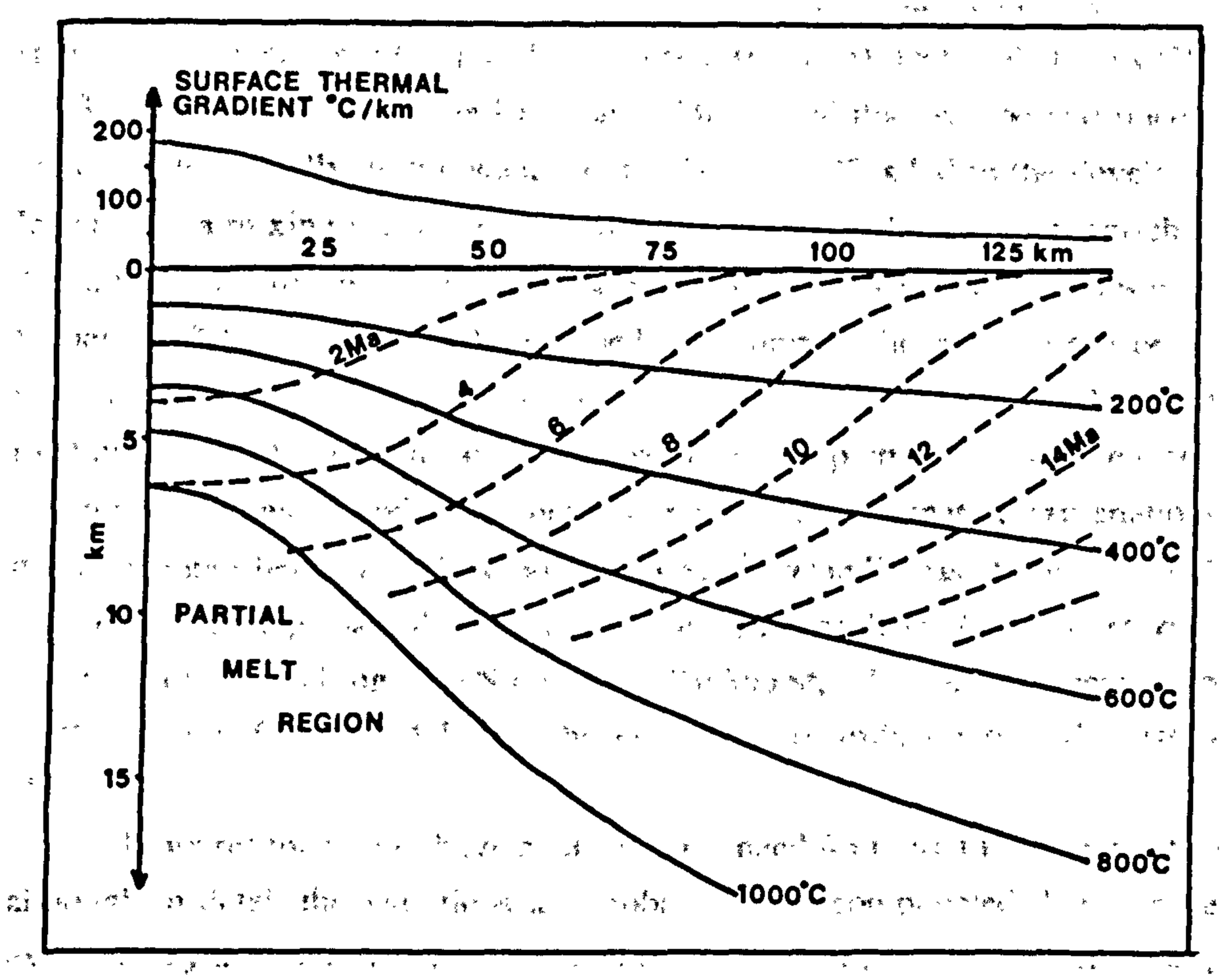


**Fig. 1.2** Crustal accretion mechanism. Section through the lithosphere across an axial rift zone, Iceland, according to the model of Pálmason (1981). Isotherms (solid lines) and isochrons (dashed lines) are shown together with a graph of surface thermal gradient plotted against distance.

## 1.2 Previous Work

### 1.2.1 General Work on Iceland

Iceland is an anomalously thick piece of axial oceanic crust (Beblo & Björnsson, 1980; Pálmason, 1981) which is widely believed to result from melting within a mantle plume under the ridge axis (Morgan, 1971; Vogt, 1971; Vink *et al.*, 1985), something which was not envisaged by early versions of plate tectonics (Wilson, 1965). From a geochemical perspective two distinct mantle sources have been identified for oceanic basalts. One is associated with plumes and ocean island basalts (OIBs). The other is associated with the majority of mid-ocean ridge basalts (MORBs) (Engel *et al.*, 1965). The source for OIBs is enriched in incompatible trace elements (higher Rb/Sr) and has a higher $^{87}Sr/^{86}Sr$ ratio than that of the MORB source (the asthenosphere; see Chapter 5 for more discussion). Detailed studies (Hart *et al.*, 1973; Schilling, 1973) on the Reykjanes ridge found that isotope and trace elements varied systematically with distance along the ridge. This led to the development, for Iceland, of a mixing model between depleted asthenosphere and an enriched plume. Thus, Iceland is distinctive in showing many of the source characteristics of OIB (e.g. higher $^{87}Sr/^{86}Sr$, lower Zr/Nb) combined with some of those of the source of MORB (e.g. a relatively large degree of melting) (Sun *et al.*, 1979). The large degree of melting involved seems to arise because a mantle plume is positioned beneath an ocean ridge. However, other authors have put forward alternative explanations for the distinctive geochemical and isotopic features of Icelandic basalts such as, phlogopite breakdown during partial melting in the asthenosphere (Flower *et al.*, 1975), disequilibrium melting (O'Nions & Pankhurst, 1974), extensive fractional crystallisation (O'Hara, 1973) or the effects of assimilation of old crust (O'Hara, 1977).

More recent studies have confirmed the need for more than one mantle source, although in detail the variations are probably more complicated than can be easily explained by a simple two-source model (O'Nions *et al.*, 1977; Schilling *et al.*, 1983). The discovery of an Icelandic $^{3}He$ anomaly led to the idea of a reservoir, probably in the lower mantle and physically separated from the asthenosphere, supplying mantle plumes. Similar situations occur in intraplate regions such as Hawaii (Condomines *et al.*, 1983; Kurz *et al.*, 1985).

Recent activity in the neovolcanic zones of Iceland gives an almost instantaneous view of magmatic activity (cf. the studies of Tertiary volcanoes by Walker (1958, 1963)). Studying recent fresh Icelandic lavas reveals a range of chemical compositions over the island (Jakobsson, 1972,1979,1980; Imsland, 1978,1983). The major regional differences are as follows: the off-axis regions are

dominantly alkaline, the SE zone is transitional to alkaline and the SW and NE zones are thoroughly sub-alkaline. Krafla is one of the typical sub-alkaline tholeiitic volcanic systems (Jakobsson, 1972). These regional differences have been explained by a selection of magmatic processes, which include differences in the degree and the average depth of mantle melting (O'Nions *et al.*, 1976; Wood, 1979,1981), changes in the extent of crystallisation (Imsland, 1978), variable magma supply rate and varied residence times (Meyer *et al.*, 1985), and the effects of interaction with hydrothermally-altered oceanic crust (Condomines *et al.*, 1983; Oskarsson *et al.*, 1985; Steinthorsson *et al.*, 1987; Macdonald *et al.*, 1987; Hemond *et al.*, 1988).

### 1.2.2. Previous work on Krafla

Geochemical investigation of Krafla began with the analysis of a small number of samples as part of larger-scale regional studies. These studies provided evidence for chemical variation induced by mantle-melting (Sigvaldason, 1974a; O'Nions *et al.*, 1976; Wood, 1979), especially from the most primitive samples. In contrast there were studies looking at the role of magma-crust interaction (O'Nions & Grönvold, 1973; Muehlenbachs et al., 1974), especially by considering the more chemically differentiated compositions. O'Nions & Grönvold (1973) and Sigvaldason (1974b) suggested that many rhyolites might be derived by partial melting of altered crust, rather than by extreme degrees of fractional crystallisation. Along similar lines Muehlenbachs *et al.* (1974) discovered anomalously low $\delta^{18}O$ values for fresh Icelandic rocks (relative to MORB) and postulated some unspecified mode of magma-crust interaction. Their evidence suggested that the extent of $^{18}O$ depletion increased with increased chemical differentiation. Various explanations were considered including direct water-magma interaction, O-exchange with the crust, and crustal assimilation (either by partial melting or whole-scale assimilation). The discovery of low-$^{18}O$ lavas provided evidence for those authors who were arguing that the "Icelandic mantle plume" was a secondary effect (O'Hara, 1977) without accepting that the presence of low-$^{18}O$ lavas could be reconciled with a mantle plume. Hattori & Muehlenbachs (1982) showed that the Krafla crust was progressively depleted in $^{18}O$ with depth as meteoric water in the Krafla hydrothermal system interacted with the crust. Hence the crust, and not just the $^{18}O$-depleted meteoric water, became an excellent source for a low-$\delta^{18}O$ signature. Further regional studies of Th, O, Sr and He isotope ratios including a few Krafla samples led to the development a crustal assimilation model (Condomines *et al.*, 1983; Hemond *et al.*, 1988).

From 1975 to 1984 there was a period of renewed volcanic activity in the Krafla volcanic system and geophysical studies of the active region were commenced almost immediately. Geochemical studies were started as well, initially on the new scoria samples. Samples from the 1975-1977 eruptions were described by Grönvold & Mäkipää (1978) and Larsen *et al.* (1979) and those from the previous volcanic eruptive cycle (1724-1729) were analysed by Grönvold (1984).

Detailed geophysical measurements revealed that there was a shallow-level magma reservoir at a depth of about 3 km below the caldera (Einarsson, 1978; Brandsdóttir & Einarsson, 1979; Tryggvason, 1986). This reservoir was observed inflating and deflating and each time this combination occurred there was an eruption or the lateral propagation of magma into dykes (Björnsson *et al.*, 1977; Björnsson *et al.*, 1979; Einarsson & Brandsdóttir, 1980). Over the time period 1975-1984 the total extension in the region, due to dyke injection, was about 9 metres (Tryggvason, 1986).

During this period K. Saemundsson (pers. comm. 1987,1988) has been working on a detailed geological map of the Krafla system, unravelling the lava flow correlations across a region that has been subjected to continued rifting. His work has enabled a detailed volcanic stratigraphy to be constructed.

## 1.3. Aims of the Project.

In the course of this project a collection of Krafla volcanic rocks has been assembled and divided into groups according to relative age. The major and trace element compositions of the samples were determined, and the variation in composition with time was assessed by comparing samples from different stratigraphic divisions. This approach allows for the magmatic evolution of the central volcano and the fissure swarm to be documented.

The compositions of the Krafla magmas are apparently the result of a number of magmatic processes. The aim of this project is to use geochemical and petrological techniques to investigate these processes and, where possible, to quantify them.

The processes may be divided simply into those occurring at depth in the mantle and those taking place in, or just beneath, the oceanic crust. Mantle processes begin with melt generation by partial melting and are followed by melt migration and accumulation. Once the magmas have accumulated, crustal (or sub-crustal) differentiation may take place by fractional crystallisation and crustal contamination or assimilation. Magma mixing also takes place and the role of "open system fractionation" will be considered with reference to the recent geophysical evidence.

Mantle melting processes appear to vary from one volcanic system to another and are reflected in variable compositions of primitive magmas. Recently these variations in magmatic compositions have been attributed to variations in the mantle potential temperature ($T_p$), which is the temperature the convecting mantle would have if it rose adiabatically to the surface without melting (Klein & Langmuir, 1987; McKenzie & Bickle, 1988). McKenzie & Bickle (1988) derived some simple empirical expressions from melting experiments, which enabled the prediction of the major-element compositions and volume of MORBs for a given $T_p$. An estimate is made here for the value of $T_p$ for NE Iceland by comparing the major-element compositions obtained during this study with the compositions predicted from the model. It is necessary, however, to allow for the effects of fractional crystallisation on the primitive compositions predicted by the model before a fair estimate of $T_p$ can be made. In broader terms the Krafla rocks are compared with other MORBs, especially those from Iceland's neighbouring submarine ridges (Sigurdsson, 1981; Schilling *et al.*, 1983) in order to evaluate the differences between plume and non-plume settings.

# Chapter 2

# Fieldwork and recent geophysical evidence

## 2.1 Aims of the fieldwork

Krafla is a distinct volcanic system (Saemundsson, 1977), consisting of a central volcano and associated fissure swarm located near Myvatn, a large shallow lake in the NE of Iceland (Figs. 1.1 and 2.1). Fieldwork, lasting a total of 2 months, was undertaken in the summers of 1987 and 1988 to collect a suite of volcanic samples from Krafla for petrographic and geochemical examination. These samples were chosen to cover the whole of the exposed history of the system, from the most recent flows (1984) to the oldest (exact age unknown) using a stratigraphic framework constructed by Dr. K. Saemundsson (pers. comm. 1987,1988; see section 2.2). The division of the samples into groups according to age allows the investigation of the magmatic evolution of the system with time. The suite shows considerable variation in chemical and mineralogical composition; the magmatic processes responsible for this variation have been examined. Also the samples were acquired from a large portion of the volcanic system in order to identify the geographic distribution of different lava compositions. Finally, time was spent in the field studying a selection of volcanological features including the results of different eruption mechanisms, rifting processes and the types and behaviour of lava flows. This rationale helps to avoid the potential pitfalls of sample selection and stratigraphy for older samples (e.g. lava flows in stream valleys and lava flowing over fault scarps).

## 2.2 Stratigraphic Framework

The volcanic history of Krafla has been divided into several time intervals (K. Saemundsson pers. comm., 1987) and the main divisions of the stratigraphy are shown in Table 2.1. The absolute time scale is poorly constrained as young tholeiites are very difficult to date (M. Condomines pers. comm., 1989). For the last 10 ka (postglacial) some radiocarbon dates on key marker horizons exist. Hekla (central volcano, S Iceland) has produced two tephra layers H3 and H5 which are identifiable over much of the country, and which have been dated at about 3000 and 7000 years BP respectively (Thorarinsson, 1960; Björnsson *et al.*, 1977). These layers are found throughout the Krafla region and enable the postglacial stratigraphy to be divided into

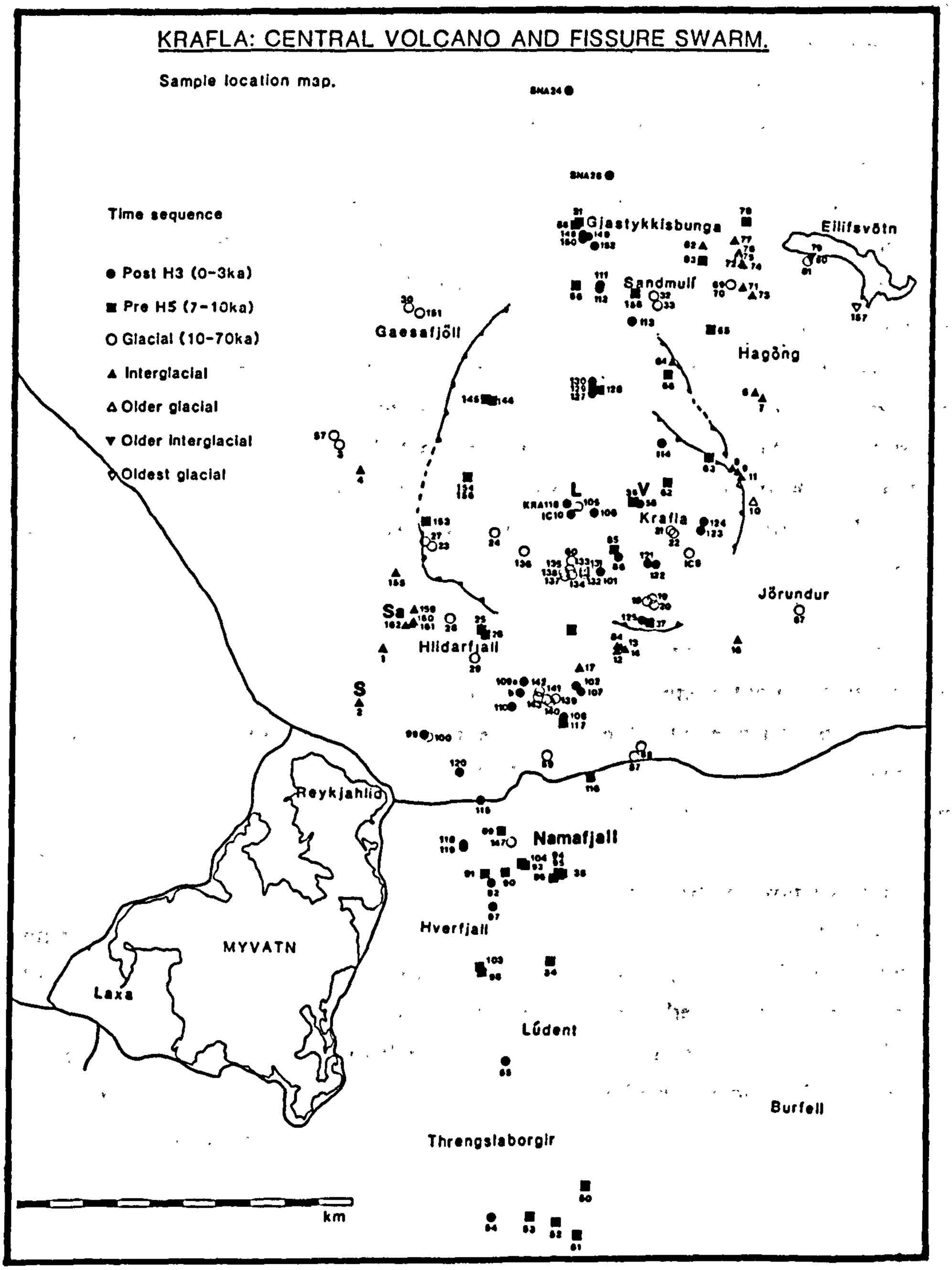


Fig. 2.1 Map of the Krafla volcanic system (see Fig. 1.1) showing the ages (see key; filled symbols are interglacial) and localities of samples. The caldera is shown by a line with small triangles. L=Leirhnjúkur, S=Sly, Sa=Saudagil and V=Víti.

three time periods. However, outside the range for radiocarbon, the Krafla rocks have only been dated by means of the glacial/interglacial record, which is distinguished by the presence or absence of subglacial volcanic products (i.e. hyaloclastite ridges and table mountains). It may be possible to tie in the glacial/interglacial stratigraphy with that of dated ice-core records (Kellogg, 1976), allowing an estimate of 70 ka to be placed on the beginning of the last glacial period (K. Grönvold pers. comm., 1987). Before that time the effect of local climatic variation and uncertainty over the glacial history of Iceland is likely to make correlation unreliable.

The postglacial time period (Divisions 1,2,3; Table 2.1) is split into three major divisions using the Hekla H3 and H5 tephra layers as marker horizons. Events younger than H3 (Division 1; Table 2.1) are relatively easily understood and correlated across the system. Six main eruptive episodes have been recognised; two of which occurred in historical time (1724-9 & 1975-84). The study of the most recent eruptive episode has implied that all such periods of volcanic activity last several years and are made up of many individual lava flows. The other post-H3 events are recorded over much of the volcanic system, from Námafjall to north of the caldera (Fig. 2.1). There appears to have been a quiescent period between H3 and H5 (Division 2; Table 2.1).

Before H5 (Division 3; Table 2.1) there was much volcanic activity in Krafla, which appears to have been concentrated around the caldera in the north and around Námafjall in the south. This has led to the suggestion that there is a separate volcanic reservoir under Námafjall (Grönvold & Mäkipää, 1978). The individual sequence of eruptions before H5 is poorly constrained; they are only bracketed between 7 ka and the end of the last glacial period (about 10 ka).

The end of the glacial period is quite well established and some of the flows on top of the latest hyaloclastite formations are probably older than 10 ka. These flows are termed finiglacial by Saemundsson (pers. comm., 1988). The glacial period (Division 4; Table 2.1) lasted for a considerable time and the beginning of this period is put at about 70 ka. Prior to the last-glacial period there are two, more distinct, glacial periods (Divisions 6,8; Table 2.1) seen in the volcanic record of Krafla, as well as two interglacial periods (Divisions 5,7; Table 2.1).

## KRAFLA STRATIGRAPHIC FRAMEWORK

| Time (years) | Division no. | |
|---|---|---|
| | 1a | Recent 1975-84 |
| | 1b | Myvatn Fires 1724-9 |
| | 1c | Dalseldar ~950 A.D. |
| | 1d | Threngslaborgir ~2050 B.P. |
| | 1e | Holseldar ~2400 B.P. |
| | 1f | Hverfjall ~2800 B.P. |
| ~3000 H3 | | |
| Quiescence | 2 | POSTGLACIAL |
| ~7000 H5 | | |
| | 3 | |
| ~10 ka | | |
| | 4 | GLACIAL |
| ~70 ka | Halaraudar welded-tuff layer: caldera collapse | |
| | 5 | LAST INTERGLACIAL |
| ~120 ka | | |
| | 6 | PREVIOUS GLACIAL |
| | 7 | PREVIOUS INTERGLACIAL |
| | 8 | OLDEST GLACIAL |

**Table 2.1** Stratigraphic framework for the Krafla volcanic system showing the different glacial and interglacial periods. Approximate ages are shown.

## 2.3 Volcanic history of Krafla

### 2.3.1 General

The Krafla fissure swarm stretches from southeast of Myvatn nearly all the way to the north coast of Iceland, covering approximately 80 km and overlapping with the fissure swarms of Theistareykir and Fremri-Námur (to the N and S of Krafla respectively; Fig. 1.1). The Krafla fissure swarm is approximately 5-10 km wide (Saemundsson, 1977) and trends about NNE-SSW.

The central volcano is commonly called Krafla, after a 800 metre high hyaloclastite mountain towards the eastern edge of the caldera. This caldera is about 8-10 km in diameter and is defined by the annular outcrop of an interglacial welded-tuff (Calderone, 1988). The main vertical motion on the caldera (about 50-100 metres) occurred during the last interglacial period, about 70 ka ago.

The total time span of the sequence in Table 2.1 has not been established, but may be of the order of 200-400 ka. For comparison, estimates of the typical life expectancy of a central volcano range from 0.3 to 2.5 Ma (Friedleifsson, 1973; Saemundsson & Noll, 1974; Jóhannesson, 1975).

The major volcanological features of the region can be divided into those occurring under glacial and interglacial conditions. The extensive ice sheets covering the NE of Iceland during the last glacial period made a major impact upon the volcanic environment and affected all forms of physical volcanism (Sigvaldason, 1968; Cas & Wright, 1987).

During interglacial times, fissure swarms and shield volcanoes are the major eruptive edifices, and produce dominantly non-explosive volcanism. Lava flows (both aa and pahoehoe) result from fire-fountaining along fissures, sometimes many kilometres in length. This mode of eruption can generate a small amount of scoria and a row of small craters may develop during the course of the fissure eruption. A good example of such a crater row is to be found from the 1724-1729 eruptions at Leirhnjúkur.

Occasionally phreatomagmatic eruptions occur, when magma interacts with groundwater. The Víti explosion crater (near the centre of the caldera) was generated during the 1724-9 eruption episode by a phreatomagmatic explosion of a small amount of rhyolite and a larger quantity of country-rock. There is another example of a phreatomagmatic crater to the E of Myvatn (Hverfjall). It is about 100 metres high and about 1 km in diameter and is made of basaltic scoria. A different type of magma-water interaction occurred at the edge of Myvatn during late postglacial times, when a lava from a nearby fissure eruption entered the lake, resulting in the formation of pseudocraters. Pseudocraters look just like small, real craters but are in

fact rootless, without any magma source. They are formed by the explosive release of water vapour trapped when the lava enters shallow water (Thorarinsson, 1953).

### 2.3.2 Postglacial

The postglacial period of Krafla began with a change from hyaloclastite formations to lava flows. However, some early flows on top of the glacial formations have been classified as "finiglacial" (K. Saemundsson pers. comm., 1988) and for the purposes of this thesis they are included in the postglacial time period. There have been 6 sets of post-H3 fissure eruptions identified across most of the volcanic system and each set probably consisted of many eruptions (cf. the recent eruptions). Before H5 there were many fissure eruptions found over the system; 13 over the central caldera area and 8 near Námafjall to the south. Some of these eruptions may be from the same eruptive event but stratigraphic control is not sufficiently good to correlate volcanic events across the whole volcanic system (K. Grönvold pers. comm., 1988).

**(a) Post Hekla H3**

**(i) 1975-1984** This most recent series of 9 eruptions, over a similar number of years, has led to a considerable advancement in the geophysical understanding of central volcano processes. This eruptive episode may therefore be used as a model for other events. For a more detailed discussion of the recent results see section 2.5. The eruptions took place along a 10 km fissure running northwards from the centre of the caldera at Leirhnjúkur. The total volume of magma erupted was about 0.2 $km^3$ and the area covered by lava flows was about 80 $km^2$, mostly in the form of pahoehoe (Björnsson, 1985). The total crustal extension over this period was about 9 metres (Tryggvason, 1986).

**(ii) 1724-1729** This eruption has been described in detail by Grönvold (1984) and is called "Myvatnseldar" in Icelandic or Myvatn Fires. The eruptive episode began in May 1724 with a rhyolitic phreatomagmatic eruption at Víti and continued with intense rifting during its early stages with little lava until August 1727. From then, until September 1729 about 0.45 $km^3$ of lava was erupted along an 11 km long discontinuous fissure, in a roughly similar position to the 1975-84 eruptions. The detailed timing of the main eruptions is not known but the episode seemed to be similar to the 1975-1984 episode. Both aa and pahoehoe lava types were formed, and flowed both to the south and to the north of the fissure; to the south the lava descended rapidly to the small village of Reykjalid, destroying buildings and entering the lake (Fig. 2.1). An account of the eruption based on the records of the local priest is given by Thoroddsen (1925).

(iii) The Dalseldar eruptive cycle occurred just before historical times in about 950 A.D. It has not been possible to distinguish individual eruptions within the cycle (cf. 1975-1984). However, this eruptive cycle has been identified over a region from Námafjall in the south to as far north as the centre of the caldera. There may be lava further north but it is not presently exposed.

(iv) The Threngslaborgir eruptive event produced flows which lie beneath those of the Dalseldar eruptions. The former are only found in the area south of Námafjall and east of Krafla (Björnsson *et al., 1977*). In this locality there is a crater row about 6 km long which erupted a considerable volume of lava (equivalent to 2-3 $km^3$ of magma) and covers an area of 220 $km^2$. An estimated age for this eruptive cycle is 2050 years BP.

(v) An eruptive event called Holseldar preceded the Threngslaborgir event and has been recognised over most of the eastern side of the volcanic system. It occurred at about 2400 years. BP.

(vi) The Hverfjall eruptive event consisted of several fissure eruptions covering Námafjall and Krafla and also has tentatively been identified tens of kilometres north of the caldera (K. Grönvold pers. comm., 1989). In the Námafjall region there was a phreatomagmatic explosion which generated a large basaltic cinder cone (about 1 km in diameter) and a variety of volcanic products, including air-fall and pyroclastic deposits.

**(b) Pre-Hekla H5**

Like the post-H3 volcanism, the pre-H5 volcanism can divided into fissure eruptions and shield volcanoes.

Shield volcanoes appear to be the result of enormous outpourings of generally primitive lava from a single volcanic edifice, which may be built up from a fissure swarm. An example of an early-postglacial shield volcano is found near Gjástykkisbunga north of the caldera (Fig. 2.1). It has been suggested that such shield volcanoes are the result of increased magmatic activity following pressure release due to the melting ice at the end of the last glacial period.

Other features of this period include an eroded basaltic cinder cone (Lúdent, Fig. 2.1) and a thick late-stage dacitic lava flow on the N side of this cone. There are other intermediate lava flows to the north of Lúdent, which form several small craters and flows.

In general the stratigraphic control for this period is poor and only 3 flows covering a large part of the region have been identified. These flows have been called K0, K1 and K2 (K. Saemundsson pers. comm., 1988) and they lie above the finiglacial flows mentioned below (section 2.3.3) and in section 2.2.

### 2.3.3 Glacial

There were several lava flows at the end of the glacial period during the ice-retreat (finiglacial). However, most of the glacial eruptive products are influenced by the presence of ice or melt-water and lie beneath these finiglacial flows. This glacial volcanism around Krafla produced three main types of landform: hyaloclastite ridges, table mountains and rhyolite domes.

The hyaloclastite ridges (or tindas) are topographically pronounced ridges, typically over 100 metres high, which consist of masses of pillow lava, breccia and glass fragments (sideromelane) erupted into a meltwater vault under the ice sheet. Some of the volcanic material may be redistributed as a result of sedimentary processes in the meltwater (Cas & Wright, 1987). In time the hyaloclastite material in time may suffer secondary alteration (or palagonitisation). However, most of the Krafla material is fresh glass or pillow fragments, containing some phenocrysts. The hyaloclastite ridges run approximately parallel to the trend of the postglacial fissure swarms and cross the whole of the Krafla region, from Námafjall in the south to Sandmulf in the north (Fig. 2.1).

The table mountains (or tuyas) are large steep-sided, flat-topped mountains (about 600-800 metres above the general topography of the region), which are thought to be subglacial equivalents to shield volcanoes (e.g. Cas & Wright, 1987). Jones (1969) proposed a mechanism for their formation, which begins with an aquatic effusive-phase producing a steep-sided pillow lava pile. The ice roof then collapses and an intraglacial lake is formed, enabling explosive volcaniclastic deposits to accumulate on top of, and around the sides of, the pillow lava pile. Finally there is an subaerial effusive phase when lavas are erupted from a vent above the meltwater, forming deltas out into the glacial lake. Gæsafjöll is an example of a table mountain near the Krafla volcanic system (Fig. 2.1).

When rhyolites erupt subglacially they melt the ice, quench and form domes and small lava bodies. The product of quenching is fragmental volcaniclastic debris (Cas & Wright, 1987; Furnes *et al.*, 1980). The outsides of such deposits are fragmental whereas the insides may be glassy and flow-banded. There are several such rhyolite domes around the edge of the Krafla caldera, for example Hlidafjall to the west of the caldera and Jörundur to the east of the caldera. Hlidafjall is 270 m in height above the general topographic level of the region (Fig. 2.1).

### 2.3.4 Last interglacial

The last interglacial period in this region is estimated to finish at about 70 ka BP and to run back to some unspecified age when the previous glacial period finished (K. Grönvold pers. comm., 1987). The glacial/interglacial history of Krafla may be correlated with Greenland ice-core records, which give an estimate of 120 ka for the start of this interglacial (Kellogg, 1976). However correlations with dated ice-core records are likely to be unreliable due to local variation in ice coverage over Iceland, making the figure of 120 ka little more than a vague estimate. The major event during this time was the formation of the Halaraudar welded-tuff layer, which is to be found in places at the top of a succession of interglacial lavas in the centre of the volcanic system. The outcrop defines an annular pattern which has led workers to believe that the layer formed during caldera collapse near the end of this interglacial period (Björnsson *et al.*, 1977; Calderone, 1988; K. Grönvold pers. comm., 1988). The layer consists of a mixture of different lava types, ranging from evolved basalt to rhyolite, as well as xenoliths, xenocrysts and phenocrysts and it was possibly rheomorphic in origin (Calderone, 1988). After this eruption the newly-formed caldera (possibly 50-100 m deep) was filled by lava flows covering the welded tuff layer in the caldera area. The glacial period followed shortly after the collapse event, leading to the removal of the obvious signs of caldera collapse by the eruption of cross-cutting N-S trending hyaloclastite ridges.

There is a considerable volume of interglacial lava over much of Krafla, exposed especially on the edges of the fissure swarm by large normal faults (e.g. the edge of Hagöng to the E of Krafla). These flows have many of the features of the younger postglacial flows but the task of correlating individual units is very difficult due to continuous rifting. During this interglacial period there were times when hyaloclastite formations were produced (e.g. Saudagil, SW of Krafla's caldera; Fig. 2.1). These bodies are of limited extent vertically and laterally and probably reflect local accumulation of ice or meltwater during an eruption.

### 2.3.5 Older time periods

Table 2.1 shows two more glacial and one interglacial period older than the interglacial period described above (section 2.3.4). There are relatively few exposures of lavas and hyaloclastite formations from these times. However, the volcanic products appear to show similar features to those from the younger periods. Outcrops of these units are restricted to the edges of the Krafla volcanic system, for example near Sly (W of Krafla) and near Eilífsvötn (E of Krafla, Fig. 2.1).

## 2.4 Sample choice and distribution

In the field, samples were selected using the stratigraphic framework developed by Saemundsson (section 2.2). The full collection of samples are listed according to sample number in Appendix I (a) and by their ages in Appendix I (b). The samples KK1 to KK37 were collected by K. Grönvold a few years before the start of this project but were not investigated geochemically. Most of the remaining specimens were collected during August 1987 and July 1988 with the assistance of K. Grönvold and K. Saemundsson. The following criteria were used in the collection of additional samples for this project:

1) Collecting the samples with the best possible stratigraphic and geographic control (i.e. samples for which the eruptive unit or time period can be determined). Some samples have been taken from different parts of the same flow as a check on flow correlation.

2) Freshness. Only the freshest samples have been collected, avoiding surficial weathering where possible and the scoriaceous tops to flows.

3) Large samples of lava were collected (approximately 5 kg each) and sub-samples weighing several hundred grams were taken for this study. The scoria samples were in general much smaller, due to a shortage of material from accurately-dated historic eruptions.

## 2.5 Recent geophysical studies

### 2.5.1 Introduction

Krafla has been geophysically investigated over a long period of time but the studies have been more intensive during the recent period of eruption and rifting (1975-84). Various studies (Björnsson *et al.*, 1977; Saemundsson, 1977; Grönvold, 1984) have shown that volcanic activity in Icelandic centres is confined to short periods of high activity followed by longer periods of quiescence. In addition, it seems that only one eruptive system in the NE neovolcanic zone is active at any one time. This implies that the average time interval between eruptive events is about 100-150 years in NE Iceland (Björnsson *et al.*, 1979).

Early geodetic surveys across the Krafla region were initiated in 1938 (Niemczyk, 1943), and remeasurement carried out in 1965, showed no significant ground deformation over that period. However, during the period 1971-5 there was considerable expansion across Krafla, which was followed by increased seismic

activity in early 1975 and culminated in an eruption in December 1975. A network of seismographic stations was set up in 1975 to monitor the seismic activity of the volcanic system and this provided advanced warning of the December 1975 eruption. Geodetic surveys deduced the horizontal and vertical components of ground deformation during this period and identified a series of inflation and deflation events centred over the caldera. A record of the deflation events is presented in Table 2.2, together with the volcanic eruptions which occurred during some of these events. This crustal motion can be explained by a shallow magma reservoir at a depth of about 3 km repeatedly filling and emptying (Björnsson, 1985). The deflation events coincided with crustal rifting, extension and northward moving earthquakes. These observations have been used as evidence to suggest that magma is laterally propagated from a central reservoir into dykes which may reach the surface and feed fissure eruptions.

From 1975 onwards renewed geothermal activity took place, primarily in the caldera region. This is likely to have been caused by the increased heat flow from a magma body at a relatively shallow level in the crust. Several drill-holes have been made in the caldera area, in order to extract geothermal power. One of these drill-holes, originally put down before 1975, was re-drilled in 1979 and it was found to be blocked by a primitive basaltic intrusion at a depth of about 1 km (K. Grönvold pers. comm., 1988). The following section (2.5.2) describes the geophysical results in more detail and the modelling undertaken by various authors.

### 2.5.2 Geophysical results

Increased seismic activity in early 1975 suggested that a rifting episode was likely to occur. Therefore, seismographic stations were installed in order to monitor the volcanic system (Björnsson *et al.*, 1977). At 11-08 am on 20th December 1975 there was a basaltic eruption at Leirhnjúkur, in the centre of the Krafla caldera. Earthquake activity quickly propagated northwards and within 2 hours at least 40 km of the fissure swarm had been activated. Later, in January 1976, there were bigger earthquakes near the coast, some 50 km north of the caldera.

Tiltmeters were installed over the caldera in order to record ground surface motion and to help to identify magma motion. The tiltmeters showed that there was an inflation event prior to December 1975 and a subsequent rapid deflation during the eruption. Following this eruption the ground surface gradually inflated over a 9 month period before suddenly deflating again (September 1976). This deflation was proceeded by another inflation/deflation pair (October 1976). Both the latter

| Date | Est. Volume | Details |
|---|---|---|
| 20.12.75 | 0.4 x $10^6$ $m^3$ | Eruption at Leirhnjúkur; earthquakes |
| 1.76 | | Fault displacement 35-50 km N of Krafla |
| 9.76 | 10 x $10^6$ $m^3$ | Small slow deflation |
| 31.10.76 | 32 x $10^6$ $m^3$ | Rapid deflation, 5-25 km N of Krafla |
| 1.77 | 21 x $10^6$ $m^3$ | Rapid deflation, 7 km N of Krafla |
| 4.77 | 1 x $10^4$ $m^3$ | Minor eruption, 3 km N of Krafla |
| 4.77 | 47 x $10^6$ $m^3$ | Very rapid deflation, associated with minor eruption |
| | | Fissures open 15-20 km S of Leirhnjúkur |
| 8.9.77 | 2 x $10^6$ $m^3$ | Eruption 1-4 km N of Leirhnjúkur |
| | | Rapid deflation |
| | | Borehole eruption, Námafjall |
| 2.11.77 | 2 x $10^6$ $m^3$ | Rapid deflation |
| 7.1.78 | 74 x $10^6$ $m^3$ | Slow deflation over 18-20 days |
| | | Earthquakes 10-45 km N of Leirhnjúkur |
| 7.78 | 37 x $10^6$ $m^3$ | Slow deflation (3 days) |
| | | Earthquakes migrate N from 3 to 30 km N of Krafla |
| 10.11.78 | 45 x $10^6$ $m^3$ | 5 days deflation; earthquakes 18-28 km N of Krafla |
| 5.79 | 44 x $10^6$ $m^3$ | 5 days deflation; earthquakes 12-23 km N of Krafla |
| 3.12.79 | <3 X $10^6$ $m^3$ | Minor deflation (4-6 days) |
| 11.2.80 | 6 x $10^6$ $m^3$ | Minor deflation (4-5 days) |
| 16.3.80 | 3 x $10^6$ $m^3$ | Eruption 1-6 km N of Leirhnjúkur |
| | 30-40 x $10^6$ $m^3$ | Rapid deflation |
| 10.7.80 | 23 x $10^6$ $m^3$ | Eruption 6.5-11 km N of Leirhnjúkur |
| | 24 x $10^6$ $m^3$ | Rapid deflation |
| 10.80 | 35 x $10^6$ $m^3$ | Eruption at Leirhnjúkur and for 7 km N |
| | 16 x $10^6$ $m^3$ | Estimate of deflation event |
| 12.80 | 5 x $10^6$ $m^3$ | Small slow deflation |
| 30.1.81 | 32 x $10^6$ $m^3$ | Eruption 6-8 km N of Leirhnjúkur |
| | 25 x $10^6$ $m^3$ | Deflation |
| 18.11.81 | ? | Eruption; lava covered 17 $km^2$ |
| | 720 x $10^6$ $m^3$ | Rapid deflation |
| 4.9.84 | 100 x $10^6$ $m^3$ | Eruption along 8.5 km fissure N of Leirhnjúkur |
| | 80-160 x $10^6$ $m^3$ | Deflation over 14 days |

**Table 2.2** A record of the deflation events during the recent eruptive cycle 1975-84 in Krafla (see Fig. 2.2).

deflations were not accompanied by eruptions and coincided with periods of substantial crustal widening.

The total subsidence caused by the emptying of the magma reservoir during deflation events (identified by tiltmeters) was much greater than the equivalent volume of lava erupted. This led Björnsson *et al.* (1977) to suggest that most of the subsidence led to the production of dykes by the lateral propagation of magma northwards out of a central magma reservoir. This would also explain the crustal extension and the propagation earthquakes as the magma flowed northwards. This behaviour was repeated about 20 times over the years 1975-1984 due to repeated rifting, eruptions and lateral propagation. The tiltmeter record is presented in Fig. 2.2, showing the inflation and deflation events. During the period from September 1984 to the present (1990) the magma reservoir has been gradually inflating, although at a much reduced rate compared with the period 1975 to 1984, and no major deflation event has occurred. This suggests that inflation may cease soon and the recent volcanic episode has nearly finished.

Other geophysical techniques have been used to study the volcanic system. In early 1977 a geodetic programme was started to measure the horizontal component of ground deformation over the Krafla system (Björnsson *et al.*, 1979). Its aim was to complement the information on the vertical motion already being obtained from the tiltmeters. Repeated length measurements revealed considerable amounts of crustal extension over a 1 km wide region in the centre of the fissure swarm and contraction in the flank zones outside this region. In addition, major fissures, taking up most of the surface crustal extension, were individually monitored for changes in their widths; these superficial surface changes observed, agreed with those measured across the rift-zone by geodetic surveying techniques (Björnsson *et al.*, 1979).

Einarsson (1978) studied regional earthquakes and discovered that the majority of these occurred in the top 4 km of the crust. He also found an S-wave shadow zone beneath the caldera (i.e. on the site of inflation and deflation). This observation confirmed the existence of a magma reservoir, which the tiltmeter data suggested was at a depth of approximately 3 km beneath the Krafla caldera. Beblo & Björnsson (1980) carried out a study of the magnetotelluric properties of the crust and mantle beneath NE Iceland and found a low resistivity zone under Krafla from 9 to 14 km. They explained this zone by the presence "of partially molten basaltic magma", probably resulting from magma accumulation following melt generation (Björnsson, 1985; Schmeling, 1985). The resistivity increased below this zone to a value compatible with the presence of partially molten asthenosphere.

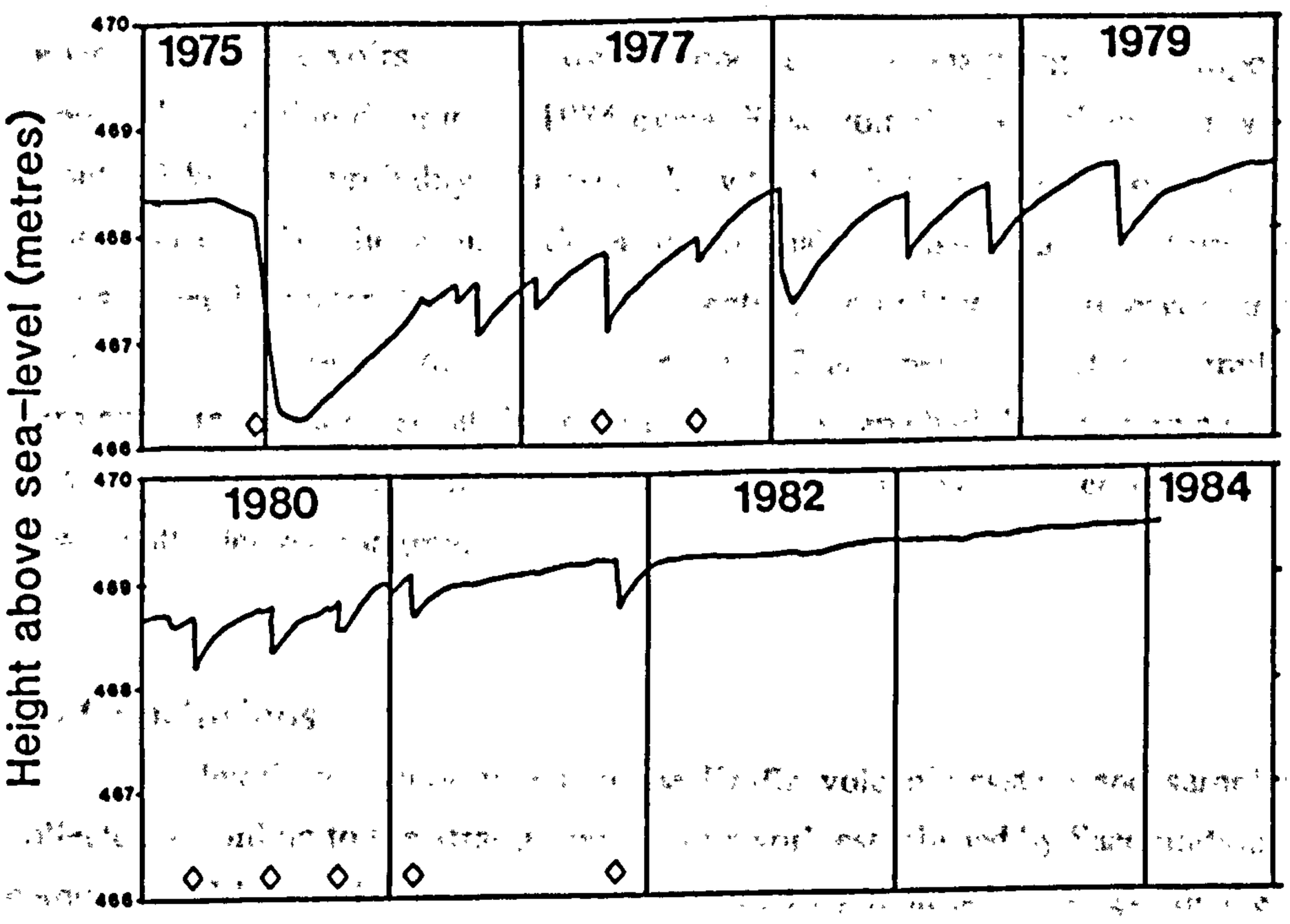


**Fig. 2.2** A record of tiltmeter readings over the Krafla caldera from 1975 to 1983 showing the inflation/deflation events of the Krafla magma reservoir (excluding 1984). Deflation events which include volcanic eruptions are shown by open diamonds (after Björnsson 1985).

Björnsson (1985) summarised the geophysical observations undertaken up to the beginning of the latest eruption (September 1984) and put forward a crustal accretion model (cf. Pálmason, 1981). He concluded that most of the new magma (approx. 85%) was added to the crust in the form of dykes. The rifting event occurred in response to the build-up of crustal tension accompanied by upwelling asthenosphere and the accumulation of magma beneath the crust. Fig. 2.3 shows Björnsson's simplified model for the Krafla volcanic system (1985, p.10159, Fig. 7).

Tryggvason (1986) considered the geophysical evidence from the latest eruption (September 1984) and described geodetic evidence for several magma reservoirs (I,II,III) at different depths beneath Krafla. The shallow reservoir (I), first identified by Einarsson (1978), was confirmed to exist at about 3 km depth. Two other deeper reservoirs (II,III) were proposed after analysing the components of ground deformation during the 1984 event. Reservoir II was positioned at a depth of about 10 km and probably corresponds with the low resistivity zone of Beblo & Björnsson (1980). The ground deformation analysis also required a third reservoir (III) at a depth greater than 20 km. The identification of the third reservoir appears to be much less well-constrained than the other 2 and need not actually imply that a permanent reservoir exists at this depth but that magma had flowed from a depth of at least 20 km before eruption. Reservoir III could then have supplied reservoir II with new mantle-derived magma.

## 2.6 Conclusions

Fieldwork was undertaken in the Krafla volcanic system and samples were collected according to the stratigraphic framework established by Saemundsson (pers. comm., 1987,1988). This framework is defined by tephrochronology for the young samples and by a sequence of glacial and interglacial volcanism for the samples older than the postglacial. Samples younger than about 3 ka BP have been placed in specific volcanic episodes, of which two are recorded historically. Older samples are less well-constrained in age and have been assigned to various glacial/interglacial time periods.

The geophysical record of the 1975-1984 eruptive episode has shown that there was a shallow magma reservoir periodically filling and emptying beneath the central volcano. This evidence may be used to constrain geochemical arguments on "open system fractionation".

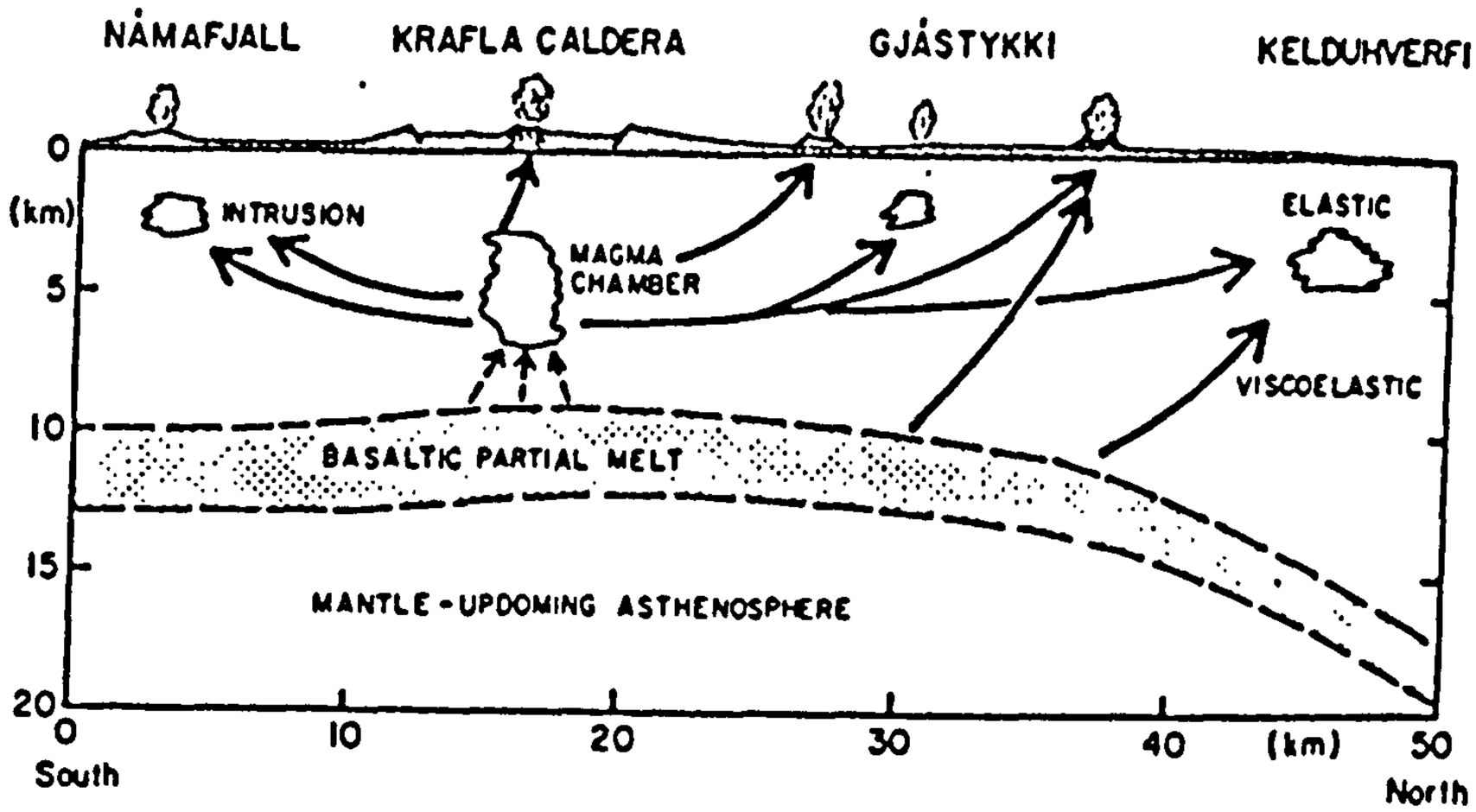


**Fig. 2.3** Cross-section through the crust and mantle of NE Iceland (from Björnsson 1985), showing the partially molten basaltic layer at the base of the crust and the upper crustal magma chamber below the Krafla caldera. Arrows indicate possible directions of magma movement during the recent rifting events.

The suite of samples may be used to investigate the chemical evolution of the volcanic system with time and the processes responsible for the range of compositions seen. The following Chapters report the results of these investigations.

# Chapter 3

# Petrography and Mineral Chemistry

## 3.1 Objectives

Krafla displays a suite of rock types, from basalt through to rhyolite, containing characteristic phenocryst and groundmass minerals. The majority of the lavas (and some hyaloclastites) have been studied in thin section, generating information about the various mineral phases present in the different rock types of the suite. The main petrographic features recorded include the nature of the mineral assemblages, rock texture, mineral size, shape and distribution. These observations were made in order to distinguish between crystals present in the magma before eruption (phenocrysts and xenocrysts) and those which crystallised from the lava during rapid cooling (groundmass). Such distinctions are often difficult to make for coarse-grained samples (Cox *et al.*, 1979; Bryan, 1983). The texture, shape and chemical composition of minerals were used to help identify those crystals which were in equilibrium with the liquid prior to eruption (phenocrysts) and those minerals which were out of equilibrium (xenocrysts). The latter are probably derived as phenocrysts from other magmas incorporated via magma mixing (Huppert & Sparks, 1980) or by assimilation of cumulate crystals (Pyle *et al.*, 1988).

The aim of the petrographic work is to define characteristic phenocryst assemblages for the different rock types of the suite. Because different phases are stable in magmas under different chemical and temperature conditions, such phase assemblages can be related to the falling temperature of the magma as it crystallises.

Previous studies on MORB-type tholeiites (e.g. Muir & Tilley, 1964; Shibata *et al.*, 1979; Sigurdsson, 1981; Schilling *et al.*, 1983; Stakes *et al.*, 1984) have found a common sequence of mineral assemblages as crystallisation proceeds; for example, olivine (ol) followed by olivine and plagioclase together (ol+plag) and later joined by clinopyroxene (ol+plag+cpx). Krafla displays a similar suite of phenocryst assemblages and these assemblages can then be used to constrain models of the chemical evolution of the magma during crystallisation, using mineral and whole-rock chemical analyses. Models based on phenocryst compositions may be used to constrain magma crystallisation paths (Chapter 4), whereas the presence of xenocrystic material (and the range of mineral compositions within samples) may help constrain the extent of magma mixing (section 3.6). However, whole-rock analyses, which reflect the chemical composition of the liquid together with any

phenocrysts and xenocrysts, in contrast to glass analyses, only provide an approximation to liquid composition (Bryan, 1983; Kuo & Kirkpatrick, 1982). It is clear that any crystal redistribution processes (usually gravity driven), which may have led to highly porphyritic lavas and unrepresentative phenocryst assemblages, will give rise to whole-rock compositions which may depart considerably from the composition of the liquid (Shibata *et al.*, 1979). Modal analysis of such samples can help to compensate for any chemical distortion. The most aphyric lavas may often help to define the best approximation to the course of liquid chemical evolution.

The main lava/hyaloclastite types are as follows: ol + plag-phyric basalts (Group 1), ol + plag + cpx-phyric basalts (Group 2), plag + cpx ± ol-phyric basalts (Group 3), plag + cpx + opx + FeTi oxides-phyric intermediates (Group 4), plag + FeTi oxides ± cpx ± fayalitic ol-phyric rhyolites (Group 5).

## 3.2 Petrographic descriptions

### 3.2.1 Olivine+plagioclase-phyric basalts

This group of lavas, which contains phenocrysts of olivine and plagioclase, is distinguished from the majority of Krafla basalts by the absence of clinopyroxene as a common phenocryst phase. The olivines are generally euhedral to subhedral in shape and range in size from 0.1 to 1 mm. There is little evidence for resorption and crystal overgrowths are also rarely seen. The plagioclase phenocrysts occur over a wider range of sizes (0.05-2 mm) than the olivine's and possess more variable morphology. Small phenocrysts are usually tabular in shape and slightly zoned, whereas the larger plagioclases are often non-tabular and complexly zoned. Typically the large plagioclase phenocrysts (or megacrysts) are composed of three parts; a resorbed core, a subhedral mantle and a thin rim or overgrowth. This morphology suggests that multiple stages of growth and resorption have occurred and that these megacrysts could also be termed xenocrysts (see section 3.2.6 for a more detailed description). The plagioclase megacrysts are, however, relatively uncommon in this group, being present in only 2 out of 15 samples. Glomeroporphyritic clusters of plagioclase and occasionally olivine and plagioclase together occur. Small crystals of spinel (<0.05mm) are found only as inclusions in olivines in several samples of this group. A photomicrograph of a typical sample (KK21) is shown in Fig. 3.1.

The groundmass consists of very fine-grained olivine, plagioclase and clinopyroxene (probably crystallised in that order), which are arranged in an intergranular to sub-ophitic texture. Apatite needles may occur as inclusions in

groundmass plagioclase. There are interstitial FeTi oxides (angular magnetite and platy ilmenite) in between the 3 main mineral phases.

### 3.2.2 Olivine+plagioclase+clinopyroxene-phyric basalts

The largest proportion of the Krafla samples contains phenocrysts of olivine, plagioclase and clinopyroxene (39 samples). Olivine phenocrysts are generally smaller than in the olivine+plagioclase-phyric samples (0.1-0.5 mm) and their shape is usually more anhedral. Resorptional boundaries are common, which may suggest that most olivine crystals have reacted with the liquid. Spinel inclusions in olivines are rarely found (2 out of 39 samples). Plagioclase phenocrysts and xenocrysts (identified by their complex morphologies) range in size from less than 0.1 mm to more than 5 mm. The largest plagioclases or megacrysts are similar to those described above (in section 3.2.1) and show signs of a xenocrystal origin. Smaller plagioclase crystals do not show such features and appear to be true phenocrysts. Such phenocrysts are often tabular in shape and are rarely zoned. Plagioclase also occurs as glomerocrysts, often with clinopyroxene and sometimes with olivine and clinopyroxene. The clinopyroxene is generally found as small, blocky, subhedral crystals (0.1-0.2 mm) in glomerocrysts. The general features of the group are shown by sample KK51 in Fig. 3.2.

The groundmass is quite variable, ranging from olivine + plagioclase + clinopyroxene + FeTi oxides to plagioclase + pyroxene (augite rimmed by pigeonite) + FeTi oxides. The pigeonite was identified by electron microprobe analysis (see section 3.5.4). In some samples (7 out of 39) the usual ragged, interstitial, groundmass opaques are replaced by larger, more equant, non-interstitial crystals (still in the groundmass), characteristic of the most Fe-enriched Icelandic tholeiites (Carmichael, 1964, 1967). These large FeTi oxide crystals appear to have crystallised early in the cooling history of the groundmass, before the plagioclase and the pyroxenes, rather than as a late-stage phase as in the other samples. Brown residual glass is also a common feature of this assemblage, associated with the FeTi oxides and fresh in all but the oldest samples .

### 3.2.3 Plagioclase+clinopyroxene±olivine-phyric basalts

The distinguishing feature of this group is the general absence of olivine as a significant phenocryst phase. Indeed Carmichael (1964) referred to this basalt type by the term "olivine-free" tholeiite. However, one sample (KK09) contains a small

quantity of forsteritic olivine probably of xenocrystal origin, since its composition ($Fo_{84}$) is much more magnesian than expected from the other minerals. Plagioclase and clinopyroxene are present in a range of sizes similar to those described in section 3.2.2. A few samples contain plagioclase megacrysts which are likely to be of xenocrystal origin. Glomerophyric clusters of plagioclase and clinopyroxene are also common.

The samples are usually sparsely porphyritic and the groundmass is fine-grained or glassy, giving rise to problems of groundmass mineral identification. However, it is possible to identify plagioclase, pyroxene (probably both augite and pigeonite) and FeTi oxides. The FeTi oxides are usually non-interstitial to the silicate phases in the groundmass and in some samples these crystals may be phenocrysts. An example of a typical member of this group is shown in a photomicrograph of KK110 in Fig. 3.3.

### 3.2.4 Plagioclase+clinopyroxene+orthopyroxene+FeTi oxides-phyric intermediate lavas

These samples are from lavas of intermediate composition (i.e. icelandites and dacites) and contain phenocrysts of orthopyroxene (hypersthene) similar to those described by Carmichael (1964) for some rocks from the Tertiary central volcano Thingmuli. The orthopyroxene may be distinguished from groundmass pigeonite by its straight extinction and lower birefringence. It is only found in these intermediate lavas. The phenocrysts are generally small (0.1-0.3 mm), subhedral in shape, and make up less than 1% by volume of the rock. Clinopyroxene occurs together with the orthopyroxene, often as glomerocrysts and is slightly more brown coloured than the basaltic clinopyroxenes described in previous sections. Plagioclase crystals range in size, from microphenocrysts (0.05-0.1 mm) to phenocrysts (about 1 mm). Plagioclase also forms glomerocrysts with the two pyroxenes. There are occasional phenocrysts of opaque oxides, which are considerably larger than the groundmass crystals. Also a few resorbed forsteritic olivines are found which are almost certainly of xenocrystal origin.

The groundmass is generally very fine-grained and consists of small plagioclase laths, opaques and pyroxene. Flow banding of the groundmass, defined by plagioclase laths, is common. Fig 3.4 shows a photomicrograph of a representative sample, KK35.

### 3.2.5 Plagioclase+opaques±clinopyroxene±Fe-rich olivine-phyric rhyolites

Samples with this assemblage are both glassy (traditionally called obsidians) and crystalline. All these samples are chemically classified as rhyolites (Chapter 4). Glassy samples may show flow-banding in thin-section. The phenocryst assemblage consists of dominantly plagioclase and opaque oxides (both found in all samples), and Fe-rich olivine and clinopyroxene (in some samples). The plagioclase crystals are usually quite large (0.5-1.0 mm) and tabular showing only slight zonation and poorly developed lamellar twins. Extinction angles are consistent with plagioclase being close to andesine in composition, which is confirmed by the discussion on mineral chemistry in section 3.5. However, unlike all the above rock types, the rhyolites show no evidence for the presence of plagioclase megacrysts. Phenocrysts of opaque oxides, 0.1-0.3 mm in size and euhedral in shape, are found but they are not modally abundant (<1%). Clinopyroxene is present in many samples and can be identified by its green colour, inclined extinction and generally elongate subhedral shape. The clinopyroxene often shows signs of resorption. It occurs in association with brown-green, Fe-rich olivine, which is generally subhedral to anhedral in shape (less elongate than the clinopyroxene), and which shows extensive resorption. Both these mafic phases are 0.1-0.3 mm in size and are much less abundant than the plagioclase (<<1% by volume).

The groundmass of the rhyolites is composed of glass, which may be devitrified. This pale brown to colourless glass is often finely flow-banded. Devitrification in some samples has led to the pervasive development of quartz spherulites. Some of the characteristic features of the rhyolites are shown in Fig. 3.5.

### 3.2.6 Plagioclase-phyric samples

The occurrence of large amounts of modal plagioclase in rocks of a wide variety of compositions, exceeding in proportion all other phenocryst phases, has been known for some time. Up to 40% modal plagioclase has been reported from both plume and non-plume settings (Bryan & Moore, 1977; Kuo & Kirkpatrick, 1982; Bryan, 1983; Meyer *et al.*, 1985).

Plagioclase-phyric rocks are quite commonly found in Krafla (13 samples contain more than 5% modal xenocrystal plagioclase) and samples containing up to 30% modal xenocrystal plagioclase have also been recorded in this study. Plagioclase occurs over a wide size range in these samples, from microlites in the groundmass (<0.05 mm), through small tabular crystals (probably phenocrysts, 0.1-0.3 mm in size) to large complexly-zoned crystals (1-5 mm), which commonly occur in clusters.

**Fig. 3.1** Example of an olivine + plagioclase-phyric lava (KK21), showing euhedral phenocrysts of olivine (**ol**), enclosing spinel (**s**) surrounded by a groundmass of ol + plag + cpx + FeTi oxides. Field of view is about 5 mm. **ppl**.

**Fig. 3.2** Example of an olivine + plagioclase + clinopyroxene-phyric lava (KK51) showing microphenocrysts of ol (**ol**) + plag (**p**) + cpx (**c**) set in a fine-grained matrix of plag + cpx + FeTi oxides. Field of view is approximately 5 mm. **ppl**.

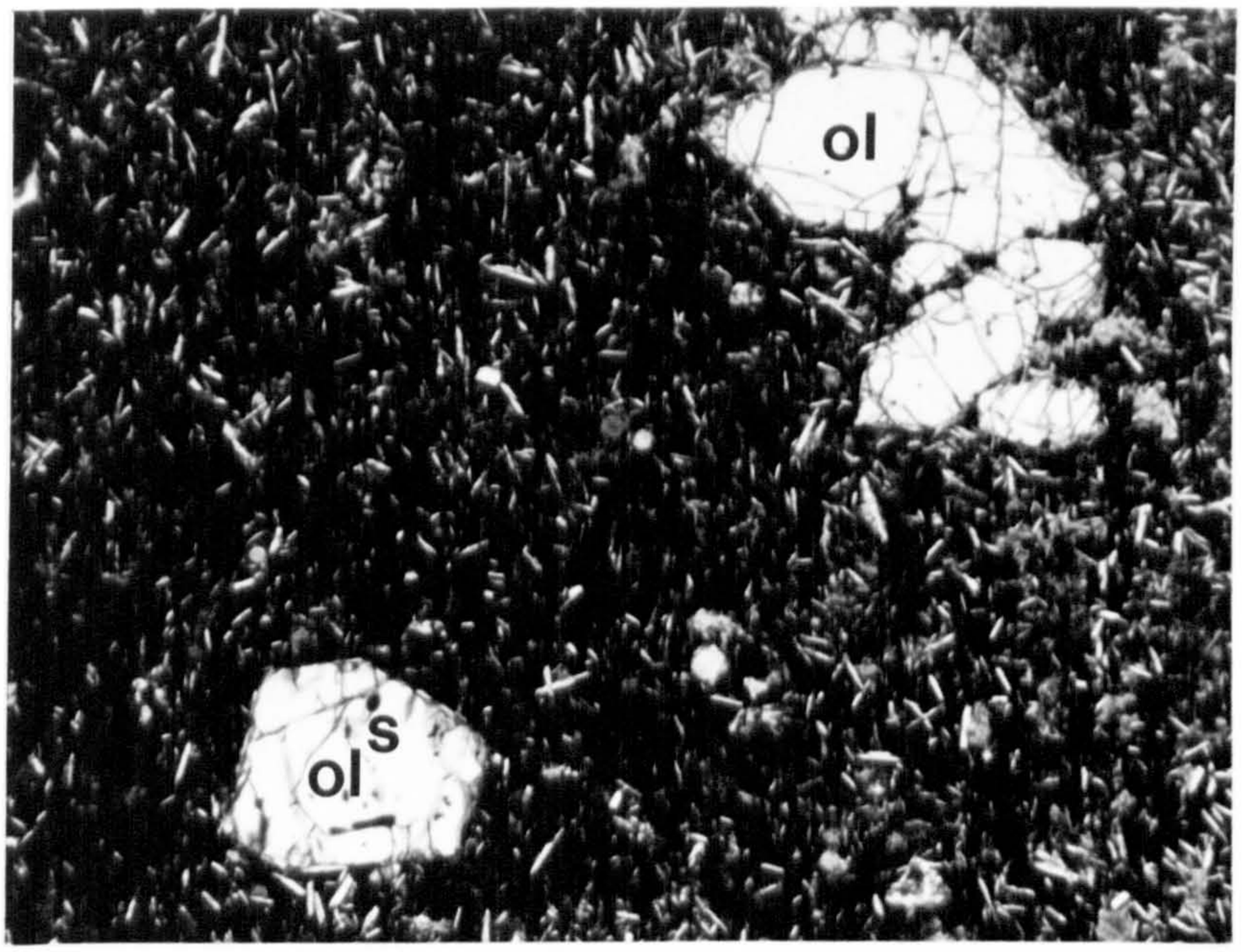
ol
s
ol

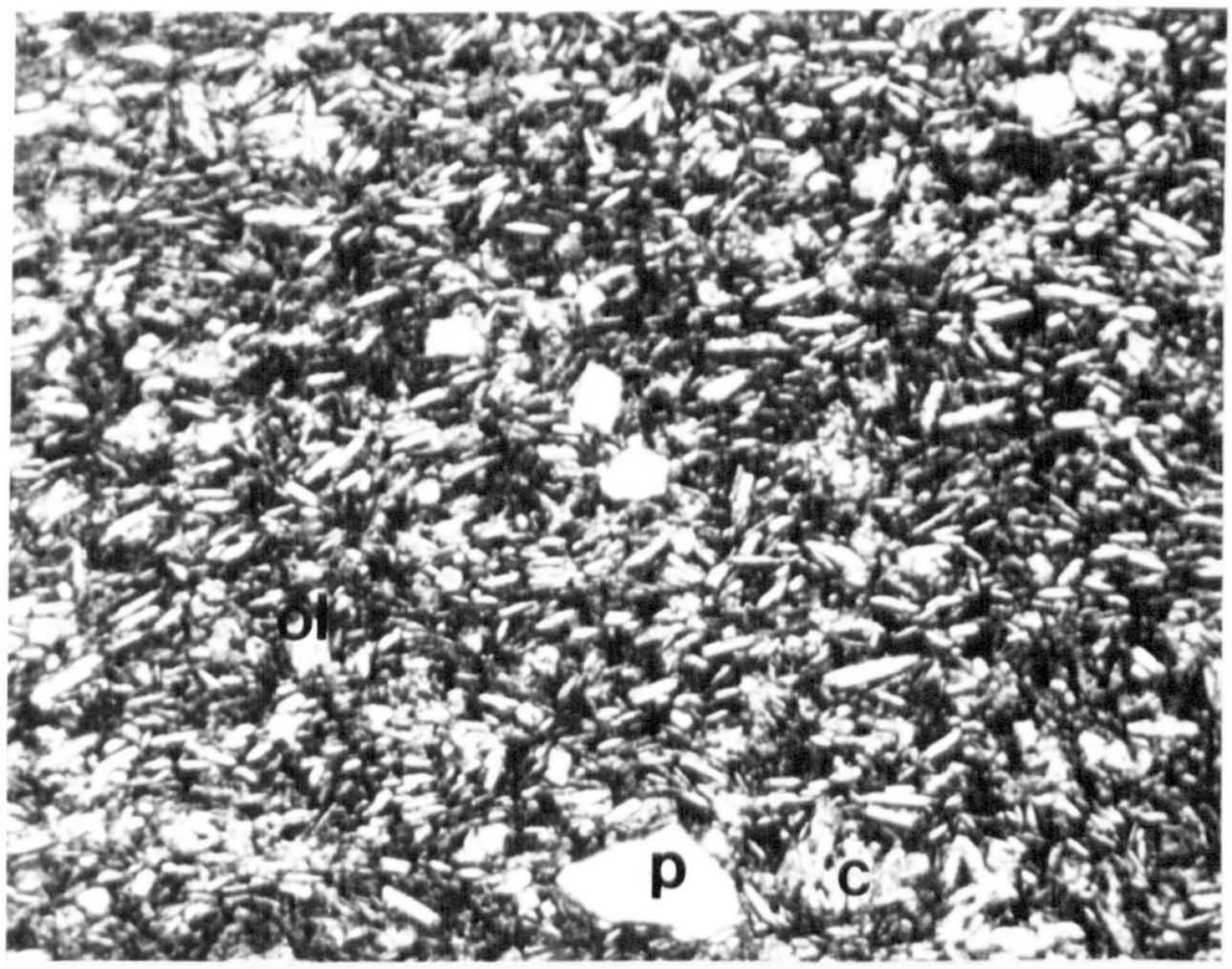
ol
p
c

**Fig. 3.3** Example of a plagioclase + clinopyroxene ± olivine-phyric lava (KK110) showing in this picture characteristic non-interstitial opaques and plagioclase laths. There is also a cluster of coarser-grained basalt containing many plagioclase laths and a larger plagioclase phenocryst (**p**). Field of view is approximately 5 mm. **ppl**.

**Fig. 3.4** Example of a plagioclase + clinopyroxene + orthopyroxene+ FeTi oxides-phyric lava (KK35) showing phenocrysts of plag (**p**), cpx (**c**), opx (**o**) and FeTi oxides (**f**), and microphenocrysts of plag set in a glassy groundmass. Field of view about 5 mm. **ppl**.

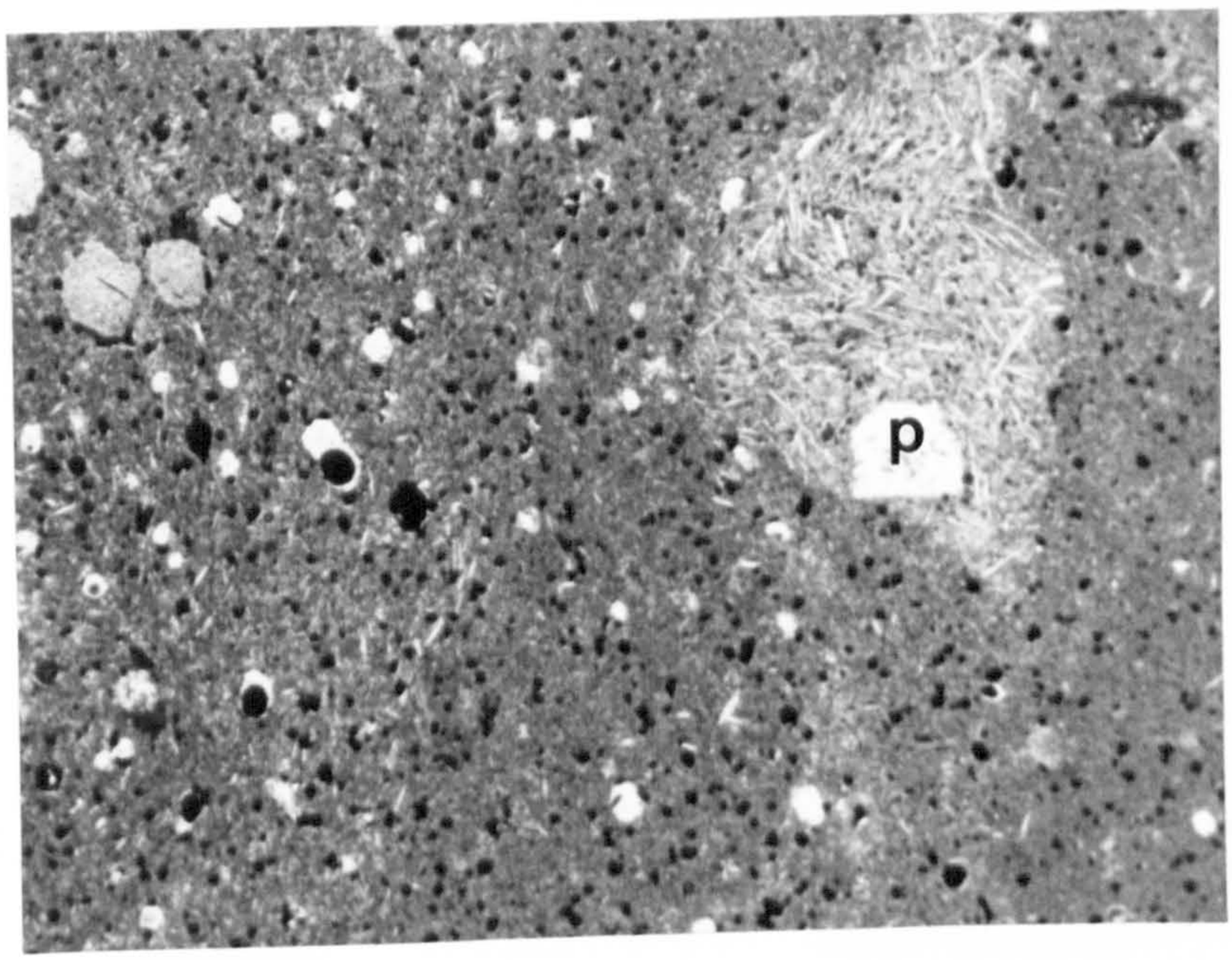
p

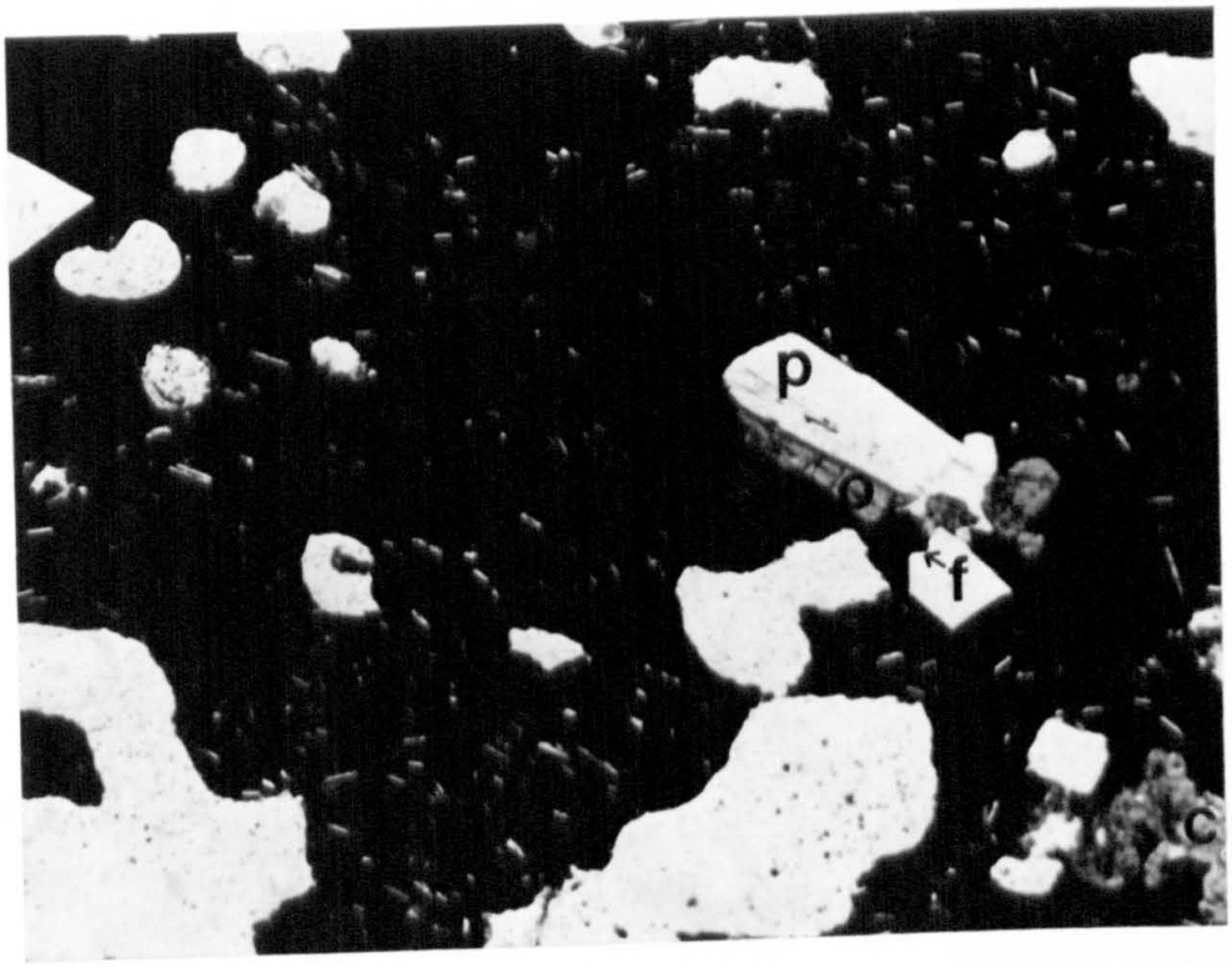
p
f
c

Fig. 3.5 Example of a plagioclase + FeTi oxides ± clinopyroxene ± fayalitic olivine-phyric lava (KK03), which shows a cluster of plag (**p**), cpx (**c**), ol (**ol**), FeTi oxides (**f**) phenocrysts set in a groundmass of devitrified glass. Field of view about 5 mm. **ppl**.

Fig. 3.6 Example of a plagioclase-phyric lava (KK18) containing a large modal proportion of plagioclase megacrysts. Note the rim (overgrowth), mantle and indication of core (filled with inclusions) of the left-hand megacryst. Field of view about 6 mm. **xpl**.

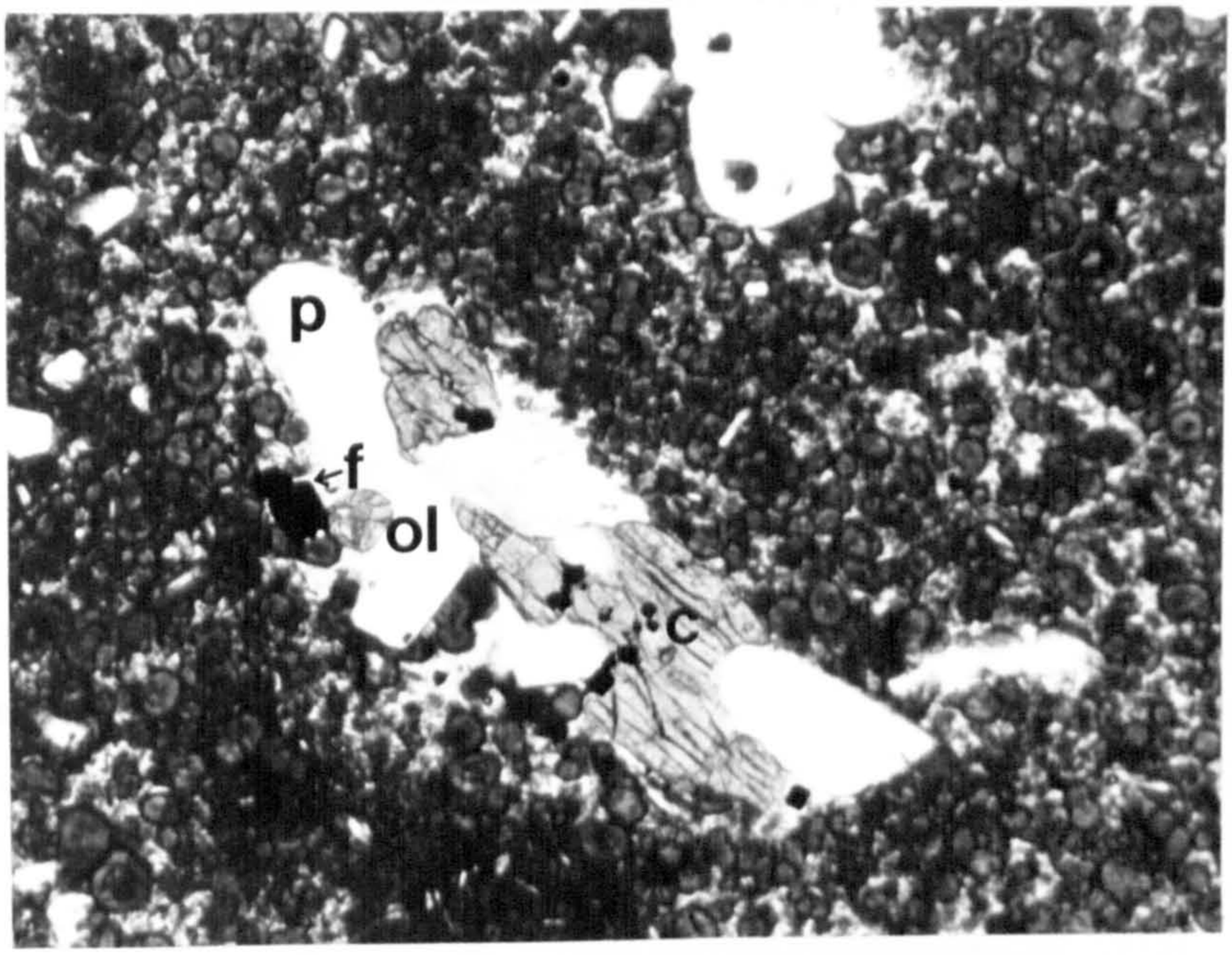
p
f
ol
c

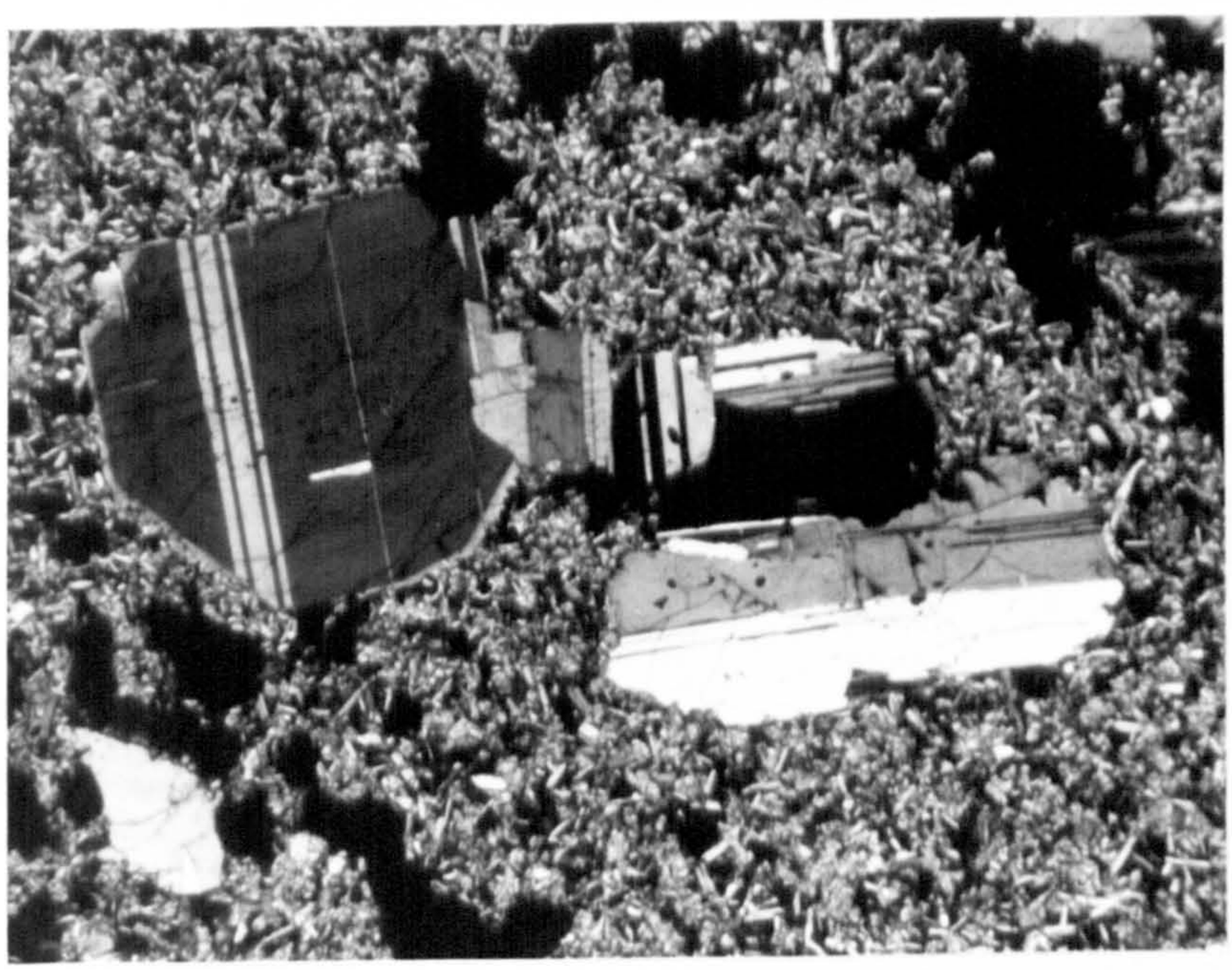

The latter dominate where the modal proportion of plagioclase is high. As described above (section 3.2.1) the largest crystals show complex internal morphologies, usually consisting of a core and a mantle, surrounded by a thin overgrowth. The core is variable in size (0.5-2 mm), but often forms the greater part of the crystal and is commonly full of melt inclusions. The core outline is usually anhedral and resorbed and is surrounded by an optically continuous mantle of tabular plagioclase. This zone also often contains many melt inclusions. The mantle is finally rimmed by a thin plagioclase overgrowth (50-250 μm thick). Each large crystal usually displays variations in extinction angle, reflecting chemical zonation. The mantle/core boundary may show either normal or reverse zonation, whereas the rims are always normally zoned. Optical identification of the core and mantle suggests that the crystals are dominantly close to bytownite ($An_{70-90}$) with an overgrowth that seems to be more sodic (see section 3.5.3 for electron microprobe results). The general texture of plagioclase-phyric lavas is shown in a photomicrograph of KK18 (Fig. 3.6).

## 3.3 Magma mixing

The geophysical evidence presented in Chapter 2 suggests that magma mixing occurs under the Krafla central volcano. This section examines the petrographic evidence in favour of magma mixing, of which there are two main lines.

1. Physical mixes of different magmas observable in hand specimen.
2. Phenocryst and xenocryst textures (and compositions).

1. If magma mixing has occurred at a sufficiently shallow level (and/or just prior to eruption) then the lava sample may contain unhomogenised regions of different bulk composition. This is best observed in hand specimens of volcanic glass (sometimes with different colours) but occasionally picked out in holocrystalline samples by variation in groundmass texture. There is one particular Krafla volcanic unit mentioned in Chapter 2, called the Halaraudar welded-tuff layer, which displays mixed glasses. These mixed-magma glasses (or rock samples) range in composition from Fe-rich basalt through to rhyolite, and contain strings of lighter-coloured rhyolite contained in darker-coloured glasses of other compositions. The glasses contain a range of mineral phases, reflecting the mixing of a Fe-rich basalt with a rhyolite (Calderone, 1988).

2. Although discrete phenocryst assemblages have been observed in the Krafla suite (indicating the progressive evolution of the magma from higher to lower temperatures) there appear to be xenocrysts of most mineral phases in many of the petrographic groups described above. The presence of large, complexly-zoned crystals of bytownite plagioclase in the majority of Krafla lavas suggests that most lavas are likely to have been subject to mixing during the course of their magmatic history (for a more detailed discussion see section 3.6).

## 3.4 Modal analysis

The case for modal analysis has been made above; namely that the chemical analysis of whole-rock samples cannot be expected always to provide the true liquid composition because of the presence of phenocrysts and xenocrysts. With its use an attempt was made to define the effects of crystal accumulation on the general trends of chemical differentiation (Chapter 4).

The modal analyses were carried out using a semi-automatic Swift point-counter attached to a standard petrological microscope (a Vickers instrument with 40, 100 and 400 times magnification). Depending on the level of precision required, between 300-600 points per thin section were counted. A table of key modal analyses is given in Appendix II. Some of the results, especially for the modal proportions of xenocrystal plagioclase, are used in Chapters 4 and 5 when the major and trace element compositions are discussed.

## 3.5 Mineral Chemistry

### 3.5.1 Rationale and analytical techniques

In order to confirm and expand on the petrographic observations made above, a number of samples from the Krafla suite were chosen for analysis by electron microprobe. Samples were chosen so as to show lava types with a wide range of phenocryst and groundmass assemblages. The electron microprobe work was performed using a Cambridge Instruments Microscan Mark V machine. Operational details and representative analyses are set out in Appendices VI (b) and III respectively.

The following section summarises the compositions of the different mineral phases present in the Krafla suite. The petrography and mineral chemical compositions are then used together to discuss the nature of crystallisation pathways and magma mixing.

### 3.5.2 Olivine

Olivine is a common phenocryst phase in the Krafla suite. It is found in most of the more primitive basalts, but is generally absent from the most Fe-rich basalts and the intermediates, but appears again in the rhyolites. This gap in the appearance of olivine corresponds to a major change in olivine composition, from relatively forsteritic compositions in the basaltic rocks ($Fo_{85}$ to $Fo_{56}$) to compositions close to fayalite (ferrohortonolite, $Fo_{13-12}$) in the rhyolites. These compositions are shown in Fig. 3.8 and discussed with reference to phase equilibria in section 3.7.3.

The olivine-bearing samples may be divided into three groups, following the petrographic subdivision of section 3.2.

1. The olivine+plagioclase-phyric group (1) (section 3.2.1) contains olivines which range in composition from $Fo_{86}$ to $Fo_{74}$. Most olivine phenocrysts are not apparently zoned. In one example studied, rims are more Fe-rich than cores, i.e. $Fo_{85}$ to $Fo_{74}$ (KK58). Unfortunately, due to its fine grain size, it was not possible to probe any groundmass olivine for comparison with the phenocrysts.
2. The olivine+plagioclase+clinopyroxene-phyric group (2) (section 3.2.2) also contains olivines with a wide range of composition, $Fo_{86}$ to $Fo_{58}$, although the minimum Fo composition is slightly lower than the above group. This observation is compatible with the appearance of clinopyroxene as a phenocryst phase at lower liquidus temperatures, together with more Fe-rich olivine and more Na-rich plagioclase (e.g. Sigurdsson, 1981; Wilkinson, 1982). Zoning is not generally observed. However, olivine in one example studied was normally zoned from a core of $Fo_{71}$ to an edge of $Fo_{63}$. The almost ubiquitous resorption of olivine phenocrysts suggests that olivine is reacting with the magma and may eventually be replaced by low-Ca pyroxene (see section 3.5.6).
3. Olivine reappears in the rhyolites (group 5), with compositions ranging from $Fo_{13}$ to $Fo_{12}$ (ferrohortonolite) in sample KK03. The other rhyolite studied (KK29) contains no olivine, only plagioclase and opaque oxide phenocrysts.

### 3.5.3 Plagioclase

Plagioclase is found in all of the Krafla rocks which have been studied. It occurs both as a phenocryst phase and as a groundmass mineral. The total observed range of plagioclase compositions is from $An_{90}$ to $An_{32}$ (see Fig. 3.7 for the feldspar compositions plotted on a An-Ab-Or molar-proportions triangular diagram).

The phenocrysts have been split into two distinct groups on the basis of size and texture (section 3.2.6). The large, complex plagioclase phenocrysts range in composition generally from $An_{80}$ to $An_{90}$ (bytownite) irrespective of the composition of the host rock. They appear to be out of equilibrium with their groundmasses in most samples. In detail, the megacryst cores have compositions from $An_{78}$ to $An_{91}$. Mantles have a similar spread of compositions but often have higher An values than cores (reverse zoning). This mantle is then surrounded by an overgrowth, whose composition is always more sodic than the mantle or core ($An_{78}$ to $An_{62}$). A typical example from KK81 has a core of $An_{87}$, mantle $An_{89}$ and overgrowth, $An_{79}$. The overgrowth compositions are close to those of smaller (0.1-0.5 mm) plagioclase phenocrysts present in the samples. The presence of the sodic overgrowth and the complex nature of the megacrysts suggests that the core and mantle are xenocrystal in origin (Kuo & Kirkpatrick, 1982). A typical plagioclase megacryst is shown in Fig. 3.6.

The smaller plagioclase phenocrysts show more variable compositions. Olivine+plagioclase-phyric lavas (group 1) have generally plagioclase phenocrysts with the highest An contents ($An_{74}$ to $An_{78}$).

The appearance of clinopyroxene as a phenocryst phase corresponds with an increase in abundance of smaller and less An-rich plagioclase phenocrysts. The olivine+plagioclase+clinopyroxene-phyric group (2) (section 3.2.2) contains a range of smaller, non-complex plagioclase with compositions ranging from $An_{89}$ to $An_{62}$, with the highest values ($>An_{80}$) only present in KK28 (a highly porphyritic basalt).

In the plagioclase+clinopyroxene±olivine-phyric samples (group 3) (section 3.2.3) the smaller plagioclase crystals vary in composition from $An_{61}$ to $An_{72}$. Again it is probable that plagioclase megacrysts are xenocrysts. They have compositions with a similar range to comparable crystals in the other assemblages. In addition sample KK12 contains a partially-resorbed phenocryst of composition $An_{45}$, which is probably xenocrystal in origin.

The orthopyroxene-bearing, intermediate, lavas (group 4) (see section 3.2.5) contain small plagioclase phenocrysts which are more Ab-rich than those in the above basalts, covering the range $An_{51}$ to $An_{73}$. There is some normal zoning in these phenocrysts, for example from $An_{68}$ to $An_{64}$ and $An_{55}$ to $An_{54}$. Gabbroic xenoliths are present in some samples, with one fragment containing plagioclase of $An_{85}$. Other plagioclase megacrysts are present as described above. Small microlites of plagioclase in the groundmass have compositions from $An_{55}$ to $An_{61}$.

No megacrysts have been observed in the rhyolites (group 5). The plagioclase phenocrysts found in them are of composition $An_{32}$ to $An_{42}$ (cf. Carmichael, 1963).

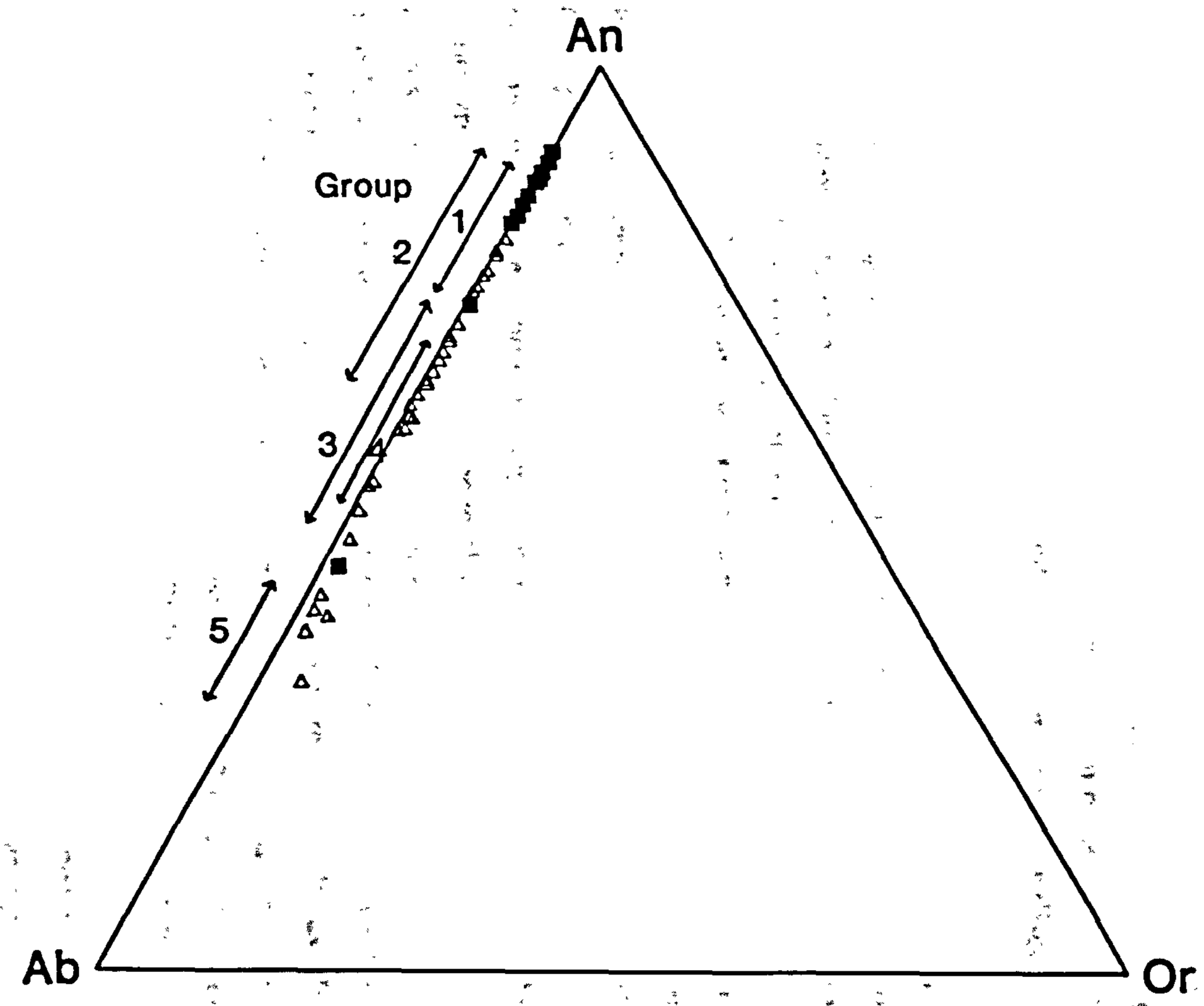


**Fig. 3.7** Triangular diagram showing the molar proportions of An, Ab and Or for selected analyses of plagioclase phenocrysts (open triangles) and xenocrysts (filled squares), identified on textural grounds. Groups 1-5 refer to the phenocryst assemblages referred to in the text.

Typically they are normally zoned but only slightly (e.g. $An_{42}$ to $An_{40}$, core to edge). No groundmass plagioclase is present.

### 3.5.4 Clinopyroxene

Clinopyroxene is present in most samples, either as a groundmass phase or as both groundmass and phenocryst phases. The exceptions are a few glassy samples which may show only phenocrystal clinopyroxene. The five main phenocryst assemblages are numbered 1 to 5, following the order of sections 3.2.1 to 3.2.5.

1. The olivine+plagioclase-phyric samples contain either very little phenocrystal clinopyroxene or none at all. The groundmass clinopyroxene is discussed at the end of this section.

2. The first common appearance of clinopyroxene as a phenocryst phase occurs in the olivine+plagioclase+clinopyroxene-phyric group of basalts. Pyroxenes are then nearly always present as phenocrysts or microphenocrysts. Core compositions vary from endiopside to augite, with a maximum of 0.4 cations per formula unit (CPFU) Fe (Fig. 3.8). Where examined, rims show a slight tendency to Fe enrichment, similar to that in the olivines described above. Variation within individual samples tends to be small and trends parallel to the Mg-CaMg edge of the pyroxene quadrilateral. Clinopyroxenes in KK68 have two extremes of composition, varying in Ca and Mg content while Fe contents are approximately constant. The Al contents of clinopyroxene phenocrysts are generally fairly low (0.08 to 0.2 CPFU Al). $Na_2O$ ranges from 0.17 to 0.30 wt%. The ratio of $Al^{IV}$ (2-Si) to $Al^{VI}$ ($\Sigma Al$-$Al^{IV}$) is generally also low, suggesting that clinopyroxene crystallisation has occurred at low pressures (Wilkinson, 1982). $TiO_2$ values are also low and increase with Fe as Mg decreases.

The clinopyroxenes from different samples define quite a broad trend with approximately constant Ca content and decreasing Mg/Fe ratios (Poldervaart & Hess, 1951; Deer *et al.*, 1966; Carmichael, 1967), which according to Lindsley (1983) represents the effects of decreasing crystallisation temperatures.

3. The clinopyroxenes in the plagioclase+clinopyroxene±olivine-phyric group (section 3.2.5) are usually more Fe-rich than those in group 2 and vary from endiopside to ferroaugite. However the most Fe-rich clinopyroxenes found in KK12 show signs of originating as xenocrysts. Some of the pyroxene is even contained within a gabbroic xenolith also including plagioclase ($An_{45}$), ilmenite and magnetite. This plagioclase is much more Ab-rich than true phenocrysts in the same sample ($An_{66}$). This difference in An content suggests that the xenolith is derived from a more evolved magma or from a cumulate sequence. In KK26 there are many

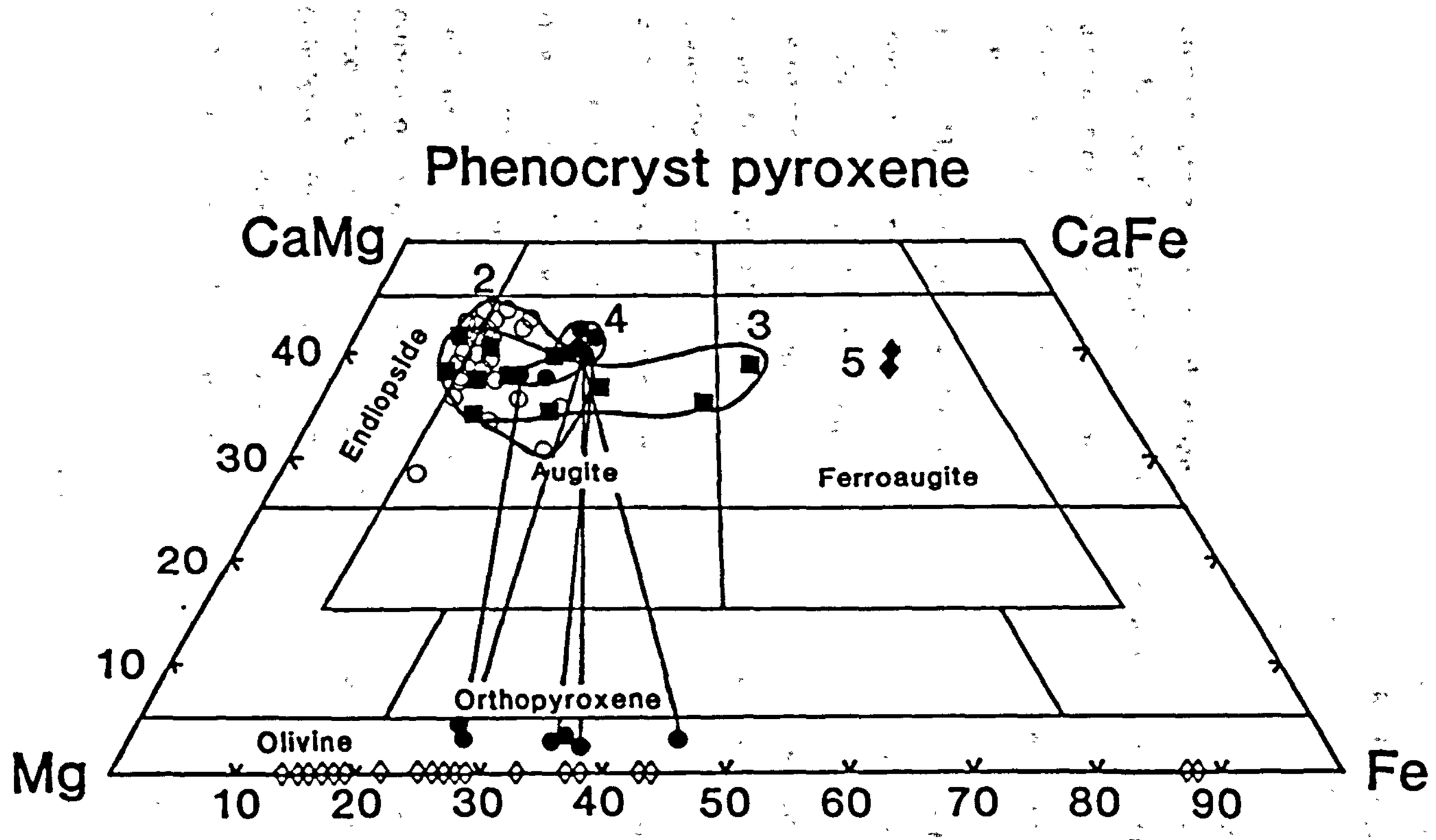


Fig. 3.8 A selection of phenocryst pyroxene analyses from Groups 2-5 (2, open circles; 3, filled squares; 4, open circles; 5, filled diamonds) plotted on the molar CaMg-CaFe-Mg-Fe quadrilateral. Selected olivine compositions are shown on the lower axis of the quadrilateral. Tie-lines indicate coexisting pairs of pyroxene phenocrysts.

clinopyroxenes in comparable gabbroic xenoliths which appear to be derived from a more basic magma than the intermediate composition of KK26 would imply. The clinopyroxenes are associated with olivine ($Fo_{84}$) and plagioclase ($An_{67}$ to $An_{72}$), again indicating a more primitive origin than expected. Despite these signs of magma mixing (section 3.6) the overall trend of this group's clinopyroxene phenocrysts is towards higher Fe contents than in group 2 (e.g. KK91 in group 1 with 0.08 to 0.20 CPFU Fe, cf. KK54 in group 2 with 0.1 to 0.12 CPFU Fe), reflecting the lower liquidus temperatures of the more differentiated magma.

The minor components of the clinopyroxenes in this group also vary; the $TiO_2$ contents are generally higher than those of the previous groups (0.29-1.30 wt% $TiO_2$), so also are the contents of $Na_2O$ (0.17-0.30 wt% $Na_2O$). $Al_2O_3$ is variable and covers a similar range to clinopyroxenes from group 2 (1.9-3.9 wt% ). $Cr_2O_3$ values are low (usually less than 0.2 wt%, with higher values from the more Mg-rich crystals from KK26).

4. The plagioclase + clinopyroxene + orthopyroxene + FeTi oxide-phyric lavas (section 3.2.4) reveal augites which are more Fe-rich than those in group 2 but similar to those in group 3, with about 15 atomic% Fe or about 0.3 CPFU (see the CaMgFe pyroxene quadrilateral in Fig. 3.8). The $Na_2O$ content of the clinopyroxenes is generally slightly higher than for the ol+plag+cpx group (0.21-0.36 wt%); $TiO_2$ is about the same; $Cr_2O_3$ is undetectable and $Al_2O_3$ covers the same range (1.6-3.3 wt%). These variations are compatible with the generally more-evolved nature of these intermediate lavas. Some obviously xenocrystal material is present in the form of gabbroic inclusions in KK08 (cf. KK26 above).

5. The clinopyroxene phenocrysts in the rhyolites (plagioclase + clinopyroxene + FeTi oxides + fayalitic olivine-phyric) are distinctly different from all the other clinopyroxenes. They lie at the low Mg-high Fe end of the trend shown in Fig 3.8, a trend which is consistent with the rhyolites having the lowest liquidus temperatures (Lindsley, 1983). Sample KK03 contains ferroaugite (with 45 atomic% Fe in Fig. 3.8), in which $Cr_2O_3$ is undetectable, MnO is high (0.92-1.00 wt% MnO), $Al_2O_3$ and $TiO_2$ lower than in other samples (0.29-0.34 wt% $TiO_2$).

The groundmasses of Krafla samples consist of up to 50% modal clinopyroxene, which may be coarsely crystalline. The compositions range from endiopside and augite through sub-calcic augite to pigeonite (Fig. 3.9). The first two types of clinopyroxene occur most frequently in groups 1 and 2. Fe, Ti and Mn increase from endiopside to augite (Fe ranging from 0.17 to 0.62 CPFU) in sample KK58. The Al contents are generally low (0.09 to 0.12 CPFU) thus justifying their plotting on a molar CaMgFe quadrilateral plot (Fig. 3.9).

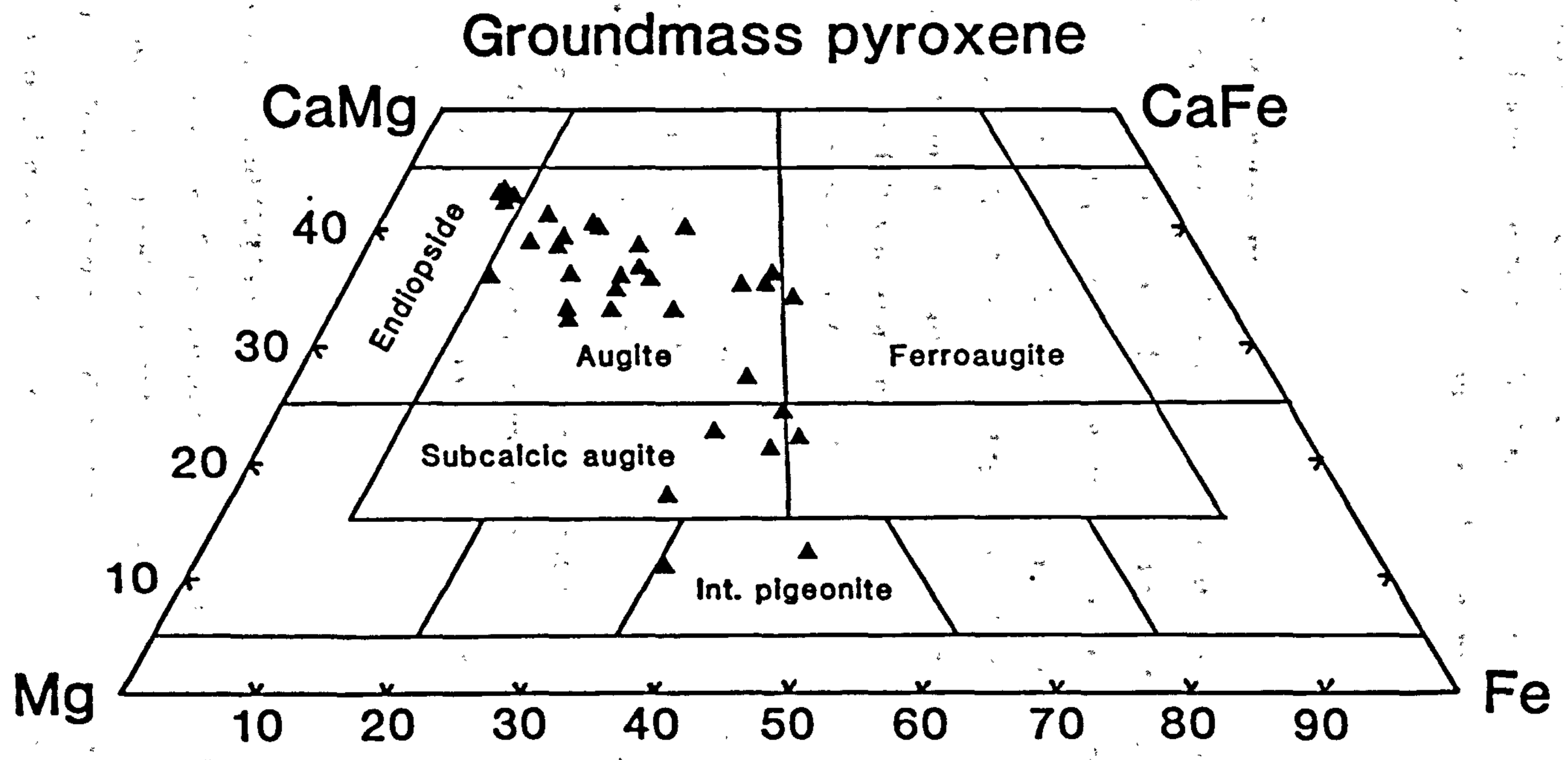


**Fig. 3.9** Groundmass pyroxene compositions on the molar CaMg-CaFe-Mg-Fe quadrilateral.

In groups 2-4 the values of Mn are higher and Cr lower than in the equivalent phenocryst clinopyroxene in these groups. Al and Na remain approximately constant. Zonation is common in groundmass clinopyroxene. The edges are rich in Fe and poor in Ca compared with the cores. The edges of some grains reach pigeonite in composition, although the fine-grained nature of the groundmass means that it is difficult to provide details of its occurrence. The pigeonite contains about 0.24 CPFU Ca (or 6.0 wt% CaO).

### 3.5.5 Orthopyroxene

Orthopyroxene is found in a small group of intermediate lavas (7 samples in total, 3 of which were examined by the electron microprobe). The mineral is only found as a phenocryst phase. It is not present in the groundmass of any Krafla samples, where another low-Ca pyroxene, pigeonite, occurs instead. Orthopyroxene ranges in composition in Mg number (Mg#) from 72 to 53 (where Mg# = atomic $Mg/(Mg+Fe^{2+})$) (bronzite to hypersthene) and contains about 0.07 Ca CPFU. Sample KK35 displays the full variation in different phenocrysts, whereas KK34 has a restricted range of compositions (Mg# 63-64). KK08 contains a single phenocryst of orthopyroxene, with an Mg# of 62. It may have been included in the rock by the mixing of magmas. The minor components of the orthopyroxene are as follows: bronzite, $TiO_2$ 0.24-0.44 wt%; $Al_2O_3$ 0.89-1.61 wt%; MnO 0.44-0.41 wt% and hypersthene, $TiO_2$ 0.20-0.35 wt%; $Al_2O_3$ 0.66-1.42wt%; MnO 0.31-0.50 wt%. The phenocrysts are not significantly zoned. Compositions are shown in Fig. 3.8. Discussion of the crystallisation temperatures implied by the compositions of coexisting orthopyroxene and clinopyroxene phenocrysts is to be found in section 3.7.1 (and Fig. 3.11).

### 3.5.6 Spinel and FeTi oxides

Three main types of opaque minerals are found in the Krafla suite of lavas; magnesiochromite, ulvöspinel-magnetite (solid solution$_{ss}$) and ilmenite-hematite$_{ss}$.

Magnesiochromite is restricted to a few samples in groups 1 and 2 containing phenocrysts of ol+plag and ol+plag+cpx. It is found only as inclusions in olivine phenocrysts. A single crystal in KK21 (group 1 lava) showed the following chemical composition: $Mg_{5.03}\ Fe^{2+}_{3.07}\ Mn_{0.11}\ Cr_{6.55}\ Al_{7.34}\ Fe^{3+}_{1.70}\ Ti_{0.15}\ Si_{0.05}\ O_{32}$. This formula was recast using the value of $Fe^{3+}$ derived from the method of Droop (1987). The spinel in KK21 is included within an olivine phenocryst of composition $Fo_{85}$. This is

in good agreement with Sigurdsson & Schilling's (1976) observation that magnesiochromites from MORBs are only stable with the most primitive magmas, in which olivine phenocrysts are Fo rich. The composition of this spinel is similar to that of spinels found in other MORBs. Rich in $Fe^{3+}$ and containing a small quantity of Ti, its composition falls near to those of the titaniferous magnesiochromites reported by Sigurdsson & Schilling (1976). A photomicrograph of olivine containing spinel inclusions is shown in Fig. 3.1.

Ulvöspinel-magnetite$_{ss}$ and ilmenite-hematite$_{ss}$ are common groundmass minerals throughout the Krafla suite, although they are most abundant in the more-evolved basalts. FeTi oxide phenocrysts, however, are restricted to the intermediate lavas and rhyolites.

Ilmenite-hematite$_{ss}$, both phenocryst and groundmass, contains a small quantity of $Fe^{3+}$ (Droop, 1987). Ilmenite-hematite$_{ss}$ phenocrysts are found in some intermediate lavas (icelandites and dacites) and rhyolites where they contain more $Fe^{3+}$ and less Mg than the groundmass ilmenite of basalts. This is a relationship consistent with derivation from a more evolved magma, at lower T and higher $fO_2$ (see section 3.7).

Ulvöspinel-magnetite$_{ss}$ crystals typically are considerably larger than ilmenite crystals. As a result, more analyses were obtained from the former. Groundmass crystals of ulvöspinel-magnetite$_{ss}$ from basalts are poorer in $Fe^{3+}$ (lower magnetite component) than in the equivalent phenocrysts from intermediate compositions and rhyolites, as is the case for ilmenite-hematite$_{ss}$. The composition of the groundmass ulvöspinel-magnetite$_{ss}$ tends towards higher values of $Fe^{3+}$, Ti and Mn but lower Al as the samples become more differentiated. The groundmass ulvöspinel-magnetite$_{ss}$ is reasonably stoichiometric in composition ($Mt_{30}Ulv_{70}$ to $Mt_{19}Ulv_{81}$), as reported from basalts from Thingmuli (Carmichael, 1967). Phenocrysts of ulvöspinel-magnetite$_{ss}$ are found in some of the same samples containing ilmenite-hematite$_{ss}$ phenocrysts. They are chemically different from groundmass ulvöspinel-magnetite, in the same way as ilmenite is different from its groundmass equivalent (i.e. higher $Fe^{3+}$ and lower Mg). The compositions of groundmass ulvöspinel-magnetite$_{ss}$ are also generally very close to stoichiometric. They range from $Mt_{50}Ulv_{50}$ to $Mt_{40}Ulv_{60}$.

Some groundmass ulvöspinel-magnetite$_{ss}$ crystals, especially from the older basalts show exsolution lamellae of ilmenite-hematite$_{ss}$. The host phase is varied in composition but usually much richer in $Fe^{3+}$ than unaltered samples from the same or comparable samples. The $Fe^{3+}$ enrichment is, however, not accompanied by decreased content of Mg and higher Mn, as might be expected from a crystal from an evolved magma.

content of Mg and higher Mn, as might be expected from a crystal from an evolved magma.

### 3.5.7 Apatite

Apatite needles are found enclosed in groundmass plagioclase in most basalts from Krafla. They are subhedral in form (5-10 μm long and 1-2 μm wide) and can be distinguished by their low birefringence and high relief. Small apatite phenocrysts have been observed in a rhyolite, KK03, in contact with magnetite phenocrysts. Because of their small size no apatite crystals have been analysed.

### 3.5.8 Alteration

All the samples from Krafla were chosen in the field to be as fresh as possible (section 2.4). However, rock specimens and thin sections were inspected for signs of alteration, in order to concentrate on the magmatic processes themselves. In fact alteration does not appear to be a problem as lava samples, especially those from the postglacial period (<10 ka), are very fresh. Only occasionally do they contain small patches of hematitic staining on the sides of vesicles. Older lavas show more common hematitic staining, occasional alteration of olivine to iddingsite and the devitrification of interstitial glass. One sample from the last interglacial period contains vesicles filled with calcite. In this case most of the olivine in the sample is altered to iddingsite.

The hyaloclastite samples are more extensively altered than the lavas and more of them contain calcite amygdales. The hyaloclastite glass may be hydrated to palagonite but altered phenocrysts are very rare. One sample (KK132) contains a low birefringence mineral (with straight extinction) in vesicles together with calcite. This mineral is likely to be thompsonite! Outline details of alteration in the Krafla samples are given in Appendix I (a).

## 3.6 Mineral chemistry: evidence for differentiation processes and magma mixing.

The rocks from Krafla appear to be divisible into several petrographic types, each of which show characteristic assemblages of phenocrysts. These assemblages together show progressive changes in mineral chemistry, consistent with their formation through gradual chemical differentiation. For example, olivine

compositions fall into two groups; $Fo_{86}$ to $Fo_{56}$ and $Fo_{13}$ to $Fo_{12}$ (see section 3.7.3 for an explanation of this bimodal distribution). Plagioclase with the form of non-megacrysts ranges from $An_{77}$ to $An_{32}$. Clinopyroxene at the same time changes from Mg-rich compositions in basalts through to Fe-rich ones in rhyolites. The apparent mineral differentiation sequence of the Krafla suite is very similar to that from many other tholeiitic volcanic systems (e.g. Mid-Atlantic Ridge (36°N), Stakes *et al.*, 1984; Iceland, Meyer *et al.*, 1985), showing similar phenocryst assemblages; for example, ol+plag and ol+plag+cpx. However, there is a major difference between Krafla and most MORB suites in that the former volcanic system generates a greater abundance of more chemically-differentiated products (see Fig. 4.21). In this respect, however, Krafla resembles the Galapagos spreading centre (Byerly *et al.*, 1976; Muehlenbachs & Byerly, 1982) which is characterised by the assemblage of plag+cpx+low-Ca pyroxene+FeTi oxides (in the low-MgO samples). These tholeiitic assemblages are generally regarded as being formed through crystal fractionation processes (e.g. Schilling *et al.*, 1983; Stakes *et al.*, 1984). Chapter 4 documents the changes in whole-rock composition and models the changes in whole-rock composition through fractional crystallisation using the nature and compositions of the observed phenocryst assemblages.

Despite the general progression from high- to low-temperature phenocryst phases, across the range of petrographic groups described above, there is considerable detailed variation in phenocryst composition even within individual samples. This is particularly noticeable for plagioclase. The textures and primitive compositions of the plagioclase megacrysts (section 3.2.6) suggest that they did not crystallise directly from the magma represented by the groundmass, but were formed elsewhere in equilibrium with a more primitive magma (i.e. they are xenocrysts).

Typical plagioclase compositions range from $An_{80}$ to $An_{90}$ in the cores and mantles. Overgrowths, although more varied, have compositions similar to those of microphenocrysts, which are likely to be in equilibrium with the groundmass. The three-part character of the plagioclase megacrysts is consistent with two changes in the crystal-growth environment (Kuo & Kirkpatrick, 1982), i.e. compatible with two magma mixing events. Several authors (e.g. Stolper & Walker, 1980; Sparks *et al.*, 1980; Huppert & Sparks, 1982; Sparks & Huppert, 1984; Meyer *et al.*, 1985) have described a possible mixing process whereby hot, dense primitive magma is injected into a more chemically-evolved magma reservoir. This results in the ponding of primitive magma beneath the more evolved magma in the chamber until fractional crystallisation has reduced the density of the former sufficiently for convective overturn and mixing to occur. Such behaviour of a magma should lead to two phases

of plagioclase growth; one prior to overturn and another in the mixed magma. This may be the explanation for the different phases of growth observed in the plagioclase megacrysts. The core and mantle compositions (both in the range $An_{80}$ to $An_{90}$) are consistent with both magmas crystallising relatively primitive compositions of plagioclase. An idealised plot of density against magma composition in Fig. 3.10 (after Sparks & Huppert, 1984) shows that the position of the appearance of plagioclase on the liquidus roughly coincides with the density minimum, suggesting that plagioclase crystallisation and convective overturn could occur over a short period of time. A possible primitive injected magma is shown at point A (Fig. 3.10) and a more evolved magma at B, i.e just crystallising plagioclase. Densities will be the same when the primitive magma has crystallised enough olivine to lower its density to point B, by which stage the more evolved magma will still be close to this point (olivine crystallisation more rapidly decreases *M* (see Fig. 3.10) than the crystallisation of ol+plag together). The resultant mixed magma may lie close to B, which means that further plagioclase crystallisation could continue outside the plagioclase cores already formed. The primitive nature of both the core and mantle zones indirectly suggests that such a mixing event occurred at considerable depth, leaving the overgrowth/mantle transition to form at a shallower level in the crust (see below). Tryggvason (1986) has identified a body of magma, accumulating beneath the oceanic crust at a depth of 8-10 km, which would be an ideal environment for these cores and mantles of plagioclase to crystallise.

The outer break between mantle and overgrowth, described earlier, is a much more pronounced compositional jump than between core and mantle. The outer break typically separates a mantle of composition $An_{85}$ from a rim of $An_{60}$-$An_{70}$. The latter compositions imply that the final stage of crystallisation took place at considerably lower temperatures (i.e. probably at shallower depths) than the cores and mantles. The thin nature of the overgrowth hints that the interval of time between the time at which it began to form and eruption was short, compared with the time required for the crystallisation of the more primitive core and mantle. Geophysical evidence from the 1975-1984 eruptive cycle confirms that shallow-level mixing occurs before eruption at a depth of about 3 km, with an average reservoir residence time of several months (Björnsson, 1985). Such a period of mixing is a plausible explanation for the generation of the thin plagioclase rims (see Chapter 7 regarding the possibility of a 2-stage crustal assimilation model).

An alternative mode of formation of some megacrysts is by the incorporation of cumulate crystals into the magma. However, most megacrysts provide little textural evidence for growth or compaction in a crystal mush.

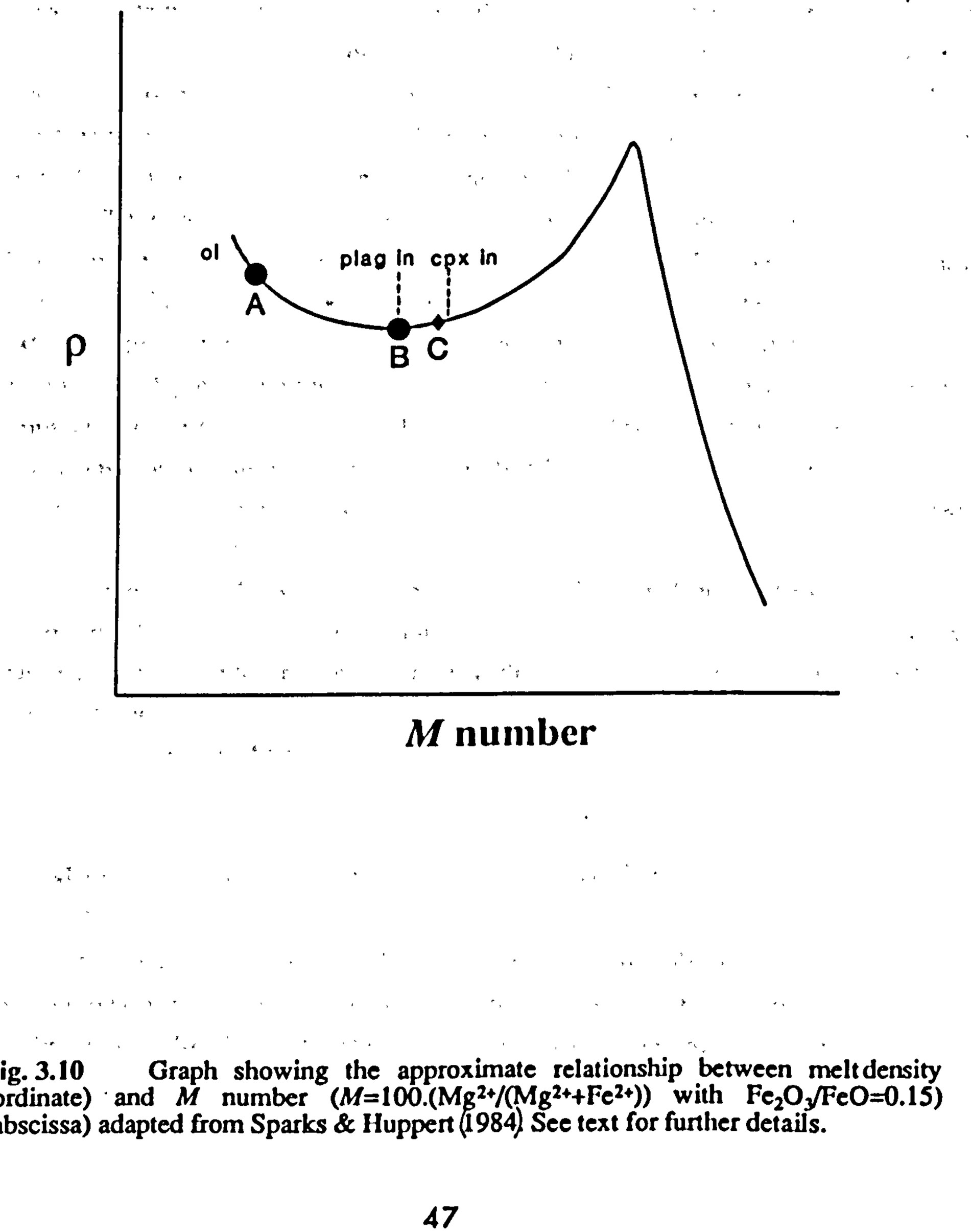


**Fig. 3.10** Graph showing the approximate relationship between melt density (ordinate) and *M* number ($M=100.(Mg^{2+}/(Mg^{2+}+Fe^{2+}))$ with $Fe_2O_3/FeO=0.15$) (abscissa) adapted from Sparks & Huppert (1984). See text for further details.

The occurrence of complex plagioclase megacrysts in *virtually all* Krafla samples (apart from the rhyolites) suggests that magma mixing has affected most compositions. This certainly is in accord with the geophysical evidence from the 1975-1984 eruptive cycle (Chapter 2).

Plagioclase is the phenocryst phase of the lowest density in the tholeiitic system (Sparks *et al.*, 1980) and the dominance of plagioclase megacrysts may reflect selective accumulation by flotation or selective removal of other denser phases (Bryan, 1983). However, McBirney & Noyes (1979) suggested that plagioclase flotation was unlikely because typical yield strengths of magmas were too high. This experimental investigation seems in direct conflict with the observation that some basalts contain large modal proportions of plagioclase, far in excess of that expected by the crystallisation of the coexisting liquid. There is little convincing evidence for plagioclase-only saturated liquids in the literature. This suggests that the plagioclase must have been added to the liquid in some manner. Flotation is probably the best way of selectively accumulating plagioclase (e.g. Cox & Mitchell, 1988).

The rhyolites contain no plagioclase xenocrysts, suggesting that rhyolitic liquids present in the Krafla magma reservoir have not mixed with primitive magmas containing plagioclase xenocrysts, perhaps as a result of rhyolite formation during extended periods of crystallisation without magma recharge. Alternatively, the absence of plagioclase xenocrysts may imply that the rhyolite was largely derived from crustal partial melting of altered wall-rock. Therefore the incorporation of plagioclase xenocrysts would be unlikely. In Chapters 5 and 7 independent lines of evidence from trace-element concentrations and ratios and isotope ratios are presented in favour of the latter argument.

As mentioned above, other minerals also show evidence that magma mixing has occurred. For instance a wide range of compositions of olivine are found in many basalts, too variable to be in equilibrium with one magma (Roeder & Emslie, 1970). However, the olivines, unlike the plagioclases, preserve few obvious textural signs of reacting with liquids of variable compositions.

## 3.7 Magma temperature, $fO_2$ and phase equilibria

### 3.7.1 General

Grönvold & Mäkipää (1978) used electron microprobe analyses of glass and mineral phases to estimate the temperature of selected Krafla magmas, following the calibrations of Roeder & Emslie (1970) for olivine-liquid equilibria, and Kudo &

Weill (1970) and Drake (1976) for plagioclase-liquid equilibria. They also estimated $fO_2$ values by the method of Roeder & Emslie (1970).

This project has concentrated on Krafla's older holocrystalline samples. Few glass analyses have been obtained, meaning that geothermometers such as those listed above cannot be applied. There is the complication that the presence of considerable intra-sample phenocryst variation in mineral chemistry suggests that the application of crystal-glass equilibria with fixed $K_d$ values may be of little use, except where textural signs of equilibrium can be confirmed (cf. Stakes *et al.*, 1984). However, despite the problems of xenocrysts and non-equilibrium phenocryst assemblages, there are two available geothermometers, which do not rely on the availability of glass analyses. They are the two-pyroxene and the $magnetite_{ss}$-$ilmenite_{ss}$ geothermometers. The latter geothermometer also may be used to constrain $fO_2$ values at the time of crystallisation.

The two-pyroxene geothermometer has limited application to the Krafla suite because only a small number of samples contain two types of pyroxene phenocryst (see section 3.2.4). However, whenever possible, temperature estimates have been made using the graphical method of Lindsley (1983), which is based on the experimental calibration of pyroxene compositions at different pressures (see Fig. 3.11). Lindsley offers a choice of different crystallisation pressures. As the crystallisation pressure is thought to be low (<3 kb), from geophysical evidence and from the lack of high pressure pyroxenes (cf. Thompson, 1987), the 1 atm calibration is probably most applicable. The ratio of $Al^{IV}/Al^{VI}$ in the pyroxene crystals can indicate the pressure of crystallisation. Low ratios found throughout the suite are typical of low-pressure pyroxenes. Lindsley's method involves recasting the minor components of the pyroxene analyses and the projection of the result onto a Wo-En-Fs plot. Since all the pyroxenes contain only small amounts of the minor components (e.g. jadeite, acmite) the resulting plot (Fig. 3.11) is similar to that of Fig. 3.8, where minor components were ignored. Estimated temperatures of the intermediate rock types containing two pyroxenes are 900°C for KK34 and 1020°C for KK35. KK08 provides an estimate of about 1150°C but as this sample contains many crystals of probable xenocrystal origin, the pyroxene pair may not be in equilibrium. Other representative analyses of clinopyroxenes (from one-pyroxene lavas) are also plotted on Fig. 3.11. A range of temperatures from 800 to 1300°C is indicated. The majority of the basalts do not exceed 1200°C.

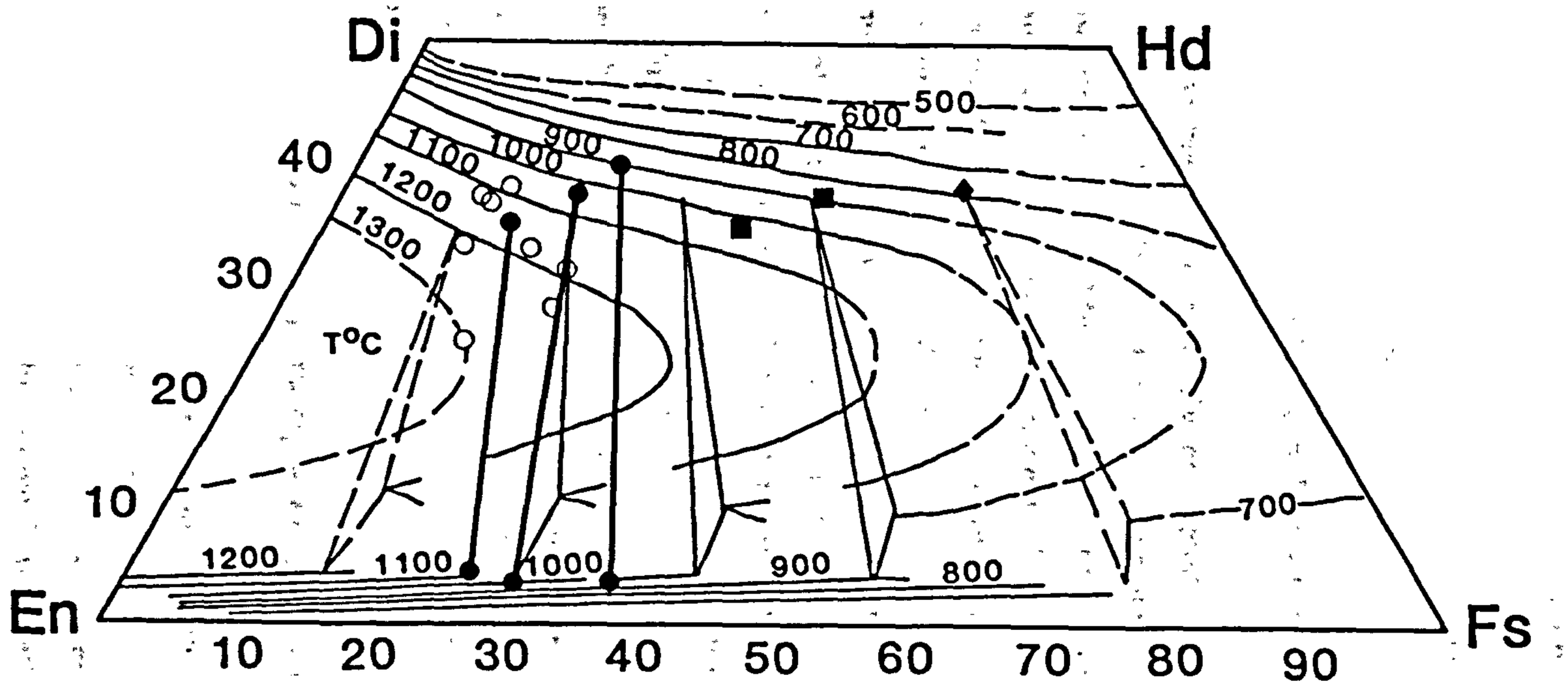


**Fig. 3.11** Representative analyses of Krafla pyroxene phenocrysts plotted according to the projection scheme of Lindsley (1983), showing the estimated crystallisation temperatures. Tie-lines indicate coexisting pairs of pyroxene phenocrysts. Symbols as in Fig. 3.8.

### 3.7.2 $fO_2$ determinations

Some coexisting examples of ilmenite and magnetite have been analysed, both from the groundmass of basalts and phenocrysts in the differentiated lavas (e.g. intermediates). The equilibria between solid solutions of ilmenite-hematite and magnetite-ulvöspinel can be used to estimate both the temperature and oxygen fugacity ($fO_2$) at the time of crystallisation. The following equilibrium reaction is a geothermometer independent of $fO_2$;

$$FeTiO_3 + Fe_3O_4 = Fe_2O_3 + Fe_2TiO_4$$

This equation has been experimentally calibrated in the system $FeO\text{-}Fe_2O_3\text{-}TiO_2$ (Buddington & Lindsley, 1964). However, ilmenite and magnetite contain other minor components (e.g. MgO, MnO) which affect the temperature estimate and some allowance must be made for these components. Buddington & Lindsley recast their analyses to allow for site occupancy of minor components and then graphically deduce the temperature of crystallisation. In contrast, Powell & Powell (1977) obtained a numerical version based on the same experimental data, in which the concentrations of the minor components can be used to assess estimates of the error on the temperature determination. Temperature estimates using this method vary from 730 to 900°C for the phenocrysts in KK34, comparable with the approximate temperature values obtained from the 2-pyroxene thermometer (section 3.7.1). The determinations, based on data from groundmass, were all performed on basalts. They range from 930 to 1070°C, either reflecting variable temperatures during basalt groundmass crystallisation or non-equilibrium conditions during quenching.

The following equation can be used to deduce a value for the $fO_2$ during crystallisation;

$$6FeTiO_3 + 2Fe_3O_4 = 6Fe_2TiO_4 + O_2$$

The minor components are the main source of uncertainty over the $fO_2$ determination in the same way as for the temperature estimates.

The method of Powell & Powell (1977) was used again and the results are presented in Fig 3.12. The log $fO_2$ values range from about -10 to -17, and lie close to the experimentally determined buffer of quartz-fayalite-magnetite (QFM) in Fig 3.12. The error bars are calculated using the method of Powell & Powell (1977). The results are similar to those obtained by Carmichael (1967) on Thingmuli.

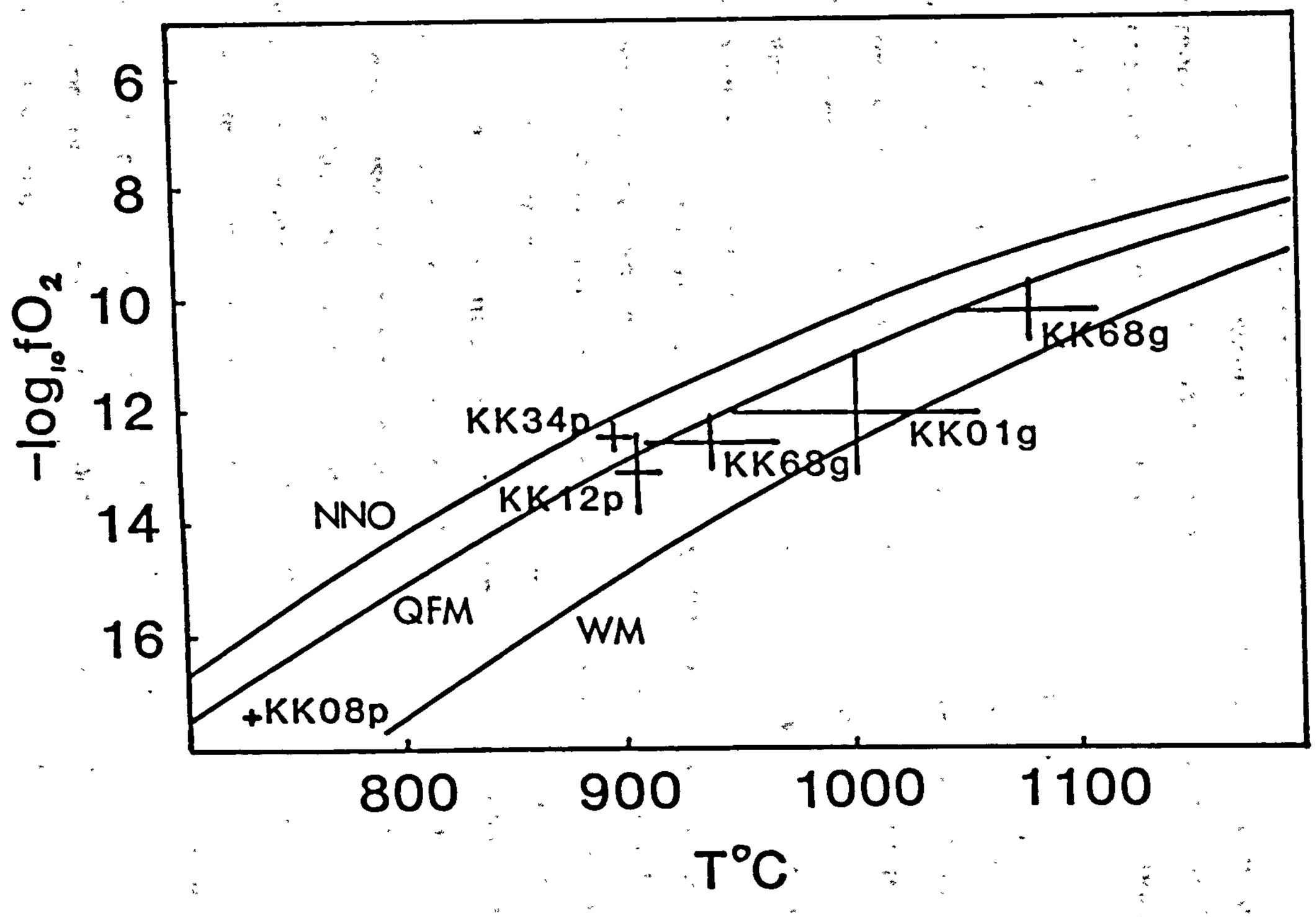


**Fig. 3.12** Iron-titanium oxide equilibration temperatures and oxygen fugacites, calculated following the method of Powell & Powell (1977). The 3 labelled curves NNO, QFM and WM represent the buffer curves nickel-nickel oxide, quartz-fayalite-magnetite and wustite-magnetite respectively (after Carmichael 1967); p = phenocryst; g = groundmass.

Studies on pillow basalts have revealed that pillow rims are considerably more reduced than QFM (Christie *et al.*, 1986) and that pillows are usually $fO_2$ zoned to QFM in the relatively oxidised cores. Hence the position of the Krafla basalts close to QFM may not reflect the oxygen fugacity of the primitive magma but instead the relatively oxidised nature of crystallisation conditions in the crust.

### 3.7.3 Phase equilibria

The petrographic assemblages described in section 3.2 can be interpreted with reference to the progressive crystallisation of phenocryst phases as the magma cools. Experimentally determined phase diagrams may help in the understanding of the course of liquid differentiation (Cox *et al.*, 1979).

The phenocryst assemblages distinguished above are; ol+plag, ol+plag+cpx, plag+cpx±ol, plag+cpx+opx+FeTi oxides, plag+cpx+fayalitic olivine+FeTi oxides. MORB data suggests that the assemblages are arranged above in an order of progressive crystallisation with decreasing magmatic temperatures (Byerly *et al.*, 1976; Byerly, 1980; Sigurdsson, 1981; Schilling et al., 1983). This is confirmed in Chapter 4 by comparing the changes in assemblage with that of the major-element compositions of the magmas.

The quaternary system Fo-Di-An-Sil at 1 atm is useful for basaltic compositions and can be used to confirm the crystallisation order of the observed phase assemblages. A possible crystallisation pathway is presented in Fig 3.13a (taken from Presnall *et al.*, 1978). Olivine is generally thought to be the first phase crystallising from most magmas derived from the mantle (Yoder, 1976). It is followed in most tholeiites by plagioclase. There is no petrographic evidence for an olivine-only assemblage from the Krafla samples, although other Icelandic volcanoes do produce lavas which seem to be in equilibrium with only olivine. The ol+plag assemblage produced at the highest temperatures of all the assemblages present in the Krafla suite is formed in Fig. 3.13a by crystallisation along the surface cdpab away from An and Fo. Clinopyroxene can begin to crystallise together with ol+plag along the join ap, and at point p olivine begins to react with the liquid forming low-Ca pyroxene (opx) instead. Under conditions of equilibrium crystallisation the liquid would stay at p until all olivine had been removed from the magma before proceeding down temperature to the eutectic minimum point m. This means that an assemblage of ol+plag+cpx+opx would be expected, as opx replaced ol. However, ol and opx are not found together, probably suggesting that equilibrium conditions are rarely obtained and that fractional crystallisation occurs.

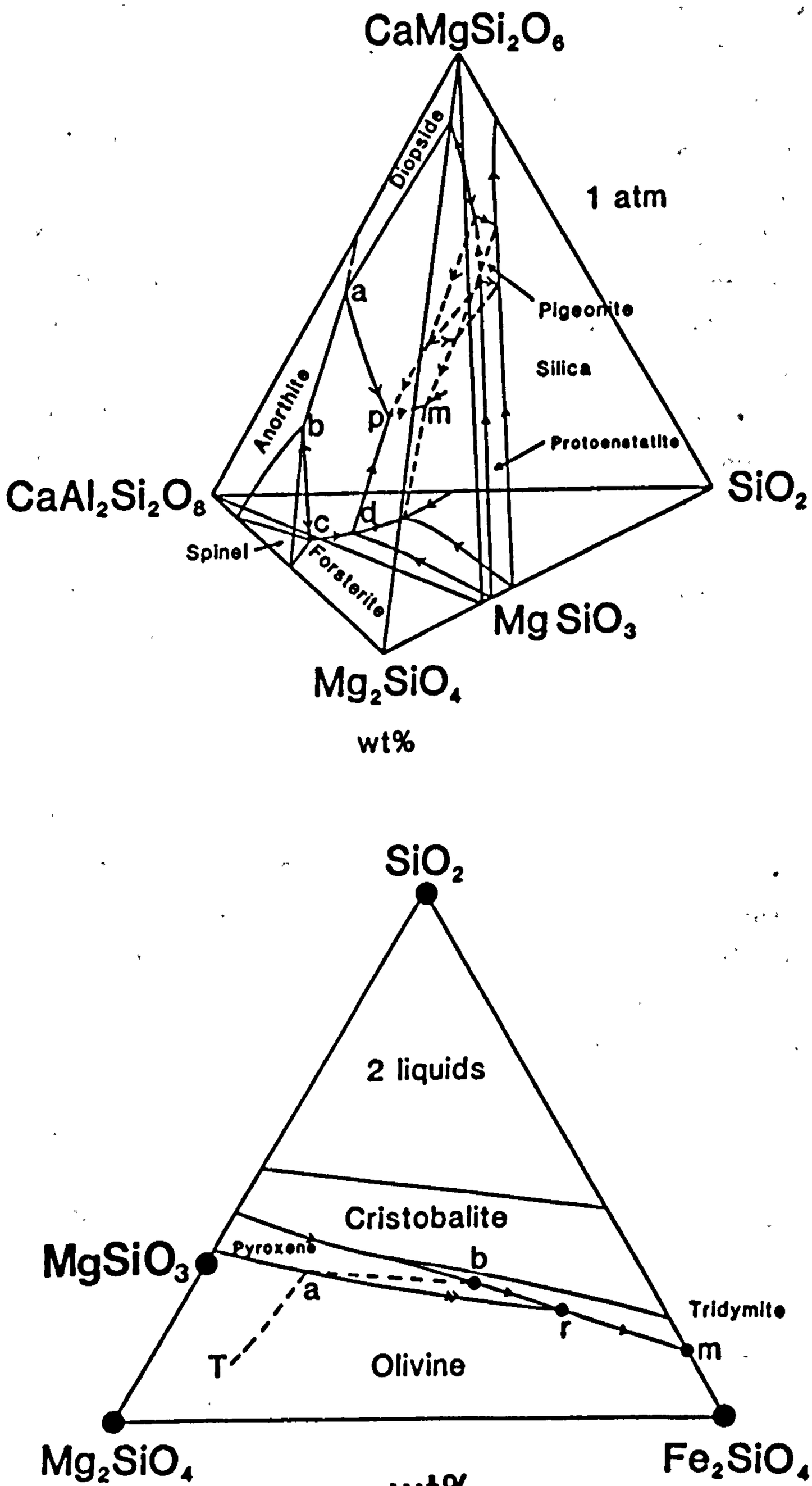


**Fig. 3.13 (a)** The forsterite-diopside-anorthite-silica system at 1 bar after Presnall *et al.* (1978), showing the likely course of liquid evolution for the Krafla suite (see text).
**(b)** The forsterite-fayalite-silica system after Bowen & Schairer (1935).

The appearance of FeTi oxides cannot be accounted for in the system Fo-Di-An-Sil (Fig. 3.13a) because the system does not include an Fe-bearing phase. However, Fig 3.13b shows the system Fo-Fa-Sil, which contains Fe. This can account for the disappearance and subsequent reappearance of olivine during fractional crystallisation of a primitive composition (see typical fractional crystallisation pathway Tabrm). When the olivine returns to the liquidus it is Fe-rich, which is consistent with the fayalitic-olivine compositions found in the Krafla rhyolites.

In the quaternary system Fo-An-Mag-Sil in Fig 3.14 the majority of 3-phase basalts would crystallise along the join BR. When the liquid reaches R olivine reacts with the liquid as described above and the crystallisation assemblage changes from ol+plag+pyroxene to plag+pyroxene+magnetite, ignoring the pyroxene type in this system. Then the liquid can differentiate further to the eutectic minimum point G. However the phases occurring at G and the exact position of this point may be inaccurate due to the absence of Na and K from this system.

These phase diagrams appear to explain many of the first-order petrographic observations of the Krafla differentiation series, which are similar to many MORB assemblages.

## 3.8 Summary

Distinct phenocryst assemblages have been identified in the Krafla lavas. Basalts contain ol+plag, ol+plag+cpx or plag+cpx±ol, whereas many lavas of intermediate composition (icelandites and dacites) have FeTi oxides and orthopyroxene phenocrysts without olivine, and the rhyolites develop a fayalitic olivine in place of orthopyroxene. These assemblages are similar to those observed in most ocean ridge tholeiite suites.

Most samples also contain complexly-zoned plagioclase megacrysts, which suggests that most lavas have seen at least two stages of magma-mixing prior to eruption. This fits well with the geophysical evidence. It is likely that the first mixing event took place at the base of the oceanic crust and was followed by shallow-level mixing shortly before eruption.

The absence of plagioclase megacrysts from the rhyolites suggests that these magmas may have been unable to mix with primitive magmas, possibly because of high crustal-level differentiation, with or without crustal assimilation.

Phase equilibria suggest that the phenocryst assemblages of Krafla can be readily explained by a process of progressive magma fractional crystallisation. Such a hypothesis is tested in Chapters 4 and 5.

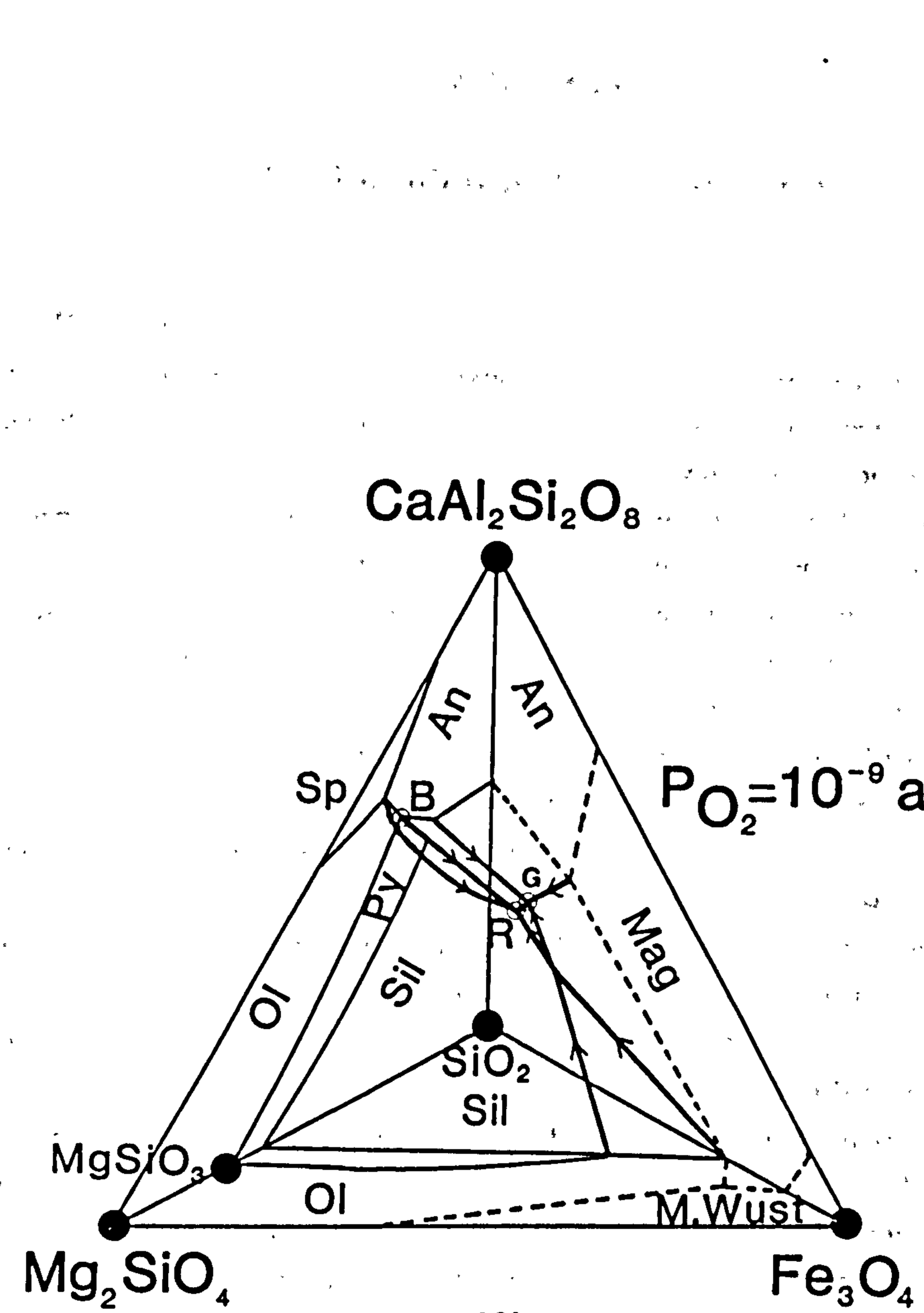


**Fig. 3.14** The phase relations of the system forsterite-anorthite-magnetite-silica at an oxygen fugacity of $10^{-9}$ atm (Roeder & Osborn 1966).

# Chapter 4

# Major-element compositions

## 4.1 Rationale

Major-element whole-rock compositions of volcanic rocks may be used to test hypotheses concerning magmatic processes. Traditionally the chemical diversity of ocean ridge rocks has been ascribed primarily to two types of process. From one viewpoint the range of compositions is considered to reflect differing extent and conditions of fractional crystallisation in shallow magma reservoirs. From the other, however, the differences are regarded as being due mostly to the melting process with the effects of fractional crystallisation being only of secondary importance. However, it seems more likely that the variation in observed compositions of ocean ridge rocks, including those of Krafla, reflect the sum of several influences. These are likely to include the two mentioned above together with the effects of magma mixing and the interaction of the magma with its surroundings (i.e. contamination or assimilation).

A range of chemical compositions of lavas/hyaloclastites is seen in the Krafla volcanic system spanning the common tholeiitic differentiation sequence of basalt, icelandite (tholeiitic andesite), dacite and rhyolite. The observed range in chemical composition is considerably larger than is usually found in the ocean ridge environment (see Fig. 4.21). This large range may be ascribed to the greater importance of shallow-level processes (e.g. fractional crystallisation and assimilation) because of the larger, more permanent magma chambers developed in the abnormally-thick Icelandic crust. Most of the lavas erupted from Krafla have compositions which are chemically too evolved to have been derived directly from the mantle (e.g. $M<68$, where $M=100.Mg/(Mg+Fe^{2+})$ and $Fe_2O_3/FeO=0.15$ is specified). However, there is evidence (presented in this Chapter and Chapter 6) that, although the effects of crystallisation processes appear to be dominant, there is a mantle-melting signature preserved behind the differentiation trends, justifying the claim that the variation in chemical compositions arises from the result of the sum of different causes.

Major-element whole-rock compositions, together with the compositions of mineral phases present as phenocrysts, can enable the hypothesis that the Krafla suite formed by fractional crystallisation to be tested in several different ways. These include the graphic use of oxide-oxide plots, computer based least-square fitting calculations, and by computer simulation of fractional crystallisation from

experimental data. It will be shown below that fractional crystallisation alone cannot explain all the features of the major-element whole-rock compositions, and that other processes need to be invoked such as magma mixing, the effects of partial melting, and crustal assimilation. The geochemical effects of the first of these processes are discussed in this Chapter. A more detailed discussion of the partial melting process in particular is left to Chapter 6, where a quantitative model for melt generation at spreading centres (McKenzie & Bickle 1988) is applied to Krafla. Evidence in favour of crustal assimilation is presented in Chapter 7.

## 4.2 Analytical details

The majority of samples collected from Krafla are fine-grained, mostly aphyric lavas. Whole-rock compositions were obtained by X-ray fluorescence (XRF) spectrometry at the University of Edinburgh and these compositions have been used in the most part directly to represent liquid compositions. The limitations of using whole-rock analyses in this way are discussed in section 4.4.2.

XRF analyses were carried out mostly on a Philips PW1450 spectrometer using a Rh-anode X-ray tube, although a few samples were analysed for major elements on a PW1480 machine using a Cr-anode tube. Details of sample preparation and analytical procedure are contained in Thirlwall (1979), Fitton & Dunlop (1985) and Wallis (1989) (also see Appendix VI (a)). Over 150 samples were analysed, covering a wide range in age (Chapter 2), rock composition and geographical location. The chemical compositions of the samples are listed in Appendix IV. Estimates of XRF accuracy and precision are given in Appendix VI (a). Analyses that were not originally collected as part of this thesis are noted in Appendix IV by crosses.

## 4.3 Classification

Volcanic rocks have been traditionally classified chemically in several ways. One name may then convey the approximate chemical composition, without the need to specify a long list of oxide concentrations (Cox *et al.*, 1979). There are three regularly used chemical classifications of this kind. The first is based on total alkalies ($Na_2O+K_2O$) and silica concentrations. It has long been recognised that such a diagram can discriminate between rock series of different petrogenetic origin. A plot of $Na_2O+K_2O$ *vs* $SiO_2$ is shown in Fig. 4.1, with the alkaline/sub-alkaline divide (Irvine & Baragar, 1971) and the Icelandic Thingmuli trend (Carmichael, 1964)

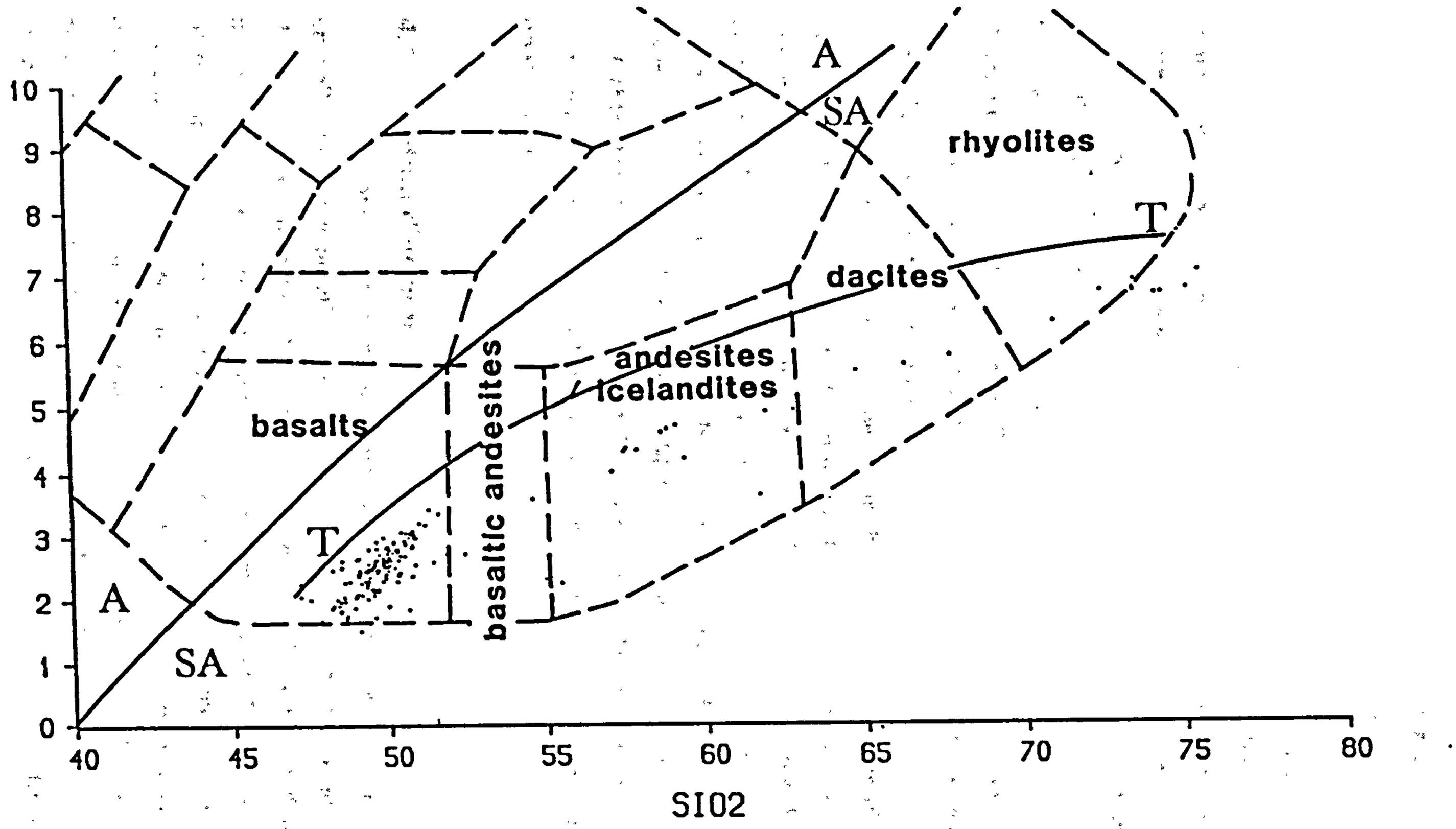


**Fig. 4.1** $Na_2O + K_2O$ *vs* $SiO_2$ for the whole Krafla suite of whole-rock compositions (dots). The trend labelled T shows the range of compositions found from Thingmuli (Carmichael 1964) and the division A/SA reflects the alkaline/sub-alkaline divide of Irvine & Baragar 1971.

shown for comparison. Krafla shows a sub-alkaline trend from basalt through to rhyolite, although most of the rocks are basaltic and cluster at values close to 50% $SiO_2$ and 2% $Na_2O+K_2O$. This cluster of points results from the relatively slow initial increase in both $SiO_2$ and alkalies during fractional crystallisation of basaltic liquids. Therefore this classification does not distinguish very well between primitive and more evolved basalt types, but it is useful for discriminating between basalts and the more-differentiated compositions (icelandites, dacites and rhyolites).

A second type of classification is based on normative mineralogy. In the tholeiitic system there is a shift from *ol*-normative compositions in the most primitive basalts through to *qz*-normative in the more evolved basalts and even more differentiated rocks. Therefore, unlike the alkali-silica classification, this scheme can distinguish between different basalts. However, normative mineralogy is difficult to use in fractional crystallisation modelling.

From this discussion it appears that both of the above classification schemes have disadvantages. However, Thompson (1973,1987) has pointed out that the MgO contents of basalts correlate well with their liquidus temperatures. Hence the MgO content of a basalt can be used to monitor the progress of fractional crystallisation. For this reason MgO is used in this thesis as a means of easily describing basalt chemistry. As an alternative to MgO one may use the magnesium number ($100.(Mg/(Mg+Fe^{2+}))$ or *M*), which is also a useful index of fractional crystallisation, although like the norm it is less easily related to the compositions of phases actually crystallising.

## 4.4 Variation diagrams

Oxide-oxide variation diagrams can be used to assess the role of fractional crystallisation in generating the observed range of volcanic products in Krafla. As discussed above in section 4.3, the major element oxides are plotted against MgO to provide an indication of the extent of differentiation (Figs. 4.2 to 4.13). The samples plotted are divided into several categories; firstly by phenocryst assemblages (see Chapter 3), secondly by phenocryst content (i.e. aphyric and phenocryst-rich), and thirdly by plotting age as in the subdivisions of Table 2.1. The graphs subdivided according to phenocryst assemblage may help qualitatively to test the fractional crystallisation hypothesis, by revealing the effects on chemical trends as different phases are removed from the liquid (section 4.4.1). Phenocryst accumulation is important since the presence of large amounts of phenocrysts can ensure that the trends seen in variation diagrams are not those representing the true liquid

compositions (section 4.4.2). The time subdivisions allow the investigation of the temporal evolution of the volcanic system (section 4.4.3).

### 4.4.1 Petrographic subdivision

The variation of major element oxides with MgO is shown in Figs. 4.2 to 4.6. The observations are summarised as follows:

(i) $SiO_2$ *vs* MgO (Fig. 4.2a). $SiO_2$ remains approximately constant (at 48 to 50 wt%) as MgO decreases from 10 to 5 wt%, but increases rapidly with further decrease of MgO. The $SiO_2$-constant part of this graph coincides with the occurrence of assemblages of phenocrysts of ol+plag and ol+plag+cpx. The $SiO_2$ content of the basalts is therefore buffered during the extraction of these phases but when, at 5 wt% MgO, ilmenite-hematite$_{ss}$ and ülvospinel-magnetite$_{ss}$ start to crystallise, the $SiO_2$ concentration of the extract is decreased.

(ii) $Al_2O_3$ *vs* MgO (Fig. 4.2b). A general decrease in $Al_2O_3$ from about 16 to 12 wt% is seen as the MgO content changes from 10 to 0 wt%. The positive correlation between $Al_2O_3$ and MgO reflects the crystallisation of plagioclase, the only fractionating phase containing significant $Al_2O_3$ (about 30%). The generally flatter trend at low values of MgO may be explained by the lower $Al_2O_3$ concentrations in Ab-rich plagioclase. Note that some samples have higher $Al_2O_3$ contents than the general trend both for basalts and intermediate rocks. Samples with higher values of $Al_2O_3$ are mostly those which have accumulated plagioclase and these are discussed in section 4.4.2.

(iii) $Fe_2O_3$ (total) *vs* MgO (Fig. 4.3a). Total Fe, reported as $Fe_2O_3^*$ (an asterisk indicates total Fe), reaches a peak in concentration (16 wt%) at about 5 wt% MgO, after which it falls to a minimum value close to 1 wt% in the rhyolites. The low values of $Fe_2O_3^*$ seen in some samples which contain between about 8 and 6 wt% MgO may be attributed to plagioclase accumulation (section 4.4.2). The increase in $Fe_2O_3^*$ from 10 to 5 wt% MgO can be understood if the crystallising assemblage contains a high proportion of plagioclase, making the composition of the bulk extract lower in Fe than that of the liquid. The change at about 5 wt% MgO is consistent with the start of crystallisation of FeTi oxides, which contain high concentrations of Fe.

(iv) CaO *vs* MgO (Fig. 4.3b). CaO is buffered at MgO contents between 10 and 8 wt%, which is consistent with an ol+plag extract assemblage (minimal cpx). The

introduction of clinopyroxene as a phenocryst phase at ~8 wt% MgO then leads to decreasing CaO values. The appearance of the FeTi oxide phenocrysts might be expected to lead to some relative increase in CaO, but this is not apparent presumably because the proportion of these minerals in the assemblage crystallising must be sufficiently small for the effect not to be seen (at least in terms of CaO).

(v) $Na_2O$ *vs* MgO (Fig 4.4a). $Na_2O$ steadily increases with decreasing MgO with the slope greatest at the lowest values of MgO. Some Na is incorporated into plagioclase, especially as the plagioclase becomes more-Ab rich with decreasing MgO, and some into clinopyroxene (however, generally very little in tholeiitic systems). Overall $Na_2O$ behaves as a moderately incompatible component, leading to the gradual increase in $Na_2O$ with differentiation.

(vi) $K_2O$ *vs* MgO (Fig. 4.4b). $K_2O$ rapidly increases with decreasing MgO, although there is considerable scatter in the basalt region (see Chapter 5). Overall the large increase in $K_2O$ from 10 wt% to 0 wt% MgO can be qualitatively explained by the absence of any phase which removes significant $K_2O$ from the liquid. However, the absolute increase with differentiation is probably too large for fractional crystallisation alone. This will be discussed below in section 4.5. The abrupt change in slope at about 5 wt% MgO is unlikely to result from any change in $K_2O$ behaviour, but results from the changing rate of removal of MgO as the FeTi oxides begin to crystallise.

(vii) $TiO_2$ *vs* MgO (Fig. 4.5a) reveals a similar trend to that of $Fe_2O_3^*$ vs MgO (Fig. 4.3a). Ti is only present in small quantities in clinopyroxene (0.3 to 1.2 wt% $TiO_2$), and therefore providing there is not too high a proportion of clinopyroxene in the phase assemblage, $TiO_2$ will increase significantly in the residual liquid during the early stages of crystallisation. At about 5 wt% MgO, and coinciding with the appearance of FeTi oxide phenocrysts, the $TiO_2$ content begins to decrease.

(viii) $P_2O_5$ *vs* MgO (Fig. 4.5b). $P_2O_5$ appears to behave in a similar way to both $Fe_2O_3^*$ and $TiO_2$, increasing as MgO changes from 10 to 5-4 wt% MgO, then decreasing to low concentrations in the rhyolites. Apatite crystallisation is the most likely cause of the decrease in $P_2O_5$, few apatite crystals have been observed. All observed tholeiitic phenocryst phases take up little $P_2O_5$, which explains the general increase in P content throughout the basaltic differentiation series.

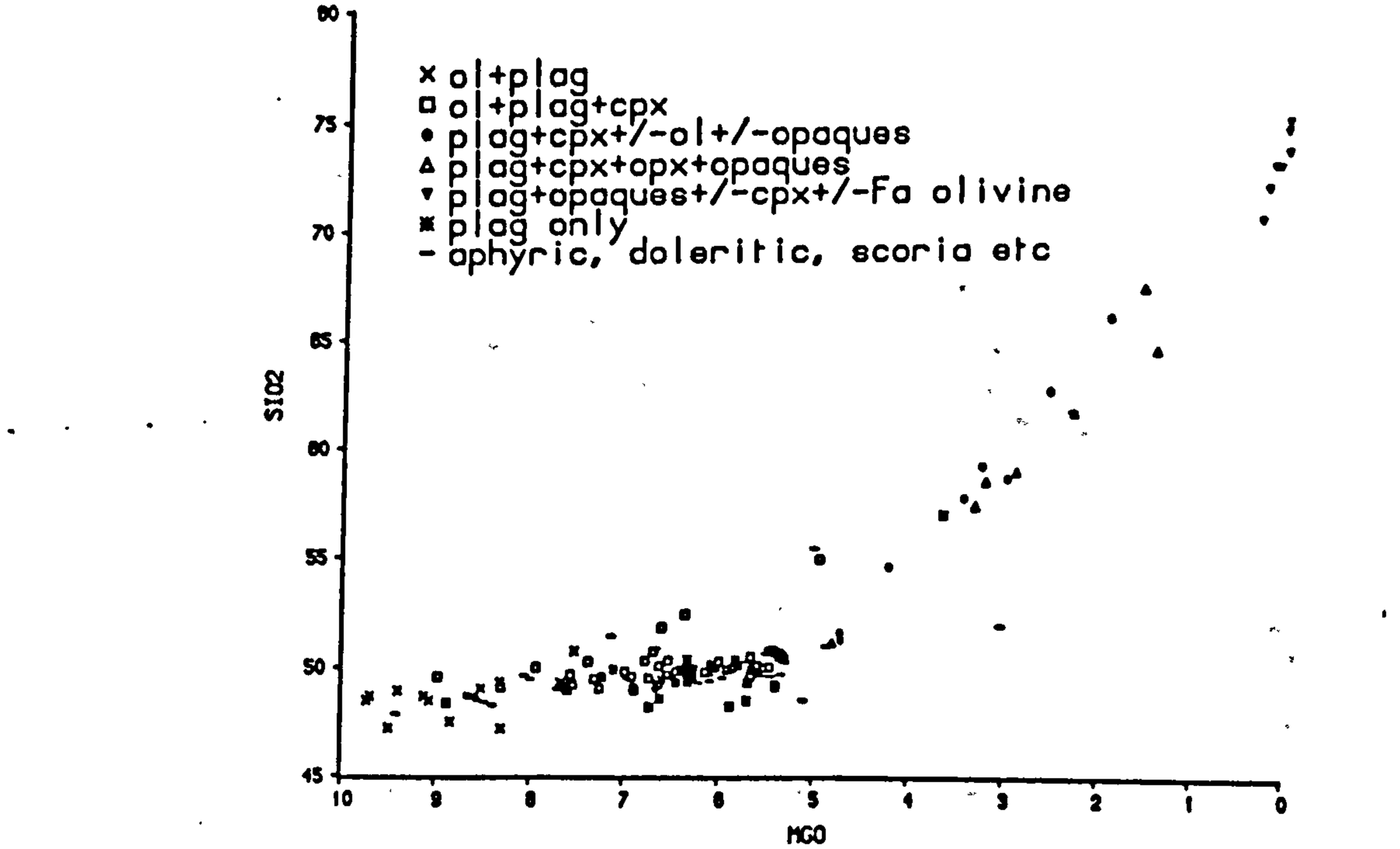


**Fig. 4.2 (a)** $SiO_2$ *vs* MgO, showing the various phenocryst assemblages (see key on diagram).
**(b)** $Al_2O_3$ *vs* MgO, details as Fig. 4.2 (a)

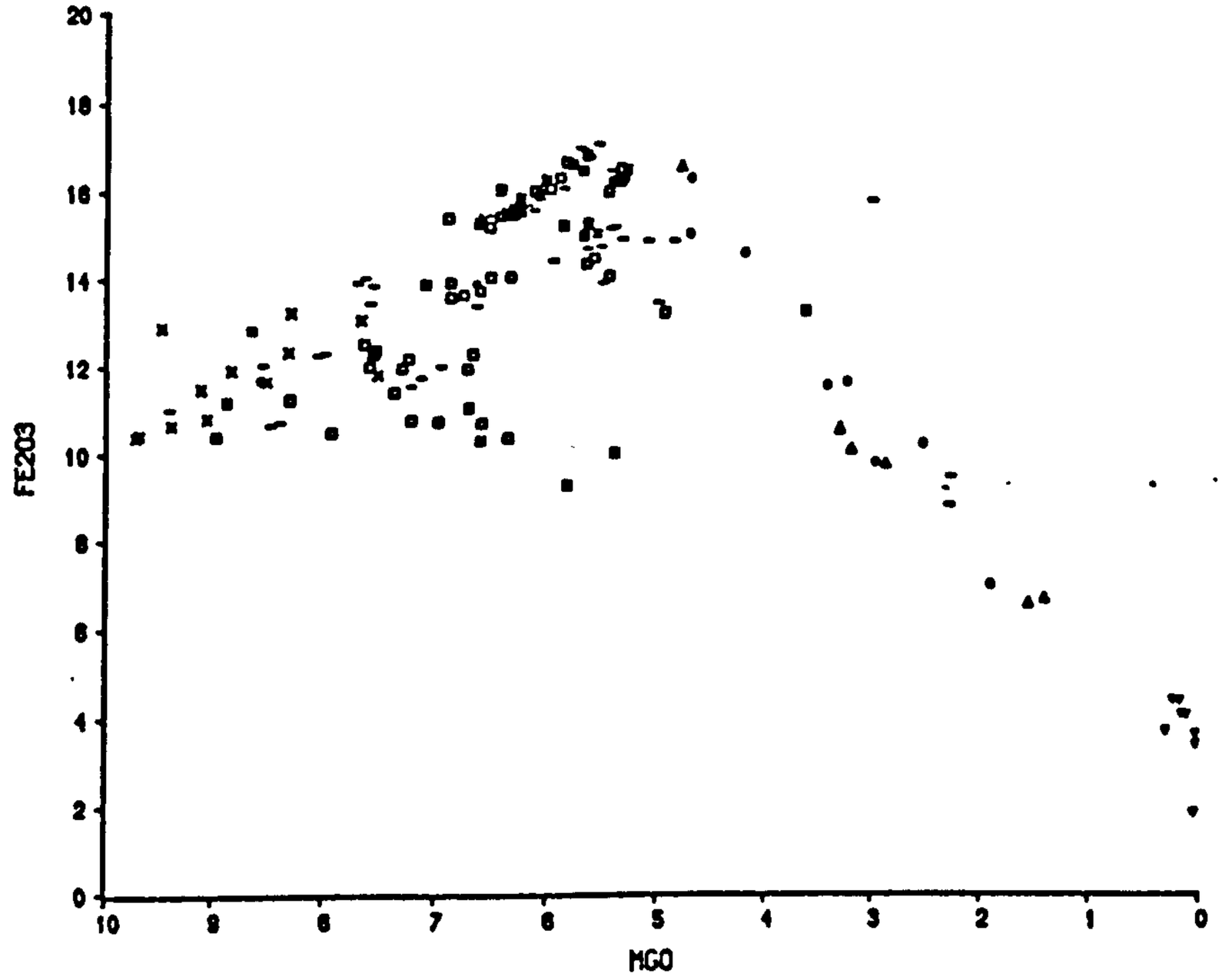


a

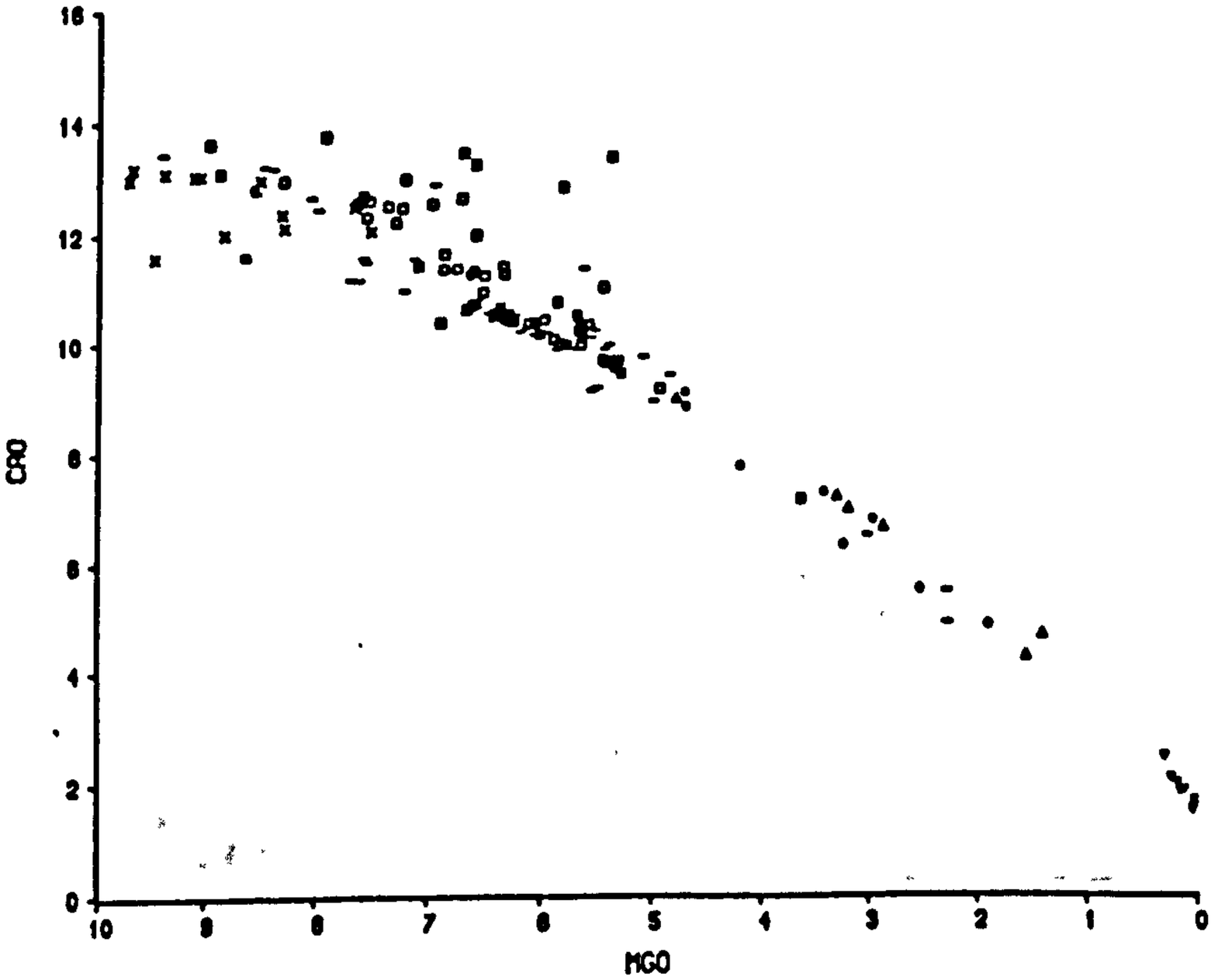


b

**Fig. 4.3 (a)** $Fe_2O_3$ (total) *vs* MgO, details as Fig. 4.2(a)
**(b)** CaO *vs* MgO, details as Fig. 4.2(a)

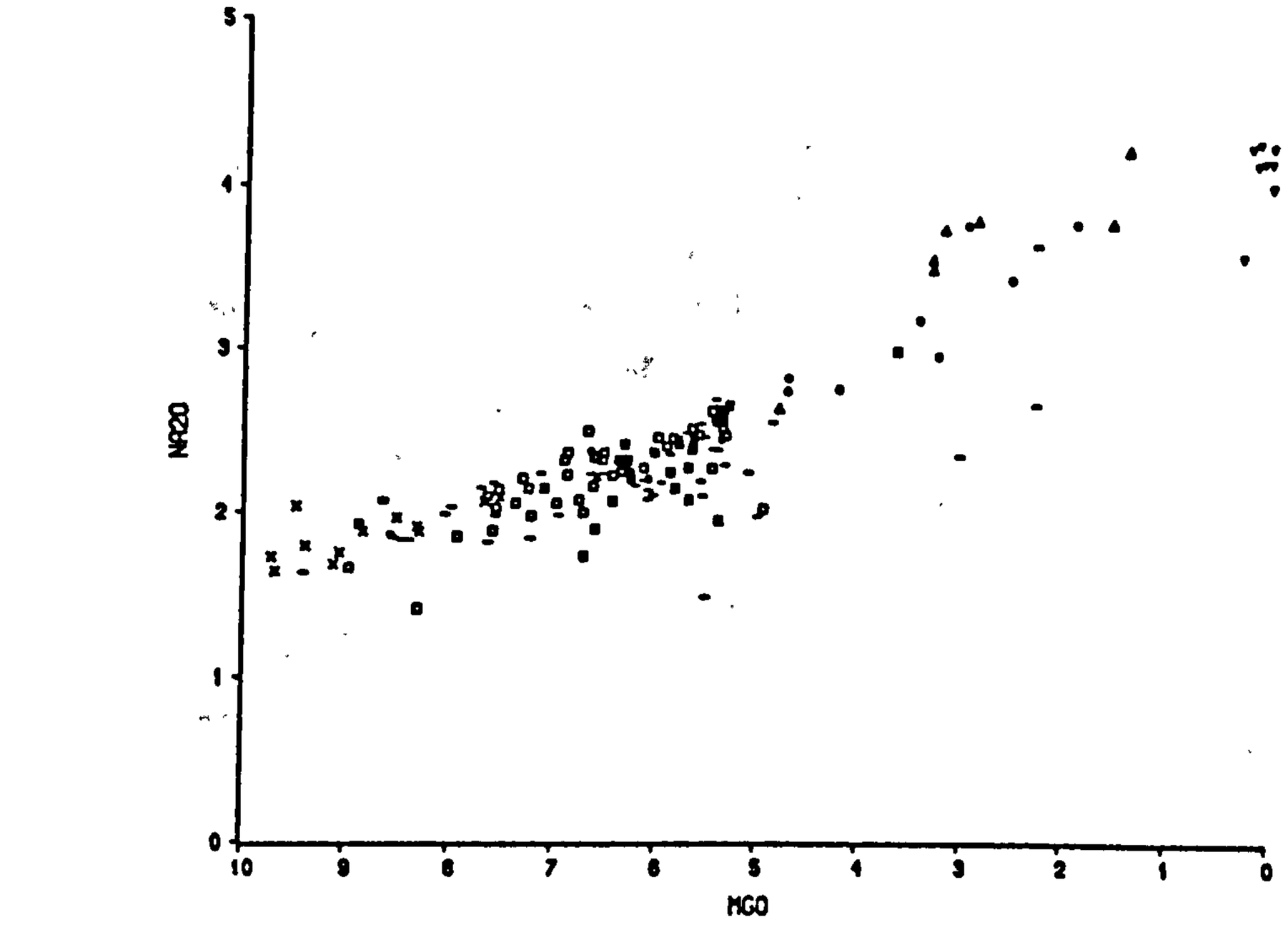


a

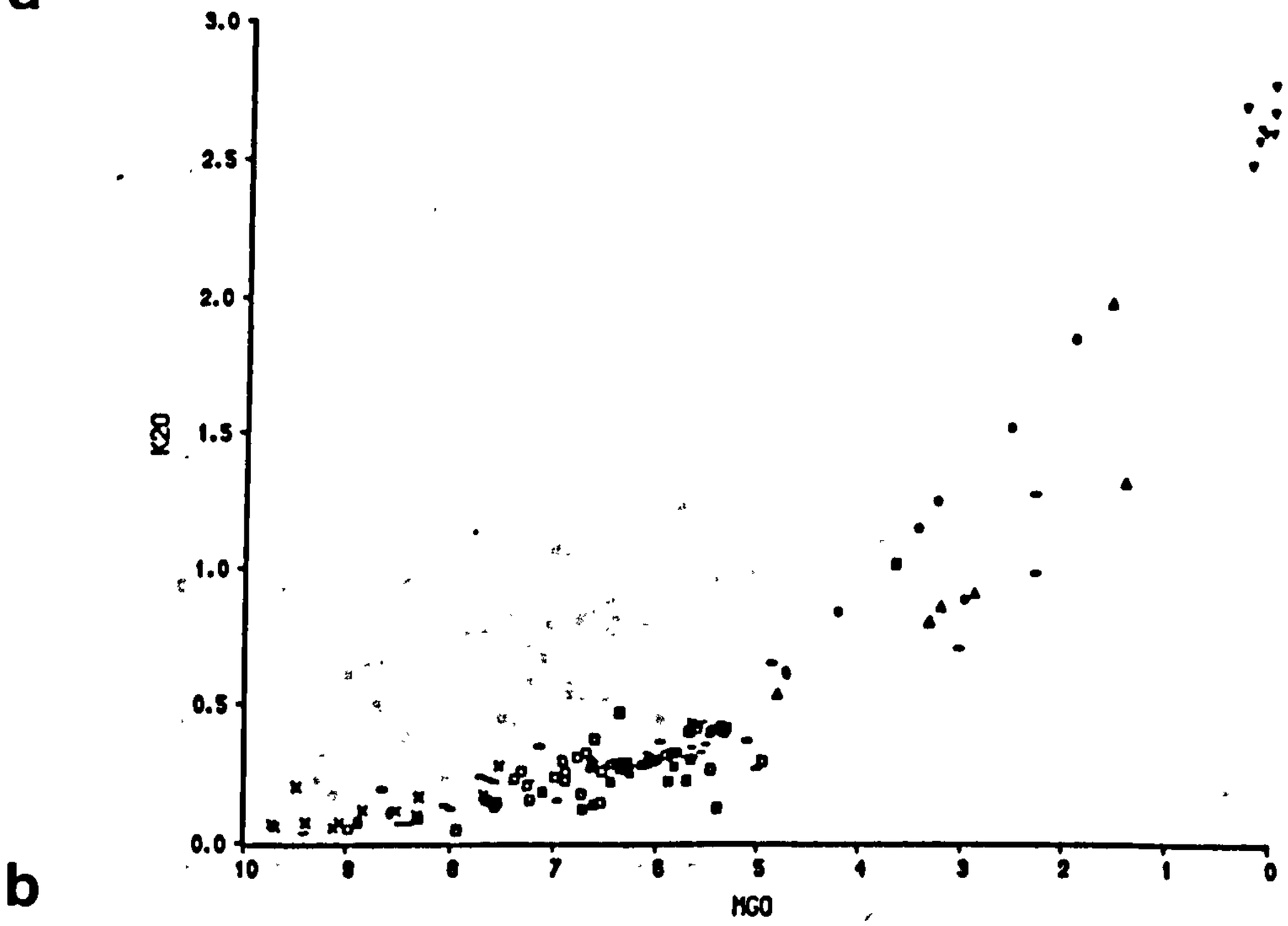


b

**Fig 4.4 (a)** $Na_2O$ *vs* MgO, details as Fig. 4.2 (a)
**(b)** $K_2O$ *vs* MgO, details as Fig. 4.2 (a)

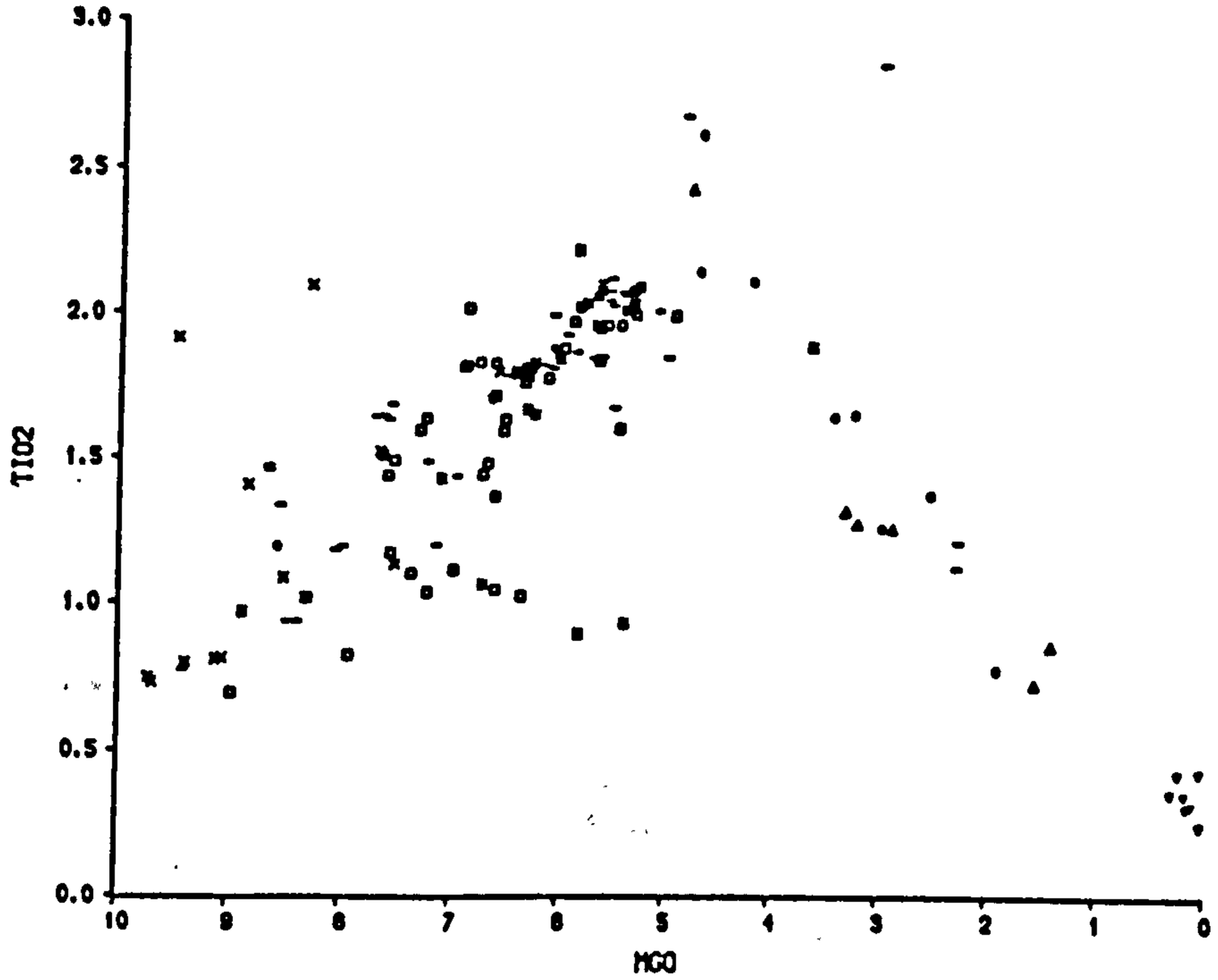


a

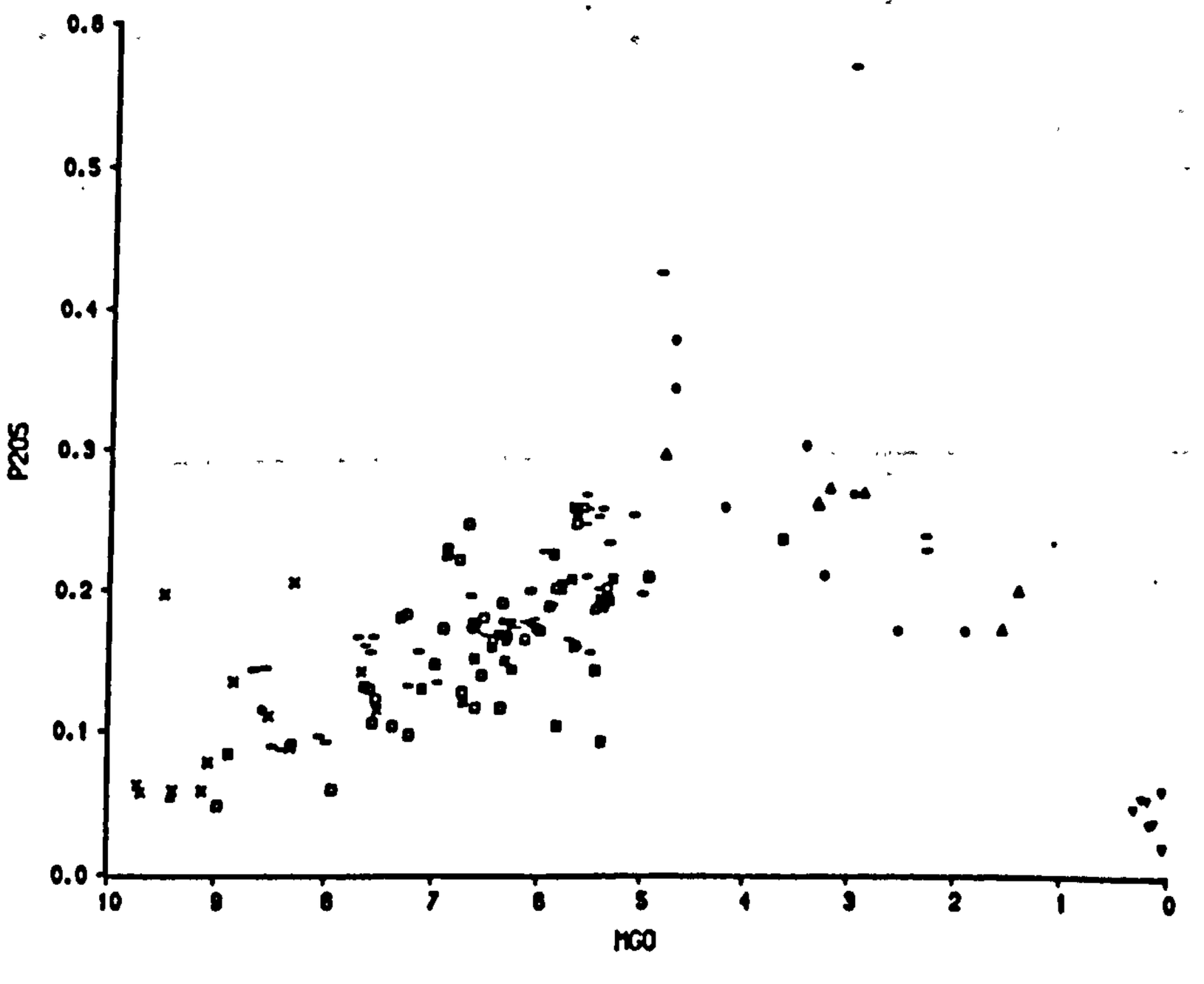


b

**Fig. 4.5 (a)** $TiO_2$ *vs* MgO, details as Fig. 4.2(a)
**(b)** $P_2O_5$ *vs* MgO, details as Fig. 4.2(a)

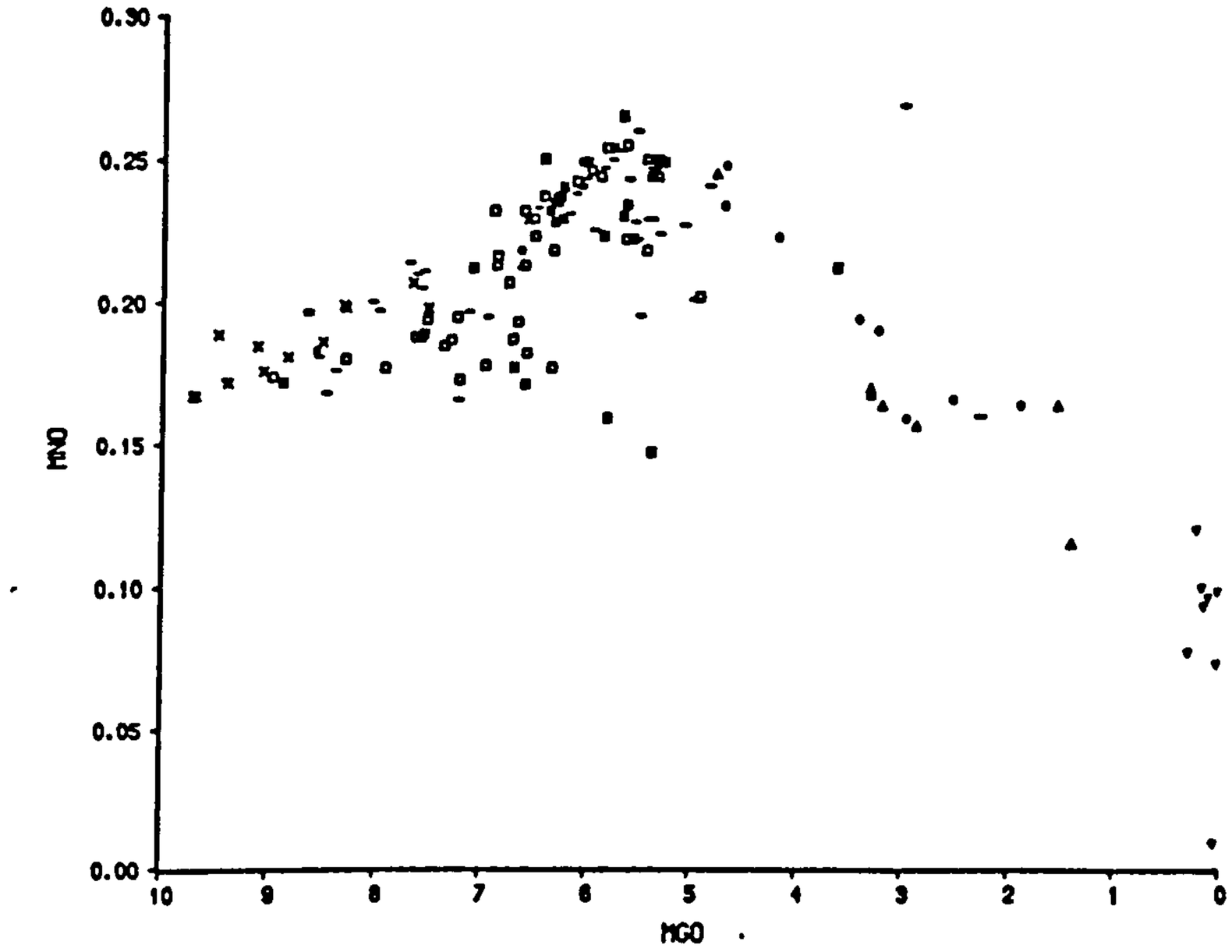


**Fig. 4.6** MnO *vs* MgO, details as Fig. 4.2(a)

(ix) MnO *vs* MgO (Fig. 4.6) follows the trends shown by $Fe_2O_3^*$ and $TiO_2$. This can be understood by the onset of crystallisation of FeTi oxides and relatively Fe-rich clinopyroxene in evolved basaltic magmas. Both of these minerals contain significant amounts of Mn substituting for $Fe^{2+}$.

### 4.4.2 Variation diagrams indicating phenocryst accumulation

Modal analysis of phenocryst content was performed on 38 Krafla lavas (see section 3.4 and Appendix II). This section relates the results of modal analysis to whole-rock compositions, in order to assess the limitations of using such compositions to represent liquid. The largest modal proportion of phenocrysts is found in the plagioclase-phyric lavas, which may contain up to 30% plagioclase by volume. Most of these plagioclase crystals are thought on textural grounds to be xenocrysts (section 3.2.6). Such plagioclase crystals contain 17-18 wt% CaO, 32-34 wt% $Al_2O_3$, and negligible quantities of $Fe_2O_3^*$, MgO, $TiO_2$, MnO and $P_2O_5$. Hence the accumulation of An-rich plagioclase will lead to an increase in CaO and $Al_2O_3$ (Figs. 4.7a,b), and to the decrease of all the other oxides mentioned. A graph of $Al_2O_3$ *vs* MgO is shown in Fig. 4.7a,b, with different symbols for varying proportions of plagioclase xenocrysts (identified texturally). It can be seen that, for a given MgO content, the rocks with the lowest $Al_2O_3$ are generally aphyric, and that those rocks with the highest $Al_2O_3$ values contain the most modal plagioclase. A vector of plagioclase accumulation is also shown in Fig 4.7a. The calculated vector values agree well with the observed modal proportions of plagioclase. Hence much of the $Al_2O_3$ spread can be explained by plagioclase accumulation. However, several samples at lower MgO values (3.5-1.5 wt% MgO) contain higher $Al_2O_3$ concentrations than the "minimum trend". Such samples (icelandites and dacites) do not contain the large quantities of the xenocrystal plagioclase found in the other $Al_2O_3$-rich samples. They do contain, however, large modal proportions of plagioclase microlites/microphenocrysts (10-20% by volume). These crystals are $An_{51}$ to $An_{55}$ in composition (KK34). Their accumulation will also lead to higher $Al_2O_3$ values and lower values of MgO, $Fe_2O_3^*$ and $TiO_2$. CaO will not be expected to increase significantly, since the relatively Ab-rich plagioclase contains much less CaO than the xenocrystal plagioclase. Mineral vectors for this accumulation are shown in Fig. 4.7a,b. The $Fe_2O_3^*$ and $TiO_2$ *vs* MgO plots are shown in Figs. 4.8a,b. The plagioclase-rich samples form a trend pointing towards the composition of the plagioclase near the origin.

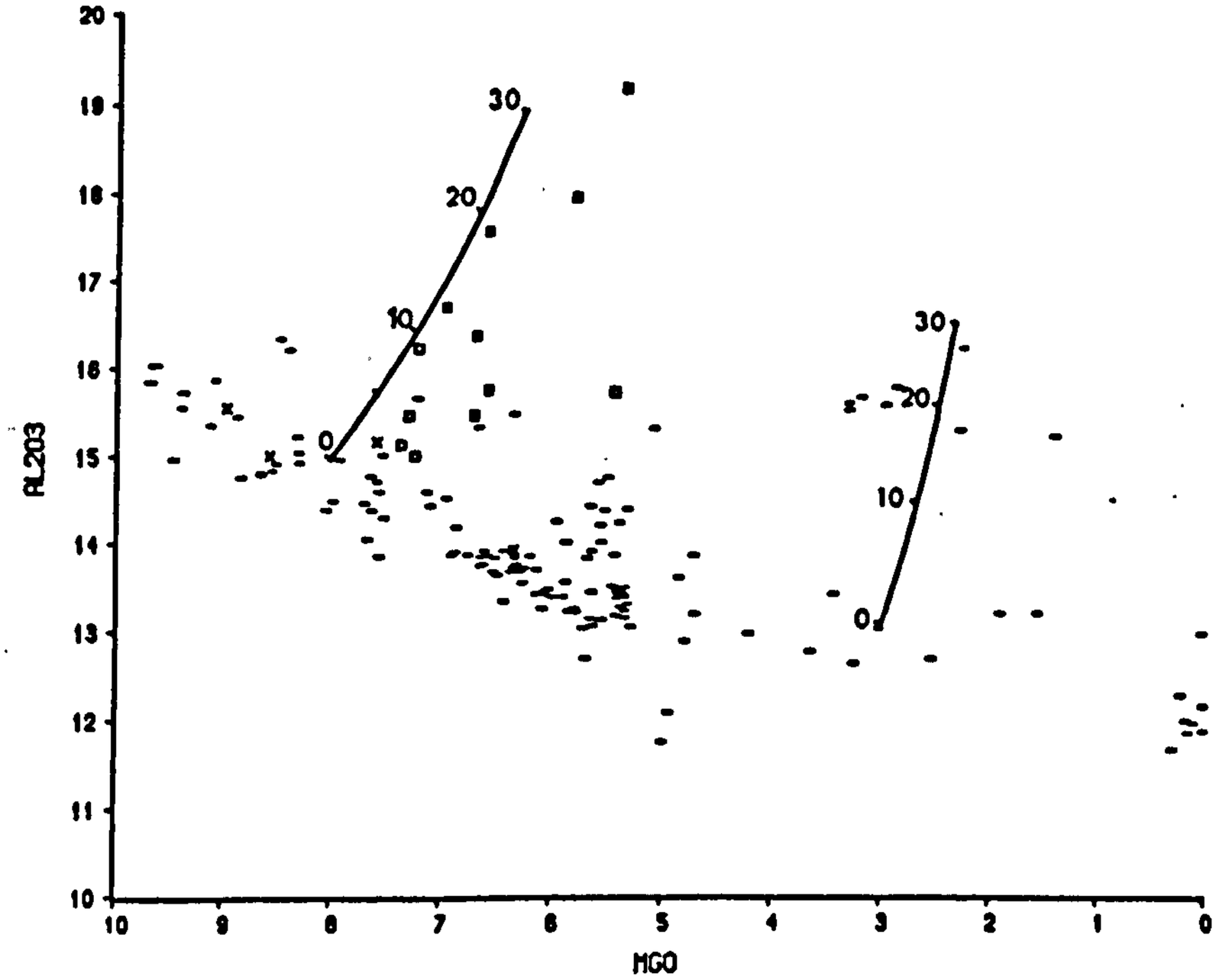


a

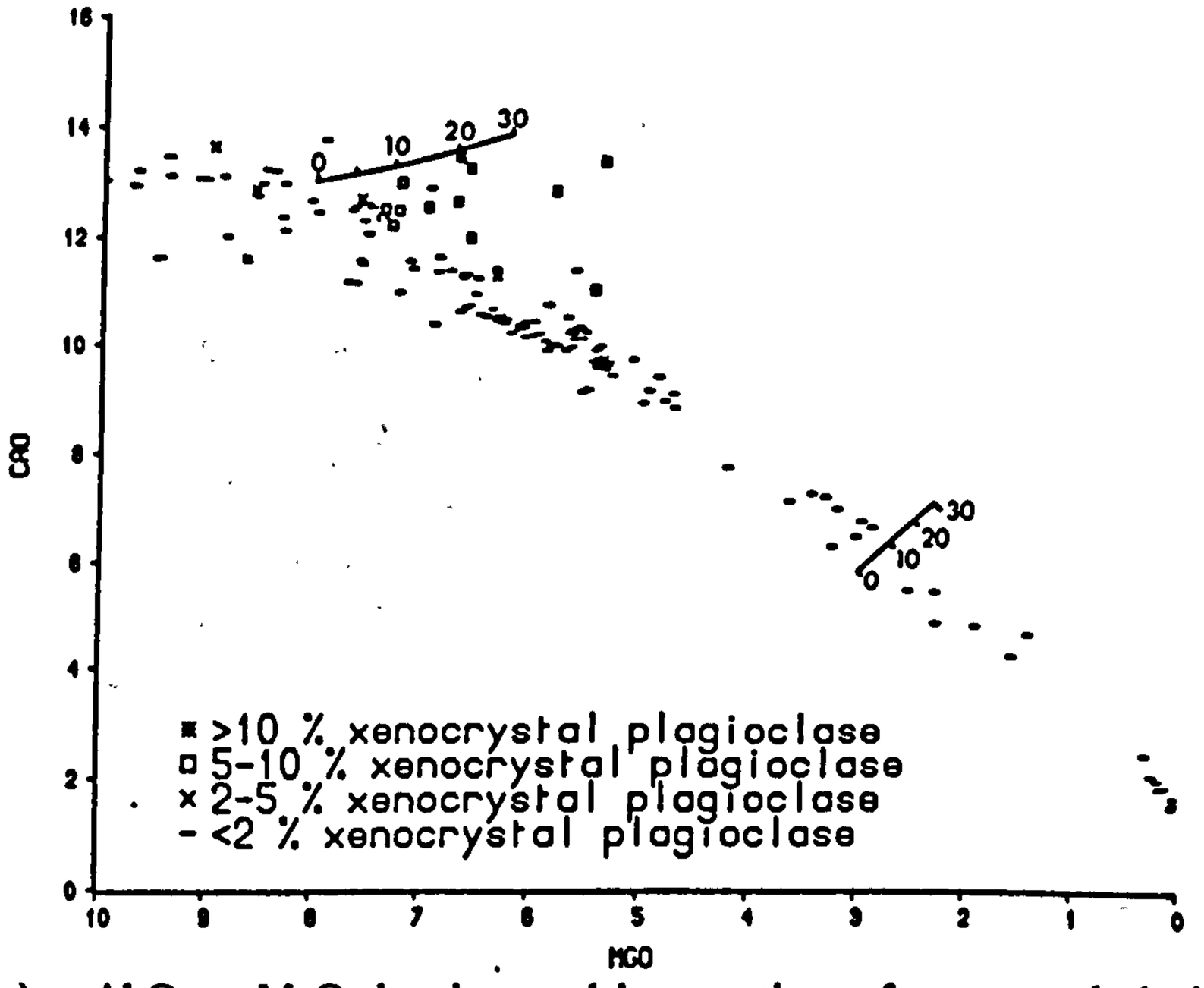


b

Fig. 4.7 (a) $Al_2O_3$ *vs* MgO showing modal proportions of xenocrystal plagioclase (key in Fig. 4.7 (b)). The numbers on the left-hand curve represent the percentage of plagioclase phenocrysts ($An_{81}$) added to a starting composition with 15 wt% $Al_2O_3$ and 8 wt% MgO. The numbers on the right-hand curve are similar but for $An_{54}$ and a starting composition of 13 wt% $Al_2O_3$, 3 wt% MgO.
(b) CaO *vs* MgO showing modal proportions of xenocrystal plagioclase. Numbers as in Fig. 4.7 (a), but for starting compositions of 13 and 6 wt% CaO for the left- and right-hand curves respectively.

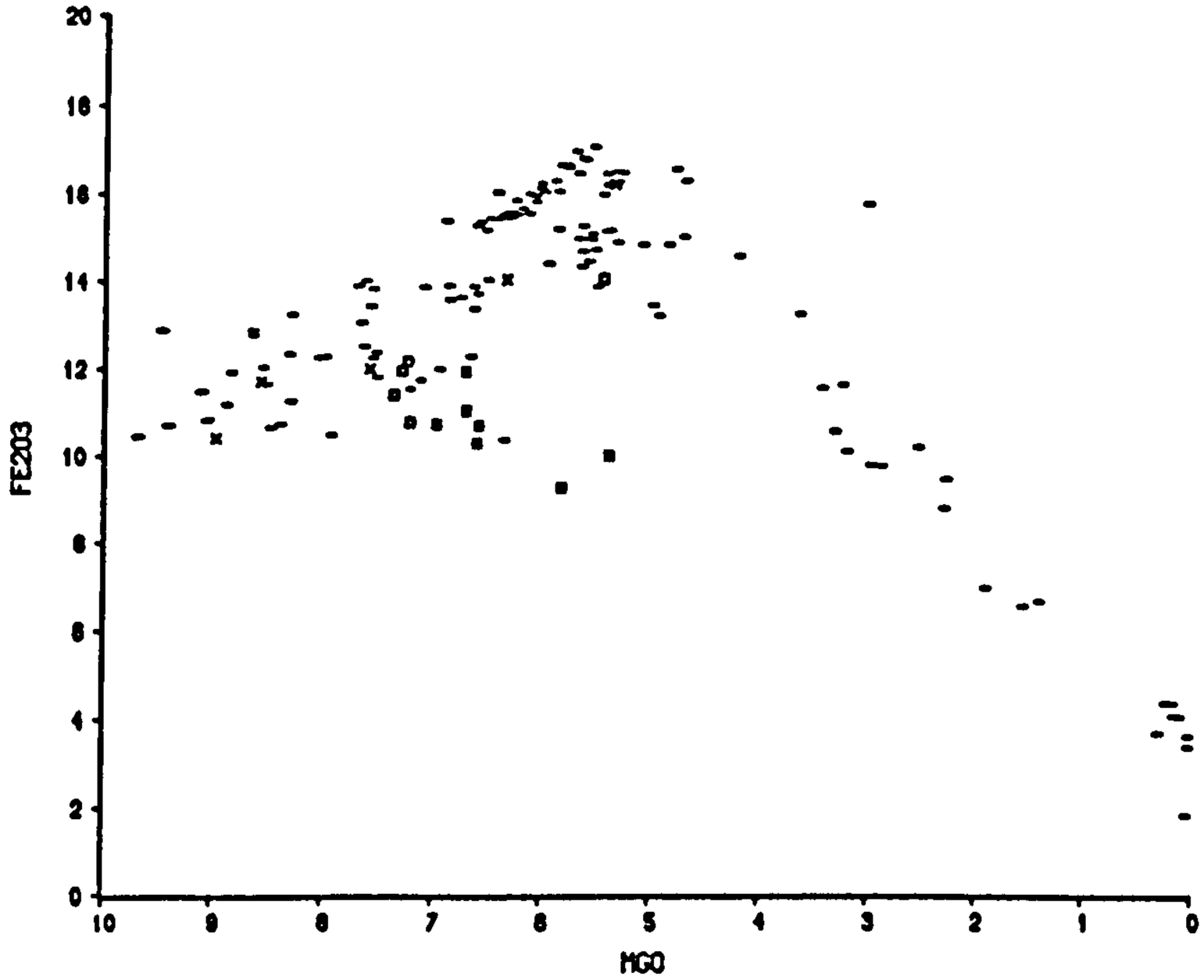


a

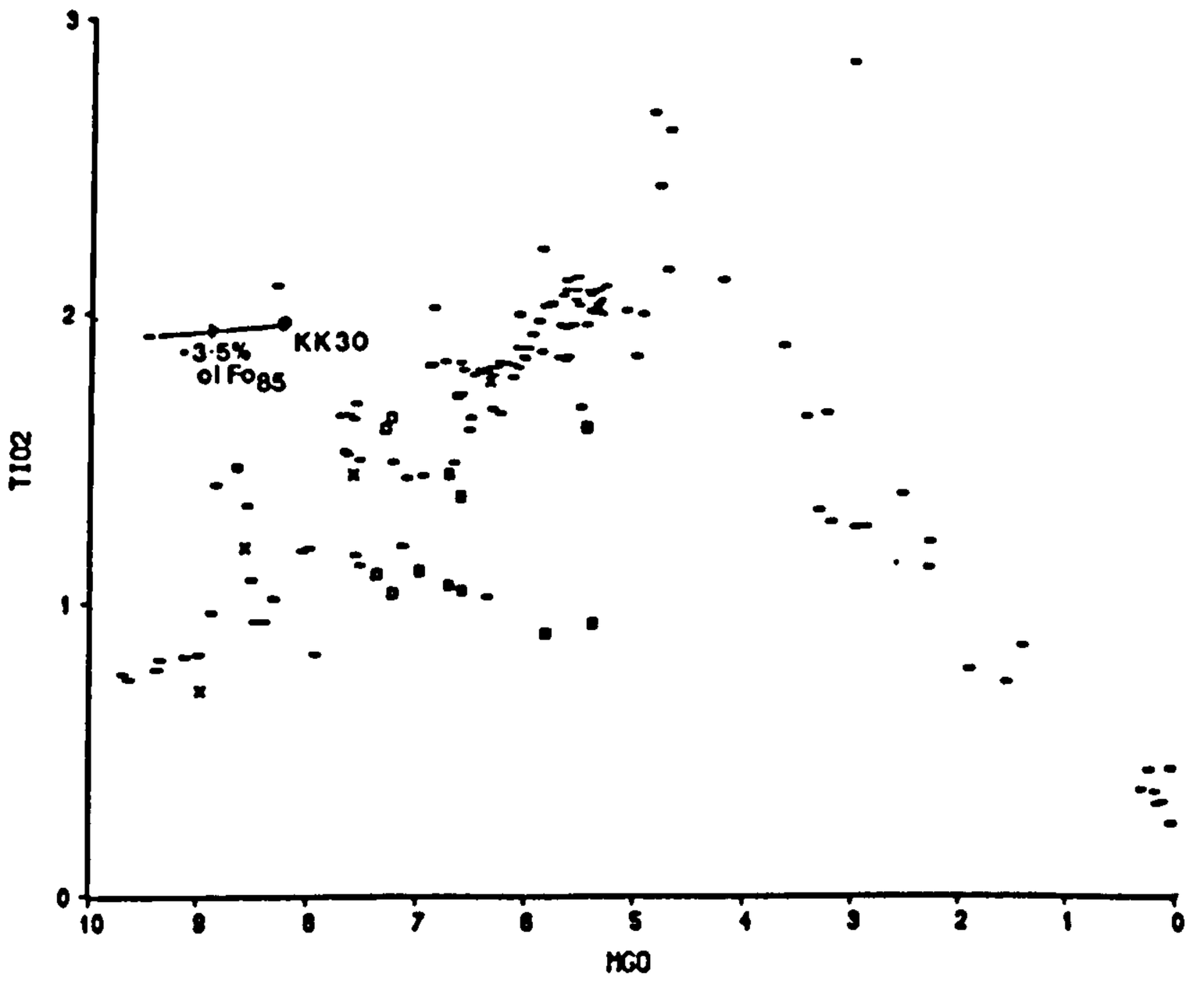


b

**Fig. 4.8 (a)** $Fe_2O_3$ (total) *vs* MgO showing modal proportions of xenocrystal plagioclase (key in Fig. 4.7b).
**(b)** $TiO_2$ *vs* MgO showing modal proportions of xenocrystal plagioclase (key in Fig. 4.7b): KK30 is corrected for 3.5% olivine phenocrysts ($Fo_{85}$).

Other phenocryst phases have accumulated in some samples, although none to such an extent as plagioclase. For example, olivine accumulation can lead only to significant increase in MgO, leaving other oxides relatively unaffected. KK30 (9.49 wt% MgO) contains approximately 3.5% modal olivine and the corrected composition is shown in Fig. 4.8b (see discussion by Biggar (1983) on phenocryst accumulation). Generally the total effect on the whole-rock chemistry is small because the modal proportions of olivine and clinopyroxene are small, and because these minerals are often found together with plagioclase (MgO~0 wt%).

### 4.4.3 Age subdivision

The time intervals used in this section are shown in Table 2.1 and cover the exposed history of Krafla. In Figs. 4.9 to 4.13 samples from Krafla are plotted, according to age, on oxide-MgO variation diagrams. It can be seen from these graphs that the 5 most recent time intervals (in Table 2.1; 0 to 120 ka BP) include samples which cover a large proportion of the total spread of MgO values. This suggests that the Krafla volcanic centre has been capable of producing a wide range of chemical compositions for at least 120 ka. The older time intervals contain too few points for plots containing them to be statistically significant.

The post-H3 (basaltic) samples, from the last 3 ka, form a coherent group in all the oxide-MgO plots (Figs. 4.9 to 4.13), with less scatter at a given MgO value than the older groups. For example, the $K_2O$ *vs* MgO plot in Fig. 4.11b shows the relatively tight cluster of these post-H3 samples. A likely explanation for the chemical coherence of the post-H3 samples is that the parental magmas supplied during this period are approximately constant in composition, and that subsequent fractional crystallisation has then produced essentially only one trend (see Fig. 5.8 for lack of variation of Zr/Y ratio over this period). Over a longer time period, variations in parental magma composition may lead to several separate differentiation trends and produce scatter on oxide-oxide variation diagrams. Such scatter is unlikely to be caused by modal variation in phenocryst content (e.g. $K_2O$ is not significantly affected by the accumulation of any tholeiitic phenocrysts). The variation in composition of the most primitive Krafla samples is discussed with reference to melting processes in Chapters 5 and 6.

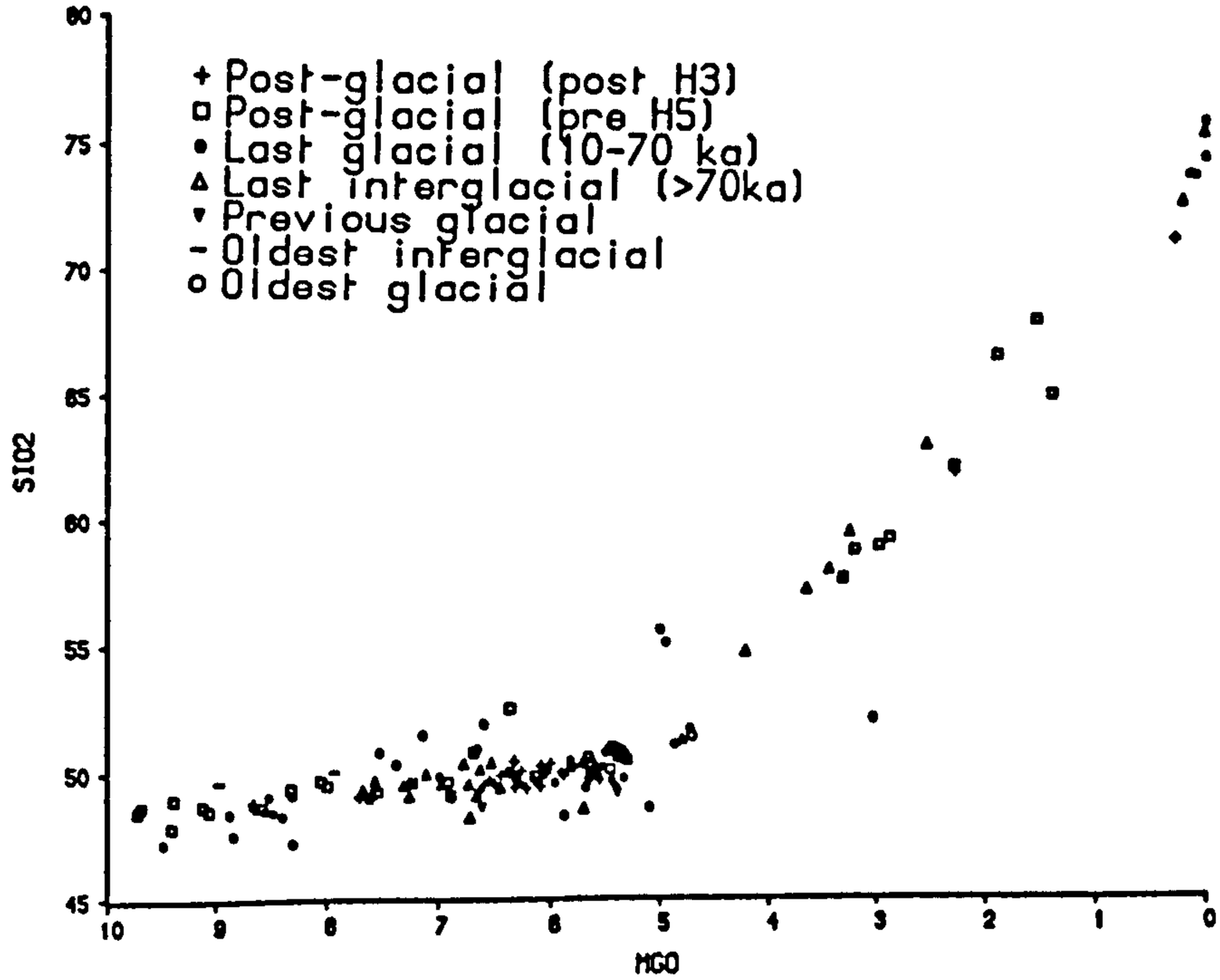


a

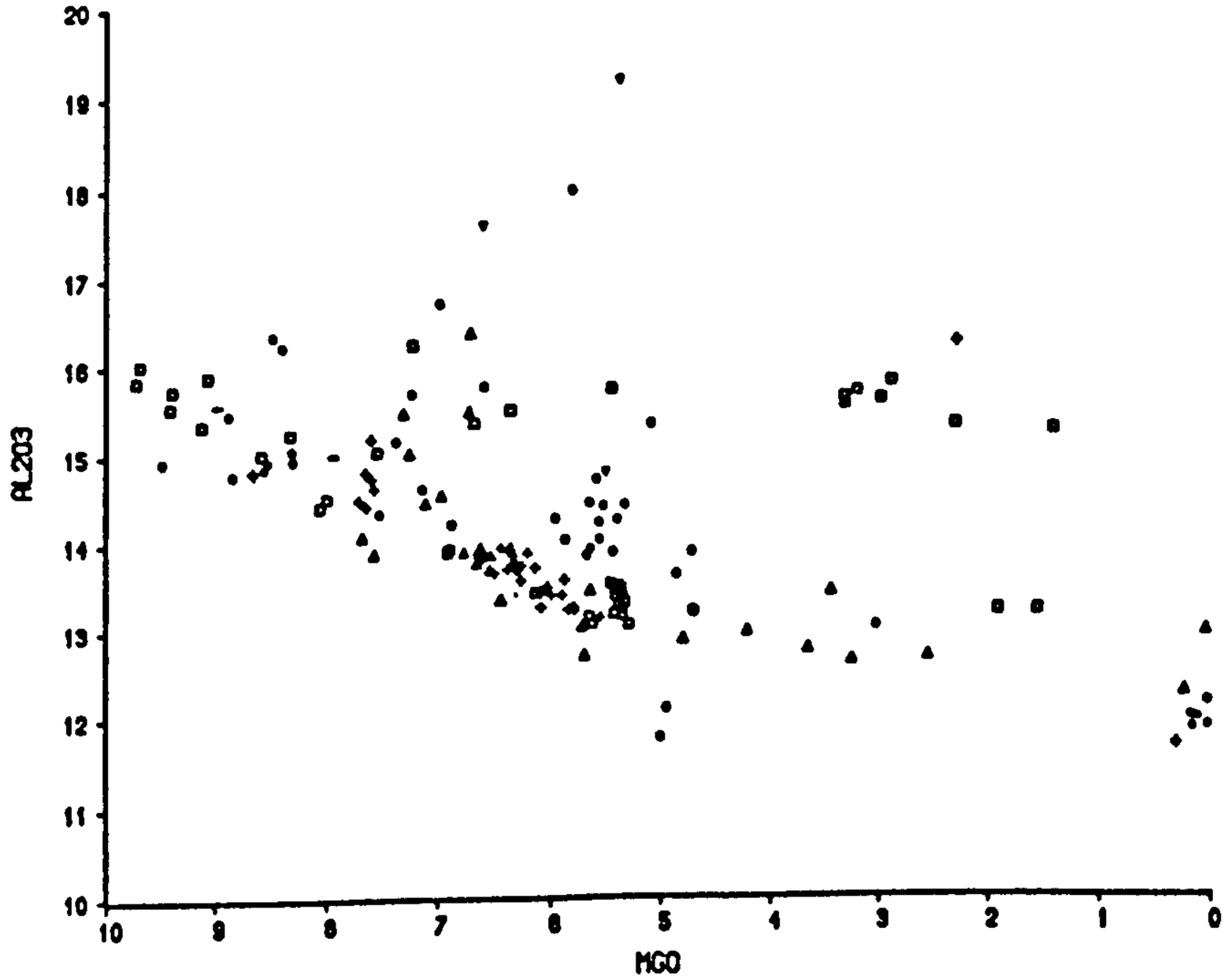


b

**Fig. 4.9 (a)** $SiO_2$ *vs* MgO, showing the variation in composition with time (see key on diagram).
**(b)** $Al_2O_3$ *vs* MgO, details as Fig. 4.9(a)

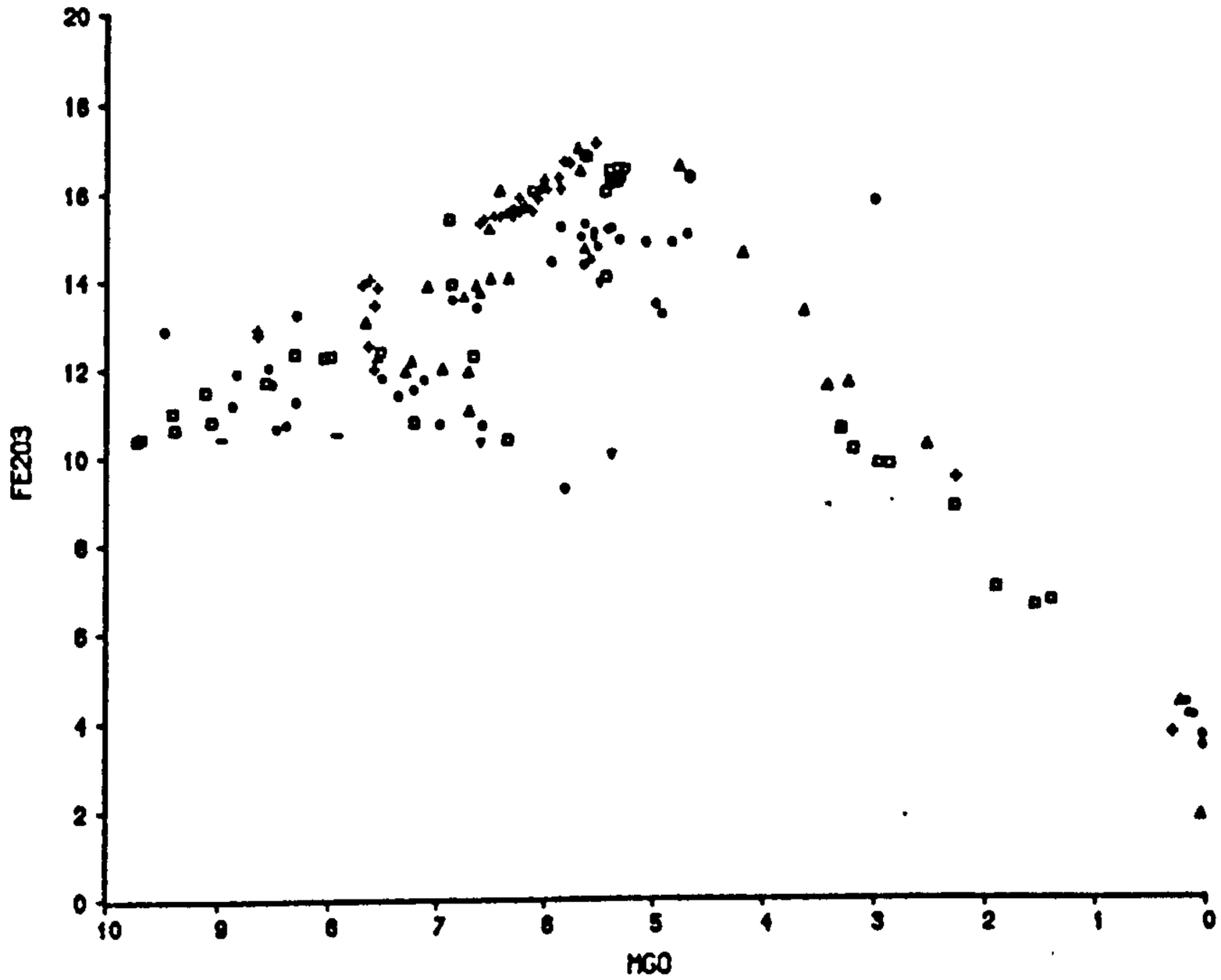


a

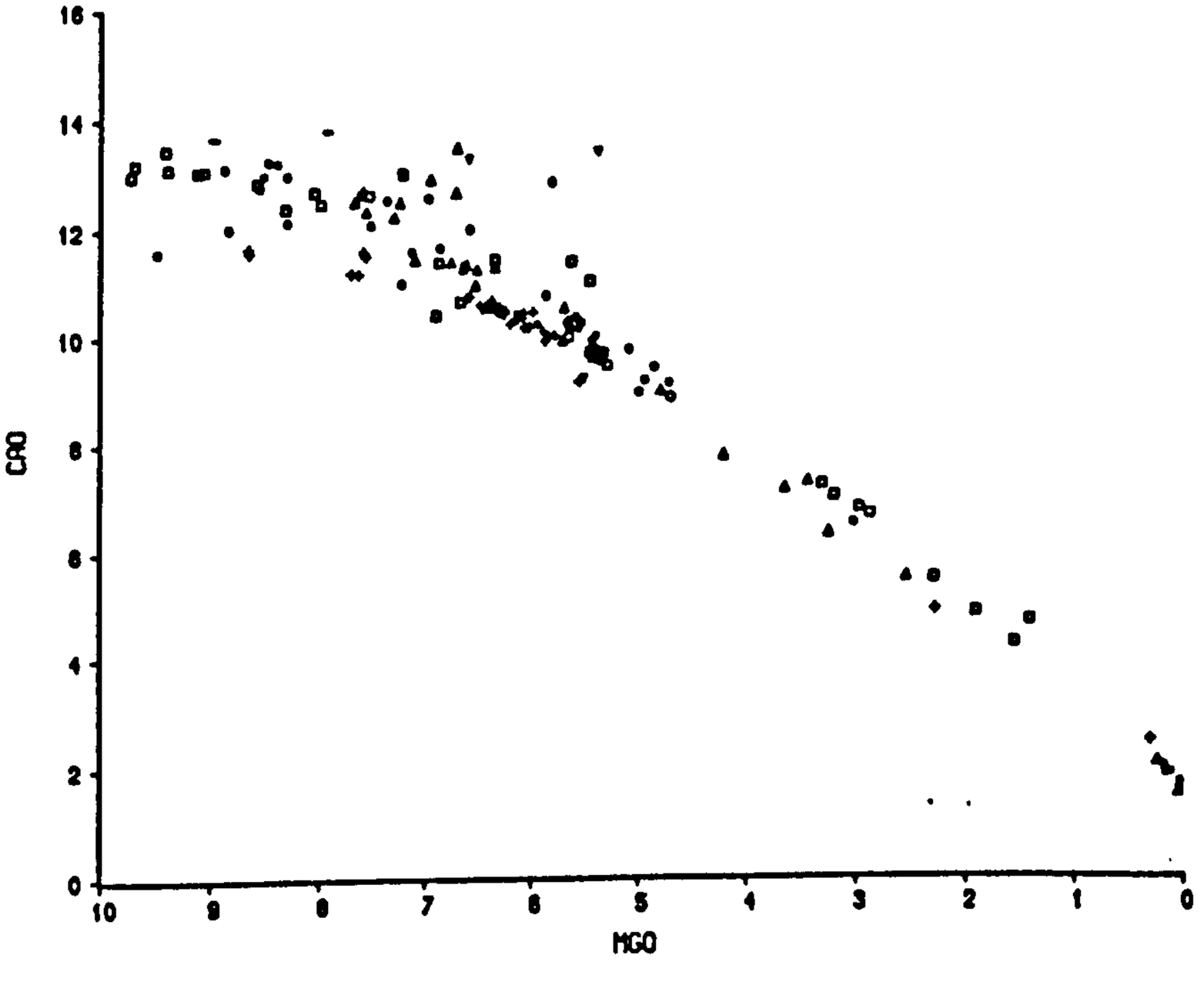


b

**Fig. 4.10 (a)** $Fe_2O_3$ (total) *vs* MgO, details as Fig. 4.9 (a)
**(b)** CaO *vs* MgO, details as Fig. 4.9 (a)

a

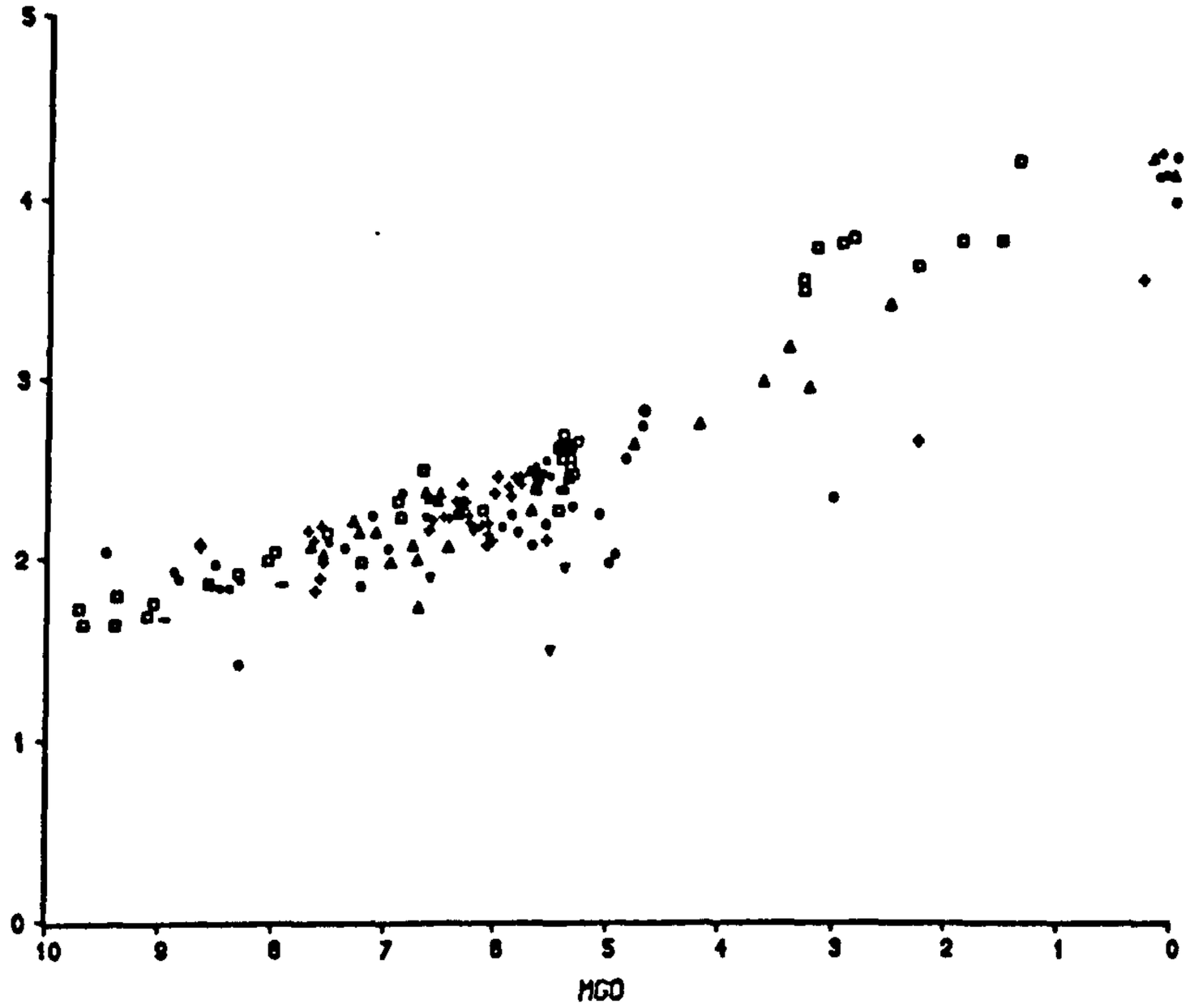


b

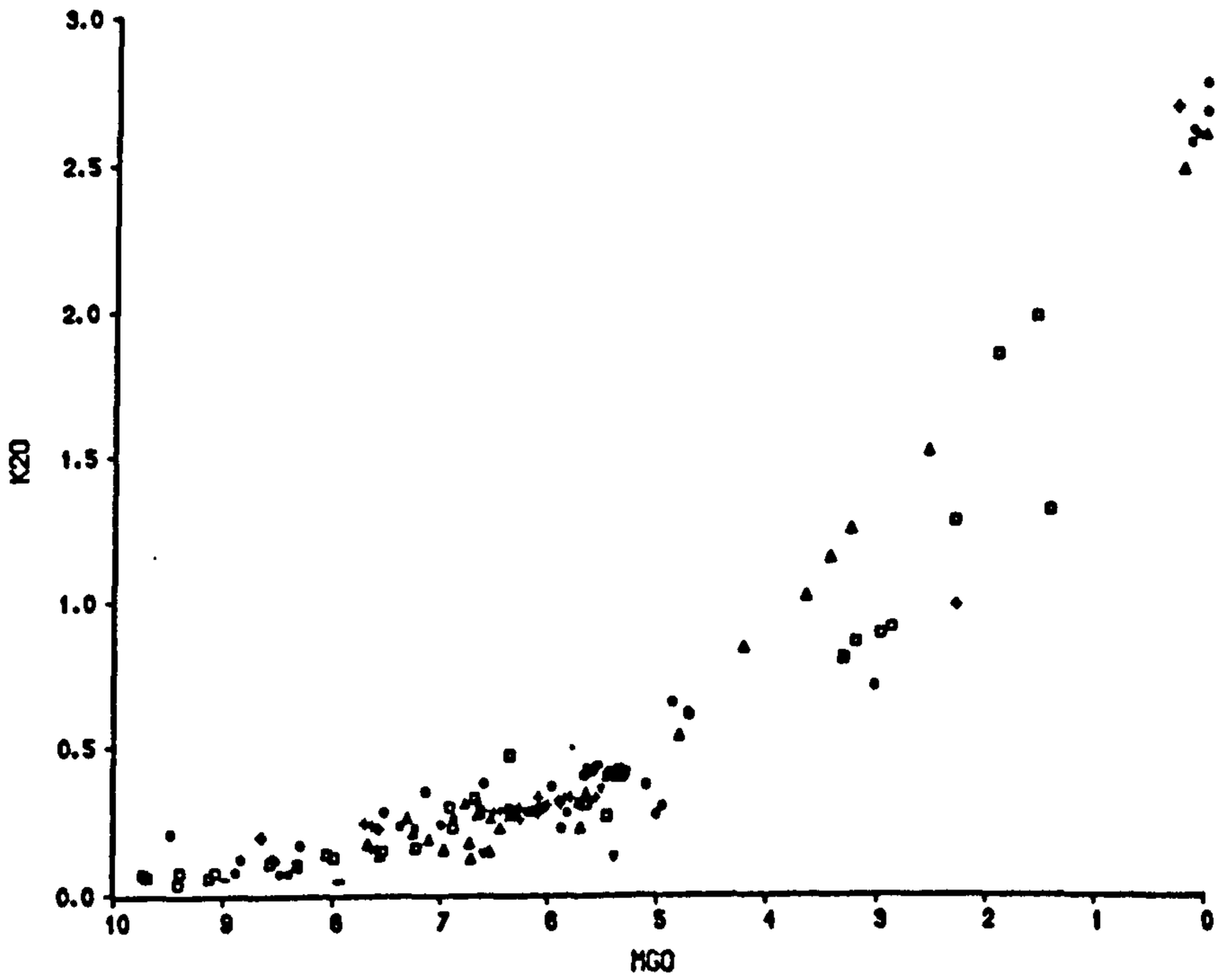


**Fig 4.11 (a)** $Na_2O$ *vs* MgO, details as Fig. 4.9(a)
**(b)** $K_2O$ *vs* MgO, details as Fig. 4.9(a)

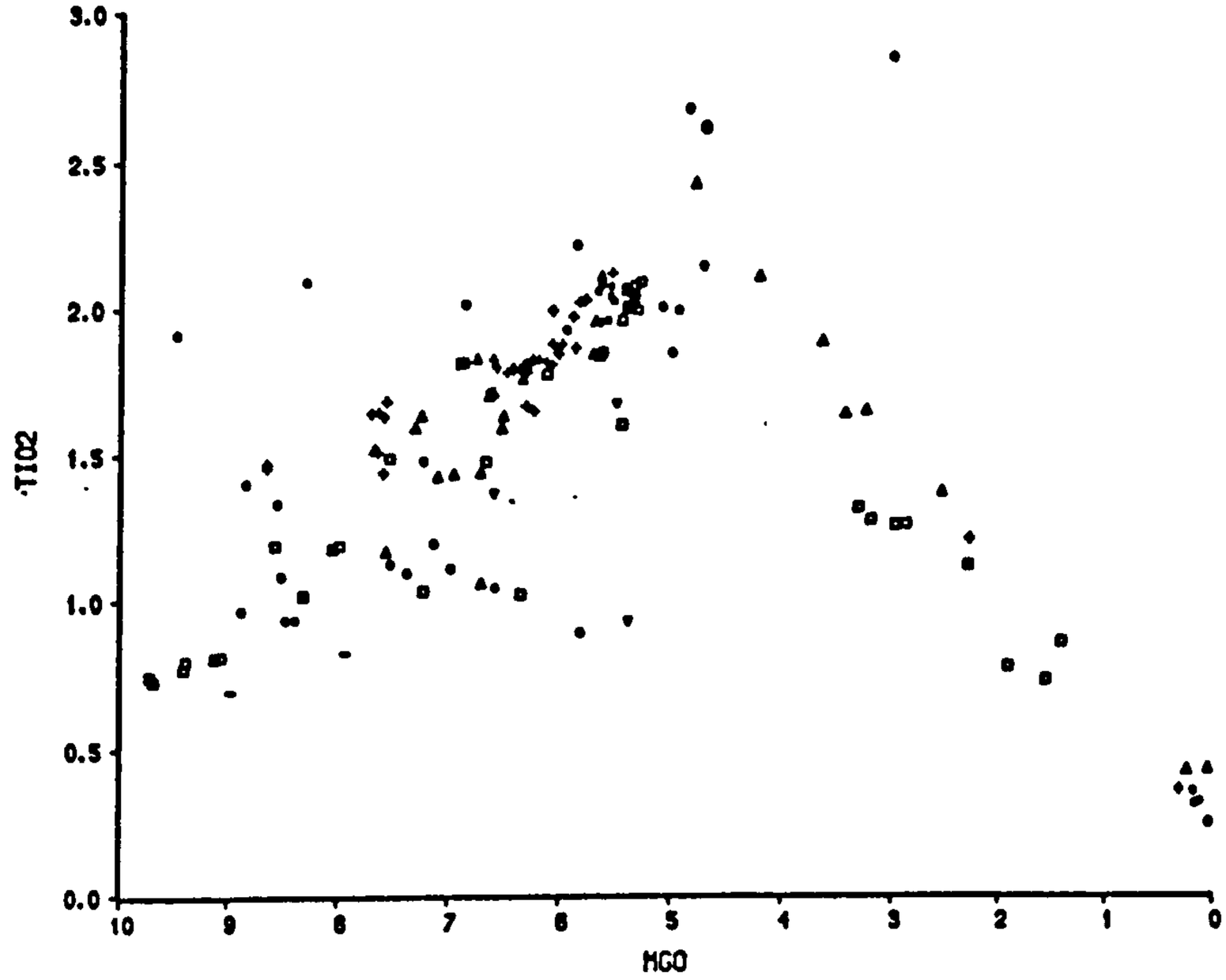


a

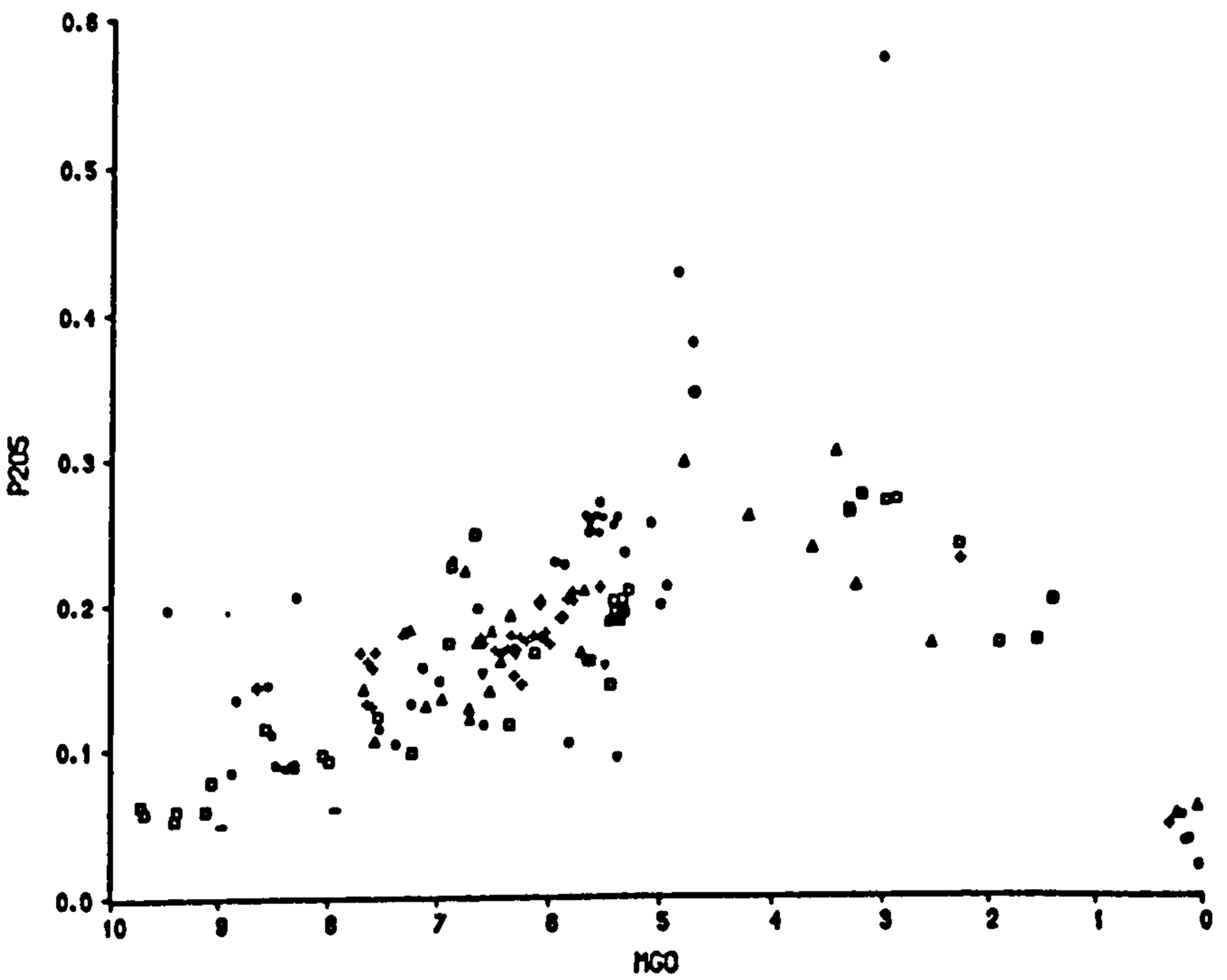


b

**Fig. 4.12 (a)** $TiO_2$ *vs* MgO, details as Fig. 4.9(a)
**(b)** $P_2O_5$ *vs* MgO, details as Fig. 4.9(a)

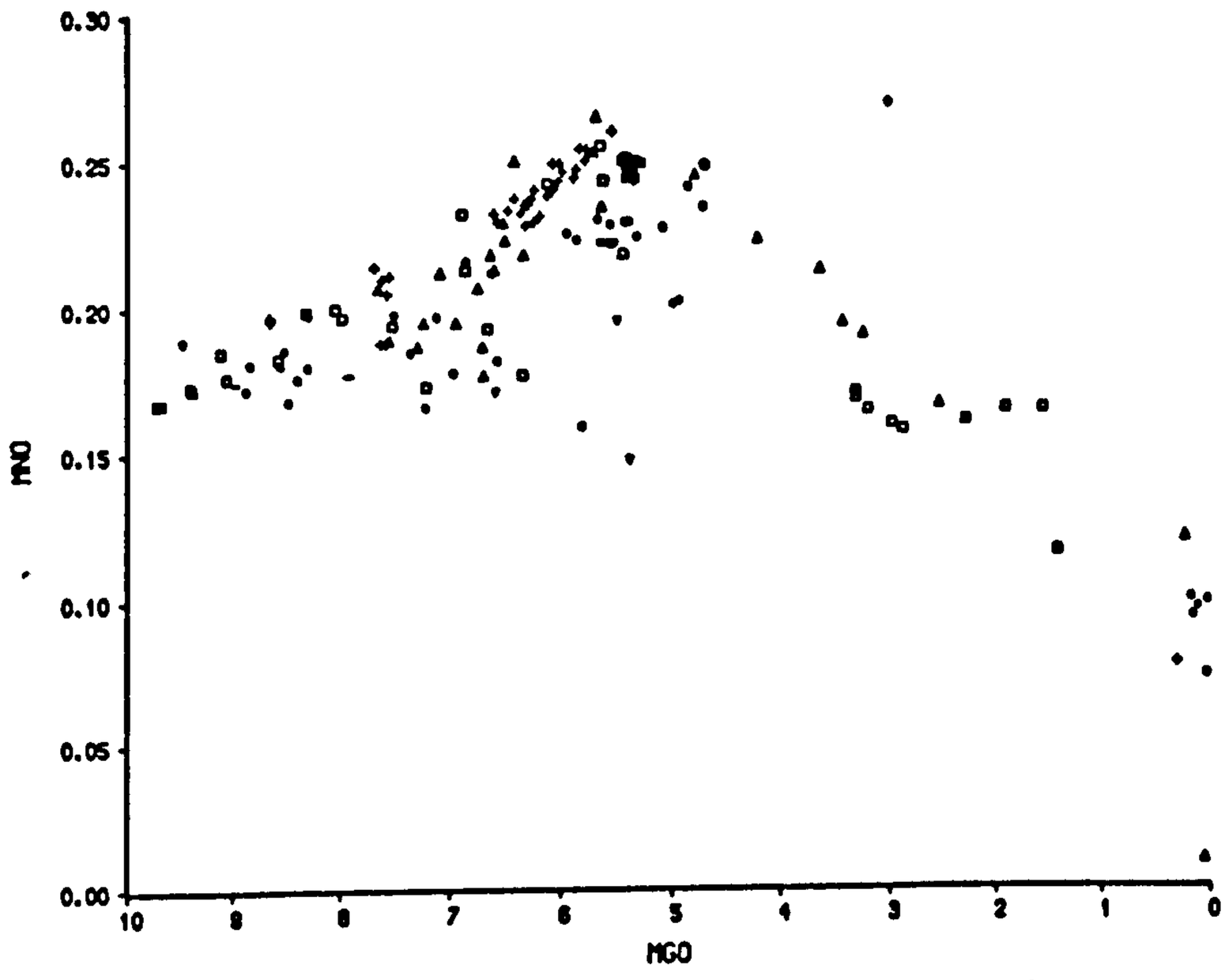


**Fig. 4.13** MnO *vs* MgO, details as Fig. 4.9(a)

### 4.4.4 Geographic variation

The variation of whole-rock composition with geographic location is shown in Fig. 4.14. The Krafla area has been split into four areas: (A) to the north of the caldera, (B) within the caldera, (C) outside and around the southern edge of the caldera, and (D) Námafjall and to the south of area (C). The areas were chosen to investigate the hypothesis that evolved compositions are concentrated around the calderas of central volcanoes (Carmichael, 1964; Saemundsson, 1977).

The results of the investigation are shown in Fig. 4.14, with four histograms of numbers of samples plotted against MgO content. It can be seen that, although all four areas cover most of the differentiation sequence (10-0 wt% MgO), there is a tendency for the areas near the caldera and just to the south of the caldera to have more evolved samples than the other two areas. This is consistent with the views of the above authors who considered that the longer-lived magma reservoirs are to be found near the caldera. Recent geophysical evidence confirms this proposition, by identifying a shallow central magma reservoir which supplies magma laterally into the fissure swarms (Björnsson, 1985).

### 4.4.5 Conclusions

The major-element whole-rock compositions appear to confirm the fractional crystallisation hypothesis for the Krafla suite. The observed phenocryst assemblages are consistent with the whole-rock chemical trends seen above, though in detail there may be phases whose crystallisation effects cannot be observed from these trends (e.g. orthopyroxene and fayalitic olivine).

It has been recognised that whole-rock analyses have their limitations when trying to understand the differentiation course of the magmatic liquid (e.g. Bryan, 1983; Thompson, 1987). However, in Figs. 4.2 to 4.8 it is shown that the aphyric samples appear to define the chemical course of liquid differentiation adequately. The chemical effects of large amounts of modal plagioclase are recorded in the $Al_2O_3$ and CaO concentrations. Other phenocryst/xenocryst phases appear to affect the chemical compositions to a lesser degree.

The geographic variation of the chemical compositions would appear to confirm the notion that more-differentiated magmas are best developed in and near to the central volcano, although more primitive compositions are found over the entire area. Such chemical zonation is consistent with the concept that longer-lasting magma reservoirs are developed towards the centre of the volcanic system.

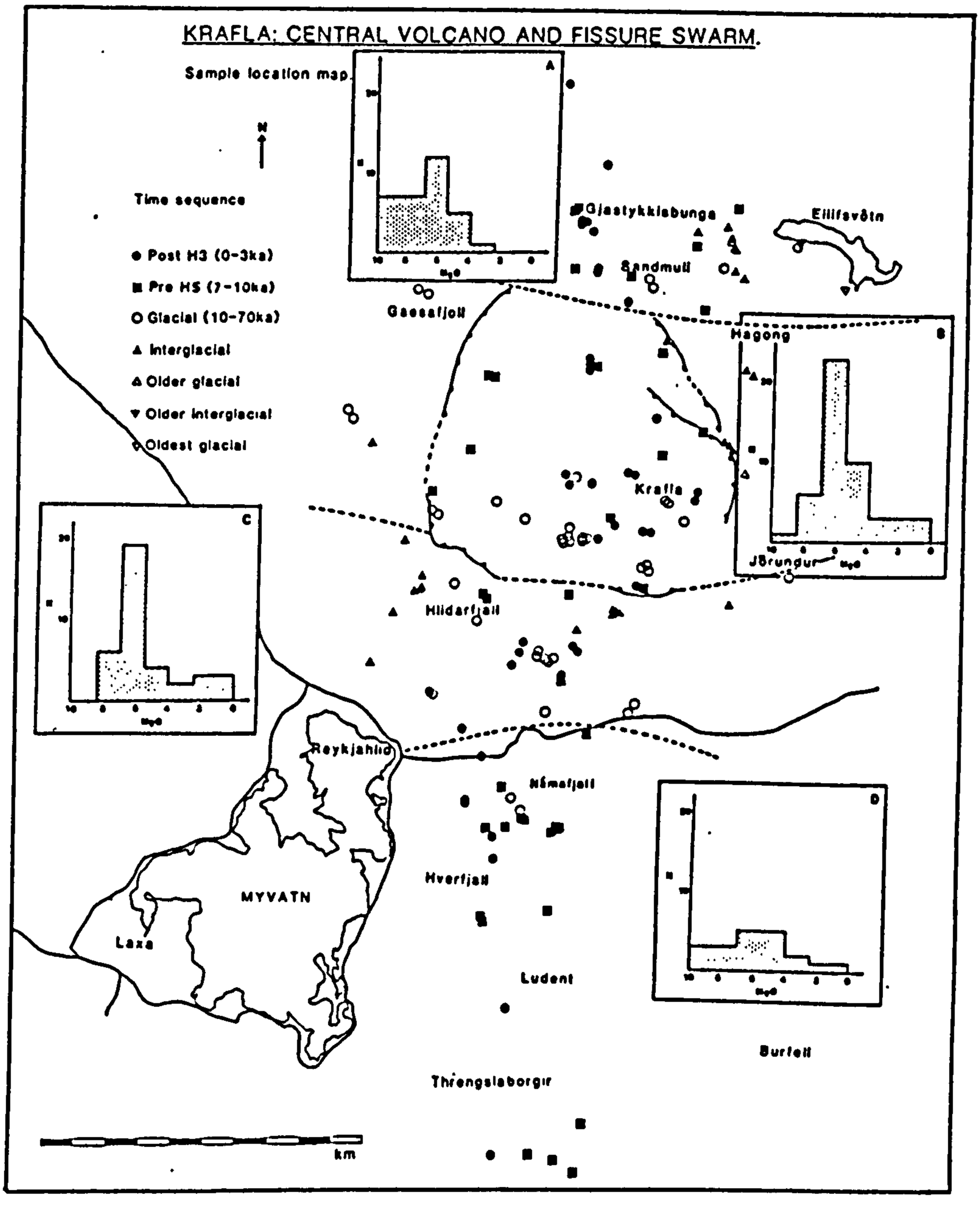


**Fig. 4.14** Variation in MgO content with geographic location in the Krafla volcanic system. The system is split into 4 areas labelled A-D (see text). Barcharts are presented in insets in the diagram showing the numbers of samples for a given area plotted against MgO.

The temporal variation in the geochemistry of the Krafla suite reveals that the volcanic system has produced a wide range of magma compositions, ranging from relatively primitive compositions to highly differentiated ones, in each time period over the last (approx.) 120 ka. There is, therefore, no evidence for the gradual chemical evolution of the central volcano with time. Prior to 120 ka the number of samples within each time period is too small for them to be statistically significant.

The compositions of the most recent lavas form the most coherent group within the suite, showing the least degree of scatter on the oxide-MgO plots. Such coherence probably reflects a more uniform parental magma sampled over a shorter time period (see Chapter 5 for a trace element perspective on parental magmas; and Chapter 6 for an analysis of the most primitive samples).

## 4.5 Least-squares estimation of proportions of crystallising phases

For a suite of rocks controlled by the fractional crystallisation of two mineral phases, it is relatively easy, by application of the lever rule in a simple mixing calculation, to deduce the proportions and relative amounts of phases crystallising (Cox *et al.*, 1979). However, where 3 or more phases are crystallising together, (which is the case for the majority of the Krafla samples) computer analysis is used to deduce the best-fit solution for the mixing calculation. Mixing programs (Wright & Doherty, 1970) perform similar calculations to a graphical application of the lever rule but use all the major element oxides at once to calculate the proportions and amounts of specified phenocryst compositions that must be removed from a primitive composition to produce a differentiated one. Here a program written by A. Walker (Univ. of Edinburgh), modified from the method of Wright & Doherty (1970) is used.

There are limitations to this kind of computer model (Cox *et al.*, 1979), some of which are listed below.

1. The compositions under investigation may be indirectly related, e.g. they follow the same fractional crystallisation path but from different batches of parental magma.
2. When a large number of phases are crystallising a wide range of solutions can arise, each of which has a good degree of fit. Some of these solutions are petrogenetically unreasonable.
3. Analytical error may be significant.
4. Other processes may be operating (e.g. partial melting of the crust), which may mean that the apparent extent of fractional crystallisation is different from that which actually took place in the liquid.

Mineral phases do not crystallise continuously and/or do not keep a fixed composition. Hence it is useful to divide up the differentiation series into a number of stages (usually on the basis of MgO content) to which average mineral compositions can be assigned. The program is then used to calculate the extent of fractional crystallisation required to explain the composition of any particular stage using the mineral compositions for that interval alone. The total differentiation sequence can then be deduced by considering the cumulative effect of all the steps. The assignment of a fixed mineral composition to a fractional crystallisation interval is clearly an approximation but a good solution to the least-squares fit is usually obtained.

The first task in setting up such a model is to select two rock compositions, which are from the volcanic suite and may be inferred to be related by fractional crystallisation. The compositions of the relevant phenocryst phases are then selected. One example is shown in Table 4.1 in which samples 84-19 and KK152 have been chosen as starting and finishing compositions respectively (Appendix IV) for the first step of modelling the differentiation series. The relevant mineral phases are ol, plag and cpx (compositions shown in Table 4.1). The program calculates the best-fit solution for these phases (Table 4.1). 13.6% fractional crystallisation of an assemblage consisting of 26.4% ol, 42.4% plag and 31.2% cpx is required to produce KK152 from 84-19. An estimate of the degree of fit of the least-squares model is given by the sum of the squares ($\Sigma r^2$) of the differences between the calculated oxide wt% and the actual rock composition. In this case $\Sigma r^2$=0.06, which is less than the generally accepted maximum value of 0.10 for a satisfactory solution (Wright, 1974). Values higher than 0.10 usually suggest that there are processes other than fractional crystallisation linking the two compositions used in the mixing calculation (e.g. Sigurdsson 1981; Stakes *et al.*, 1984).

The whole differentiation sequence is shown in Table 4.1. About 90% cumulative fractional crystallisation (f.c.) is required to produce KK03 (rhyolite, 0.19 wt% MgO) from 84-19 (basalt, 8.66 wt% MgO). This is consistent with values obtained by other workers on comparable suites of rocks. For example, Byerly (1980) investigated the differentiation pathway of a suite from the Galapagos spreading centre and found that 76.4% f.c. is necessary to generate a rhyodacite from a basalt with 9.0 wt% MgO.

The proportions of phases used in the f.c. steps are also shown in Table 4.1. The average basaltic crystallisation assemblage from Krafla is 20.2% ol, 48.8% plag, 31.0% cpx, which is reasonably close to that obtained by Meyer *et al.* (1985) for the NE region of Iceland. The relative amount of olivine in the assemblage falls as the samples become more evolved, whereas the proportions of plagioclase and

| Sample | MgO wt% | Δ%fc | Total% | ol. | plag. | cpx. | ap. | mt. | ilm. | opx. |
|---|---|---|---|---|---|---|---|---|---|---|
| 84-19/KK152 | 8.66-7.58 | 13.6 | 13.6 | 26.4 | 42.4 | 31.2 | 0.0 | 0.0 | 0.0 | 0.0 |
| KK152/84-05 | 7.58-5.86 | 31.7 | 41.0 | 20.2 | 54.4 | 25.4 | 0.0 | 0.0 | 0.0 | 0.0 |
| 84-05/KK08 | 5.86-4.81 | 18.0 | 51.6 | 12.1 | 42.6 | 45.3 | 0.0 | 0.0 | 0.0 | 0.0 |
| KK08/KK35 | 4.81-3.32 | 30.9 | 66.6 | 0.0 | 17.5 | 47.4 | 0.65 | 29.3 | 0.0 | 5.1 |
| KK35/KK03 | 3.32-0.19 | 60.8 | 86.9 | 11.0 | 59.1 | 11.3 | 0.79 | 3.7 | 2.2 | 11.9 |



Note: Representative mineral analyses were used for this model, where possible from one of the two samples in each step. Mineral analyses are contained in Appendix III.

84-19/KK152: ol. $Fo_{81}$, plag. $An_{77}$, cpx. Mg#=80
KK152/84-05: ol. $Fo_{70}$, plag. $An_{77}$, cpx. Mg#=80
84-05/KK08: ol. $Fo_{70}$, plag. $An_{77}$, cpx. Mg#=80
KK08/KK35: plag. $An_{67}$, cpx Mg#=69, opx Mg#=71, ap. (see Deer *et al.*, 1966), mt. Appendix III.
KK35/KK03: ol. $Fo_{13}$, plag. $An_{61}$, cpx. Mg#=69, opx. #Mg=71, ap., mt., (as above), ilm. see Appendix III.

$\Sigma r^2$ terms were 0.057, 0.071, 0.025 0.087 & 0.143 respectively for the above steps.

**Table 4.1** Least-squares estimation of the proportions of crystallising phases.

clinopyroxene are more variable. This variability may result from trying to find a fractional crystallisation model for samples derived from different parental magmas. In order to minimise the effects of different parental magmas, the first 3 samples were selected from the same eruptive event. Unfortunately, no individual eruptive event seems to have produced lavas spanning the whole compositional range, so samples from other events have to be taken to complete the sequence.

$\Sigma r^2$ values range from 0.025 to 0.143 and are shown in Table 4.1. It is significant to note that the largest $\Sigma r^2$ value comes from the increment KK35 to KK03 (icelandite to rhyolite), of which the major contribution is provided by $K_2O$ ($r^2$=0.08). $K_2O$ is present in greater concentration in the rhyolite than can be accounted for by the f.c. of the icelandite. The excess of $K_2O$ in the rhyolite cannot be explained by changing the phase assemblage, as $K_2O$ is close to being perfectly incompatible in all possible mineral phases. It would require 68.8% f.c. of the icelandite (0.81 wt% $K_2O$) to produce a rhyolite with 2.60 wt% $K_2O$, which is in excess of the model value of 60.8%.

There are several possible explanations for this $K_2O$ discrepancy, including:

1. Open system fractionation (i.e. a magma chamber which is periodically replenished, tapped, and fractionated: e.g. O'Hara, 1977; O'Hara & Mathews, 1981; Cox, 1988)
2. Crustal assimilation (e.g. by partial melting of altered wall-rock)
3. Variation in extent of mantle partial melting.

All 3 of these possibilities are considered; (1) in section 4.7, (2) in section 7.1.6 and (3) in sections 5.5 and 6.1.2.

## 4.6 Computer Modelling

### 4.6.1 Background

Chemical equilibria between mineral phases and silicate liquids have been the subject of a considerable amount of experimental study over the last 30 years (e.g. O'Hara, 1968a; Roeder & Emslie, 1970; Langmuir & Hanson, 1981). They are particularly relevant to the understanding of magma crystallisation (e.g. Biggar, 1983; Ford *et al.*, 1983), since the behaviour of a liquid of given composition can be predicted if mineral-melt equilibria are known (with equilibria expressed as partition coefficients). It is possible to simulate both equilibrium and fractional crystallisation by using the partition coefficients for mineral/melt equilibria of different elements. Fractional crystallisation is modelled by the sequential removal of small amounts of phases formed by equilibrium crystallisation.

A computer program (MAGMAS) written by Dr C.E.Ford of the University of Edinburgh was used to model the fractional crystallisation of 3 relatively primitive lava compositions (84-19, KK30 and KK78). This program is similar to one written by Nathan & Van Kirk (1978) but the former has the merit of being based on a large collection of experimental data on the basaltic system obtained mostly in Edinburgh. MAGMAS allows a choice of pressure (or range of pressures) over which the fractional crystallisation is to be simulated. In this case a range of pressures was used (see Table 4.2), in order to derive the most realistic crystallisation conditions.

### 4.6.2 Results

The results are summarised in Table 4.2, which shows the appearance of phases on the liquidus as a function of the MgO content of the liquid for different pressures. This program only has enough information to model the crystallisation of olivine, plagioclase and clinopyroxene successfully. Therefore the calculations are stopped at about 5 wt% MgO with the appearance of FeTi oxide phenocrysts. $fO_2$ values were set in the program using a fixed value of $Fe_2O_3/FeO=0.15$.

The computer model suggests that olivine will be the only phase initially on the liquidus for all the samples, although, petrographically plagioclase is also present in the phenocryst assemblage. Changes of pressure appear not to change the situation and plagioclase remains absent from the initial liquidus for a range of pressures. Altering the $fO_2$ value does not seem to make a significant difference. Alternatively there may be a small difference between the whole-rock chemical composition and that of the true liquid composition due to the acknowledged presence of olivine phenocrysts. The latter explanation would seem to be the more plausible (see section 4.4.2).

It can be seen in Table 4.2 that at low pressure (0 and 2 kb) plagioclase comes in as a liquidus phase before clinopyroxene. However, at higher pressures saturation in clinopyroxene is achieved before saturation in plagioclase. Different samples reach plagioclase and clinopyroxene saturation over a range of MgO contents, probably reflecting variable starting compositions. The chemical fit between experimentally-predicted compositions and the Krafla compositions is also shown in Table 4.2. Some oxides (e.g. $Na_2O$ and $K_2O$) change little with pressure of crystallisation, whereas others (especially $Al_2O_3$, CaO, $SiO_2$) are sensitive to changes in pressure. The pressure dependence of the $Al_2O_3$, CaO, $SiO_2$ differentiation trends appears to arise from the effect of pressure on the position of cpx appearance on the liquidus. Clinopyroxene contains a relatively large amount of CaO and $SiO_2$, and a

a)

| Pressure | $SiO_2$ | $Al_2O_3$ | $Fe_2O_3$ | CaO | $Na_2O,K_2O$ |
|---|---|---|---|---|---|
| 1 atm | OK | Low | OK | High | OK |
| 2 kb | OK | OK | High | High | OK |
| 5 kb | Low | High | High | OK | OK |
| 3.5-1.0 kb | OK | OK | Sl.High | Sl.High | OK |

Sl.=Slighly

b)

| 84-19<br>Pressure | $ol_{in}$ | $plag_{in}$ | $cpx_{in}$ |
|---|---|---|---|
| 1 atm | 8.69 | 7.91 | 6.70 |
| 2 kb | 8.69 | 7.75 | 7.74 |
| 5 kb | 8.12 | 7.54 | 8.69 |
| 3.5-1.0 kb | 8.69 | 7.69 | 8.53 |
| **KK30** | | | |
| 1 atm | 9.56 | 8.30 | 7.01 |
| 2 kb | 9.56 | 8.14 | 7.84 |
| 5 kb | 9.56 | 8.05 | 9.09 |
| 3.5-1.0 kb | 9.56 | 8.06 | 8.61 |
| **KK78** | | | |
| 1 atm | 9.72 | 9.72 | 8.70 |
| 2 kb | 9.72 | 9.56 | 9.72 |
| 5 kb | 8.91 | 9.05 | 9.72 |
| 3.5-1.0 kb | 9.32 | 9.26 | 9.72 |

**Table 4.2** Results of the fractional crystallisation modelling using the computer program MAGMAS. The upper table (a) shows the overall fit between the model data and the Krafla data for different oxides. The lower tables (b) present the liquidus positions (in MgO wt%) for the 3 starting compositions 84-19, KK30 and KK78 at different pressures.

relatively small amount of $Al_2O_3$ when compared with plagioclase. This means that early clinopyroxene crystallisation leads to lower CaO and $SiO_2$ values but higher $Al_2O_3$ values in the residual liquid than for the case of delayed clinopyroxene crystallisation. At 2 kb the fit between predicted and observational data is slightly better than for 0 kb, with a close agreement for $Al_2O_3$, $Na_2O$ and $K_2O$ but a poorer fit for CaO and $Fe_2O_3^*$. At 5 kb the CaO discrepancy is removed, but $SiO_2$ and $Fe_2O_3^*$ are respectively too low and much too high in concentration. Thus 2 kb seems to be the best estimate of fixed pressure.

Geophysical evidence suggests (see Chapter 2), however, that crystallisation at one fixed pressure is unlikely. It is reasonable to expect the crystallisation pressure to fall with increasing differentiation (a plausible range of pressures of crystallisation is from 0 to 3.5 kb, i.e.≡0-9 km). The effect of variable crystallisation pressure (3.5 to 1 kb at 50% f.c.) is to produce earlier clinopyroxene-saturation (in 84-19 and KK78) and later more extensive plagioclase crystallisation. A reasonable fit is achieved between the predicted and actual compositions, although as for the 2 kb case, CaO is still slightly too high in the more differentiated samples. Plots of $SiO_2$, $Al_2O_3$, $Fe_2O_3^*$ (converted from FeO and $Fe_2O_3$), CaO, $Na_2O$ and $K_2O$ against MgO are shown in Figs. 4.15 to 4.17.

This modelling appears to favour the crystallisation of clinopyroxene at an earlier stage (higher pressures) than that observed petrographically. One possible explanation for this disagreement would be for early-formed crystals of clinopyroxene to react with the liquid at lower pressure. Although, if this were the case, it is surprising that there is no petrographic evidence for early cpx crystallisation, even in the form of eroded phenocryst cores. This problem is discussed further in the next section. The overall proportions of the phases in the crystallisation assemblage (up to 5-6 wt% MgO) range from: 17-25% ol, 50-52% plag, 23-33% cpx. These values are similar to those given above for the average basaltic phenocryst assemblage of 20% ol, 48% plag and 31% cpx for the least-squares method.

## 4.7 Magma mixing

Several lines of evidence are presented below which suggest that magma mixing has played a role in the generation of the observed range of major-element compositions in the Krafla suite, although data presented in Section 4.4 show qualitatively how fractional crystallisation is the dominant cause of the Krafla major-element trends.

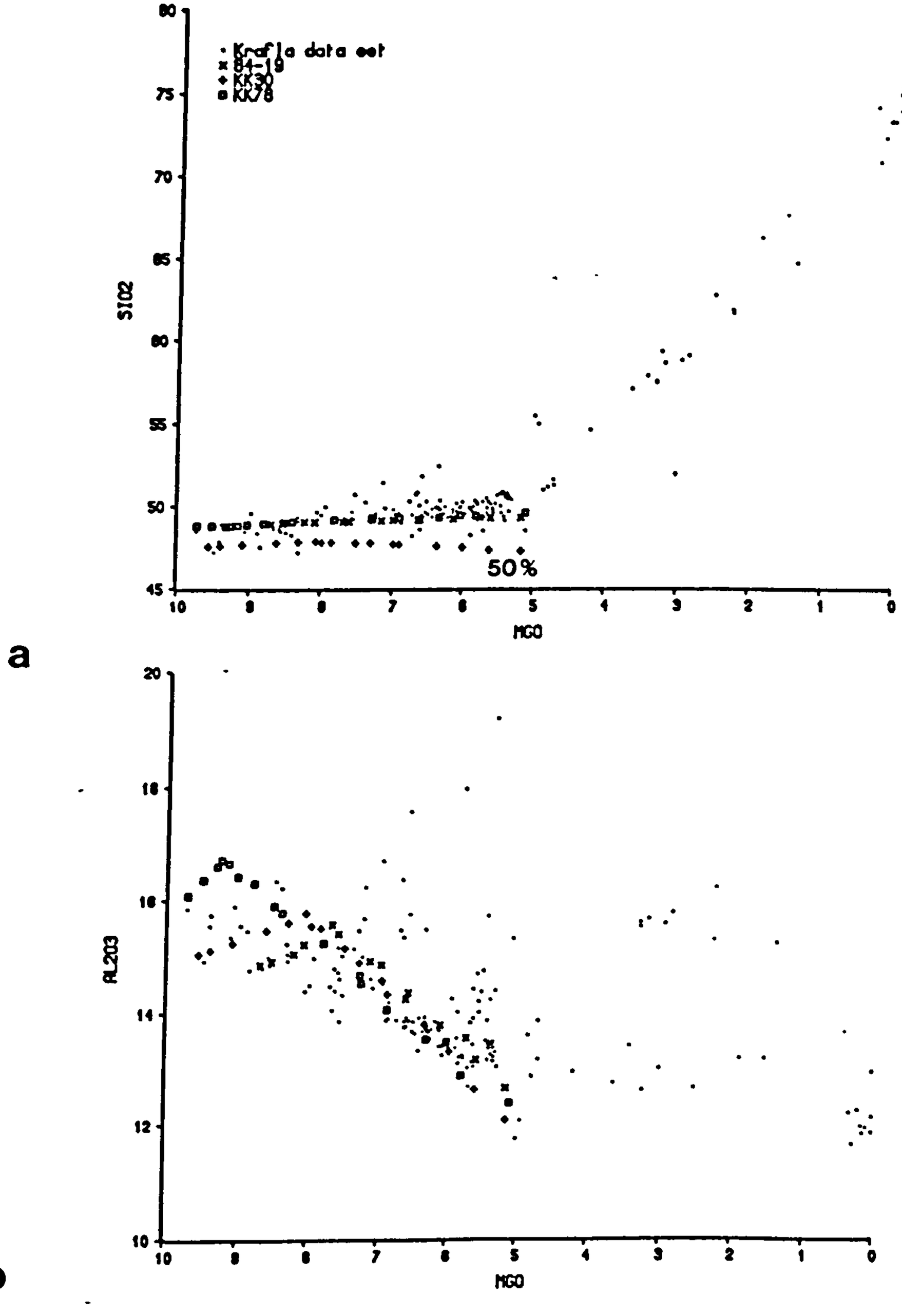


**Fig. 4.15** (a) $SiO_2$ *vs* MgO for the Krafla data (dots) and for the fractional crystallisation trends determined by computer modelling for 3 samples 84-19 (cross), KK30 (plus) and KK78 (open square). Pressure of crystallisation ranges from 3.5 kbar at 0% fractional crystallisation to 1 kbar at 50% f.c.
(b) $Al_2O_3$ *vs* MgO, details as Fig. 4.15 (a).

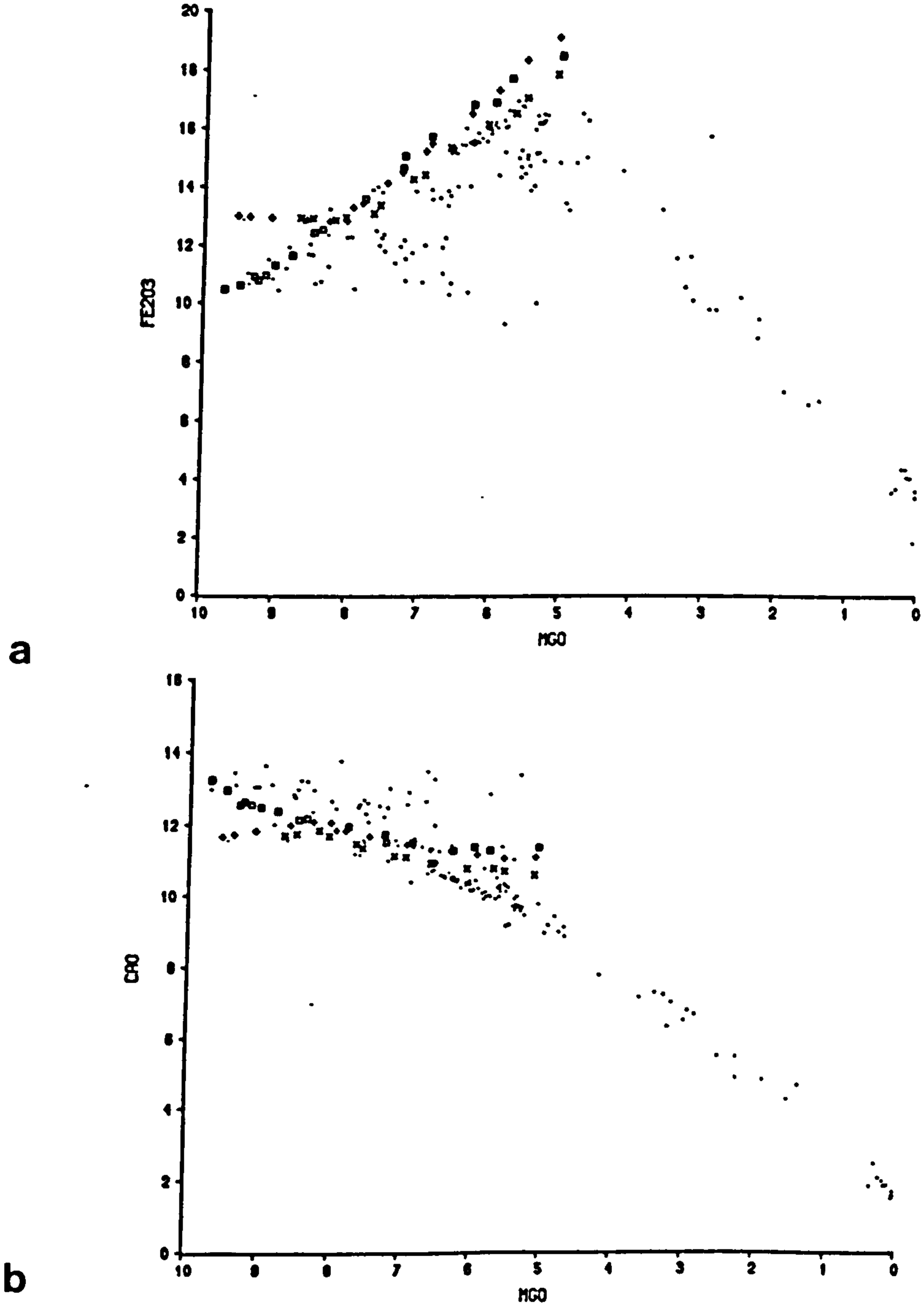


Fig. 4.16 (a) $Fe_2O_3$ (total) *vs* MgO, details as Fig. 4.15(a)
(b) CaO *vs* MgO, details as Fig. 4.15(a)

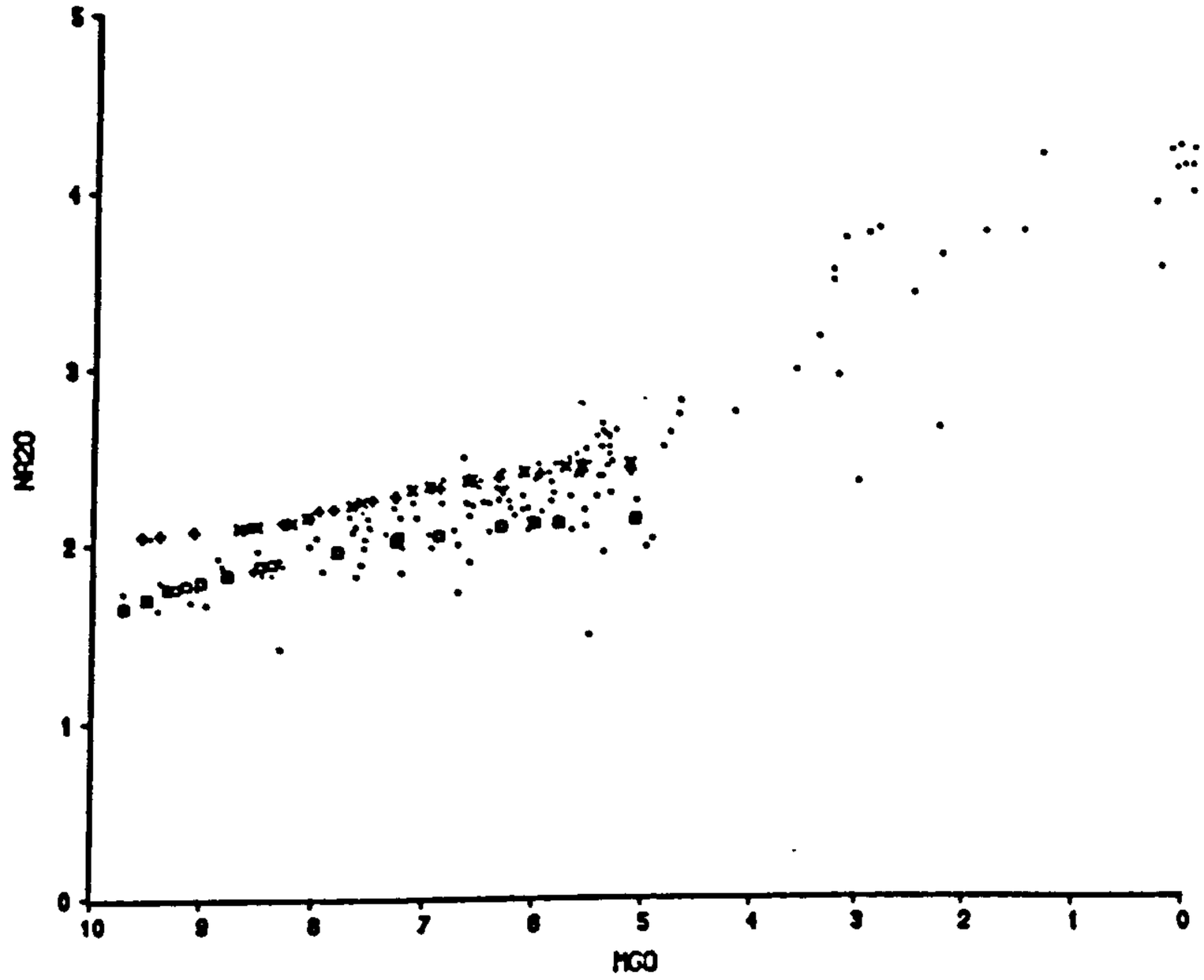


a

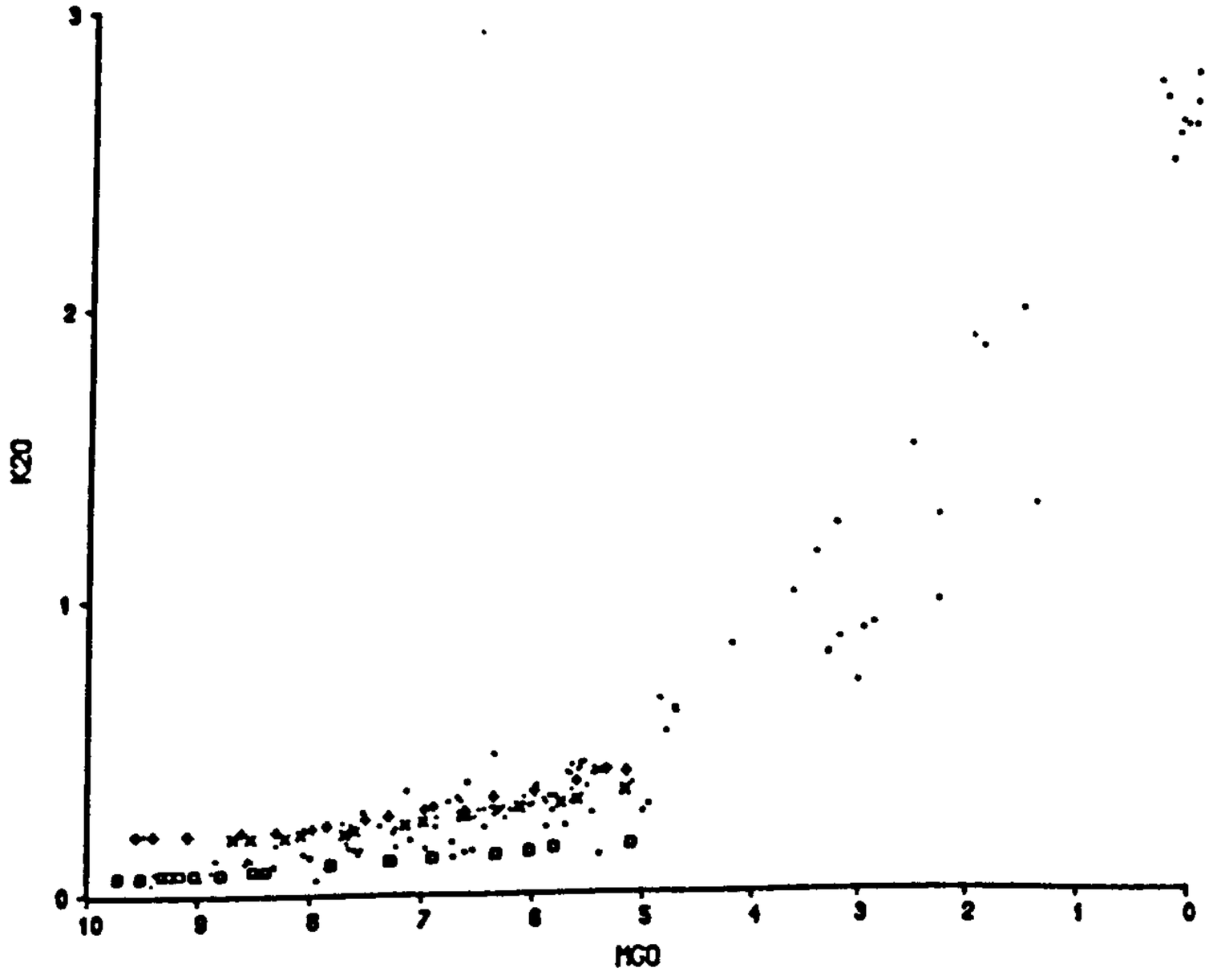


b

**Fig. 4.17 (a)** $Na_2O$ *vs* MgO, details as Fig. 4.15(a)
**(b)** $K_2O$ *vs* MgO, details as Fig. 4.15(a)

The modelling presented in sections 4.5 and 4.6 requires that more clinopyroxene should crystallise in generating the observed Krafla trends than is found petrographically. For example, all least-square fitting attempts starting with relatively-primitive compositions require a considerable proportion of clinopyroxene fractionation in order to obtain a satisfactory fit (section 4.5). This observation is consistent with the plot of $CaO/Al_2O_3$ *vs* MgO in Fig. 4.18, which suggests that at least some cpx fractionation appears necessary to explain the high-MgO part of this trend, although there is a considerable amount of scatter. The absence of clinopyroxene phenocrysts from a sizeable number of Krafla samples (Group 1, Chapter 3), which appear to need cpx fractionation to explain their chemical evolution, is a manifestation of the "clinopyroxene paradox" (Dungan & Rhodes, 1978; Walker *et al.*, 1979; Francis, 1986). Several possible explanations have been put forward to explain this problem (section 4.5), two of which relate to the role of magma mixing (see also section 5.5). The third explanation considers the effects of variation in mantle-melting processes (see sections 5.5 and 6.1.2).

One possible answer to the clinopyroxene paradox is provided by the chemical effects of magma mixing. Let a relatively-primitive magma (ol+plag-phyric) mix with a more evolved magma crystallising ol+plag+cpx. The resulting mixture may lie in the ol+plag field (providing the phase boundary is appropriately curved) and begin to dissolve clinopyroxene. After the mixed magma has erupted it may retain no petrographic evidence of clinopyroxene phenocrysts but still show geochemical evidence for cpx fractionation (Dungan & Rhodes, 1978). If this explanation is correct, however, it is difficult to understand why there are not at least some clinopyroxene phenocrysts with resorbed cores, similar to textures seen, for example, in the plagioclase megacrysts.

Another way of looking at the effects of magma mixing is to project major-element compositions of lava samples onto phase diagrams. Fig. 4.19 shows the experimentally-determined plagioclase-saturated liquidus surfaces in the system diopside-olivine-silica together with Krafla compositions, projected using the equations derived by Walker *et al.* (1979). Most of the Krafla suite, like other ocean ridge tholeiites, plots close to the ol+plag+cpx cotectic. Some of the evolved rocks (icelandites, dacites) plot along the low-Ca pyroxene + cpx + plag boundary. However, not all of the basalt samples lie on the ol + plag + cpx cotectic - a sizeable proportion of the data set lies within the cpx + plag field. Many MORBs also lie within this field and it was suggested by Walker *et al.* (1979) that these samples result from mixing a primitive basalt close to the cotectic (point A in Fig. 4.19) with an evolved composition near the low-Ca pyroxene saturation point (B). The curvature of

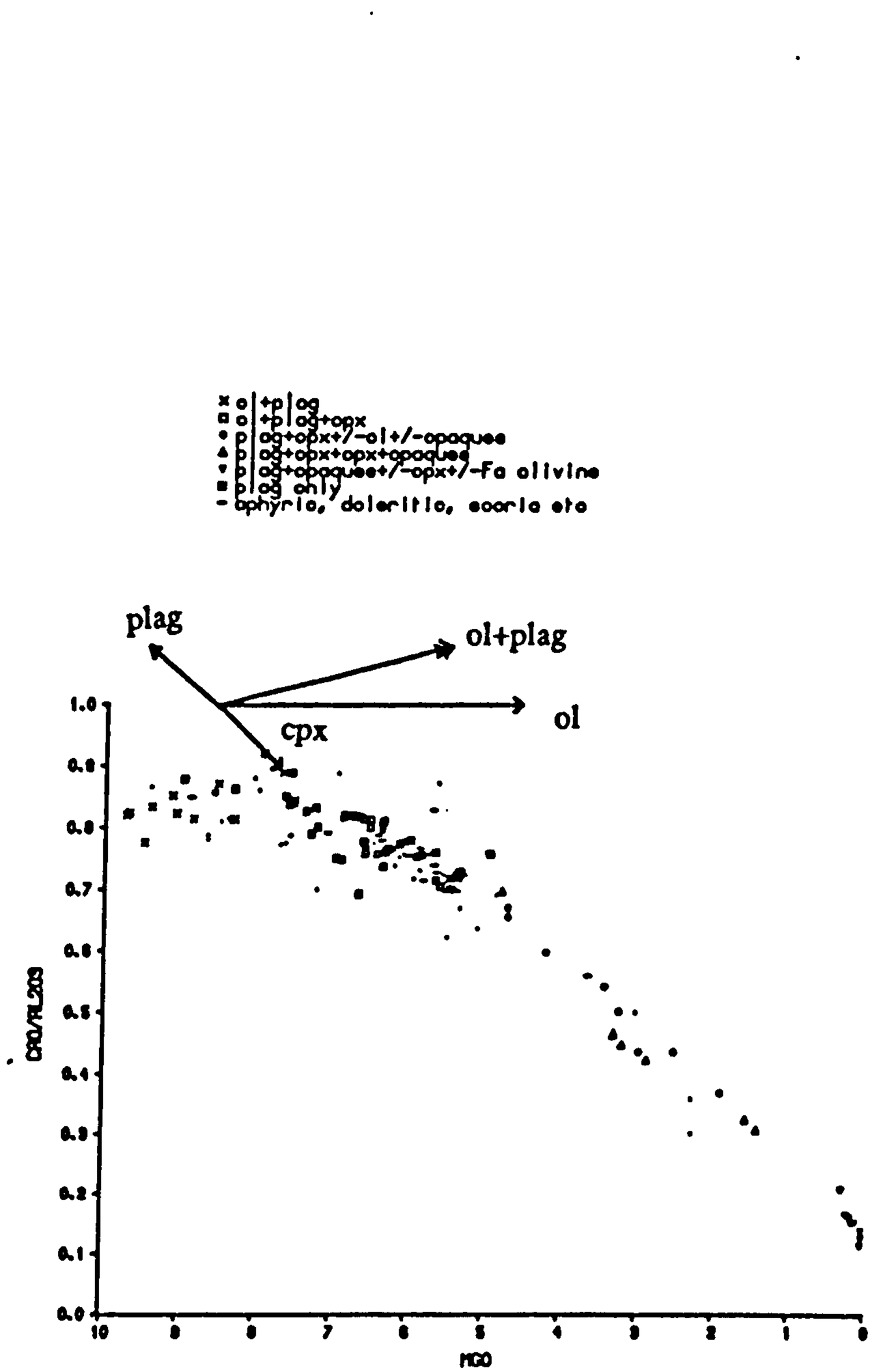


**Fig. 4.18** $CaO/Al_2O_3$ *vs* MgO, subdivided according to petrographic subgroups. "Vectors" show approximate changes with 10% fractional crystallisation of olivine, plagioclase, ol+plag, and clinopyroxene (mineral compositions appropriate for a lava containing 8.5 wt% MgO).

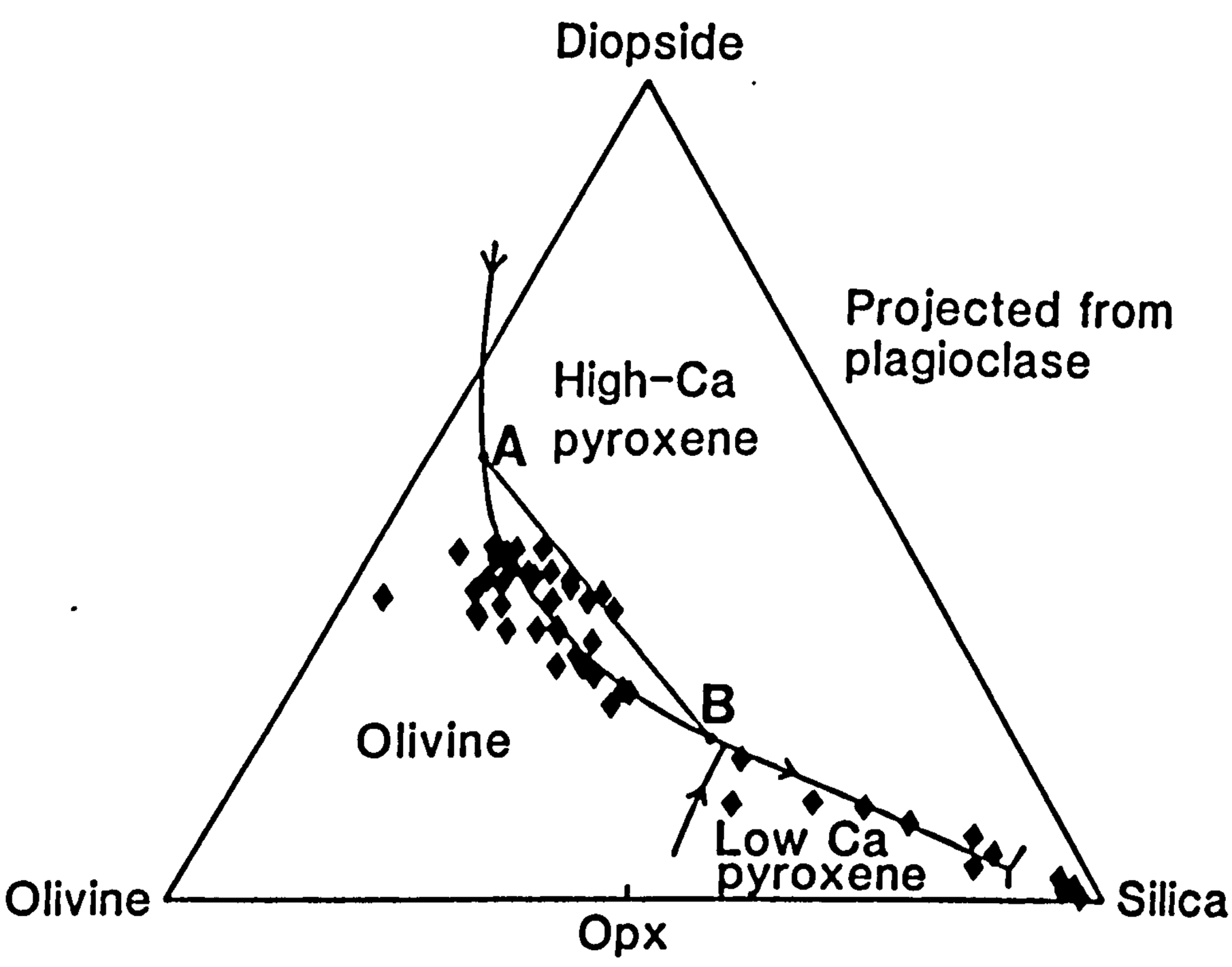


Fig. 4.19 Triangular diagram of diopside-olivine-silica projected from plagioclase, at 1 bar (QFM buffer), after Walker *et al.* (1979). A representative selection of Krafla analyses have been used to show the range of Krafla compositions found, plotted according to the scheme of Walker *et al.* (1979), where all the Fe is converted to $Fe^{2+}$ before using the projection equations.

the phase boundaries is then apparently responsible for the mixture lying in the cpx + plag field. Other authors have suggested that there are problems with this interpretation (e.g. Wilkinson, 1982; Thompson, 1987). For example Thompson (1987) has cast doubt on the $fO_2$ values used in the experiments performed by Walker *et al.* (1979). The arguments of Walker *et al.* (1979) are in conflict with those of Dungan & Rhodes (1978). Although both groups agree on the importance of magma mixing in generating some chemical features of MORBs, it would seem that the hypothesis of Walker *et al.* (1979) cannot explain the "clinopyroxene paradox". In particular, the general scatter of the basalts about the cotectic casts doubt on the interpretation of Walker *et al.* (1979). Hence it appears that attention should be focussed on mantle-melting processes when seeking an explanation of the clinopyroxene paradox (e.g. Francis 1986).

One particular welded-tuff layer from Krafla shows evidence from major-element concentrations for mixing between an evolved basalt (5-6 wt% MgO) and rhyolite. Hand-specimen evidence in favour of shallow-level mixing immediately prior to eruption is discussed in section 3.3. This unit contains a similar range of compositions produced by mixing to those samples from Askja described by Sigurdsson & Sparks (1981) and Macdonald *et al.* (1987). Evidence for magma mixing is shown in a plot of $P_2O_5$ *vs* $TiO_2$ (Fig. 4.20). The overall "loop shape" of all the data from Krafla is consistent with the incompatibility of both $TiO_2$ and $P_2O_5$ before crystallisation of FeTi oxides and apatite occurs. At the top of the loop the $P_2O_5$ concentration continues to increase while $TiO_2$ remains constant, suggesting that some $TiO_2$ is being extracted into FeTi oxides prior to apatite crystallisation. Hence the icelandites and dacites do not plot in the same position as the basalts on this plot but form the "upper limb" of the loop shape in Fig. 4.20. Intermediate compositions from the welded-tuff layer, which show evidence for mixing do not follow this "upper limb" but coincide with the basalt field, lying on an inferred mixing-line between evolved basalt and rhyolite (MgO contents shown in Fig. 4.20). Unfortunately the $P_2O_5$ concentration of the rhyolite (one of the supposed end-members in the mixing process) in the tuff was not obtained but it is likely to be similar to that in all the other Krafla rhyolites.

**Mixing models**

Open system fractionation is the process whereby a magma chamber is periodically replenished (R), tapped (T), and fractionated (F) (hence the name RTF; e.g. see Cox, 1988). O'Hara (1977) and O'Hara & Mathews (1981) who developed a numerical model for this process, claimed that the observed compositions of rocks

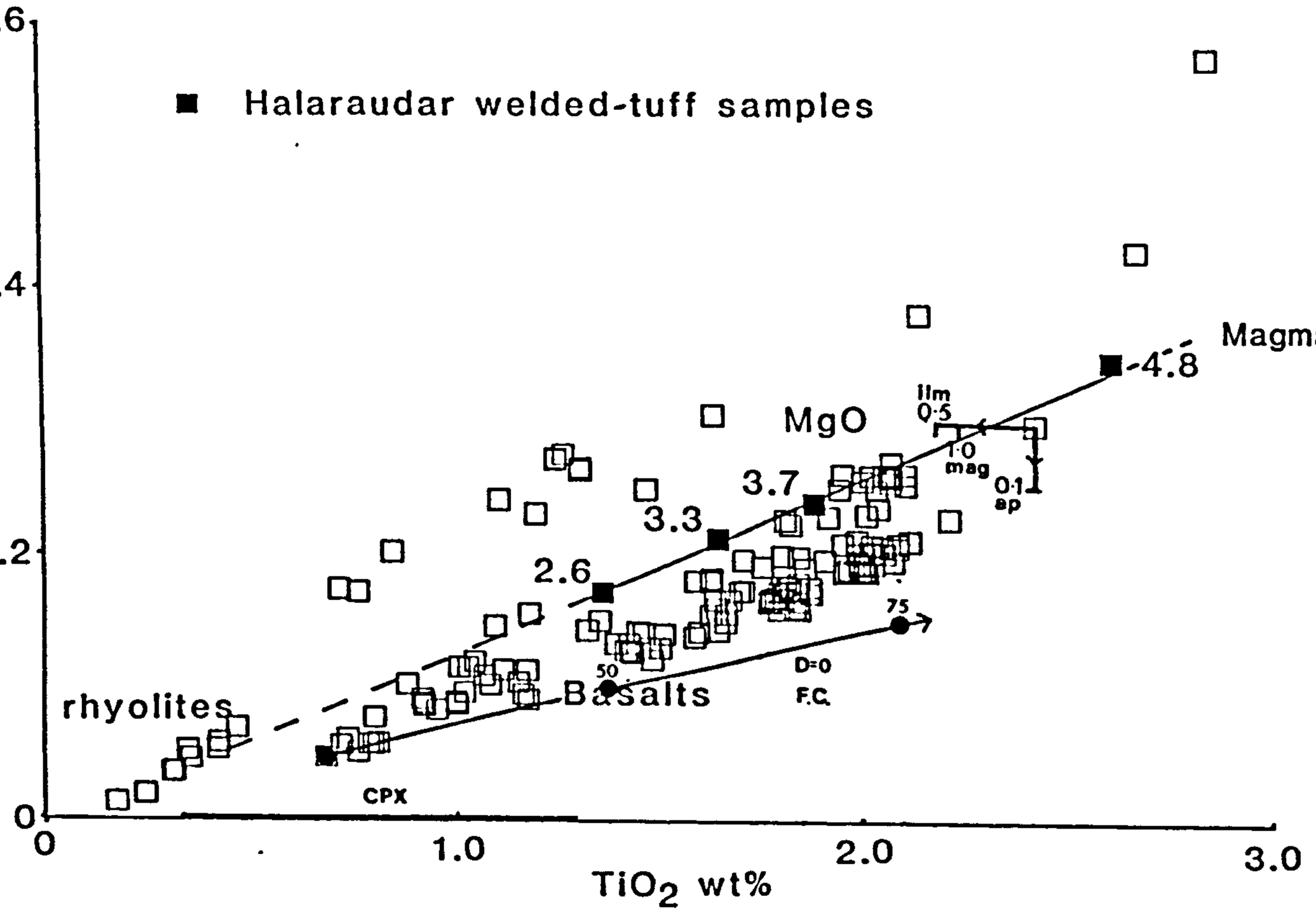


**Fig. 4.20** $P_2O_5$ *vs* $TiO_2$, showing samples from the Halaraudar welded-tuff layer (filled squares) and the remaining samples from the Krafla volcanic system (open squares). The line represents a mixing-line between evolved basalt and rhyolite (dashed to the estimated rhyolitic end-member). The crystallisation "vectors" represent the fractional crystallisation of apatite (ap), ilmenite-hematite (ilm) and ulvöspinel-magnetite(mag)from the composition shown. (%f.c. shown next to vectors)

cannot be properly used to deduce the extent of fractional crystallisation linking two compositions because each of the two compositions reflects a different steady-state condition of an RTF magma reservoir. In particular, it has been postulated that open system fractionation, given many episodes of magma replenishment, can lead to enrichment in incompatible components (i.e. elements which do not enter crystallising mineral phases). The behaviour of the incompatible trace elements is discussed in Chapter 5. However, the major-element compositions are less affected by open system behaviour than the incompatible trace elements (O'Hara & Mathews, 1981), so justifying delay in testing the RTF or open system fractionation model until Chapter 5.

In summary, magma mixing appears necessary to explain some aspects of the major-element compositional trends not easily explicable by fractional crystallisation (see further discussion in section 5.4). However, the clinopyroxene paradox is difficult to explain by magma-mixing processes. For an alternative explanation, see the discussion on the effects of mantle-melting processes on the compositions of the most primitive Krafla samples in Chapters 5 and 6.

## 4.8 Comparisons with other ocean ridge tholeiites

A large data-base of major-element compositions from ocean ridge tholeiites has been assembled over the past few years (e.g. Melson *et al.*, 1977; Sigurdsson, 1981; Schilling *et al.*, 1983). The Krafla suite can be compared with this global data-base.

The most obvious difference between tholeiites from Krafla and ocean ridge tholeiites, in general, is that the Krafla suite contains many more evolved compositions than are normally found at ocean ridges (Fig. 4.21). It has been suggested that the differentiated nature of the Krafla suite is a result of the development of permanent magma reservoirs within and beneath the (thick) Icelandic crust. This factor can allow for longer periods of differentiation between eruptions than in other oceanic ridge environments and therefore a greater abundance of more evolved compositions. Crustal assimilation will also aid the generation of more differentiated volcanic products (see Chapter 7).

The Galapagos spreading centre is a comparable example where highly differentiated magma has evolved in an ocean ridge environment. Byerly (1980) reported the occurrence of a suite of rocks ranging from relatively primitive ol + plag-phyric basalts (9.0 wt% MgO) through to rhyodacites (1.6 wt% MgO), covering most of the range of MgO values of the Krafla suite. In particular, the Galapagos suite has

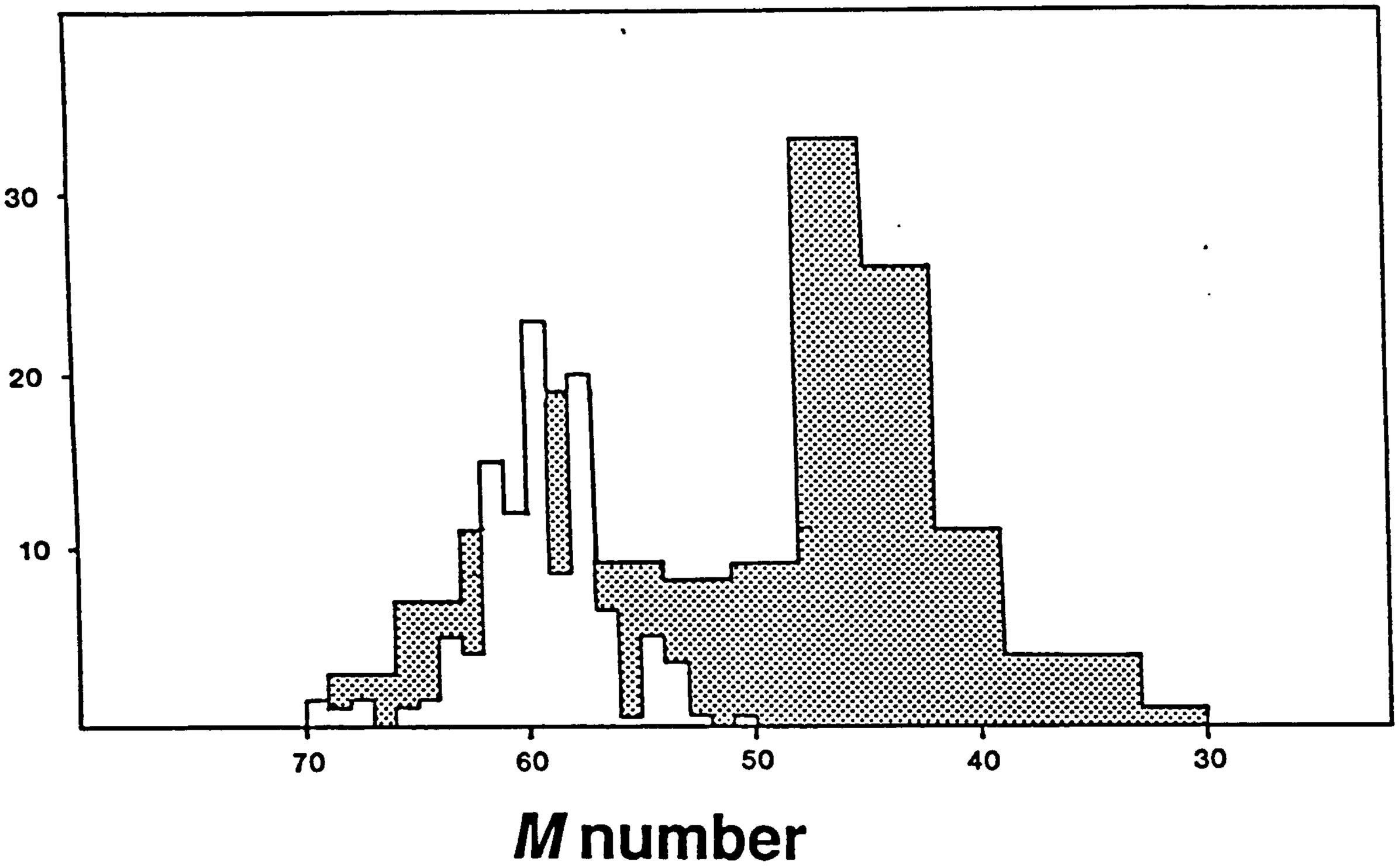


Fig. 4.21 Sample abundance plotted against *M* number (*M*=100.($Mg^{2+}$/($Mg^{2+}$+$Fe^{2+}$)) where $Fe_2O_3$/FeO=0.15) for samples with M≥30 from the Krafla data set (dark) and from a selection of MORB samples (white) taken from Wilkinson (1982). Note that the number of samples for the MORB data set is halved.

similar major-element trends to those described above. It is rare, however, for rocks more differentiated than evolved basalt (5-6 wt% MgO) to be found at ocean ridges.

It has been recognised for some time now that there are distinctive features of MORB chemistry, which cannot easily be explained by fractional crystallisation from a single parental basaltic composition (e.g. Bryan & Moore, 1977; Langmuir *et al.*, 1977; Bryan, 1979). Variations in the composition of both the mantle source and the melt generated by partial melting of that source have often been cited as explanations for such differences (e.g. Sun *et al.*, 1979; Wood, 1979; Sigurdsson, 1981; Natland, 1989). Sigurdsson (1981) recognised two distinct major-element trends in MORB data from the N. Atlantic: group A from 29-35°N and 54-70°N with lower $Na_2O$ and $SiO_2$ and higher $FeO^*$ (where $FeO^*$ is total Fe expressed as $Fe^{2+}$), and group B from 35-53°N and 71-73°N with higher $Na_2O$ and $SiO_2$, and lower $FeO^*$. The Krafla basalts fall into group A. Such differences in MORB compositions are highly unlikely to be caused by crystallisation processes. Recently, however, it has been recognised that the major-element compositions of primitive MORBs are likely to be controlled by the temperature and flow regime of the mantle undergoing partial melting as it ascends beneath the ocean ridges. Klein & Langmuir (1987) showed that there was correlation between zero-age water depth and the composition of erupted basalts, after correcting for low pressure fractional crystallisation. Assuming isostatic compensation at a depth of 200 km, they related the differences in water depth to variable mantle temperature, such that shallow areas traditionally associated with "hot spots", like Iceland, represent areas of hotter than average, decompressing, asthenospheric mantle. McKenzie & Bickle (1988) and Watson & McKenzie (submitted, 1990) produced a more rigorous mathematical model for the upwelling process and combined it with a parameterisation of available experimental melting data. They explained the differences in MORB composition by varying the mantle potential temperature ($T_p$) (see Chapter 1 for definition). Their results were consistent with those of Klein & Langmuir (1987). After correction for different extents of fractional crystallisation, $Na_2O$ and $FeO^*$ serve as useful indicators of $T_p$. High concentrations of $FeO^*$ (at 8.0 wt% MgO, written as $FeO^*_{8.0}$) together with low $Na_2O_{8.0}$ correspond to high values of $T_p$. Krafla has on average a value of $2.0 \pm 0.3$ wt% for $Na_2O_{8.0}$ and $10.7 \pm 1.4$ wt% for $FeO^*_{8.0}$, consistent with a $T_p$ of about 1580°C, which is at the high end of the spectrum of values from oceanic ridge tholeiites (mean value 1280°C). Such a high value of $T_p$ fits with the traditional idea of a mantle plume or "hot spot" beneath Iceland. A more detailed analysis of the conditions of melting is undertaken in Chapter 6.

## 4.9 Conclusions

It appears that fractional crystallisation can explain many aspects of the major element whole-rock compositions of the Krafla suite. Major-element variation diagrams are reasonably consistent with the fractional crystallisation of the observed phenocryst phases.

Least-squares modelling of the compositional trends suggests that there is an excess of $K_2O$ in the rhyolites, over and above that which can be reasonably expected due to simple closed-system fractional crystallisation. This may be due either to open system fractionation and/or to crustal assimilation. Numerical modelling of fractional crystallisation based on experimental data suggests that crystallisation over a range of pressures (average about 2 kb) gives the best fit with the observed Krafla compositions.

Geophysical evidence (from the recent eruptive cycle) has shown that magma mixing is a significant process in the central volcano environment. Magma mixing may explain some aspects of the major-element compositions, e.g. the need for more clinopyroxene fractionation than is petrographically observed. However, there are difficulties in using the above mixing models to explain the absence of clinopyroxene. Instead, there may be another explanation for the clinopyroxene paradox; namely samples which are thought to be related solely by fractional crystallisation may be in fact products of different degrees of melting. This is explored further in Chapter 6.

The Krafla suite contains many more evolved compositions than are typically found at ocean ridges. The production of differentiated lavas is consistent with the development of a longer-lived magma reservoir beneath the Krafla central volcano. Also there are differences in composition (e.g. $Na_2O$, $FeO^*$) between ocean ridge tholeiites which cannot readily be explained by crystallisation or magma mixing processes. Such differences probably reflect regional differences in mantle potential temperature rather than mantle heterogeneity (e.g. Natland, 1989). Krafla's basalts are consistent with the presence of a high mantle potential temperature beneath Iceland. This fits with the widely accepted notion of a mantle plume or "hot spot" beneath Iceland.

# Chapter 5

# Trace-element compositions

## 5.1 Rationale

The term trace element is generally applied only to those elements whose abundances are no greater than 1000 ppm (Henderson, 1982). Such elements do not generally form major rock-forming minerals themselves but instead are contained in specific crystallographic sites in common mineral phases. Some trace elements have a high degree of preference for certain sites in the crystal lattices of particular minerals and are thus removed from the magma during fractional crystallisation of those minerals (i.e. they are compatible in those phases). Other trace elements which are not removed from the magma during the fractional crystallisation, preferring to remain in the magma, are incompatible in these minerals. The final concentration of a trace element achieved during fractional crystallisation, whether compatible or incompatible with the given crystallising assemblage, depends upon the nature and proportions of the minerals crystallising from the liquid, and on its original concentration in the magma. With only a small proportion of a phase crystallising with a high degree of compatibility for a trace element (e.g. apatite for Ce) increasing concentrations of that trace element with differentiation may still result (i.e. net incompatibility). In addition the phase assemblages also alter with differentiation, causing many elements to change from being incompatible to compatible during the course of crystallisation. Examples of such behaviour for the Krafla suite are shown below. Although trace elements are fractionated during crystallisation processes, they show similar types of behaviour during melting. However, in the case of melting, of either mantle or crust, the incompatible trace elements rapidly enter the magma (and therefore decrease in concentration during the melting process) while compatible elements are held back (and so increase in concentration with the extent of melting).

The usefulness of data on trace-element concentrations arises from this variability of behaviour. Given a knowledge of the preference of the minerals for certain trace elements during melting or crystallisation, and the proportions of the phases involved, then this knowledge may be used to produce models of differentiation or melting processes. The preference of a mineral for a given trace element is commonly expressed by means of a partition coefficient, $K_D$ (the concentration of an element in a given mineral divided by the concentration of the element in the coexisting liquid at equilibrium). The behaviour of an element during

fractional crystallisation depends upon the overall value of D (the bulk distribution coefficient) for the phenocryst assemblage. For example, Ni is highly compatible with olivine and clinopyroxene (both with $K_D>>1$) but incompatible in plagioclase, resulting in net compatibility in the assemblage. Hence Ni decreases rapidly in concentration in the residual liquid during fractional crystallisation. In contrast, Rb which has very small values of $K_D$ ($\rightarrow 0$) in olivine, plagioclase and clinopyroxene, always increases in the residual liquid (net incompatibility $D<0$).

Modelling fractional crystallisation or various types of melting process is, however, not simple because D- and $K_D$-values are not that well known for some elements (e.g. Y, U, Th in most phases) and in any event D-values may continuously change during differentiation (or melting) as a function of temperature and changing crystal and liquid composition. Modelling, in the first instance, can only safely proceed as far as the reliability of the D-values allows. Despite this reservation, however, some quantitative tests of differentiation and melting processes can be made using trace-element concentrations and their ratios.

In this Chapter trace-element concentrations are used to help understand the magmatic processes occurring in the Krafla volcanic system. Firstly, most of the trace elements are plotted against MgO in order to assess the proposition that the Krafla volcanic suite is largely produced by variable amounts of fractional crystallisation. Secondly, other magmatic processes are considered; namely crustal assimilation, magma mixing (i.e. open system fractionation in periodically replenished magma chambers) and mantle melting processes. Mantle-melting processes are also considered in Chapter 6.

## 5.2 Analytical techniques

The concentrations of trace elements in whole-rock samples have been determined in three separate ways:

(1) By X-ray fluorescence (XRF) spectrometry for the trace elements Ni, Cr, V, Sc, Cu, Zn, Sr, Rb, Zr, Nb, Ba, Y, $La^*$, $Ce^*$, $Nd^*$, $Th^*$ and Pb. Elements marked with an asterisk have also been analysed by one of the other two techniques listed below. The analytical techniques are described in Appendix VIa and the concentrations of the elements are given in Appendix IVb. It should be noted that the determinations of the last five elements (La to Pb) in the above list are associated with considerable analytical errors for many of the Krafla samples. Details of analytical reproducibility and typical detection limits are also given in Appendix VIa.

(2) By isotope dilution for Th and U (see Appendix VIf); data are given in Table 7.3.

(3) By inductively-coupled plasma (ICP) atomic emission spectrometry for most of the rare-earth elements (REE) (see Appendix V for REE concentrations, and Appendix VIc for analytical procedures, estimated errors and a comparison with the XRF results).

## 5.3 Results

### 5.3.1 Variation diagrams against MgO

The trace-element results are presented in the form of variation diagrams plotted against MgO (Figs. 5.1 to 5.6). Only selected REE analysed by ICP (e.g. La, Nd, Eu, Lu), are shown in these diagrams. The remaining REE analysed by ICP, are plotted for selected samples in chondrite-normalised REE diagrams (Figs. 5.7 and 5.12).

The trace element *vs* MgO variation diagrams may be divided into three categories according to the bulk compatibility or incompatibility of the trace elements within the phenocryst assemblage. These are discussed in turn below.

**(a) Compatible (10-0 wt% MgO): Ni, Cr**

**Ni and Cr *vs* MgO** (Fig. 5.1 a,b). The concentrations of Ni and Cr are controlled by the crystallisation of olivine and pyroxene (principally clinopyroxene; orthopyroxene is of lesser relevance to the Krafla suite, in which opx phenocrysts only appear in icelandites and dacites; see Chapter 3). There is still ~40 ppm Ni in rocks of 5 wt% MgO, whereas Cr concentrations by this stage are close to zero. The remaining Ni is removed by further pyroxene crystallisation.

**(b) Incompatible then compatible (with the division at 8 or 5 wt% MgO): V, Sc, Cu, Zn, Sr**

**V *vs* MgO** (Fig. 5.1 c). The concentration of V mirrors the variation shown by $TiO_2$ (Fig. 4.5a), with V behaving as an incompatible element from 10 to 5 wt% MgO (some V enters ol and cpx; but little is taken into plag) but following the addition of FeTi oxides to the phase assemblage, V changes, at ~5 wt% MgO, to being a compatible trace element. Some samples plot off the general ∧-shape of the line of variation, reflecting the accumulation of plagioclase xenocrysts (cf. Fig. 4.5a).

**Sc *vs* MgO** (Fig. 5.2 a). The behaviour of Sc is slightly different from that of V, in that the maximum values of Sc concentration are reached earlier in the crystallisation sequence than for V. The initial increase in Sc concentration is consistent with the assemblage ol+plag (±minimal cpx; see Chapter 4) fractionating. However, the onset

of cpx crystallisation at ~8 wt% MgO leads to a buffering of the Sc concentration, as a result of the generally higher $K_D$ values for Sc in cpx. At ~5 wt% MgO, the Sc concentration begins to decrease due to the high $K_D$ value of Sc in FeTi oxides.

**Cu *vs* MgO** (Fig. 5.2 b). The behaviour of Cu roughly mirrors V, although there is considerable scatter, possibly reflecting the variable concentrations of sulphide mineral phases in the samples.

**Zn *vs* MgO** (Fig. 5.2 c). The concentration of Zn increases as the MgO content of the lavas decreases from 10 to 5 wt% (although some Zn enters ol, much less enters plag and cpx; hence $D_{Zn} < 1$). From 5 to 0 wt% MgO, the Zn concentration decreases, consistent with the crystallisation of FeTi oxides and, to a lesser extent, with orthopyroxene in the evolved liquids.

**Sr *vs* MgO** (Fig. 5.3 a). The Sr concentration increases from 10 to 5 wt% MgO, then gradually decreases from 5-0 wt% MgO. The change in concentration would appear to reflect the increasing role of plagioclase crystallisation and the increase in the $K_D$ value of Sr in plagioclase at lower liquidus temperatures (Sun *et al.*, 1974).

**(c) Incompatible (10-0 wt% MgO): Rb, Ba, Nb, Zr, Y, La-Lu, Th, U.**

**Rb *vs* MgO** (Fig. 5.3 b). Rb is a highly incompatible trace element over the whole range of the differentiation series, which is consistent with the known $K_D$ values of Rb for all the appropriate phenocryst phases crystallising in the Krafla suite. The increase in Rb concentration is most easily seen in the range 5-0 wt% MgO, where the absolute changes in concentration are greatest (see below for discussion on these changes in concentration). From 10-5 wt% MgO the Rb concentrations show considerable scatter but values generally increase. The scatter is unlikely to be the result of crystallisation processes (see below). For example two basalts, each with about 8.5 wt% MgO may have Rb concentrations which differ from each other by a factor of about 3 to 4. However, some of the scatter at high values of MgO may be due to analytical error (see Appendix VIa). In addition, there is some scatter in the Rb concentrations from 3-1 wt% MgO, with a distinct sub-group with lower Rb concentration (which mostly consists of the samples with higher $Al_2O_3$ concentrations described in Chapter 4). The low-Rb values are consistent with the presence of significant amounts of plagioclase microphenocrysts ($An_{50-55}$), which may be expected to contain little Rb. This reduces the Rb content compared with that expected from an aphyric sample. Generally, this same group of samples has higher concentrations of Sr, consistent with their high content of plagioclase of composition $An_{50-55}$.

**Ba *vs* MgO** (Fig. 5.3 c). Ba shows very similar behaviour to Rb, except that there is much more scatter for any given value of MgO. This is probably caused by the increased analytical uncertainty in the determination of the Ba concentration by XRF spectrometry (see Appendix VI (a)). Ba, like Rb, is essentially incompatible in the relevant tholeiitic crystallising phases.

**Nb, Zr and Y *vs* MgO** (Figs. 5.4 a,b,c). All these elements increase in a similar fashion from 10-0 wt% MgO, showing some scatter across the range of values of MgO. Zr and Nb are similarly incompatible in tholeiitic mineral phases, but Y is less incompatible reflecting the incorporation of some Y into FeTi oxides and cpx.

**La and Nd *vs* MgO** (Figs. 5.5 a,b). La and Nd are comparable to Nb and Zr respectively, being highly incompatible in the tholeiitic assemblage. Modelling of the crystallisation of REE is undertaken in section 5.3.3 below.

**Eu *vs* MgO** (Fig. 5.5 c). For the interval 10-5 wt% MgO, Eu is slightly less incompatible than La and Nd, but is markedly more compatible for the interval 5 to 0 wt% MgO with values remaining at approximately the same, or even slightly lower, Eu concentrations for the whole of this interval. This can be understood by the increase in the value of $K_D$ for Eu in plagioclase (and clinopyroxene) at lower temperatures (e.g. Schnetzler & Philpotts, 1970; Sun *et al.*, 1974; Henderson, 1982). The behaviour of Eu during differentiation is shown in Fig. 5.7 by a chondrite-normalised REE variation diagram for a suite of Krafla samples (84-19, KK152, 84-05, KK60, KK35, KK56) ranging from 8.7 to 0.3 wt% MgO. It reveals the development of an Eu anomaly in samples with less than 4-5 wt% MgO (i.e. a decrease in concentration of Eu relative to the other REE).

**Lu *vs* MgO** (Fig. 5.6 a). This element is moderately incompatible in tholeiitic phenocryst phases (less so than La and Nd) and is approximately similar to Y (Fig. 5.4 c).

**Th, U *vs* MgO** (Figs. 5.6 b,c) Both Th and U are highly incompatible and show similar trends to Rb (and $K_2O$; see Chapter 4). The increase in Th and U concentrations over the range 5-0 wt% MgO is difficult to reconcile with the extent of fractional crystallisation suggested by major element least-squares modelling (see section 4.5). Discussion is continued in the next section.

### 5.3.2 Time variation

As for the concentrations of the major elements, the majority of the trace-element concentrations are plotted against MgO according to their ages (in Figs. 5.1 to 5.4), excluding the REE, Th and U for which there are insufficient analyses of

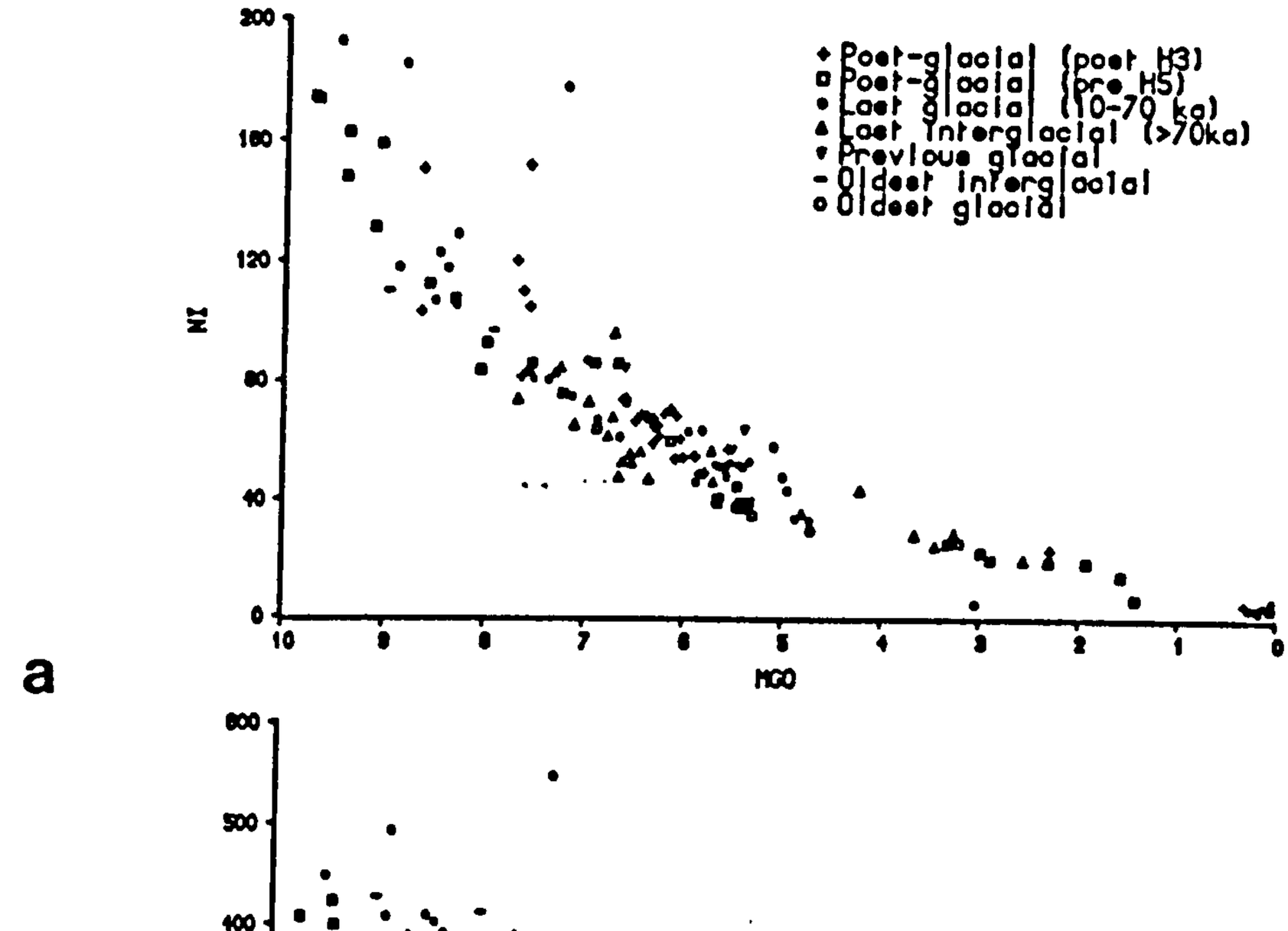


a

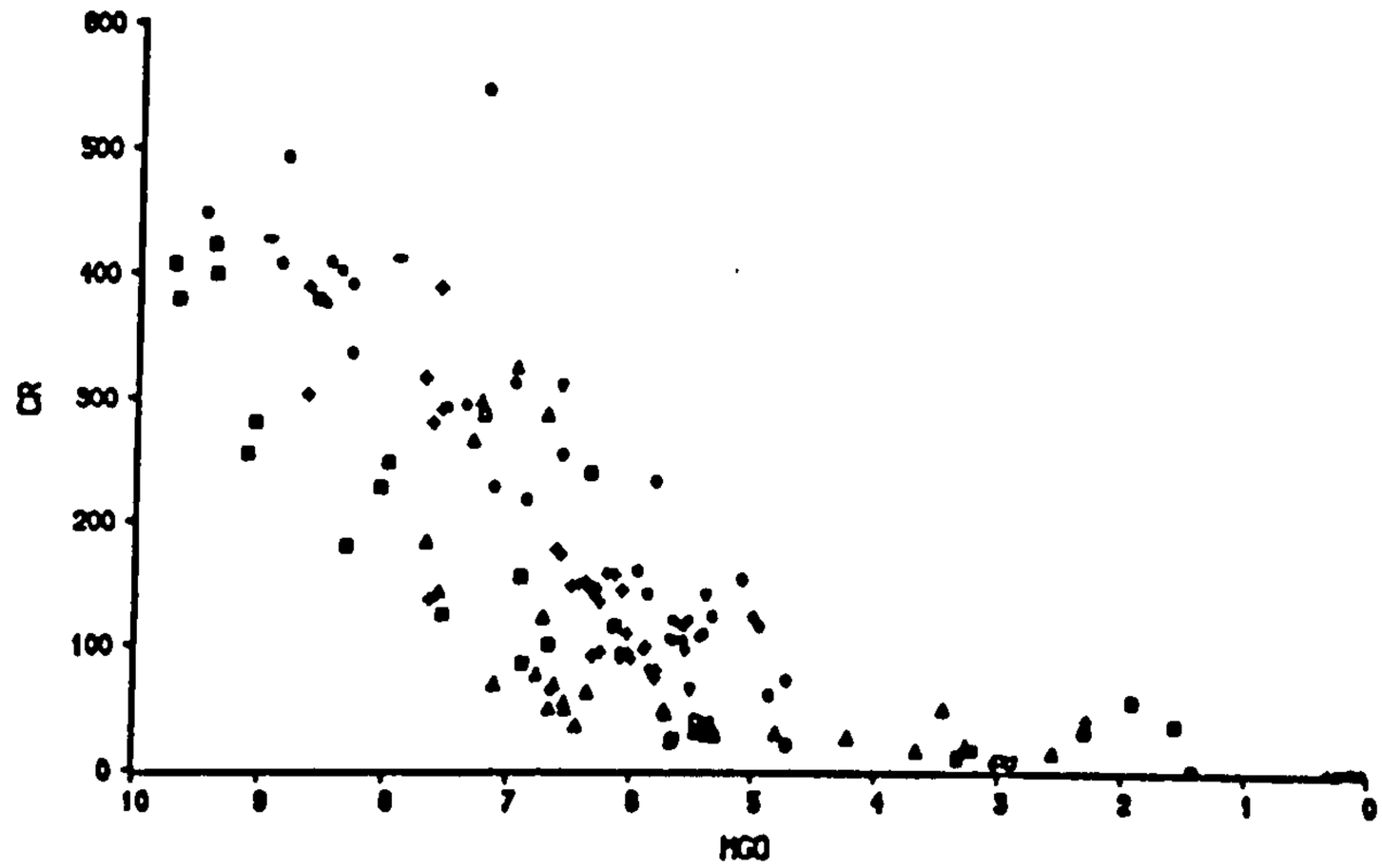


b

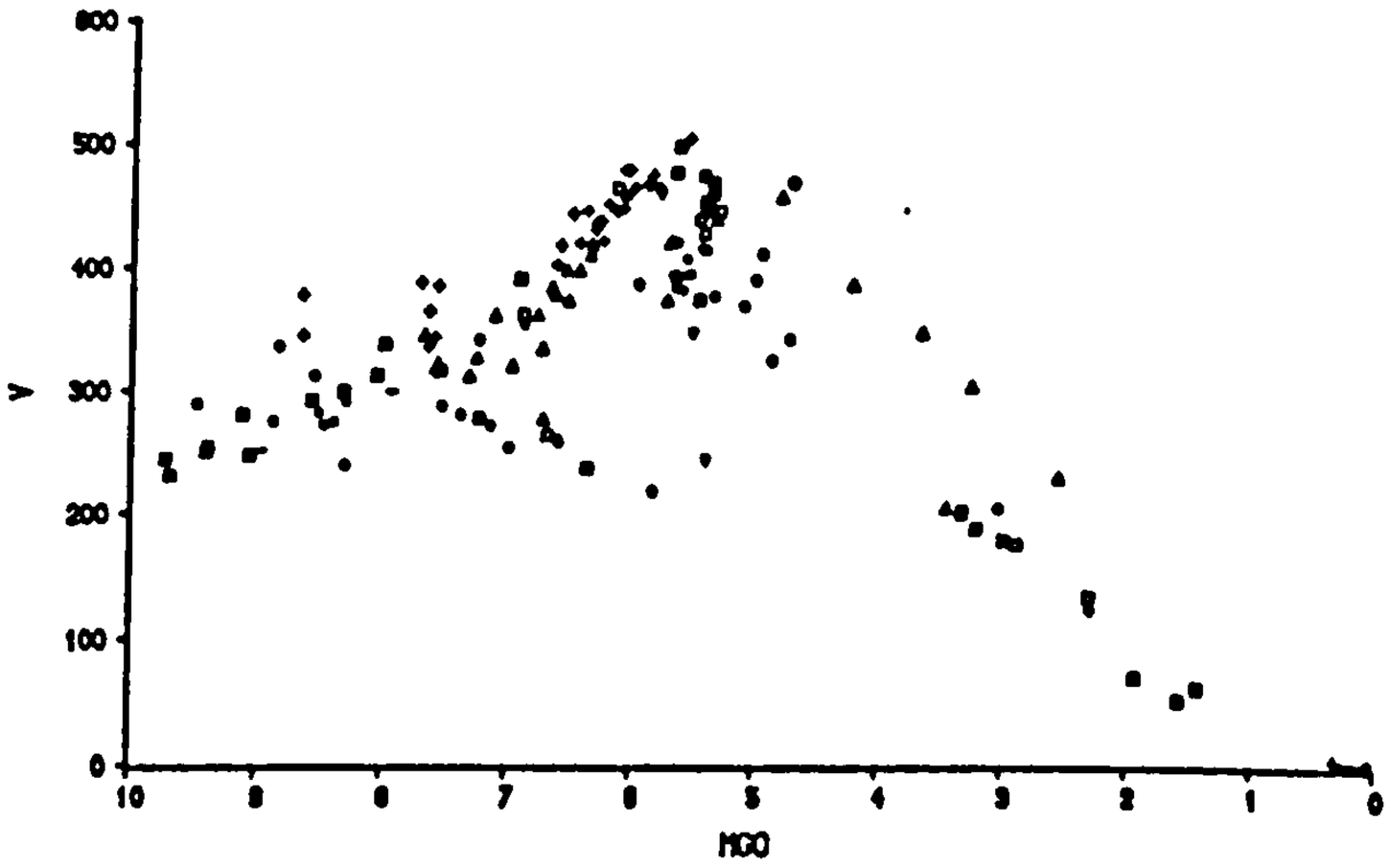


C

**Fig. 5.1 (a)** Ni (ppm) *vs* MgO (wt%); samples plotted according to age: see key.
**(b)** Cr *vs* MgO; for details see Fig. 5.1 (a)
**(c)** V *vs* MgO; for details see Fig. 5.1 (a)

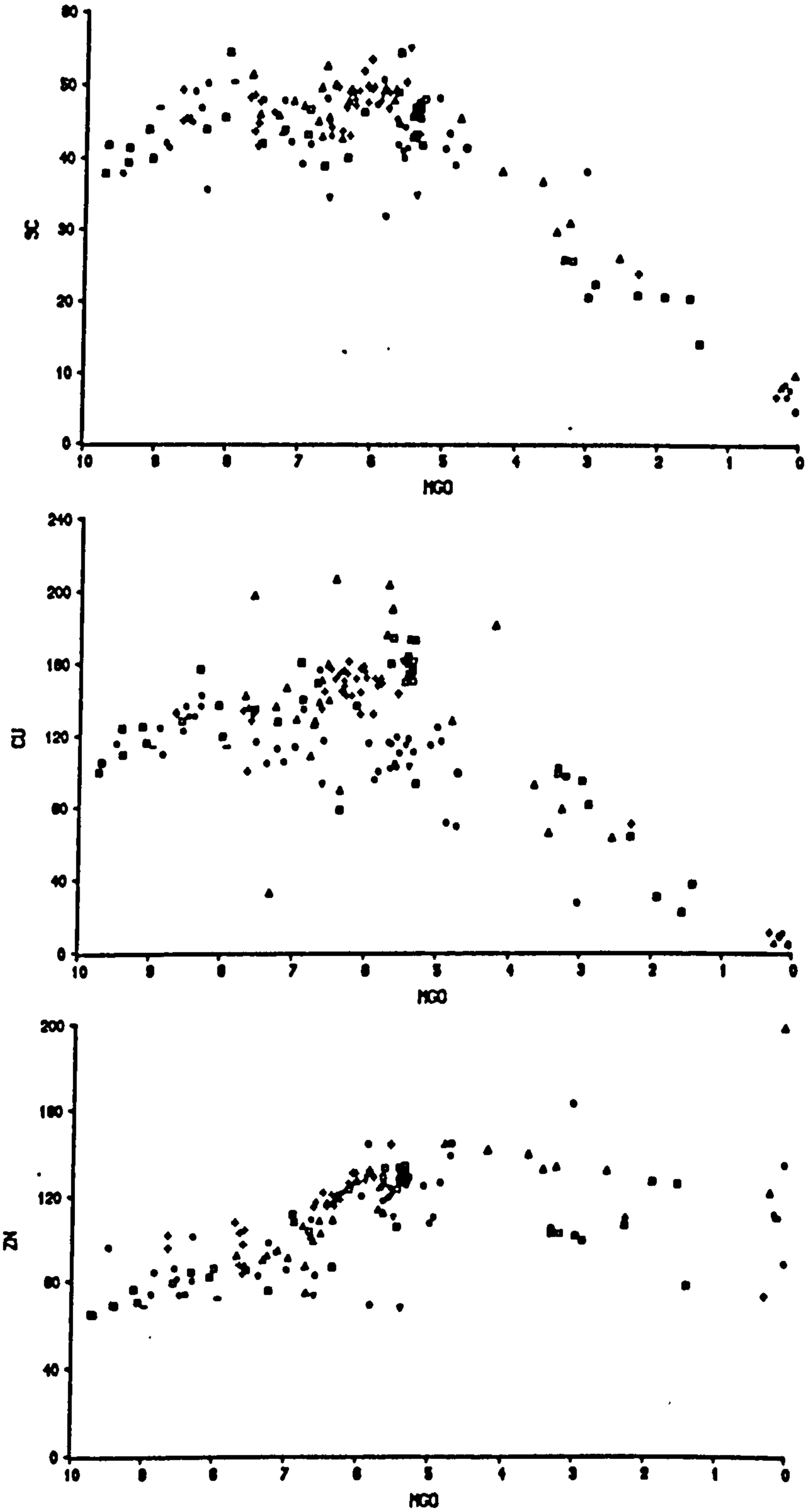


Fig. 5.2 (a) Sc *vs* MgO; for details see Fig. 5.1 (a)
(b) Cu *vs* MgO; for details see Fig. 5.1 (a)
(c) Zn *vs* MgO; for details see Fig. 5.1 (a)

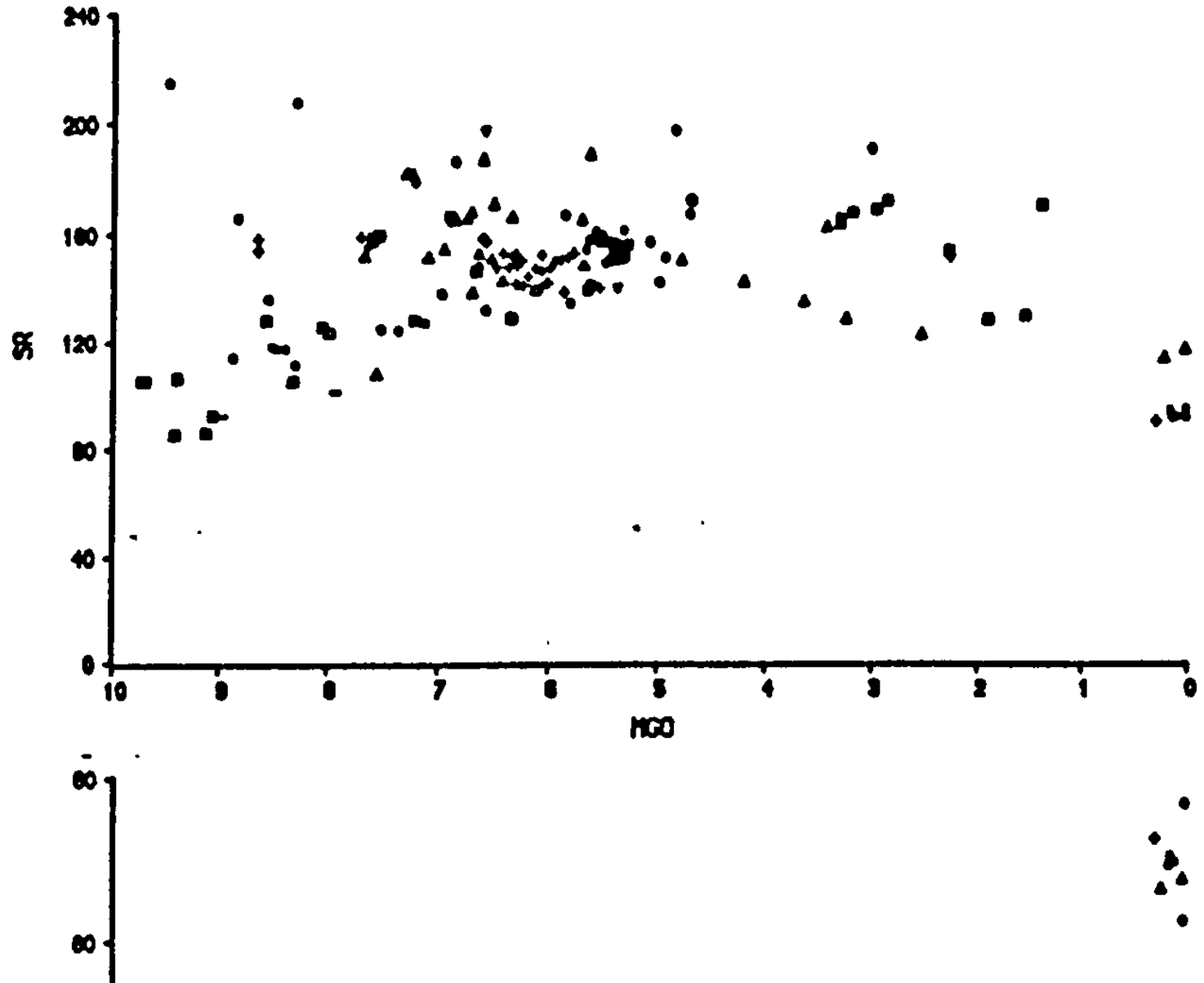


a




b

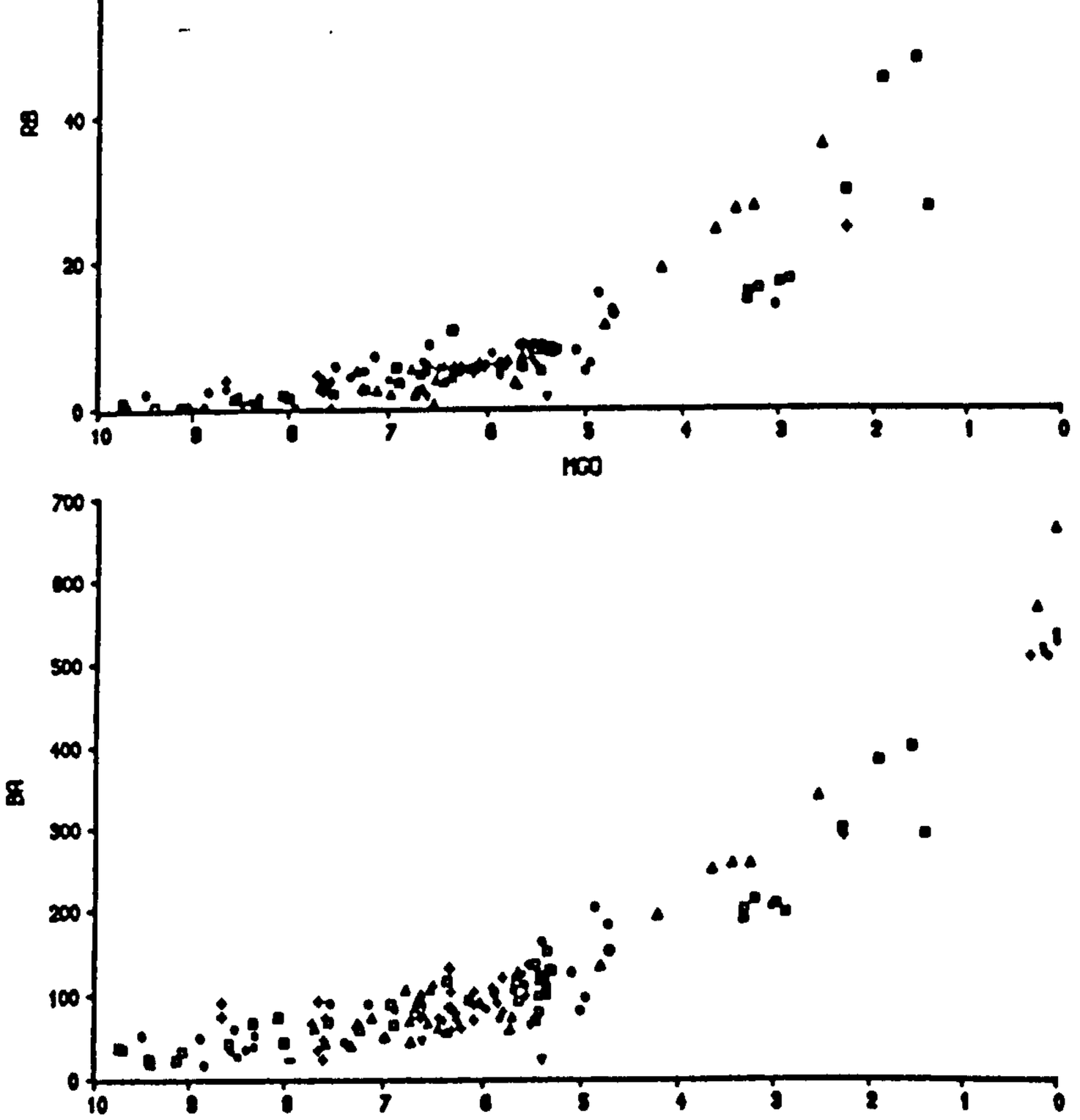


c

**Fig. 5.3 (a)** Sr *vs* MgO; for details see Fig. 5.1 (a)
**(b)** Rb *vs* MgO; for details see Fig. 5.1 (a)
**(c)** Ba *vs* MgO; for details see Fig. 5.1 (a)

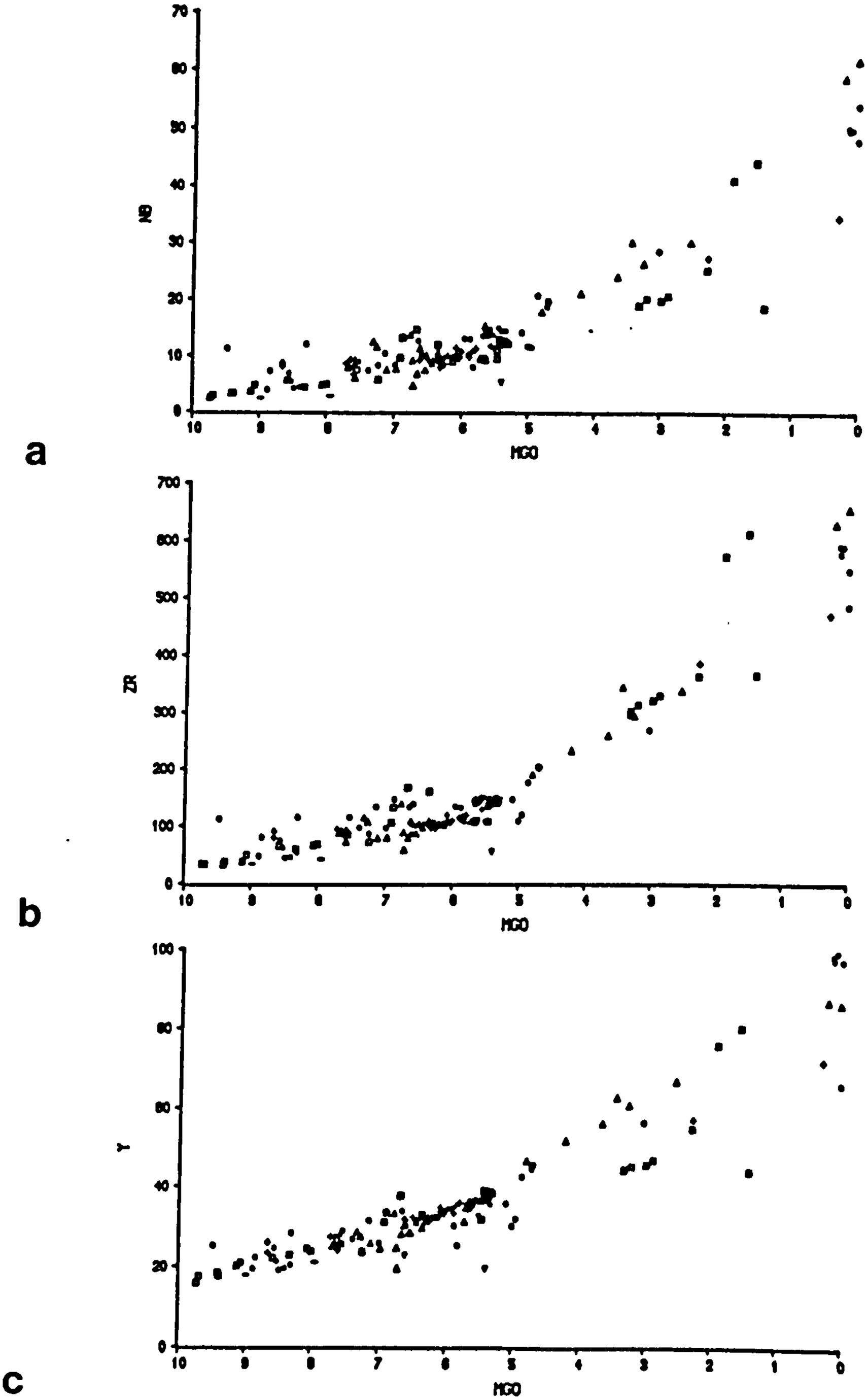


Fig. 5.4 (a) Nb *vs* MgO; for details see Fig. 5.1 (a)
(b) Zr *vs* MgO; for details see Fig. 5.1 (a)
(c) Y *vs* MgO; for details see Fig. 5.1 (a)

a

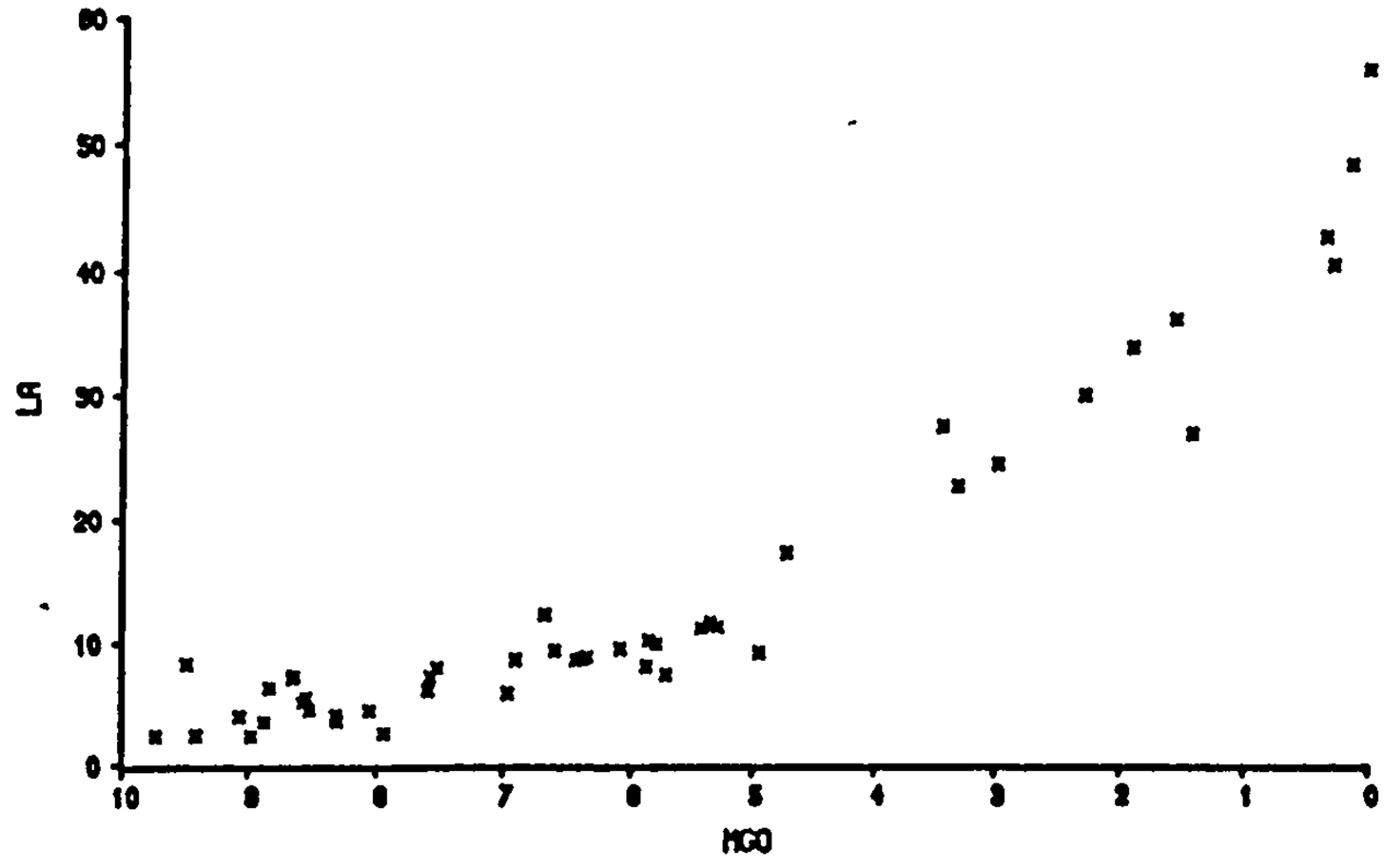


b

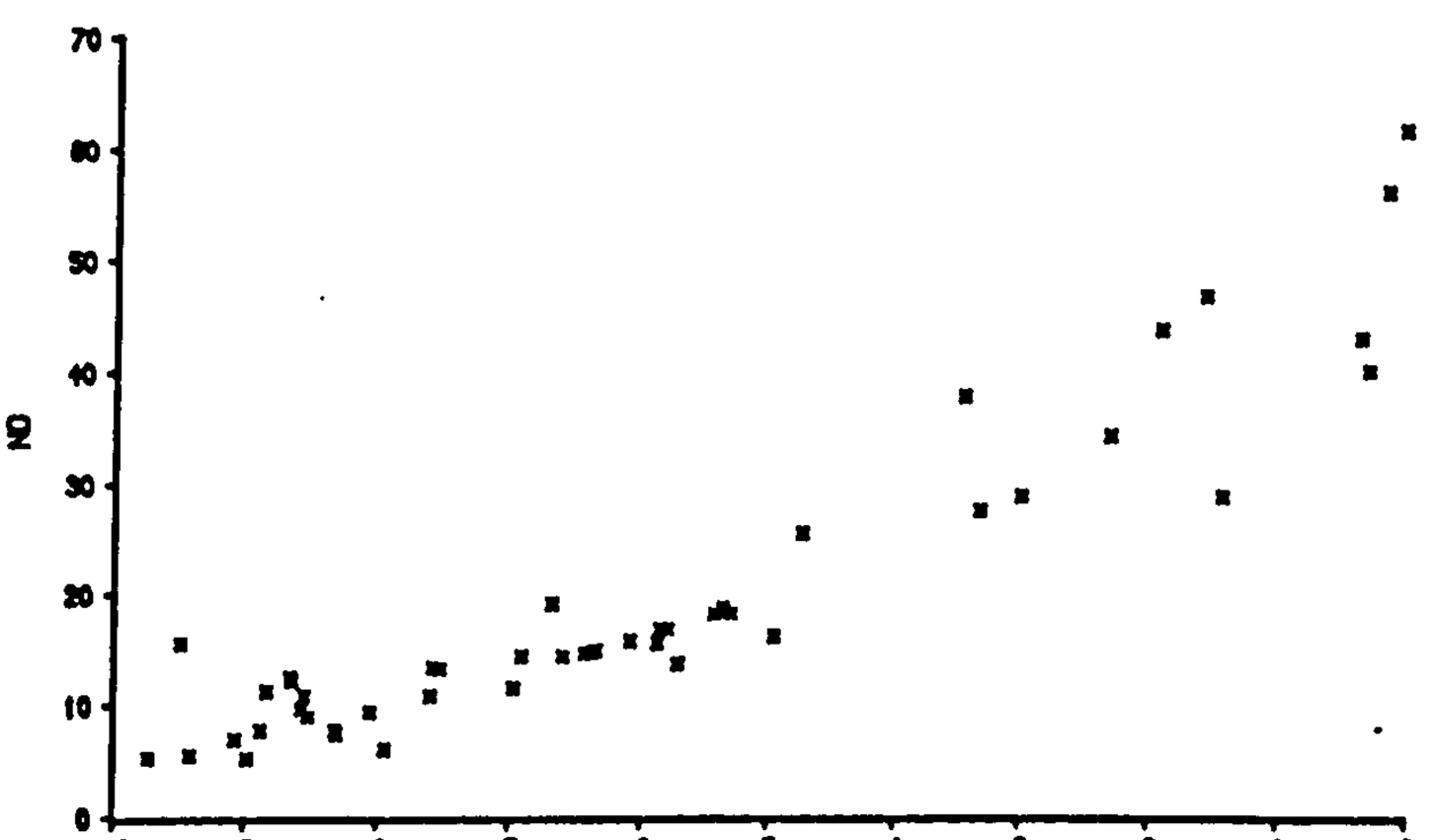


C

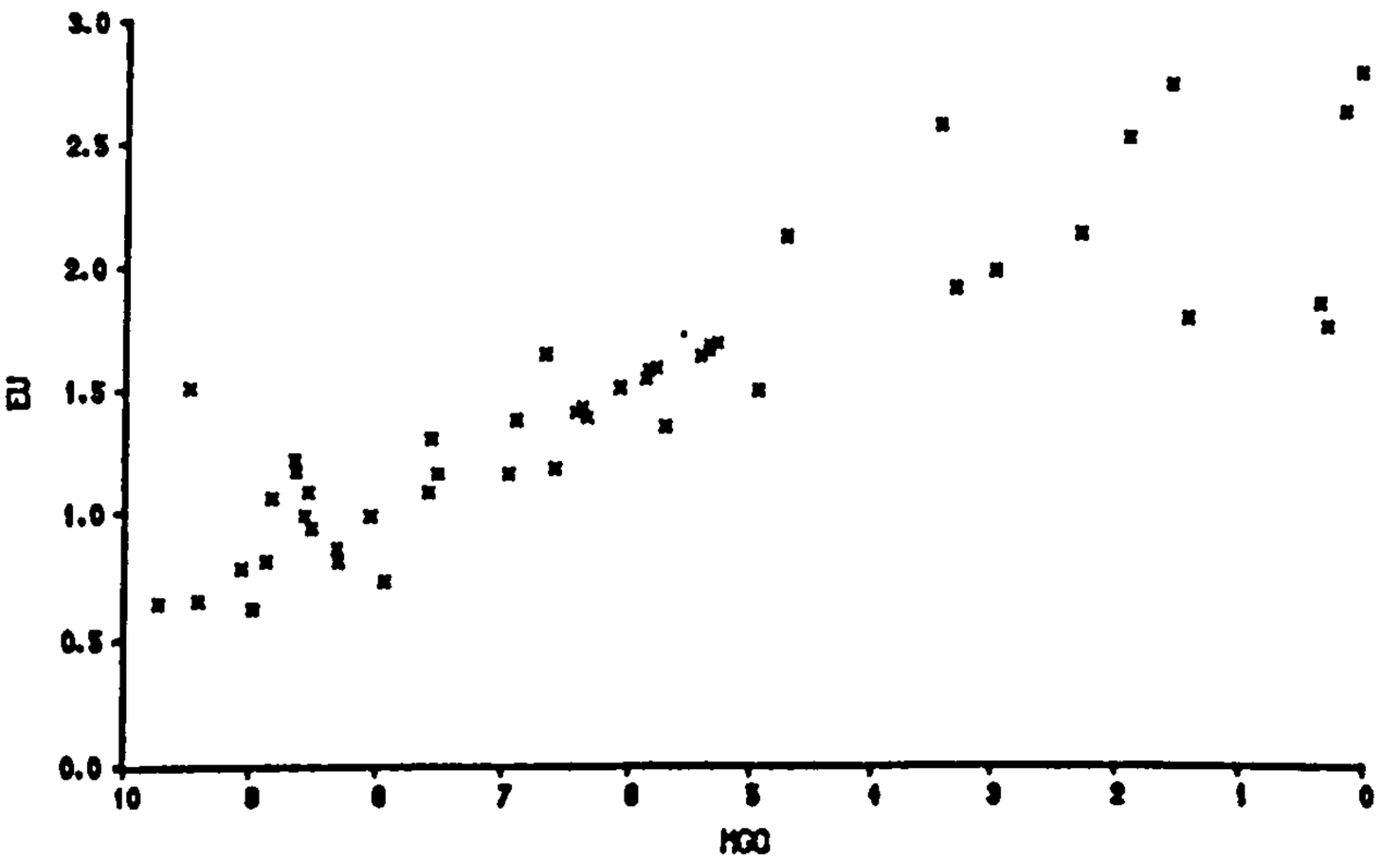


Fig. 5.5 (a) La (ppm) *vs* MgO (wt%); for selected Krafla samples.
(b) Nd *vs* MgO; for details see Fig. 5.5(a)
(c) Eu *vs* MgO; for details see Fig. 5.5(a)

a

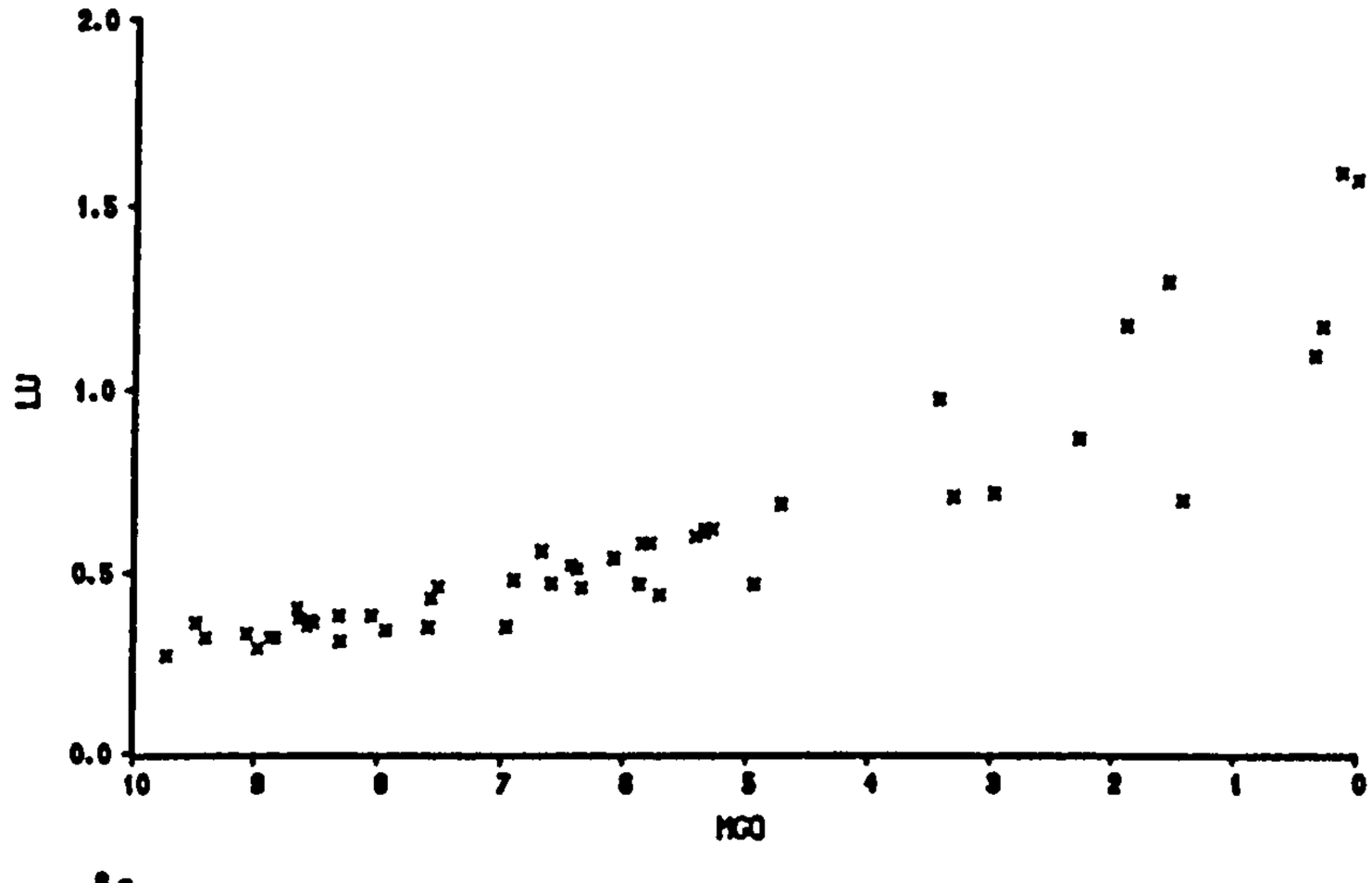


b

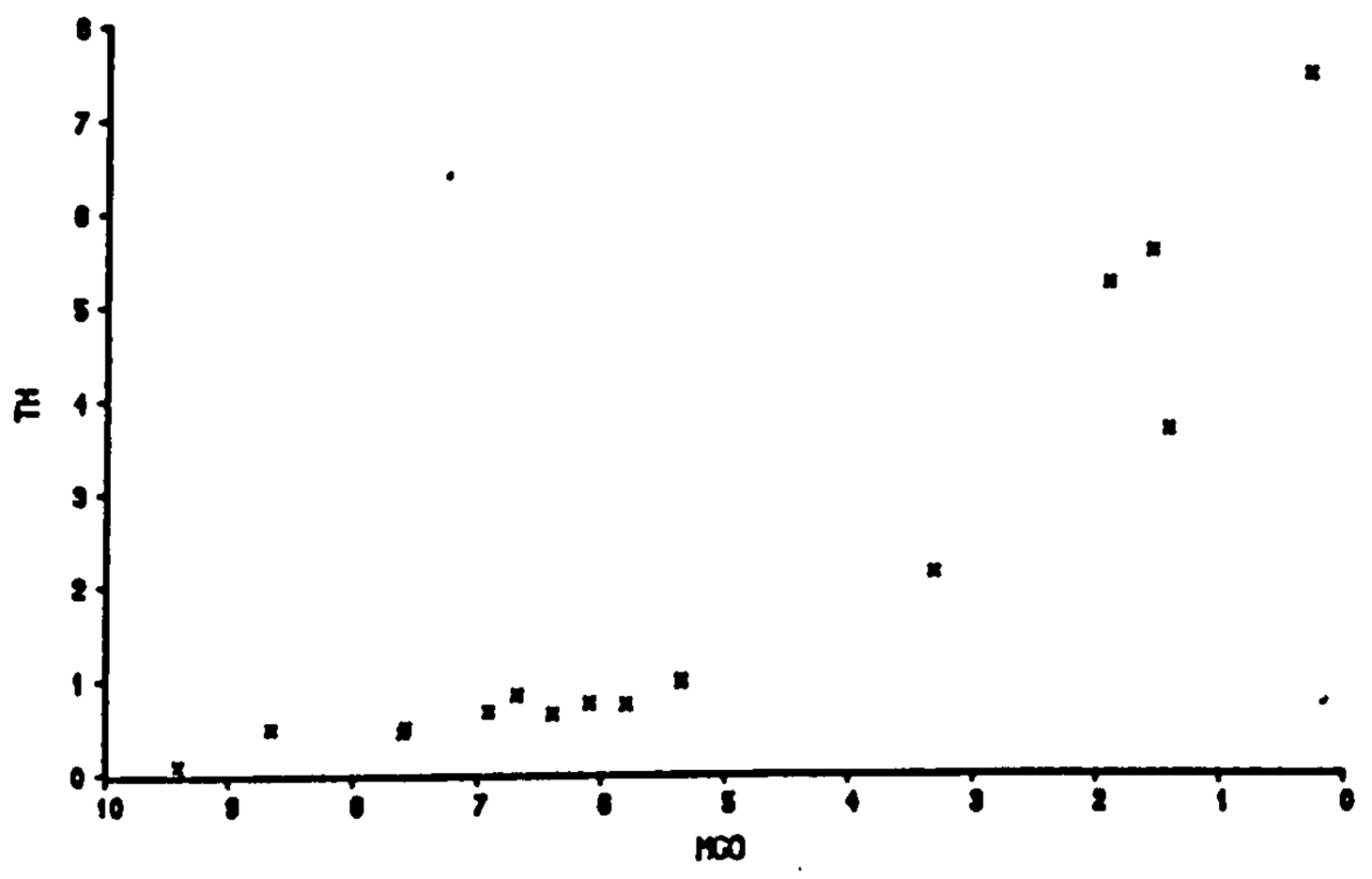


C

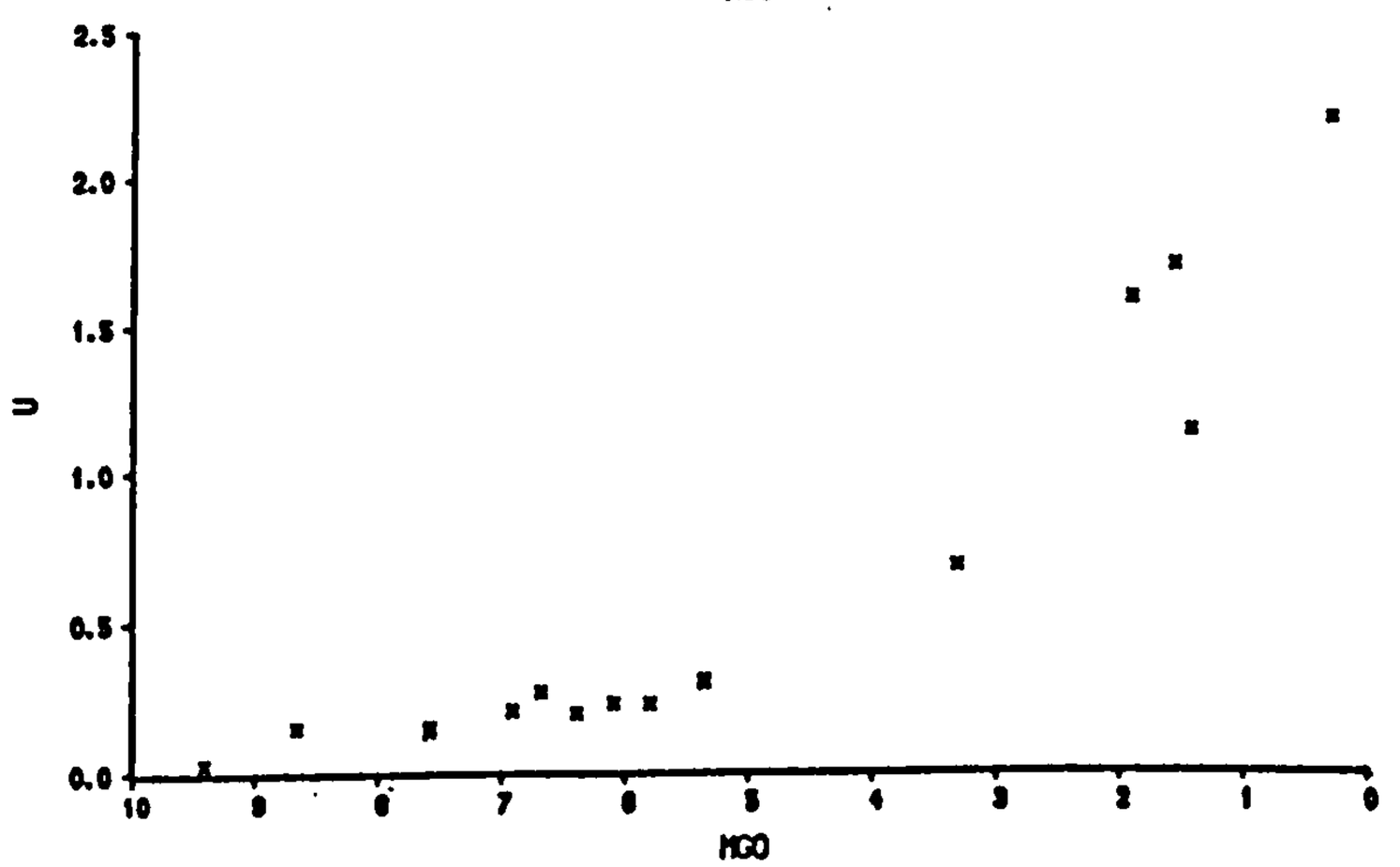


Fig. 5.6 (a) Lu *vs* MgO; for details see Fig. 5.5(a)
(b) Th *vs* MgO; for details see Fig. 5.5(a)
(c) U *vs* MgO; for details see Fig. 5.5(a)

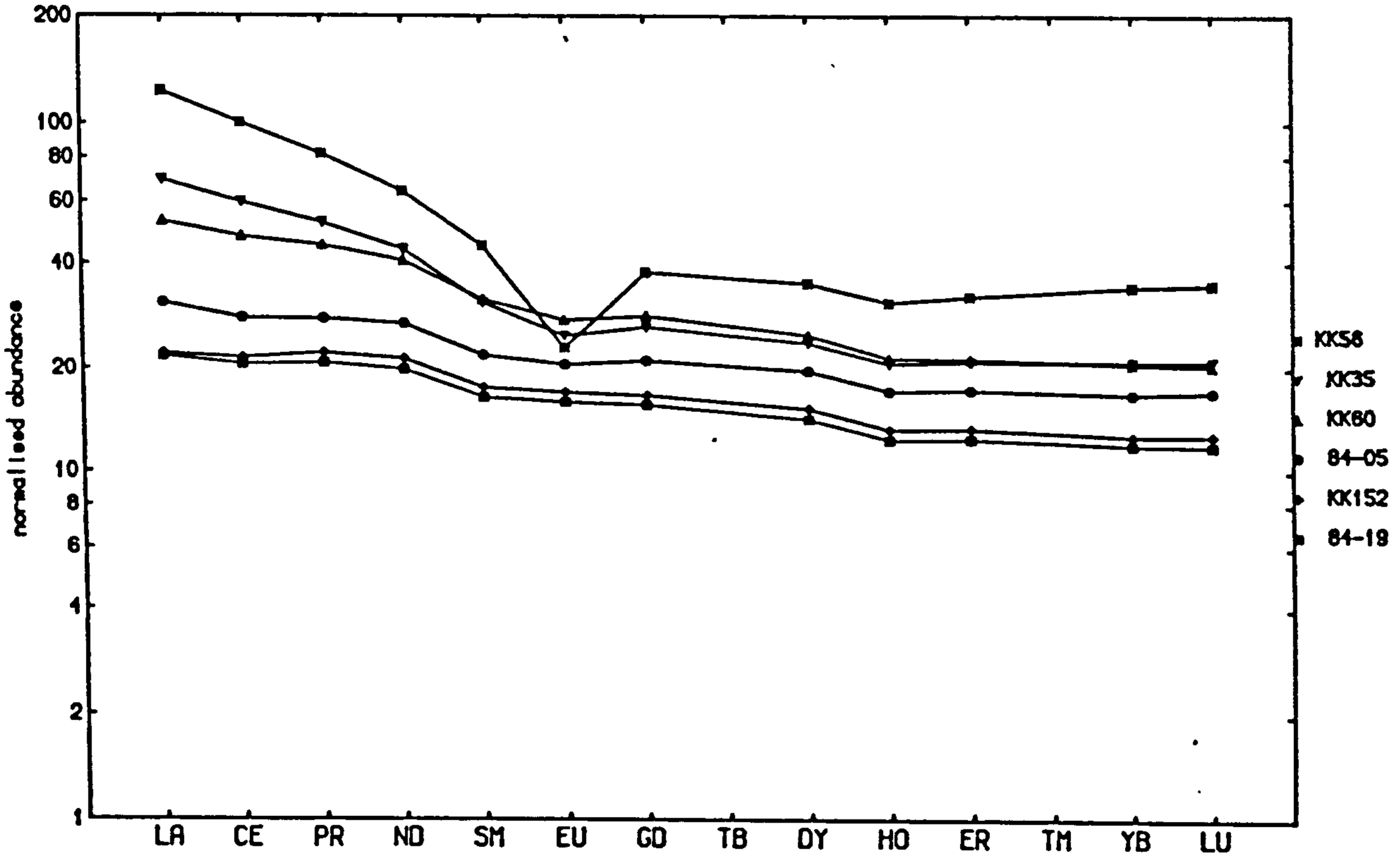


Fig. 5.7 REE variation diagram (chondrite normalised, after Nakamura 1974; modified according to J.N. Walsh pers. comm. 1989) for selected Krafla samples containing a range of different MgO contents (84-19, 8.66 wt% MgO; KK152, 7.58 wt% MgO; 84-05, 5.86 wt% MgO; KK60, 4.73 wt% MgO; KK35, 3.32 wt% MgO; KK56, 0.31 wt% MgO).

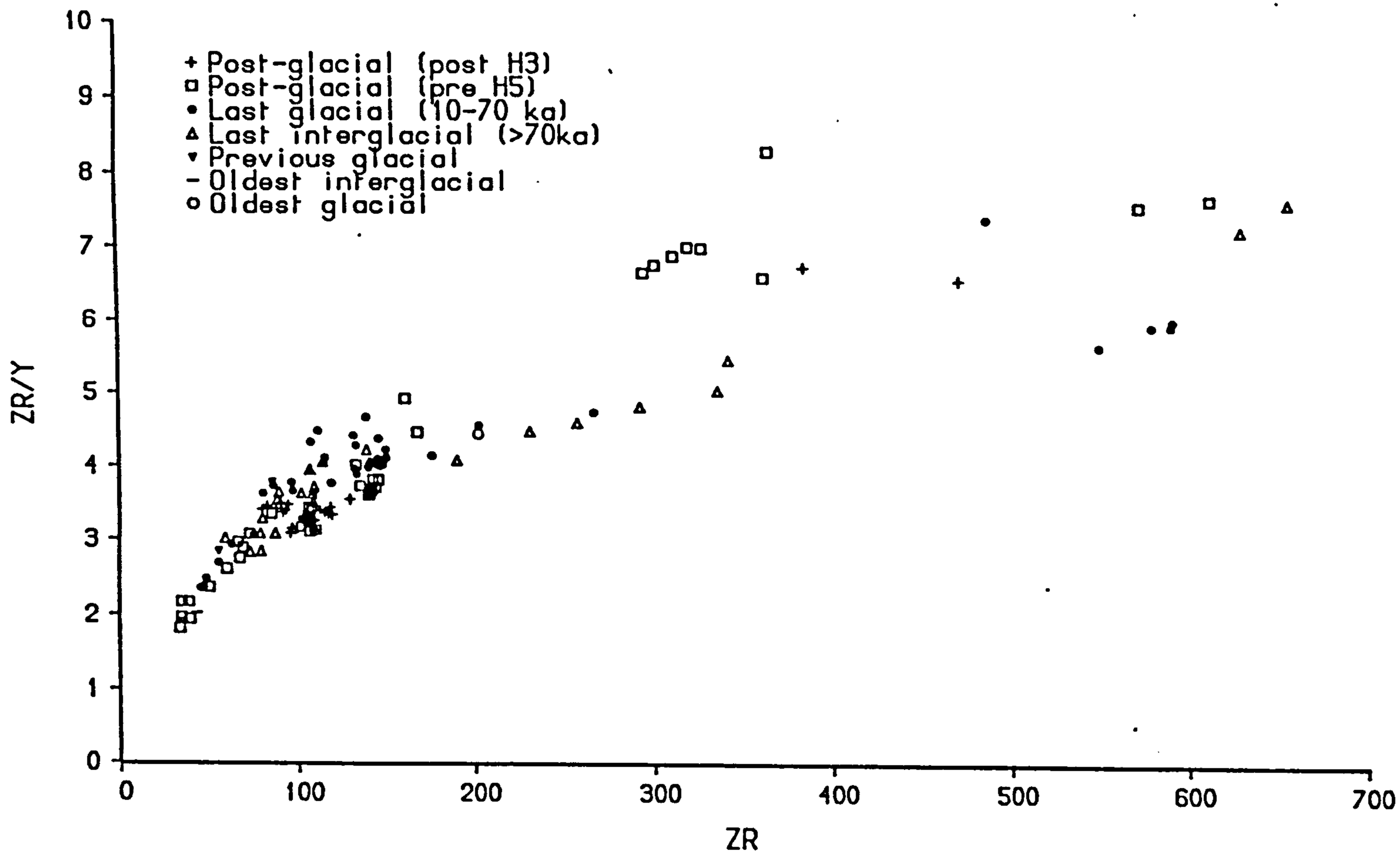


**Fig. 5.8** **Zr/Y *vs* Zr (ppm) plotted according to age (see key).**

older samples. There is little sign of obvious variation in trace-element concentration with time. The samples from the post-H3 period (the last 3000 years), however, form a coherent group with less scatter than for the other time periods (especially for the incompatible trace elements). This is confirmed in Fig. 5.8, where Zr/Y is plotted against Zr (cf. $K_2O$ *vs* MgO in Fig. 4.11b). This plot shows that over the last 3000 years the Zr/Y ratios of the basalts are reasonably constant, when compared with the total range in Zr/Y ratios for all the Krafla basalts. Whatever process produces the range of Zr/Y ratios evidently has had an approximately constant effect over this 3000 year interval. As the Zr/Y ratio in the basalts appears to be largely a function of the partial melting processes in the mantle beneath NE Iceland (see below), samples from the last 3000 years probably represent the product of constant melting conditions over this time interval (or the same batch of magma from a subcrustal magma reservoir). In the older time interval (pre-H5, 7-10 ka) there is no such uniformity of Zr/Y ratios.

### 5.3.3 Discussion on the role of fractional crystallisation

The trace-element variation diagrams described above are qualitatively consistent with the fractional crystallisation hypothesis set out in Chapters 3 and 4 (cf. Wood *et al.* 1979 for the whole of Iceland). There are, however, some points concerning the trace element data which appear to be inconsistent with differentiation through only fractional crystallisation.

Firstly, there is considerable scatter in most diagrams showing the variation of trace-element concentrations with MgO. Most of this variation is unlikely to be caused by phenocryst accumulation, especially for the incompatible trace elements (an obvious exception to this statement concerns plagioclase and is discussed in section 5.3.1). Secondly for any given MgO content, the Krafla rocks show highly variable ratios of more incompatible to less incompatible trace elements (e.g. see Fig. 5.10).

Various processes have been suggested to explain the scatter in the variation diagrams and the variable trace element ratios. These processes are listed below, in the order in which they are discussed:

**(a) Closed-system fractional crystallisation.**

**(b) *In situ* crystallisation.**

**(c) Crustal assimilation (or crustal melting).**

**(d) Magma mixing (i.e. open system fractionation in a periodically replenished magma chamber(s)).**
**(e) Mantle partial melting.**

Processes (a), (b) and (c) are discussed in the remainder of this section but (d) and (e) are discussed below in sections 5.4 and 5.5 respectively. Melting processes are also discussed in Chapter 6.

**(a) Closed-system fractional crystallisation**

Given the relevant $K_D$ values for the analysed trace elements, it is possible to test the fractional crystallisation hypothesis proposed in Chapters 3 and 4 (modelling restricted here to the closed-system case). At the present time, many partition coefficient data are poorly constrained and all data used here are taken from the literature (e.g. from the compilation by Henderson, 1982). Examples of values of $K_D$ used to model ol, plag, cpx crystallisation in the basalts are given in Table 5.1.

Two samples from the September 1984 Krafla eruption are chosen to test the fractional crystallisation hypothesis (84-19 and 84-05). Major element modelling, similar to that shown in Table 4.1, reveals that sample 84-05 can be produced from 84-19 by about 40% fractional crystallisation of an average assemblage of 22% ol, 51% plag and 27% cpx. Trace element modelling is carried out (Table 5.1) using these crystallisation proportions for selected REE as representative elements with sufficient partition coefficient data (references given in Table 5.1). The concentration of $K_2O$ is also modelled, since it appears to be one of the most incompatible elements present in basalts. The maximum and minimum concentrations of these elements obtained after 40% fractional crystallisation of sample 84-19 are calculated using a range of acceptable $K_D$ values. Apart from La, whose $K_D$ values are more poorly constrained, the results show that the changes in REE (and $K_2O$) concentrations appear to be consistent with magmatic evolution by closed-system fractional crystallisation, within the relatively large limits set by uncertainty in $K_D$ values. Errors quoted for the calculated concentrations reflect only the approximate initial analytical errors on the trace-element concentrations, scaled up to allow for fractional crystallisation. The real uncertainty in the modelling is much more likely to arise from uncertainty in the appropriate $K_D$ values.

Trace-element behaviour consistent with closed-system fractional crystallisation is not, however, always found. An example is shown in Table 5.2, where trace-element concentrations from KRA118 (an evolved basalt) and KK56 (a rhyolite) are compared. Again these samples are taken from the same eruptive cycle

| Element/Oxide | Olivine | Plagioclase | Clinopyroxene | D | +Conc.$_{Res}$ | $Conc. |
|---|---|---|---|---|---|---|
| La | 0.009*<br>0.011 | 0.14<br>0.14 | 0.08<br>0.22 | 0.095<br>0.153 | 11.2<br>10.9 | 10.2 |
| Nd | 0.007<br>0.010 | 0.02<br>0.20 | 0.32<br>1.3 | 0.098<br>0.455 | 19.7<br>16.4 | 16.9 |
| Sm | 0.003<br>0.015 | 0.02<br>0.20 | 0.43<br>1.8 | 0.225<br>0.975 | 4.9<br>3.4 | 4.4 |
| Dy | 0.009<br>0.014 | 0.01<br>0.20 | 0.56<br>1.46 | 0.158<br>0.499 | 7.4<br>6.2 | 6.7 |
| Er | 0.009<br>0.017 | 0.02<br>0.24 | 0.53<br>1.3 | 0.155<br>0.477 | 4.3<br>3.6 | 3.9 |
| $K_2O$ | | | | 0.001* | 0.32 | 0.33 |

Data from Gast 1968, Irving 1978, Henderson 1982, and * estimated.

+ = Resultant concentration is based on 40% fractional crystallisation of an assemblage of 22% ol, 51% plag and 27% cpx from sample 84-19, using the above $K_D$ values.
$ = Actual concentration in sample 84-05, which least-squares modelling suggests is derived from 40% fractional crystallisation of sample 84-19.

**Table 5.1** Modelling fractional crystallisation using selected trace elements (samples 84-19 and 84-05).

| Sample | MgO wt% | Rb | Th | U | Zr | Nb | Y | La | Sm | Lu | Sr | Ni | Cr |
|---|---|---|---|---|---|---|---|---|---|---|---|---|---|
| KRA118 | 6.09 | 6.1 | 0.74 | 0.23 | 118 | 11 | 34 | 9.49 | 4.23 | 0.54 | 152 | 68 | 145 |
| KK56 | 0.31 | 72 | 7.48 | 2.20 | 472 | 35 | 72 | 40.5 | 9.1 | 1.18 | 90 | 4.8 | 1.0 |
| E.F. | | 11.8 | 10.1 | 9.7 | 4.0 | 3.1 | 2.1 | 4.3 | 2.1 | 2.2 | | | |

E.F. (enrichment factor) is the ratio of the trace element concentration in the rhyolite divided by the basalt.

**Table 5.2** A comparison of trace element concentrations from samples KRA118 (evolved basalt) and KK56 (rhyolite) from the 1724-29 eruption.

in an attempt to minimise other sources of variation. Major-element modelling, similar to that performed using compositions KK08 and KK03 in Table 4.1, suggests that about 80% fractional crystallisation of KRA118 could produce a residual liquid equivalent to KK56. However, the concentrations of Rb, Th and U are all enriched more than can be explained by closed-system fractional crystallisation. These elements show an ~10-fold variation in concentration, compared with a 4-5 fold variation for other incompatible trace elements such as La, Nb and Zr (which are in fact consistent with 80% fractional crystallisation). Such excess concentrations of the most incompatible trace elements may be explained by open system fractionation processes (see section 5.4 where, however, this is judged to be of limited importance), by *in situ* crystallisation, or by assimilation of a partial melt of altered crust.

**(a) *In situ* crystallisation**

Langmuir (1989) proposed a model to explain the major and trace element characteristics of magmas which have undergone chemical fractionation between a magma reservoir and a cumulate pile. In these circumstances the concentrations of the more incompatible trace elements in the trapped liquid might be expected to be increased compared with the concentrations of the more compatible elements. Under appropriate circumstances a proportion of the trapped liquid may be returned to the main magma body, increasing the concentrations of the most incompatible elements over and above that expected by closed-system fractional crystallisation. This process is probably untestable for most volcanic suites, without information on cumulate processes, especially given the lack of data on the fractionation factors between a crystal mush and liquid during the proposed *in situ* crystallisation process.

**(b) Crustal assimilation**

Crustal assimilation can lead to enhanced concentrations of the most incompatible trace elements, providing the assimilant contains high enough concentrations of these elements. The wall-rocks of the magma reservoir may include evolved rocks such as rhyolite. Rhyolite contains high concentrations of incompatible trace elements, including both those traditionally regarded as being mobile (e.g. Rb) and relatively immobile during alteration (e.g. Th). Bulk assimilation of such material can lead to excess concentrations of the most incompatible trace elements. Alternatively, assimilation of a partial melt derived from basaltic wall-rock can lead to similar excess concentrations of the most incompatible trace elements, providing the degree of partial melting is sufficiently low and the wall rocks are not themselves

too depleted in incompatible trace elements (i.e. cumulates are unsuitable contaminants).

The importance of the assimilation of highly evolved rocks (e.g. rhyolites, granophyres) by basaltic magma at the margins of the magma reservoir(s) has been suggested for Askja by Macdonald *et al.* (1987) (cf. Sigurdsson, 1977). In general the proportion of such rock types available for assimilation in central volcanoes like Krafla is small, and the walls are likely to be dominated by evolved basalts. Therefore, it would seem highly unlikely that the enrichment in the most incompatible trace elements in the differentiated lavas could be caused by assimilation of a pre-existing Rb-, Th-, U-enriched assimilant. This suggests that of the possibilities set out above, partial melting of on average basaltic crust is the most likely explanation for the excess concentrations of Rb, Th and U.

To produce increased concentrations of Rb, Th and U over and above those of the other incompatible trace elements by assimilation demands that a small degree of melting occurs during the assimilation process. For example, 10% partial melting of a basalt made of a simple ol+plag+cpx+Fe-Ti oxides assemblage using D=0.095 for La and D=0.001 for Th generates a melt with a Th/La ratio about twice as high as the parent basalt. By the late-stages of differentiation, the addition of a relatively large amount of the assimilant may lead to an increased Th/La ratio in the residual liquid. Of course, in practice, the solution to such a problem is probably much more complex because the partition coefficients for altered basalt will be different from those of a simple assemblage of ol, plag, cpx and FeTi oxides and may involve Th, La partitioning between a melt and hydrated minerals such as amphibole. It appears from preliminary experimental work by M. Fisk (pers. comm., 1990) that silicic partial melts generated during partial melting experiments of hydrated, altered DSDP samples tend to form along veins originally formed during sea-floor alteration. This suggests that a simple treatment of the melting process may not be realistic. In similar experimental work, Spulber & Rutherford (1983) produced a rhyolite by 10% partial melting of an evolved basalt at 1 kbar $P_{H2O}$. The concentration of $K_2O$ in experimental rhyolite was found to be very similar to $K_2O$ concentrations in rhyolites from the axial-rift zones of Iceland, suggesting that rhyolites might be derived by partial melting of the hydrothermally-altered crust, rather than by closed-system fractional crystallisation of basaltic magma. However, recently Thy *et al.*, (1990) have pointed out that the concentrations of $FeO^*$ and $Al_2O_3$ in partial melts of basalt, in contrast to $K_2O$ are highly sensitive to the value of $P_{H2O}$ in the experiment. In particular, Thy *et al.* (1990) show that the concentrations of $FeO^*$ and $Al_2O_3$ in axial-rift rhyolites

appear to be consistent with the partial melting of basalts with $P_{Total}$ = 1-3 kbar and $P_{H2O}$ < 1 kbar (see also Chapter 7).

## 5.4 Magma mixing (open system fractionation processes)

Magma mixing has often been invoked to explain scatter in variation diagrams or triangular plots (see section 4.7; e.g. Dungan & Rhodes, 1978; Walker *et al.*, 1979; Defant & Neilsen, 1990) and the cyclic nature of modal layering in intrusions (e.g. Wilson, 1982). Without evidence for the exact nature of the magmas being mixed (cf. Macdonald *et al.*, 1987), it is difficult to quantify the chemical effects of mixing. The nature of any phenocrysts may, however, provide valuable evidence as to the nature of the different magmas involved. Unfortunately does not indicate the proportions of the different liquid components concerned in the mixing. Sparks & Marshall (1986) discussed the fluid dynamics of the mixing of tholeiitic liquids and the effects of mixing on the range of chemical compositions observed in the erupted liquids. The main variables are the temperatures and the viscosities of the magmas. Silicic melts, whether formed by partial melting of the wall-rock, or by extensive fractional crystallisation, are much cooler (200-400°C) and more viscous than basaltic magmas. This means that only small proportions of silicic magma can be added to relatively primitive magmas (e.g. with a temperature of 1200°C) without the viscosity of the resultant magma increasing so much as to prevent eruption. More differentiated basaltic magmas are cooler and more viscous than more primitive ones, and can be mixed with greater proportions of silicic melt, whilst still forming a liquid mixture. Sparks & Marshall (1986) showed that the most differentiated basaltic and silicic magmas can mix in any proportion and still generate a liquid. The overall effects are such that certain proportions of tholeiitic magmas are unlikely to form liquid mixtures, shown by what Sparks & Marshall (1986) call the "mixing prohibited" regions of chemical variation diagrams. This is best shown in variation diagrams of type (b) above, e.g. V, Sc, Cu or $TiO_2$ *vs* MgO. $TiO_2$ *vs* MgO is used by the above authors (Fig. 5.9), who show, for example, that a 50:50 mixture of primitive basalt (~9 wt% MgO) and rhyolite lies in the "mixing prohibited" region. As shown in Fig. 5.1c (for V *vs* MgO) and Fig. 4.5a ($TiO_2$ *vs* MgO) the Krafla data appear to conform with such a mixing model, prohibiting the mixing of certain proportions of different magma types. The samples cutting across the ∧-shape (seen in Figs. 4.5a and 5.1c) are those with large modal abundances of plagioclase xenocrysts and do not reflect mixed magmas. The model, however, assumes that silicic and mafic magmas are equally available to form mixtures. However, the absence of large quantities of silicic melt in

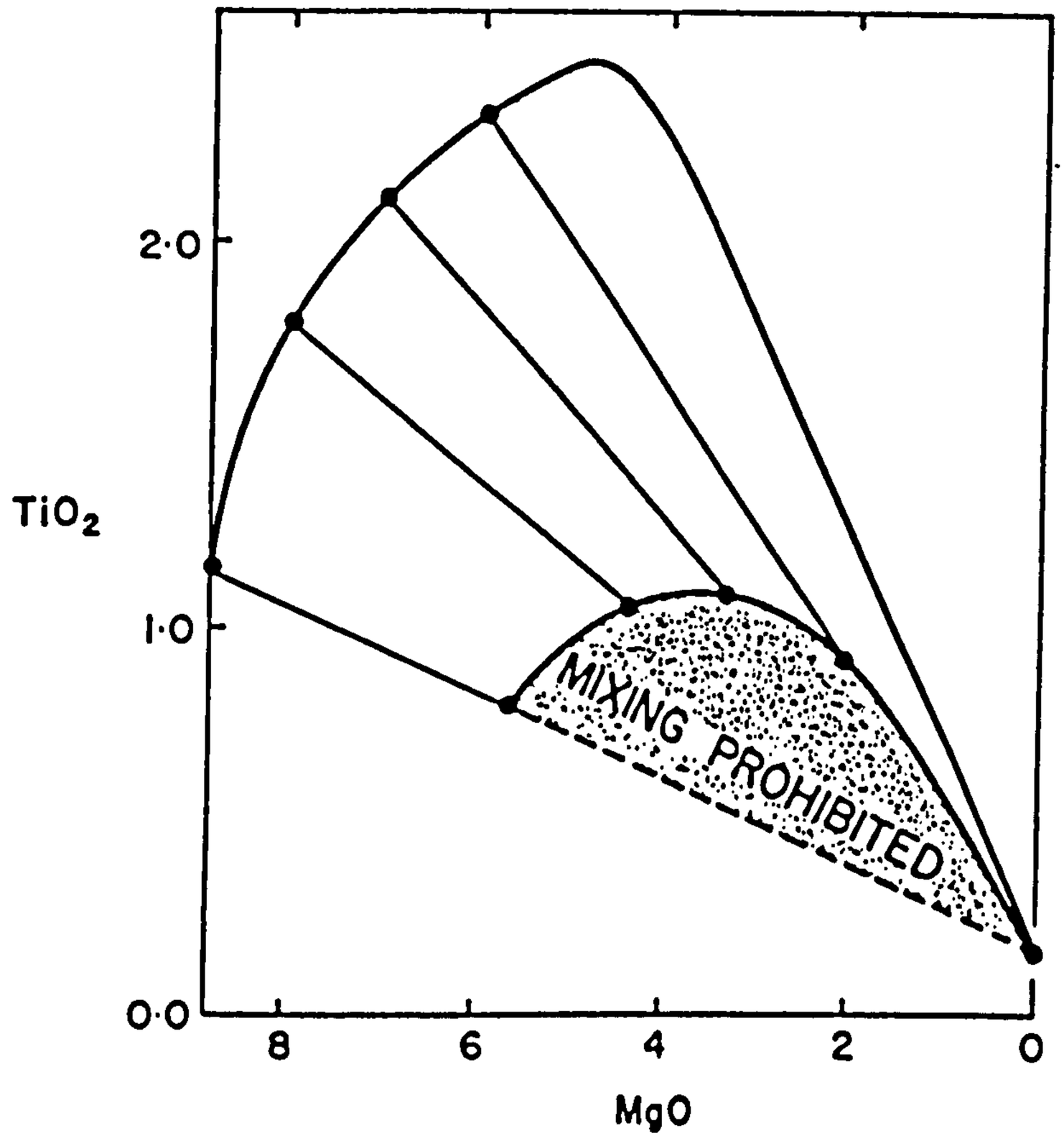


**Fig. 5.9** Schematic plot of $TiO_2$ and MgO (but could represent V *vs* MgO), showing region in which magma mixing is prohibited. The uppermost curve defines the tholeiitic liquid line of descent. Mixing lines from mafic magmas along this curve are constructed with the silicic end member. The mixture which contains the maximum proportion of silicic magma and which still remains a liquid is plotted along the tie line. A curve joining the locus of these compositions bounds the region which magma mixing is prohibited (Diagram taken from Fig. 13, Sparks & Marshall 1986).

the Krafla system decreases the chance of producing mixtures with high proportions of the silicic end-member (cf. some other Icelandic central volcanoes, e.g. Torfajökull, McGarvie, 1984; D. McGarvie pers. comm., 1989). In addition, if the magma reservoir is zoned due to differences in density (Sparks *et al.*, 1980), then the different magmas may be physically isolated and therefore unable to mix. This may mean that less dense silicic magma at the roof of the chamber may be unable to mix with the most primitive basaltic magmas being intruded into the reservoir during replenishment events (cf. Huppert & Sparks, 1980; Sparks *et al.*, 1984) but able to mix with differentiated basalts already in the reservoir which lie ponded immediately beneath the silicic magmas (Campbell & Turner, 1987; S.Day pers. comm., 1990).

The phenomenon of magma mixing has also been addressed from a geochemical point of view. O'Hara (1977) and O'Hara & Mathews (1981) developed a model (section 4.7) for open system fractionation in a periodically replenished magma chamber (PRMC). Given certain mixing conditions (e.g. numbers of mixing cycles, proportions of magma input/output/crystallised), their model is capable of enhancing the concentrations of the most incompatible trace elements and increasing the ratios of more incompatible to less incompatible trace elements so, effectively "decoupling" the incompatible trace elements from the major elements.

At first sight such a model would seem to be particularly appropriate to the Krafla volcanic system because recent eruptions have shown that long-lived magma PRMCs are likely to exist in or beneath the Icelandic crust (Björnsson, 1985; Tryggvason, 1986) and that repeated episodes of magma mixing and quiescence take place in such magma reservoirs. However, it is uncertain precisely what changes in magma composition can be caused by magma mixing (especially for the most incompatible trace elements). The model of O'Hara & Mathews (1981) predicts that the major-element compositions of the magma in the PRMC will readily reach a steady-state condition (i.e. the composition of the magma is significantly changed by a small number of mixing-crystallisation cycles). This is consistent with the above discussion on the fluid dynamics of mixing, which suggests that a wide variety of major element compositions can be formed by magma mixing, even if the absolute range in compositions is in fact a result of fractional crystallisation. In contrast to the compatible major elements, O'Hara & Mathews's (1981) model suggests that trace element ratios (e.g. Zr/Y or La/Sm) are only altered by a large number of mixing-crystallisation cycles (e.g. they may reach a steady-state condition in, say, 1000-10000 cycles). The recent Krafla eruptions consisted of some 20 mixing events in a magma reservoir at a depth of about 3 km (see Chapter 2) and such events appear to have occurred approximately every 500 years for at least the last 3000 years. Hence,

over the past 150,000 years there may have been about 6000 individual mixing events. According to the model this is a large enough number of events to fractionate Zr from Y, or La from Sm. However, the record of Krafla compositions through the volcano's history suggests that there is no observable change in the degree of enrichment in the more incompatible trace elements with time (e.g. see Fig. 5.8 for Zr/Y ratios plotted against Zr concentrations), although change would be expected from O'Hara & Mathews' model.

Galer & O'Nions (1986) present a strong argument against the O'Hara & Mathews model, based on the observed excess of ($^{230}$Th) in most MORBs (see Chapter 7 for more details of the generation of excess ($^{230}$Th)). The former authors suggest that for excess ($^{230}$Th) to exist in any MORB, including Icelandic rocks, then the average magma reservoir residence time for Th must be no more than $10^4$ to $10^5$ years (as the half-life of $^{230}$Th is 75.2 ka). Yet in the O'Hara & Mathews model the average time for Th to reach a steady state, because of its extremely low value of D, is greater than $5x10^4$ cycles or equivalent to more than 1 Ma in the life of a central volcano.

In conclusion, it would appear that magma mixing processes are not capable of significantly driving the fractionation of trace elements relative to one another. Hence, some other process must be sought to explain the range in trace-element concentrations such as shown by the differences in La/Sm or Zr/Y ratios (see section 5.5). The major-element compositions appear, however, to be much more easily altered by mixing processes, although certain mixtures appear unlikely on fluid dynamic grounds. This is a conclusion consistent with the geophysical evidence from the recent eruptions (Chapter 2) and the range of phenocryst compositions seen in the Krafla samples (Chapter 3).

## 5.5 Trace-element evidence for mantle processes

Partial melting processes are best inferred when the effects of crustal processes are minimal. Minimising these effects can be achieved by choosing only the least-differentiated basaltic samples in a suite (e.g. Langmuir et al., 1977), or by attempting to correct for the effects of fractional crystallisation to a common MgO content (e.g. Klein & Langmuir, 1987). The latter approach is however likely to be unreliable when processes apart from fractional crystallisation (±magma mixing) may affect the differentiation sequence (e.g. crustal assimilation). The former method also has a disadvantage, in that the Krafla volcanic system has produced dominantly evolved basalts (see Fig. 4.21) and the number of relatively primitive samples is quite

small. If the samples with >8 wt% MgO are selected from the data base then it appears from that the effects of clinopyroxene fractionation can largely be ignored (see below and Chapter 6), leaving only olivine and plagioclase as important fractionating phases. Such a group of high-MgO samples are plotted in Fig. 5.10, showing a plot of Zr/Y *vs* Zr. It can be seen that the most primitive samples tend to fall to the left-hand (or low Zr) side of the array of the Krafla data, ranging considerably in both Zr concentration and Zr/Y ratio. The samples with higher Zr concentrations generally have the lower MgO contents, which would appear to be the result of fractional crystallisation. The samples containing more than 8 wt% MgO vary in Zr concentration by a factor of about 4; Zr/Y ratios vary by a factor of over 2.5. Such variation would require an inconceivably large amount of clinopyroxene fractional crystallisation (over 75%; cf. discussion on "phantom clinopyroxene" crystallisation in section 4.7), and would be impossible to explain by olivine and/or plagioclase fractionation. This suggests that the variation may be a result of melting processes and/or source variation. The Sr and Nd isotope ratios, however, suggest little scope for altering source characteristics, (see Chapter 7), leaving only variation in mantle partial melting processes as a likely explanation for the differences in trace element ratios. In addition, the Zr/Y ratios of the most primitive samples correlate with their La/Sm ratios (see Fig. 5.11). Considerable variation in La/Sm ratios of MORB samples from an area with constant Sr and Nd-isotope ratios has been reported before from both plume and non-plume environments, e.g. from Iceland (O'Nions *et al.*, 1976; Wood *et al.*, 1979) and the mid-Atlantic (Langmuir *et al.*, 1977). Hence, as concluded above, such local variation in trace element ratios looks likely to result from partial melting processes rather than variation in source characteristics. A selection of models which may explain the variation in trace-element concentrations and ratios are examined below, ranging from fractional melting to equilibrium batch melting. Examination of the causes of the variation in major element composition (for samples with more than 8 wt% MgO) is left until Chapter 6 and discussed in the light of a quantitative model for melt generation (McKenzie & Bickle, 1988).

**(i) Batch melting** generates a given proportion of melt in one melting event, which is removed in one batch. This is one of the simplest types of melting model and all experimental studies produce melt in such a way. Experimental studies suggest that most tholeiites can be produced by between 8-30% batch melting of an appropriate mantle source (e.g. Bender *et al.*, 1978; Jaques & Green, 1980; references in Klein & Langmuir, 1987). As an example of the effects of batch melting, consider the REE, La

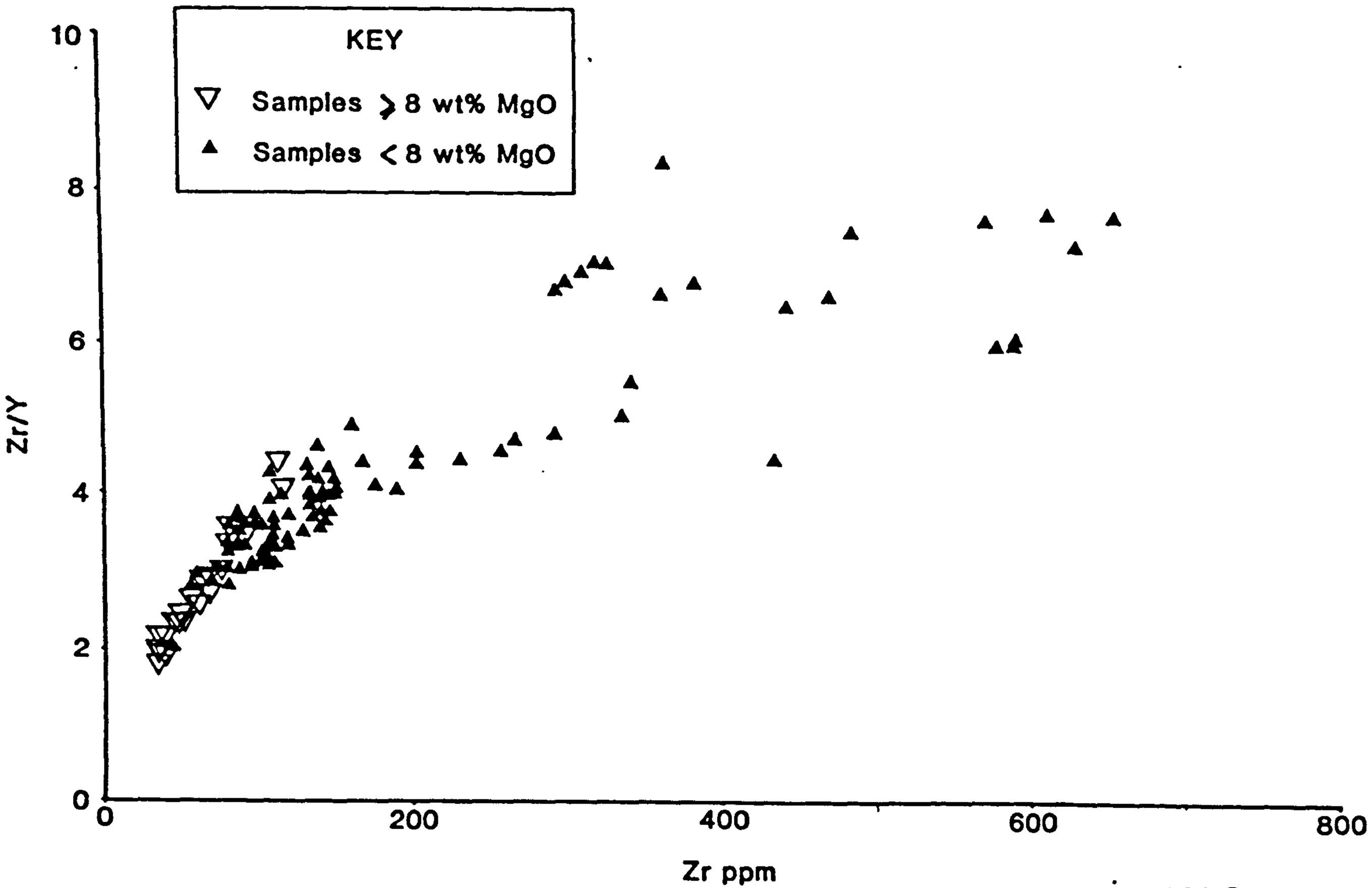


**Fig. 5.10** *Zr/Y vs Zr* (ppm) showing the samples containing at least 8 wt% MgO (open inverted triangles) and less than 8 wt% MgO (filled smaller triangles).

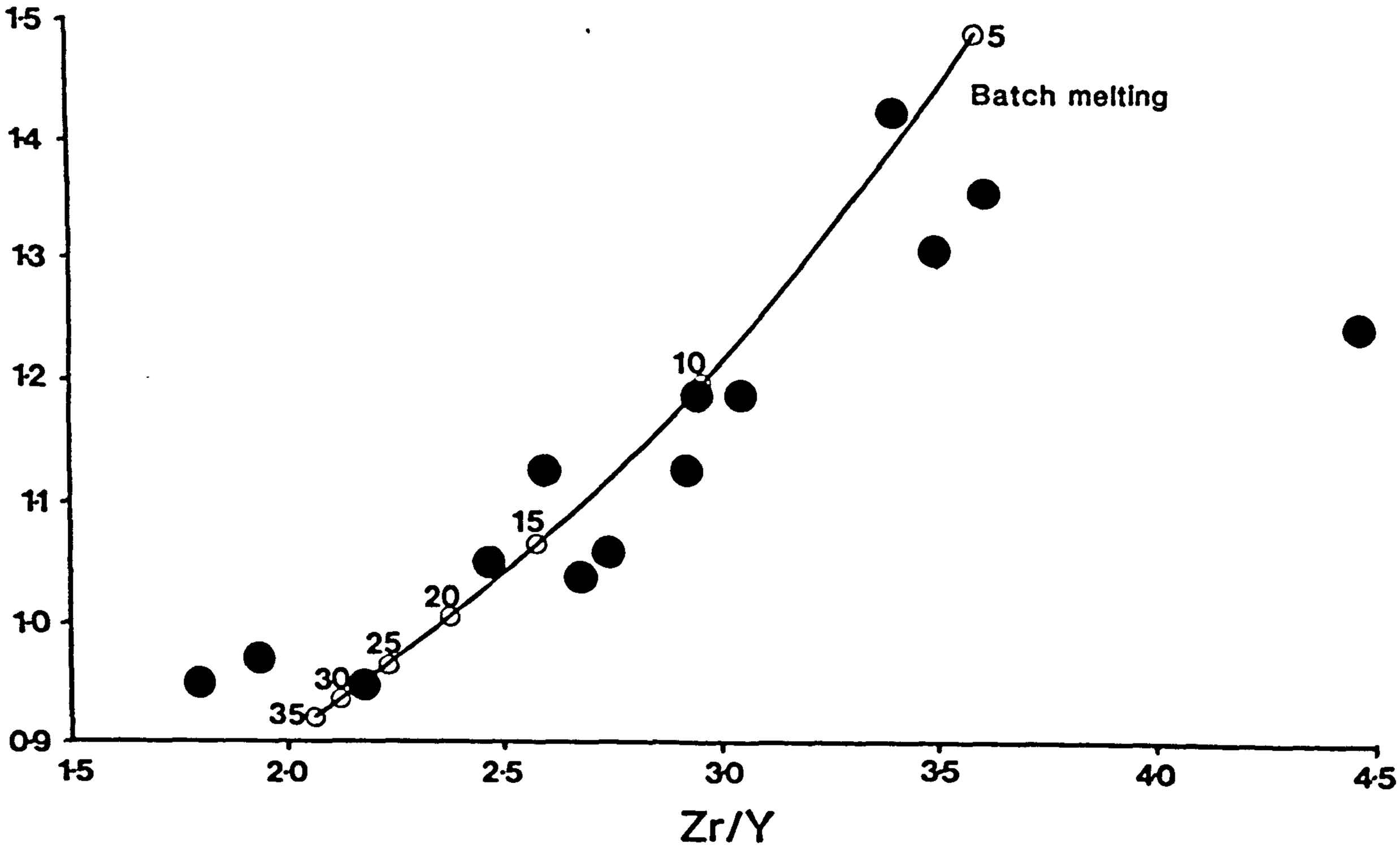


Fig. 5.11 (La/Sm) (chondrite-normalised as in Fig. 5.7) plotted against Zr/Y for samples containing at least 8 wt% MgO (see Fig. 5.10). The curve shown represents a batch melting model (% partial melting indicated from 5% to 35%; see Table 5.3 for details).

and Sm and the elements Zr and Y, although there are fewer data on partition coefficients for the latter elements. A simple batch melting model is presented in Table 5.3. The proportions of mantle phases entering the melt, and the proportions of mineral phases in the mantle source are modified from Wood (1981). Generating the range of $(La/Sm)_{(chondrite\ normalised)}$ values (0.95-1.45) seen in the Krafla basalts with MgO > 8 wt% (see Fig. 5.12) would require a range in the proportion of partial melt generated by batch melting from 0.05 to 0.35. Such extreme limits to the degree of partial melting are probably not acceptable, given the major-element compositions of the Krafla lavas/hyaloclastites (see Chapter 6). Even with this relatively wide range in the degree of melting, the absolute concentrations of La and Sm in the magmas vary too much to fit. Increased values of $K_D$ for Sm may be used to increase the range of values of (La/Sm) but only at the expense of keeping the concentrations of Sm too low to be useful. As several authors have pointed out (e.g. Langmuir *et al.*, 1977; Wood, 1981), batch melting models apparently fail to generate the range of required REE ratios and concentrations, when realistic parameters are used.

(ii) **Fractional or Rayleigh melting**, unlike batch melting involves instantaneous melt extraction. This mechanism therefore removes most of the incompatible trace elements in the first stages of melting, leaving the later formed melts with very low concentrations of all but the most compatible trace elements. Since this is not observed, pure fractional melting is probably unrealistic (e.g. Langmuir et al., 1977; Cox *et al.*, 1979).

(iii) **Incremental fractional melting** has been suggested (Cox *et al.*, 1979) as an alternative to pure fractional melting so as not to secure the removal of all the most incompatible trace elements in the first melt formed, and at the same time allow fractionation of the more incompatible from the less incompatible trace elements (e.g. La from Sm). The increment of melting, however, must be sufficiently small (e.g. 1-3%) in order to generate the range of trace element ratios seen in the Krafla data. In this case incremental melting gives rise to the same problem as pure fractional melting, namely that the mantle source has a much reduced incompatible trace element budget in the later stages of melting, which are needed to generate the major-element compositions of MORB.

(iv) **Dynamic melting** was proposed by Langmuir et al. (1977) as an alternative to the melting models discussed above. In this model the melt is produced in small increments; some of the melt is extracted leaving the remainder of the melt with the

| f | La ppm | Sm ppm | $(La/Sm)_n$ | Zr ppm | Y ppm | Zr/Y |
|---|---|---|---|---|---|---|
| 0.05 | 10.37 | 4.29 | 1.49 | 105.3 | 29.3 | 3.59 |
| 0.10 | 5.71 | 2.97 | 1.18 | 71.4 | 24.4 | 2.93 |
| 0.15 | 3.94 | 2.27 | 1.07 | 54.1 | 21.0 | 2.58 |
| 0.20 | 3.01 | 1.84 | 1.01 | 43.5 | 18.3 | 2.38 |
| 0.25 | 2.44 | 1.55 | 0.97 | 36.4 | 16.3 | 2.23 |
| 0.30 | 2.04 | 1.33 | 0.94 | 31.3 | 14.7 | 2.13 |
| 0.35 | 1.76 | 1.17 | 0.925 | 27.4 | 13.3 | 2.06 |

The batch melting model uses a mantle source of $Ol_{55}\ Cpx_{15}\ Opx_{25}\ Gt_5$, melting proportions of $Ol_{15}\ Cpx_{50}\ Opx_{25}\ Gt_{10}$ (adapted from Wood 1981) and values of D and P (in the batch melting equation) of D(La=0.011, Sm=0.05, Zr=0.05, Y=0.15) and P(La=0.036, Sm=0.2, Zr=0.10, Y=0.25) taken from Arth & Hanson (1975); Hanson (1977); Frey *et al.* (1978); Pearce & Norry (1979); Wood (1981).

**Table 5.3** A batch melting model for the elements La, Sm, Zr and Y.

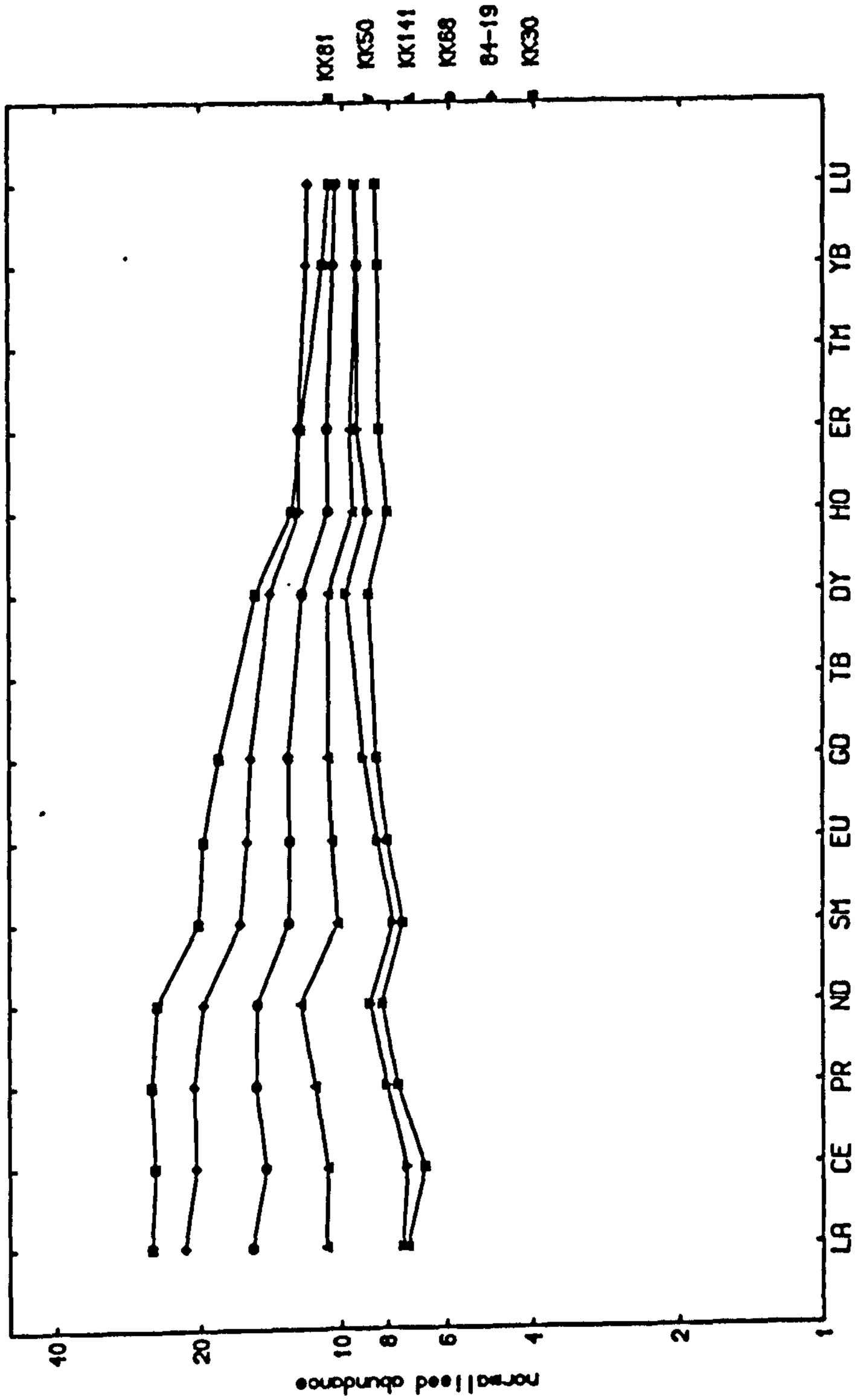


Fig. 5.12 REE variation diagram (chondrite normalised as in Fig. 5.7) for selected samples containing at least 8 wt% MgO (KK81, KK50, KK141, KK68, 84-19 and KK30).

mantle residue. The extracted melt is then allowed to equilibrate with the mantle further up the melting column. Langmuir *et al.* (1977) claim that such a model can produce variable ratios of $(La/Sm)_{(chondrite\ normalised)}$, whilst retaining realistic REE concentrations in the larger degree melts. Fig. 5.13 shows the results of a simple melting model apparently fitting the requirements of their model of "dynamic melting" using a garnet lherzolite source. It should be noted that no attempt has been made, given all of the uncertainties involved, to model the effects of re-equilibration with the mantle. Garnet appears to be necessary in the source to buffer concentrations of the heavy REE. This model requires that only half of the melt present in the mantle (1% in total) is actually extracted, the remainder is mixed with the next increment of melt produced. This process is repeated. However, it appears that this model suffers from the same deficiency as the other models listed above; namely that the degrees of melting in the model required to generate the range in $(La/Sm)_{(chondrite\ normalised)}$ ratios are too small to fit with degrees of melting estimated from the major element compositions (too few details are provided by the above authors for a conclusion to be reached in its case).

The above discussion suggests that most simple melting models (i.e. perfect equilibrium melting, where melts do not move relative to the source, and perfect fractional melting, where melts move instantaneously away from the source) are unlikely to match real melting processes where melts move "at a finite rate and continuously interact with the matrix they pass through" (Richter, 1986). Recent work on the physics of melt extraction (Scott & Stevenson, 1984; McKenzie, 1984; Richter & McKenzie, 1984; McKenzie, 1985a) suggests that the melting process may be capable of causing chemical fractionation between melt and the matrix through which the melt is flowing. The main difficulty in the past with the concept of fractionating trace elements during melting lay with the idea that melt could not be extracted until a critical melt proportion of, say, 5-10% was reached. It is now, however, widely recognised that melt can probably be extracted at melt fractions of less than 1%, depending upon the viscosity of the melt, thus theoretically enabling fractionation of most elements. Richter (1986) developed a model for continuous melt segregation from a deformable matrix for elements of different degrees of incompatibility. He found that the more incompatible trace elements appear to be derived from smaller degrees of melting for a given source composition than the less incompatible trace elements. This reflects the lesser interaction of the highly incompatible elements moving through a matrix, following melt generation. More compatible elements, in contrast, can continuously exchange with the matrix. Such types of process would appear to be consistent with the wide variations in ratios of concentrations of more to

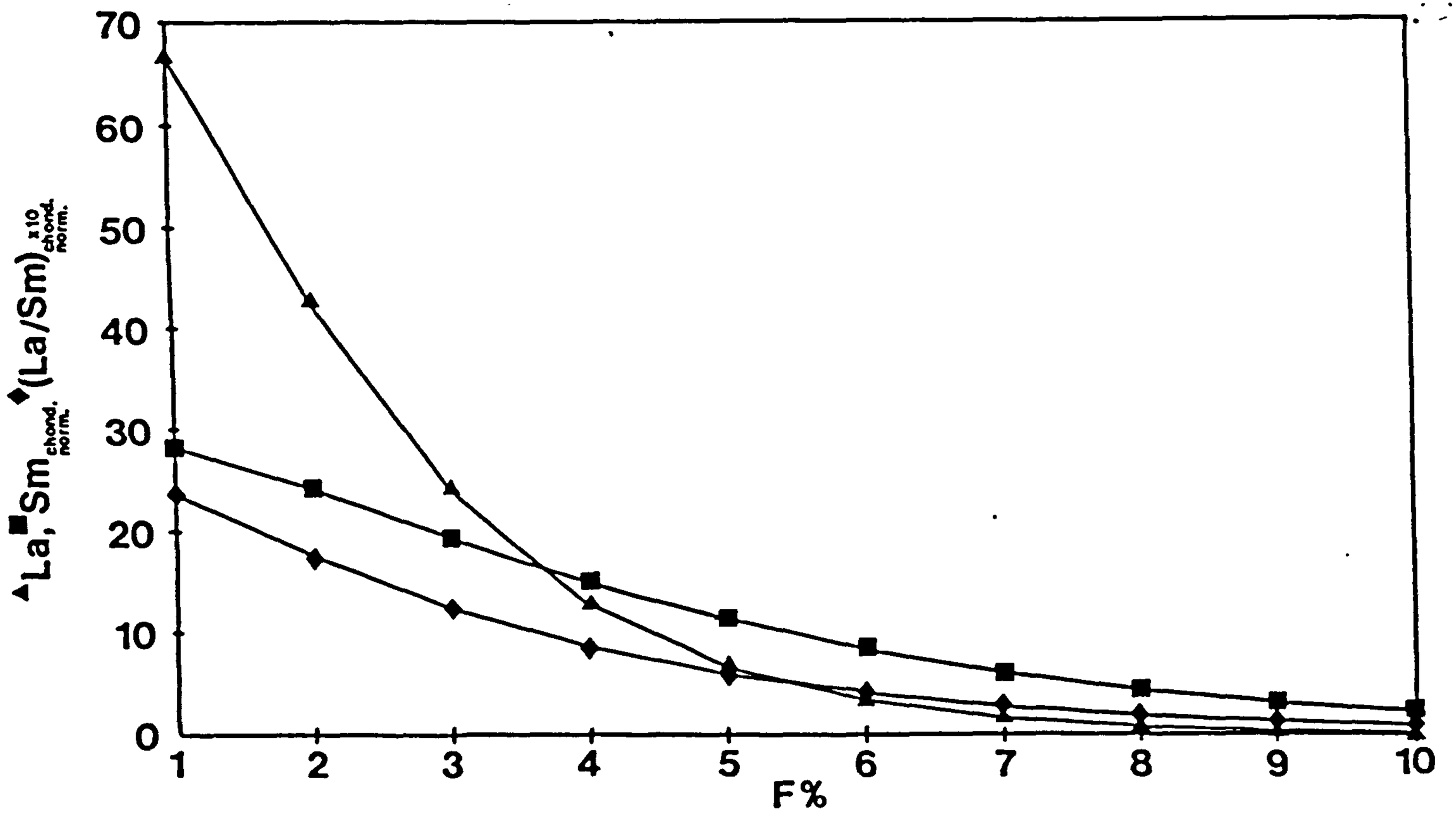


Fig. 5.13 Incremental batch melting model showing the variation of La, Sm and (La/Sm) with the extent of partial melting (see text for details; La, Sm concentrations and (La/Sm) ratios normalised after Nakamura 1974).

less incompatible trace elements (cf. Ribe & Smooke, 1987; Ribe, 1988). In detail, however, the melting process remains poorly understood, especially regarding its effects on trace-element concentrations and ratios.

Galer & O'Nions (1986) reinforced the view that melting processes may be able to fractionate most trace elements from one another. They cited the extreme example of fractionating Th from U. Both elements appear to have very similar and small partition coefficients (e.g. Benjamin et al., 1978; Henderson, 1982) and appear to fractionate only where very small degrees of melting occur (e.g. <2% if controlled by clinopyroxene-melt equilibria; McKenzie, 1985b). Most MORB, including those from Iceland (as explained in Chapter 7), show excess quantities of ($^{230}$Th) which appear to have resulted from chemical fractionation of Th from U during the melting process, i.e. during very small degrees of melting. However, as explained above, the overall degree of melting responsible for the Icelandic basalts, as seen by the major elements, may be as high as 25%. This apparent contradiction can be rationalised (even if not, as yet, quantitatively modelled) by accepting a process of melting which allows the incompatible trace-element budget to be controlled at depth by small degrees of melting, possibly at the edges of a mantle plume (Oxburgh, 1980) while the major elements are dominated by much larger degrees of melting at much shallower levels in the plume. Indeed Galer & O'Nions (1986) suggest that volatiles and/or accessory phases may control the behaviour of the most incompatible trace elements. For a given temperature, a "wet solidus" would occur at much greater depths than a dry one (e.g. Green, 1973; Olafsson & Eggler, 1983) and allow the breakdown of phases of amphibole (or phlogopite) to form very small degrees of melt rich in the most incompatible trace elements. Thus adiabatically-upwelling mantle would meet the wet solidus at much greater depths than the dry peridotite solidus and produce small volumes of melt rich in the most incompatible elements. The mantle would then meet the dry solidus at shallower levels in the mantle, generating larger volumes of melt whose character would be dominated by the major elements. There appears, however, to be a conflict here with the Krafla data, which show a correlation between the degree of melting (as indicated by the Zr/Y ratio) and the average pressure of melting (e.g. FeO*; see Fig. 5.14 and Chapter 6). This suggests that the major and trace-element concentrations are indeed "coupled" (cf. Viereck *et al.*, 1989).

In conclusion, the melting process appears to be able to fractionate most trace elements from one another. Thus it appears that the trace element-characteristics of primitive basalts (e.g. the ratio of a highly incompatible to less incompatible trace element) probably reflect differences in the degree of melting or the *"differential*

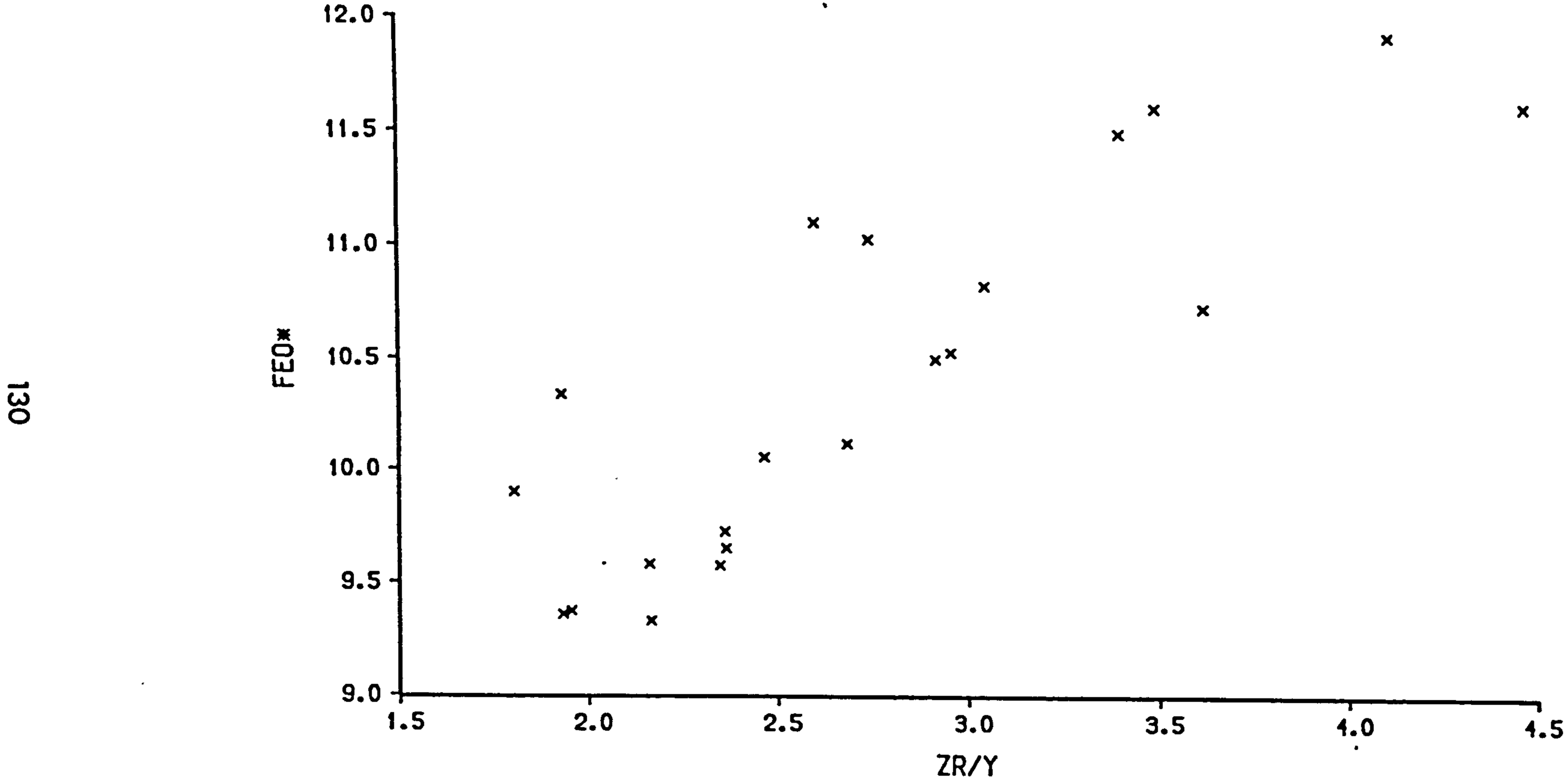


**Fig. 5.14** FeO (total) *vs* Zr/Y for samples containing at least 8 wt% MgO.

*sampling of small melt fractions"* by mantle plumes (Galer & O'Nions 1986). This will be considered again in the next part of this section when the differences and similarities in trace element ratios and concentrations between Krafla basalts and other MORBs are discussed.

**Comparisons of the trace element compositions of Krafla basalts with other MORBs.**

The distinctive trace element characteristics of Icelandic basalts have been recognised for a considerable period of time (e.g. Schilling, 1973). It was noted in this regard that Icelandic rocks show many of the characteristics of OIB (Fig. 5.15). This similarity is also revealed by the Sr- and Nd-isotope ratios - see Chapter 7. In addition, large-scale surveys of Iceland (e.g. O'Nions & Grönvold, 1973; O'Nions *et al.*, 1976; Meyer *et al.*, 1985) revealed that most Icelandic basalts (including those from Krafla) show flat or light-REE (LREE) enriched patterns (see Fig. 5.12), in contrast to the dominance of LREE-depleted patterns in most "normal" MORBs (as defined by lower $^{87}Sr/^{86}Sr$ ratios). One explanation is that the Icelandic basalts may be derived from a source which is more enriched in incompatible elements than the source of most MORBs (i.e. from a "mantle plume"; i.e. E-MORB). The enriched source appears to be similar in composition to estimates for the composition of the "primitive" or primordial mantle (Hoffmann, 1988), consistent with the idea of mantle material from a deeper (lower) mantle-reservoir melting to produce magma beneath Iceland. But as referred to above, trace-element concentrations and even their ratios (traditionally used to "map" source variations) appear to be vulnerable to fractionation during mantle melting (e.g as summarised by Thompson 1987). Hence, it is possible that the differences in trace element ratios of Krafla basalts compared with many other MORBs may result from differential sampling of small melt fractions by a mantle plume (Oxburgh, 1980; Galer & O'Nions, 1986). However, such an argument cannot explain the isotopic differences between different MORBs.

These differences are perhaps best shown on a chondrite normalised "spiderdiagram" or "spidergram", where incompatible trace elements are plotted in their estimated order of decreasing incompatibility from left to right (Fig. 5.15). Two Krafla samples are shown (KK50 and KK30) which represent the least and most incompatible-element enriched samples respectively. Also shown are an average N-MORB (depleted in incompatible-trace elements) and an average OIB (D. James and J.G. Fitton, unpublished data; Fitton *et al.*, 1990 submitted). The Krafla samples, although showing a spread in their degrees of enrichment in the more incompatible trace elements, have profiles more like those of OIB than N-MORB, with a distinctive

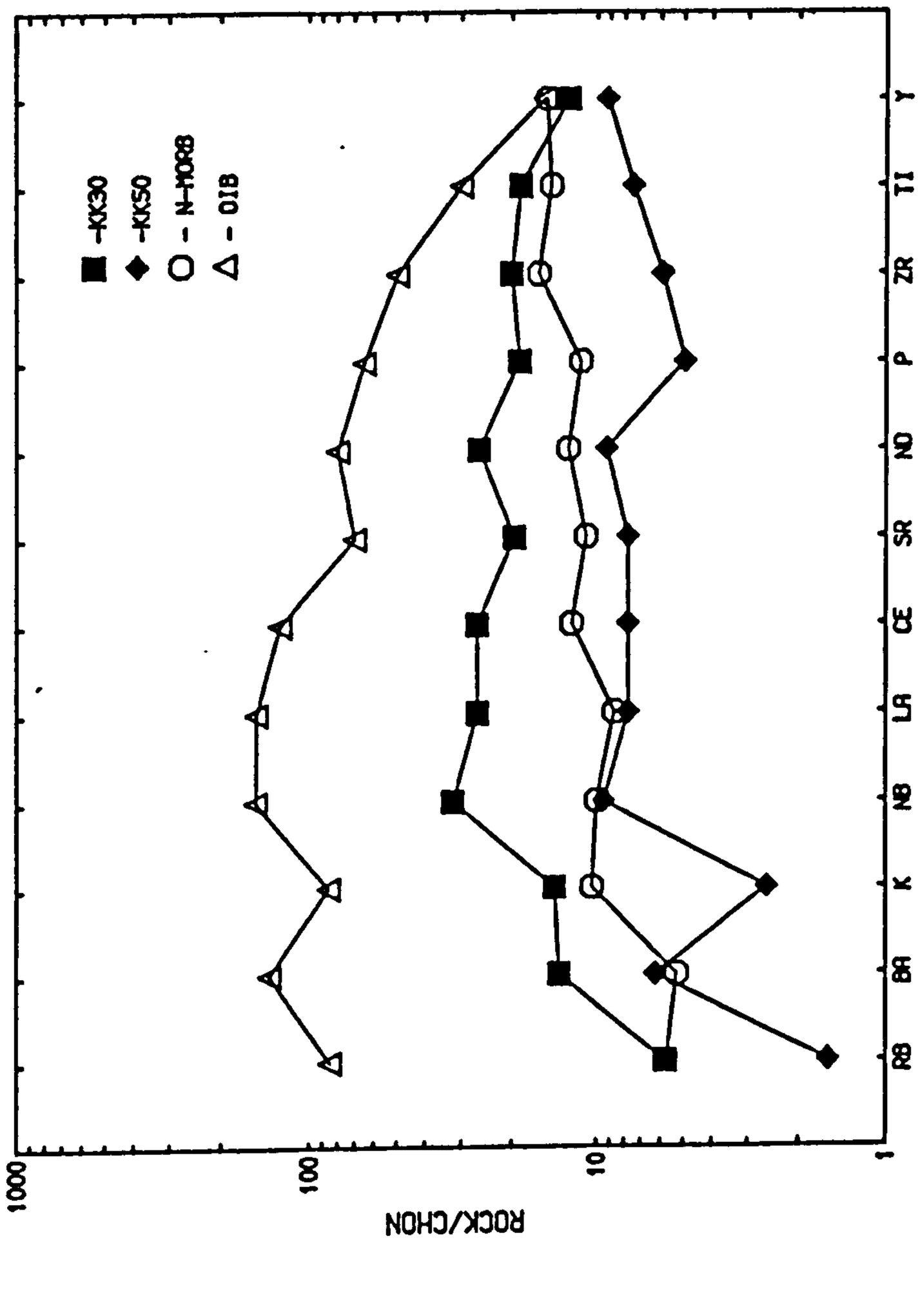


Fig. 5.15 "Spiderdiagram" showing the chondrite normalised (normalising factors from Sun 1980) concentrations of two Krafla samples (KK30, filled squares; and KK50, filled diamonds), a mean N-MORB composition (open circle) and a mean OIB composition (open triangle).

peak at Nb and a trough at K. The differences in trace-element concentrations between KK30 and KK50 probably depend upon the degree of melting because the more incompatible elements show greater differences in concentration than the less incompatible elements (see Fig. 5.11). In contrast, the differences in concentration of elements next to each other in the spiderdiagram, as shown by peaks or troughs, are more likely to result from source differences. This particular point is open to debate.

## 5.6 Conclusions

The trace-element compositions of the Krafla suite suggest that fractional crystallisation is the dominant factor controlling the differentiation process. However, the high concentrations of Th, U and Rb in the Krafla rhyolites, which are above that expected by simple closed-system fractional crystallisation, can be most easily explained by the assimilation of a crustal partial-melt rich in these elements.

Open system fractionation has often been used by other authors to explain the excess concentrations of the most incompatible trace elements. The Krafla data set shows no evidence of enrichment in concentrations of incompatible trace elements with time, a condition inconsistent with the open system fractionation model.

The least-differentiated Krafla basalts appear to preserve evidence of mantle-melting processes. In particular it seems that simple melting models (e.g. batch melting or fractional melting) are unable to reproduce the range of trace-element concentrations seen in the high-MgO samples from Krafla. More complex melting models may more successfully reproduce the Krafla data by requiring that the melt fraction in equilibrium with the matrix never exceeds a few percent (e.g. "dynamic melting").

The Krafla samples also show distinctive chondrite-normalised trace element patterns on "spiderdiagrams". The patterns are similar to that of average OIB, although the actual concentrations may be significantly less than that of OIB. This suggests that Krafla may share the same source as OIB (e.g. perhaps by the involvement of the lower mantle) and/or that there was differential sampling of small melt fractions by a mantle plume.

# Chapter 6
# Mantle melting: Application of the model of McKenzie & Bickle (1988)

## 6.1. Introduction and evidence for a major-element mantle-melting signature

### 6.1.1. Introduction

In earlier Chapters (4 and 5) it was suggested that the compositions of basalts from Krafla are not solely the result of fractional crystallisation from a single parental magma. The implication is that some process(es) was operating to produce a variety of parental magma compositions. In recent years systematic variations in major- and trace-element compositions of MgO-rich basalts have been ascribed by many workers to melting processes and variations in mantle source composition (e.g. Gast, 1968; Schilling, 1975; O'Nions *et al.*, 1976; Langmuir *et al.*, 1977; Kay & Hubbard, 1978; Sun *et al.*, 1979; Basaltic Volcanism Study Project, 1981). A study of trace elements which are moderately to highly incompatible in mantle phases is most useful in identifying variation in mantle processes (e.g. Langmuir *et al.*, 1977; Wood, 1979; Wood, 1981). However, major-element concentrations have also been used to document changes in degree and depth of melting (e.g. Bryan, 1979; Sun *et al.*, 1979; Sigurdsson, 1981; Schilling *et al.*, 1983; Klein & Langmuir, 1987).

As explained in section 4.8, systematic global variations in major-element compositions of MORB has been recognised (e.g. Klein & Langmuir, 1987). In particular, Klein & Langmuir (1987) showed that there was a clear correlation between the water depth at the ridge axis and the composition of erupted basalts after correction for low-pressure fractional crystallisation. They suggested variations in the major-element compositions of the least-differentiated MORB result from melting the mantle over a range of temperatures. It is possible, instead, that the observed variation in major-element composition of MORB results from global variation in the major-element composition of the mantle (cf. Natland, 1989). However, the clear correlation between ridge depth and MORB composition is compelling evidence in favour of a theory which links the thermal structure of the mantle with the melt composition. McKenzie & Bickle (1988) emphasised this point and produced a more rigorous mathematical model (cf. Klein & Langmuir, 1987) for the melting process, relating variation in MORB composition to differences in mantle potential temperature.

In this chapter, major-element compositions of the most MgO-rich Krafla basalts, least affected by fractional crystallisation (see Chapters 4 and 5) are compared with experimental melting data. It is shown that the least-differentiated Krafla samples preserve evidence for differences in the degree and depth of partial melting. These primitive compositions are also compared with the melt compositions calculated by the model of McKenzie & Bickle (1988) for different mantle potential temperatures ($T_p$), allowing an estimate to be made of the $T_p$ beneath NE Iceland. In addition, the melt thickness calculated using McKenzie & Bickle's (1988) model is compared with estimates of the Icelandic crustal thickness. There are, however, discrepancies between the Krafla compositions and the melt compositions as calculated by the model. These discrepancies may be qualitatively explained by the importance of large volumes of small degree melt fractions provided at depth within the Iceland plume.

### 6.1.2 Major element mantle-melting evidence

Evidence in favour of mantle-melting processes is best revealed in the least-differentiated samples (see also discussion in Chapter 5), allowing the chemical effects of fractional crystallisation and assimilation to be minimised. For this reason, only basalts with more than 8 wt% MgO are considered when investigating melting processes in this Chapter. A cut-off of 8 wt% MgO should eliminate most of the effects of plagioclase and clinopyroxene fractional crystallisation (plag and cpx join the liquidus assemblage at about 8-9 wt% MgO; see discussion in section 4.7; cf. Klein & Langmuir, 1987). Crystallisation of olivine, however, cannot be eliminated from consideration since the MgO content of the "parental" Krafla melt(s) is not known. Olivine fractionation does, however, have a smaller effect on the compositions of the magmas than do plag and cpx.

Figures 6.1 to 6.3 show several variation diagrams for 21 samples with at least 8 wt% MgO. In Fig. 6.1a $TiO_2$ is shown to correlate with $K_2O$ (cf. Bryan, 1979), with the values of $TiO_2$ and $K_2O$ varying by factors of 3 and 5 respectively. Over 80% fractional crystallisation of olivine, plagioclase and clinopyroxene (see the "vectors" in Fig. 6.1a) would be required to generate the range of $TiO_2$ and $K_2O$ values observed (e.g. KK30, 0.20 wt% and KK50, 0.04 wt% $K_2O$; cf. estimated error of $<\pm 0.01$ wt%). This extent of fractional crystallisation is, of course, inconsistent with the high concentrations of Ni, Cr and MgO (see Chapter 5) and therefore variable concentrations of $K_2O$ and $TiO_2$ may be more easily explained by variable degrees of

mantle partial melting or source variation (cf. section 4.7). Both $K_2O$ and $TiO_2$ are incompatible in most major mantle phases and are thus highly sensitive to changes in the degree of melting (see discussion on the incompatible trace elements in Chapter 5). The plot of $FeO^*$ *vs* $Na_2O$ (Fig. 6.1b) is also difficult to reconcile with simple fractional crystallisation, since the variation in these oxides demands at least 40% fractional crystallisation of cpx (and more crystallisation if ol and plag are included); whilst numerical modelling of fractional crystallisation and petrographic observations suggest that little plag or cpx crystallisation can have occurred (possibly <10%), leaving olivine as the only potential crystallising phase in any quantity. However, as will be shown below, fractional crystallisation of olivine alone is inconsistent with the trends shown in Figs. 6.1 to 6.3. It is easier to understand this trend by invoking variations in the melting process, whereby samples with higher concentrations of $FeO^*$ are derived from melts formed at, on average, higher pressure (e.g. Jaques & Green, 1980; Langmuir & Hanson, 1980). However, the positive correlation between $Na_2O$ and $FeO^*$ suggests that melts formed at higher pressure also represent smaller degrees of melting. This appears to be confirmed by the positive correlation between $K_2O$ and $FeO^*$ (Fig. 6.2a) (e.g. KK30: 0.20 wt% $K_2O$, 11.6 wt% $FeO^*$; KK50 0.04 wt% $K_2O$, 9.89 wt% $FeO^*$).

Fig. 6.2b shows a slight negative correlation between $Al_2O_3$ and $Na_2O$ which can be explained by fractional crystallisation of ol+plag+cpx. However, a large amount of fractional crystallisation of these three phases (possibly >80%) would be needed to generate the trend observed in Fig. 6.2b. Olivine crystallisation alone would tend to increase both $Na_2O$ and $Al_2O_3$, in contrast to the observed trend. However, experimental evidence suggests that the melt concentrations of both $Na_2O$ and $Al_2O_3$ should increase as the degree of melting decreases, although there is some disagreement regarding the variation of the $Al_2O_3$ concentration in mantle-derived melts with pressure - see Table 6.1. Similarly, a plot of CaO *vs* $Na_2O$ (Fig. 6.3a) shows a very slight negative correlation, consistent with fractional crystallisation of ol+plag+cpx, although the extent of crystallisation required to explain the trend is probably unrealistic (cf. $FeO^*$ *vs* $Na_2O$ in Fig. 6.1b). In contrast, evidence from experimental melting studies suggests that if this trend is due to melting processes then there should be a positive correlation between these two oxides, with melts derived by small degrees of melting containing relatively high concentrations of both CaO and $Na_2O$. Fig. 6.3b shows a slight positive correlation between CaO and $Al_2O_3$: such a trend may be consistent with either fractional crystallisation of plag±cpx±ol or with differences in the degree of partial melting (i.e. high CaO and $Al_2O_3$ for small

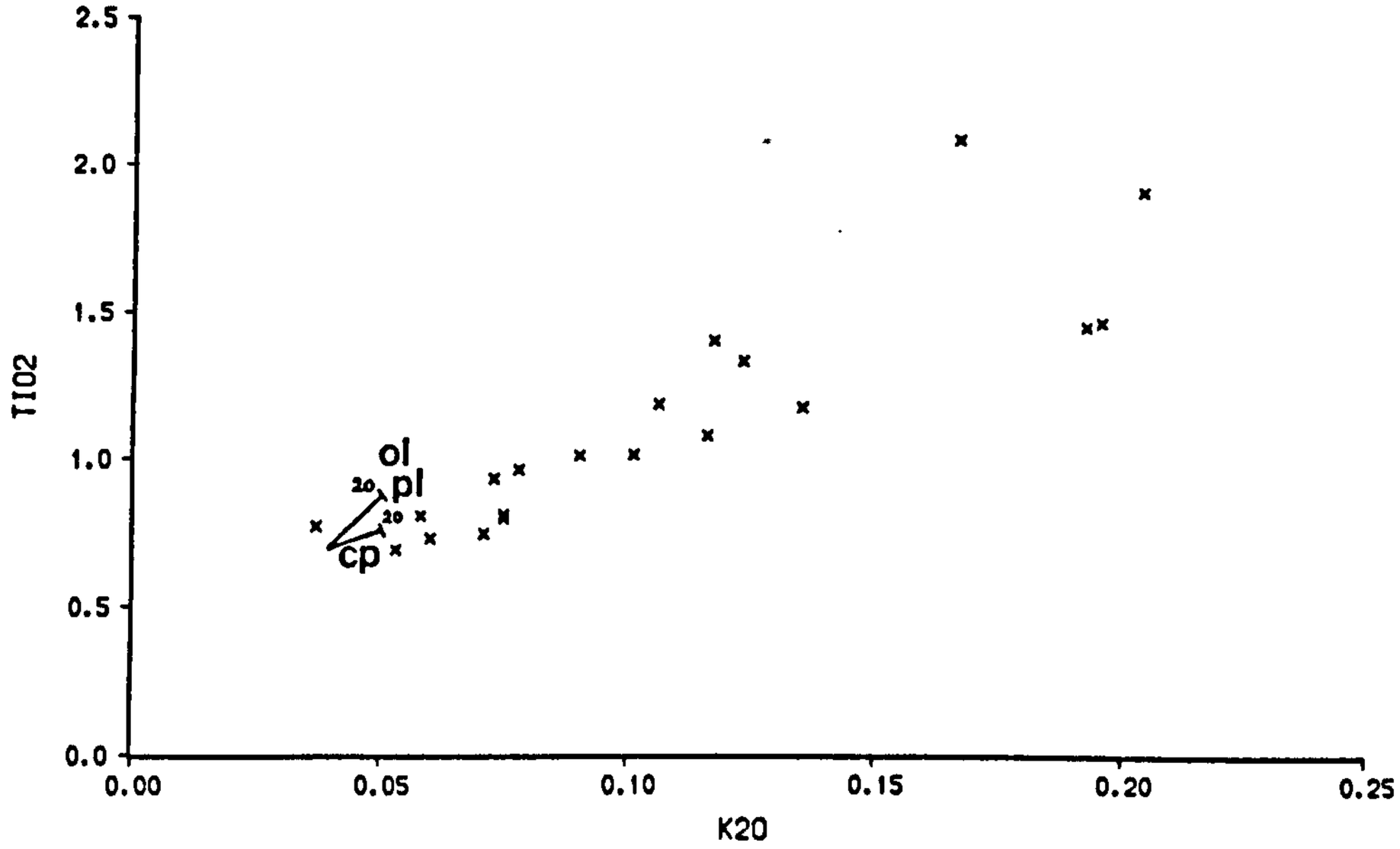


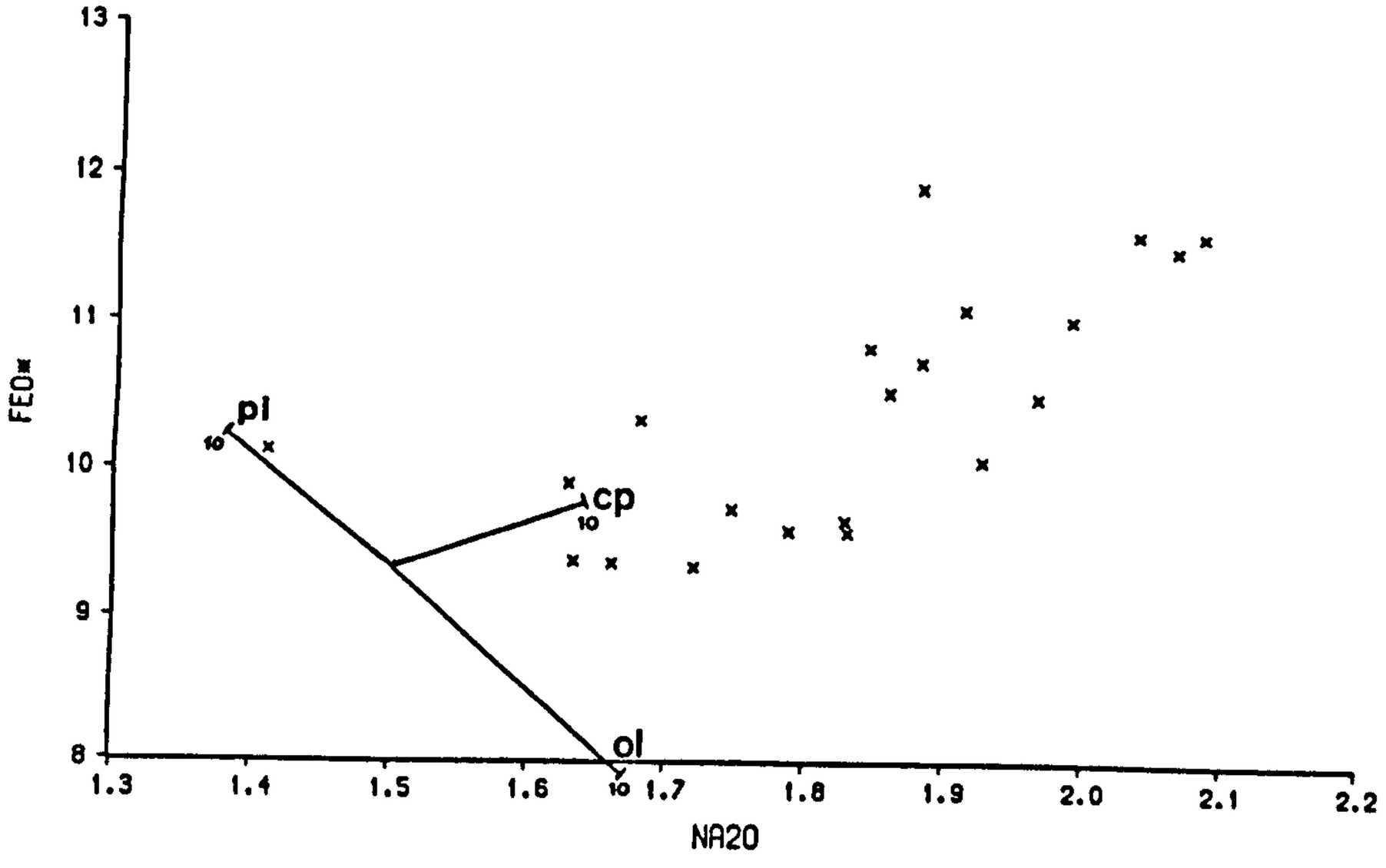


**Fig. 6.1** (a) $TiO_2$ *vs* $K_2O$ for samples containing at least 8 wt% MgO. Lines indicate 20% fractional crystallisation of olivine (ol), plagioclase (pl) and clinopyroxene (cp) from a starting composition of 0.04 wt% $K_2O$ and 0.7 wt% $TiO_2$. (b) FeO (total) *vs* $Na_2O$; as for Fig. 6.1 (a) but for 10% fractional crystallisation from a starting composition of 9.3 wt% FeO (total) and 1.5 wt% $Na_2O$.

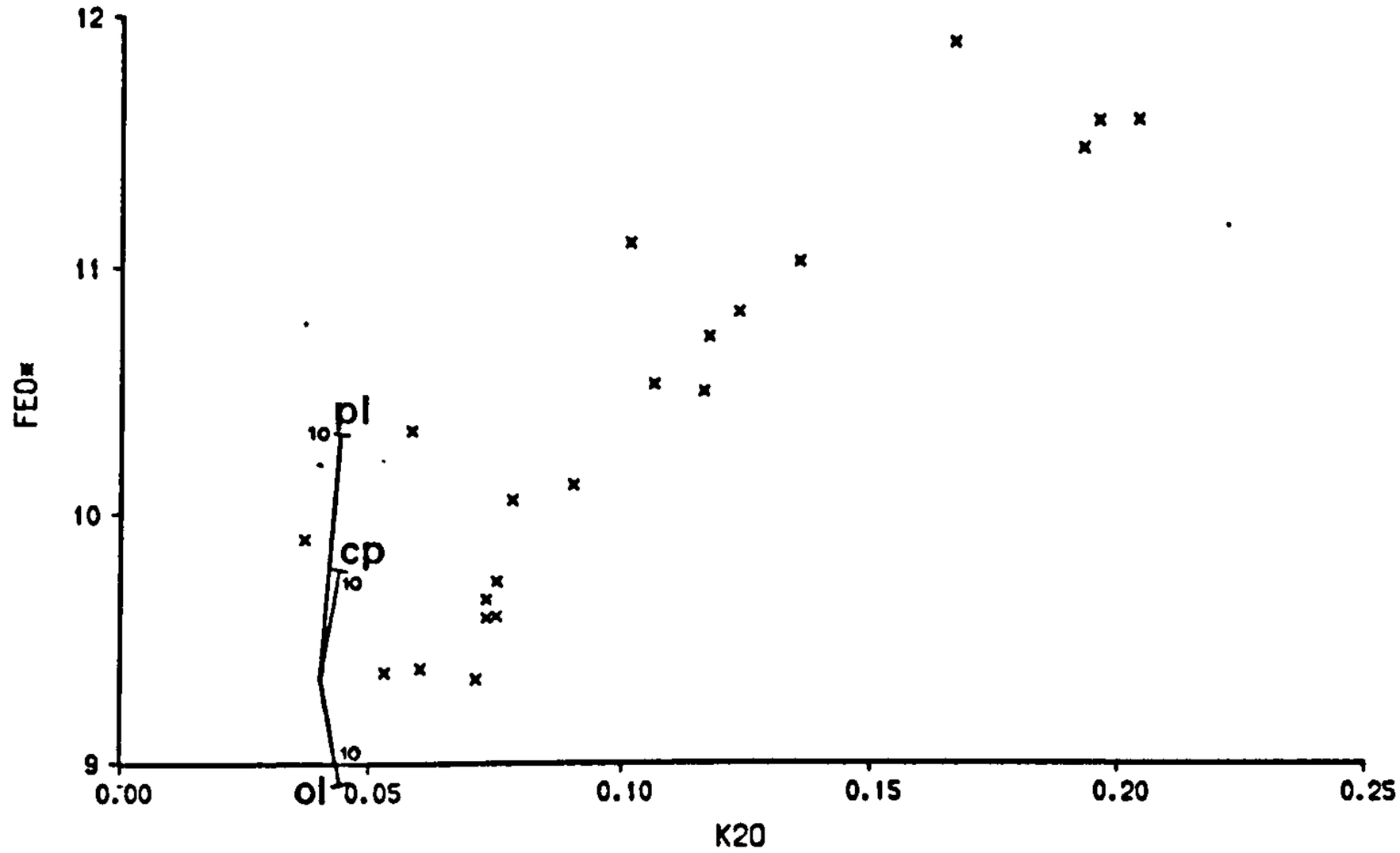


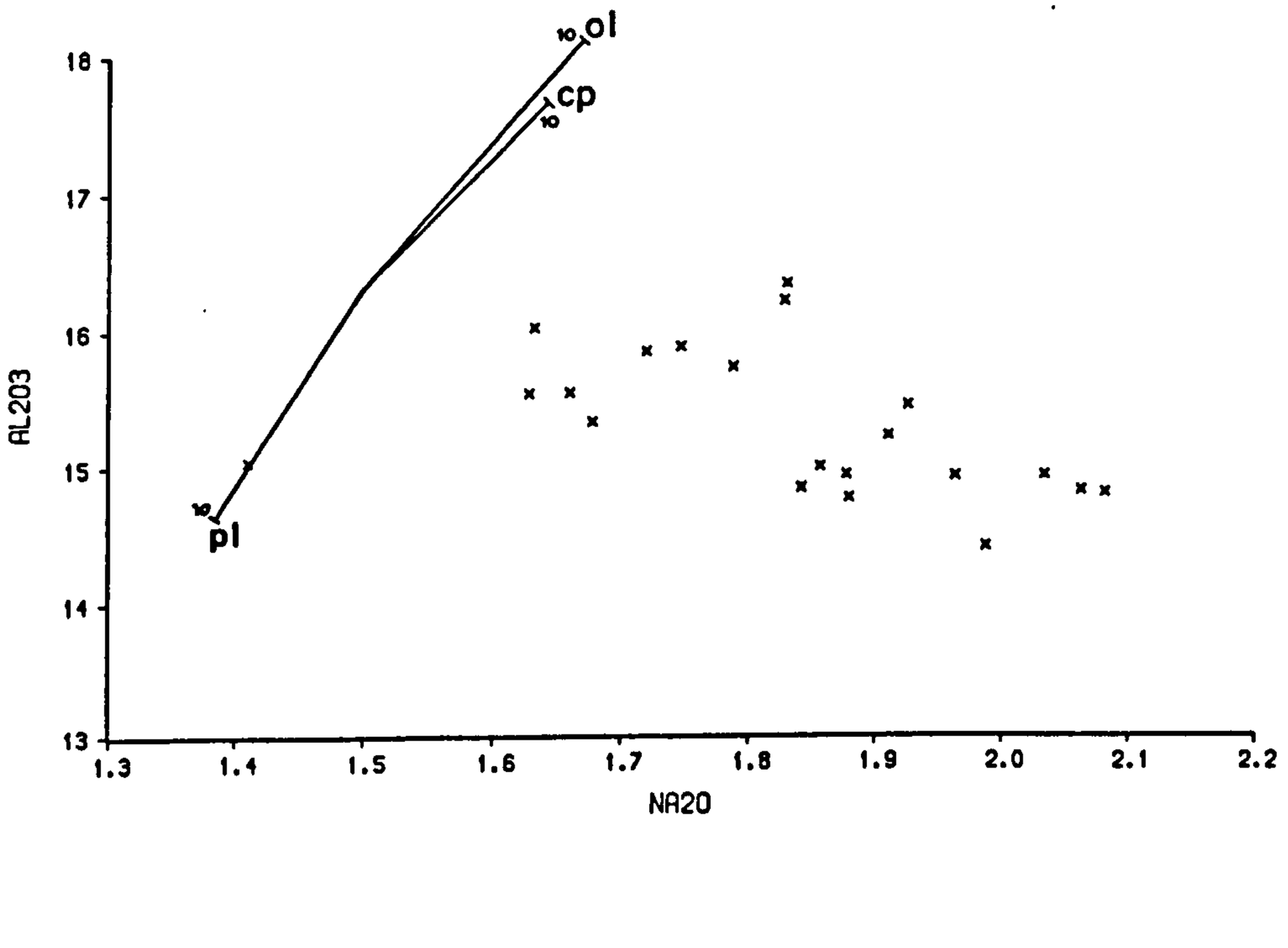


Fig. 6.2 (a) FeO (total) *vs* $K_2O$; as for Fig. 6.1 (a) but for 10% fractional crystallisation from a starting composition of 9.3 wt% FeO (total) and 0.04 wt% $K_2O$.
(b) $Al_2O_3$ *vs* $Na_2O$; as for Fig. 6.1 (a) but for 10% fractional crystallisation from a starting composition of 16.3 wt% $Al_2O_3$ and 1.5 wt% $Na_2O$.

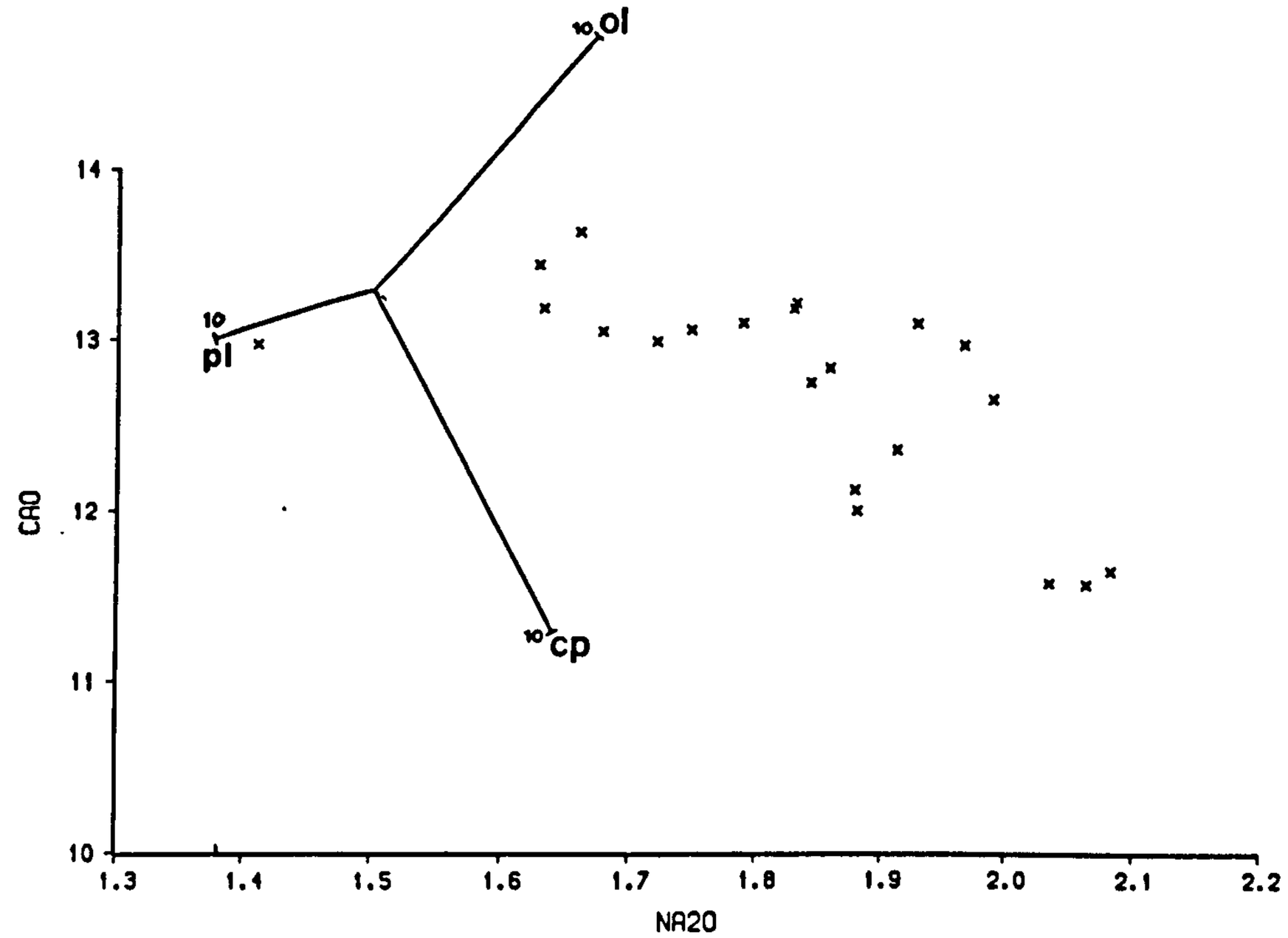


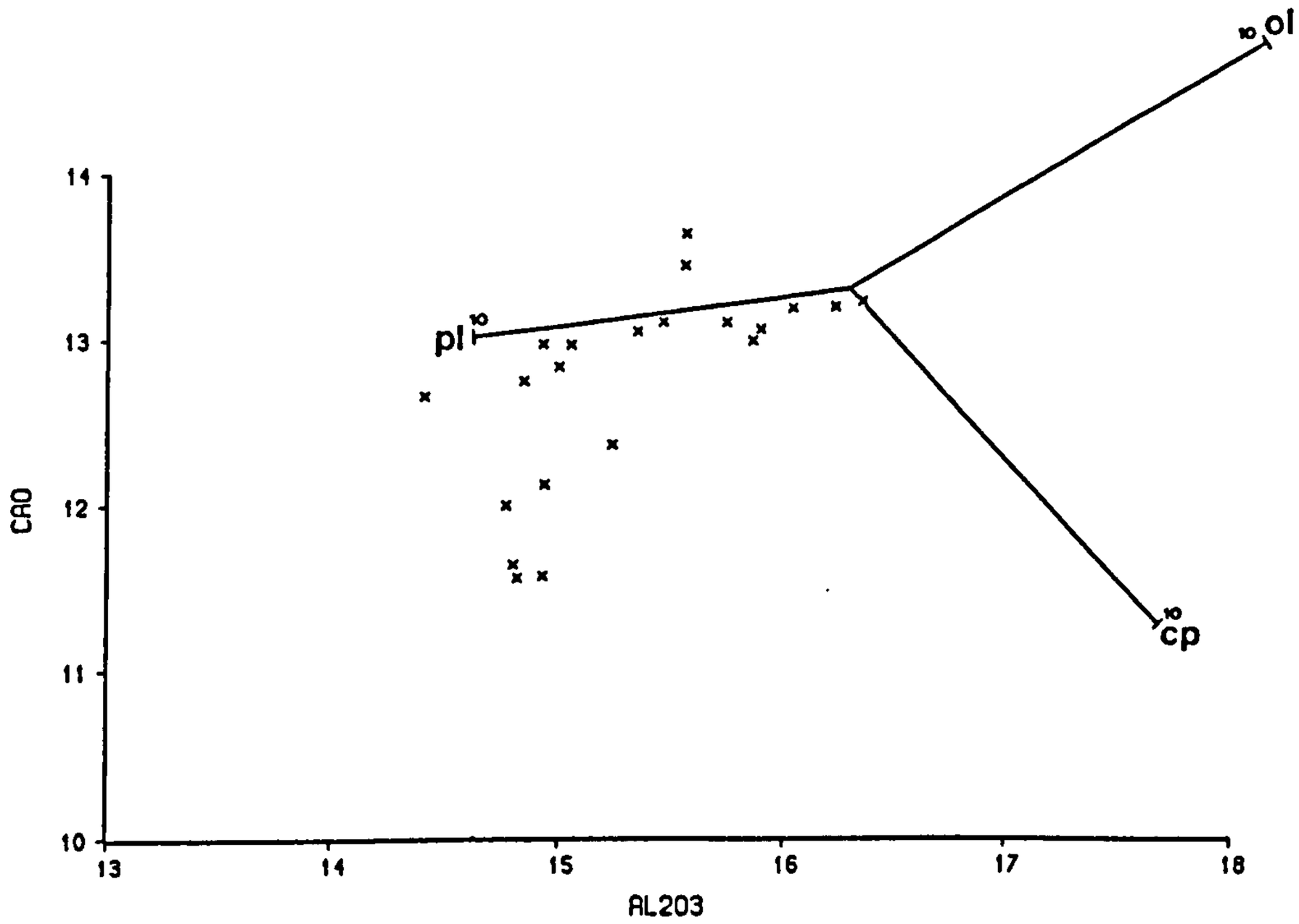


**Fig. 6.3 (a)** CaO *vs* $Na_2O$; as for Fig. 6.1 (a) but for 10% fractional crystallisation from a starting composition of 13.3 wt% CaO and 1.5 wt% $Na_2O$.
**(b)** CaO *vs* $Al_2O_3$; as for Fig. 6.1 (a) but for 10% fractional crystallisation from a starting composition of 13.3 wt% CaO and 16.3 wt% $Al_2O_3$.

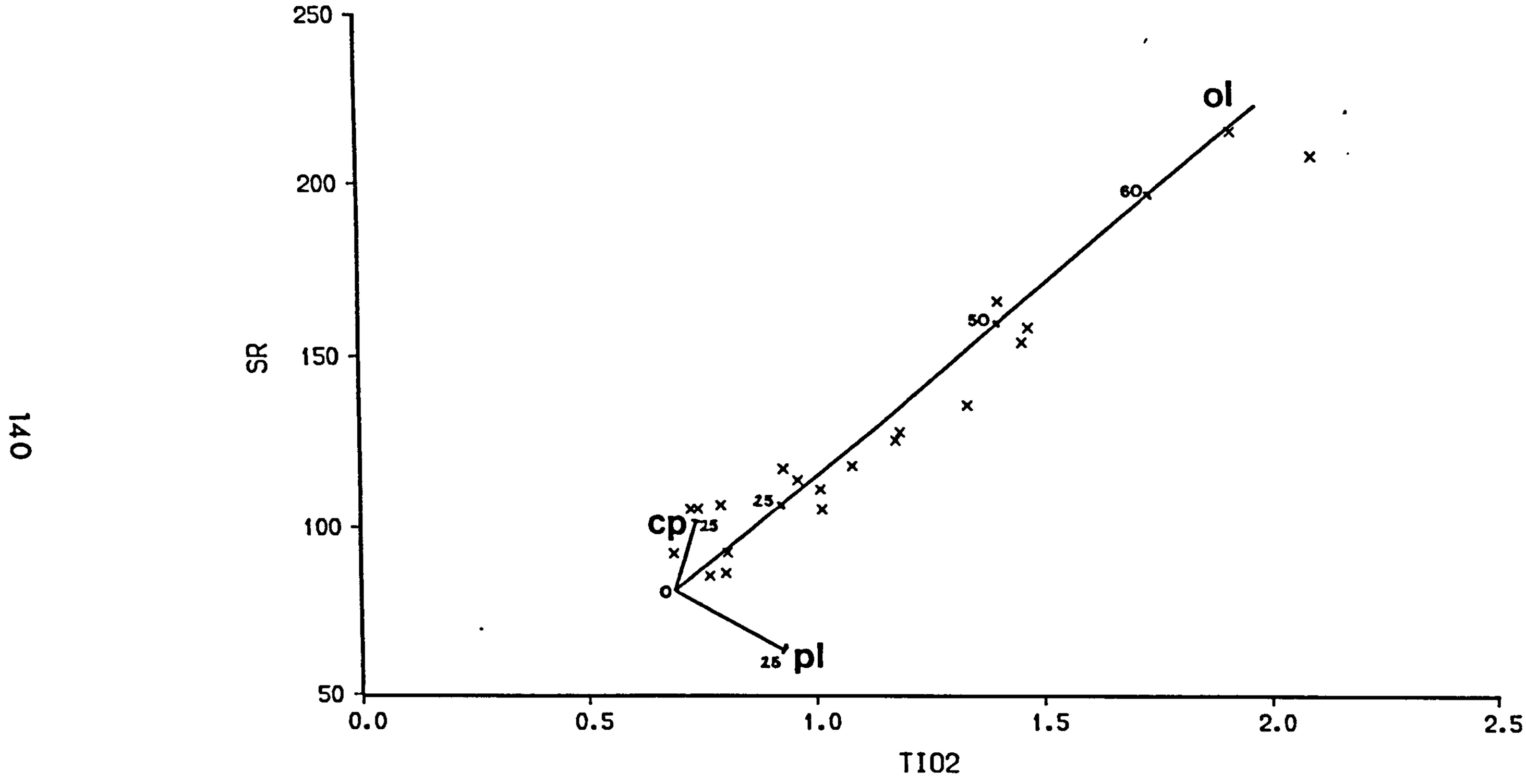


Fig. 6.4 Sr *vs* $TiO_2$ for samples with at least 8 wt% MgO. Fractional crystallisation of olivine (ol), plagioclase (pl) and clinopyroxene (cp); numbers indicate % fractional crystallisation. D values used for Ti are ol, 0.01; pl, 0.01; cp, 0.8: and for Sr; ol, 0.01; pl, 1.8; cp, 0.14.

degrees of melting) (see section 6.1.3). However, a plot of Sr *vs* $TiO_2$ (Fig. 6.4) suggests that little plagioclase fractional crystallisation can have occurred in the evolution of these least-differentiated Krafla samples, because Sr shows a clear positive correlation with $TiO_2$ (with the extrapolated Sr *vs* $TiO_2$ trend passing through the origin, inconsistent with any significant amount of plagioclase fractional crystallisation).

In conclusion, the variation in composition of the samples with more than 8 wt% MgO is highly unlikely to reflect solely fractional crystallisation processes for the following four reasons:

(a) An unreasonable amount of ol+plag+cpx fractional crystallisation would be required to explain the variation diagrams in Figs. 6.1 to 6.3.

(b) There is little petrographic evidence for substantial amounts of cpx fractionation (although note the possible role of cpx fractionation at higher pressures, providing it dissolves at low pressure).

(c) The Sr *vs* $TiO_2$ plot in Fig. 6.4 suggests that little plagioclase fractionation can have occurred.

(d) The trends are also inconsistent with only olivine crystallisation.

In contrast, it appears that the most primitive Krafla samples preserve evidence for variation in the degree and pressure of partial melting in the mantle (see section 6.1.3).

### 6.1.3. Melting systematics - experimental evidence

There has been a considerable amount of attention focussed on the composition of basaltic melts formed by equilibrium partial melting of experimental charges of anhydrous peridotite (e.g. O'Hara, 1968a; Mysen & Kushiro, 1977; Presnall *et al.*, 1979; Jaques & Green, 1980; Fujii & Scarfe, 1985). Table 6.1 is a summary of the behaviour of the key major element oxides during partial melting, compiled from Klein & Langmuir (1987) and McKenzie & Bickle (1988; derived from their point average melt compositions). These results are based primarily on the experiments of Ito & Kennedy (1967); Green & Ringwood (1967); Jaques & Green (1980); Stolper (1980); Harrison (1981); Takahashi & Kushiro (1983); and Takahashi (1986). The behaviour of the oxides is expressed in terms of the melt fraction present during batch melting of the peridotite sample.

| Melting systematics |
| --- |
| $SiO_2$ for constant MgO; increases with X, decreases with P |
| $Al_2O_3$ decreases with X, decreases with increasing P (or no P dependence for parameterisation a, McKenzie & Bickle 1988) |
| FeO* is constant with X at constant P; increases with increasing P (McKenzie & Bickle; FeO* decreases slightly with increasing X, until cpx is melted out, then it increases) |
| MgO increases with X at constant P; increases with increasing P |
| $Na_2O$ decreases with X (no apparent P dependence) |
| CaO increases with X, while cpx is residual (McKenzie & Bickle find that CaO decreases with X, while cpx is residual; parameterisation c gives CaO decreasing for increasing P) |
| $TiO_2$ and $K_2O$ behave as highly incompatible elements |

Table 6.1 Melting systematics for anhydrous peridotite (compiled from Klein & Langmuir, 1987 and McKenzie & Bickle, 1988); X is the melt fraction present in the experiments.

The experimental results summarised in Table 6.1 show that the compositions of basaltic melts depend upon the average degree and pressure of melting. The variation in composition of the most primitive lavas from Krafla, as shown in Figs. 6.1 to 6.3, is generally consistent with the melting behaviour of peridotite as given in Table 6.1. In particular, the positive correlations between $Na_2O$, $TiO_2$, and $K_2O$ suggest that the basalts are derived by variable degrees of partial melting. A sample such as KK30 (with high $Na_2O$, $TiO_2$, $K_2O$) may represent a smaller degree of partial melting than, say, KK50 (with low $Na_2O$, $TiO_2$, $K_2O$). Those samples from Krafla, like KK30, which apparently formed by smaller degrees of melting also contain higher concentrations of $FeO^*$. $FeO^*$ is little affected by the degree of melting, at least while cpx, garnet or spinel is a residual phase and therefore seems to be most sensitive to the average pressure of melting. Since high values of $Na_2O$ occur in samples with high values of $FeO^*$, small degrees of melting appear to occur at higher average pressures of melting than samples with low $Na_2O$ (cf. Fig. 5.14, showing the correlation between Zr/Y and $FeO^*$). The differences in CaO and $Al_2O_3$ concentrations between samples such as KK30 and KK50 do not appear to be consistent with the melting systematics (see Table 6.1), and may indicate plagioclase fractionation. However, the Sr *vs* $TiO_2$ plot (Fig. 6.4) suggests this is not likely to be the case. Alternatively the discrepancies between the melting systematics and the Al2O3 and CaO concentrations of the Krafla samples may reflect problems in the understanding of the behaviour of these oxides during peridotite melting at high pressures (see below).

The proposition that the major-element trends may be explained by different degrees of partial melting is confirmed by least-squares modelling using samples KK30 and KK50. It is found that KK50 (apparently the sample produced by the largest degree of melting) may be produced from KK30 (smallest degree of melting) by the addition of 60 wt% of a mixture of roughly equal proportions of clinopyroxene and garnet. This suggests that if KK30, for example, is formed by 15% partial melting then KK50 can be produced by 24% partial melting, consuming roughly equal proportions of garnet and clinopyroxene. This treatment is obviously a considerable simplification to the actual melting process since this modelling assumes that the melting process is performed in a single batch and also assumes that the compositions of the melts formed during partial melting are the same as those of the actual mineral phases found in the source.

**Global comparisons (see also section 4.8)**

When compared to other MORB, Krafla basalts generally have lower mean values of $SiO_2$ and $Na_2O$, and higher mean values of $FeO^*$ consistent with their derivation from higher average degrees of melting at greater than average pressures (cf. Klein & Langmuir, 1987). The other major element oxides have proved less useful in discriminating between basalts from different regions, because of their sensitivity to the degree of partial melting. However, Klein & Langmuir (1987) also report significant global variation in the $CaO/Al_2O_3$ ratios of basalts, after correction for fractional crystallisation of ol, plag and cpx. Samples from shallow ridges generally have high values of $CaO/Al_2O_3$, whereas samples from deep ridges have low values. Rocks from Krafla have high values of $CaO/Al_2O_3$ (typically 0.78-0.88 for basalts >8 wt% MgO), which is again consistent with large degrees of melting at higher temperatures. According to Klein & Langmuir (1987) the high value of $CaO/Al_2O_3$ reflects larger degrees of melting in the Iceland plume at higher average pressures of melting. In contrast with this McKenzie & Bickle's (1988) model (parameterisation a) predicts little variation in the $CaO/Al_2O_3$ of melts generated at different values of $T_p$ (see section 6.3.1).

The larger average degrees of melting near plumes appear to be confirmed by studies on dredged abyssal peridotite samples (e.g. Dick *et al.*, 1984; Michael & Bonatti 1985). This is shown by the fact that the concentrations of Ti and Zr are lower in clinopyroxenes in peridotite samples from plume environments (e.g. Iceland, Azores) than from non-plume environments. In addition, the concentrations of Ti and Zr in the clinopyroxenes decrease as the modal abundance of clinopyroxene in the samples falls, consistent with increasing degrees of melting near plumes (Johnson *et al.*, 1990).

## 6.2 A quantitative model for melt generation

### 6.2.1. Background

Recent developments in the understanding of the physics of melt generation and extraction at spreading ridges have allowed considerable steps to be taken towards a quantitative model for melt generation at ocean ridges (e.g. Ahern & Turcotte, 1979; Foucher *et al.*, 1982; Richter & McKenzie, 1984; McKenzie, 1984; McKenzie & Bickle, 1988). Most spreading ridges are best regarded as passive features where two plates are separating, with the mantle upwelling in response to the plate separation, rather than because each ridge has a mantle plume beneath it (Watts

*et al.*, 1985). This idea allows melting at ridges to be treated in a simpler manner than for the dynamic case of mantle plumes, where the motion of mantle within the plume has to be considered (Ribe & Smooke, 1987; Liu & Chase, in press 1990; Watson & McKenzie, submitted 1990). As will be discussed below, melting beneath Iceland almost certainly involves a mantle plume, superimposed on the normal ridge structure, although, for simplicity Iceland will be regarded as a simple passive spreading system (albeit with hotter mantle beneath it). The implications of using this model rather than a more numerically-complex dynamic model (so far unsolved) are briefly discussed below.

The model used in this Chapter was produced by McKenzie & Bickle (1988), with the results generated by computer programs written by the above authors and modified by D.M.Latin to run on the Edinburgh "EMAS" computer system. The first premise of the model is that melting at a ridge occurs by adiabatic decompression. This is likely to be a fair assumption, given that the Péclet number of the ridge system is much greater than unity, i.e. heat transport is dominated by advection rather than by conduction. McKenzie & Bickle (1988) also assume that the decompression during adiabatic upwelling is isentropic and that the change in entropy on melting ($\Delta S$) is 250 J $kg^{-1}°C^{-1}$.

The temperature of the adiabatically upwelling mantle is depth dependent and is therefore best expressed in terms of potential temperature ($T_p$). The $T_p$ of the mantle determines the pressure at which the mantle crosses the solidus and begins to melt. In particular, hotter mantle begins to melt at greater pressures than cooler mantle. Once melt has formed then the temperature of the adiabatically upwelling mantle and melt is a function of the melt fraction present, due to the latent heat of melting. Hence McKenzie & Bickle's model calculates both the melt fraction and the resultant geotherm iteratively.

The model divides the melting process into two simple stages. Firstly the top of a column of asthenosphere, equal in thickness to the thickness of the lithospheric plate in thermal equilibrium (~120 km), is brought to the surface and allowed to melt. No relative motion is allowed between melt and matrix during melting. The melt is removed and ponded. The melt so produced should be equivalent to the average thickness and average composition of the oceanic crust. This division into a two-stage process is obviously not physically realistic since it is likely that melt begins to be extracted once a small melt fraction has formed (McKenzie, 1984; Ribe, 1985; McKenzie, 1985a,b; Galer & O'Nions, 1986). This model also assumes that the melt once formed does not re-equilibrate with the mantle above it in the melting column

(see discussion in Chapter 5). The advantage of this simplified melting scheme is that it enables the composition of melts to be predicted from a parameterisation of experimentally-determined batch-melting experiments. This would not have been possible if a physically more plausible process had been chosen (e.g. Rayleigh melting or "dynamic" melting). The limitations of selecting a batch-melting model are referred to below.

If a small portion of mantle (at a given place in the melting column) is converted from solid into melt, by increasing the melt fraction from X to X + dX, then the composition of this melt increment is called the instantaneous melt composition, c. The increments of instantaneous melt, c, may be integrated for a single portion of mantle at constant pressure over a range of different melt fractions. This integrated composition is called the point average composition $C_p$, and is equivalent to the batch-melt composition as determined in experimental studies. These point average compositions can be integrated over the whole melting column (weighted according to the melt fraction present at any given depth) to give the point and depth average composition $C_{pd}$. This is the average composition of all the melt formed in the melting-column.

All these melt compositions (and probably the melt volume) are in fact dependent upon the exact nature of the melting process: if melt is derived by Rayleigh melting or even "dynamic melting" then the composition of the melt will obviously be different from the case of equilibrium batch melting (cf. Chapter 5 for trace elements). However, in order to use experimental data, McKenzie & Bickle (1988) have to assume batch melting, even if Rayleigh or "dynamic" melting is more likely.

The compositions of the batch melts (point average compositions) are taken from experimental melting studies on garnet peridotite (or similar compositions). The choice of experimental starting composition significantly affects the concentrations of some oxides in the melt, especially for the most incompatible elements. This may explain some of the disagreement between various workers over the melting systematics (see section 6.1.3).

The solidus and liquidus temperatures of these experiments are first parameterised as a function of pressure. Then the melt fraction present in the experiments is parameterised as a function of pressure and temperature (by using the dimensionless temperature T′ as defined by McKenzie & Bickle (1988), which is independent of the pressure). The experimental melting compositions (point averages) are then parameterised as functions of T′ and pressure, allowing the point & depth average composition to be calculated. Only MgO, FeO* and $SiO_2$ were found to be

pressure dependent (in parameterisation a in Table A1 of McKenzie & Bickle (1988), which shows the best fit with the MORB data). The pressure dependence of $SiO_2$ arises indirectly from the model since it is calculated by subtracting all the other components from 100%, but is consistent with phase equilibria. McKenzie & Bickle (1988) attempted to make the concentrations of CaO and $Al_2O_3$ pressure dependent but the relevant parameterisation, c, fits the MORB data less well. The estimated errors for parameterisation (a) are shown in Table 6.2. The most successful parameterisation (a) generally produces a satisfactory fit with the most primitive MORB compositions, apart from for $K_2O$ and $TiO_2$. All 3 of McKenzie & Bickle's (1988) parameterisations fail to reproduce the expected melting behaviour of $K_2O$ (and to a lesser extent also $TiO_2$), due to the poor quality of the experimental data and the large variation in the concentrations of $K_2O$ and $TiO_2$ in the starting material.

### 6.2.2 Results

McKenzie & Bickle's (1988) model allows the calculation of the instantaneous, point average, and point & depth average melt compositions formed in the melting column. This section is primarily concerned with the point & depth average compositions, which represent the average composition produced from the whole melting system. The instantaneous melt composition is simply a convenient mathematical representation used in modelling the melting process, derived from the (batch melting) point average compositions. It may bear no close resemblance to melts formed from any given part of the mantle. As has been shown above in sections 6.1.2 and 6.1.3 the point average compositions appear to be useful in understanding the variation in the major element concentrations of the least differentiated Krafla rocks.

The point & depth average compositions are shown in Table 6.2 for different values of $T_p$. McKenzie & Bickle (1988) showed that the point & depth average composition for a $T_p$ of 1280°C is reasonably similar to that of the compositions of the most primitive MORB samples. They concluded, therefore, that the least-differentiated MORBs probably represent primary melts (cf. Green & Ringwood, 1967; O'Hara, 1968b; Presnall *et al.*, 1979; Stolper, 1980). McKenzie & Bickle's (1988) model suggests that large amounts of fractional crystallisation are unnecessary in the formation of the least-differentiated MORBs.

However, the point & depth average compositions of melts formed from mantle with greater values of $T_p$ have increased concentrations of MgO. For example,

if $T_p$ = 1480°C, then the point & depth average melt composition contains ~17 wt% MgO. This is a picritic composition and requires the crystallisation of extensive amounts of olivine before the magma has a similar Fe/Mg ratio to that of least-differentiated lavas actually erupted. McKenzie & Bickle's (1988) model implies that most basalts derived from mantle with a high value of $T_p$ must have undergone significant crystal fractionation before eruption.

**Changes in model melt compositions with $T_p$**

The main effect of increasing the value of $T_p$ from 1280°C through to 1580°C is to increase the concentrations of MgO and FeO* at the expense of all the other oxides. In particular, $Na_2O$ falls from 2.16 wt% at 1280°C, to 1.51 wt% at 1580°C. The reason for the decreasing concentration of $Na_2O$ (and also the other oxides, except for MgO and FeO*) results from the increase in the mean extent of melting, which changes from 13.5% at 1280°C to 24.5% at 1580°C. This means that increased amounts of olivine and orthopyroxene are entering the melt as the value of $T_p$ increases (especially from 1480 to 1580°C, where the proportion of melt generated in the absence of residual cpx is increased), leading to a dilution of all the other components in the melt except MgO and FeO*. It should be noted that different values of $T_p$ in McKenzie & Bickle's model (parameterisation a) fail to generate significant variation in the $CaO/Al_2O_3$ ratio of the melts produced (cf. Klein & Langmuir, 1987).

**Thickness of the oceanic crust**

McKenzie & Bickle's model allows the calculation of melt thickness as a function of the value of $T_p$. Average MORB with a crustal thickness of about 7 km is generated by mantle with a $T_p$ of 1280°C. Due to the uncertainties in the mean oceanic crustal thickness and in the correct value of $\Delta S$, Latin (1990) showed that the likely error is ±40°C. The amount of melt produced is much increased at higher values of $T_p$; e.g. 27 km for 1480°C and 40 km for 1580°C. The higher resistivity layer (i.e. the crust) in NE Iceland is estimated to be about 9 to 16 km thick (Beblo & Björnsson 1980; Björnsson 1985). However, measurements of crustal thickness made in the active rifting zones are likely to underestimate the total amount of melt formed, because the melt presently being generated in the mantle will not be included in the thickness estimate. A more realistic estimate of the total melt formed may be obtained from the off-axis crustal thickness, although this thickness does in fact measure the

melt thickness at some time in the past. Bott & Gunnarsson (1980), using seismic refraction surveys, showed that the crustal thickness in eastern Iceland is about 30 km. This melt thickness is consistent with a value of $T_p$ of about 1480°C (McKenzie & Bickle, 1988).

### 6.2.3. Effects of fractional crystallisation on the results of the model

It has been suggested by various authors (e.g. Courtney & White, 1986; Klein & Langmuir, 1987; Ribe & Smooke, 1987; White & McKenzie, 1989) that mantle plumes are considerably hotter than the average mantle which generates the majority of MORB. Such a mantle plume with an estimated $T_p$ of 1480°C has been suggested for Iceland, both to explain the increased thickness of the oceanic crust and the distinctive chemical composition of the lavas (e.g. McKenzie & Bickle, 1988; White, 1990). However, the effects of fractional crystallisation from a high-MgO starting composition (from mantle with a high value of $T_p$) must be considered before a reasonable comparison can be made between the compositions of Icelandic lavas and McKenzie & Bickle's (1988) point & depth average compositions.

The effects of fractional crystallisation on McKenzie & Bickle's point & depth average compositions for $T_p$ values of 1380, 1480 and 1580°C are presented in section 6.3.1. Fractional crystallisation is modelled using the computer program, MAGMAS (as in section 4.6). A pressure of 3.5 kbar is chosen for the modelling, approximately equivalent to that of the pressure at the apparent base of the oceanic crust beneath NE Iceland, as determined by resistivity measurements (Beblo & Björnsson, 1980). MAGMAS predicts that olivine will be the only liquidus phase for the 1380, 1480 and 1580°C compositions until plagioclase and clinopyroxene are added to the liquidus below 10 wt% MgO (see Figs. 6.5 to 6.8). A variable pressure of fractional crystallisation is unlikely to make a significant difference to the path of liquid evolution, at least while olivine is the only liquidus phase.

The concentrations of most of the oxides in the model compositions change considerably during fractional crystallisation (Figs. 6.5 to 6.8), necessitating correction for fractional crystallisation before attempting to compare Krafla rocks (containing 8-10 wt% MgO) with McKenzie & Bickle's (1988) calculated compositions. The effects of fractional crystallisation are discussed further in section 6.3.

## 6.3 A comparison between the model compositions and the Krafla compositions

### 6.3.1. Results

McKenzie & Bickle's (1988) model compositions contain up to 20 wt% MgO (for 1580°C). It is therefore necessary to account for the differentiation processes which must operate to bring predicted compositions into line with Krafla compositions containing 8-10 wt% MgO. The computer program MAGMAS has been used to correct for the effects of fractional crystallisation and the results of this program are shown in Table 6.2 and Figs. 6.5 to 6.8. The pressure of fractional crystallisation appears to have little effect on the corrected compositions (at least when considering compositions in the range 8-10 wt% MgO). A pressure of 3.5 kbar is felt to be most consistent with estimates of the crustal thickness near Krafla, providing most differentiation occurs at the base of the crust.

Table 6.2 shows that the (f.c. corrected) melt compositions generated at highest values of $T_p$ (1480-1580°C) seem to fit better with the Krafla compositions, although some elements show a poor degree of fit for all values of $T_p$. The degree of fit is judged by comparing the f.c. corrected model compositions with the total spread of Krafla compositions, rather than by comparing the model compositions with an average Krafla composition, which might be significantly affected by sample bias and/or the effects of mixing processes.

Most noticeable is the fact that the f.c. corrected compositions have concentrations of $SiO_2$ which are higher than those observed in Krafla. This suggests that $SiO_2$ is of little use in estimating a value of $T_p$, although the highest $T_p$ values give the closest degree of fit. Reasons for the discrepancy in $SiO_2$ concentrations between model and Krafla compositions are suggested below. The errors in calculating the model values of $K_2O$ and $TiO_2$ are very large, in fact greater than the actual concentrations predicted by the model. This means that both these oxides are little use for comparative purposes, leaving $Al_2O_3$, CaO, $FeO^*$ and $Na_2O$ as the key oxides to be considered.

Both $Al_2O_3$ and CaO vary considerably in the uncorrected point & depth average compositions; decreasing with increasing $T_p$. However, as the value of $T_p$ increases so does the amount of fractional crystallisation needed to reduce the MgO content of the primary melt to that actually seen in the Krafla suite. This extra fractional crystallisation needed for the higher-MgO melts, compared with the lower-MgO melts, leads to a considerable reduction in the differences in concentrations of $Al_2O_3$ and CaO in the f.c. corrected compositions at different values of $T_p$. This

argument also applies to the $Na_2O$ concentrations. The uncorrected $Na_2O$ values range from 2.16 to 1.51 wt% (for $T_p$ = 1280°C to 1580°C respectively) but after correction for fractional crystallisation the differences in composition are much smaller than originally calculated by the model (cf. Figs. 15a and 15c in McKenzie & Bickle, 1988), who ignore the effects of fractional crystallisation on the compositions derived from mantle with values of $T_p$ from 1380 to 1580°C). For example, the fractional crystallisation correction for the 1580°C composition changes its $Na_2O$ value from 1.51 to 2.11 wt% (see Table 6.2).

In contrast with this behaviour, $FeO^*$, is largely unaffected by fractional crystallisation (of olivine, which is the only phase crystallising up to the 8-10 wt% MgO region) and initial differences in $FeO^*$ concentration as a result of variable $T_p$ values, are clearly preserved in the corrected model compositions. The f.c. corrected value of $FeO^*$ increases with increasing $T_p$, in a similar fashion to the uncorrected values of $FeO^*$.

The Krafla primitive compositions (>8 wt% MgO) do vary in composition (see discussion above). This variation may be explained qualitatively by changes in composition due to differences in the extent and pressure of partial melting in the mantle. The ranges in concentration of the major oxides in samples with > 8 wt% MgO are shown in Table 6.2.

As is shown below, the Krafla compositions appear to agree most closely with model compositions derived from higher values of $T_p$, i.e. more than 1280°C (see Figs. 6.5 to 6.8). The Krafla compositions probably fit, within the error on the predicted compositions, with compositions derived from a range of $T_p$ values from 1380 to 1580°C.

$SiO_2$ is higher in all the model compositions than it is in the Krafla compositions, although the higher potential temperature compositions fit most closely with the Krafla data (e.g. for $T_p$ = 1580°C; 51.2±1.2 wt% $SiO_2$ for the predicted compositions cf. 47.2-49.7 wt% $SiO_2$ for the Krafla data). The $SiO_2$ concentration of the uncorrected 1580°C composition, for example, is much closer to that of the Krafla data than the f.c. corrected composition, since the effect of olivine fractional crystallisation is to increase the $SiO_2$ concentration of the melt. The Krafla analyses have a more variable $Al_2O_3$ concentration than the model compositions, perhaps reflecting local melting variation. This variation makes comparison between Krafla and model data difficult and $Al_2O_3$ appears of little comparative use (Fig. 6.5). The high $FeO^*$ contents of the least-differentiated Krafla lavas are consistent with a high

a)

| McKenzie & Bickle (1988) model compositions | | | | | | | | |
|---|---|---|---|---|---|---|---|---|
| | 1280°C | 1380°C | 1380°C$_{corr}$ | 1480°C | 1480°C$_{corr}$ | 1580°C | 1580°C$_{corr}$ | 1580°C$_{lid\ corr}$ |
| $SiO_2$ | 51.89 | 50.94 | 52.96 | 49.34 | 52.18 | 48.03 | 51.23 | 50.78 |
| $Al_2O_3$ | 14.57 | 12.92 | 15.69 | 11.70 | 15.14 | 10.85 | 15.22 | 15.68 |
| $FeO^*$ | 8.53 | 9.07 | 8.92 | 9.75 | 9.40 | 10.40 | 10.32 | 10.09 |
| MgO | 10.26 | 13.94 | 8.16 | 17.27 | 8.45 | 20.01 | 8.34 | 8.10 |
| CaO | 11.01 | 9.93 | 10.84 | 9.04 | 11.61 | 8.40 | 11.68 | 12.02 |
| $Na_2O$ | 2.16 | 1.83 | 2.28 | 1.63 | 2.11 | 1.51 | 2.11 | 2.18 |
| $K_2O$ | 0.25 | 0.22 | 0.28 | 0.21 | 0.27 | 0.19 | 0.27 | 0.28 |
| $TiO_2$ | 0.92 | 0.74 | 0.88 | 0.65 | 0.83 | 0.60 | 0.84 | 0.86 |

b)

| Krafla compositions (≥8 wt% MgO) | |
|---|---|
| $SiO_2$ | 47.20-49.65 |
| $Al_2O_3$ | 14.40-16.34 |
| $FeO^*$ | 9.32-11.60 |
| MgO | 8.00-9.73 |
| CaO | 11.58-13.64 |
| $Na_2O$ | 1.41-2.08 |
| $K_2O$ | 0.04-0.20 |
| $TiO_2$ | 0.69-2.09 |
| MnO | 0.17-0.20 |
| $P_2O_5$ | 0.05-0.21 |

corr = corrected for the effects of fractional crystallisation (at 3.5 kbar).
lid = melting does not occur in the top 10 km of the melting column.

Table 6.2 (a) Variation of point & depth average melt composition with mantle potential temperature ($T_p$) using McKenzie & Bickle's (1988) model, including correction for fractional crystallisation to approximately 8 wt% MgO (using MAGMAS).
(b) The range of major-element compositions for Krafla samples containing at least 8 wt% MgO.

value of $T_p$ (e.g. 1480°C or 1580°C in Table 6.2). Similarly the mean value of FeO* for the whole data-set (corrected to 8 wt% MgO; in the manner of Klein & Langmuir, 1987) of 10.7±1.4 wt% FeO* (1 s.d.) is consistent with such a high value of $T_p$ (Fig. 6.6). Likewise, CaO generally fits better with the higher-$T_p$ melt compositions (e.g. 1480°C, 1580°C) because the compositions derived at higher $T_p$ values appear to begin crystallising plag and cpx at lower values of MgO (see Fig. 6.7). $Na_2O$ concentrations vary considerably in the least-differentiated samples from Krafla (1.41-2.08 wt%; although the lowest value may represent alteration during hyaloclastite formation). The average value of $Na_2O$ (corrected to 8 wt% MgO) for the whole data-set (cf. Klein & Langmuir 1987) is 2.0±0.3 (1 s.d.). This is more consistent with a higher value of $T_p$ than with a lower value, although the Krafla compositions are lower than any of the f.c. corrected compositions. Thus, it appears that when magmas containing 8-10 wt% MgO are compared then the effects of fractional crystallisation will mask compositional differences which are apparent in primary, unfractionated, model compositions. Although mantle of different $T_p$ value may result in different primary magma compositions, these differences may be removed by the differences in the extent of fractional crystallisation. In addition, the differences in $Na_2O$ concentration in compositions formed at different values of $T_p$ (after correcting for the effects of fractional crystallisation) are less than the mean error on $Na_2O$ in the parameterisation (Fig. 6.8). Values of $TiO_2$ and $K_2O$, as discussed above, are little use in discriminating between different values of $T_p$.

It should be pointed out that although these Krafla compositions suggest that the mantle beneath NE Iceland has a higher than normal value of $T_p$ (>1280±40°C), the differences in $T_p$ are not necessarily seen on some of the diagrams as used by McKenzie & Bickle (1988). The Krafla data are plotted on a triangular diagram (Fig. 6.9) taken from McKenzie & Bickle (1988; Fig. 13a), which shows that the Krafla data (> 8 wt% MgO) lie in the middle of the MORB field (data from Elthon, 1989; >9 wt% MgO) and sit on top of the 1280°C melting curve, rather than plotting near the 1380, 1480 or 1580°C melting curves as might be expected from the above discussion. However, this can be explained by considering the effects of fractional crystallisation on the initial model compositions. The 1580°C composition, for example, will initially crystallise only olivine, and take the residual liquid directly away from the olivine corner of the triangular diagram towards the Krafla and MORB data. Hence this diagram will only discriminate between different $T_p$ values, if the primary melt compositions are preserved. This also applies to the other triangular

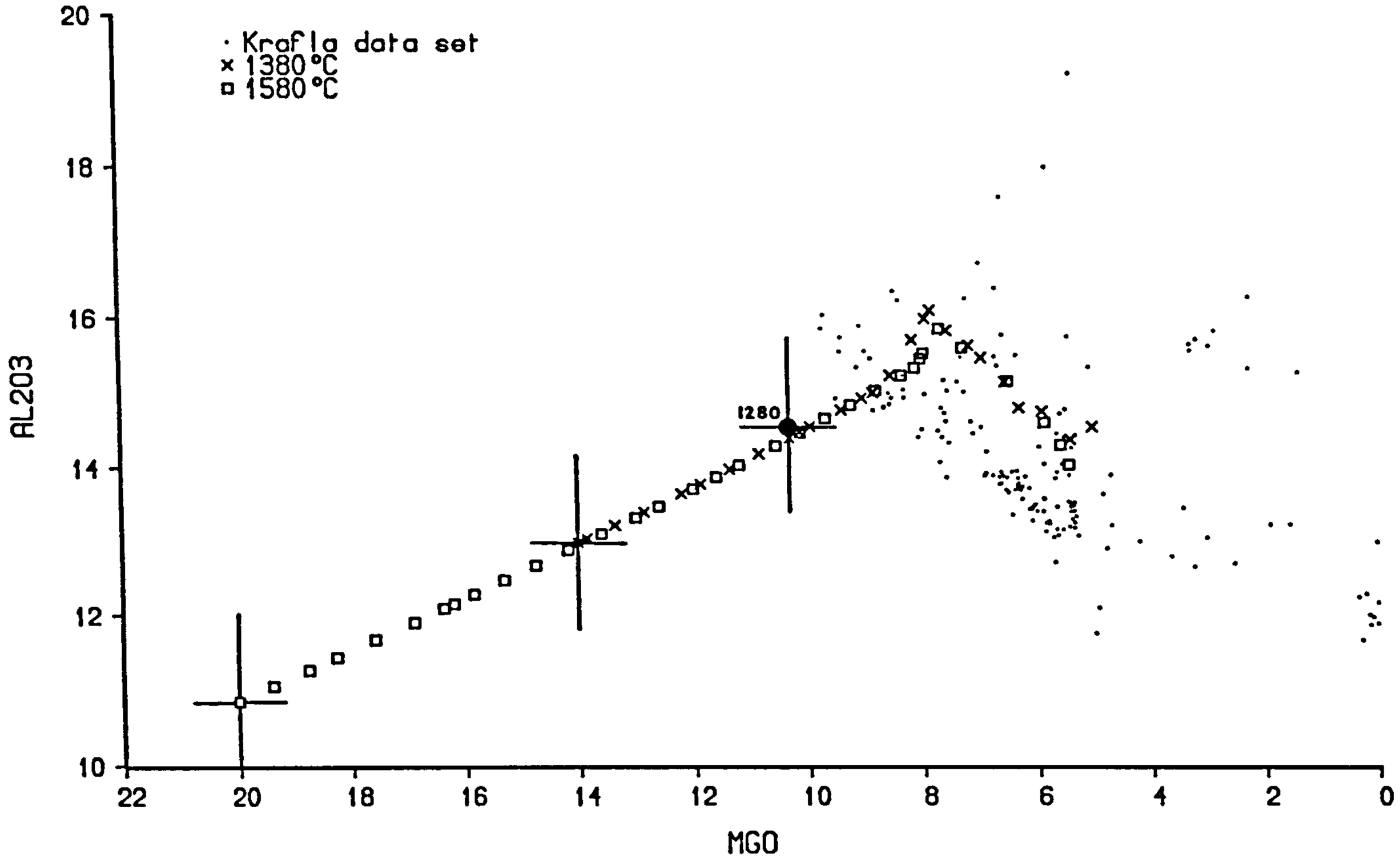


Fig. 6.5 $Al_2O_3$ *vs* MgO showing McKenzie & Bickle (1988) model compositions (with 1σ error bars on model primitive composition; 1280°C, filled circle; 1380°C, crosses; 1580°C, open squares) and the effects of fractional crystallisation using the program MAGMAS on the 1380°C and 1580°C compositions (greater than 5 wt% MgO).

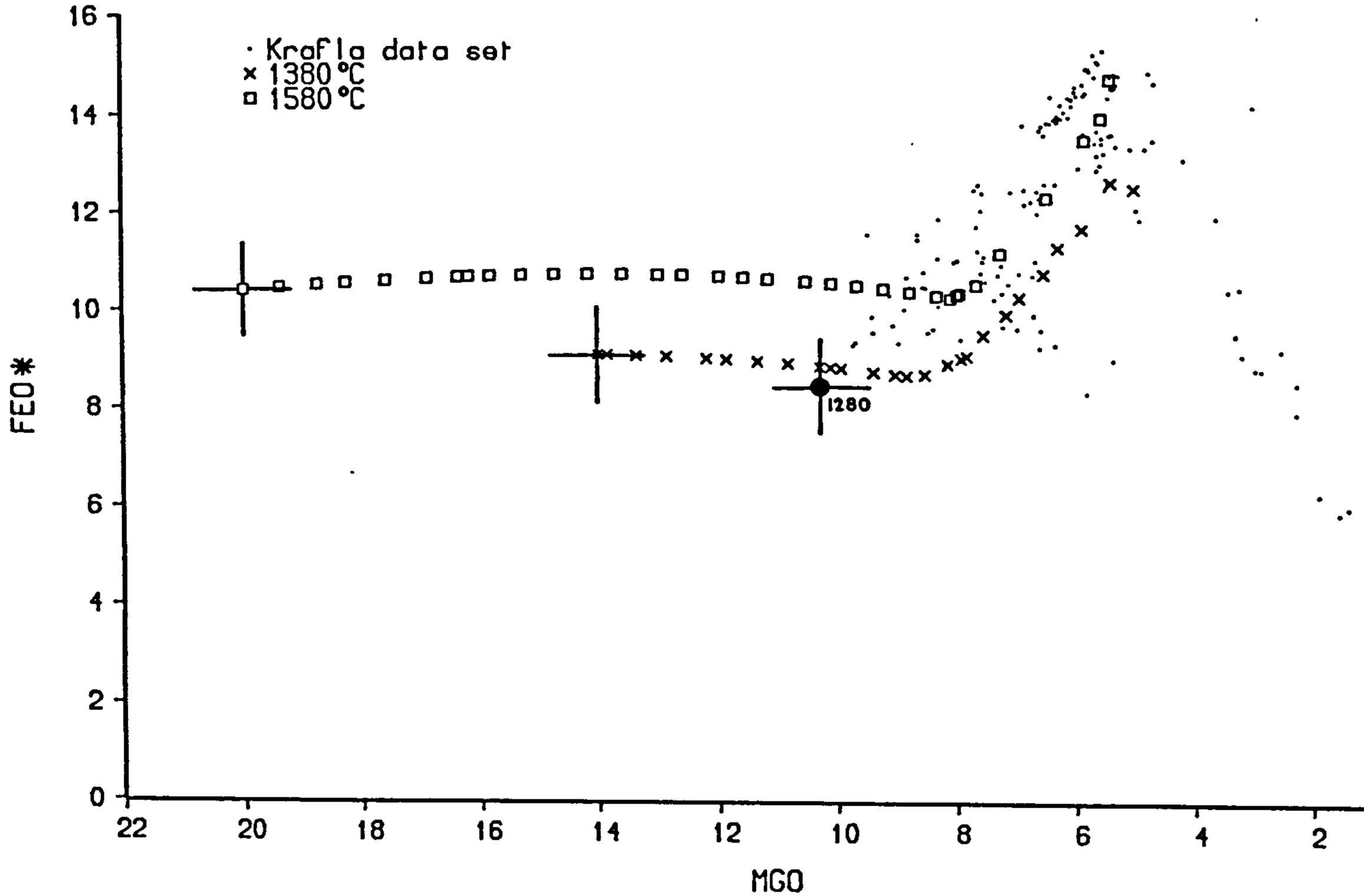


**Fig. 6.6** FeO (total) *vs* MgO; details as for Fig. 6.4.

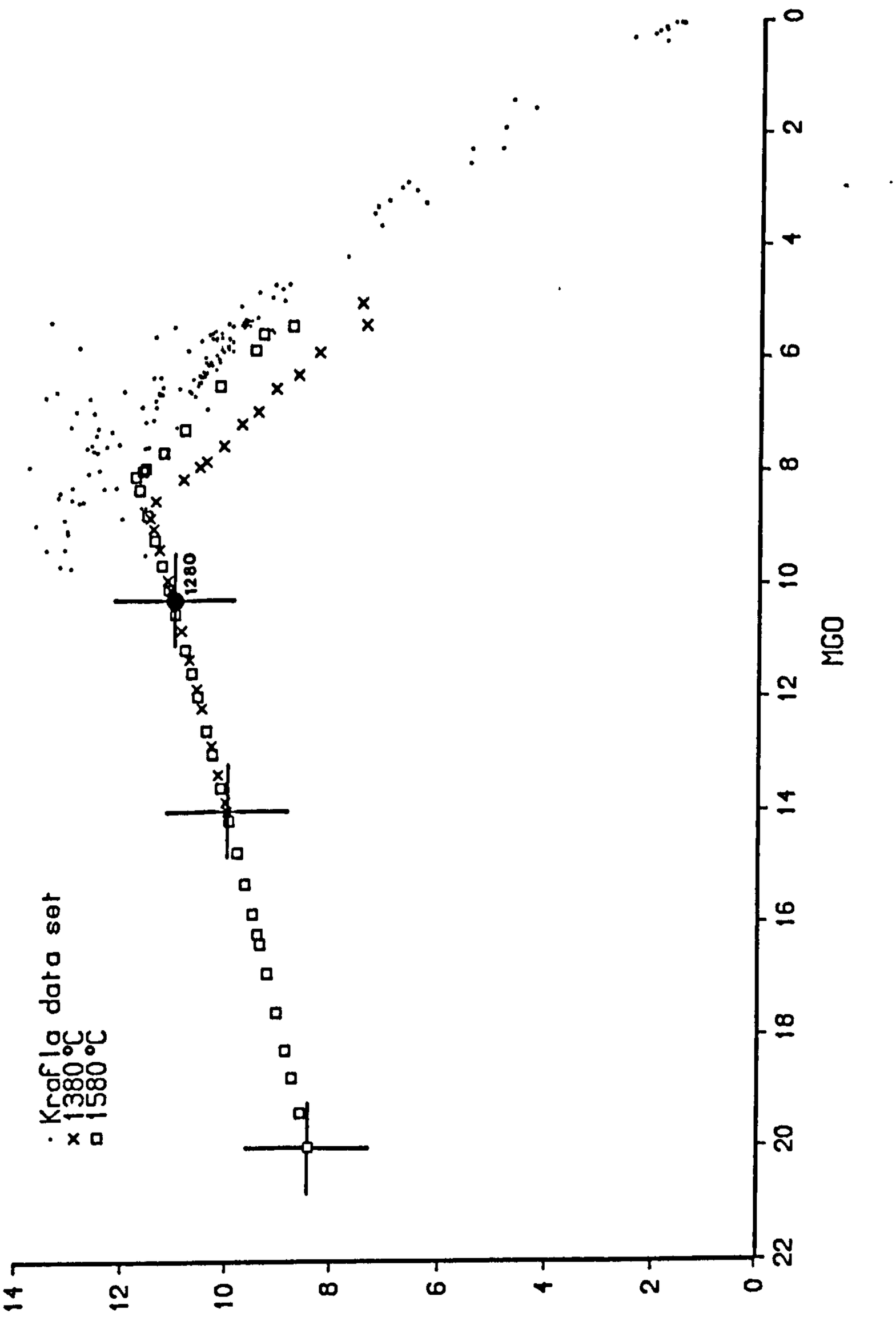


Fig. 6.7 CaO *vs* MgO; details as for Fig. 6.4.

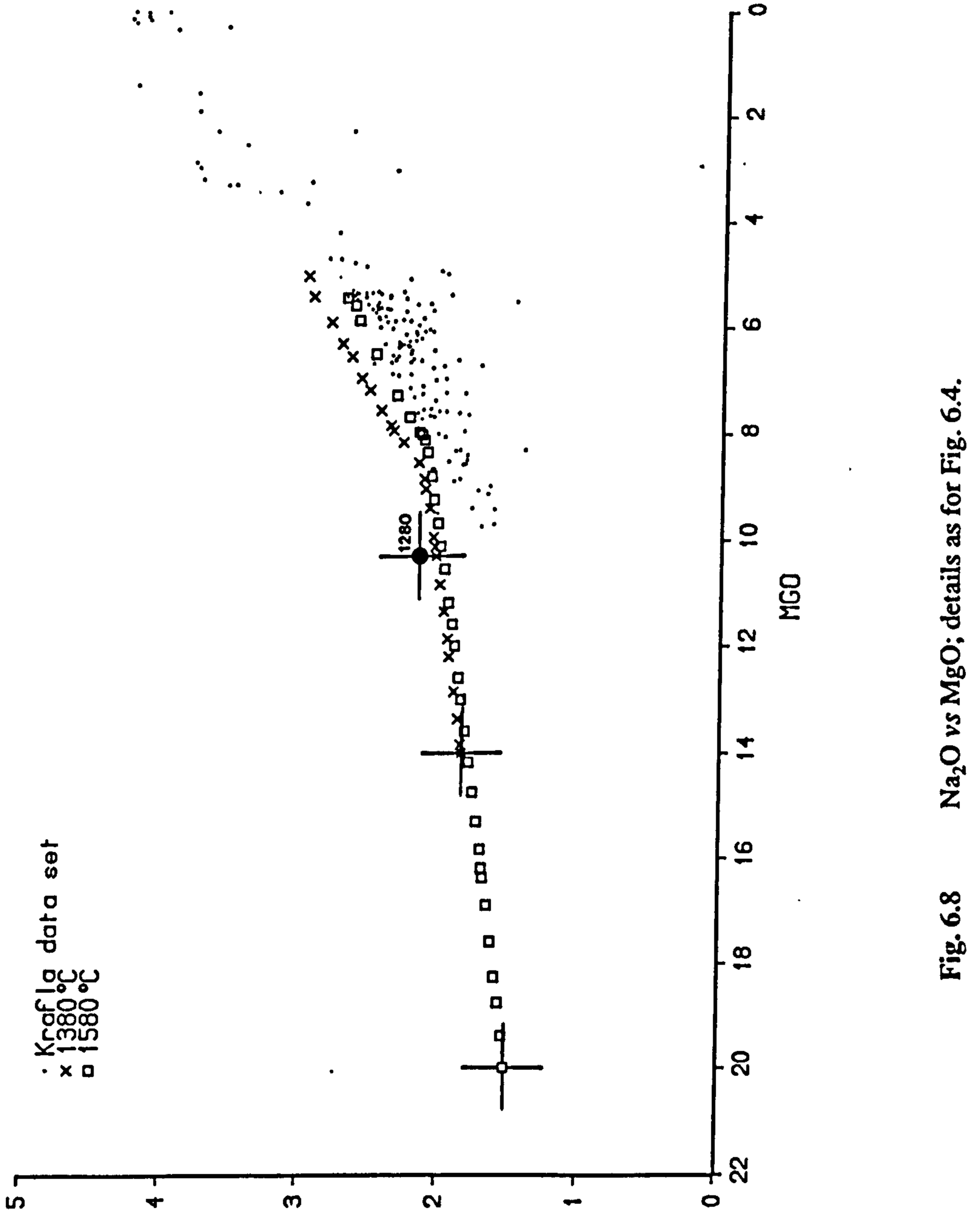


Fig. 6.8 $Na_2O$ *vs* MgO; details as for Fig. 6.4.

**Fig. 6.9** Projection from plagioclase into the field ol-plag-qtz, after McKenzie & Bickle (1988), using the scheme of Walker *et al.* (1979). MORB data (>9 wt% MgO) are taken from Elthon (1989) (open circles) and Krafla data (≥8 wt% MgO) (filled squares) all lie over the 1280°C melting line (solid line) of McKenzie & Bickle (1988). The calculated line of cpx-out is shown by a dashed line, crossing the melting curves in filled circles. The point & depth average compositions are shown by circles containing crosses. Fractional crystallisation of olivine from the 1580°C point & depth average composition is shown by an arrow.

diagrams used by McKenzie & Bickle (1988) in support of the 1280°C $T_p$ value for average MORB.

In conclusion, despite the above reservation regarding the model of McKenzie & Bickle (1988), the compositions of the least-differentiated Krafla samples do appear to favour a higher than normal value of $T_p$, of approximately 1480°C (see discussion over FeO* below). The thickness of melt generated by mantle with such a value of $T_p$ is consistent with the crustal thickness of Iceland.

**Discrepancies between the observed and predicted compositions**

There are several discrepancies between the compositions and melt thicknesses predicted by the model of McKenzie & Bickle (1988) and those observed in Krafla. Possible explanations for these discrepancies are as follows:

**(a) Melting model; batch melting assumption**
**(b) Melting continues to the surface of the Earth**
**(c) Dynamic effects of a mantle plume**
**(d) Pressure dependence of Al and Na concentrations at high pressures**

(a) In order to utilise experimental data, McKenzie & Bickle's (1988) model assumes that melting occurs by equilibrium batch melting. It is thought, however, that the actual melting process is probably closer to Rayleigh or "dynamic" melting (see Chapter 5), in that the maximum melt fraction present before extraction may be as small as 2% (e.g. McKenzie, 1985b; see Chapter 7 for the discussion on the generation of excess ($^{230}$Th)). Application of a batch-melting model is unlikely to reproduce the concentrations of the most incompatible major elements successfully (e.g. K, Ti, P), in the same way as for the incompatible trace elements (see Chapter 5). In addition to affecting the concentrations of the most incompatible elements, the amount of melt generated appears to be dependent on the particular melting model chosen (e.g. McKenzie & Bickle, 1988; Watson & McKenzie, submitted 1990; Latin, 1990). The effects on melt volume of melting processes other than batch melting are unfortunately difficult to quantify. Batch melting will probably overestimate the melt volume.

(b) McKenzie & Bickle's (1988) model also assumes that melting occurs from the dry peridotite solidus continuously to the surface of the Earth. This assumption ignores

the presence of oceanic crust; for melting is unlikely to continue beyond the base of the crust, and may even cease at greater depths (Klein & Langmuir, 1987). In the case of normal thickness oceanic crust, this assumption may have little effect on the composition of the magmas produced, removing only a small proportion of the largest degree melts (i.e. those generated at the lowest pressures). However, in regions of thicker oceanic crust (e.g. Iceland), there may be a discrepancy between the composition as predicted by melting with a "lid", and the composition as calculated by McKenzie & Bickle (1988). The effects of applying a 10km thick "lid" to the melting column, simply by integrating the point average melt compositions without any contributions from the top of the melt column, are shown in Table 6.2. This method is an approximation to the actual effects of a "lid" but gives a first-order indication of the changes in composition of the integrated melt composition when the melts derived at low pressures are removed from the integration. The concentrations of $FeO^*$ and $SiO_2$ decrease in the f.c. corrected 1580°C melt composition with a "lid" and the concentrations of all the other oxides increase. The fit between the Krafla compositions and the model compositions is only significantly improved for $SiO_2$, suggesting that although the application of a "lid" to the melting column may be relevant, the effects of a "lid" are not enough to explain all the chemical differences between the Krafla and model data.

(c) It is most important to note that the model does not consider the dynamic effect of a mantle plume, i.e. passing more mantle into the melting column than would be expected by passive adiabatic upwelling. The presence of a plume, therefore, tends to increase the melt thickness for a given value of $T_p$. In addition, there should be considerable lateral variation in $T_p$ across a broad mantle plume (White & McKenzie, 1989), with lower values of $T_p$ near the edges of the plume. Watson & McKenzie (submitted, 1990) modelled the Hawaiian plume using a stationary steady-state axisymmetric plume, with a central $T_p$ value of 1546°C, under a solid conducting lithospheric lid. They calculated the mean Hawaiian tholeiite composition by integrating the melt compositions produced across the plume at different values of $T_p$. In addition, they modified McKenzie & Bickle's (1988) parameterisation (a) to take better account of the melts generated by small degrees of melting at higher pressure, by including primitive Hawaiian tholeiite data in their parameterisation. This significantly improved the fit between model and Hawaiian compositions. However, this step is apparently an example of circularity, but Watson & McKenzie justify their use of the Hawaiian data by stressing that its inclusion hardly modifies the fit of the

overall parameterisation and still enables them to generate MORB. In particular the concentrations of $Na_2O$ and $Al_2O_3$ are decreased and FeO* is increased by the new version of the parameterisation.

Watson & McKenzie also show that the presence of a plume enhances the proportion of the melt in the point & depth average composition derived by small degrees of melting. The increased proportion of melt derived by small degrees of melting probably arises from the edges of the plume at depth (Oxburgh, 1980), where the values of $T_p$ (and hence the extent of melting) are lower than in the centre of the plume. The extra contribution from small melt fractions from the edges of the Icelandic plume may lead to increased concentrations of, for example, $K_2O$, $TiO_2$ and the more incompatible trace elements (e.g. enrichment in LREE over HREE). However, since the primitive Krafla samples show a correlation between FeO* and $K_2O$ (Fig. 6.2a), this may imply that the relatively high FeO* values (and low $SiO_2$ values, which are also pressure and melt fraction dependent) in the Krafla basalts also reflect the preferential sampling of small melt fractions under the Iceland plume (cf. O'Hara, 1985) rather than solely the effects of high mantle potential temperature (cf. Galer & O'Nions' (1986) argument in Chapter 5, regarding trace element characteristics of MORB).

As mentioned above, an additional effect of the presence of a mantle plume is to alter the volume of melt produced for a given mantle potential temperature. If the rate of plume upflow exceeds the rate of passive plate separation then more melt will be produced for a given $T_p$ than the model of McKenzie & Bickle (1988) will predict. Unfortunately the numerical solution to the above problem remains unsolved.

(d) The most successful parameterisation of McKenzie & Bickle (parameterisation (a)) does not contain pressure dependence for the melt concentrations of Al and Na. However, Walter & Presnall (1990) show that the jadeite component in clinopyroxene becomes significant at higher pressures. This means that melt derived at high pressure is likely to have a lower concentrations of $Al_2O_3$ and $Na_2O$ than the concentrations originally calculated by McKenzie & Bickle (1988). This may mean that a lower estimate of $T_p$ can be made for the Krafla suite, when compared with the original model of McKenzie & Bickle (1988).

### 6.3.2. Conclusions

Application of the model of McKenzie & Bickle for melt generation suggests that the mean mantle potential temperature beneath NE Iceland is higher than for most MORBs. The Krafla compositions are consistent with a value of $T_p$ of at least 1380°C, and may require a $T_p$ as high as 1580°C. This value of $T_p$ is estimated from the model compositions after correction for fractional crystallisation. The effects of correcting for fractional crystallisation are to reduce the ability of the McKenzie & Bickle model to discriminate between different values of $T_p$. The values of $Na_2O$ and $Al_2O_3$ are generally too high for any reasonable estimate of $T_p$, although the concentrations of these oxides are more consistent with a higher estimate of the value of $T_p$. $FeO^*$ is little affected by fractional crystallisation, and probably provides the best discriminator of mantle potential temperature.

The primitive Krafla compositions calculated by the model for a 1580°C value of $T_p$ contain ~20 wt% MgO (and 17% for 1480°C), and therefore must undergo substantial amounts of olivine fractional crystallisation before eruption. The steady-state crustal thickness of Iceland is about 30 km, which would be consistent with a value of $T_p$ of about 1480°C. Discrepancies between the model compositions and the Krafla compositions may be explained by the dynamic effects of melting in a mantle plume and/or by differential sampling by the plume of melt derived from small melt fractions (e.g. leading to increased $FeO^*$ concentrations). These effects could lead to a lower estimate for $T_p$ for NE Iceland, but are difficult to quantify.

## 6.4 Conclusions

Primitive lavas from Krafla show evidence for mantle processes, which appear consistent with data from experimental melting studies. The Krafla compositions appear to be derived from variable amounts of melting at different pressures, with the smallest degree melts being generated at the highest pressures. The incompatible elements (e.g. $K_2O$) appear to be "coupled" to the major elements (e.g. $FeO^*$) (cf. Schilling, 1975; White & Schilling, 1978; Viereck *et al.*, 1989).

The model of McKenzie & Bickle (1988) calculates the compositions of melts generated at ocean ridges by passive upwelling for different values of $T_p$. The effects of fractional crystallisation are considered before comparing the Krafla primitive compositions with those of the model compositions. After correction for fractional crystallisation the model is much less able to discriminate between melts derived from different values of $T_p$. However, the Krafla compositions seem most consistent with a

$T_p$ of about 1480°C. Discrepancies between predicted and observed compositions may be qualitatively explained by considering the effects of the shape, flow and thermal structure of a mantle plume on the volume and composition of melt.

# Chapter 7

# Isotope geochemistry

## 7.1 Oxygen isotopes

### 7.1.1 Background

Analysis of $^{18}O/^{16}O$ ratios (commonly expressed as $\delta^{18}O_{SMOW}$ - hereafter written as $\delta^{18}O$) can help considerably in the understanding of igneous phenomena (Faure, 1986; Taylor & Sheppard, 1986), enabling the investigation of processes, such as crustal assimilation, which show little effect on the major- or trace-element concentrations. Although the absolute range of igneous $\delta^{18}O$ values is small (-2 to +16‰) the relative differences between rocks in a suite have petrogenetic significance. A range of $\delta^{18}O$ values results from the action of one or more of the following types of process:

(1) Mantle melting processes and the effects of source heterogeneity
(2) Closed-system effects during magmatic crystallisation
(3) Open-system effects during magmatic crystallisation (e.g. crustal assimilation)
(4) Disequilibrium effects and magma mixing
(5) Effects of volatiles
(6) All these magmatic processes may be succeeded by sub-solidus alteration of the rocks they produce.

These different types of process have distinct effects on the oxygen isotope ratios of magmas, which are discussed with reference to the Krafla data in section 7.1.5. The $\delta^{18}O$ values are best combined with other geochemical data (e.g. major and trace-element compositions and other isotopic ratios) in order to extract the maximum amount of information about magma genesis. Accordingly the $\delta^{18}O$ values are discussed in this way.

Generally most magmatic values of $\delta^{18}O$ lie in the range +5 to 11‰, with MORB values forming a relatively tight cluster about 5.7±0.3‰. Taylor & Sheppard (1986) pointed out that unusual circumstances are probably required to explain $\delta^{18}O$ values less than +5.5‰. However, lower temperature effects, such as those involved in point 6 above, must be first eliminated before proceeding to invoke special processes (cf. Taylor & Forester, 1971,1979). In Iceland many fresh volcanic samples have low $\delta^{18}O$ values (+1.8 to +5.7‰, which do not however appear to be explicable by low-temperature effects, because the rocks are so fresh and phenocrysts seem to be

in isotopic equilibrium with the groundmass. Hence it looks likely that these low $\delta^{18}O$ values represent true magmatic values. Muehlenbachs *et al.* (1974) pointed out that some kind of interaction with crust previously depleted in $^{18}O$ by hydrothermal activity was plausibly capable of generating such low $\delta^{18}O$ values. It is possible that comparable processes occur more widely (Gregory & Taylor, 1981) but are only distinguished in Iceland by the combination of sub-aerial rifting and low $\delta^{18}O$ values of meteoric water characteristic of high latitudes.

This section concerns the $\delta^{18}O$ values of fresh recent Krafla lavas. The $\delta^{18}O$ data are combined with other geochemical information in order to investigate the $^{18}O$-depletion process.

Most Krafla lavas have few phenocrysts (<3%), although some samples contain plagioclase in greater modal proportions (section 3.2.6). Plagioclase crystals were separated from the groundmass for samples containing sufficient quantities of phenocrysts and analysed for their $\delta^{18}O$ values. Unfortunately because of the relatively fine-grained nature of the Krafla lavas, no other phenocryst phases are readily separable from Krafla samples.

The $\delta^{18}O$ analysis of phenocryst phases is capable of revealing the temperature of the $^{18}O$-depletion process (O'Neil, 1986). Mineral-melt $^{18}O/^{16}O$ fractionation factors are small at magmatic temperatures, which mean that minerals crystallised from a melt initially low in $^{18}O$ will have $\delta^{18}O$ values close to that of the magma they are in equilibrium with (as recorded by the whole-rock analysis). However, if sub-solidus exchange has occurred plagioclase phenocrysts are unlikely to have $\delta^{18}O$ values similar to the whole-rock because plagioclase more rapidly exchanges oxygen with an external fluid than other tholeiitic mineral phases. Hence at say 400-500°C plagioclase in these circumstances is the phase most depleted in $^{18}O$.

### 7.1.2 Analytical techniques

Selected lava and scoria samples from Krafla were analysed for oxygen isotope ratios. Samples were chosen to cover the full range of chemical compositions from Krafla (from the least-differentiated basalts through to rhyolites) across the whole of the volcanic system (from the caldera to the fissure swarms). Only relatively recent material which showed no signs of alteration (as estimated from handspecimen and thin section) was used for $\delta^{18}O$ analysis. Therefore, most of the material analysed consisted of postglacial scoria or lava (avoiding the oxidised tops of flows). Several samples from the recent eruptive cycle (1975-84) were collected within hours of eruption and are compared with older postglacial lava flows. Only one sample of

postglacial rhyolite (KK56) has been collected from the Krafla volcanic centre. Therefore, in order to increase the $\delta^{18}O$ data available on the most differentiated products, several glacial obsidians have also been analysed. These obsidians come from the cores of glacial domes and are free from obvious signs of alteration. Apart from these obsidians, glacial samples were generally avoided in order to minimise the chances of confusing low values of $\delta^{18}O$ arising from the effects of surficial interaction of magma/rock and meteoric water with low magmatic values.

$\delta^{18}O$ analyses were undertaken at the S.U.R.R.C. (East Kilbride). Details of the analytical procedures are given in Borthwick & Harmon (1982). Obtaining reproducible results was a problem for some samples. It has been noted by several authors (e.g. Taylor & Sheppard, 1986; Halliday *et al.*, 1988) that this is especially the case for samples containing a high proportion of mafic minerals. Longer furnace reaction times appeared to improve the reproducibility for some samples. Generally, at least three separate aliquots of powder were analysed from each sample in the attempt to achieve reproducible results. The results of the analyses of separate aliquots were averaged when they were within $\pm 0.2‰$ of each other. If necessary more determinations of the same powder were made until a consistent result was obtained. This was most difficult for the most iron-rich samples, or the evolved basalts.

The quartz standard NBS28 was analysed and gave a $\delta^{18}O$ value +9.4‰, which compares reasonably with values obtained in other laboratories (A.E.Fallick personal communication, 1988).

### 7.1.3 Results

**a) Whole-rock samples**

The $\delta^{18}O$ results of selected Krafla postglacial lavas (and some glacial obsidians) are shown in Table 7.1a. $\delta^{18}O$ values vary from +1.0 to +4.7‰. The Krafla results are all less than the range of values for MORBs (+5.7±0.3‰; Taylor & Sheppard, 1986). These Krafla $\delta^{18}O$ results are similar to those presented by Muehlenbachs *et al.* (1974), Condomines *et al.* (1983) and Hemond *et al.* (1988). The above authors addressed the problem of low-$^{18}O$ lava by studying oxygen isotope ratios on a regional scale. This thesis is concerned with the lava $\delta^{18}O$ variation within one volcanic centre, eliminating the need to consider regional factors and allowing concentration on the $^{18}O$-depletion process in greater detail.

**(b) Plagioclase mineral separates**

Mineral separates of plagioclase were obtained from Krafla samples which contain more than approximately 2% modal plagioclase phenocrysts/xenocrysts. The samples were divided into those from the postglacial period and those from the last glacial period. Plagioclase phenocrysts/xenocrysts were separated from other phases and from the groundmass using electromagnetic separation techniques (using a Frantz Isodynamic magnetic separator - model L1) as described by Dymoke (1988). The crystals were further subdivided by using sieves of the mesh range 80-120. Petrographic observations made in Chapter 3 suggest however that crystals of this size are xenocrystal ($An_{80-90}$) (i.e. in chemical disequilibrium) and may not necessarily be in isotopic equilibrium with the present groundmass. True plagioclase phenocrysts (i.e. those in chemical equilibrium with the groundmass) are much more difficult to separate from the Krafla rocks because they tend to be much smaller.

The results are shown in Table 7.1b. $\delta^{18}O$ values range from +4.1 to +5.1‰ and there is no noticeable difference between glacial and postglacial samples. Differences between whole-rock and mineral $\delta^{18}O$ values {$\Delta^{18}O$} are also shown in Table 7.1b and range from +1.25 to -0.02‰ (cf. average error of $\pm$0.4‰). Samples from the glacial period have generally larger $\Delta^{18}O$ values than from the postglacial period (average of +0.7‰ for glacial samples compared with +0.3‰ for postglacial samples).

The $\Delta^{18}O$ values from the postglacial period are within error consistent with $^{18}O$-depletion at magmatic temperatures (Kyser, 1986). However, detailed interpretation based on these values should be undertaken with caution because all these plagioclase samples are xenocrystal in origin and may tell little about the $^{18}O$-depletion of the surrounding groundmass. The glacial samples appear to show in 3 cases (out of only 4 in total) higher values of $\Delta^{18}O$ than are consistent with magmatic depletion (i.e. at 1100-1200°C, $\Delta^{18}O$ should be of the order of $\pm$0.5‰). This may be the result of the interaction of surface waters directly with the magma, and not sub-solidus O-isotope exchange, which would tend to preferentially lower the plagioclase values relative to the groundmass. Alternatively it is possible that the glacial xenocrysts have a different origin from the postglacial xenocrysts. As there are few suitable plagioclase-bearing samples available for study, this hypothesis is difficult to test.

a) Whole-rock samples

| Sample | MgO wt% | $\delta^{18}O$ | C/NC |
|---|---|---|---|
| KK58 | 9.73 | 4.33 | NC |
| KK50 | 9.41 | 4.67 | NC |
| 84-19 | 8.66 | 4.38 | NC |
| SNA24 | 8.65 | 4.54 | NC |
| SNA26 | 7.71 | 4.22 | C |
| KK54 | 7.65 | 4.14 | NC |
| KK55 | 7.60 | 4.18 | NC |
| 84 | 7.60 | 4.14 | C |
| KK152 | 7.58 | 3.81 | C |
| KK92 | 6.91 | 3.70 | NC |
| KK51 | 6.68 | 3.80 | NC |
| KK148 | 6.63 | 3.86 | NC |
| KK115 | 6.44 | 3.76 | C |
| KK113 | 6.39 | 3.92 | C |
| KK130 | 6.27 | 3.38 | C |
| KRA118 | 6.09 | 3.74 | C |
| 84-05 | 5.86 | 4.05 | C |
| KK101 | 5.80 | 4.20 | C |
| KK37 | 5.36 | 3.19 | C |
| KK107 | 5.36 | 2.99 | C |
| KK35 | 3.32 | 3.46 | NC |
| KK26 | 1.92 | 2.11 | C |
| KK25 | 1.57 | 1.87 | C |
| KK34 | 1.43 | 3.28 | NC |
| KK56 | 0.31 | 2.19 | C |
| KK67 | 0.17 | 0.97 | C |
| IC9 | 0.04 | 2.38 | C |
| KK29 | 0.04 | 1.53 | C |

Errors for $\delta^{18}O$ are approximately $\pm$ 0.2 ‰.
C = sample from near the caldera or the central area.
NC = sample from north and south of the central area.

b) Plagioclase separates

| Sample | $\delta^{18}O_{plag}$ | $\delta^{18}O_{wr}$ | $\Delta$ | PG/G |
|---|---|---|---|---|
| KK18 | 4.56 | 3.31 | 1.25 | G |
| KK28 | 4.48 | 3.54 | 0.96 | G |
| KK33 | 4.44 | 3.38 | 1.06 | G |
| KK19 | 4.30 | 3.98 | 0.32 | G |
| KK32 | 4.11 | 4.13 | -0.02 | G |
| KK55 | 4.31 | 4.18 | 0.13 | PG |
| KK54 | 4.12 | 4.14 | -0.02 | PG |
| KK50 | 5.08 | 4.67 | 0.39 | PG |
| KK51 | 4.31 | 3.80 | 0.51 | PG |
| KK92 | 4.17 | 3.70 | 0.47 | PG |

$\Delta = \delta^{18}O_{plag} - \delta^{18}O_{wr}$ (‰)
PG/G = postglacial/glacial sample

**Table 7.1** O-isotope ratio results for selected samples from the postglacial and last glacial periods.

### 7.1.4 Variation of $\delta^{18}O$ values with whole-rock composition and geographic location.

$\delta^{18}O$ values (whole-rock unless otherwise stated) are plotted against MgO in Fig. 7.1. There is a good correlation between the $\delta^{18}O$ value and the MgO content of the lavas/obsidians. At high values of MgO (e.g. 8.6-9.7 wt%) the $\delta^{18}O$ values range from +4.4 to +4.7‰ (considerably less than values for most MORBs). The $\delta^{18}O$ values decrease as MgO falls, reaching values as low as +1.0 to 2.4‰ in the rhyolites. There is considerable scatter in the values of $\delta^{18}O$ at a fixed MgO content. For example, at 6 wt% MgO the total variation in $\delta^{18}O$ is about 1.0‰, and between 2 and 0 wt% MgO about 1.4‰. This scatter is more than would be expected solely from analytical error (about $\pm$0.2‰).

A graph of $\delta^{18}O$ *vs* $K_2O$ is shown in Fig. 7.2, in order to compare the data from this study with those obtained by Muehlenbachs *et al.* (1974). The $\delta^{18}O$ values decrease as $K_2O$ values increase, confirming the relationship discovered by Muehlenbachs *et al.* (1974). However this plot shows that the Krafla $\delta^{18}O$ *vs* $K_2O$ trend is clearer than that shown by Muehlenbachs *et al.*'s (1974) data. This is probably because this study has concentrated on data from one volcanic system, thus minimising regional differences in $K_2O$.

**(b) Geographic variation**

The distribution of $\delta^{18}O$ values with geographic location is shown in Fig. 7.3. The $\delta^{18}O$ values are generally lower nearer the caldera, although there are higher values present as well. This poor correlation between $\delta^{18}O$ and geographic location contrasts with the relatively clear correlation between $\delta^{18}O$ and MgO. Therefore, the lower values of $\delta^{18}O$ on average near the caldera (see Fig. 4.14) may reflect the greater abundance of more-differentiated lavas in that position than in the fissure system. As is discussed below, the formation of evolved magmas is aided by the assimilation process, suggesting that greater amounts of assimilation occur near the caldera. Evidence from Askja (Macdonald et al., 1987) shows that basalts erupted 60 km north of the caldera have much higher $\delta^{18}O$ values than similarly-evolved examples in the caldera (+5.5‰ cf. +3.0 to 3.6‰). The data from Askja suggest that either the $^{18}O$-depletion process is localised relatively close to the caldera or the source of $^{18}O$-depleted material is restricted to areas near the caldera. Unfortunately no volcanic material was collected from Krafla at a comparable distance to the Askja example.

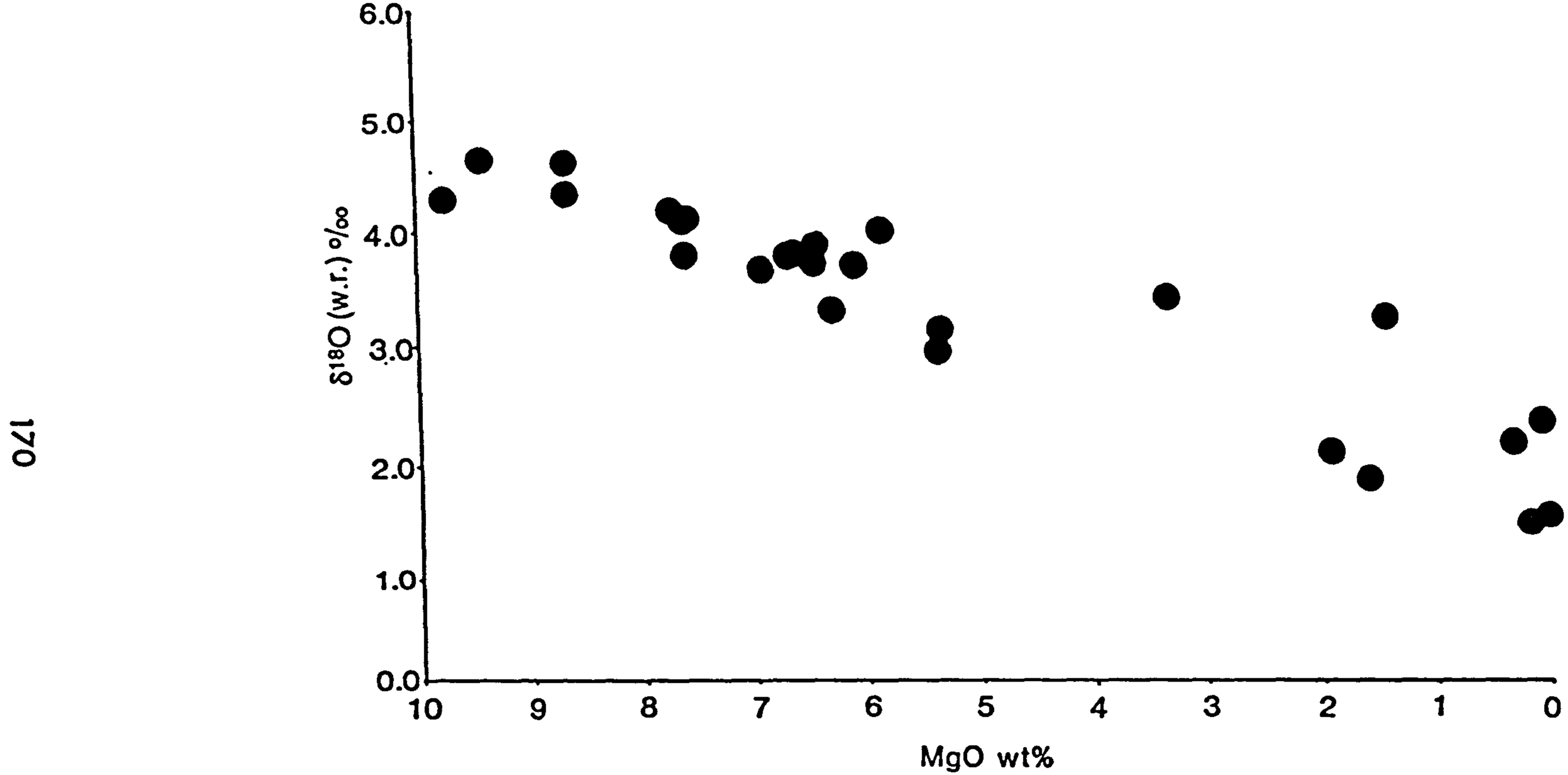


Fig. 7.1 $\delta^{18}O$ values (‰) (whole-rock) plotted against MgO (wt%) for postglacial and some glacial samples (glassy rhyolites). Approximate errors on the $\delta^{18}O$ values are ±0.2‰.

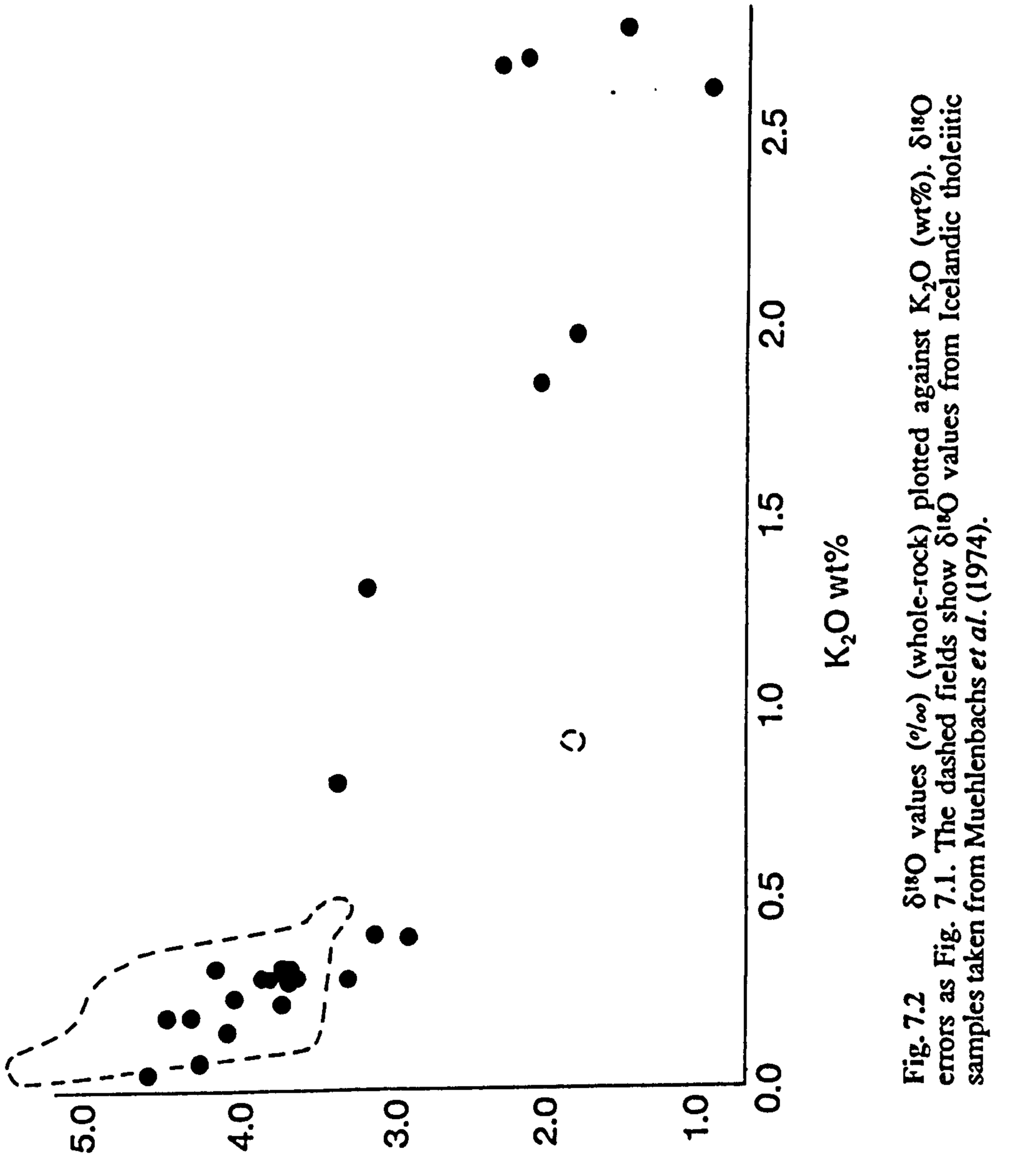


Fig. 7.2 $\delta^{18}O$ values (‰) (whole-rock) plotted against $K_2O$ (wt%). $\delta^{18}O$ errors as Fig. 7.1. The dashed fields show $\delta^{18}O$ values from Icelandic tholeiitic samples taken from Muehlenbachs *et al.* (1974).

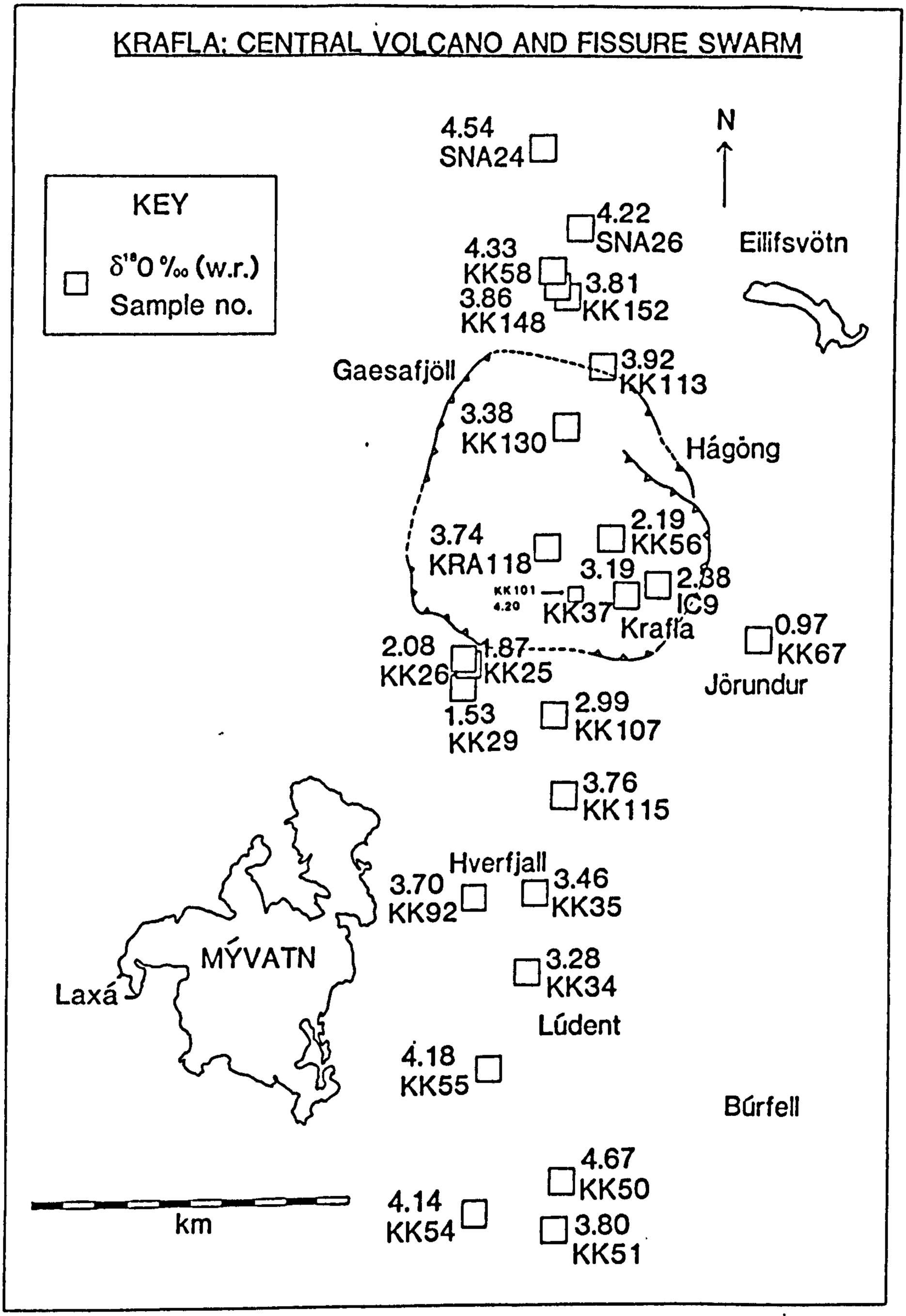


Fig. 7.3 The distribution of $\delta^{18}O$ values (‰) (whole-rock) with geographic location in the Krafla volcanic system. $\delta^{18}O$ errors as Fig. 7.1.

### 7.1.5 Origin of low-$^{18}O$ lavas

Low-$^{18}O$ lavas have been identified from several localities (Taylor & Sheppard, 1986) but Iceland provides some of the most well-known examples. The Krafla suite of lavas is similarly depleted in $^{18}O$ when compared with those samples analysed by Muehlenbachs *et al.* (1974) and Hemond *et al.* (1988). There have been several possible models proposed for the production of low-$^{18}O$ lavas, at the surface, or near it (or even kilometres below):

(1) Sub-solidus alteration by meteoric fluids
(2) Low-$^{18}O$ primary mantle melts (perhaps associated with a mantle plume)
(3) Direct interaction of low-$^{18}O$ meteoric water with magma
(4) Partial fusion of oceanic crust
(5) Bulk assimilation of oceanic crust (as in (4))

**(1) Sub-solidus alteration**

There are several reasons to believe that the Krafla low-$^{18}O$ lavas represent low-$^{18}O$ magmas and are not the result of sub-solidus alteration processes (see section 7.1.1). Firstly these lavas and scoria fragments are very fresh. Some of the scoria samples were collected within hours of eruption (e.g. 84-19, 84 and 84-05) and show $\delta^{18}O$ values comparable to older postglacial lava flows (for a given MgO content). Secondly, because plagioclase $\delta^{18}O$ values are usually higher than whole-rock values the $^{18}O$-depletion process is unlikely to have occurred at lower than magmatic temperatures. Thirdly, the correlation between $\delta^{18}O$ and MgO suggests that the depletion process is related to processes that produce magma differentiation. Such a correlation is hard to explain if $^{18}O$-depletion takes place by interaction of rock and meteoric water.

**(2) Low-$^{18}O$ primary mantle melts**

The mantle source beneath Iceland from which its basalts are derived has long been recognised to be slightly different from the MORB sources to the north and south of the island (see section 7.3). It has been suggested that the development of low-$^{18}O$ lavas might be directly caused by low-$^{18}O$ mantle beneath Iceland or through the activity of special O-isotope fractionation processes during melting. However, Muehlenbachs *et al.* (1974) and Sigvaldason (1974a) effectively dismissed this idea in an investigation of the distribution of $\delta^{18}O$ values across the whole of Iceland. The discovery of low $\delta^{18}O$ values and "normal MORB" $\delta^{18}O$ values within kilometres of each other is difficult to reconcile with the model of a low-$^{18}O$ mantle source, unless the mantle (±special processes) has had varied values of $\delta^{18}O$ over length scales of

only a few kilometres. This opinion is strengthened by the $\delta^{18}O$ correlation with MgO, which would be very difficult to explain by source variation.

**(3) Direct interaction of low-$^{18}O$ meteoric water with magma.**

Several authors have suggested that changes in $\delta^{18}O$ value by direct water interaction are unlikely, although a few studies suggest that in special circumstances it may be possible (e.g. Lipman & Friedman, 1975; Hildreth, 1981). Taylor & Forester (1979) presented data from the Skaergaard intrusion suggesting that meteoric water from the intrusion's hydrothermal system does not enter the magma body until the magma has solidified. There is no evidence that $\delta^{18}O$ values of mineral separates indicate lower than normal-mantle $\delta^{18}O$ values of the magma (such information is gained from studying minerals with slow rates of isotopic exchange with external fluids, which can preserve original magmatic $\delta^{18}O$ values, even after considerable hydrothermal alteration). Most of the intrusion, however, does show evidence (from minerals with faster rates of isotopic exchange) for interaction with meteoric water at sub-solidus temperatures. Hence Taylor & Forester (1979) concluded that the meteoric fluids did not enter the magma body until it was solid, and fluid penetration could occur along fractures.

In addition, Taylor & Sheppard (1986) suggested that the large volume of water required to achieve $^{18}O$-depletion observed in the Icelandic lavas was inconsistent with the relatively dry nature of the Icelandic magmas. Marsh (pers. comm. in Taylor & Sheppard (1986)) also proposed that this was improbable in any event as the time required to diffuse water in the required quantity into a magma body was about $10^4$ times longer than the time required for the magma to crystallise completely. This argument is based on the ratio of the chemical diffusivity of water in basaltic magma ($\sim 10^{-6}$ $cm^2s^{-1}$) to the magma's thermal diffusivity ($\sim 10^{-2}$ $cm^2s^{-1}$)

**(4) and (5) Crustal assimilation**

Both partial fusion and bulk assimilation of low-$^{18}O$ country rock coupled to fractional crystallisation can generate lower $\delta^{18}O$ values in magmas as crystallisation proceeds (i.e. at lower values of MgO). The following discussion centres on (a) the sources of low $\delta^{18}O$ material and (b) the possible mechanism for producing low-$^{18}O$ lavas.

**(a) Source**

The country rock surrounding the Krafla central volcano is highly depleted in $^{18}O$ as a result of hydrothermal alteration (Hattori & Muehlenbachs, 1982). This hydrothermal alteration is generally restricted to the areas around the central magma reservoir(s), which have developed large hydrothermal convective systems (e.g. Carmichael, 1964). Previous workers have shown that the Icelandic crust is

progressively depleted in $^{18}O$ with depth as a result of isotopic exchange with low-$^{18}O$ meteoric water (Hattori & Muehlenbachs, 1982). Indeed, Hattori & Muehlenbachs (1982) examined drill-core material taken from the centre of the Krafla caldera, which consisted of hydrothermally-altered basalt, granophyre and hyaloclastite. The $\delta^{18}O$ value of the core material decreased with depth from -3‰ at 500m to -10‰ at 2 km. The $\delta^{18}O$ values of the country rock at deeper levels in the Icelandic crust remain unknown. However, Gregory & Taylor (1981) looked at the variation of $\delta^{18}O$ with depth in the Semail ophiolite. They found that the $\delta^{18}O$ values decreased with depth for the first few km (as for Krafla) and then increased to normal-mantle values at the base of the oceanic crust. It is possible that the same type of variation occurs under Krafla, although there is a substantial body of opinion which questions the analogy between ophiolites and "normal" ocean ridges (especially with regard to the very different type of hydrothermal system in a submarine environment as compared to a subaerial setting; S.Day pers. comm., 1990). Gregory & Taylor's study suggests that the $\delta^{18}O$ values at depths of about 2 km beneath Krafla may be close to the minimum crustal value. Macdonald *et al.* (1987) appeared to confirm this minimum crustal value by reporting that highly $^{18}O$-depleted silicic xenoliths from Askja reached a minimum value of -10‰. In addition, Muehlenbachs *et al.* (1974) pointed out that -10‰ is close to the theoretical minimum value of $\delta^{18}O$ that could be generated by closed-system equilibrium exchange of oxygen at crustal temperatures between an infinite reservoir of Icelandic meteoric water (about -12 to -13 ‰) and country rock. It should be noted that open-system effects could lead to even more $^{18}O$-depleted country rock (Gregory & Taylor, 1981; Gregory & Criss, 1986).

These lines of evidence suggest that the crust beneath Krafla is varied in $\delta^{18}O$ value and probably reaches a minimum value at 2-3 km depth, corresponding with the top of the observed crustal magma reservoir. Hence crustal assimilation at the top of the magma reservoir would involve the most $^{18}O$-depleted assimilant (about -10‰). The depletion process, however, could altematively occur at greater depths, as a result of the assimilation of less $^{18}O$-depleted crust (or assimilation could occur over a whole range of depths).

**(b) Mechanism**

Bowen (1922) discussed the problem of crustal assimilation in some detail. He pointed out that crustal assimilation can be regarded as a 3 end-member process (rather than just 2), although there is evidence that this is not always the case for some continental flood basalts (e.g. Cox & Hawkesworth, 1985). The 3 end-members are (1) the magma, (2) the country rock, and (3) the cumulate. Hence assimilation appears to be thermally linked to fractional crystallisation as a result of using the

reach the temperature of the magma body (say 1100°C) using 150 cal/g (i.e. 600x0.25, temperature interval x specific heat) and is probably augmented by 75 cal/g of latent heat of melting to achieve complete dissolution, making a total of 225 cal/g. This heat can be supplied by crystallising 2.25g of magma with a latent heat of crystallisation of 100 cal/g (equivalent to a value of r of 0.44, where r = ratio of the mass of assimilant added to the mass of cumulate formed). This result gives the maximum possible value of r; if the assimilation process is less efficient then the value is smaller. In this simple heat balance the value of r is critically dependent upon the starting temperature of the country rock. If the temperature is considerably higher, then the value of r may be much increased, even as high as 1. However, although increased values of r may make assimilation in principle more efficient at greater depths, the $\delta^{18}O$ values of the country rock may well be less negative (nearer to normal mantle values; as in Gregory & Taylor, 1981). Thus, the overall effect of crustal assimilation on $\delta^{18}O$ values near the base of the crust may not be as significant as assimilation of more $^{18}O$-depleted crust at much shallower levels. Overall, there are unfortunately few constraints on the value of r during the assimilation process.

The major-element composition of the assimilant is another unknown in the assimilation process. It is primarily a function of the composition of the country rock and the degree of melting involved in the assimilation process. At low pressures (1 kbar) Spulber & Rutherford (1983) showed that, for example, about 10% partial melting of a quartz tholeiite ($MgO = 7.0\%$: $K_2O = 0.44\%$) in hydrous conditions produces a melt composition similar to many Icelandic rhyolites. At higher pressures (5 kbar) Helz (1973, 1976) produced a similar range of compositions (from rhyolite to icelandite) depending upon the degree of melting. However, as discussed in Chapter 5, melting in water-poor systems (Thy *et al.*, 1990) seems to reproduce the compositions of Icelandic axial-rift rhyolites (especially for iron oxide) better than the hydrous conditions used by Helz (1973, 1976). The effect of the country rock composition seems to be less important, for Helz (1976) showed that the melt composition (apart for the incompatible elements like K; see discussion in Chapter 5) does not depend much on the country rock's composition. Obviously rhyolitic country rock can be produced by 100% melting of an existing rhyolite, and produce a similar major-element composition to say 10% partial melting of a basalt. The country rock around the Krafla magma reservoir(s) is probably highly variable in chemical composition, but on average, if present activity near the centre of the volcanic centre is a reliable indicator of past activity, then evolved basalts (5-7 wt% MgO) should be the dominant rock type.

The degree of melting appears to be the main variable controlling the major-element composition of the assimilant. Values for the degree of melting may vary from 10% (or possibly less) in the case of generating rhyolites to 100% for bulk assimilation; where country rock undergoes total dissolution, perhaps following stoping into the magma body. In the case of bulk assimilation, the country rock's minerals tend to be out of equilibrium with the surrounding magma and react, with the heat supplied by fractional crystallisation (Bowen, 1922).

The results of assimilation by partial melting (irrespective of the degree of melting) is to introduce low-$^{18}O$ material into the magma and lower the $\delta^{18}O$ value of the magma as it crystallises. Hence crustal assimilation can, in principle, explain the oxygen isotope signature of the Krafla suite, as a result of the coupling of assimilation with fractional crystallisation (AFC). As will be explained in section 7.1.6, the major-element composition of the assimilant (for a given $\delta^{18}O$ value) does not affect the extent of magma $^{18}O$-depletion, because the oxygen concentrations of magma, assimilant and cumulates are approximately the same. Indeed there is no reason why the $^{18}O$-depletion process should not be the result of assimilation of a variety of assimilant compositions. It is possible that bulk assimilation occurs at deeper levels in the crust (associated with the early stages of fractional crystallisation) and that smaller extents of partial melting are restricted to the hydrated roof zone of the shallow magma reservoir (Taylor & Sheppard, 1986).

Assimilation (at any degree of melting) hardly alters the liquid line of descent (Bowen, 1922; Ghiorso & Carmichael, 1985), at least as far as the major elements are concerned (see Chapter 5 for a discussion about the trace elements, which seem to favour assimilation of a relatively small-degree partial melt). Bowen (1922) showed that assimilation merely drives the magma more rapidly along its usual differentiation pathway and tends to enhance the formation of late-stage differentiates (see Fig. 4.21 which confirms that the Krafla suite is relatively chemically differentiated compared to other ocean ridge tholeiites, possibly as the result of assimilation).

In summary, crustal assimilation appears to be the most plausible mechanism for generating low-$^{18}O$ magmas. However, it may be possible to discriminate between assimilation at different degrees of melting by considering the concentrations of the most incompatible trace elements (and $K_2O$) and the Th-isotope ratios. Small degrees of partial melting will tend to enhance the concentrations of the most incompatible trace elements and lead to even lower Th-isotope ratios in the most differentiated magmas than is possible for bulk assimilation. This is discussed further in sections 7.2 and 7.4.

### 7.1.6 $\delta^{18}O$ modelling

Taylor (1980) and De Paolo (1981) developed a simple mass-balance model for assimilation coupled to fractional crystallisation (AFC) in a magma reservoir. They used the following equation to model the change in $\delta^{18}O$ ($\delta_{magma}$) with progressive AFC.

$$\delta_{magma} = (\delta_a - \Delta/r)(1 - f^{(r/(1-r))})$$

The variables are as follows: $\delta_a$ is the $\delta^{18}O$ value of assimilant; $\Delta = \delta^{18}O_{cumulate} - \delta^{18}O_{melt}$; r is the ratio by weight of the amount of assimilant digested to the amount of cumulate formed; and f is the amount of liquid remaining in the system.

The resulting $\delta^{18}O$ value of the magma as expressed by the above equation is not dependent on the chemical composition of the assimilant because the above equation assumes that most rocks have approximately the same oxygen concentration. Hence this form of modelling will not discriminate between different assimilants, but for a given $\delta^{18}O$ value of the assimilant, can suggest the extent of assimilation required to explain the Krafla trend.

The above equation assumes constant values of r, $\Delta$ and $\delta_a$. The assumption of a constant value of r may not be valid. The value of r may vary with time or with the depth of assimilation. In the first instance r is taken to be constant, although a 2-stage model is explored below when modelling the Th-isotope ratios.

It has already been shown (section 7.1.5) that $\delta_a$ is variable in the Icelandic crust but that a value of -10‰ is likely to reflect crustal assimilation near the top of the crustal magma-reservoir. This value is used in the modelling in this section but other values of $\delta_a$ are also considered because assimilation may take place over a range of depths.

The value of f is derived from the least-squares modelling of major-element compositions (Section 4.5). Additionally, some allowance has to be made for the effects of fractional crystallisation from the assumed starting composition with $\delta^{18}O$=+5.5‰ to the least-differentiated Krafla basalts observed. The least-squares model gives a value of approximately 90% fractional crystallisation for the observed sequence basalt-rhyolite (or f = 0.1). After allowing for fractional crystallisation from the assumed starting composition f may fall to as low as 0.05. The use of values of f derived from major-element modelling is an approximation, since the least-squares method ignores the effects of assimilation. However, providing the amount of assimilation is small compared to the extent of fractional crystallisation, then the

difference is likely to be minimal. This assumption appears to be justified since other volcanic suites, which show no evidence for assimilation, suggest similar extents of fractional crystallisation for the sequence basalt-rhyolite. Δ is probably small and slightly negative for the cumulate phases crystallising from the basalts. But the appearance of magnetite on the liquidus means that Δ becomes slightly more negative for the sequence evolved basalt to rhyolite. For example, Muehlenbachs & Byerly (1982) measured $\Delta_{(Mag\text{-}melt)}$ at -3.7‰. However, as the O-isotope fractionation factor for the bulk phenocryst assemblage is likely to be close to zero for the whole differentiation series (Muehlenbachs & Byerly, 1982), the assumption of a value of $\Delta = 0$‰ is likely to be reasonably good.

The results of the O-isotope modelling are given in Table 7.2. As $\delta_a$ becomes more positive then the values of r consistent with the Krafla data also increase (i.e. more efficient assimilation is needed with a less $^{18}O$-depleted assimilant). For $\delta_a$=-10‰, the appropriate values of r (which give $\delta^{18}O$ values of 1.0-2.4‰ in the rhyolites after 90-95% fractional crystallisation, f.c.) range from 0.14 to 0.20 for 90% f.c. and 0.11-0.16 for 95% f.c. According to the model, values of $\delta_a$ greater than -4‰ cannot generate the full range of $\delta^{18}O$ values seen in the Krafla suite, however large a value of r is considered.

### 7.1.7 Conclusions

The Krafla suite of lavas shows anomalously low whole-rock $\delta^{18}O$ values when compared with normal MORB values. This observation is consistent with the analyses of other authors who have undertaken regional studies of the $\delta^{18}O$ values of Icelandic lavas. The $\delta^{18}O$ values correlate with MgO content; the least differentiated Krafla basalts show $\delta^{18}O$ values in the range +4.4 to +4.7‰, whereas the rhyolites vary from +1.0 to +2.4‰. Plagioclase xenocrysts have $\delta^{18}O$ values from +4.1 to +5.1‰, which are probably consistent with $^{18}O$-depletion at magmatic temperatures.

The $\delta^{18}O$ *vs* MgO correlation is consistent with some mechanism of crustal assimilation, although magma mixing may in part explain the relative linearity of the $\delta^{18}O$ *vs* MgO plot (Fig. 7.1). Magma mixing appears to be necessary for the efficient distribution of the assimilant in the magma reservoir. The source of low-$^{18}O$ material is thought to be previously hydrothermally-altered $^{18}O$-depleted country rock. O-isotope analysis of drill-core material suggests that the country rock at the top of the Krafla magma reservoir is likely to have a d18O value of about -10‰. For greater depths in the crust the $\delta^{18}O$ value of the country rock is very poorly constrained. As regards the mechanism of assimilation, the only reasonable heat source for the process

| $\delta_a$(‰) | -5 | -6 | -8 | -10 |
|---|---|---|---|---|
| r (f=0.1) | 0.30-0.49 | 0.24-0.37 | 0.18-0.26 | 0.14-0.20 |
| (f=0.05) | 0.24-0.43 | 0.19-0.31 | 0.14-0.22 | 0.11-0.16 |

Range of values of r are given for $\delta_{magma}$ = -1.9 and -3.7‰.



Table 7.2 Results of the assimilation fractional crystallisation modelling using the O-isotope ratios. See text for details.

is the latent heat of crystallisation of the magma. The major-element composition of the assimilant cannot be determined from studying the O-isotope ratios. However, experiments suggest that the assimilant is likely to be rhyolitic in composition.

The $\delta^{18}O$ variation with differentiation (Fig. 7.1) is modelled by a simple AFC equation. The major unknowns in the simple model are the values of r and $\delta_a$. The value of r is probably the more poorly-constrained of the two variables (i.e. only weakly constrained on thermal grounds), although $\delta_a$ is also not well constrained if crustal assimilation occurs over a range of depths. So assuming values for all the other variables apart from r in the AFC equation, then the model predicts for $\delta_a$=-10‰ that r ranges from 0.11-0.20. The maximum value of $\delta_a$ consistent with the Krafla O-isotope data is about -5‰, for which r has to be at least 0.49.

The calculated values of r and $\delta_a$ may be subsequently used to model the changes in ($^{230}Th/^{232}Th$) activity ratio and Th concentration with differentiation (section 7.2), in order to investigate the degree of melting involved in the assimilation process.

## 7.2 Th isotopes

### 7.2.1 Background to U-series disequilibrium studies

Radioactive disequilibria between $^{238}U$ and the daughter nuclides in its decay series have been known for a considerable period of time (e.g. Joly, 1909; Oversby & Gast, 1968). A decay series will reach radioactive equilibrium (referred to as secular equilibrium) across the whole chain within 4-5 half-lives of the longest-lived intermediate nuclide (Faure, 1986; Condomines *et al.*, 1988). At that point the activities of all the members of the chain will be equal (i.e. $\lambda_i N_i$ = constant, where $\lambda$ is the decay constant and N is the number of atoms present of a given nuclide). The time to achieve equilibrium between 2 successive members of the chain depends on the half life of the parent nuclide.

In the $^{238}U$ decay series, $^{238}U$ decays successively to $^{234}Th$ and $^{234}Pa$, both of which establish equilibrium relatively quickly (3-4 months). Therefore, the next decay product $^{234}U$ can be considered to be a daughter of $^{238}U$. $^{230}Th$ ($t_{1/2}$ = 75.2 ka) is in turn the daughter product of $^{234}U$ and has been found in many rocks to be in radioactive disequilibrium with $^{234}U$ (i.e. $(^{230}Th) \neq (^{234}U)$ where ( ) = activity of nuclide). Since for most volcanic rocks $(^{234}U) = (^{238}U)$ (Condomines *et al.*, 1988), then $^{230}Th$ can be effectively considered to be a daughter of $^{238}U$. In most MORBs and Ocean Island Basalts (OIBs) $(^{230}Th)$ is greater than $(^{238}U)$, which means there is more $^{230}Th$ present in the rock than can be expected from the decay of $^{238}U$ now contained

within that sample. It is thought that this disequilibrium results from the chemical fractionation of Th from U during the last 300 ka, leaving excess ($^{230}$Th) over that expected from ($^{238}$U). Partial melting of the mantle is the only plausible magmatic process capable of fractionating Th from U during the formation of MORBs and OIBs. Indeed McKenzie (1985b) calculated that for Th-U fractionation to occur during magma formation only about 2% melt (or less) can be present in the mantle during partial melting (prior to melt accumulation). Chapters 5 and 6 contain further discussion on melting processes.

It is necessary for the magma transfer time to be relatively short (compared with the $t_{1/2}$ of $^{230}$Th) for ($^{230}$Th) disequilibrium to be detectable. The following equation shows the decrease in ($^{230}$Th) values with time:

$$(^{230}Th/^{232}Th) = (^{238}U/^{232}Th)(1 - e^{-\lambda t}) + (^{230}Th/^{232}Th)_o(e^{-\lambda t})$$

where t is the decay time under consideration, $\lambda$ is half-life of $^{230}$Th, $(^{230}Th/^{232}Th)_o$ is the initial Th-isotope activity ratio and ($^{230}$Th/$^{232}$Th) is the activity ratio at the present day. The values of ($^{230}$Th) are normalised to ($^{232}$Th), which has such a long $t_{1/2}$ that it can be safely regarded as a stable element over short time scales.

In addition, radioactive disequilibrium between $^{226}$Ra and $^{238}$U was observed in some East Pacific Rise samples by MacDougall & Rubin (1987) suggesting that magma transfer and chamber residence times are short compared with the half-life of $^{226}$Ra (1600 years). However, Krishnaswami *et al.* (1984) found no excess ($^{226}$Ra) from a sample of basalt from the 1981 Krafla eruptions. A note of caution should be added here, for Krishnaswami *et al.* (1984) also reported little or no ($^{230}$Th) excess from the same sample, which is in direct conflict with data from equivalent samples analysed during the course of this thesis and others previously analysed (Condomines *et al.*, 1981b; Hemond *et al.*, 1988). So, in the absence of other reliable $^{226}$Ra data, the matter looks open to debate. In general to preserve ($^{230}$Th) excesses requires short periods between magma generation and eruption.

As mentioned above, it is commonly thought that excess ($^{230}$Th) directly reflects the extent of chemical fractionation between U and Th during melting (McKenzie, 1985b; Condomines *et al.*, 1988). A useful way of recording this Th-U fractionation is to plot a graph of ($^{230}$Th/$^{232}$Th) *vs* ($^{238}$U/$^{232}$Th). Secular equilibrium exists when ($^{230}$Th) = ($^{238}$U), which is represented by a straight-line of gradient 1 in Fig. 7.5 (called the equiline). It is assumed that the mantle lies on the equiline prior to melting (i.e. no other Th-U fractionation events have occurred during the preceding 300ka). On melting it appears that Th is preferentially incorporated into the melt

compared with U (changing the value of ($^{238}U/^{232}Th$)), whereas the Th isotopes themselves are not fractionated, leaving ($^{230}Th/^{232}Th$) the same in source and partial melt. The effect of partial melting of the mantle producing MORBs and OIBs is to alter the melt's position on the "isochron diagram" approximately horizontally away from the equiline (to the left since the Th/U ratio increases in the melt) (see discussion in Chapter 5).

After the melting event, excess ($^{230}Th$) decays, reducing the value of ($^{230}Th/^{232}Th$) in the magma/lava but leaving ($^{238}U/^{232}Th$) practically constant due to the relatively short time-scale compared to the half-lives of $^{238}U$ and $^{232}Th$. Thus with time the positions of the samples and/or magma move vertically down the graph in Fig. 7.5, approaching the equiline in about 300 ka. For samples less than about 10 ka old it is not necessary to apply an age correction to deduce the original magmatic values of ($^{230}Th/^{232}Th$) because the change in ($^{230}Th/^{232}Th$) is less than the analytical error. However, the effect of variable magma residence time in generating the range of Krafla ($^{230}Th/^{232}Th$) values cannot be ruled out because the Icelandic crust is thicker than normal oceanic crust (see Chapter 2). This idea is considered below. However many MORBs, unlike those from Iceland, are generated in settings with no evidence for long-term magma reservoirs, which may mean it is safe to assume that the ($^{230}Th/^{232}Th$) value of the magma directly reflects the ($^{230}Th/^{232}Th$) of the mantle source at the time of melt generation.

Condomines *et al.* (1981a) showed that there is a negative correlation between ($^{230}Th/^{232}Th$) and $^{87}Sr/^{86}Sr$ for MORBs and OIBs and suggested that the ($^{230}Th/^{232}Th$) values of the magma reflect that of the mantle source from which the magmas are generated. Low values of ($^{230}Th/^{232}Th$) indicate low present-day Th/U ratios in the source. By contrast, low $^{87}Sr/^{86}Sr$ values for the same MORB source represent low time-integrated Rb/Sr ratios. Williams & Gill (1989) have qualified such discussion about sources by proposing that the melting process may itself be responsible for generating different ($^{230}Th/^{232}Th$) values (by "slow" melting of a source which is already undergoing preferential extraction of Th from U). It should be noted that these effects are probably much smaller in magnitude than the total range in ($^{230}Th/^{232}Th$) values seen in MORBs and OIBs, which almost certainly correspond to differences in their mantle sources.

Previous work on Iceland has shown that the lavas lie on the "Sr-Th array" between those of most MORBs and OIBs, with higher values of $^{87}Sr/^{86}Sr$ and lower values of ($^{230}Th/^{232}Th$) than most MORBs. This difference from MORB probably reflects the less-depleted mantle source originating in a plume (see section 7.3). Although discussion so far has centred on melting in the mantle, the Icelandic

($^{230}Th/^{232}Th$) data suggest that other processes apart from those in the mantle are operating. Faure (1986) summarised the range of processes which may modify the Th isotope activity ratio of a magma after formation. These processes include "phenocryst formation, vapour fractionation, crustal assimilation and interaction with seawater" (Faure, 1986).

A selection of Krafla rocks has been analysed for Th-isotope activity ratios in order to investigate these secondary magmatic processes, (e.g. the effects of crustal assimilation).

### 7.2.2 Analytical techniques

A collection of Krafla whole rock samples covering the range of compositions of the suite was analysed to determine ($^{230}Th/^{232}Th$) and ($^{238}U/^{232}Th$) activity ratios, and Th and U concentrations. The techniques used for this thesis were similar to those described by Condomines *et al.* (1981b), and were carried out at the University of Clermont-Ferrand, France. Analytical details, modifications and typical errors are given in Appendix VI (f). As explained in the previous section, ($^{230}Th/^{232}Th$) values decrease with age after eruption. Thus only samples younger than 10 ka were analysed in order to avoid age-correction of the Th-isotope data.

### 7.2.3 Results

The ($^{230}Th/^{232}Th$) and ($^{238}U/^{232}Th$) activity ratios and concentrations of Th and U are shown in Table 7.3, together with the MgO contents of the lavas. Values of ($^{230}Th/^{232}Th$) vary from 0.955±10 to 1.145±17 (±1σ counting statistics) and ($^{238}U/^{232}Th$) range from 0.89 to 1.02 (~±2%). The latter values are equivalent to Th/U (wt) ratios of 3.40 to 2.97. The Th and U concentrations vary from 0.086 and 0.029 ppm respectively in the most magnesian basalt analysed (KK50), to 7.48 and 2.20 ppm for Th and U in a rhyolite (KK56). The Th and U concentrations are discussed specifically in Chapter 5.

In general, ($^{230}Th/^{232}Th$) values decrease with decreasing MgO, although there is some scatter in the data (Fig. 7.4). The Krafla data are plotted on a "isochron diagram" of ($^{230}Th/^{232}Th$) *vs* ($^{238}U/^{232}Th$) (Fig. 7.5). These data can be compared with other Icelandic Th-isotope analyses from regional studies (see the oval shape from Hemond *et al.*, 1988, in Fig. 7.5). The Krafla trend varies mostly in ($^{230}Th/^{232}Th$), whereas ($^{238}U/^{232}Th$) stays relatively constant, so that the data spread across the oval shape defined by the data of Hemond *et al.* (1988) towards the equiline. ($^{230}Th/^{232}Th$)

| Sample | MgO(wt%) | Th(ppm) | U(ppm) | ($^{230}Th/^{232}Th$) | ($^{238}U/^{232}Th$) |
|---|---|---|---|---|---|
| KK50 | 9.73 | 0.086 | 0.029 | | 1.023 |
| 84-19 | 8.66 | 0.484 | 0.150 | 1.13±2 | 0.940 |
| KK55 | 7.60 | 0.447 | 0.137 | 1.09±2 | 0.930 |
| KK152 | 7.58 | 0.499 | 0.151 | | 0.916 |
| KK92 | 6.91 | 0.662 | 0.204 | 1.145±17 | 0.937 |
| KK51 | 6.68 | 0.832 | 0.266 | 1.026±11 | 0.971 |
| KK113 | 6.39 | 0.628 | 0.194 | 1.094±13 | 0.937 |
| KRA118 | 6.09 | 0.738 | 0.227 | 1.109±11 | 0.933 |
| KK101 | 5.80 | 0.725 | 0.224 | 1.094±12 | 0.939 |
| KK37 | 5.36 | 0.981 | 0.302 | 1.048±15 | 0.935 |
| KK107 | 5.36 | 0.956 | 0.293 | 1.065±15 | 0.931 |
| KK35 | 3.32 | 2.14 | 0.679 | 0.987±8 | 0.962 |
| KK26 | 1.92 | 5.24 | 1.59 | 0.99±1 | 0.921 |
| KK25 | 1.57 | 5.59 | 1.70 | 1.003±7 | 0.923 |
| KK34 | 1.43 | 3.67 | 1.14 | 0.986±9 | 0.942 |
| KK56 | 0.31 | 7.48 | 2.20 | 0.955±10 | 0.892 |

$(^{238}U/^{232}Th) = 3.034/(Th/U)_{wt}$

Table 7.3 MgO (wt%), Th and U (ppm) and ($^{230}Th/^{232}Th$), ($^{238}U/^{232}Th$) activity ratios for selected postglacial samples.

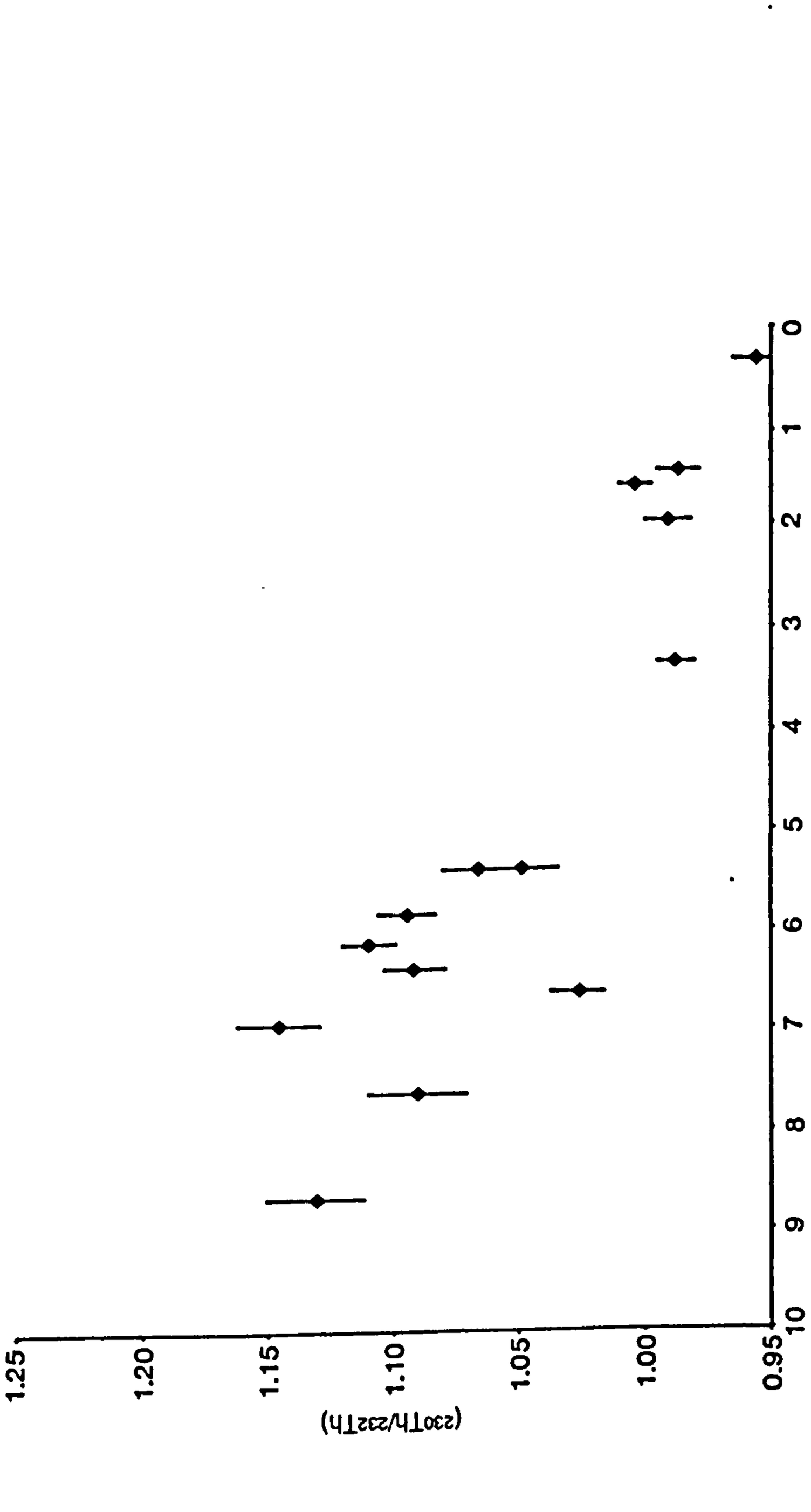


Fig. 7.4 ($^{230}Th/^{232}Th$) (activity ratios) plotted against MgO (wt%) for selected postglacial samples. ($^{230}Th/^{232}Th$) error bars represent 1σ counting statistics.

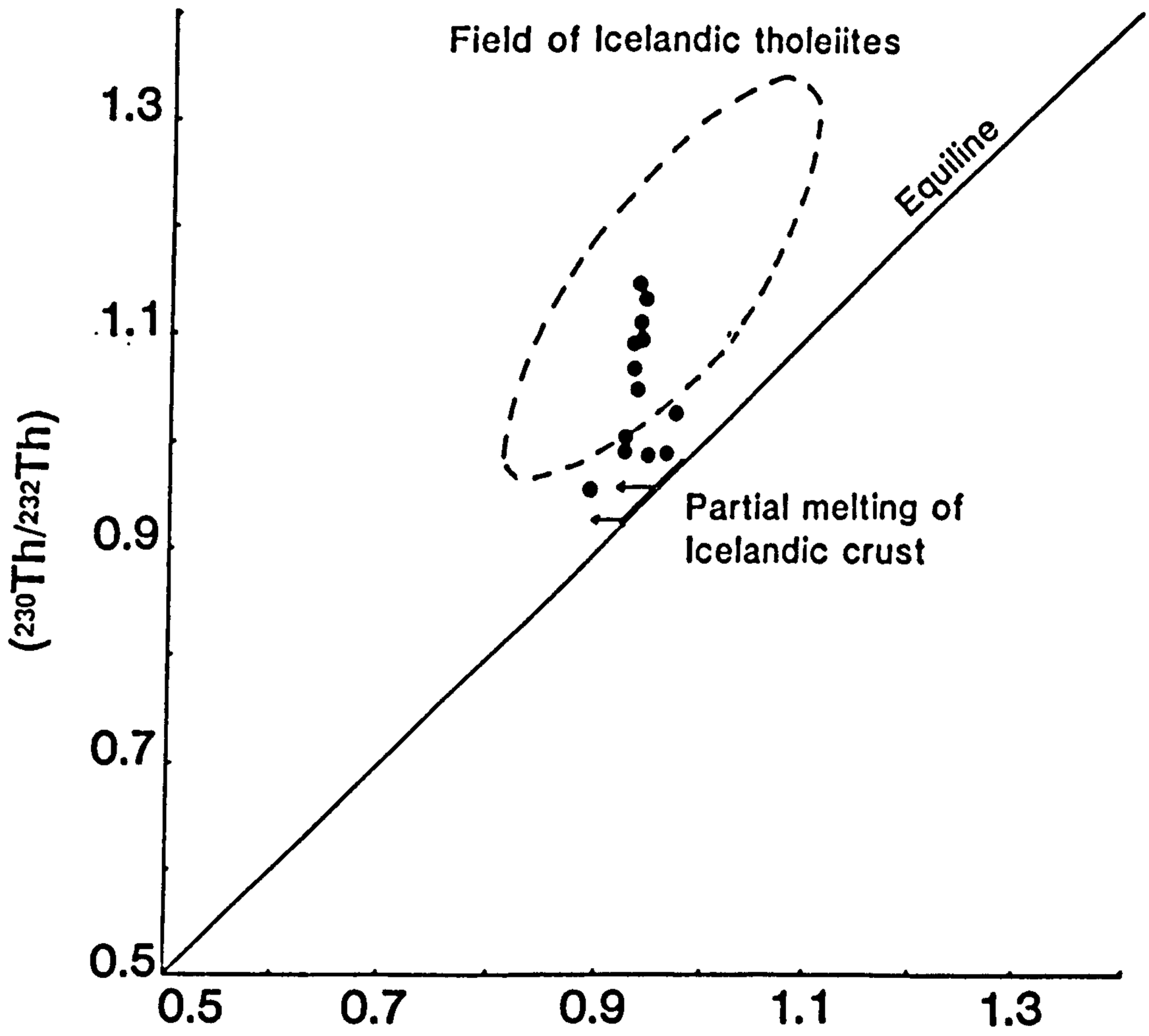


Fig. 7.5 ($^{230}Th/^{232}Th$) *vs* ($^{238}U/^{232}Th$) or the "isochron diagram" for the samples plotted in Fig. 7.4. The oval field containing Icelandic data is taken from Hemond *et al.* (1988). Errors as in Fig. 7.4 and ~±2% for the ($^{238}U/^{232}Th$) values.

activity ratios appears to correlate with $\delta^{18}O$ ratios (see Fig. 7.6), although there is a large amount of scatter.

### 7.2.4 Discussion

The Krafla data, as presented on the "isochron diagram" in Fig 7.5, suggest that there is at least one process changing the ($^{230}Th/^{232}Th$) values after magma generation. This idea is suggested by the vertical trend of the Krafla data towards the equiline in the "isochron diagram", and the correlations of ($^{230}Th/^{232}Th$) with MgO and $\delta^{18}O$. The correlation between ($^{230}Th/^{232}Th$) and $\delta^{18}O$ would be consistent with the same process generating low ($^{230}Th/^{232}Th$) values as produces low $\delta^{18}O$ lavas (Hemond *et al.*, 1988). It is possible, but perhaps unlikely, that two mechanisms have independently contributed to the variation in values of $\delta^{18}O$ and ($^{230}Th/^{232}Th$).

Five possible processes for producing low $\delta^{18}O$ values were suggested in section 7.2. These processes are now discussed in the light of the ($^{230}Th/^{232}Th$) data, together with an additional process; namely variable magma residence time.

**(1) Sub-solidus alteration**

The ($^{230}Th/^{232}Th$) correlation with $\delta^{18}O$ is difficult to understand if $\delta^{18}O$ values are the result of sub-solidus exchange with heated meteoric water. This is because meteoric water only contains trace amounts of Th, and rocks do not appear to release much Th into the water on alteration.

**(2) Primary mantle differences**

The ($^{230}Th/^{232}Th$) correlation with MgO (again as for the $\delta^{18}O$ case) appears to rule out this suggestion from serious consideration.

**(3) Direct interaction of meteoric water.**

Again, like in case (1) above, meteoric water contains very low concentrations of Th available to change the Th-isotope ratio of the magma, suggesting that this mechanism is unlikely.

**(4) (5) Crustal assimilation**

Both assimilation by partial fusion of the crust and bulk assimilation would be compatible with the ($^{230}Th/^{232}Th$) results. Hemond *et al.* (1988) pointed out that low values of ($^{230}Th/^{232}Th$) would be expected at depth in the crust. A subsidence rate of 0.5-1.0 $cm^{-1}$ $yr^{-1}$ in the rift zone would produce rocks close to radioactive equilibrium at depths of between of 1.5-3 km. Since a magma reservoir has been identified at a depth of about 3 km under Krafla, then the wall rock available for assimilation is likely to be in radioactive equilibrium. Progressive assimilation of such material will lead to lower ($^{230}Th/^{232}Th$) values as fractional crystallisation proceeds.

Partial fusion of wall-rock leads to enhanced Th concentrations in the assimilant as Th is highly incompatible in most mineral phases. Hence assimilation by low degrees of melting of the crust gives rise to more efficient reduction in the ($^{230}Th/^{232}Th$) values with differentiation than for bulk assimilation, where the Th concentration of the assimilant, although possibly variable due to the presence of different rock types, is not enhanced by the assimilation process. However, both these processes can generate low ($^{230}Th/^{232}Th$) values in the rhyolites when combined with fractional crystallisation given an appropriate value of r. The "isochron diagram" (Fig. 7.5) shows the position of the old Icelandic crust (in secular equilibrium > 300 ka). Assimilation of old Icelandic crust will lead to progressively lower values of ($^{230}Th/^{232}Th$). The field of the data of Hemond *et al.* (1988) from Icelandic basalts is shown in Fig. 7.5, with more evolved compositions plotting to the lower left of the oval field. The Krafla suite defines a more coherent trend (with less change in ($^{238}U/^{232}Th$)) than the regional data.

(6) Variable magma-residence time

This mechanism can potentially explain the correlation of ($^{230}Th/^{232}Th$) with MgO. The ($^{230}Th/^{232}Th$) values will decrease with time through the gradual decay of excess unsupported ($^{230}Th$). For this process to be viable there has to be enough time for the ($^{230}Th/^{232}Th$) values of the Krafla magmas to decrease from greater than 1.14 to lower than 1.00. This would require more than 130 ka of crystallisation, which would superficially appear to be inconsistent with the observation that on average an eruptive cycle occurs once every 500 years. Also the time needed for fractional crystallisation of the magma (Brikowski & Norton, 1989) is likely to be substantially less than the 130 ka necessary to change the ($^{230}Th/^{232}Th$) values. It should be noted that geophysical evidence from the recent eruptive cycle suggests that magma is coming from depths greater than 20 km over a time period of months prior to the eruptions, suggesting that magma residence time in crustal reservoirs is relatively short (Tryggvason, 1986). Additionally, the correlation between ($^{230}Th/^{232}Th$) and $\delta^{18}O$ suggests that the isotopic ratios are likely to be controlled by the same process. However, it is conceivable that the isotopic ratios could be controlled independently. For example, the ($^{230}Th/^{232}Th$) values could be a function of variable magma residence time, whereas the $\delta^{18}O$ values could be a function of a different process which happens to be time dependent (e.g. direct fluid interaction).

In summary, processes (4),(5) and (6) all could possibly explain the variation in ($^{230}Th/^{232}Th$) values, whereas processes (1),(2) and (3) are highly unlikely mechanisms. However, process (6) seems implausible due to the long times required for the decay of excess ($^{230}Th$), but could be combined with the assimilation processes

(4) and (5). Crustal assimilation (4),(5) seems to provide the most satisfactory way of explaining both the low $\delta^{18}O$ and low ($^{230}Th/^{232}Th$) values in Krafla magmas. However, the above discussion does not indicate the composition of the contaminant. Therefore, a simple model for crustal assimilation is presented in section 7.2.5, in an attempt to calculate the composition of the contaminant.

### 7.2.5 Modelling

The ($^{230}Th/^{232}Th$) activity ratios and Th concentrations can be modelled by means of simple AFC equations, in a similar fashion to the O-isotope data (section 7.1.6). De Paolo (1981) developed a series of equations for a crystallising magma body assimilating its country rock. It is convenient to make a number of simplifying assumptions to a general AFC model that do not significantly reduce its usefulness. These simplifications allow the easy solution of the relevant equations. The equation below (Wilson, 1989, after De Paolo, 1981) may be used to model the change in Th concentration during the AFC process.

$$C_{res} = C_o.F + (r/(r-1+D)).C_a.(1-F)$$

$$\text{where } F = f^{-((r-1+D)/(r-1))}$$

$C_{res}$, $C_o$ and $C_a$ are respectively the Th concentrations in the resultant contaminated magma, the initial magma, and the assimilant (partial melt or rock). All the other variables in the above equations have been defined in the same way as for the O-isotope modelling in section 7.1.6.

De Paolo (1981) also derived an equation for the changes in isotope ratios (in this case, Th) during the AFC process. This equation is given below:

$$(^{230}Th/^{232}Th)_{res} = \{(^{230}Th/^{232}Th) - (^{230}Th/^{232}Th)_a\}.C_o.F/C_{res} + (^{230}Th/^{232}Th)_a$$

The values of $C_{res}$ and F are taken from the first equation in this section and the subscripts res, o, a on the ($^{230}Th/^{232}Th$) values are used as above.

These equations are based on a number of simplifying assumptions:

(1) The magma body is assumed to undergo perfect fractional crystallisation, with a constant value of D. The values of f are taken from major-element modelling, with an additional correction to account for approximately 30% fractional crystallisation from the chosen starting composition $(^{230}Th/^{232}Th)_o = 1.25$ and $\delta^{18}O = +5.5‰$ to the least-differentiated Krafla basalts (4.4-4.7‰). The total amount of fractional

crystallisation required for the sequence primary basalt to rhyolite is, therefore, estimated to be 90-95% (i.e. f=0.05-0.10). As mentioned above, major-element modelling may itself introduce errors, since the least-squares method ignores the effects of AFC. The effects of magma mixing are also not considered in this model; see earlier comments on the role of mixing in AFC processes. A constant value of D=0 for Th is also assumed.

(2) The assumption of constant r is necessary for the use of the equations as expressed above. This may not be valid when dealing with crystallisation over a range of depths and temperatures (see section 7.1.6).

(3) In the first instance, a constant value of $C_a$ is assumed throughout the AFC process. Again this may not be valid for assimilation over a range of different depths.

(4) A fixed value of $C_o$ is used in each AFC model. Knowledge of mantle-melting processes suggests that this assumption is far from valid. However, since many of the samples analysed for O- and Th-isotope ratios come from the last 3000 years, which appear to suggest approximately constant degrees of melting, then this assumption may be reasonable.

(5) Constant values of $(^{230}Th/^{232}Th)_a$ and $(^{230}Th/^{232}Th)_o$ are used. It is possible that the value of $(^{230}Th/^{232}Th)_o$ is variable (Williams & Gill, 1989; Othman & Allègre, 1990; see discussion above). However, this problem is probably secondary in importance when compared to the others considered in this section, since the effects of these differences in $(^{230}Th/^{232}Th)_a$ and $(^{230}Th/^{232}Th)_o$ values are small compared to the differences in values of r, $\delta_a$, $C_o$ and $C_a$. A value of $(^{230}Th/^{232}Th)_o$ of 1.25 is used, which is consistent with data from Icelandic picrites and from the least-differentiated MORBs (Condomines *et al.*, 1981a; Hemond *et al.*, 1988). $(^{230}Th/^{232}Th)_a$ is taken to be 0.93. This is deduced from the $(^{230}Th/^{232}Th)$ values that average Krafla basalts would have at secular equilibrium, assuming that Th and U are not fractionated during hydrothermal alteration (i.e. equal to the average $(^{238}U/^{232}Th)$ value for Krafla basalts). As in section 7.1.6, a value of $\delta_a$=-10‰ is used in the modelling, although the effects of different values of $\delta_a$ are considered.

The AFC equations were written into a FORTRAN computer program (see Appendix VII). This program uses a range of values of r, $C_o$ and $C_a$ (for constant values of $\delta_a$ and $(^{230}Th/^{232}Th)_{a,o}$) and calculates values of $C_{res}$ for increments of 5% reduction in the mass of the original magma. Then the calculated values of $C_{res}$ are used in the second equation to deduce the values of $(^{230}Th/^{232}Th)_{res}$ during the AFC process. The values of $\delta_a$ are calculated from the equation given in section 7.1.6. The value of r used in the Th-isotope modelling is taken from the O-isotope modelling. This series of calculations is repeated for different values of r, $C_o$, $C_a$ and the results

are expressed in matrix form. The resultant matrix is screened to eliminate individual AFC models with combinations of r, $C_o$, $C_a$ which do not have values of $(^{230}Th/^{232}Th)_{res}$ within the range 0.95 to 1.00 at f=0.05-0.10. The same process is repeated for the $\delta^{18}O$ values using limits of +1.0 and +2.5‰ at f=0.05-0.10.

### A comparison of model data with the Krafla data

The model data and the Krafla data may be conveniently compared on a plot of $(^{230}Th/^{232}Th)$ *vs* $\delta^{18}O$. For $\delta_a$=-10‰, satisfactory solutions reaching both low values of $\delta^{18}O$ and $(^{230}Th/^{232}Th)_{res}$ at f=0.05-0.1 are achieved using values of r=0.15-0.20 and $C_a$=3-5 ppm (see Table 7.2 for the $\delta^{18}O$ results). Note that the range of values of r is slightly different from that in Table 7.2. This is because the modelling results have to be consistent with both the O- and Th-isotope ratios, and the Th concentrations found in the rhyolites instead of just the O-isotope data. Of all the models fitting the requirements of the AFC program, the best fitting single-stage model (A) is shown in Fig. 7.6, with $C_o$=0.15 ppm, $C_a$=4 ppm and r=0.16. However, this model curve does not pass through the high values of both $(^{230}Th/^{232}Th)_{res}$ and $\delta^{18}O$ in the less-differentiated Krafla samples. Other single-stage model curves generated by the AFC program (not shown here) also show this discrepancy. For example, a less $^{18}O$-depleted assimilant (e.g. $\delta_a$=-5‰) will generate low $\delta^{18}O$, low $(^{230}Th/^{232}Th)$ rhyolites if r=0.30-0.33 and $C_a$=2 ppm but still with the same curvature in a $(^{230}Th/^{232}Th)$ *vs* $\delta^{18}O$ plot. This implies that increasing the value of $\delta_a$ requires more efficient assimilation and a lower concentration of Th in the assimilant.

The above discrepancy for the single-stage model may be overcome by dividing the AFC process into two stages (see model B in Fig. 7.6); modelling the basaltic crystallisation sequence with f=0.4, followed by a value of f=0.25 for a second stage of differentiation producing the more evolved compositions (i.e. evolved-basalt to rhyolite). In this 2-stage model it is assumed that $\delta_a$ is constant. The AFC program finds the values of $C_a$, $C_o$ and r which fit most consistently with the Krafla data. For example if $\delta_a$=-10‰, the first stage may be successfully modelled with values of $C_o$=0.15 ppm, $C_a$=1 ppm and r=0.18. Similar solutions are found for different values of $\delta_a$, but with altered values of r (as noted above). The second stage takes its starting conditions from the first stage of the AFC process, using the values of $C_o$, $(^{230}Th/^{232}Th)_o$ and $\delta_{magma}$ deduced for a value of f=0.4. The best-fit solution for the second stage is $C_a$=7 ppm and r=0.15. It can be seen that the 2-stage model (Fig. 7.6) fits the Krafla data better than the single-stage model.

The values of $C_a$ required by the two AFC models discussed above are much greater than expected from the existence of only bulk assimilation of the crust under

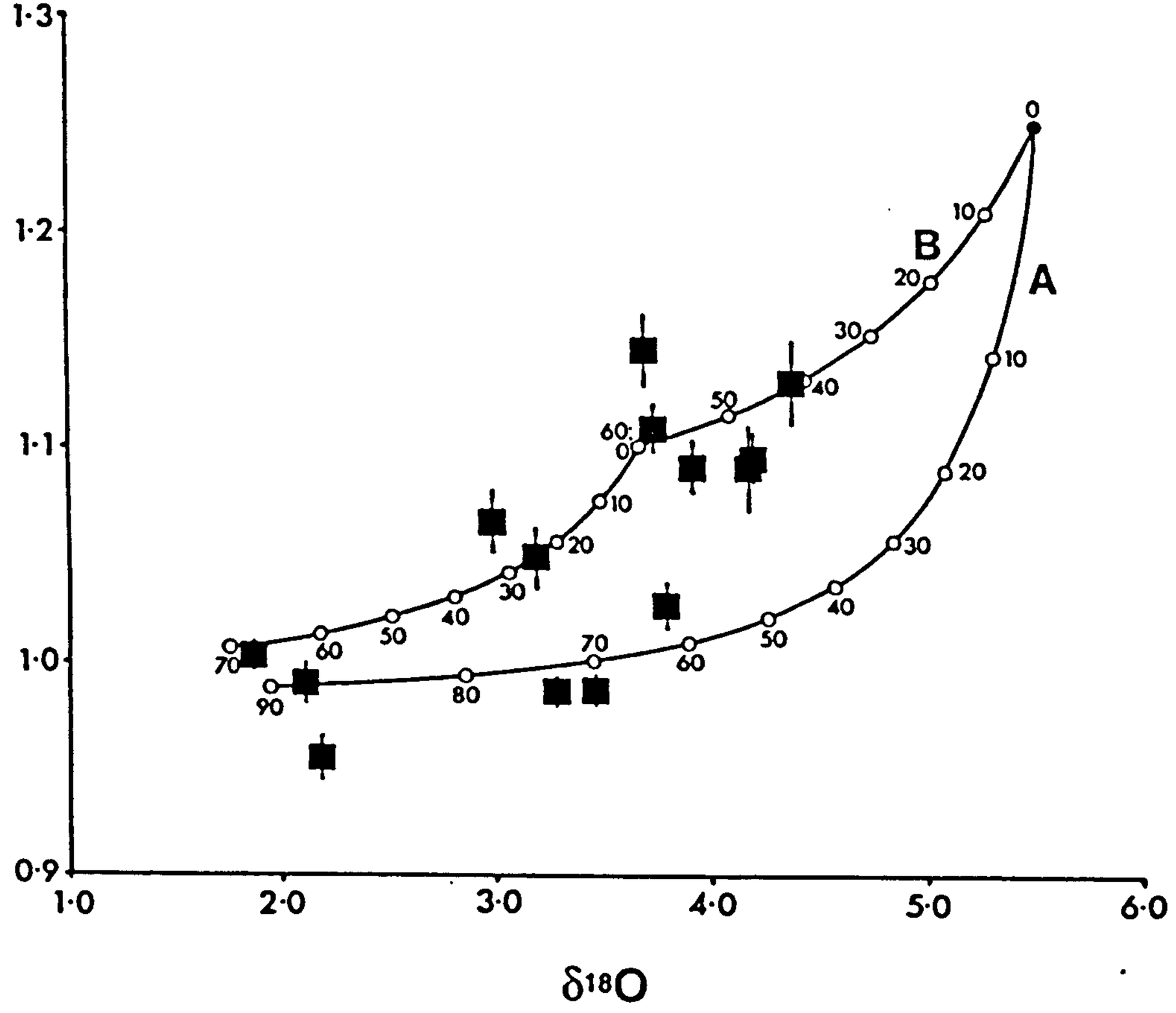


Fig. 7.6 ($^{230}Th/^{232}Th$) *vs* $\delta^{18}O$ values (‰) (whole-rock) for selected postglacial samples. Error bars for ($^{230}Th/^{232}Th$) as in Fig. 7.6. Model A is a single-stage AFC model using $(^{230}Th/^{232}Th)_o$=1.25, r=0.16, $C_o$=0.15 ppm, $C_a$=4 ppm. Model B is a 2-stage model. The 1st stage (60% f.c.) has $(^{230}Th/^{232}Th)_o$=1.25, r=0.18, $C_o$=0.15 ppm, $C_a$=1 ppm. The 2nd stage (70% f.c.) has $(^{230}Th/^{232}Th)_o$=1.10, r=0.15, $C_o$=0.70 ppm, $C_a$=7 ppm. Both models use $\delta_a$=-10‰, $\Delta$=0‰. Numbers represent the percentage of liquid crystallised (divided into 2 separate stages for the 2-stage model). Errors as in Figs. 7.1 and 7.4.

Krafla, which is likely to be on average basaltic in composition (i.e. Th < 1 ppm). The high-Th concentration of the assimilant suggests that the assimilation takes place by partial fusion of the crust; with the exception of the first stage in the 2-stage model, which would fit with 100% fusion of an evolved-basalt containing 1 ppm Th. The degree of melting involved in forming the assimilant (and hence the major-element composition of the assimilant) is difficult to assess from the values of $C_a$ because the crust itself is heterogeneous in Th concentration. But evidence from trace element ratios in Chapter 5 suggests that the assimilation process has to fractionate Th, U and Rb from La (or Zr), especially in the more-evolved compositions. This is unlikely to be possible with more than 10% crustal partial fusion, a conclusion consistent with a rhyolitic contaminant. For the single-stage model (A; Fig. 7.6) the value of $C_a$ (4 ppm), for $\delta_a$=-10‰, however, is somewhat lower than that found in the Krafla rhyolites (about 7 ppm). But since the Krafla rhyolites themselves appear to be the end-product of AFC processes, there is no reason why the assimilant Th content should bear any resemblance to that of the Krafla rhyolites. The 2-stage model (B; Fig 7.6), which fits more closely with the Krafla O- and Th-isotope data, suggests that during the early stages of differentiation the Krafla magma assimilates a contaminant with a relatively low-Th concentration followed by a high-Th contaminant during the later stages of differentiation. The high-Th concentration for the contaminant in the second stage is consistent with a rhyolitic major-element composition and can explain the fractionation of Th, U and Rb from La in the formation of the rhyolites.

### 7.2.6 Conclusions

The ($^{230}Th/^{232}Th$) activity ratios from postglacial lavas vary from 0.95 to 1.15. ($^{230}Th/^{232}Th$) values correlate with MgO contents and $\delta^{18}O$ values, suggesting that the ($^{230}Th/^{232}Th$) variation is a function of the same crustal processes that generate the low $\delta^{18}O$ values. As it was argued for the $\delta^{18}O$ variation, the Th-isotope data are probably best explained by crustal assimilation coupled to fractional crystallisation (AFC). Variable magma reservoir residence time may, however, be a very small contributory factor to the change in ($^{230}Th/^{232}Th$) values from basalt to rhyolite.

Modelling of the Th-isotope data requires knowledge of several variables. Simple AFC equations are used to show that bulk crustal assimilation is highly unlikely to account for the overall changes in ($^{230}Th/^{232}Th$) values and Th concentrations with differentiation from basalt through to rhyolite. If assimilation occurs at the top of the seismically-identified magma reservoir (with $\delta_a$=-10‰), then the combined O-Th isotope data can be explained by assimilation of crust with 3-5

ppm Th in a single-stage model (with r = 0.15-0.20). The plot of ($^{230}Th/^{232}Th$) *vs* $\delta^{18}O$ (Fig. 7.6) suggests that there is a considerable discrepancy between the single-stage model and the observed Krafla compositions at high values of ($^{230}Th/^{232}Th$) and $\delta^{18}O$. This may imply that the assumption of constant r, $\delta_a$ and $C_a$ during the AFC process is invalid because crustal assimilation occurs over a range of conditions (cf. Condomines *et al.*, 1983). A better fit between model and Krafla compositions is obtained for a 2-stage AFC model, with a relatively low-Th concentration assimilant for the initial stages of differentiation (1 ppm). In the second stage a much higher Th concentration is required to fit the Krafla data (7 ppm). Using a relatively high-Th concentration assimilant for only the later stages of differentiation can explain the increased Th/La ratios in the icelandites, dacites and rhyolites when compared to the basalts.

## 7.3 Sr- and Nd-isotope geochemistry

### 7.3.1 Rationale

The isotopic compositions of Sr and Nd have been widely used to study the origin of igneous rocks. They provide information about the sources from which the magmas are derived and the processes by which their chemical and isotopic compositions are modified (Faure, 1986).

Ocean ridge samples have mean values of $^{87}Sr/^{86}Sr = 0.70280$ and $^{143}Nd/^{144}Nd = 0.513100$, although there are significant geographic differences (O'Nions & Pankhurst, 1974; Schilling *et al.*, 1983). The main causes of these differences are thought to be:

(1) Differences in the time-integrated ratios of Rb/Sr and Sm/Nd of the mantle source:

(2) Assimilation or isotope exchange of magma with rocks from the oceanic crust.

In particular, Icelandic basalts have higher $^{87}Sr/^{86}Sr$ and lower $^{143}Nd/^{144}Nd$ values than most MORBs. Many authors (e.g. Hart *et al.*, 1973; O'Nions & Pankhurst, 1974; Zindler *et al.*, 1979; O'Nions *et al.*, 1977) have invoked source differences to explain the variation in Sr-Nd isotope ratios (i.e. explanation 1). In this model, magma from regions such as Iceland with high values of $^{87}Sr/^{86}Sr$ (and low $^{143}Nd/^{144}Nd$) is supplied by mantle plumes possibly originating in the lower mantle (cf. the "Sr-Th array" in section 7.2.1). In contrast, other authors (e.g. O'Hara, 1977; Oskarsson *et al.*, 1985; Steinthorsson *et al.*, 1987; Hemond *et al.*, 1988) favour crustal processes (explanation 2) to generate the higher Icelandic $^{87}Sr/^{86}Sr$ ratios through the assimilation of hydrothermally-altered oceanic crust. However, it is not clear if Icelandic crust altered by meteoric water actually has the enhanced $^{87}Sr/^{86}Sr$ values to

make it a suitable contaminant. It should be noted that the latter group of workers has not investigated variation in $^{87}Sr/^{86}Sr$ with $^{143}Nd/^{144}Nd$. If this variation in $^{87}Sr/^{86}Sr$ is caused by crustal assimilation then values of $^{143}Nd/^{144}Nd$ themselves should remain unaffected (see below for justification).

Sr- and Nd-isotopic data are presented (in section 7.3.3) from a selection of recent rocks from Krafla (all young enough to avoid the need for age-correction). The aim of the rest of this Chapter is to assess to which the Krafla Sr-Nd isotopic data can be explained by crustal processes identified by the variation in the Th-, O-isotope ratios, or alternatively the extent to which they reflect mantle source variation.

### 7.3.2 Analytical techniques

$^{87}Sr/^{86}Sr$ and $^{143}Nd/^{144}Nd$ ratios were determined for 14 Krafla samples from the postglacial and last glacial time periods. Most of the samples were also analysed for O- and Th-isotope ratios. The same rationale for sample choice was followed for the Sr- and Nd-isotope ratio determinations as for the other isotopic systems. The chemical preparation and the analyses were undertaken at the S.U.R.R.C. (East Kilbride). Analytical techniques performed are described in Appendix VI (d) and essentially follow those described by Dymoke (1988). Standard NBS987 gave an $^{87}Sr/^{86}Sr$ value of 0.71028±1 during the course of this study. All the $^{87}Sr/^{86}Sr$ values presented in this thesis are quoted renormalised to an $^{87}Sr/^{86}Sr$ value of 0.71022 for NBS987 following usual conventions.

### 7.3.3 Results

The Sr- and Nd-isotope ratios are shown in Table 7.4. As explained in section 7.3.1, all the samples are young enough to avoid the need to correct for age. Values of $^{87}Sr/^{86}Sr$ vary from 0.70309±3 to 0.70326±3. $^{143}Nd/^{144}Nd$ values range from 0.512982±37 to 0.513111±22. A plot of $^{143}Nd/^{144}Nd$ *vs* $^{87}Sr/^{86}Sr$ (Fig. 7.7) shows a vague negative correlation, although the total range in $^{143}Nd/^{144}Nd$ values is only about twice the worst error estimate. Values of $^{87}Sr/^{86}Sr$ are plotted against MgO (Fig. 7.8) and show no obvious relationship. Indeed the $^{87}Sr/^{86}Sr$ values of the least differentiated samples (basalts > 8 wt% MgO) cover the whole range of the Krafla values. There is a slight negative correlation between $^{87}Sr/^{86}Sr$ and $\delta^{18}O$ (Fig. 7.9), with the Krafla rhyolites plotting at low values of $\delta^{18}O$ and high values of $^{87}Sr/^{86}Sr$. Four early postglacial samples (7-10 ka) (KK35,KK50,KK51,KK55) from a restricted

| Sample | MgO(wt%) | $^{87}Sr/^{86}Sr$ | $^{143}Nd/^{144}Nd$ |
|---|---|---|---|
| KK58 | 9.73 | 0.70320±3 | 0.513111±22 |
| KK30 | 9.49 | 0.70326±3 | 0.513025±18 |
| KK50 | 9.41 | 0.70309±3 | 0.513087±20 |
| 84-19 | 8.66 | 0.70319±3 | 0.512982±37 |
| KK55 | 7.60 | 0.70311±3 | 0.513054±20 |
| KK152 | 7.58 | 0.70320±4 | 0.513049±42 |
| KK92 | 6.91 | 0.70320±3 | 0.513037±40 |
| KK51 | 6.68 | 0.70317±3 | 0.513068±21 |
| KRA118 | 6.09 | 0.70324±4 | 0.513032±21 |
| KK37 | 5.36 | 0.70317±3 | 0.513047±34 |
| KK35 | 3.32 | 0.70314±3 | 0.513079±22 |
| KK26 | 1.92 | 0.70321±4 | 0.513051±37 |
| KK56 | 0.31 | 0.70322±3 | 0.513021±21 |
| IC9 | 0.04 | 0.70324±3 | 0.513050±33 |

Table 7.4 MgO (wt%), $^{87}Sr/^{86}Sr$ & $^{143}Nd/^{144}Nd$ results for selected samples from the postglacial and last glacial periods.

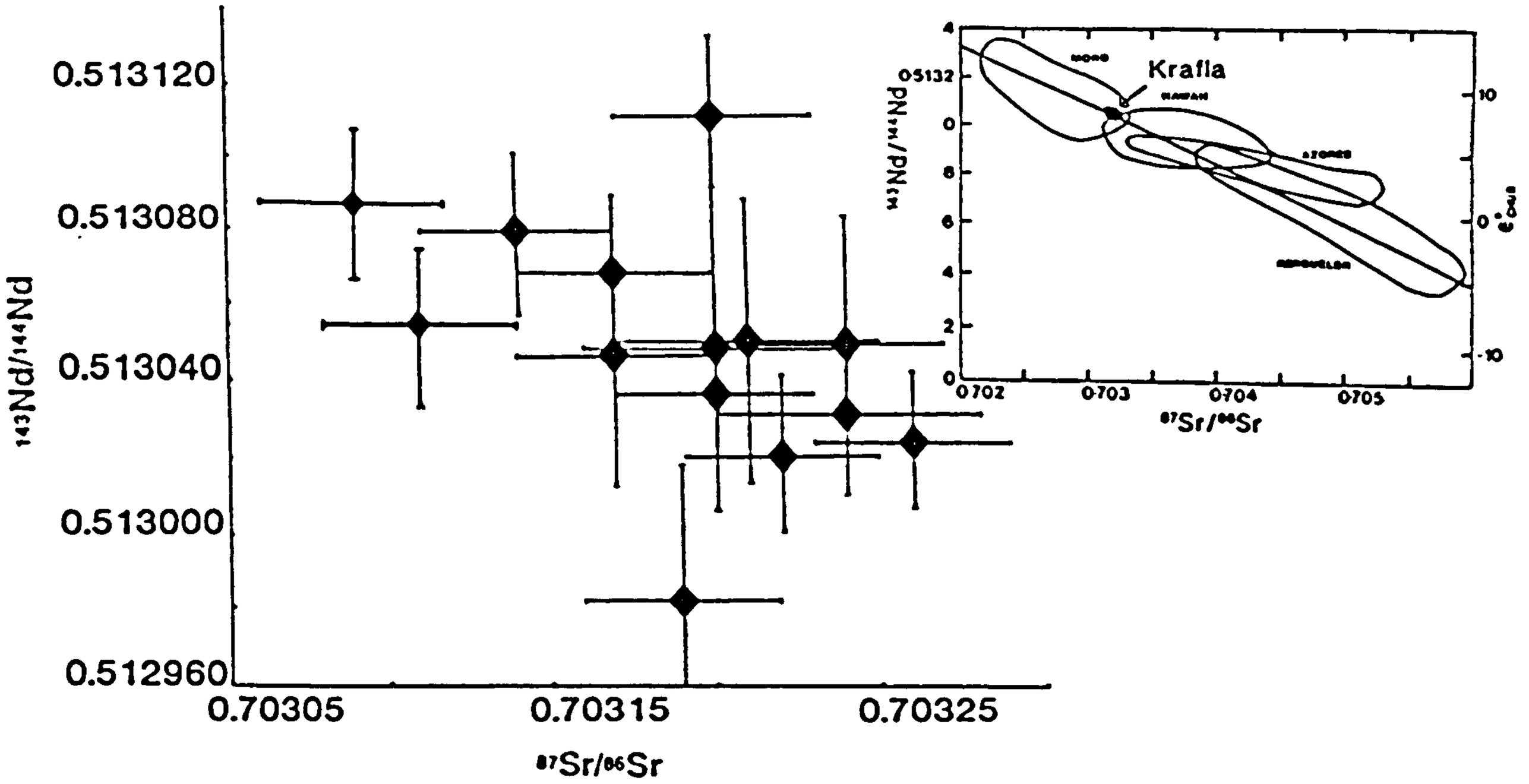


Fig. 7.7 $^{143}Nd/^{144}Nd$ *vs* $^{87}Sr/^{86}Sr$ for selected Krafla rocks (postglacial and last glacial). Error bars indicate 2σ precision. Inset shows the position of the Krafla samples compared with other oceanic basalts, adapted from Faure (1986).

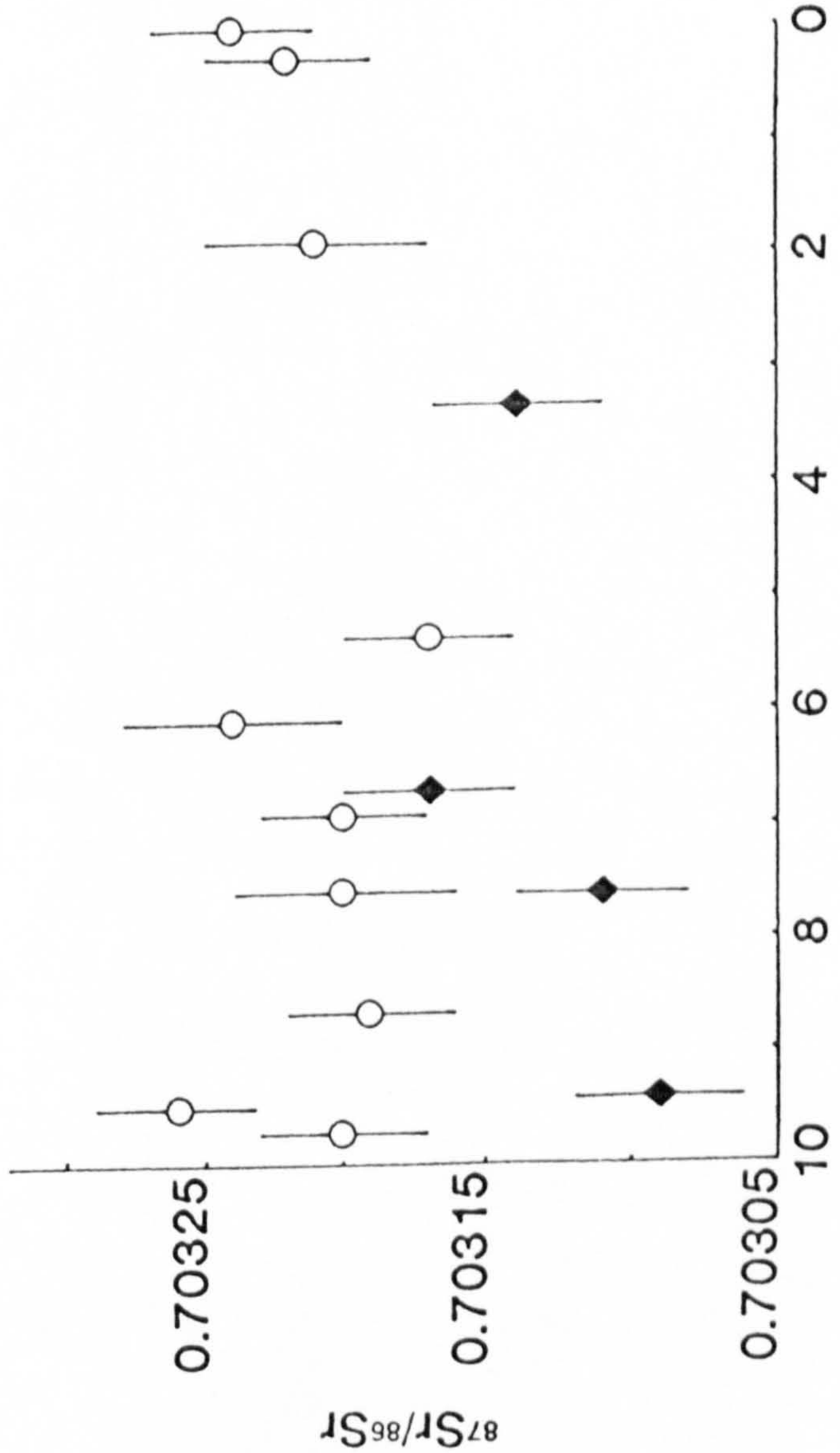


Fig. 7.8 $^{87}Sr/^{86}Sr$ *vs* MgO (wt%) for selected Krafla rocks (postglacial and last glacial). Samples shown by black diamonds are from the area S of Lúdent. Error bars as in Fig. 7.7.

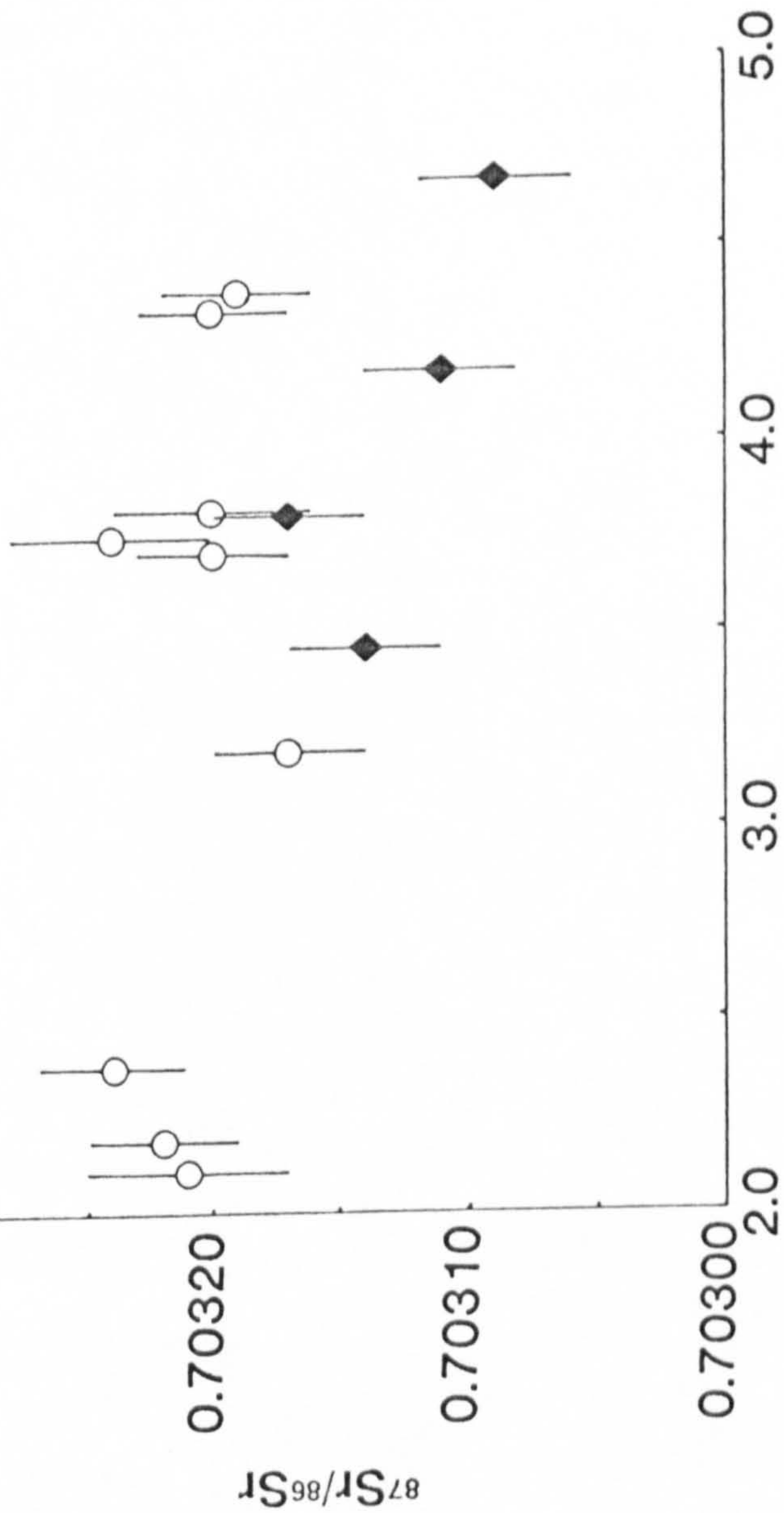


Fig 7.9 $^{87}Sr/^{86}Sr$ *vs* $\delta^{18}O$ values (‰) (whole-rock) for the samples shown in Fig. 7.8 excluding KK30. Samples shown by black diamonds are from the area S of Lúdent. Errors as Figs. 7.1 and 7.7.

geographic area to the S of Lúdent show lower values of $^{87}Sr/^{86}Sr$ (0.70309 to 0.70317) than the other Krafla samples irrespective of MgO contents or $\delta^{18}O$ value.

### 7.3.4 Discussion

The range in $^{87}Sr/^{86}Sr$ and $^{143}Nd/^{144}Nd$ values is relatively small compared with the total variation seen in and around Iceland (Hemond *et al.*, 1988) but is greater than the analytical error of the determinations (Fig. 7.7). The rough negative correlation between $^{143}Nd/^{144}Nd$ and $^{87}Sr/^{86}Sr$ suggests that most of the limited Sr-Nd isotope ratio variation may reflect mantle processes (as shown by the "Sr-Nd array"; O'Nions *et al.*, 1977) and not crustal processes. These arguments are developed below.

(1) Source

The $^{87}Sr/^{86}Sr$ values of hydrothermally-altered crust under Krafla are not known. It has been suggested that the hydrothermal alteration increases the value of $^{87}Sr/^{86}Sr$ of the Icelandic crust (Hemond *et al.*, 1988). Hemond *et al.* suggested that the hydrothermal interaction of Icelandic meteoric water ($^{87}Sr/^{86}Sr$ value of about 0.709) with fresh rocks could produce higher $^{87}Sr/^{86}Sr$ values in the altered material. However, the Sr concentration in Iceland meteoric water is likely to be in the order of parts per billion (cf. Sr in seawater of 100-200 ppm). So even if meteoric water has a $^{87}Sr/^{86}Sr$ of 0.709, then the overall budget of Sr in the altered crust is likely to be dominated by the Sr in the rocks (100-200 ppm) leading to only small changes in isotopic composition in the altered rocks.

An alternative process for increasing crustal $^{87}Sr/^{86}Sr$ values has been suggested (e.g. Steinthorsson *et al.*, 1987). If the Rb/Sr ratio of part of the crust is significantly increased, for example by forming rhyolites, then given sufficient time, the rhyolites' $^{87}Sr/^{86}Sr$ values can be increased. In practice it is difficult to envisage such a method working, because it would take at least 7.6 Ma to produce the highest measured Krafla value of $^{87}Sr/^{86}Sr$ from the lowest (using $^{87}Rb/^{86}Sr = 2.12$ as present in a rhyolite). This figure is an extremely low estimate of the necessary time, because the $^{87}Sr/^{86}Sr$ value of the assimilant necessary to produce the range of Krafla values by crustal assimilation would have to be considerably greater than the highest $^{87}Sr/^{86}Sr$ value in the suite, because the efficiency of the assimilation process is not likely to be high (see above). The age of the crust in the NE neovolcanic zone is unlikely to be more than 4-5 Ma (Saemundsson, 1974), which suggests that this is not a reasonable method for producing high crustal $^{87}Sr/^{86}Sr$ values.

The values of $^{143}Nd/^{144}Nd$ ratios are even less likely to change significantly as the crust ages due to the long half-life of $^{147}Sm$. The Icelandic crust is enriched in Nd relative to Sm, due to the greater incompatibility of Nd over Sm during partial melting and fractional crystallisation. In time, therefore, the $^{143}Nd/^{144}Nd$ ratio of the crust will increase more slowly (or if the crustal value of Sm/Nd = 0, then it stays constant) than the mantle source from which the lavas were originally generated, which is thought to have a relatively high ratio of Sm/Nd. Hence after a given time the crust will have a lower $^{143}Nd/^{144}Nd$ than the magmas being erupted, assuming the mantle source evolves steadily with time, according to its relatively high Sm/Nd ratio. The time required, however, to produce the total range of Krafla values, assuming the limiting case of Sm/Nd = 0 for the Krafla material, would need to be at least 100 Ma! This suggests that the Krafla differences in $^{143}Nd/^{144}Nd$ value are the result of mantle processes.

**(2) The effects of assimilation**

It would seem from the above discussion that the variation in $^{87}Sr/^{86}Sr$ and $^{143}Nd/^{144}Nd$ values from Krafla is highly unlikely to be caused by crustal processes but rather is a function of small variations in the mantle source. The total variation in Sr- and Nd-isotope ratios is small when compared with the total range of values seen in MORBs (Fig. 7.7). The poor correlation between $^{143}Nd/^{144}Nd$ and $^{87}Sr/^{86}Sr$ is perhaps not surprising when the limited total range of ratios is compared with the error estimates (Fig. 7.7). The lack of correlation between $^{87}Sr/^{86}Sr$ and MgO (Fig. 7.8) confirms that the AFC processes documented earlier do not seem to have altered the $^{87}Sr/^{86}Sr$ values significantly. The plot $^{87}Sr/^{86}Sr$ *vs* $\delta^{18}O$ (Fig. 7.9) gives a vague negative correlation but this probably results from the presence of a group of samples with low $^{87}Sr/^{86}Sr$ values at high $\delta^{18}O$ values (and high MgO), which may be derived from a slightly different mantle source. These samples with low values of $^{87}Sr/^{86}Sr$ come from a specific geographic area (S of Lúdent) and have large ranges in MgO content and $\delta^{18}O$ values. These features are consistent with low Sr-isotopic ratios reflecting a different mantle source for the lavas of this area, i.e. the different Sr-isotopic ratios have nothing to do with crustal processes.

There is a little evidence in this study in favour of the Sr-isotope ratios of Icelandic rhyolites being affected by crustal assimilation. However, other workers have recognised that Icelandic rhyolites have $^{87}Sr/^{86}Sr$ values at the high end of the total range of values of $^{87}Sr/^{86}Sr$ (O'Nions & Grönvold, 1973; Wood *et al.*, 1979; Condomines *et al.*, 1983). If the rhyolites are generated by fractional crystallisation directly from basalts with a range of values of $^{87}Sr/^{86}Sr$ reflecting variation in the

mantle source, then it is difficult to understand why the rhyolites have only high values of $^{87}Sr/^{86}Sr$. This suggests that the higher $^{87}Sr/^{86}Sr$ values in the rhyolites may reflect a component of Sr-contamination. This Sr-isotope contamination may be only detectable at extreme extents of differentiation when the Sr concentration in rhyolitic magma has fallen compared with that of most basalts.

### 7.3.5 Conclusions

The Krafla Sr-Nd isotopic data suggest that the observed variation in $^{87}Sr/^{86}Sr$ and $^{143}Nd/^{144}Nd$ ratios is mostly the result of mantle source variation. There appears to be little evidence in favour of changing $^{87}Sr/^{86}Sr$ values as a result of crustal assimilation. However, crustal assimilation may be necessary to explain the consistently higher $^{87}Sr/^{86}Sr$ values found in Icelandic rhyolites in general, although there is no specific evidence for this effect from the Krafla samples as reported in this study.

## 7.4 Conclusions

Postglacial rocks from Krafla show significant variation in O- and Th-isotopic ratios, which is consistent with crustal assimilation of low $\delta^{18}O$, low $(^{230}Th/^{232}Th)$ relatively old hydrothermally-altered oceanic crust. Additionally the $\delta^{18}O$ and $(^{230}Th/^{232}Th)$ values correlate positively with lava MgO contents, suggesting that crustal assimilation is likely to be coupled to fractional crystallisation. Magma mixing, which appears to be essential for effective assimilation throughout a volcanic suite, can explain the approximately straight-line nature of the $\delta^{18}O$ *vs* MgO plot (Fig. 7.1). Modelling the O- and Th-isotope data requires knowledge of the $\delta^{18}O$ and $(^{230}Th/^{232}Th)$ values and Th concentrations of the primary (uncontaminated) magma and the assimilant, as well as the efficiency of assimilation and the amount of liquid remaining. Given reasonable values for the above variables (e.g. $\delta_a$=-10‰) the results of the modelling suggest that the assimilant has a higher concentration of Th than thought to be present in average crust under Krafla. This implies that the crustal assimilation process occurs through relatively small degrees of partial melting of a basaltic wall-rock. Such a process can also explain the enrichment in the most incompatible elements above that expected by closed-system fractional crystallisation. An assimilant containing a relatively high Th concentration is consistent with its having a rhyolitic (or dacitic) composition. Sr- and Nd-isotope ratios vary little in the analysed postglacial and glacial samples from Krafla. Such

lack of variation is consistent with the assimilation of relatively young crust in the neovolcanic zone, which has had little time to evolve to higher $^{87}Sr/^{86}Sr$ and lower $^{143}Nd/^{144}Nd$ values.

# Chapter 8

# Conclusions

Two major igneous processes have been considered in this thesis. Firstly, the process of crustal assimilation, identified by various workers on a regional scale (e.g. Hemond *et al.*, 1988), has been confirmed from isotopic and other geochemical data to be operating in the Krafla volcanic system. The study has shown that Th- and O-isotope ratios both correlate positively with the MgO contents of the lavas, suggesting that assimilation is coupled to fractional crystallisation. The results of modelling the AFC process confirm that assimilation is likely to take place by a relatively small degree of partial melting of the crust (cf. Hemond *et al.*, 1988). The trace element data were also shown to be consistent with this model.

Secondly, considerable variation in the major- and trace-element compositions of the least differentiated lavas/hyaloclastites from Krafla was identified (cf. Bryan, 1979). This variation is consistent with variable degrees of partial melting at different average pressures in the mantle. For example, the positive correlation between the concentrations of $FeO^*$ and $K_2O$ in the least-differentiated basalts (>8 wt% MgO) suggests that basalts which are derived from relatively small degrees of melting are also generated at relatively high pressures (cf. Klein & Langmuir, 1987). In addition, the study has shown that the concentrations of $FeO^*$, $K_2O$, $Na_2O$ and $TiO_2$ correlate positively with the concentrations of incompatible trace elements and the ratios of concentrations of more to less incompatible trace elements. It has been suggested that these observations imply that the concentrations of the incompatible trace elements are "coupled" in some way to the major-element concentrations. The Krafla compositions have also been compared with the compositions calculated by a model for melt generation during adiabatic decompression (McKenzie & Bickle, 1988). This comparison suggested that the Krafla compositions are derived from asthenospheric mantle with a potential temperature of about 1480°C. However, it was also shown that application of the model of McKenzie & Bickle (1988) is less able to distinguish between basalts produced from mantle with different potential temperatures than was originally supposed.

## Summary

Fieldwork was undertaken in the Krafla volcanic system (as outlined in Chapter 2) and a suite of lava and hyaloclastite samples was collected from the last 4

interglacial periods and 3 glacial periods. This suite of samples covers a range in composition from basalts containing approximately 10 wt% MgO through to rhyolites with less than 0.4 wt% MgO.

Petrographic observations are documented in Chapter 3, and reveal a variety of phenocryst assemblages; (1) ol+plag, (2) ol+plag+cpx, (3) plag+cpx±ol, (4) plag+cpx+opx+FeTi-oxides, (5) plag+FeTi-oxides±fayalitic olivine±cpx, (6) plag only. Phenocryst assemblage (1) is generally found in samples containing the highest MgO contents, while the other groups occur at progressively lower MgO contents (with some overlap between the groups). These observations are consistent with magma differentiation via fractional crystallisation. Samples containing only plagioclase phenocrysts have a range of whole-rock compositions and the majority of these plagioclase phenocrysts appear to be xenocrystal in origin. The xenocrysts generally have compositions which range from $An_{80}$ to $An_{90}$, as is consistent with their derivation from relatively undifferentiated basaltic magmas (cf. Kuo & Kirkpatrick, 1982; Sparks *et al.*, 1984). It appears that plagioclase xenocrysts are incorporated into all Krafla lava types, with the exception of the rhyolites, by the mixing of relatively primitive magmas with more evolved ones. Repeated magma mixing is consistent with recent geophysical studies on the Krafla volcanic system, which have identified an inflating/deflating magma reservoir. The absence of plagioclase xenocrysts from the rhyolites implies that the rhyolites are either formed in isolation from mixing with the most primitive magmas, or that a substantial component of the rhyolites is derived by partial melting of the crust (O'Nions & Grönvold, 1973).

Major- and trace-element compositions of rocks from the Krafla suite are generally consistent with their origin through fractional crystallisation (see Chapters 4 and 5). The oxide or element variation diagrams plotted against MgO confirm that fractional crystallisation of the observed phenocryst phases can qualitatively explain the variation in compositions. Least-squares modelling of selected Krafla samples agrees with the idea of differentiation through closed-system fractional crystallisation. However, there is an excess of $K_2O$ in the rhyolites, which may be due to open system fractionation and/or crustal assimilation. The excess of $K_2O$ is also shown by the concentrations of Th, U and Rb. Numerical modelling of fractional crystallisation based on experimental data suggests that crystallisation over a range of pressures from 3.5 to 1 kbar can explain the differentiation trends.

Magma mixing may explain some aspects of the major- and trace-element compositions. Compatible major and trace elements are likely to be most readily affected by magma mixing. This process may explain some of the scatter in variation

diagrams and triangular plots (cf. Defant & Neilsen, 1990). The Krafla data fit with the model of Sparks & Marshall (1986) which shows that certain proportions of different liquids are unlikely to form mixtures which can be erupted. This results in "mixing forbidden" regions on element variation diagrams. However, the overall diversity of compositions in the suite is likely to result from fractional crystallisation processes. The incompatible elements may also be affected by mixing processes, although the importance of magma mixing in changing incompatible element concentrations and ratios of concentrations appears to be limited, confirming the view of Langmuir (1989) and in conflict with the model of O'Hara & Mathews (1981). The Krafla suite of rocks shows no evidence for progressive changes in incompatible element ratios with time, which would be expected from the open system fractionation model of O'Hara & Mathews (1981).

It was shown in Chapters 5 and 6 that the least-differentiated Krafla samples show varied concentrations of both major and trace elements. For example the primitive samples show positive correlations between concentrations of $Na_2O$, $K_2O$, $TiO_2$ and $FeO^*$. In addition the same samples show variable chondrite-normalised REE patterns and a range of Zr/Y ratios. Such variation is most unlikely to be a result of fractional crystallisation processes. Instead, results of experimental studies suggest that the differences in major-element concentrations are better explained by varied degrees of melting at different pressures, so that samples with higher concentrations of $Na_2O$, $K_2O$, $TiO_2$ and $FeO^*$ reflect smaller degrees of melting at higher than average pressure. In contrast, those samples with lower concentrations of these oxides appear to be derived from larger degrees of melting at a lower average pressure. The trace-element concentrations and ratios of concentrations also correlate with the above major-element concentrations. For example, samples with the highest concentrations of the most incompatible trace elements have the highest concentrations of $Na_2O$, $K_2O$, $TiO_2$ and $FeO^*$, suggesting that the concentrations of the incompatible trace elements are "coupled" in some way with the major element concentrations.

Various melting models can be used to explain the range in concentrations of the incompatible trace elements. However, as other workers have found for other suites of ocean ridge rocks (e.g. Langmuir *et al.*, 1977), relatively simple models such as batch melting or fractional melting fail to reproduce the observed range of trace element concentrations and ratios of concentrations. More complex melting models requiring only a small proportion of melt in equilibrium with the matrix at any given time, linked with the continuous extraction of melt (e.g. the "dynamic" melting of Langmuir *et al.*, 1977) may be required to help solve the problem of the varied

concentrations of trace element concentrations and ratios of concentrations in MORB suites.

The Krafla samples show distinctive chondrite-normalised spiderdiagrams (i.e. E-MORB patterns). The patterns are similar to that of average OIB, although the actual concentrations may be significantly less than those in OIB. This similarity of spiderdiagram pattern may suggest that the Krafla basalts share the same source as OIB. This appears to be confirmed by the relatively high $^{87}Sr/^{86}Sr$ and low $^{143}Nd/^{144}Nd$ values in rocks from the Krafla suite (see Chapter 7).

As shown in Chapter 6, the major-element compositions of the least-differentiated Krafla basalts are also distinctive, with higher concentrations of FeO*, and lower concentrations of $Na_2O$ and $SiO_2$; they lie to one extreme of the spectrum of MORB compositions. A recent model for melt generation at ridges (McKenzie & Bickle, 1988) suggests that the mantle beneath NE Iceland is considerably hotter than the mantle generating normal-thickness ocean ridges. The model suggests that the Krafla compositions are most consistent with a value of mantle potential temperature of about 1480°C, although in fact the Krafla compositions are within error of both 1380°C and 1580°C potential temperatures. This higher than average mantle potential temperature implies that the degree of melting and average pressure of melting beneath NE Iceland are greater than for the majority of MORBs, which may explain the lower than average concentrations of $Na_2O$ and $SiO_2$, and higher average concentrations of FeO* in the Krafla samples. A model mantle potential temperature of 1480°C should generate ~30km of melt, in agreement with estimates for the steady-state crustal thickness of Iceland. There are, however, discrepancies between the model compositions and the Krafla compositions, which may be rationalised by considering some of the assumptions used in the melt generation model. Firstly the model utilises experimental data derived by batch melting, when other lines of evidence (e.g. trace element ratios, excess ($^{230}Th$)) suggest that the actual melting process is more complicated. Secondly, the model treats Iceland as a simple passive-spreading system and does not take into account the motion of a mantle plume and the likely preferential incorporation of melt derived from small fractions at high pressure (cf. Watson & McKenzie, submitted 1990). The presence of a plume will, for a given value of $T_p$, increase the melt thickness, increase the average depth of melting and decrease the size of the average melt fraction. Thirdly, there appear to be some inadequacies in McKenzie & Bickle's (1988) parameterisation at the high pressures needed for a mantle plume, particularly for elements such as Al and Na. If a jadeite component in clinopyroxene becomes

significant at high pressures, then the melts formed at depth are likely to have lower concentrations of $Al_2O_3$ and $Na_2O$ than predicted by McKenzie & Bickle's model.

Postglacial (and some glacial) samples from Krafla show lower whole-rock $\delta^{18}O$ values than those commonly found in MORB samples, as other regional studies have found for Icelandic samples (e.g. Muehlenbachs *et al.*, 1974; Condomines *et al.*, 1983; Hemond *et al.*, 1988). The Krafla samples have $\delta^{18}O$ values ranging from +1.0 to 4.7‰ (cf. 5.7±0.3‰ for MORB), which are consistent with an origin for the Krafla suite through the interaction of crystallising primary magmas with low-$^{18}O$ hydrothermally-altered crust (cf. Muehlenbachs *et al.*, 1974) . The positive correlation between $\delta^{18}O$ and MgO (Fig. 7.1) suggests, however, that the low $\delta^{18}O$ values result from the linking of fractional crystallisation with crustal assimilation. That mixing processes in a shallow magma reservoir may also play a role is indicated by the straight-line nature of the $\delta^{18}O$ *vs* MgO plot (cf. Campbell & Turner, 1987).

Modelling the variation in $\delta^{18}O$ values in the Krafla suite requires knowledge of the likely $\delta^{18}O$ value of the crustal assimilant. This information is in part supplied by a drill-core sampling the crust above the Krafla magma chamber. The cored material reveals values of $\delta^{18}O$ that become progressively more negative with depth, reaching a value of about -10‰ at 2km (Hattori & Muehlenbachs, 1982). This value of -10‰ may be fairly realistic for the assimilant if the process occurs at the top of the seismically-identified magma reservoir (3 km depth). If this value of $\delta^{18}O$ is used in fitting an AFC model to the Krafla data, then the efficiency of the assimilation process is estimated to be between 10 and 20%.

In addition to this variation in O-isotope ratios, postglacial rocks from Krafla show decreasing values of ($^{230}Th/^{232}Th$) with decreasing values of MgO. This positive correlation is consistent with the assimilation of relatively old crust, i.e. crust old enough to be close to secular equilibrium (cf. Hemond *et al.*, 1988). While, it is possible that variable magma residence time could have caused the correlation between ($^{230}Th/^{232}Th$) and MgO, the crystallisation times required seem unreasonably long compared with the average time between eruptions. The AFC model may be extended also to cover the Th-isotope ratios and Th concentrations. This combined O-Th modelling suggests that crustal assimilation through the generation and incorporation of melts derived through relatively small degrees of partial melting coupled with fractional crystallisation is best able to explain decreasing values of both $\delta^{18}O$ and ($^{230}Th/^{232}Th$) with decreasing MgO. At the same time this process is capable of generating the high concentrations of Th in the most differentiated products, above those expected by closed-system fractional crystallisation.

The Sr- and Nd-isotope ratios in Chapter 7 show only limited variation in values, which is likely to be caused by primary differences in mantle isotopic ratios, rather than by crustal assimilation (in contrast with the views expressed by Steinthorsson *et al.*, 1987 and Hemond *et al.*, 1988).

In conclusion, therefore, the range of compositions in the Krafla suite appears to be the result of fractional crystallisation processes, in agreement with Wood *et al.* (1979). However, crustal assimilation also aids the generation of highly-differentiated rock types (Bowen, 1922; Ghiorso & Carmichael, 1985). As stated above, the major-element compositions of the least-differentiated Krafla samples suggest that the mantle beneath NE Iceland has a higher than normal potential temperature. This higher than normal temperature appears consistent with the presence of a mantle plume (cf. McKenzie & Bickle, 1988; White, 1990). However, the Krafla basalts also have distinctive trace element characteristics and Sr- and Nd-isotope ratios (E-MORB), which may imply that the plume temperature anomaly is accompanied by a different source from that supplying normal MORB and/or the preferential sampling of melts derived from a small melt fraction in a mantle plume. However, the Sr- and Nd-isotope characteristics of the Krafla samples are difficult to explain by the preferential incorporation of small melt fractions alone.

The presence of a mantle plume has led to thicker than normal oceanic crust. In turn, the thicker crust has allowed the development of long-lived magma reservoirs, which can produce a greater abundance of more differentiated rocks through longer periods of fractional crystallisation. As mentioned above, the crustal rocks surrounding the magma reservoirs have been hydrothermally altered by low $\delta^{18}O$ meteoric water. This altered wall-rock may be assimilated by the magma to produce the low $\delta^{18}O$ signature seen in the fresh Icelandic lavas. Hence, it could be argued that the Icelandic mantle plume is responsible, albeit rather indirectly, for the anomalously low $\delta^{18}O$ lavas.

## Suggestions for further work

The present study has shown that crustal assimilation is a significant process in the origin of the Krafla lavas, especially for more-differentiated compositions. However, it is debatable just how widespread the crustal assimilation process is under other ocean ridges. The identification of crustal assimilation in Iceland appears to be a consequence of subaerial spreading combined with a supply of low $\delta^{18}O$ meteoric water. However, such a supply of low $\delta^{18}O$ water is not generally available for

submarine oceanic crust. In contrast, crustal Th-isotopic ratios are independent of the topographic location of the spreading centre and only depend upon the age of the crust. Therefore, if crustal assimilation indeed occurs more widely than has been thought then it should be possible to identify its action from the change in ($^{230}Th/^{232}Th$) activity ratios with MgO (e.g. compare slow and fast spreading ridges).

New analytical techniques have recently been developed which can produce much higher precision in the determination of Th- and O-isotope ratios (e.g. Collerson *et al.*, 1989; Sharp, 1990). This could allow the determination of the ($^{230}Th/^{232}Th$) values of the most primitive Krafla samples. This would greatly help understanding of the nature of the melting process, especially with the role played by melts derived by small degrees of melting in the Icelandic plume (cf. Williams & Gill, 1989; Othman & Allègre, 1990).

In turn, higher precision O-isotope analyses, when combined with Th-isotope analyses could be used to investigate the variation of AFC processes over a short timescale and develop a more detailed model for the assimilation process. In addition, the combination of Ra- and Th-isotope analyses could allow an estimate to be made of magma residence-times for the Krafla suite.

Krafla provides a rare opportunity to study the temporal variation of ocean ridge processes, albeit modified by the presence of a mantle plume. The present study has identified no obvious changes in lava/hyaloclastite compositions with time. However, the dating at present is poor. If the ages of the samples were better known, for example by using AMS radiocarbon dating on organic fragments at the bases of lava flows and/or Th-isotopic analysis on mineral separates, then it would be feasible to look for changes in magmatic processes over shorter time periods than is possible at present. It may then be possible to identify temporal variations in the degree of partial melting or the character of the source.

# REFERENCES


Abbey S., 1980. Studies in "standard samples" for use in the general analysis of silicate rocks and minerals. Part 6: 1979 edition of "usable" values. *Geol. Surv. Canad. Paper*, 80-14.

Ahern J.L. & Turcotte D.L., 1979. Magma migration beneath an ocean ridge. *Earth planet. Sci. Lett.* 45, 115-122.

Arth J.G. & Hanson G.N., 1975. Geochemistry and origin of the early Precambrian crust of northeastern Minnesota. *Geochim. cosmochim. Acta* 39, 325-362.

Basaltic Volcanism Study Project, 1981. *Basaltic Volcanism on the Terrestrial Planets*. Pergamon Press, New York, 1286pp.

Beblo M. & Björnsson A., 1980. A model of electrical resistivity beneath NE Iceland, correlation with temperature. *J. Geophys.* 47, 164-190.

Bender J.F., Hodges F.N. & Bence A.E., 1978. Petrogenesis of basalts from the project FAMOUS area: an experimental study from 0 to 15 kbars. *Earth planet. Sci. Lett.* 41, 277-302.

Benjamin T.M., Heuser W.R. & Burnett D.S., 1978. Laboratory studies of actinide partitioning relevant to $^{244}Pu$ chronometry. *Proc. 9th Lunar Planet. Sci. Conf.*, 1393-1406.

Biggar G.M., 1983. Crystallisation of plagioclase, augite and olivine in synthetic systems and in tholeiites. *Miner. Mag.* 47, 161-176.

Björnsson A., 1985. Dynamics of crustal rifting in NE Iceland. *J. geophys. Res.* 90, 10151-10162.

Björnsson A., Saemundsson K., Einarsson P., Tryggvason E. & Grönvold K., 1977. Current rifting episode in north Iceland. *Nature* 266, 318-323

Björnsson A., Johnsen G., Sigurdsson S., Thorbergsson G. & Tryggvason E., 1979. Rifting of the plate boundary in N.Iceland 1975-78. *J. geophys. Res.* 84, 3029-3038.

Borthwick J. & Harmon R.S., 1982. A note regarding $ClF_3$ as an alternative to $BrF_5$ for oxygen isotope analysis. *Geochim. cosmochim. Acta* 46, 1665-1668.

Bott M.H.P. & Gunnarsson K., 1980. Crustal structure of the Iceland-Faeroe ridge. *J. Geophys.* 47, 221-227.

Bowen N.L., 1922. The behavior of inclusions in igneous magmas. *J. Geol.*. 30, 512-570.

Bowen N.L. & Schairer J.F., 1935. The system MgO-FeO-$SiO_2$. *Am. J. Sci. 4th Ser.* 29, 151-217.

Brandsdóttir B. & Einarsson P., 1979. Seismic activity associated with the September 1977 deflation of the Krafla central volcano in NE Iceland. *J. Volcanol. geotherm. Res.* 6, 197-212.

Brikowski T. & Norton D., 1989. Influence of magma chamber geometry on hydrothermal activity at mid-ocean ridges. *Earth planet. Sci. Lett.* 93, 241-255.

Bryan W.B., 1979. Regional variation and petrogenesis of basalt glasses from the FAMOUS area, Mid-Atlantic Ridge. *J. Petrology* 20, 293-325.

Bryan W.B., 1983. Systematics of modal phenocryst assemblages in submarine basalts: petrologic implications. *Contr. Miner. Petrol.* 83, 62-74.

Bryan W.B. & Moore J.G., 1977. Compositional variations of young basalts in the Mid-Atlantic Rift valley near latitude 36°49'. *Geol. Soc. Am. Bull.* 88, 556-570.

Buddington A.F. & Lindsley D.H., 1964. Iron-titanium oxide minerals and synthetic equivalents. *J. Petrology* 5, 310-357.

Byerly G.R., 1980. The nature of differentiation trends in some volcanic rocks from the Galapagos Spreading Center. *J. geophys. Res.* 85, 3797-3810.

Byerly G., Melson W.G. & Vogt P.R., 1976. Rhyodacites, andesites, ferrobasalts and ocean tholeiites from the Galapagos Spreading Center. *Earth planet. Sci. Lett.* 30, 215-221.

Calderone G., 1988. Halaraudar welded-tuff layer. *Initial Report of the Nordic Volcanological Institute.*

Campbell I.H. & Turner J.S., 1987. A laboratory investigation of assimilation at the top of a basaltic magma chamber. *J. Geol.* 95, 155-172.

Carmichael I.S.E., 1963. The crystallisation of feldspar in volcanic acid liquids. *Q. J. Geol. Soc. Lond.* 119, 95-131.

Carmichael I.S.E., 1964. The petrology of Thingmuli, a Tertiary volcano in Eastern Iceland. *J. Petrology* 5, 435-60.

Carmichael I.S.E., 1967. The mineralogy of Thingmuli, a Tertiary central volcano in Eastern Iceland. *Am. Miner.* 52, 1815-1841.

Cas R.A.F. & Wright J.V., 1987. *Volcanic successions, modern and ancient.* Allen & Unwin Ltd., London, 487 pp.

Christie D.M., Carmichael I.S.E. & Langmuir C.H., 1986. Oxidation states of mid ocean ridge basalt glasses. *Earth planet. Sci. Lett.* 79, 397-411.

Collerson K.D., Williams R.W. & Gill J.B., 1989. High precision $^{232}Th/^{230}Th$ ratio measurement by thermal ionization mass spectrometer. *Terra Abstracts* 1, 156.

Condomines M., Morand P. & Allègre C.J., 1981a. $^{230}Th$-$^{238}U$ radioactive disequilibria in tholeiites from the FAMOUS zone (Mid-Atlantic Ridge, 36°50'N): Th and Sr isotopic geochemistry. *Earth planet. Sci. Lett.* 55, 247-256.

Condomines M., Morand P., Allègre C.J. & Sigvaldason G.E., 1981b. $^{230}Th$-$^{238}U$ disequilibria in historical lavas from Iceland. *Earth planet. Sci. Lett.* 55, 393-406.

Condomines M., Tanguy J.C., Kieffer G. & Allègre C.J., 1982. Magmatic evolution of a volcano studied by $^{230}Th$-$^{238}U$ disequilibrium and trace element systematics: the Etna case. *Geochim. cosmochim. Acta* 46, 1397-1416.

Condomines M., Grönvold K., Hooker P.J., Muehlenbachs K., O'Nions R.K., Oskarsson N. & Oxburgh E.R., 1983. He, O, Sr & Nd isotope relationships in Icelandic volcanics. *Earth planet. Sci. Lett.* 66, 125-136.

Condomines M., Hemond C. & Allègre C.J., 1988. U-Th-Ra radioactive disequilibria and magmatic processes. *Earth planet. Sci. Lett.* 90, 243-263.

Courtney R.C. & White R.S., 1986. Anomalous heat flow and geoid across the Cape Verde Rise: evidence of dynamic support from a thermal plume in the mantle. *Geophys. J.R. astron. Soc.* 87, 815-868. .

Cox K.G., 1988. Numerical modelling of a randomized RTF magma chamber: A comparison with Continental Flood basalt sequences. *J. Petrology* 29, 681-697.

Cox K.G. & Hawkesworth C.J., 1985. Geochemical stratigraphy of the Deccan Traps at Mahabaleshwar, Western Ghats, India, with implications for open system magmatic processes. *J. Petrology* 26, 355-377.

Cox K.G. & Mitchell C., 1988. Importance of crystal settling in the differentiation of Deccan Trap basaltic magmas. *Nature* 333, 447-449.

Cox K.G., Bell J.D. & Pankhurst R.J., 1979. *The interpretation of igneous rocks.* Allen & Unwin, London.

Deer W.A., Howie R.A. & Zussman J., 1966. *An introduction to the rock forming minerals.* Longman, London.

Defant M.J. & Neilsen R.L., 1990. Interpretation of open system petrogenetic processes: Phase equilibria constraints on magma evolution. *Geochim. cosmochim. Acta* 54, 87-102.

De Paolo D.J., 1981. Trace element and isotopic effects of combined wallrock assimilation and fractional crystallisation. *Earth planet. Sci. Lett.* 53, 189-202.

Dick H.J.B., Fisher R.L. & Bryan W.B., 1984. Mineralogic variability of the uppermost mantle along mid-ocean ridges. *Earth planet. Sci. Lett.* 69, 88-106.

Drake M.J., 1976. Plagioclase-melt equilibria. *Geochim. cosmochim. Acta* 40, 457-465.

Droop G.T.R., 1987. A general equation for estimating Fe3+ concentrations in ferromagnesian silicates and oxides from microprobe analyses, using stoichiometric criteria. *Miner. Mag.* 51, 431-5.

Dungan M.A. & Rhodes J.M., 1978. Residual glass and melt inclusions in basalts from DSDP Legs 45 and 46: evidence for magma mixing. *Contr. Miner. Petrol.* 67, 417-431.

Dymoke P.L., 1988. Geochronological and petrological studies of the thermal evolution of the Dalradian, SW Scottish, Highlands. Unpubl. Ph.D. thesis, Univ. of Edinburgh.

Einarsson P., 1978. S-wave shadows in the Krafla caldera in NE Iceland, evidence for a magma chamber in the crust. *Bull. Volcanol.* 41, 187-195.

Einarsson P. & Brandsdóttir B., 1980. Seismological evidence for lateral magma intrusion during the July 1978 deflation of the Krafla volcano in NE-Iceland. *J. Geophys.* 47, 160-165.

Elthon D., 1989. Pressure of origin of primary mid-ocean ridge basalts. *In*: Norry M.J. & Weaver S.D. (eds.) *Magmatism in the Ocean Basins. Spec. Pub. Geol. Soc. London* 42, 125-136.

Engel A.E., Engel C.G. & Havens R.G., 1965. Chemical characteristics of oceanic basalts and the upper mantle. *Bull. Geol. Soc. Am.* 76, 719-34.

Faure G., 1986. *Principles of isotope geology*. 2nd edition. John Wiley & Sons, Inc., New York.

Fitton J.G. & Dunlop H.M., 1985. The Cameroon line, West Africa and its bearing on the origin of oceanic and continental alkali basalts. *Earth planet. Sci. Lett.* 72, 23-38.

Fitton J.G., James D.E. & Thirlwall M.F., 1984. *A user's guide to the X-ray fluorescence analysis of rock samples*. Unpubl. report, 2nd edition, Univ. of Edinburgh.

Fitton J.G., James D.E. & Leeman W.P., 1990. Basic magmatism associated with late Cenozoic extension in the western United States: Compositional variations in space and time. Submitted to *J. geophys. Res.*

Flower M.F.J., Schmincke H.-U., & Thompson R.N., 1975. Phlogopite stability and the $^{87}Sr/^{86}Sr$ step in the basalts along the Reykjanes Ridge. *Nature* 254, 404-405.

Ford C.E., Russell D.G., Craven J.A. & Fisk M.R., 1983. Olivine-liquid equilibria: temperature, pressure and composition dependence of the crystal/liquid cation partition coefficients for Mg, $Fe^{2+}$, Ca and Mn. *J. Petrology* 24, 256-265.

Foucher J.P., Le Pichon X. & Sibuet J.C., 1982. The Ocean-Continent transition in the uniform lithosphere stretching model: role of partial melting in the mantle. *Philos. Trans. R. Soc. Lond. Ser.* A305, 27-43.

Francis D., 1986. The pyroxene paradox in MORB glasses - a signature of picritic parental magmas? *Nature* 319, 586-589.

Frey F.A., Green D.H. & Roy S.D., 1978. Integrated models of basalt petrogenesis: A study of quartz tholeiites to olivine melilitites from south eastern Australia utilizing geochemical and experimental petrological data. *J. Petrology* 19, 463-513.

Friedleifsson I.B., 1973. Petrology and structure of the Esja Quaternary volcanic region, SW Iceland. Unpubl. D.Phil. thesis, Oxford University.

Fujii T. & Scarfe C.M., 1985. Composition of liquids coexisting with spinel lherzolite at 10 kbar and the genesis of MORBs. *Contr. Miner. Petrol.* 90, 18-28.

Furnes H., Friedleifsson I.B. & Atkins F.B., 1980. Subglacial volcanics - on the formation of acid hyaloclastites. *J. Volcanol. geotherm. Res.* 8, 95-110.

Galer S.J.G. & O'Nions R.K., 1986. Magmagenesis and the mapping of chemical and isotopic variations in the mantle. *Chem. Geol.* 56, 45-61.

Gast P.W., 1968. Trace element fractionation and the origin of tholeiitic and alkaline magma types. *Geochim. cosmochim. Acta* 32, 1057-1086.

Ghiorso M.S. & Carmichael I.S.E., 1985. Chemical mass transfer in magmatic processes II. Applications in equilibrium crystallisation, fractionation and assimilation. *Contr. Miner. Petrol.* 90, 121-141.

Green D.H., 1973. Experimental melting studies on a model upper mantle composition at high pressure under water saturated and undersaturated conditions. *Earth planet. Sci. Lett.* 19, 37-53.

Green D.H. & Ringwood A.E., 1967. The genesis of basaltic magmas. *Contr. Miner. Petrol.* 15, 103-190.

Gregory R.T. & Taylor H.P., 1981. An oxygen isotope profile in a section of Cretaceous oceanic crust, Samail Ophiolite, Oman: evidence for $\delta^{18}O$ buffering of the oceans by deep (>5km) seawater-hydrothermal circulation at mid-ocean ridges. *J. geophys. Res.* 86, 2737-2755.

Gregory R.T. & Criss R.E., 1986. Isotopic exchange in open and closed systems. *In:* Valley J.W., Taylor H.P. & O'Neil J.R., (eds.), *Stable isotopes in high temperature geological processes.* Min. Soc. Am. Reviews in Mineralogy 16, Washington.

Grönvold K. & Mäkipää H., 1978. Chemical composition of Krafla lavas 1975-77, *Nordic Volcanological Institute Report* 7816.

Grönvold K., 1984. Myvatn fires 1724-1729 chemical composition of the lava. *Nordic Volcanological Institute Report* 8401.

Gudmundsson A., 1988. Formation of collapse calderas. *Geology* 16, 808-810.

Halliday A.N., Dickin A.P., Fallick A.E. & Fitton J.G., 1988. Mantle dynamics: A Nd,Sr,Pb and O isotopic study of the Cameroon Line volcanic chain. *J. Petrology* 29, 181-211.

Hanson G.N., 1977. Geochemical evolution of the sub-oceanic mantle. *J. Geol. Soc. Lond.* 134., 235-253.

Harrison W.J., 1981. Partitioning of REE between minerals and coexisting melts during partial melting of a garnet lherzolite. *Am. Miner.* 66, 242-59.

Hart S.R., Schilling J.-G. & Powell J.L., 1973. Basalts from Iceland and along the Reykjanes Ridge. Sr isotope geochemistry. *Nature Phys. Sci.* 246, 104-107.

Hattori K. & Muehlenbachs K., 1982. Oxygen isotope ratios of the Icelandic crust. *J. geophys. Res.* 87, 6559-6565.

Helz R.T., 1973. Phase relations of basalts in their melting range $p_{H2O}$ = 5 kb as a function of oxygen fugacity. Part I, Mafic phases. *J. Petrology* 14, 249-302.

Helz R.T., 1976. Phase relations of basalts in their melting range $p_{H2O}$ = 5 kb as a function of oxygen fugacity. Part I, Melting compositions. *J. Petrology* 17, 139-193.

Hemond C., Condomines M., Fourcade S., Allègre C.J., Oskarsson N. & Javoy M., 1988. Th, Sr & O isotopic geochemistry in recent tholeiites from Iceland: crustal influence on mantle derived magmas. *Earth planet. Sci. Lett.* 87, 273-285.

Henderson P., 1982. *Inorganic geochemistry*. Pergamon Press, Oxford.

Hildreth W., 1981. Gradients in silicic magma chambers: implications for lithospheric magmatism. *J. geophys. Res.* 86, 10153-10192.

Hoffmann A.W., 1988. Chemical differentiation of the Earth: the relationship between mantle, continental crust, and oceanic crust. *Earth planet. Sci. Lett.* 90, 297-314.

Huppert H.E. & Sparks R.S.J., 1980. The fluid dynamics of a basaltic magma chamber replenished by influx of hot, dense ultrabasic magma. *Contr. Miner. Petrol.* 75, 279-289.

Huppert H.E., Sparks R.S.J. & Turner J.S., 1982. Replenished magma chambers: effects of compositional zonation and input rates. *Earth planet. Sci. Lett.* 57, 345-357.

Imsland P., 1978. The petrology of Iceland: some general remarks. *Nordic Volcanological Institute Report* 7808.

Imsland P., 1983. Iceland and the ocean floor. Comparison of the magmatic rocks and some volcanic features. *Contr. Miner. Petrol.* 83, 31-37.

Irvine T.N. & Baragar W.R.A., 1971. A guide to the classification of common volcanic rocks. *Can. J. Earth Sci.* 8, 523-548.

Irving A.J., 1978. A review of experimental studies of crystal/liquid trace element partitioning. *Geochim. cosmochim. Acta* 42, 743-770.

Ito K. & Kennedy G.C., 1967. Melting and phase relations in a natural peridotite to 40 kilobars. *Am. J. Sci.* 265, 519-538.

Jakobsson S.P., 1972. Chemistry and distribution pattern of Recent basaltic rocks in Iceland. *Lithos.* 5, 365-386.

Jakobsson S.P., 1979. Petrology of recent basalts of the eastern volcanic zone, Iceland. *Acta. Nat. Islandica* 26, 1-103.

Jakobsson S.P., 1980. Outline of the petrology of Iceland. *Jökull* 29, 57-73.

Jaques A.L. & Green D.H., 1980. Anhydrous melting of peridotite at 0-15 kb pressure and the genesis of tholeiitic basalts. *Contr. Miner. Petrol.* 73, 287-310.

Jóhannesson H., 1975. Structure and petrochemistry of the Reykjadalur central volcano and the surrounding areas, Midwest Iceland. Unpubl. Ph.D. thesis, University of Durham.

Johnson K.T.M., Dick H.J.B. & Shimizu N., 1990. Melting in the oceanic upper mantle: An ion microprobe study of diopsides in abyssal peridotites. *J. geophys. Res.* 95, 2661-2678.

Joly J., 1909. On the radioactivity of certain lavas. *Philos. Mag.* 18.

Jones J.G., 1969. Intraglacial volcanoes of the Laugarvatn region southwest Iceland I. *Q. J. Geol. Soc. Lond.* 124, 197211.

Kay R.W. & Hubbard N.J., 1978. Trace elements in ocean ridge basalts. *Earth planet. Sci. Lett.* 38, 95-116.

Kellogg T.B., 1976. Late quaternary climatic changes: evidence from deep-sea of Norwegian and Greenland seas. *Geol. Soc. Am. Mem.* 145, 77-110.

Klein E.M. & Langmuir C.H., 1987. Global correlations of ocean ridge basalt chemistry with axial depth and crustal thickness. *J. geophys. Res.* 92, 8089-8115.

Krishnaswami S., Turekian K.K. & Bennett J.T., 1984. The behavior of $^{232}Th$ and $^{238}U$ decay chain nuclides during magma formation and volcanism. *Geochim. cosmochim. Acta* 48, 505-511.

Kudo A.M. & Weill D.F., 1970. An igneous plagioclase thermometer. *Contr. Miner. Petrol.* 25, 52-65.

Kuo L.-C. & Kirkpatrick R.J., 1982. Pre-eruption history of phyric basalts from DSDP Legs 45 and 46: Evidence from morphology and zoning patterns in plagioclase. *Contr. Miner. Petrol.* 79, 13-27.

Kurz M.D., Meyer P.S. & Sigurdsson H., 1985. Helium isotopic systematics within the neovolcanic zones of Iceland. *Earth planet. Sci. Lett.* 74, 291-305.

Kyser T.K., 1986. Stable isotope variations in the mantle. *In*: Valley J.W., Taylor H.P. & O'Neil J.R., (eds.), *Stable isotopes in high temperature geological processes.* Min. Soc. Am. Reviews in Mineralogy 16, Washington.

Langmuir C.H., 1989. Geochemical consequences of *in situ* crystallization. *Nature* 340, 199-205.

Langmuir C.H. & Hanson G.N., 1980. An evaluation of major element heterogeneity in the mantle sources of basalts. *Philos. Trans. R. Soc. Lond. Ser.* A297, 383-407.

Langmuir C.H. & Hanson G.N., 1981. Calculating mineral-melt equilibria with stoichiometry, mass balance and single-component distribution coefficients. *In*: Newton R.C., Navrotsky A. & Wood B.J. (eds.), *Thermodynamics of Minerals and Melts*, New York: Springer-Verlag, 247-271.

Langmuir C.H., Bender J.F., Bence A.E., Hanson G.N. & Taylor S.R., 1977. Petrogenesis of basalts from the FAMOUS area; Mid-Atlantic Ridge. *Earth planet. Sci. Lett.* 36, 133-156.

Larsen G., Grönvold K. & Thorarinsson S., 1979. Volcanic eruption through a geothermal borehole at Námafjall, Iceland. *Nature* 278, 707-710.

Latin D.M., 1990. The relationship between extension and magmatism in the North Sea Basin. Unpubl. Ph.D. thesis Univ. of Edinburgh.

Lindsley D.H., 1983. Pyroxene thermometry. *Am. Miner.* 68, 477-493.

Lipman P.W. & Friedman I., 1975. Interaction of meteoric water with magma: An oxygen isotope study of ash-flow sheets from southern Nevada. *Geol. Soc. Am. Bull.* 86, 695-702.

Liu M. & Chase C.G., 1990. Evolution of Hawaiian basalts: a hotpsot melting model. *Earth planet. Sci. Lett.* in press.

Macdonald K.C., 1982. Mid-ocean ridges: fine scale tectonic, volcanic and hydrothermal processes within the plate boundary zone. *Ann. Rev. Earth Planet. Sci.* 10, 155-90.

Macdonald R., Sparks R.S.J., Sigurdsson H., Mattey D.P., McGarvie D.W. & Smith R.L., 1987. The 1875 eruption of Askja volcano Iceland: combined fractional crystallisation and selective contamination in the generation of rhyolitic magma. *Miner. Mag.* 51, 183-202.

MacDougall J.D. & Rubin K., 1987. Implications of uranium series disequilibrium in MORB for the timescale of melt generation. *IUGG Abstract (Vancouver)* 2, 401.

McBirney A.R. & Noyes R.M., 1979. Crystallisation and layering of the Skaergaard Intrusion. *J. Petrology* 20, 487-554.

McGarvie D.W., 1984. Torfajökull: A volcano dominated by magma mixing. *Geology* 12, 685-688.

McKenzie D., 1984. The generation and compaction of partially molten rock. *J. Petrology* 25, 713-765.

McKenzie D., 1985a. The extraction of magma from the crust and mantle. *Earth planet. Sci. Lett.* 74, 81-91.

McKenzie D., 1985b. $^{230}Th$-$^{238}U$ disequilibrium and melting processes beneath ridge axes. *Earth planet. Sci. Lett.* 72, 149-157.

McKenzie D.P. & Bickle M.J., 1988. The volume and composition of melt generated by extension of the lithosphere. *J. Petrology* 29, 625-679.

Melson W.G., Byerly G.R., Nelson J.A., O'Hearn T., Wright T.L. & Vailler T., 1977. A catalog of major element chemistry of abyssal volcanic glasses. *Smithsonian Contrib. Earth. Sci.* 19, 31-60.

Meyer P.S., Sigurdsson H. & Schilling J-G., 1985. Petrological and geochemical variations along Iceland's neovolcanic zones. *J. geophys. Res.* 90, 10043-10072.

Michael P.J. & Bonatti E., 1985. Peridotite composition from the North Atlantic: regional and tectonic variations and implications for partial melting. *Earth planet. Sci. Lett.* 73, 91-104.

Moorbath S. & Walker G.P.L., 1963. Strontium isotope investigation of igneous rocks from Iceland. *Nature* 207, 837-40.

Morgan W.J., 1971. Convection plumes in the lower mantle. *Nature* 230, 42-3.

Muehlenbachs K. & Byerly G., 1982. $^{18}O$ - Enrichment of silicic magmas caused by crystal fractionation at the Galapagos Spreading Center. *Contr. Miner. Petrol.* 79, 76-79.

Muehlenbachs K., Anderson A.T. & Sigvaldason G.E., 1974. Low-$O^{18}$ basalts from Iceland. *Geochim. cosmochim. Acta* 38, 577-588.

Muir I.D. & Tilley C.E., 1964. Basalts from the northern part of the rift zone of the Mid-Atlantic Ridge. *J. Petrology* 5, 409-434.

Mysen B.O. & Kushiro I., 1977. Compositional variations of coexisting phases with the degree of melting of peridotite in the upper mantle. *Am. Miner.* 62, 843-865.

Nakamura N., 1974. Determination of REE, Ba, Fe, Mg, Na and K in carbonaceous and ordinary chondrites. *Geochim. cosmochim. Acta* 38, 757-775.

Nathan H.D. & Van Kirk C.K., 1978. A model of magmatic crystallization. *J. Petrology* 19, 66-94.

Natland J.H., 1989. Partial melting of a lithologically heterogeneous mantle: inferences from crystallisation histories of magnesian abyssal tholeiites from the Squeiros Fracture Zone. *In*: Norry M.J. & Weaver S.D. (eds.) *Magmatism in the Ocean Basins. Spec. Pub. Geol. Soc. London* 42, 41-70.

Niemczyk O., 1943. *Spalten auf Island.* Konrad Wittwer, Stuttgart.

O'Hara M.J., 1968a. The bearing of phase equilibria studies in synthetic and natural systems on the origin and evolution of basic and ultrabasic rocks. *Earth Sci. Rev.* 4, 69-133.

O'Hara M.J., 1968b. Are any ocean floor basalts primary magma? *Nature* 220, 683-686.

O'Hara M.J., 1973. Non-primary magmas and dubious mantle plume beneath Iceland. *Nature* 243, 507-8.

O'Hara M.J., 1977. Geochemical evolution during fractional crystallisation of a periodically refilled magma chamber. *Nature* 266, 503-507.

O'Hara M.J., 1985. Importance of the "shape" of the melting regime during partial melting of the mantle. *Nature* 314, 58-62.

O'Hara M.J. & Mathews R.E., 1981. Geochemical evolution of an advancing, periodically tapped, continuously fractionated magma chamber. *J. geol. Soc. Lond.* 138, 237-277.

Olafsson M. & Eggler D.H., 1983. Phase relations of amphibole-carbonate and phlogopite-carbonate peridotite: Petrologic constraints on the asthenosphere. *Earth planet. Sci. Lett.* 64, 305-315.

O'Neil J.R., 1986. Theoretical and experimental aspects of isotopic fractionation. *In*: Valley J.W., Taylor H.P. & O'Neil J.R., (eds.), *Stable isotopes in high temperature geological processes.* Min. Soc. Am. Reviews in Mineralogy 16, Washington.

O'Nions R.K. & Grönvold K., 1973. Petrogenetic relationships of acid and basic rocks in Iceland: Sr isotopes and REEs in late and postglacial volcanics. *Earth planet. Sci. Lett.* 19, 397-409.

O'Nions R.K. & Pankhurst R.J., 1974. Petrogenetic significance of isotope and trace element variations in volcanic rocks from the Mid-Atlantic. *J. Petrology* 15, 603-634.

O'Nions R.K., Pankhurst R.J. & Grönvold K., 1976. Nature and development of basalt magma beneath Iceland and the Reykjanes Ridge. *J. Petrology* 17, 315-338.

O'Nions R.K., Hamilton P.J. & Evensen N.M., 1977. Variations in $^{143}Nd/^{144}Nd$ and $^{87}Sr/^{86}Sr$ ratios in oceanic basalts. *Earth planet. Sci. Lett.* 34, 13-22.

Oskarsson N., Steinthorsson S. & Sigvaldason G.E., 1985. Iceland geochemical anomaly: origin, volcanotectonics, chemical fractionation and isotope evolution of the crust. *J. geophys. Res.* 90, 10011-10025.

Othman D.B. & Allègre C.J., 1990. U-Th isotopic systematics at 13°N east Pacific ridge segment. *Earth planet. Sci. Lett.* 98, 129-137.

Oversby V.M. & Gast P.W., 1968. Lead isotope compositions and U-decay series disequilibrium in recent volcanic rocks. *Earth planet. Sci. Lett.* 5, 199-206.

Oxburgh E.R., 1980. Heat flow and magma genesis. *In*: Hargreaves R.B. (ed.) *Physics of Magmatic Processes.* New Jersey: Princeton University Press, 161-199.

Pálmason G., 1973. Kinematics and heat flow in a volcanic rift zone, with application to Iceland. *Geophys. J. R. Astron. Soc.*, 33, 451-481.

Pálmason G., 1981. Crustal rifting, and related thermo-mechanical processes in the lithosphere beneath Iceland. *Geol. Rundsch.* 270, 244-260.

Pearce J.A. & Norry M.J., 1979. Petrogenetic implications of Ti, Zr, Y and Nb variations in volcanic rocks. *Contr. Miner. Petrol.* 69, 33-47.

Poldervaart A. & Hess H.H., 1951. Pyroxenes in the crystallisation of basaltic magma. *J. Geol.* 59, 474-489.

Powell R. & Powell M., 1977. Geothermometry and oxygen barometry using coexisting iron-titanium oxides: a reappraisal. *Miner. Mag.* 41, 257-263.

Presnall D.C., Dixon S.A., Dixon J.R., O'Donnell T.H., Brenner N.L., Schrock R.L. & Dycus D.W., 1978. Liquidus phase relations on the join diopside-forsterite-anorthite from 1 atm to 20 kbar: their bearing on the generation and crystallization of basaltic magma. *Contr. Miner. Petrol.* 66, 203-220.

Presnall D.C., Dixon J.R., O'Donnell T.H. & Dixon S.A., 1979. Generation of mid-ocean ridge tholeiites. *J. Petrology* 20, 3-35.

Pyle D.M., Ivanovich M. & Sparks R.S.J., 1988. Magma-cumulate mixing identified by U-Th disequilibrium dating. *Nature* 331, 157-159.

Ribe N.M., 1985. The generation and composition of partial melts in the Earth's mantle. *Earth planet. Sci. Lett.* 73, 361-376.

Ribe N.M., 1988. Dynamical geochemistry of the Hawaiian plume. *Earth planet. Sci. Lett.* 88, 37-46.

Ribe N.M. & Smooke M.D., 1987. A stagnation-point flow model for melt extraction from a mantle plume. *J. geophys. Res.* 92, 6437-6443.

Richter F.M., 1986. Simple models for trace element fractionation during melt segregation. *Earth planet. Sci. Lett.* 77, 333-344.

Richter F.M. & McKenzie D.P., 1984. Dynamical models for melt segregation from a deformable matrix. *J. Geol.* 93, 729-740.

Roeder P.L. & Osborn E.F., 1966. Experimental data for the system $MgO$-$FeO$-$Fe_2O_3$-$CaAl_2Si_2O_8$-$SiO_2$. *Am. J. Sci.* 264, 428-480.

Roeder P.L. & Emslie R.F., 1970. Olivine-liquid equilibrium. *Contr. Miner. Petrol.* 29, 275-289.

Russell D.G., 1985. Experimental and petrological studies of phenocryst assemblages in Scottish Permo-Carboniferous basaltic rocks. Unpubl. Ph.D. thesis, Univ. of Edinburgh.

Saemundsson K., 1974. Evolution of the axial rifting zone in northern Iceland and the Tjörnes Fracture Zone. *Geol. Soc. Am. Bull.* 85, 495-504.

Saemundsson K., 1977. Fissure swarms and central volcanoes of the neovolcanic zones of Iceland. *In*: Bowes D.R. & Leake B.E. (eds.), *Crustal evolution in northwestern Britain and adjacent regions. Geol. J. Spec. Issue* 10, 415-432.

Saemundsson K. & Noll H., 1974. K/Ar ages of rocks from Husafell, western Iceland and the development of the Husafell central volcano. *Jökull* 24, 40-59.

Schilling J.-G., 1973. Iceland mantle plume: geochemical study of Reykjanes Ridge. *Nature* 242, 565-573, 1973.

Schilling J.-G., 1975. Rare earth variations across "normal" ridge, 29°S, and East Pacific Rise, 2-19°S, and evidence on the composition of the underlying low-velocity layer. *J. geophys. Res.* 80, 1459-1473.

Schilling J.-G., Zajac M., Evans R., Johnston T., White W., Devine J.D. & Kingsley R., 1983. Petrologic and geochemical variation along the Mid-Atlantic Ridge from 29°N to 73°N. *Am. J. Sci.* 283, 510-586.

Schmeling H., 1985. Partial melt below Iceland: A combined interpretation of seismic and conductivity data. *J. geophys. Res.* 90, 10105-10116.

Schnetzler C.C. & Philpotts J.A., 1970. Partition coefficients of rare-earth elements between igneous matrix material and rock-forming mineral phenocrysts - II. *Geochim. cosmochim. Acta* 34, 331-340.

Scott D.R. & Stevenson D.J., 1984. Magma solitons. *Geophys. Res. Lett.* 11, 1161-1164.

Sharp Z.D., 1990. A laser-based microanalytical method for the *in situ* determination of oxygen isotope ratios of silicates and oxides. *Geochim. cosmochim. Acta* 54, 1353-1358.

Shibata T., Delong S.E. & Walker D., 1979. Abyssal tholeiites from the Oceanographer Fracture Zone: I. Petrology and fractionation. *Contr. Miner. Petrol.* 70, 89-102.

Sigurdsson H., 1977. Generation of Icelandic rhyolites by melting plagiogranites in the oceanic layer. *Nature* 269, 25-28.

Sigurdsson H., 1981. First order major element variation in basalt glasses from the Mid-Atlantic Ridge 29-73°N, *J. geophys. Res.* 86, 9483-9502.

Sigurdsson H. & Schilling J.-G., 1976. Spinels in Mid-Atlantic Ridge basalts: Chemistry and occurrence. *Earth planet. Sci. Lett.* 29, 7-20.

Sigurdsson H. & Sparks R.S.J., 1981. The petrology of rhyolitic and mixed magma ejecta from the 1875 eruption of Askja Iceland. *J. Petrology* 22, 41-84.

Sigvaldason G.E., 1968. Structure and products of subaquatic volcanoes in Iceland. *Contr. Miner. Petrol.* 18, 1-16.

Sigvaldason G.E., 1974a. Basalts from the centre of the assumed Icelandic mantle plume. *J. Petrology* 15, 497-524.

Sigvaldason G.E., 1974b. The petrology of Hekla and origin of silicic rocks in Iceland. The eruption of Hekla 1947-48. *Soc. Sci. Islandica* 5, 1-44.

Sparks R.S.J. & Huppert H.E., 1984. Density changes during fractional crystallisation of basaltic magmas: fluid dynamic implications. *Contr. Miner. Petrol.* 85, 300-309.

Sparks R.S.J. & Marshall L.A., 1986. Thermal and mechanical constraints on mixing between mafic and silicic magmas. *J. Volcanol. geotherm. Res.* 29, 99-124.

Sparks R.S.J., Meyer P. & Sigurdsson H., 1980. Density variation amongst MORBs: implications for magma mixing and the scarcity of primitive lavas. *Earth planet. Sci. Lett.* 46, 419-430.

Sparks R.S.J., Huppert H.E. & Turner J.S., 1984. The fluid dynamics of evolving magma chambers. *Phil. Trans. R. Soc. Lond.* A310, 511-534.

Spulber S.D. & Rutherford M.J., 1983. The origin of rhyolite and plagiogranite in oceanic crust: an experimental study. *J. Petrology* 24, 1-25.

Stakes D.S., Shervais J.W. & Hopson C.A., 1984. The volcanic-tectonic cycle of the FAMOUS and AMAR valleys, Mid-Atlantic Ridge (36°47'): Evidence from basalt glass and phenocryst compositional variations for a steady state magma chamber beneath the valley midsections, AMAR3. *J. geophys. Res.* 89, 6995-7028.

Steinthorsson S., Oskarsson N., Arnorsson S. & Gunnlaugsson E., 1987. Metasomatism in Iceland: Hydrothermal alteration and remelting of oceanic crust. *In*: Helgeson H.C. (ed.) *Chemical Transport in Metasomatic Processes* 355-387. D. Reidel Publishing Company.

Stolper E., 1980. A phase diagram for mid-ocean ridge basalts: preliminary results and implications for petrogenesis. *Contr. Miner. Petrol.* 74, 13-27.

Stolper E. & Walker D., 1980. Melt density and the average composition of basalt. *Contr. Miner. Petrol.* 74, 7-12.

Sun C.-O., Williams R.J. & Sun S.-S., 1974. Distribution coefficients for Eu and Sr for plagioclase-liquid and clinopyroxene-liquid equilibria in oceanic ridge basalt: an experimental study. *Geochim. cosmochim. Acta* 38, 1415-1433.

Sun S.-S., 1980. Lead isotopic study of young volcanic rocks from mid-ocean ridges, ocean islands and island arcs. *Philos. Trans. R. Soc. Lond. Ser.* A297, 409-445.

Sun S.-S., Merit R.W. & Sharaskin A.Y., 1979. Geochemical characteristics of MORBs. *Earth planet. Sci. Lett.* 44, 119-138.

Sweatman T.R. & Long J.V.P., 1969. Quantitative electron probe microanalysis of rock-forming minerals. *J. Petrology* 10, 332-379.

Takahashi E., 1986. Melting of a dry peridotite KLB-1 up to 14GPa: Implications on the origin of peridotitic upper mantle. *J. geophys. Res.* 91, 9367-9382.

Takahashi E. & Kushiro I., 1983. Melting of a dry peridotite at high pressures and basalt magma genesis. *Am. Miner.* 68, 859-879.

Taylor H.P., 1980. The effects of assimilation of country rocks by magmas on $^{18}O/^{16}O$ and $^{87}Sr/^{86}Sr$ systematics in igneous rocks. *Earth planet. Sci. Lett.* 47, 243-254.

Taylor H.P. & Forester R.W., 1971. Low-$^{18}O$ igneous rocks from the intrusive complexes of Skye, Mull and Ardnamurchan, western Scotland. *J. Petrology* 12, 465-497.

Taylor H.P. & Forester R.W., 1979. An oxygen and hydrogen isotope study of the Skaergaard intrusion and its country rocks: a description of a 55 Ma old fossil hydrothermal system. *J. Petrology* 20, 355-419.

Taylor H.P. & Sheppard S., 1986. Igneous rocks: I. Processes of isotopic fractionation and isotope systematics. *In*: Valley J.W., Taylor H.P. & O'Neil J.R., (eds.), *Stable isotopes in high temperature geological processes*. Min. Soc. Am. Reviews in Mineralogy 16, Washington.

Thirlwall M.F., 1979. The petrochemistry of the British Old Red Sandstone volcanic province. Unpubl. Ph.D. thesis, Univ. of Edinburgh.

Thompson R.N., 1973. One-atmosphere melting behaviour and nomenclature of terrestrial lavas. *Contr. Miner. Petrol.* 41, 197-204.

Thompson R.N., 1987. Phase-equilibria constraints on the genesis and magmatic evolution of oceanic basalts. *Earth Sci. Rev.* 24, 161-210.

Thorarinsson S., 1953. The crater groups in Iceland. *Bull. Volcanol.* 14 3-44.

Thorarinsson S., 1960. On the Geology and Geophysics of Iceland. In: *Guide to Excursion* 60, Int. Geol. Congr., Reykjavik 1960.

Thoroddsen T., 1925. Die Gesichte der islandischen Vulkanen. Copenhagen.

Thy P., Beard J.S. & Lofgren G.E., 1990. Experimental constraints on the origin of Icelandic rhyolites. *J. Geol.* 98, 417-421.

Tryggvason E., 1986. Multiple magma reservoirs in a rift zone volcano: ground deformation and magma transport during the September 1984 eruption of Krafla, Iceland. *J. Volcanol. geotherm. Res.* 28, 1-44.

Viereck L.G., Flower M.F.J., Hertogen J., Schmincke H.-U. & Jenner G.A., 1989. The genesis and significance of N-MORB sub-types. *Contr. Miner. Petrol.* 102, 112-126.

Vink G.E., Morgan W.J. & Vogt P.R., 1985. The Earth's hot spots. *Scientific American* 252, 50-57.

Vogt P.R., 1971. Asthenosphere motion recorded by the ocean floor south of Iceland. *Earth planet. Sci. Lett.* 13, 153-60.

Walker D., Shibata T. & DeLong S.E., 1979. Abyssal tholeiites from the Oceanographer Fracture Zone: II Phase equilibria and mixing. *Contr. Miner. Petrol.* 70, 111-125.

Walker G.P.L., 1958. The geology of the Reydarfjördur area, E. Iceland. *Q. J. Geol. Soc. Lond.* 114, 367-393.

Walker G.P.L., 1963. The Breiddalur central volcano, eastern Iceland. *Q. J. Geol. Soc. Lond.* 119, 29-63.

Wallis S.M., 1989. Petrology and geochemistry of Upper Carboniferous-Lower Permian rocks in Scotland. Unpubl. Ph.D. thesis, Univ. of Edinburgh.

Walsh J.N., Buckley F. & Barker J., 1981. The simultaneous determination of the rare-earth elements in rocks using inductively coupled plasma source spectrometry. *Chem. Geol.* 33, 141-153.

Walter M.J. & Presnall D.C., 1990. Melting relations of simplified lherzolite in the system $CaO-MgO-Al_2O_3-SiO_2-Na_2O$ (CMASN) at pressures from 14 to 28 kbar - Application to MORB petrogenesis. *EOS* 71, 648.

Watson S. & McKenzie D., 1990. Melt generation by plumes: A study of Hawaiian Volcanism. Submitted to *J. Petrology*.

Watts A.B., McKenzie D.P., Parsons B.E. & Roufosse M., 1985. The relationship between gravity and bathymetry in the Pacific Ocean. *Geophys. J. R. astron. Soc.* 83, 263-298.

White M.W. & Schilling J.-G., 1978. The nature and origin of geochemical variation in Mid-Atlantic Ridge basalts from the Central North Atlantic. *Geochim. cosmochim. Acta* 42, 1501-1506.

White R.S., 1990. Initiation of the Iceland Plume and Opening of the North Atlantic. *In*: A.J. Tankard & H.R. Balkwill (eds.) Extensional Tectonics and stratigraphy of the North Atlantic margins. *AAPG Memoir* 46, 149-154.

White R.S. & McKenzie D., 1989. Magmatism at rift zones: The generation of volcanic continental margins and flood basalts. *J. geophys. Res.* 94, 7685-7729.

Wilkinson J.F.G., 1982. The genesis of mid-ocean ridge basalt. *Earth Sci. Rev.*, 18, 1-57.

Williams R.W. & Gill J.B., 1989. Effects of partial melting on the uranium decay series. *Geochim. cosmochim. Acta* 53, 1607-1619.

Wilson A.H., 1982. The geology of the Great "Dyke", Zimbabwe: the ultramafic rocks. *J. Petrology* 23, 240-292.

Wilson J.T., 1965. Submarine fracture zones, aseismic ridges and the ICSU line: proposed western margin of the E. Pacific ridge. *Nature* 207, 907-11.

Wilson M., 1989. *Igneous Petrogenesis*. Unwin Hyman Ltd., London, 466pp.

Wood D.A., 1979. Dynamic partial melting: its application to the petrogenesis of basalts erupted in Iceland, the Faeroe Islands, the Isle of Skye and the Troodos Massif. *Geochim. cosmochim. Acta* 43, 1032-1046.

Wood D.A., 1981. Partial melting models for the petrogenesis of Reykjanes Peninsula basalts, Iceland: implications for the use of trace elements and strontium and neodymium isotope ratios to record inhomogeneties in the upper mantle. *Earth planet. Sci. Lett.* 52, 183-190.

Wood D.A., Joron J.-L., Treuil M., Norry M. & Tarney J., 1979. Elemental and Sr isotope variations in basic lavas and the surrounding ocean floor. *Geochim. cosmochim. Acta* 70, 319-339.

Wright T.L., 1974. Presentation and interpretation of chemical data for igneous rocks. *Contr. Miner. Petrol.* 48, 233-248.

Wright T.L. & Doherty P.C., 1970. A linear programming and least squares computer method for solving petrographic mixing problems. *Geol. Soc. Am. Bull.* 81, 1995-2008, 1970.

Yoder H.S., 1976. *Generation of basaltic magma*. National Academy of Sciences, Washington.

Zindler A., Hart S.R., Frey F.A., Jakobsson S.P., 1979. Nd and Sr isotope ratios and rare earth element abundances in Reykjanes Peninsula basalts evidence for mantle heterogeneity beneath Iceland. *Earth planet. Sci. Lett.* 45, 249-262.

# APPENDICES

# Appendix I (a):

## List of samples collected with their ages and phenocryst phases (see key).

**KEY:**
Ages as shown in Appendix I (b)
Phenocrysts: o=olivine, p=plagioclase, c=clinopyroxene, op= orthopyroxene, s=spinel, m=magnetite
hy=hyaloclastite, aph=aphyric, sc=scoria, dol=doleritic, var=variable
0=fresh, 1=slightly altered (brown stains on insides of vesicles), 2=devitrified glass, slightly altered olivines, 3=calcite/zeolite filled vesicles, devitrified glass, altered olivine, plagioclase.

| Sample | Age | Location | Phenocrysts |
|---|---|---|---|
| KK01 | 5 | Lava from Lambadalur between Thorsteinsdalur and Seljadalur | o p (c) 3 |
| KK02 | 5 | Lava from Sly | o p c 2 |
| KK03 | 4 | Rhyolite from Gaesafjallahali | o p c m 2 |
| KK04 | 5 | Hrafnabjorg basaltic sample collected in Gaesadalur | o p c 2 |
| KK06 | 5 | Rhyolite from Hagong (holocrystalline) | o p c m 2 |
| KK07 | 5 | As KK06 but hyalocrystalline | p m 1 var 2 |
| KK08 | 5 | Halaraudar welded tuff at Hagong (upper part) | o p c op 1 |
| KK09 | 5 | As KK08 but from red layer near base | p c 1 |
| KK10 | 6 | Hyaloclastite from Hagong | hy |
| KK11 | 5 | Lava from Hagong | (o) p c 2 |
| KK12 | 5 | Lower lava from Halaskogarfjall | p c m 2 |
| KK13 | 5 | As KK12 but upper lava flow | p 1 |
| KK14 | 5 | Halaraudar welded tuff at Halaskogarfjall | o p c 3 |
| KK16 | 5 | Jorundargrjot lava next above old clays | o p 1 |
| KK17 | 5 | Hlidardalur porphyritic lava | o p 2 |
| KK18 | 4 | Porphyritic lava from Sandabotnafjall | p 1 |
| KK19 | 4 | Lava from Sandabotnafjall | o p c 0 |
| KK20 | 4 | As KK19 | o p c 0 |
| KK21 | 4 | Krafla pillow fragment | o s p 3 |
| KK22 | 4 | Krafla tuff fragment | hy |
| KK23 | 5 | Krokottuvotn porphyritic lava | o p c 1 |
| KK24 | 4 | Ytri Bjargholl tuff sample | hy |
| KK25 | 3 | Dacite lava from N of Hlidarfjall (holocrystalline) | p c op 0 |
| KK26 | 3 | As KK25 but glassy sample | o p c (op) 0 |
| KK27 | 4 | Sample from dyke cutting Halaraudar S of Krokottuvotn | aph 0 |
| KK28 | 4 | Porphyritic lava near NW corner of Hlidarfjall | o p c 0 |
| KK29 | 4 | Rhyolite from Hlidarfjall | p m 2 |
| KK30 | 4 | Gaesafjoll from top lava cover | o s p 0 |
| KK31 | 3 | Gjastykkisbunga lava flow | dol |
| KK32 | 4 | Basaltic sample in hyaloclastite from Sandmulf | o p 0 |
| KK33 | 4 | As KK32 but porphyritic | o p c 0 |
| KK34 | 3 | Dacite from Hraunbunga | p c op m 0 |
| KK35 | 3 | Icelandite from N of Lúdent | p c op m 0 |
| KK36 | 3 | Basaltic scoria from near Víti | sc |
| KK37 | 3 | Very thin lava south of Sandbotnafjall | p 0 |
| KK50 | 3 | Lava S of Hvannfell (S of Lúdent) | dol 0 var 1 |
| KK51 | 3 | Lava S of Storihnjúkur (S of Lúdent) | o p c 0 |
| KK52 | 3 | Lava from just W of KK51 | o p 2 |
| KK53 | 3 | Lava from just W of KK52 | o p 2 |
| KK54 | 1d | Lava from S end of Threngslaborgir | o p c 0 var 1 |
| KK55 | 1d | As KK54 but from N end of crater row | o p c 0 var 1 |
| KK56 | 1b | Pumice from Víti (1724) | sc |

| | | | |
|---|---|---|---|
| KK57 | 4 | As KK03 | o p c m 2 |
| KK58 | 3 | As KK31 | o p 0 var 1 |
| KK59 | 4 | Hyaloclastite basalt fragment from N of Namafjall (Skogahilid) | p 1 |
| KK60 | 4 | As KK59 but from W of Thrihymingar (3.5 km W of Krafla) | p 0 |
| KK62 | 3 | K2 lava from S of Graddabunga | aph 1 |
| KK63 | 4 | Basalt fragment in hyaloclastite from Graddabunga | o p c 0 |
| KK64 | 5 | Lava from beneath Halaraudar, S of Hagangnadalur | aph 2 |
| KK65 | 3 | K1 lava E of Hagangnadalur | o p c 1 |
| KK66 | 3 | K2 lava exposed by fault S of Hagangnadalur | (c) aph 0 |
| KK67 | 4 | Obsidian from Jörundur | p 0 var 1 |
| KK68 | 3 | Lava from W of Raudafellsborgir | o p 1 |
| KK69 | 4 | Hyaloclastite glass from ridge W of Hagangnahali | hy |
| KK70 | 4 | As KK69 but basalt fragment | o p c 0 |
| KK71 | 5 | Basalt from Hagangnahali | (o) p c 1 |
| KK72 | 5 | Basalt from beneath KK71 | p (c) 1 |
| KK73 | 5 | Dyke from ridge to the E of KK71,72 | o p c 2 |
| KK75 | 6 | Porphyritic basalt hyaloclastite samples from Hagangnahali | o p dol 1 |
| KK76 | 6 | As KK75 | p dol 0 |
| KK77 | 5 | Volcanic bomb from Halaraudar, Hagangnahali | p 0 |
| KK78 | 3 | Basalt from S of Afangamor | o p 0 var 1 |
| KK79 | 7 | Lower basalt flow below hyaloclastite, S of Eilifsvötn | o p (c) 2 |
| KK80 | 4 | Dyke feeder to hyaloclastite, S of Eilifsvötn | dol 1 |
| KK81 | 7 | As KK79, but upper flow | o p (c) 0 |
| KK82 | 5 | Basalt flow E of Hrútafjallarandir | o p (c) 1 |
| KK83 | 3 | K2 basalt flow, as KK82 | aph 1 |
| KK84 | 5 | Lowest basalt flow from Halaskógafjall | p 3 |
| KK85 | 3 | K0 basalt flow from edge of the quarry at Leibomar | p 0 |
| KK86 | 3 | Acid scoria, near KK85 | sc |
| KK87 | 4 | Basalt from hyaloclastite from ridge at Sandfell | dol 0 |
| KK88 | 4 | As KK87 but from E-W trending ridge | o p c 0 |
| KK89 | 3 | Porphyritic lava from NE Hrossaborg, Namafjall | (o) p c 1 |
| KK90 | 3 | Basaltic lava from Beinihryggur, Namafjall | o p c 0 |
| KK91 | 3 | Basalt from crater row E of KK90 | p c 0 |
| KK92 | 1c | Basalt from W of Beinihryggur | o p c 0 var 1 |
| KK93 | 3 | Basalt from Svörtuborgir, Namafjall | aph 0 |
| KK94 | 3 | Icelandite from Heidarspordshóll (upper unit) | p c (op) 0 |
| KK95 | 3 | Lower unit of KK94 flow | p c op m 0 |
| KK96 | 3 | Icelandite from main crater of KK94 | p c op m 0 |
| KK97 | 1c | Basaltic lava from NE of Hverfjall | o p c 0 |
| KK98 | 3 | Basaltic lava from Lúdent row, SE of Hverfjall | p c op m 0 |
| KK99 | 1f | Basaltic lava from Eldá | p 0 |
| KK100 | 4 | Basaltic fragment from hyaloclastite from Eldá | (o) p c 0 |
| KK101 | 1c | Basaltic lava from near power plant, Krafla | o p c 0 |
| KK102 | 1c | Basaltic lava from Hlidardalur (same crater as KK101?) | p 0 |
| KK103 | 3 | Basaltic lava from SE of Hverfjall | o p (c) 0 |
| KK104 | 3 | Porphyritic basaltic lava from W of Beinihryggur | dol 0 |
| KK105 | 4 | Tuff from Leirhnjúkur | by o p c 3 |
| KK106 | 1f | Basaltic lava from Leirhnjúkur | (o) p 0 |
| KK107 | 1c | Basaltic lava as for KK102 but from ridge crater | aph 0 |
| KK108 | 1c | As KK107 but further S | o p c 0 |
| KK109a | 1f | Basaltic lava from E of Hlidarfjall: scoriaceous top | p 0 |
| KK109b | 1f | As KK109a but solid lava (middle of flow) | p 0 |
| KK110 | 1f | Basaltic lava from S of KK109 (Halsar) | p c 0 |
| KK111 | 1f | Scoria from near Raudafellsborgir | sc |
| KK112 | 1f | As KK111 but basaltic lava | p 1 |
| KK113 | 1e | Basaltic lava from Sandmuli | p 0 |

| | | | |
|---|---|---|---|
| KK114 | 1e | Basaltic lava from car track W of Graddabunga | aph 1 |
| KK115 | 1f | Basaltic lava from opposite diatomite plant | o p c 0 |
| KK116 | 3 | Basaltic lava from W of Storihnjúkur (flowed to Dalborg) | o p 1 |
| KK117 | 3 | Basaltic lava from Hlidardalur | (o) p c 1 |
| KK118 | 1f | Scoria from quarry near Hrossaborg | sc |
| KK119 | 1f | Brown scoria (later in eruption) as KK118 | sc |
| KK120 | 1f | Basaltic lava from N of diatomite plant | p 0 |
| KK121 | 1b | Víti pumice from S slopes of Krafla | sc |
| KK122 | 1b | Basaltic scoria from KK121 | sc |
| KK123 | 1e | Oldest unit to basalt flow to E of Krafla | p 0 |
| KK124 | 1e | Younger flow of KK123 | (o) p c 0 |
| KK125 | 1e | Basaltic lava from Sandbotnaskard | (p) (c) 0 |
| KK126 | 1f? | Pumice deposit (in soil) from S of Arnarhóll | sc |
| KK127 | 3 | Basal flow to basaltic sequence at Raudkollur | aph 1 |
| KK128 | 3 | Thin basalt flow (xenolith rich) above KK127 | (o) p (c) 0 |
| KK129 | 1f | Welded basaltic airfall, scoriaceous base (at KK127) | sc |
| KK130 | 1f | Solid lava of KK129 | p 1 |
| KK131 | 4 | Hyaloclastite glass from E of Thrihyrningar | hy |
| KK132 | 4 | Basalt block from next ridge W of KK131 | p 3 |
| KK133 | 4 | As KK132, basalt blocks | p 1 |
| KK134 | 4 | Tuff from Thrihyrningar | hy |
| KK135 | 4 | Basalt blocks from KK134 | aph 0 |
| KK136 | 4 | Tuff from island in Myvatn fires lava, Sata | hy |
| KK137 | 4 | Dyke sample from W of Thrihyrningar | aph 1 |
| KK138 | 4 | Tuff from KK137 | hy |
| KK139 | 4 | Basalt fragment in hyaloclastite from Nonbungar | (o) p c 2 |
| KK140 | 4 | Tuff from next ridge W of KK139 | hy |
| KK141 | 4 | Basaltic fragment from KK140 | hy |
| KK142 | 4 | Glass from pillow rind, from next ridge W of KK140 (Halsar) | dol 1 |
| KK143 | 4 | Porphyritic basalt from pillows as KK142 | hy |
| KK144 | 3 | Basalt from E of Gaesafjöll (568 m spot height) | o p c 0 |
| KK145 | 3 | Shiny aphyric basalt from near KK144 | o p c 1 |
| KK147 | 4 | Pillow rind glass from W of Svörtuborgir | sc |
| KK148 | 1f | Basaltic lava from N of Ethóll | o p c 0 |
| KK149 | 1f | Scoria from KK148 | sc |
| KK150 | 1f | Basaltic lava fom E of KK148 | o s p (c) 0 |
| KK151 | 4 | Basaltic lava from the top of Gaesafjöll (table mountain) | o s p dol 1 |
| KK152 | 1a | Scoria from the final phase of 1984 eruption | sc |
| KK153 | 3 | Porphyritic basaltic flow N of Krókóttuvötn | (o) p c 0 |
| KK154 | 3 | Basaltic sample from N of Hvannstod | aph 0 |
| KK155 | 5 | Basaltic sample from the E of Austari-Vididalshuvik | (o) p c 0 |
| KK156 | 3 | As KK154, but from S | (o) p c 0 |
| KK157 | 8 | Basaltic block from hyaloclastite S of Eilifsvötn | p c 0 |
| KK158 | 3 | Basaltic lava from Sandmuli | dol 0 var 1 |
| KK159 | 5 | Basalt flow, NE end of Saudagil (S side) | o p c 0 |
| KK160 | 5 | Next flow down to KK159 (from further SW down Saudagil) | aph 2 |
| KK161 | 5 | As KK160, but lower flow (flow banded) | dol 2 |
| KK162 | 5 | Icelandite hyaloclastite (solid) underneath KK159-161 | p c (op) 1 |
| K2 | ? | Granophyre from Krafla | n/a |
| IC9 | 4 | Obsidian from Hrafntinnuhryggur | n/a |
| IC10 | 1a | Scoria sample from 1981 eruption | sc |
| SNA24 | 1a | Scoria sample from 1980 eruption, N of caldera (Hituhólar) | sc |
| SNA26 | 1a | Scoria sample from 1980 eruption, N of caldera (Snagi) | sc |
| 84-05 | 1a | Scoria sample from 1984 eruption, caldera | sc |
| 84-19 | 1a | Scoria sample from 1984 eruption, N of caldera | sc |
| KRA118 | 1b | Scoria sample from Leirhnjúkur | sc |

# Appendix I (b):

Samples collected from the Krafla volcanic system are arranged below according to age (following Table 2.1).

<u>POSTGLACIAL</u>:

1. (a) Recent (1975-84)

84, 84-05, 84-19, 152 (1984)
IC10 (1981)
SNA24, SNA26 (1980)

(b) 1724-29

KK56, KK121, KK122, KRA118

(c) Dalseldar

KK92, KK97, KK101, KK102, KK107, KK108

(d) Threngslaborgir

KK54, KK55

(e) Holseldar

KK113, KK114, KK123, KK124, KK125

(f) Hverfjall

KK99, KK106; KK109A,B; KK110, KK111, KK112, KK115, KK118, KK119, KK120, KK129, KK130, KK148, KK149, KK150

2. Quiescent period

3. (a) Early postglacial

KK25, KK26, KK31, KK34, KK35, KK37, KK50, KK51, KK52, KK53, KK58, KK62, KK65, KK66, KK78, KK83, KK85, KK86, KK89, KK90, KK91, KK93, KK94, KK95, KK96, KK98, KK103, KK116, KK117, KK126, KK127, KK128, KK144, KK154, KK156, KK158

(b) Finiglacial

KK68, KK145, KK153

**4. GLACIAL**

KK03, KK18, KK19, KK20, KK21, KK22, KK24, KK27, KK28, KK29, KK30, KK32, KK33, KK59, KK60, KK63, KK67, KK69, KK70, KK80, KK87, KK88, KK100, KK105, KK131, KK132, KK133, KK134, KK135, KK136, KK137, KK138, KK139, KK140, KK141, KK142, KK143, KK146, KK147, KK151

**5. INTERGLACIAL**

KK01, KK02, KK04, KK06, KK07, KK08, KK09, KK11, KK12, KK13, KK14, KK16, KK17, KK16, KK17, KK23, KK64, KK71, KK72, KK73, KK77, KK82, KK84, KK155, KK159, KK160, KK161, KK162

**6. PREVIOUS GLACIAL**

KK10, KK74, KK75, KK76

**7. PREVIOUS INTERGLACIAL**

KK79, KK81

**8. OLDEST GLACIAL**

KK157

## Appendix II:

Modal analyses of key Krafla samples (see section 3.4 for more details) are presented here:

| Sample | %xplag | %plag | %oliv (opx) | %cpx | %FeTi ox (sp) |
|---|---|---|---|---|---|
| KK03 | | 7.0 | 0.5 | <0.5 | <0.5 |
| KK17 | 10.0 | | | | |
| KK18 | 25.0 | | | | |
| KK21 | | | 3.2 | | 0.1(sp) |
| KK23 | 12.0 | <1.0 | | <0.5 | |
| KK28 | 12.0 | 1.0 | | <0.5 | |
| KK30 | | 3.0 | 3.5 | | |
| KK33 | 16.0 | 2.0 | 2.0 | 3.5 | |
| KK51 | | 5.0 | 3.0 | 1.5 | |
| KK52 | | 5.0 | 3.0 | | |
| KK54 | 3.0 | | 1.5 | 2.0 | |
| KK65 | 6.5 | | | | |
| KK68 | 3.5 | 5.5 | 5.0 | | |
| KK71 | 6.5 | | 1.0 | | |
| KK73 | | 2.5 | 0.5 | 4.5 | |
| KK75 | 7.5 | 9.0 | 1.5 | | |
| KK76 | 28.5 | | | | |
| KK81 | 4.0 | 3.0 | 2.0 | 1.5 | |
| KK89 | 5.5 | 1.0 | 0.5 | 1.5 | |
| KK90 | | 3.5 | 1.0 | 1.0 | |
| KK91 | 2.0 | 1.0 | | 2.0 | |
| KK99 | 1.0 | | | | |
| KK105 | | <0.5 | <0.5 | <0.5 | |
| KK108 | | 1.0 | 1.0 | 1.0 | |
| KK109a | | <1.0 | | | |
| KK110 | | 3.0 | | 0.5 | |
| KK113 | 1.0 | | | | |
| KK115 | | 1.0 | 0.5 | 1.0 | |
| KK130 | | 3.0 | | | |
| KK139 | | 2.0 | | 1.0 | |
| KK141 | 2.0 | | | | |
| KK145 | | 0.5 | | 0.5 | |
| KK148 | | 2.5 | 0.5 | 1.0 | |
| KK150 | | 1.5 | 1.0 | <0.5 | |
| KK153 | 10.0 | <0.5 | | 1.0 | |
| KK157 | | <0.5 | | 1.0 | |
| KK159 | 3.0 | | | | |
| KK162 | | 1.0 | <0.5(opx) | <0.5 | |

The abbreviations in the above table are as follows:
xplag: xenocrystal plagioclase; plag: phenocrystal plagioclase
ol: olivine, cpx: clinopyroxene, FeTi ox: FeTi oxides
sp: spinel, opx: orthopyroxene (all phenocryst phases).

Analyses with minimal or undetectable amounts of phases are shown with blank spaces. Generally amounts below 0.5% by volume are at the limits of resolution.

# Appendix III:

## Olivine+plagioclase-phyric basalts (Section 3.2.1)

P=phenocryst, X=xenocryst G=groundmass, C=centre, M=middle, E=edge, IL=ilmenite, UM=ülvospinel-magnetite

### Olivine

| KK21 | | | KK58 | |
|---|---|---|---|---|
| | P1E | P2C | P1C | P1E |
| $SiO_2$ | 39.97 | 39.50 | 39.64 | 38.24 |
| $Al_2O_3$ | 0.05 | 0.04 | 0.06 | 0.06 |
| FeO | 13.33 | 15.72 | 14.06 | 24.02 |
| MnO | 0.15 | 0.17 | 0.20 | 0.36 |
| MgO | 46.98 | 44.90 | 45.38 | 37.57 |
| CaO | 0.26 | 0.34 | 0.35 | 0.01 |
| Total | 100.73 | 100.67 | 99.69 | 100.65 |
| | | | | |
| Si | 0.990 | 0.990 | 0.995 | 0.997 |
| Al | 0.001 | 0.001 | 0.002 | 0.002 |
| Fe | 0.276 | 0.329 | 0.295 | 0.524 |
| Mn | 0.003 | 0.004 | 0.004 | 0.008 |
| Mg | 1.733 | 1.677 | 1.698 | 1.460 |
| Ca | 0.007 | 0.009 | 0.010 | 0.011 |
| Total | 3.010 | 3.010 | 3.004 | 3.002 |
| | | | | |
| %Fo. | 86 | 83 | 85 | 74 |

### Plagioclase

| KK21 | | | KK58 | | |
|---|---|---|---|---|---|
| | P1C | P2C | P1C | P1E | P2C |
| $SiO_2$ | 49.77 | 48.77 | 46.73 | 46.81 | 48.24 |
| $Al_2O_3$ | 29.90 | 31.31 | 32.99 | 33.34 | 31.81 |
| FeO | 0.90 | 0.66 | 0.25 | 0.29 | 0.26 |
| MgO | 0.37 | 0.27 | 0.23 | 0.21 | 0.28 |
| CaO | 15.01 | 15.84 | 18.01 | 18.20 | 16.71 |
| $Na_2O$ | 2.91 | 2.62 | 1.43 | 1.36 | 2.16 |
| $K_2O$ | 0.10 | 0.01 | 0.00 | 0.01 | 0.01 |
| Total | 98.95 | 99.48 | 99.62 | 100.22 | 99.48 |
| | | | | | |
| Si | 9.223 | 9.001 | 8.642 | 8.611 | 8.903 |
| Al | 6.533 | 6.813 | 7.193 | 7.230 | 6.922 |
| Fe | 0.139 | 0.102 | 0.038 | 0.045 | 0.040 |
| Mg | 0.101 | 0.075 | 0.063 | 0.058 | 0.077 |
| Ca | 2.979 | 3.132 | 3.569 | 3.587 | 3.305 |
| Na | 1.047 | 0.930 | 0.514 | 0.485 | 0.774 |
| K | 0.023 | 0.008 | 0.000 | 0.001 | 0.003 |
| Total | 20.046 | 20.061 | 20.018 | 20.017 | 20.025 |
| | | | | | |
| %An. | 74 | 77 | 87 | 88 | 81 |

KK58

Plagioclase

| | G1 | G2 |
|---|---|---|
| $SiO_2$ | 53.52 | 48.33 |
| $Al_2O_3$ | 28.77 | 31.33 |
| FeO | 0.89 | 0.66 |
| MgO | 0.19 | 0.34 |
| CaO | 12.71 | 15.93 |
| $Na_2O$ | 4.68 | 2.57 |
| $K_2O$ | 0.09 | 0.06 |
| Total | 100.85 | 99.22 |
| | | |
| Si | 9.667 | 8.955 |
| Al | 6.127 | 6.844 |
| Fe | 0.135 | 0.102 |
| Mg | 0.052 | 0.093 |
| Ca | 2.459 | 3.162 |
| Na | 1.638 | 0.923 |
| K | 0.021 | 0.014 |
| Total | 20.099 | 20.092 |
| | | |
| %An. | 60 | 77 |

Clinopyroxene

KK58

| | G1 | G2 | G3 |
|---|---|---|---|
| $SiO_2$ | 52.58 | 49.05 | 51.15 |
| $Al_2O_3$ | 2.23 | 1.89 | 2.30 |
| FeO | 5.50 | 18.77 | 10.11 |
| MnO | 0.10 | 0.37 | 0.23 |
| MgO | 16.97 | 10.89 | 16.27 |
| CaO | 21.18 | 16.41 | 17.26 |
| $Na_2O$ | 0.20 | 0.24 | 0.20 |
| $K_2O$ | 0.00 | 0.02 | 0.01 |
| Total | 99.60 | 99.82 | 98.15 |
| | | | |
| Si | 1.935 | 1.920 | 1.931 |
| Al | 0.097 | 0.087 | 0.103 |
| Fe | 0.169 | 0.615 | 0.319 |
| Mn | 0.003 | 0.012 | 0.007 |
| Mg | 0.930 | 0.636 | 0.916 |
| Ca | 0.835 | 0.688 | 0.698 |
| Na | 0.014 | 0.018 | 0.014 |
| K | 0.000 | 0.000 | 0.000 |
| Total | 4.007 | 4.011 | 4.011 |
| Mg#. | 85 | 51 | 69 |

Opaque phases

| KK21 | | KK58 |
|---|---|---|
| | SP1 | UM1 |
| $SiO_2$ | 0.19 | 0.43 |
| $TiO_2$ | 0.87 | 25.96 |
| $Al_2O_3$ | 25.68 | 1.39 |
| $Cr_2O_3$ | 34.17 | 0.01 |
| FeO | 23.53 | 65.92 |
| MnO | 0.52 | 0.40 |
| MgO | 13.94 | 0.18 |
| Total | 99.60 | 94.30 |
| | | |
| Si | 0.006 | 0.134 |
| Ti | 0.019 | 6.058 |
| Al | 0.917 | 0.510 |
| Cr | 0.819 | 0.003 |
| $Fe^{2+}$ | 0.384 | 14.002 |
| $Fe^{3+}$ | 0.213 | 3.101 |
| Mn | 0.014 | 0.105 |
| Mg | 0.629 | 0.084 |
| Total | 3.000 | 24.000 |

**Olivine+plagioclase+clinopyroxene-phyric basalts (Section 3.2.2)**

Olivine

| KK01 | | | KK04 | |
|---|---|---|---|---|
| | P1 | P2 | P1 | P2 | P3 |
| $SiO_2$ | 38.42 | 36.93 | 35.53 | 37.67 | 35.66 |
| $Al_2O_3$ | 0.05 | 0.07 | 0.04 | 0.08 | 0.07 |
| FeO | 25.74 | 30.43 | 37.30 | 24.67 | 33.54 |
| MnO | 0.27 | 0.35 | 0.48 | 0.41 | 0.50 |
| MgO | 36.07 | 30.43 | 26.53 | 38.05 | 30.93 |
| CaO | 0.35 | 0.34 | 0.28 | 0.36 | 0.34 |
| Total | 100.90 | 100.60 | 100.16 | 101.23 | 101.03 |
| | | | | | |
| Si | 1.006 | 1.004 | 0.997 | 0.981 | 0.974 |
| Al | 0.002 | 0.002 | 0.008 | 0.003 | 0.002 |
| Fe | 0.563 | 0.738 | 0.875 | 0.537 | 0.767 |
| Mn | 0.006 | 0.008 | 0.011 | 0.009 | 0.012 |
| Mg | 1.407 | 1.233 | 1.109 | 1.477 | 1.260 |
| Ca | 0.010 | 0.010 | 0.008 | 0.010 | 0.010 |
| Total | 2.994 | 2.995 | 3.002 | 3.017 | 3.024 |
| %Fo. | 71 | 63 | 56 | 73 | 62 |

| KK28 | | | KK51 | | KK54 |
|---|---|---|---|---|---|
| | P1 | P2 | P1 | P2 | P1 |
| $SiO_2$ | 39.90 | 39.22 | 38.52 | 43.74 | 37.49 |
| $Al_2O_3$ | 0.24 | 0.05 | 0.05 | 0.08 | 0.06 |
| FeO | 17.64 | 15.23 | 20.80 | 16.52 | 26.03 |
| MnO | 0.26 | 0.24 | 0.31 | 0.26 | 0.38 |
| MgO | 41.55 | 43.54 | 40.89 | 43.74 | 35.61 |
| CaO | 0.37 | 0.35 | 0.28 | 0.33 | 0.36 |
| Total | 99.95 | 98.64 | 100.84 | 100.83 | 99.93 |
| | | | | | |
| Si | 1.013 | 1.001 | 0.998 | 1.000 | 0.995 |
| Al | 0.007 | 0.002 | 0.002 | 0.002 | 0.002 |
| Fe | 0.375 | 0.325 | 0.446 | 0.346 | 0.578 |
| Mn | 0.006 | 0.005 | 0.007 | 0.006 | 0.009 |
| Mg | 1.573 | 1.656 | 1.562 | 1.635 | 1.409 |
| Ca | 0.010 | 0.010 | 0.008 | 0.009 | 0.010 |
| Total | 2.983 | 2.998 | 3.012 | 2.998 | 3.004 |
| | | | | | |
| %Fo. | 81 | 84 | 72 | 78 | 71 |

| KK54 | | KK55 | KK68 | | |
|---|---|---|---|---|---|
| | P2C | P1 | P1C | P2C | P3C |
| $SiO_2$ | 43.74 | 38.33 | 39.76 | 37.44 | 39.29 |
| $Al_2O_3$ | 0.08 | 0.05 | 0.10 | 0.08 | 0.09 |
| FeO | 16.52 | 18.06 | 15.80 | 29.56 | 20.70 |
| MnO | 0.26 | 0.27 | 0.23 | 0.44 | 0.33 |
| MgO | 43.74 | 41.89 | 44.83 | 33.90 | 40.96 |
| CaO | 0.33 | 0.35 | 0.33 | 0.36 | 0.36 |
| Total | 100.83 | 98.95 | 101.04 | 101.78 | 101.74 |
| | | | | | |
| Si | 1.000 | 0.990 | 0.992 | 0.992 | 0.996 |
| Al | 0.002 | 0.002 | 0.003 | 0.002 | 0.003 |
| Fe | 0.346 | 0.390 | 0.330 | 0.655 | 0.439 |
| Mn | 0.006 | 0.006 | 0.005 | 0.010 | 0.007 |
| Mg | 1.635 | 1.612 | 1.668 | 1.338 | 1.548 |
| Ca | 0.009 | 0.010 | 0.009 | 0.010 | 0.010 |
| Total | 2.998 | 3.009 | 3.006 | 3.007 | 3.002 |
| | | | | | |
| %Fo | 82 | 80 | 83 | 67 | 78 |

| KK81 | | | KK108 | | KK148 |
|---|---|---|---|---|---|
| | P1 | P2 | P1C | P2C | P1C |
| $SiO_2$ | 38.11 | 35.86 | 36.29 | 38.80 | 40.22 |
| $Al_2O_3$ | 0.04 | 0.06 | 0.04 | 0.02 | 0.11 |
| FeO | 25.84 | 36.79 | 34.25 | 23.07 | 13.66 |
| MnO | 0.36 | 0.52 | 0.44 | 0.32 | 0.16 |
| MgO | 37.37 | 28.15 | 28.96 | 39.62 | 46.45 |
| CaO | 0.34 | 0.34 | 0.31 | 0.28 | 0.28 |
| Total | 102.07 | 101.72 | 100.28 | 102.12 | 100.88 |
| | | | | | |
| Si | 0.988 | 0.987 | 1.000 | 0.991 | 0.995 |
| Al | 0.001 | 0.002 | 0.001 | 0.000 | 0.003 |
| Fe | 0.560 | 0.847 | 0.789 | 0.493 | 0.282 |
| Mn | 0.008 | 0.012 | 0.010 | 0.007 | 0.003 |
| Mg | 1.444 | 1.155 | 1.190 | 1.509 | 1.712 |
| Ca | 0.009 | 0.010 | 0.009 | 0.008 | 0.007 |
| Total | 3.011 | 3.012 | 2.999 | 3.008 | 3.004 |
| | | | | | |
| %Fo. | 72 | 57 | 60 | 75 | 86 |

| KK148 | | | |
|---|---|---|---|
| | P1E | P2C | P3C |
| $SiO_2$ | 37.90 | 36.11 | 38.90 |
| $Al_2O_3$ | 0.07 | 0.07 | 0.04 |
| FeO | 26.62 | 32.90 | 20.68 |
| MnO | 0.40 | 0.49 | 0.28 |
| MgO | 36.52 | 31.02 | 40.98 |
| CaO | 0.34 | 0.36 | 0.30 |
| Total | 101.86 | 101.35 | 101.18 |
| | | | |
| Si | 0.989 | 0.989 | 0.992 |
| Al | 0.002 | 0.002 | 0.001 |
| Fe | 0.581 | 0.745 | 0.441 |
| Mn | 0.009 | 0.011 | 0.006 |
| Mg | 1.420 | 1.252 | 1.558 |
| Ca | 0.009 | 0.010 | 0.008 |
| Total | 3.010 | 3.010 | 3.007 |
| | | | |
| %Fo. | 71 | 63 | 78 |

Plagioclase

| KK01 | | | | | KK04 |
|---|---|---|---|---|---|
| | X1C | X1M | X1E | G1 | |
| $SiO_2$ | 47.48 | 46.72 | 52.99 | 52.25 | 49.92 |
| $Al_2O_3$ | 32.77 | 32.83 | 28.89 | 28.39 | 30.17 |
| FeO | 0.28 | 0.29 | 0.64 | 0.90 | 1.03 |
| MgO | 0.19 | 0.19 | 0.18 | 0.15 | 0.19 |
| CaO | 17.52 | 17.72 | 13.19 | 12.87 | 14.34 |
| $Na_2O$ | 1.69 | 1.56 | 4.13 | 4.21 | 3.30 |
| $K_2O$ | 0.02 | 0.00 | 0.09 | 0.12 | 0.11 |
| Total | 99.95 | 99.31 | 100.10 | 98.89 | 99.06 |
| | | | | | |
| Si | 8.740 | 8.666 | 9.631 | 9.630 | 9.235 |
| Al | 7.110 | 7.179 | 6.191 | 6.168 | 6.580 |
| Fe | 0.043 | 0.045 | 0.098 | 0.139 | 0.160 |
| Mg | 0.052 | 0.051 | 0.049 | 0.041 | 0.053 |
| Ca | 3.456 | 3.522 | 2.568 | 2.542 | 2.843 |
| Na | 0.604 | 0.560 | 1.454 | 1.504 | 1.183 |
| K | 0.005 | 0.000 | 0.021 | 0.029 | 0.025 |
| Total | 20.010 | 20.025 | 20.011 | 20.053 | 20.079 |
| | | | | | |
| %An. | 85 | 86 | 64 | 62 | 70 |

| KK04 | | KK28 | | | KK51 |
|---|---|---|---|---|---|
| | P2 | X1C | X1E | G1 | P1 |
| $SiO_2$ | 45.35 | 46.04 | 52.17 | 50.61 | 51.93 |
| $Al_2O_3$ | 34.10 | 33.47 | 27.59 | 30.76 | 28.98 |
| FeO | 0.63 | 0.47 | 1.84 | 0.78 | 1.00 |
| MgO | 0.16 | 0.18 | 1.49 | 0.34 | 0.25 |
| CaO | 17.33 | 17.92 | 13.36 | 15.03 | 13.29 |
| $Na_2O$ | 1.42 | 1.22 | 3.36 | 2.84 | 3.72 |
| $K_2O$ | 0.03 | 0.00 | 0.08 | 0.03 | 0.06 |
| Total | 99.04 | 99.32 | 99.88 | 100.43 | 99.28 |
| | | | | | |
| Si | 8.450 | 8.550 | 9.566 | 9.219 | 9.538 |
| Al | 7.491 | 7.326 | 5.964 | 6.606 | 6.275 |
| Fe | 0.098 | 0.072 | 0.282 | 0.119 | 0.153 |
| Mg | 0.045 | 0.051 | 0.407 | 0.093 | 0.069 |
| Ca | 3.460 | 3.566 | 2.625 | 2.933 | 2.616 |
| Na | 0.512 | 0.440 | 1.196 | 1.004 | 1.326 |
| K | 0.008 | 0.000 | 0.019 | 0.008 | 0.014 |
| Total | 20.074 | 20.007 | 20.059 | 19.984 | 19.995 |
| | | | | | |
| %An. | 62 | 89 | 68 | 74 | 66 |

| KK51 | | KK54 | | | KK55 |
|---|---|---|---|---|---|
| | P2 | P1C | P2C | X1C | X1C |
| $SiO_2$ | 49.80 | 47.93 | 53.71 | 46.05 | 46.14 |
| $Al_2O_3$ | 31.06 | 31.86 | 26.23 | 33.19 | 33.23 |
| FeO | 0.54 | 0.62 | 1.92 | 0.50 | 0.48 |
| MgO | 0.24 | 0.25 | 0.38 | 0.17 | 0.22 |
| CaO | 14.89 | 16.18 | 12.47 | 17.71 | 17.64 |
| $Na_2O$ | 2.96 | 2.28 | 4.13 | 1.32 | 1.41 |
| $K_2O$ | 0.05 | 0.02 | 0.21 | 0.01 | 0.02 |
| Total | 99.57 | 99.14 | 99.04 | 98.95 | 99.14 |
| | | | | | |
| Si | 9.147 | 8.884 | 9.908 | 8.581 | 8.582 |
| Al | 6.726 | 6.962 | 5.705 | 7.291 | 7.285 |
| Fe | 0.083 | 0.097 | 0.296 | 0.078 | 0.074 |
| Mg | 0.067 | 0.068 | 0.105 | 0.047 | 0.061 |
| Ca | 2.931 | 3.213 | 2.465 | 3.536 | 3.516 |
| Na | 1.055 | 0.818 | 1.476 | 0.478 | 0.509 |
| K | 0.013 | 0.004 | 0.048 | 0.004 | 0.005 |
| Total | 20.023 | 20.046 | 20.002 | 20.014 | 20.032 |
| | | | | | |
| %An. | 66 | 73 | 87 | 90 | 77 |

KK55

| | X2C | X2E | P1 | P2 | X1C |
|---|---|---|---|---|---|
| $SiO_2$ | 46.16 | 45.29 | 45.88 | 49.21 | 45.10 |
| $Al_2O_3$ | 33.44 | 34.03 | 33.52 | 31.19 | 34.20 |
| FeO | 0.36 | 0.38 | 0.63 | 0.94 | 0.39 |
| MgO | 0.25 | 0.25 | 0.16 | 0.17 | 0.21 |
| CaO | 17.79 | 18.09 | 17.66 | 15.32 | 18.28 |
| $Na_2O$ | 1.41 | 1.19 | 1.51 | 2.75 | 1.03 |
| $K_2O$ | 0.01 | 0.00 | 0.01 | 0.02 | 0.00 |
| Total | 99.43 | 99.22 | 99.40 | 99.59 | 99.21 |
| | | | | | |
| Si | 8.560 | 8.427 | 8.526 | 9.066 | 8.395 |
| Al | 7.311 | 7.464 | 7.343 | 6.774 | 7.505 |
| Fe | 0.057 | 0.059 | 0.098 | 0.145 | 0.060 |
| Mg | 0.069 | 0.068 | 0.045 | 0.046 | 0.059 |
| Ca | 3.534 | 3.607 | 3.516 | 3.024 | 3.646 |
| Na | 0.508 | 0.428 | 0.544 | 0.982 | 0.372 |
| K | 0.002 | 0.000 | 0.002 | 0.005 | 0.000 |
| Total | 20.040 | 20.054 | 20.075 | 20.041 | 20.038 |
| | | | | | |
| %An. | 90 | 77 | 87 | 75 | 91 |

KK81

KK108

| | X2C | X2M | X2E | P1E | P1C |
|---|---|---|---|---|---|
| $SiO_2$ | 46.16 | 45.29 | 47.87 | 48.29 | 51.28 |
| $Al_2O_3$ | 33.44 | 34.03 | 31.67 | 31.68 | 29.87 |
| FeO | 0.36 | 0.38 | 0.96 | 0.70 | 0.67 |
| MgO | 0.25 | 0.25 | 0.19 | 0.20 | 0.21 |
| CaO | 17.79 | 18.09 | 15.96 | 15.59 | 13.61 |
| $Na_2O$ | 1.41 | 1.19 | 2.30 | 2.50 | 3.66 |
| $K_2O$ | 0.01 | 0.00 | 0.02 | 0.03 | 0.05 |
| Total | 99.43 | 99.22 | 98.98 | 99.00 | 99.36 |
| | | | | | |
| Si | 8.560 | 8.427 | 8.896 | 8.951 | 9.408 |
| Al | 7.311 | 7.464 | 6.939 | 6.923 | 6.460 |
| Fe | 0.057 | 0.059 | 0.149 | 0.108 | 0.103 |
| Mg | 0.069 | 0.068 | 0.054 | 0.055 | 0.058 |
| Ca | 3.534 | 3.607 | 3.179 | 3.097 | 2.677 |
| Na | 0.508 | 0.428 | 0.831 | 0.900 | 1.303 |
| K | 0.002 | 0.000 | 0.005 | 0.007 | 0.013 |
| Total | 20.040 | 20.054 | 20.052 | 20.041 | 20.020 |
| | | | | | |
| %An. | 87 | 89 | 79 | 77 | 67 |

| | KK108 | | KK148 | | |
|---|---|---|---|---|---|
| | P2C | P3C | P1C | P2C | P3C |
| $SiO_2$ | 50.48 | 52.34 | 48.71 | 51.79 | 51.29 |
| $Al_2O_3$ | 29.36 | 28.77 | 31.46 | 28.99 | 28.48 |
| FeO | 1.46 | 1.05 | 0.68 | 1.02 | 0.94 |
| MgO | 0.42 | 0.22 | 0.20 | 0.18 | 0.21 |
| CaO | 13.24 | 13.02 | 15.55 | 13.67 | 13.20 |
| $Na_2O$ | 3.76 | 4.04 | 2.49 | 3.55 | 3.83 |
| $K_2O$ | 0.05 | 0.07 | 0.04 | 0.11 | 0.10 |
| Total | 98.76 | 99.51 | 99.13 | 99.30 | 98.06 |
| | | | | | |
| Si | 9.359 | 9.589 | 9.009 | 9.518 | 9.544 |
| Al | 6.418 | 6.213 | 6.859 | 6.281 | 6.247 |
| Fe | 0.226 | 0.160 | 0.105 | 0.156 | 0.146 |
| Mg | 0.115 | 0.060 | 0.054 | 0.049 | 0.059 |
| Ca | 2.632 | 2.557 | 3.082 | 2.692 | 2.632 |
| Na | 1.350 | 1.434 | 0.892 | 1.266 | 1.383 |
| K | 0.011 | 0.017 | 0.010 | 0.025 | 0.024 |
| Total | 20.112 | 20.030 | 20.012 | 19.987 | 20.035 |
| | | | | | |
| %An. | 66 | 64 | 77 | 68 | 65 |

Clinopyroxene

| KK01 | | | KK04 | | |
|---|---|---|---|---|---|
| | G1 | G2 | P1C | P2C | G1 |
| $SiO_2$ | 50.41 | 51.43 | 52.90 | 51.11 | 50.93 |
| $TiO_2$ | 0.35 | 0.75 | 0.33 | 0.43 | 0.73 |
| $Al_2O_3$ | 1.09 | 2.10 | 2.04 | 3.02 | 7.54 |
| $Cr_2O_3$ | 0.01 | 0.04 | 0.26 | 0.40 | 0.02 |
| FeO | 19.28 | 13.00 | 6.86 | 5.93 | 15.21 |
| MnO | 0.32 | 0.27 | 0.20 | 0.16 | 0.36 |
| MgO | 10.19 | 14.27 | 19.00 | 16.94 | 10.15 |
| CaO | 15.26 | 17.31 | 17.85 | 20.96 | 14.15 |
| $Na_2O$ | 0.02 | 0.27 | 0.17 | 0.20 | 1.14 |
| Total | 98.83 | 99.46 | 99.61 | 99.15 | 100.25 |
| | | | | | |
| Si | 1.963 | 1.941 | 1.939 | 1.897 | 1.901 |
| Ti | 0.032 | 0.021 | 0.009 | 0.012 | 0.020 |
| Al | 0.087 | 0.094 | 0.088 | 0.132 | 0.332 |
| Cr | 0.000 | 0.001 | 0.008 | 0.012 | 0.000 |
| Fe | 0.628 | 0.411 | 0.210 | 0.184 | 0.475 |
| Mn | 0.011 | 0.009 | 0.006 | 0.005 | 0.011 |
| Mg | 0.591 | 0.803 | 1.038 | 0.937 | 0.565 |
| Ca | 0.637 | 0.700 | 0.701 | 0.833 | 0.566 |
| Na | 0.024 | 0.020 | 0.012 | 0.015 | 0.083 |
| Total | 3.974 | 4.000 | 4.010 | 4.027 | 3.953 |
| | | | | | |
| Mg#. | 48 | 66 | 83 | 84 | 54 |

| KK04 | KK28 | | | KK51 |
|---|---|---|---|---|
| | G2 | P1C | P2C | P3C | X1C |
| $SiO_2$ | 51.95 | 50.79 | 52.97 | 53.62 | 50.26 |
| $TiO_2$ | 0.49 | 0.49 | 0.34 | 0.35 | 1.28 |
| $Al_2O_3$ | 1.87 | 3.96 | 2.02 | 2.15 | 3.55 |
| $Cr_2O_3$ | 0.10 | 0.90 | 0.36 | 0.23 | 0.25 |
| FeO | 9.24 | 5.68 | 6.43 | 8.82 | 8.22 |
| MnO | 0.26 | 0.16 | 0.17 | 0.27 | 0.20 |
| MgO | 16.35 | 15.93 | 18.29 | 20.07 | 15.38 |
| CaO | 19.26 | 20.53 | 18.25 | 13.76 | 20.03 |
| $Na_2O$ | 0.21 | 0.23 | 0.15 | 0.18 | 0.27 |
| Total | 99.73 | 98.67 | 98.97 | 99.44 | 99.45 |
| | | | | | |
| Si | 1.933 | 1.890 | 1.932 | 1.959 | 1.876 |
| Ti | 0.014 | 0.014 | 0.014 | 0.010 | 0.036 |
| Al | 0.082 | 0.174 | 0.111 | 0.092 | 0.156 |
| Cr | 0.003 | 0.026 | 0.010 | 0.007 | 0.007 |
| Fe | 0.288 | 0.177 | 0.209 | 0.269 | 0.257 |
| Mn | 0.008 | 0.005 | 0.006 | 0.008 | 0.006 |
| Mg | 0.907 | 0.883 | 0.946 | 1.092 | 0.856 |
| Ca | 0.768 | 0.819 | 0.759 | 0.538 | 0.801 |
| Na | 0.015 | 0.015 | 0.014 | 0.013 | 0.019 |
| Total | 4.018 | 4.004 | 4.001 | 3.988 | 4.016 |
| | | | | | |
| Mg#. | 76 | 83 | 82 | 80 | 77 |

| KK51 | | KK54 | | KK55 | |
|---|---|---|---|---|---|
| | G1 | P1C | P2C | P1C | P2C |
| $SiO_2$ | 52.42 | 52.40 | 51.55 | 52.62 | 50.35 |
| $TiO_2$ | 0.45 | 0.43 | 0.64 | 0.38 | 0.87 |
| $Al_2O_3$ | 6.56 | 2.23 | 2.90 | 1.93 | 4.21 |
| $Cr_2O_3$ | 0.01 | 0.32 | 0.17 | 0.27 | 0.42 |
| FeO | 17.82 | 6.04 | 7.53 | 6.01 | 6.92 |
| MnO | 0.39 | 0.18 | 0.22 | 0.17 | 0.19 |
| MgO | 15.25 | 17.28 | 17.49 | 18.02 | 16.54 |
| CaO | 7.26 | 20.15 | 18.40 | 19.97 | 19.80 |
| $Na_2O$ | 1.37 | 0.21 | 0.20 | 0.21 | 0.23 |
| Total | 101.53 | 99.24 | 99.08 | 99.57 | 99.53 |
| | | | | | |
| Si | 1.916 | 1.935 | 1.911 | 1.935 | 1.865 |
| Ti | 0.012 | 0.012 | 0.018 | 0.011 | 0.024 |
| Al | 0.282 | 0.097 | 0.127 | 0.084 | 0.184 |
| Cr | 0.000 | 0.009 | 0.005 | 0.008 | 0.012 |
| Fe | 0.544 | 0.186 | 0.233 | 0.185 | 0.215 |
| Mn | 0.012 | 0.006 | 0.007 | 0.005 | 0.006 |
| Mg | 0.830 | 0.951 | 0.966 | 0.988 | 0.913 |
| Ca | 0.284 | 0.583 | 0.731 | 0.787 | 0.786 |
| Na | 0.097 | 0.015 | 0.014 | 0.015 | 0.017 |
| Total | 3.979 | 4.008 | 4.012 | 4.016 | 4.021 |
| | | | | | |
| Mg#. | 60 | 84 | 81 | 84 | 81 |

| KK81 | | KK108 | | | KK148 |
|---|---|---|---|---|---|
| | P1C | P1C | P2C | P3C | P1C |
| $SiO_2$ | 52.01 | 51.25 | 50.41 | 49.52 | 52.30 |
| $TiO_2$ | 0.38 | 0.66 | 0.86 | 1.16 | 0.37 |
| $Al_2O_3$ | 3.35 | 2.93 | 3.04 | 4.03 | 1.95 |
| $Cr_2O_3$ | 0.53 | 0.25 | 0.24 | 0.20 | 0.37 |
| FeO | 5.69 | 10.08 | 12.80 | 12.09 | 9.31 |
| MnO | 0.15 | 0.29 | 0.33 | 0.30 | 0.25 |
| MgO | 16.65 | 16.65 | 16.83 | 15.35 | 18.19 |
| CaO | 20.69 | 17.24 | 14.46 | 16.37 | 16.11 |
| $Na_2O$ | 0.18 | 0.24 | 0.23 | 0.29 | 0.26 |
| Total | 99.64 | 99.60 | 99.20 | 99.32 | 99.11 |
| | | | | | |
| Si | 1.912 | 1.908 | 1.896 | 1.866 | 1.941 |
| Ti | 0.011 | 0.019 | 0.024 | 0.033 | 0.010 |
| Al | 0.145 | 0.129 | 0.135 | 0.179 | 0.085 |
| Cr | 0.015 | 0.007 | 0.007 | 0.006 | 0.011 |
| Fe | 0.175 | 0.314 | 0.402 | 0.381 | 0.289 |
| Mn | 0.005 | 0.009 | 0.010 | 0.009 | 0.008 |
| Mg | 0.913 | 0.924 | 0.943 | 0.862 | 1.006 |
| Ca | 0.815 | 0.687 | 0.583 | 0.661 | 0.641 |
| Na | 0.013 | 0.018 | 0.016 | 0.021 | 0.019 |
| Total | 4.003 | 4.014 | 4.017 | 4.019 | 4.010 |
| | | | | | |
| Mg#. | 84 | 75 | 70 | 69 | 78 |

KK148

| | P1E | G1 |
|---|---|---|
| $SiO_2$ | 52.49 | 50.97 |
| $TiO_2$ | 0.43 | 0.96 |
| $Al_2O_3$ | 2.28 | 2.54 |
| $Cr_2O_3$ | 0.40 | 0.02 |
| FeO | 8.42 | 16.45 |
| MnO | 0.22 | 0.43 |
| MgO | 17.23 | 13.17 |
| CaO | 18.07 | 15.25 |
| $Na_2O$ | 0.28 | 0.38 |
| Total | 99.82 | 100.18 |
| | | |
| Si | 1.936 | 1.931 |
| Ti | 0.012 | 0.027 |
| Al | 0.099 | 0.113 |
| Cr | 0.012 | 0.001 |
| Fe | 0.160 | 0.521 |
| Mn | 0.007 | 0.014 |
| Mg | 0.947 | 0.744 |
| Ca | 0.714 | 0.619 |
| Na | 0.020 | 0.028 |
| Total | 4.007 | 3.998 |
| | | |
| Mg#. | 86 | 59 |

Opaque phases

| KK01 | | KK04 | KK54 | KK68 | |
|---|---|---|---|---|---|
| | UMG1 | ILG | UMG1 | ILG | UMG1 |
| $SiO_2$ | 0.11 | 0.26 | 0.26 | 0.34 | 0.18 |
| $TiO_2$ | 23.80 | 51.21 | 23.09 | 49.78 | 24.17 |
| $Al_2O_3$ | 2.06 | 0.17 | 2.08 | 0.27 | 1.69 |
| $Cr_2O_3$ | 0.10 | 0.00 | 0.08 | 0.01 | 0.06 |
| FeO | 67.91 | 46.04 | 69.25 | 46.75 | 68.21 |
| MnO | 0.35 | 0.31 | 0.45 | 0.50 | 0.38 |
| MgO | 1.03 | 1.13 | 1.10 | 0.89 | 1.55 |
| Total | 95.37 | 99.11 | 96.30 | 98.58 | 96.24 |
| | | | | | |
| Si | 0.030 | 0.007 | 0.077 | 0.000 | 0.060 |
| Ti | 5.430 | 0.970 | 5.204 | 0.948 | 5.450 |
| Al | 0.740 | 0.007 | 0.735 | 0.085 | 0.600 |
| Cr | 0.011 | 0.000 | 0.018 | 0.000 | 0.000 |
| $Fe^{2+}$ | 12.910 | 0.928 | 12.677 | 0.910 | 12.690 |
| $Fe^{3+}$ | 4.320 | 0.042 | 4.681 | 0.080 | 4.400 |
| Mn | 0.090 | 0.007 | 0.114 | 0.011 | 0.090 |
| Mg | 0.470 | 0.043 | 0.493 | 0.033 | 0.690 |
| Total | 24.000 | 2.000 | 24.000 | 2.000 | 24.000 |

| KK68 | | KK81 | | KK148 |
|---|---|---|---|---|
| | UMG2 | UMG | UMG1 | UMG1 |
| $SiO_2$ | 0.19 | 0.21 | 0.16 | 0.18 |
| $TiO_2$ | 27.66 | 49.34 | 20.82 | 20.03 |
| $Al_2O_3$ | 1.64 | 0.17 | 1.65 | 2.00 |
| $Cr_2O_3$ | 0.05 | 0.04 | 0.10 | 0.03 |
| FeO | 65.10 | 46.57 | 69.57 | 70.77 |
| MnO | 0.40 | 0.47 | 0.33 | 0.44 |
| MgO | 0.96 | 2.54 | 1.99 | 1.07 |
| Total | 96.01 | 99.27 | 94.63 | 94.54 |
| | | | | |
| Si | 0.090 | 0.004 | 0.047 | 0.058 |
| Ti | 6.300 | 0.921 | 4.741 | 4.587 |
| Al | 0.580 | 0.005 | 0.588 | 0.715 |
| Cr | 0.000 | 0.000 | 0.024 | 0.010 |
| $Fe^{2+}$ | 13.830 | 0.818 | 11.799 | 12.031 |
| $Fe^{3+}$ | 2.670 | 0.148 | 5.815 | 5.994 |
| Mn | 0.100 | 0.010 | 0.085 | 0.116 |
| Mg | 0.430 | 0.094 | 0.901 | 0.488 |
| Total | 24.000 | 2.000 | 24.000 | 24.000 |

**Plagioclase+clinopyroxene±olivine basalts (Section 3.2.3)**

**Olivine**

**KK26**

| | X1C |
|---|---|
| $SiO_2$ | 39.10 |
| $Al_2O_3$ | 0.05 |
| FeO | 15.73 |
| MnO | 0.18 |
| MgO | 45.27 |
| CaO | 0.30 |
| Total | 100.63 |
| | |
| Si | 0.981 |
| Al | 0.002 |
| Fe | 0.330 |
| Mn | 0.004 |
| Mg | 1.693 |
| Ca | 0.008 |
| Total | 3.018 |
| | |
| %Fo. | 84 |

Plagioclase

KK09

| | X1C | P1C | P2C | P2E | P3C |
|---|---|---|---|---|---|
| $SiO_2$ | 46.98 | 52.17 | 50.52 | 51.65 | 52.17 |
| $Al_2O_3$ | 33.30 | 29.62 | 30.20 | 29.68 | 29.62 |
| FeO | 0.64 | 0.95 | 0.86 | 0.90 | 0.95 |
| MgO | 0.20 | 0.15 | 0.15 | 0.16 | 0.15 |
| CaO | 17.62 | 13.66 | 14.62 | 13.98 | 13.66 |
| $Na_2O$ | 1.60 | 3.95 | 3.35 | 3.80 | 3.95 |
| $K_2O$ | 0.04 | 0.13 | 0.09 | 0.11 | 0.13 |
| Total | 100.38 | 100.64 | 99.79 | 100.30 | 100.64 |
| | | | | | |
| Si | 8.634 | 9.470 | 9.272 | 9.417 | 9.470 |
| Al | 7.213 | 6.339 | 6.534 | 6.379 | 6.339 |
| Fe | 0.098 | 0.144 | 0.132 | 0.138 | 0.144 |
| Mg | 0.054 | 0.041 | 0.042 | 0.045 | 0.041 |
| Ca | 3.470 | 2.658 | 2.876 | 2.731 | 2.658 |
| Na | 1.570 | 1.389 | 1.191 | 1.342 | 1.389 |
| K | 0.010 | 0.031 | 0.022 | 0.026 | 0.031 |
| Total | 20.050 | 20.071 | 20.068 | 20.078 | 20.025 |
| | | | | | |
| %An. | 86 | 65 | 70 | 67 | 65 |

KK12 KK26

| | X1C | P1C | X2 | P1C | P2C |
|---|---|---|---|---|---|
| $SiO_2$ | 46.04 | 51.17 | 56.80 | 51.38 | 50.51 |
| $Al_2O_3$ | 33.15 | 29.70 | 26.20 | 30.01 | 30.70 |
| FeO | 0.67 | 0.87 | 0.59 | 0.68 | 0.89 |
| MgO | 0.13 | 0.16 | 0.16 | 0.26 | 0.32 |
| CaO | 17.92 | 13.79 | 9.47 | 13.54 | 14.49 |
| $Na_2O$ | 1.42 | 3.85 | 6.13 | 3.56 | 3.12 |
| $K_2O$ | 0.02 | 0.12 | 0.32 | 0.12 | 0.10 |
| Total | 99.38 | 99.66 | 99.59 | 99.56 | 100.13 |
| | | | | | |
| Si | 8.562 | 9.388 | 10.280 | 9.404 | 9.228 |
| Al | 7.269 | 6.424 | 5.590 | 6.476 | 6.613 |
| Fe | 0.105 | 0.133 | 0.089 | 0.105 | 0.136 |
| Mg | 0.036 | 0.044 | 0.017 | 0.072 | 0.087 |
| Ca | 3.571 | 2.711 | 1.835 | 2.656 | 2.837 |
| Na | 0.513 | 1.370 | 2.150 | 1.263 | 1.105 |
| K | 0.005 | 0.029 | 0.075 | 0.027 | 0.022 |
| Total | 20.062 | 20.099 | 20.038 | 20.003 | 20.029 |
| | | | | | |
| %An. | 87 | 66 | 45 | 67 | 72 |

| KK26 | | | | | KK91 |
|---|---|---|---|---|---|
| | X1C | X1E | P3C | P4C | P1C |
| $SiO_2$ | 46.13 | 53.15 | 55.45 | 51.69 | 52.71 |
| $Al_2O_3$ | 34.23 | 29.17 | 28.02 | 30.09 | 28.45 |
| FeO | 0.49 | 0.93 | 0.42 | 0.84 | 0.93 |
| MgO | 0.22 | 0.16 | 0.03 | 0.21 | 0.19 |
| CaO | 17.80 | 12.46 | 10.03 | 13.69 | 12.65 |
| $Na_2O$ | 1.37 | 4.11 | 5.61 | 3.59 | 4.44 |
| $K_2O$ | 0.01 | 0.19 | 0.24 | 0.14 | 0.09 |
| Total | 100.27 | 100.17 | 99.83 | 100.30 | 99.46 |
| | | | | | |
| Si | 8.486 | 9.643 | 10.013 | 9.405 | 9.655 |
| Al | 7.425 | 6.240 | 5.965 | 6.455 | 6.144 |
| Fe | 0.076 | 0.141 | 0.066 | 0.127 | 0.142 |
| Mg | 0.061 | 0.044 | 0.009 | 0.057 | 0.051 |
| Ca | 3.508 | 2.423 | 1.966 | 2.670 | 2.483 |
| Na | 0.489 | 1.446 | 1.941 | 1.268 | 1.575 |
| K | 0.003 | 0.044 | 0.055 | 0.032 | 0.022 |
| Total | 20.048 | 19.982 | 20.038 | 20.018 | 20.072 |
| | | | | | |
| %An. | 88 | 62 | 50 | 67 | 61 |

| KK91 | |
|---|---|
| | X1C |
| $SiO_2$ | 46.52 |
| $Al_2O_3$ | 32.64 |
| FeO | 0.73 |
| MgO | 0.12 |
| CaO | 17.37 |
| $Na_2O$ | 1.65 |
| $K_2O$ | 0.02 |
| Total | 99.05 |
| | |
| Si | 8.666 |
| Al | 7.169 |
| Fe | 0.114 |
| Mg | 0.034 |
| Ca | 3.467 |
| Na | 0.594 |
| K | 0.004 |
| Total | 20.049 |
| | |
| %An. | 85 |

Clinopyroxene

| KK09 | | KK12 | | KK26 | |
|---|---|---|---|---|---|
| | P1C | P1C | X2 | P1C | P2C |
| $SiO_2$ | 52.70 | 50.11 | 49.40 | 51.52 | 51.42 |
| $TiO_2$ | 0.41 | 1.30 | 0.42 | 0.48 | 0.52 |
| $Al_2O_3$ | 1.97 | 2.35 | 1.39 | 2.91 | 3.70 |
| $Cr_2O_3$ | 0.17 | 0.05 | 0.02 | 0.20 | 0.72 |
| FeO | 7.44 | 13.95 | 19.88 | 8.30 | 6.05 |
| MnO | 0.19 | 0.32 | 0.87 | 0.22 | 0.15 |
| MgO | 16.98 | 14.05 | 9.30 | 18.85 | 17.25 |
| CaO | 20.17 | 17.52 | 17.94 | 16.76 | 20.11 |
| $Na_2O$ | 0.21 | 0.27 | 0.28 | 0.17 | 0.21 |
| Total | 100.24 | 99.91 | 99.51 | 99.40 | 100.13 |
| | | | | | |
| Si | 1.937 | 1.899 | 1.942 | 1.902 | 1.885 |
| Ti | 0.011 | 0.037 | 0.012 | 0.013 | 0.014 |
| Al | 0.085 | 0.105 | 0.064 | 0.127 | 0.160 |
| Cr | 0.005 | 0.001 | 0.000 | 0.006 | 0.021 |
| Fe | 0.229 | 0.442 | 0.654 | 0.256 | 0.185 |
| Mn | 0.006 | 0.010 | 0.029 | 0.007 | 0.005 |
| Mg | 0.930 | 0.794 | 0.545 | 1.037 | 0.942 |
| Ca | 0.794 | 0.711 | 0.756 | 0.663 | 0.790 |
| Na | 0.015 | 0.020 | 0.021 | 0.013 | 0.015 |
| Total | 4.014 | 4.020 | 4.024 | 4.024 | 4.018 |
| | | | | | |
| Mg#. | 80 | 64 | 45 | 80 | 84 |

KK91

| | P1C | P2C |
|---|---|---|
| $SiO_2$ | 49.82 | 50.42 |
| $TiO_2$ | 1.12 | 0.97 |
| $Al_2O_3$ | 3.85 | 3.22 |
| $Cr_2O_3$ | 0.11 | 0.08 |
| FeO | 10.66 | 11.94 |
| MnO | 0.24 | 0.29 |
| MgO | 14.93 | 16.12 |
| CaO | 18.85 | 16.44 |
| $Na_2O$ | 0.30 | 0.24 |
| Total | 99.88 | 99.72 |
| | | |
| Si | 1.867 | 1.889 |
| Ti | 0.032 | 0.027 |
| Al | 0.170 | 0.124 |
| Cr | 0.003 | 0.002 |
| Fe | 0.334 | 0.374 |
| Mn | 0.008 | 0.009 |
| Mg | 0.834 | 0.900 |
| Ca | 0.757 | 0.660 |
| Na | 0.022 | 0.018 |
| Total | 4.026 | 4.021 |
| | | |
| Mg#. | 71 | 71 |

Opaque phases

KK12

| | ILX | UMX | UMG2 |
|---|---|---|---|
| $SiO_2$ | 0.18 | 0.17 | 0.19 |
| $TiO_2$ | 49.90 | 20.42 | 27.66 |
| $Al_2O_3$ | 0.09 | 1.11 | 1.64 |
| $Cr_2O_3$ | 0.00 | 0.08 | 0.05 |
| FeO | 48.63 | 73.34 | 65.10 |
| MnO | 0.63 | 0.75 | 0.40 |
| MgO | 0.75 | 0.37 | 0.96 |
| Total | 100.19 | 96.24 | 96.01 |
| | | | |
| Si | 0.000 | 0.050 | 0.000 |
| Ti | 0.937 | 4.640 | 6.300 |
| Al | 0.000 | 0.390 | 0.580 |
| Cr | 0.000 | 0.020 | 0.090 |
| $Fe^{2+}$ | 0.900 | 12.340 | 13.830 |
| $Fe^{3+}$ | 0.115 | 6.200 | 2.670 |
| Mn | 0.013 | 0.190 | 0.100 |
| Mg | 0.028 | 0.170 | 0.430 |
| Total | 2.000 | 24.000 | 24.000 |

**Plagioclase+clinopyroxene+orthopyroxene+FeTi oxides-phyric intermediates (section 3.2.4)**

Plagioclase

| KK08 | | | | | KK34 |
|---|---|---|---|---|---|
| | X1 | P1C | X1C | X2C | P1C |
| $SiO_2$ | 50.16 | 50.88 | 46.74 | 46.03 | 54.02 |
| $Al_2O_3$ | 29.77 | 29.42 | 32.38 | 32.95 | 28.52 |
| FeO | 0.88 | 0.90 | 0.48 | 0.58 | 0.49 |
| MgO | 0.21 | 0.17 | 0.26 | 0.17 | 0.06 |
| CaO | 14.54 | 13.70 | 17.12 | 17.53 | 10.95 |
| $Na_2O$ | 3.43 | 3.82 | 1.97 | 1.68 | 5.15 |
| $K_2O$ | 0.07 | 0.11 | 0.02 | 0.02 | 0.11 |
| Total | 99.06 | 98.99 | 98.98 | 98.98 | 99.29 |
| | | | | | |
| Si | 9.280 | 9.399 | 8.706 | 8.588 | 9.835 |
| Al | 6.493 | 6.406 | 7.111 | 7.247 | 6.121 |
| Fe | 0.136 | 0.139 | 0.075 | 0.091 | 0.074 |
| Mg | 0.057 | 0.046 | 0.071 | 0.049 | 0.017 |
| Ca | 2.883 | 2.711 | 3.417 | 3.506 | 2.136 |
| Na | 1.231 | 1.370 | 0.712 | 0.608 | 1.817 |
| K | 0.016 | 0.026 | 0.004 | 0.006 | 0.025 |
| Total | 20.097 | 20.096 | 20.096 | 20.095 | 20.025 |
| | | | | | |
| %An. | 70 | 66 | 83 | 85 | 54 |

| KK34 | | KK35 | | | |
|---|---|---|---|---|---|
| | P2C | X1C | P1C | P1E | P2C |
| $SiO_2$ | 55.03 | 46.44 | 53.38 | 52.99 | 54.72 |
| $Al_2O_3$ | 28.03 | 33.09 | 29.94 | 29.22 | 28.20 |
| FeO | 0.37 | 0.72 | 0.67 | 0.68 | 0.46 |
| MgO | 0.06 | 0.06 | 0.14 | 0.13 | 0.08 |
| CaO | 10.55 | 17.50 | 13.96 | 13.33 | 11.46 |
| $Na_2O$ | 5.41 | 1.70 | 3.60 | 4.10 | 5.17 |
| $K_2O$ | 0.15 | 0.04 | 0.10 | 0.10 | 0.14 |
| Total | 99.61 | 99.55 | 100.19 | 100.55 | 100.23 |
| | | | | | |
| Si | 9.966 | 8.615 | 9.426 | 9.595 | 9.882 |
| Al | 5.988 | 7.237 | 6.425 | 6.238 | 6.004 |
| Fe | 0.056 | 0.111 | 0.101 | 0.103 | 0.069 |
| Mg | 0.016 | 0.015 | 0.037 | 0.034 | 0.021 |
| Ca | 2.047 | 3.478 | 2.724 | 2.585 | 2.218 |
| Na | 1.902 | 0.612 | 1.271 | 1.440 | 1.812 |
| K | 0.035 | 0.010 | 0.023 | 0.023 | 0.033 |
| Total | 20.009 | 20.078 | 20.008 | 20.018 | 20.038 |
| | | | | | |
| %An. | 51 | 85 | 68 | 64 | 55 |

| KK35 | |
|---|---|
| | P2E |
| $SiO_2$ | 51.28 |
| $Al_2O_3$ | 28.85 |
| FeO | 1.01 |
| MgO | 0.05 |
| CaO | 12.55 |
| $Na_2O$ | 4.37 |
| $K_2O$ | 0.20 |
| Total | 98.49 |
| | |
| Si | 9.512 |
| Al | 6.309 |
| Fe | 0.156 |
| Mg | 0.049 |
| Ca | 2.495 |
| Na | 1.571 |
| K | 0.047 |
| Total | 20.143 |
| | |
| %An. | 61 |

Clinopyroxene

| KK08 | | | | KK34 | KK35 |
|---|---|---|---|---|---|
| | X1C | P1C | X2C | P1C | P1C |
| $SiO_2$ | 50.27 | 51.35 | 51.33 | 50.50 | 50.82 |
| $TiO_2$ | 0.45 | 0.58 | 0.54 | 0.68 | 0.68 |
| $Al_2O_3$ | 3.42 | 2.41 | 1.59 | 2.47 | 2.35 |
| $Cr_2O_3$ | 0.95 | 0.21 | 0.04 | 0.00 | 0.00 |
| FeO | 5.82 | 9.61 | 10.92 | 12.23 | 12.20 |
| MnO | 0.18 | 0.26 | 0.28 | 0.31 | 0.34 |
| MgO | 16.97 | 16.52 | 15.70 | 13.49 | 14.30 |
| CaO | 20.05 | 18.46 | 18.31 | 19.84 | 18.94 |
| $Na_2O$ | 0.21 | 0.30 | 0.21 | 0.27 | 0.30 |
| Total | 98.33 | 99.73 | 98.95 | 99.79 | 99.94 |
| | | | | | |
| Si | 1.880 | 1.913 | 1.938 | 1.912 | 1.915 |
| Ti | 0.013 | 0.016 | 0.015 | 0.019 | 0.019 |
| Al | 0.151 | 0.106 | 0.071 | 0.110 | 0.104 |
| Cr | 0.028 | 0.006 | 0.001 | 0.000 | 0.000 |
| Fe | 0.182 | 0.299 | 0.345 | 0.387 | 0.384 |
| Mn | 0.006 | 0.008 | 0.009 | 0.010 | 0.011 |
| Mg | 0.946 | 0.917 | 0.883 | 0.761 | 0.803 |
| Ca | 0.804 | 0.737 | 0.741 | 0.805 | 0.765 |
| Na | 0.016 | 0.022 | 0.015 | 0.020 | 0.022 |
| Total | 4.025 | 4.026 | 4.019 | 4.024 | 4.024 |
| | | | | | |
| Mg#. | 84 | 75 | 68 | 66 | 68 |

| KK35 | |
|---|---|
| | P2C |
| $SiO_2$ | 51.42 |
| $TiO_2$ | 0.62 |
| $Al_2O_3$ | 3.25 |
| $Cr_2O_3$ | 0.01 |
| FeO | 10.35 |
| MnO | 0.30 |
| MgO | 14.73 |
| CaO | 19.01 |
| $Na_2O$ | 0.36 |
| Total | 100.04 |
| | |
| Si | 1.915 |
| Ti | 0.017 |
| Al | 0.143 |
| Cr | 0.000 |
| Fe | 0.322 |
| Mn | 0.010 |
| Mg | 0.817 |
| Ca | 0.758 |
| Na | 0.026 |
| Total | 4.009 |
| | |
| Mg#. | 70 |

Orthopyroxene

| KK08 | | KK34 | KK35 | |
|---|---|---|---|---|
| | P1C | P1C | P1C | P2C |
| $SiO_2$ | 52.88 | 52.31 | 53.56 | 51.49 |
| $TiO_2$ | 0.44 | 0.20 | 0.24 | 0.31 |
| $Al_2O_3$ | 1.61 | 0.66 | 0.89 | 1.13 |
| $Cr_2O_3$ | 0.05 | 0.00 | 0.03 | 0.02 |
| FeO | 17.44 | 23.23 | 18.16 | 27.79 |
| MnO | 0.41 | 0.57 | 0.44 | 0.71 |
| MgO | 25.14 | 21.97 | 25.49 | 17.92 |
| CaO | 2.26 | 1.57 | 1.72 | 1.64 |
| $Na_2O$ | 0.05 | 0.03 | 0.04 | 0.03 |
| Total | 100.29 | 99.73 | 100.56 | 101.04 |
| | | | | |
| Si | 1.932 | 1.956 | 1.953 | 1.958 |
| Ti | 0.012 | 0.006 | 0.007 | 0.009 |
| Al | 0.070 | 0.029 | 0.038 | 0.051 |
| Cr | 0.001 | 0.000 | 0.000 | 0.000 |
| Fe | 0.533 | 0.726 | 0.554 | 0.884 |
| Mn | 0.013 | 0.018 | 0.014 | 0.023 |
| Mg | 1.369 | 1.224 | 1.386 | 1.016 |
| Ca | 0.088 | 0.063 | 0.067 | 0.067 |
| Na | 0.003 | 0.002 | 0.003 | 0.002 |
| Total | 4.022 | 4.025 | 4.022 | 4.009 |
| | | | | |
| Mg#. | 72 | 63 | 71 | 53 |

Opaque phases

| KK08 | | | KK34 | |
|---|---|---|---|---|
| | ILP | UMP | ILP | UMP |
| $SiO_2$ | 0.25 | 0.48 | 0.08 | 0.21 |
| $TiO_2$ | 50.03 | 17.93 | 49.28 | 17.30 |
| $Al_2O_3$ | 0.15 | 1.54 | 0.53 | 1.88 |
| $Cr_2O_3$ | 0.00 | 0.08 | 0.00 | 0.07 |
| FeO | 46.00 | 74.31 | 47.25 | 74.57 |
| MnO | 0.45 | 0.41 | 0.53 | 0.43 |
| MgO | 1.47 | 0.62 | 1.95 | 1.33 |
| Total | 98.35 | 95.34 | 99.26 | 95.79 |
| | | | | |
| Si | 0.006 | 0.144 | 0.002 | 0.062 |
| Ti | 0.951 | 4.085 | 0.924 | 3.893 |
| Al | 0.005 | 0.549 | 0.005 | 0.664 |
| Cr | 0.002 | 0.019 | 0.000 | 0.018 |
| $Fe^{2+}$ | 0.893 | 12.608 | 0.843 | 11.256 |
| $Fe^{3+}$ | 0.080 | 6.213 | 0.142 | 7.405 |
| Mn | 0.010 | 0.105 | 0.011 | 0.109 |
| Mg | 0.055 | 0.279 | 0.073 | 0.594 |
| Total | 2.000 | 24.000 | 2.000 | 24.001 |

**Plagioclase±clinopyroxene±FeTi oxides±fayalitic olivine-phyric rhyolites (section 3.2.5)**

**Olivine**

**KK03**

| | P1C | P2C |
|---|---|---|
| $SiO_2$ | 30.48 | 30.82 |
| $Al_2O_3$ | 0.06 | 0.06 |
| FeO | 62.28 | 62.81 |
| MnO | 1.94 | 2.01 |
| MgO | 5.26 | 5.09 |
| CaO | 0.39 | 0.36 |
| Total | 100.41 | 101.16 |
| | | |
| Si | 0.991 | 0.995 |
| Al | 0.002 | 0.002 |
| Fe | 1.693 | 1.695 |
| Mn | 0.054 | 0.055 |
| Mg | 0.255 | 0.245 |
| Ca | 0.014 | 0.012 |
| Total | 3.008 | 3.004 |
| | | |
| %Fo. | 13 | 12 |

**Plagioclase**

| | KK03 | | | KK29 | |
|---|---|---|---|---|---|
| | P1C | P1E | P2C | P1C | P2C |
| $SiO_2$ | 58.05 | 58.65 | 59.28 | 59.04 | 60.68 |
| $Al_2O_3$ | 26.07 | 26.00 | 25.35 | 26.42 | 24.73 |
| FeO | 0.40 | 0.41 | 0.37 | 0.48 | 0.40 |
| MgO | 0.03 | 0.03 | 0.02 | 0.03 | 0.02 |
| CaO | 8.42 | 8.14 | 7.56 | 8.33 | 6.93 |
| $Na_2O$ | 6.33 | 6.54 | 6.76 | 6.74 | 7.55 |
| $K_2O$ | 0.28 | 0.29 | 0.34 | 0.63 | 0.78 |
| Total | 99.61 | 100.08 | 99.73 | 101.68 | 101.11 |
| | | | | | |
| Si | 10.440 | 10.490 | 10.621 | 10.431 | 10.745 |
| Al | 5.527 | 5.482 | 5.354 | 5.503 | 5.163 |
| Fe | 0.060 | 0.062 | 0.056 | 0.072 | 0.059 |
| Mg | 0.008 | 0.008 | 0.003 | 0.008 | 0.006 |
| Ca | 1.623 | 1.559 | 1.451 | 1.578 | 1.315 |
| Na | 2.209 | 2.268 | 2.347 | 2.308 | 2.592 |
| K | 0.063 | 0.066 | 0.078 | 0.141 | 0.176 |
| Total | 19.933 | 19.936 | 19.915 | 20.042 | 20.058 |
| | | | | | |
| %An. | 42 | 40 | 37 | 39 | 32 |

Clinopyroxene

KK03

| | P1C | P2C |
|---|---|---|
| $SiO_2$ | 48.72 | 48.40 |
| $TiO_2$ | 0.30 | 0.34 |
| $Al_2O_3$ | 0.82 | 0.79 |
| $Cr_2O_3$ | 0.00 | 0.00 |
| FeO | 26.16 | 25.97 |
| MnO | 1.00 | 0.92 |
| MgO | 5.53 | 5.15 |
| CaO | 17.39 | 18.02 |
| $Na_2O$ | 0.19 | 0.21 |
| Total | 100.11 | 99.80 |
| | | |
| Si | 1.960 | 1.957 |
| Ti | 0.009 | 0.010 |
| Al | 0.039 | 0.037 |
| Cr | 0.000 | 0.000 |
| Fe | 0.880 | 0.878 |
| Mn | 0.039 | 0.031 |
| Mg | 0.332 | 0.310 |
| Ca | 0.750 | 0.781 |
| Na | 0.015 | 0.016 |
| Total | 4.019 | 4.022 |
| | | |
| Mg#. | 27 | 26 |

Opaque phases

KK03

| | PC |
|---|---|
| SiO2 | 0.13 |
| TiO2 | 19.95 |
| Al2O3 | 1.48 |
| Cr2O3 | 0.01 |
| FeO | 74.66 |
| MnO | 0.74 |
| MgO | 0.40 |
| Total | 97.37 |
| | |
| Si | 0.039 |
| Ti | 4.469 |
| Al | 0.518 |
| Cr | 0.004 |
| Fe2+ | 12.144 |
| Fe3+ | 6.459 |
| Mn | 0.187 |
| Mg | 0.180 |
| Total | 24.000 |

# APPENDIX IV:

## Whole-rock analyses

## (a) Major-element concentrations

### Loss-on-ignition values.

The following loss-on-ignition (LOI) values were determined. All other samples show negligible LOI values. Analyses in Appendices IV and V are presented uncorrected for LOI.

KK7, 0.8: KK10, 2.1: KK22, 0.8; KK56, 3.7; KK67, 1.1; KK84, 1.6; KK86, 0.9; KK105, 4.1; KK118, 1.1; KK121, 3.5; KK132, 5.2. (Values in wt%)

| Sample | wt% SiO2 | Al2O3 | Fe2O3 | MgO | CaO | Na2O | K2O | TiO2 | MnO | P2O5 | Total |
|---|---|---|---|---|---|---|---|---|---|---|---|
| KK1 | 49.63 | 13.68 | 15.18 | 6.54 | 10.94 | 2.32 | 0.14 | 1.59 | 0.23 | 0.14 | 100.39 |
| KK2 | 49.90 | 14.44 | 13.86 | 7.11 | 11.43 | 2.15 | 0.18 | 1.43 | 0.21 | 0.13 | 100.83 |
| KK3 | 73.50 | 11.99 | 4.34 | 0.19 | 1.97 | 4.14 | 2.57 | 0.35 | 0.10 | 0.05 | 99.19 |
| KK4 | 49.66 | 13.86 | 12.27 | 7.57 | 12.32 | 2.03 | 0.13 | 1.17 | 0.19 | 0.11 | 99.29 |
| KK6 | 75.17 | 12.97 | 1.82 | 0.05 | 1.50 | 4.15 | 2.60 | 0.42 | 0.01 | 0.06 | 98.75 |
| KK7 | 72.47 | 12.28 | 4.38 | 0.25 | 2.07 | 4.24 | 2.48 | 0.42 | 0.12 | 0.05 | 98.75 |
| KK8 | 51.15 | 12.89 | 16.58 | 4.81 | 8.99 | 2.64 | 0.53 | 2.43 | 0.25 | 0.30 | 100.55 |
| KK9 | 62.85 | 12.68 | 10.22 | 2.55 | 5.51 | 3.42 | 1.52 | 1.37 | 0.17 | 0.17 | 100.48 |
| KK10 | 50.63 | 14.77 | 13.91 | 5.52 | 9.19 | 1.48 | 0.35 | 1.67 | 0.20 | 0.16 | 97.87 |
| KK11 | 49.47 | 15.46 | 11.95 | 7.31 | 12.22 | 2.21 | 0.26 | 1.60 | 0.19 | 0.18 | 100.84 |
| KK12 | 54.63 | 12.98 | 14.61 | 4.22 | 7.76 | 2.75 | 0.84 | 2.11 | 0.22 | 0.26 | 100.39 |
| KK13 | 48.49 | 12.70 | 16.50 | 5.70 | 10.51 | 2.27 | 0.22 | 1.96 | 0.27 | 0.21 | 98.83 |
| KK14 | 59.39 | 12.64 | 11.65 | 3.26 | 6.32 | 2.96 | 1.25 | 1.65 | 0.19 | 0.21 | 99.52 |
| KK16 | 49.31 | 14.06 | 13.07 | 7.68 | 12.50 | 2.07 | 0.17 | 1.52 | 0.21 | 0.14 | 100.72 |
| KK17 | 48.18 | 16.38 | 11.03 | 6.71 | 13.46 | 1.73 | 0.12 | 1.06 | 0.18 | 0.12 | 98.95 |
| KK18 | 50.36 | 17.97 | 9.26 | 5.83 | 12.83 | 2.15 | 0.28 | 0.89 | 0.16 | 0.10 | 99.83 |
| KK19 | 50.28 | 15.13 | 11.40 | 7.38 | 12.51 | 2.06 | 0.23 | 1.10 | 0.19 | 0.10 | 100.37 |
| KK20 | 50.76 | 14.31 | 11.80 | 7.53 | 12.07 | 2.09 | 0.28 | 1.13 | 0.20 | 0.11 | 100.28 |
| KK21 | 47.50 | 14.76 | 11.91 | 8.84 | 12.01 | 1.88 | 0.12 | 1.40 | 0.18 | 0.13 | 98.73 |
| KK22 | 49.52 | 15.67 | 11.54 | 7.24 | 10.98 | 1.84 | 0.22 | 1.48 | 0.17 | 0.13 | 98.79 |
| KK23 | 49.51 | 15.46 | 11.94 | 6.72 | 12.64 | 2.00 | 0.17 | 1.44 | 0.19 | 0.13 | 100.20 |
| KK24 | 49.71 | 14.40 | 14.93 | 5.34 | 9.64 | 2.29 | 0.42 | 2.05 | 0.22 | 0.24 | 99.23 |
| KK25 | 67.75 | 13.20 | 6.55 | 1.57 | 4.28 | 3.78 | 1.99 | 0.72 | 0.16 | 0.17 | 100.19 |
| KK26 | 66.33 | 13.20 | 6.98 | 1.92 | 4.87 | 3.78 | 1.85 | 0.77 | 0.16 | 0.17 | 100.03 |
| KK27 | 50.16 | 14.39 | 14.76 | 5.54 | 10.26 | 2.47 | 0.43 | 2.03 | 0.22 | 0.26 | 100.51 |
| KK28 | 51.84 | 15.76 | 10.69 | 6.60 | 11.98 | 2.34 | 0.37 | 1.04 | 0.18 | 0.12 | 100.91 |
| KK29 | 75.55 | 12.15 | 3.37 | 0.04 | 1.56 | 4.25 | 2.78 | 0.24 | 0.07 | 0.02 | 100.02 |
| KK30 | 47.20 | 14.92 | 12.89 | 9.49 | 11.58 | 2.03 | 0.20 | 1.91 | 0.19 | 0.20 | 100.60 |
| KK31 | 48.92 | 15.73 | 10.64 | 9.39 | 13.10 | 1.79 | 0.08 | 0.79 | 0.17 | 0.06 | 100.67 |
| KK32 | 49.02 | 14.92 | 11.66 | 8.52 | 12.98 | 1.96 | 0.12 | 1.08 | 0.19 | 0.11 | 100.55 |
| KK33 | 49.82 | 16.71 | 10.73 | 6.99 | 12.55 | 2.06 | 0.24 | 1.11 | 0.18 | 0.15 | 100.52 |
| KK34 | 64.82 | 15.25 | 6.68 | 1.43 | 4.70 | 4.22 | 1.32 | 0.86 | 0.12 | 0.20 | 99.58 |
| KK35 | 57.47 | 15.54 | 10.60 | 3.32 | 7.23 | 3.50 | 0.81 | 1.32 | 0.17 | 0.26 | 100.23 |
| KK36 | 49.46 | 14.49 | 12.30 | 8.00 | 12.46 | 2.03 | 0.12 | 1.19 | 0.20 | 0.09 | 100.33 |
| KK37 | 50.64 | 13.16 | 16.24 | 5.36 | 9.65 | 2.56 | 0.41 | 2.03 | 0.25 | 0.19 | 100.49 |
| KK50 | 47.84 | 15.54 | 10.99 | 9.41 | 13.45 | 1.63 | 0.04 | 0.77 | 0.17 | 0.05 | 99.89 |
| KK51 | 50.74 | 15.34 | 12.27 | 6.68 | 10.63 | 2.50 | 0.32 | 1.48 | 0.19 | 0.25 | 100.41 |
| KK52 | 48.47 | 15.88 | 10.80 | 9.07 | 13.06 | 1.75 | 0.08 | 0.81 | 0.18 | 0.08 | 100.16 |
| KK53 | 48.66 | 15.33 | 11.48 | 9.12 | 13.05 | 1.68 | 0.06 | 0.80 | 0.19 | 0.06 | 100.43 |
| KK54 | 49.13 | 14.78 | 12.51 | 7.65 | 12.56 | 2.10 | 0.16 | 1.51 | 0.19 | 0.13 | 100.71 |
| KK55 | 48.95 | 15.16 | 11.99 | 7.60 | 12.69 | 1.89 | 0.15 | 1.44 | 0.19 | 0.13 | 100.18 |
| KK56 | 71.00 | 11.66 | 3.67 | 0.31 | 2.45 | 3.57 | 2.70 | 0.35 | 0.08 | 0.05 | 95.84 |
| KK57 | 73.49 | 11.97 | 4.06 | 0.12 | 1.85 | 4.15 | 2.60 | 0.31 | 0.10 | 0.04 | 98.68 |

| | | | | | | | | | | | |
|---|---|---|---|---|---|---|---|---|---|---|---|
| KK58 | 48.47 | 15.85 | 10.36 | 9.73 | 12.99 | 1.72 | 0.07 | 0.74 | 0.17 | 0.06 | 100.16 |
| KK59 | 48.21 | 14.02 | 15.22 | 5.88 | 10.77 | 2.24 | 0.22 | 2.22 | 0.22 | 0.23 | 99.24 |
| KK60 | 51.61 | 13.88 | 15.05 | 4.73 | 9.10 | 2.74 | 0.62 | 2.15 | 0.23 | 0.38 | 100.48 |
| KK62 | 50.41 | 13.06 | 16.51 | 5.30 | 9.45 | 2.66 | 0.41 | 2.09 | 0.25 | 0.21 | 100.35 |
| KK63 | 48.97 | 14.20 | 13.57 | 6.88 | 11.64 | 2.37 | 0.25 | 2.02 | 0.22 | 0.23 | 100.34 |
| KK64 | 49.90 | 13.45 | 14.72 | 5.65 | 10.22 | 2.47 | 0.34 | 2.11 | 0.23 | 0.25 | 99.35 |
| KK65 | 49.57 | 16.24 | 10.77 | 7.24 | 13.00 | 1.98 | 0.15 | 1.03 | 0.17 | 0.10 | 100.25 |
| KK66 | 50.55 | 13.28 | 16.21 | 5.40 | 9.71 | 2.64 | 0.41 | 2.01 | 0.25 | 0.19 | 100.64 |
| KK67 | 73.53 | 11.86 | 4.08 | 0.17 | 1.83 | 4.27 | 2.62 | 0.31 | 0.09 | 0.04 | 98.79 |
| KK68 | 48.61 | 14.99 | 11.69 | 8.58 | 12.84 | 1.86 | 0.11 | 1.19 | 0.18 | 0.11 | 100.15 |
| KK69 | 48.51 | 15.33 | 14.87 | 5.10 | 9.76 | 2.25 | 0.37 | 2.01 | 0.23 | 0.26 | 98.68 |
| KK70 | 49.61 | 14.43 | 14.36 | 5.66 | 10.31 | 2.51 | 0.40 | 1.95 | 0.22 | 0.25 | 99.71 |
| KK71 | 49.05 | 15.00 | 12.17 | 7.26 | 12.48 | 2.15 | 0.20 | 1.64 | 0.20 | 0.18 | 100.33 |
| KK72 | 49.04 | 13.75 | 13.89 | 6.65 | 11.26 | 2.38 | 0.27 | 1.70 | 0.22 | 0.17 | 99.33 |
| KK73 | 50.08 | 13.93 | 13.72 | 6.62 | 11.33 | 2.34 | 0.27 | 1.72 | 0.21 | 0.17 | 100.39 |
| KK75 | 48.58 | 17.58 | 10.29 | 6.61 | 13.26 | 1.90 | 0.14 | 1.36 | 0.17 | 0.15 | 100.04 |
| KK76 | 49.15 | 19.18 | 10.01 | 5.40 | 13.37 | 1.95 | 0.12 | 0.93 | 0.15 | 0.09 | 100.34 |
| KK77 | 57.10 | 12.77 | 13.27 | 3.66 | 7.15 | 2.99 | 1.02 | 1.89 | 0.21 | 0.24 | 100.31 |
| KK78 | 48.65 | 16.03 | 10.41 | 9.69 | 13.19 | 1.63 | 0.06 | 0.73 | 0.17 | 0.06 | 100.61 |
| KK79 | 50.01 | 14.97 | 10.48 | 7.94 | 13.77 | 1.85 | 0.05 | 0.82 | 0.18 | 0.06 | 100.11 |
| KK80 | 51.00 | 13.62 | 14.87 | 4.87 | 9.41 | 2.56 | 0.65 | 2.68 | 0.24 | 0.43 | 100.32 |
| KK81 | 49.56 | 15.55 | 10.40 | 8.98 | 13.64 | 1.66 | 0.05 | 0.69 | 0.17 | 0.05 | 100.74 |
| KK82 | 50.32 | 13.85 | 14.04 | 6.53 | 11.25 | 2.37 | 0.26 | 1.63 | 0.22 | 0.18 | 100.64 |
| KK83 | 50.77 | 13.44 | 16.26 | 5.43 | 9.75 | 2.69 | 0.40 | 2.00 | 0.25 | 0.19 | 101.18 |
| KK84 | 49.35 | 13.34 | 16.04 | 6.44 | 10.52 | 2.07 | 0.22 | 1.80 | 0.25 | 0.16 | 100.19 |
| KK85 | 50.83 | 13.50 | 16.22 | 5.43 | 9.66 | 2.56 | 0.41 | 2.01 | 0.24 | 0.20 | 101.05 |
| KK86 | 61.98 | 15.31 | 8.81 | 2.30 | 5.48 | 3.64 | 1.28 | 1.12 | 0.16 | 0.24 | 100.32 |
| KK87 | 51.43 | 14.60 | 11.75 | 7.14 | 11.57 | 2.24 | 0.35 | 1.19 | 0.20 | 0.16 | 100.62 |
| KK88 | 50.85 | 13.85 | 13.38 | 6.65 | 11.32 | 2.23 | 0.31 | 1.71 | 0.21 | 0.20 | 100.72 |
| KK89 | 50.03 | 15.73 | 14.08 | 5.46 | 11.02 | 2.27 | 0.26 | 1.60 | 0.22 | 0.14 | 100.83 |
| KK90 | 50.76 | 13.52 | 16.02 | 5.47 | 9.71 | 2.62 | 0.40 | 1.96 | 0.25 | 0.19 | 100.90 |
| KK91 | 50.76 | 13.46 | 16.25 | 5.38 | 9.72 | 2.45 | 0.40 | 2.02 | 0.25 | 0.19 | 100.86 |
| KK92 | 49.58 | 13.88 | 15.39 | 6.91 | 10.40 | 2.32 | 0.29 | 1.82 | 0.23 | 0.17 | 101.00 |
| KK93 | 50.76 | 13.38 | 16.22 | 5.42 | 9.72 | 2.65 | 0.40 | 2.00 | 0.25 | 0.20 | 101.00 |
| KK94 | 58.84 | 15.60 | 9.80 | 2.99 | 6.77 | 3.77 | 0.89 | 1.26 | 0.16 | 0.27 | 100.36 |
| KK95 | 57.54 | 15.63 | 10.58 | 3.33 | 7.22 | 3.56 | 0.80 | 1.32 | 0.17 | 0.26 | 100.40 |
| KK96 | 58.67 | 15.69 | 10.12 | 3.22 | 7.01 | 3.74 | 0.86 | 1.28 | 0.16 | 0.27 | 101.03 |
| KK97 | 50.00 | 13.23 | 16.67 | 5.85 | 10.00 | 2.46 | 0.32 | 2.02 | 0.25 | 0.20 | 101.00 |
| KK98 | 59.14 | 15.81 | 9.78 | 2.89 | 6.67 | 3.80 | 0.91 | 1.26 | 0.16 | 0.27 | 100.67 |
| KK99 | 50.36 | 13.72 | 15.62 | 6.33 | 10.46 | 2.42 | 0.27 | 1.67 | 0.24 | 0.15 | 101.21 |
| KK100 | 50.14 | 14.71 | 14.49 | 5.60 | 10.37 | 2.48 | 0.41 | 1.96 | 0.22 | 0.26 | 100.62 |
| KK101 | 50.22 | 13.25 | 16.67 | 5.80 | 10.02 | 2.46 | 0.32 | 2.03 | 0.25 | 0.21 | 101.24 |
| KK102 | 50.11 | 13.22 | 16.62 | 5.79 | 10.00 | 2.42 | 0.32 | 2.04 | 0.25 | 0.20 | 100.98 |
| KK103 | 50.67 | 13.23 | 16.54 | 5.36 | 9.56 | 2.62 | 0.42 | 2.08 | 0.25 | 0.20 | 100.92 |

| | | | | | | | | | | | |
|---|---|---|---|---|---|---|---|---|---|---|---|
| KK104 | 49.22 | 15.02 | 12.37 | 7.55 | 12.61 | 2.14 | 0.15 | 1.49 | 0.19 | 0.12 | 100.86 |
| KK105 | 49.08 | 15.04 | 11.24 | 8.31 | 12.97 | 1.41 | 0.09 | 1.01 | 0.18 | 0.09 | 99.42 |
| KK106 | 49.36 | 13.77 | 15.62 | 6.32 | 10.54 | 2.29 | 0.27 | 1.81 | 0.24 | 0.17 | 100.39 |
| KK107 | 50.81 | 13.50 | 16.30 | 5.36 | 9.65 | 2.62 | 0.40 | 2.01 | 0.24 | 0.19 | 101.08 |
| KK108 | 49.93 | 13.39 | 16.32 | 5.91 | 10.09 | 2.41 | 0.31 | 1.97 | 0.24 | 0.19 | 100.77 |
| KK109A | 49.57 | 13.69 | 15.56 | 6.29 | 10.43 | 2.32 | 0.28 | 1.81 | 0.24 | 0.17 | 100.35 |
| KK109B | 49.83 | 13.84 | 15.46 | 6.34 | 10.46 | 2.31 | 0.29 | 1.81 | 0.23 | 0.17 | 100.73 |
| KK110 | 49.95 | 13.74 | 15.56 | 6.35 | 10.52 | 2.31 | 0.29 | 1.81 | 0.24 | 0.18 | 100.94 |
| KK111 | 49.81 | 13.56 | 16.08 | 5.88 | 9.91 | 2.35 | 0.30 | 1.87 | 0.25 | 0.19 | 100.20 |
| KK112 | 50.00 | 13.48 | 16.27 | 6.03 | 10.19 | 2.37 | 0.29 | 1.84 | 0.25 | 0.17 | 100.89 |
| KK113 | 49.96 | 13.68 | 15.52 | 6.39 | 10.67 | 2.32 | 0.29 | 1.79 | 0.23 | 0.17 | 101.02 |
| KK114 | 49.52 | 13.65 | 15.45 | 6.50 | 10.59 | 2.24 | 0.28 | 1.78 | 0.23 | 0.17 | 100.40 |
| KK115 | 49.85 | 13.93 | 15.44 | 6.44 | 10.56 | 2.23 | 0.28 | 1.79 | 0.24 | 0.17 | 100.91 |
| KK116 | 49.33 | 15.22 | 12.33 | 8.32 | 12.36 | 1.91 | 0.10 | 1.01 | 0.20 | 0.09 | 100.88 |
| KK117 | 50.50 | 13.39 | 16.31 | 5.36 | 9.63 | 2.52 | 0.41 | 2.03 | 0.24 | 0.20 | 100.60 |
| KK118 | 49.39 | 13.26 | 15.84 | 6.09 | 10.34 | 2.08 | 0.27 | 1.81 | 0.24 | 0.20 | 99.52 |
| KK119 | 49.62 | 13.71 | 15.58 | 6.15 | 10.31 | 2.20 | 0.28 | 1.82 | 0.24 | 0.18 | 100.07 |
| KK120 | 49.99 | 13.73 | 15.54 | 6.26 | 10.49 | 2.21 | 0.25 | 1.65 | 0.24 | 0.14 | 100.50 |
| KK121 | 61.77 | 16.25 | 9.47 | 2.29 | 4.90 | 2.66 | 0.99 | 1.21 | 0.16 | 0.23 | 99.93 |
| KK122 | 49.63 | 13.14 | 17.08 | 5.56 | 9.15 | 2.10 | 0.32 | 2.12 | 0.26 | 0.21 | 99.57 |
| KK123 | 49.83 | 13.68 | 15.48 | 6.31 | 10.55 | 2.32 | 0.28 | 1.78 | 0.24 | 0.17 | 100.64 |
| KK124 | 50.28 | 13.39 | 16.07 | 6.00 | 10.45 | 2.46 | 0.30 | 1.88 | 0.25 | 0.17 | 101.24 |
| KK125 | 50.20 | 13.42 | 15.98 | 6.09 | 10.44 | 2.20 | 0.30 | 1.88 | 0.25 | 0.18 | 100.93 |
| KK127 | 50.89 | 13.18 | 16.49 | 5.44 | 9.59 | 2.56 | 0.41 | 2.06 | 0.25 | 0.20 | 101.07 |
| KK128 | 49.80 | 13.42 | 16.02 | 6.14 | 10.39 | 2.27 | 0.28 | 1.78 | 0.24 | 0.17 | 100.51 |
| KK129 | 49.90 | 13.47 | 16.15 | 6.04 | 10.18 | 2.11 | 0.29 | 1.85 | 0.24 | 0.18 | 100.42 |
| KK130 | 49.54 | 13.56 | 15.86 | 6.27 | 10.42 | 2.25 | 0.29 | 1.83 | 0.23 | 0.18 | 100.43 |
| KK131 | 49.60 | 13.88 | 15.16 | 5.45 | 9.92 | 2.39 | 0.42 | 2.08 | 0.23 | 0.25 | 99.38 |
| KK132 | 49.34 | 13.84 | 14.99 | 5.69 | 10.24 | 2.08 | 0.40 | 2.06 | 0.23 | 0.26 | 99.13 |
| KK133 | 49.95 | 13.92 | 15.28 | 5.66 | 10.13 | 2.41 | 0.43 | 2.08 | 0.23 | 0.26 | 100.34 |
| KK134 | 49.37 | 14.25 | 15.19 | 5.41 | 10.00 | 2.39 | 0.41 | 2.07 | 0.23 | 0.26 | 99.57 |
| KK135 | 49.82 | 14.02 | 15.11 | 5.57 | 10.14 | 2.55 | 0.43 | 2.08 | 0.22 | 0.27 | 100.21 |
| KK136 | 51.97 | 13.03 | 15.81 | 3.04 | 6.50 | 2.35 | 0.71 | 2.85 | 0.27 | 0.57 | 97.09 |
| KK137 | 49.90 | 14.22 | 14.98 | 5.58 | 10.31 | 2.19 | 0.41 | 2.04 | 0.23 | 0.25 | 100.10 |
| KK138 | 49.54 | 14.26 | 14.41 | 5.97 | 10.23 | 2.18 | 0.36 | 1.92 | 0.23 | 0.23 | 99.33 |
| KK139 | 55.00 | 12.09 | 13.22 | 4.95 | 9.16 | 2.03 | 0.29 | 1.99 | 0.20 | 0.21 | 99.14 |
| KK140 | 48.40 | 16.34 | 10.63 | 8.48 | 13.23 | 1.83 | 0.07 | 0.93 | 0.17 | 0.09 | 100.17 |
| KK141 | 48.35 | 15.45 | 11.17 | 8.88 | 13.11 | 1.93 | 0.08 | 0.96 | 0.17 | 0.08 | 100.18 |
| KK142 | 48.47 | 14.83 | 12.02 | 8.55 | 12.75 | 1.84 | 0.12 | 1.33 | 0.18 | 0.14 | 100.26 |
| KK143 | 48.25 | 16.22 | 10.72 | 8.39 | 13.19 | 1.83 | 0.07 | 0.93 | 0.18 | 0.09 | 99.86 |
| KK144 | 50.54 | 13.31 | 16.32 | 5.33 | 9.68 | 2.48 | 0.40 | 2.00 | 0.25 | 0.19 | 100.50 |
| KK145 | 49.06 | 13.91 | 13.90 | 6.89 | 11.38 | 2.24 | 0.22 | 1.82 | 0.21 | 0.23 | 99.85 |
| KK147 | 55.49 | 11.75 | 13.45 | 5.01 | 8.94 | 1.98 | 0.27 | 1.85 | 0.20 | 0.20 | 99.13 |
| KK148 | 49.25 | 13.78 | 15.29 | 6.63 | 10.71 | 2.17 | 0.29 | 1.83 | 0.23 | 0.18 | 100.33 |

| | | | | | | | | | | | |
|---|---|---|---|---|---|---|---|---|---|---|---|
| KK149 | 49.32 | 13.86 | 15.70 | 6.21 | 10.23 | 2.17 | 0.28 | 1.83 | 0.23 | 0.17 | 100.00 |
| KK150 | 49.46 | 13.87 | 15.38 | 6.59 | 10.75 | 2.22 | 0.28 | 1.80 | 0.23 | 0.17 | 100.75 |
| KK151 | 47.19 | 14.93 | 13.23 | 8.30 | 12.13 | 1.88 | 0.17 | 2.09 | 0.20 | 0.21 | 100.31 |
| KK152 | 49.31 | 14.61 | 13.83 | 7.58 | 11.51 | 1.98 | 0.22 | 1.68 | 0.21 | 0.17 | 101.09 |
| KK153 | 52.46 | 15.49 | 10.36 | 6.36 | 11.42 | 2.25 | 0.47 | 1.02 | 0.18 | 0.12 | 100.11 |
| KK154 | 50.28 | 13.06 | 16.79 | 5.64 | 11.38 | 2.45 | 0.31 | 1.85 | 0.24 | 0.16 | 102.16 |
| KK155 | 50.31 | 13.88 | 13.63 | 6.77 | 11.38 | 2.08 | 0.31 | 1.83 | 0.21 | 0.22 | 100.62 |
| KK156 | 50.50 | 13.14 | 16.83 | 5.67 | 9.98 | 2.39 | 0.30 | 1.84 | 0.26 | 0.16 | 101.07 |
| KK157 | 51.30 | 13.20 | 16.33 | 4.72 | 8.84 | 2.82 | 0.61 | 2.62 | 0.25 | 0.34 | 101.02 |
| KK158 | 49.65 | 14.40 | 12.25 | 8.06 | 12.66 | 1.99 | 0.14 | 1.18 | 0.20 | 0.10 | 100.61 |
| KK159 | 49.94 | 13.93 | 14.05 | 6.35 | 11.29 | 2.26 | 0.26 | 1.76 | 0.22 | 0.19 | 100.26 |
| KK160 | 50.29 | 13.04 | 16.98 | 5.72 | 9.91 | 2.49 | 0.31 | 1.85 | 0.25 | 0.17 | 101.01 |
| KK161 | 49.51 | 14.53 | 11.98 | 6.97 | 12.90 | 1.98 | 0.15 | 1.43 | 0.20 | 0.13 | 99.78 |
| KK162 | 57.89 | 13.43 | 11.57 | 3.45 | 7.28 | 3.18 | 1.16 | 1.64 | 0.19 | 0.30 | 100.09 |
| K2 | 74.37 | 12.23 | 3.55 | 0.37 | 1.83 | 3.94 | 2.75 | 0.47 | 0.08 | 0.07 | 99.65 |
| IC9 | 74.18 | 11.88 | 3.60 | 0.04 | 1.67 | 4.00 | 2.68 | 0.24 | 0.10 | 0.02 | 98.40 |
| IC10 | 48.96 | 14.40 | 14.03 | 7.64 | 11.16 | 1.82 | 0.23 | 1.65 | 0.21 | 0.16 | 100.26 |
| SNA24 | 48.60 | 14.81 | 12.76 | 8.65 | 11.57 | 2.06 | 0.19 | 1.46 | 0.20 | 0.14 | 100.44 |
| SNA26 | 49.01 | 14.47 | 13.91 | 7.71 | 11.18 | 2.16 | 0.24 | 1.64 | 0.21 | 0.17 | 100.70 |
| 84 | 49.08 | 14.72 | 13.43 | 7.60 | 11.58 | 2.18 | 0.22 | 1.63 | 0.21 | 0.16 | 100.80 |
| 84-05 | 49.63 | 13.12 | 16.13 | 5.86 | 10.14 | 2.29 | 0.33 | 2.05 | 0.24 | 0.21 | 100.00 |
| 84-19 | 48.76 | 14.79 | 12.88 | 8.66 | 11.65 | 2.08 | 0.20 | 1.47 | 0.20 | 0.14 | 100.82 |
| KRA118 | 49.69 | 13.44 | 15.99 | 6.09 | 10.17 | 2.14 | 0.32 | 1.99 | 0.24 | 0.20 | 100.27 |

# APPENDIX IV:

## Whole-rock analyses

## (b) Trace-element concentrations

| Sample | ppm V | Ba | Sc | La | Nd | Ce | Cr | Ni |
|---|---|---|---|---|---|---|---|---|
| KK1 | 396.6 | 65.5 | 49.9 | 4.6 | 11.8 | 14.6 | 54.2 | 55.2 |
| KK2 | 360.4 | 72.0 | 47.7 | -0.4 | 8.3 | 17.4 | 68.4 | 65.0 |
| KK3 | 1.2 | 519.4 | 8.4 | 52.9 | 61.7 | 129.2 | 0.9 | 3.4 |
| KK4 | 322.8 | 42.4 | 45.9 | 4.3 | 5.0 | 10.9 | 143.0 | 83.8 |
| KK6 | 1.6 | 666.4 | 9.7 | 41.1 | 58.0 | 112.2 | -0.8 | 3.5 |
| KK7 | 1.8 | 569.2 | 8.0 | 54.5 | 59.6 | 126.5 | 0.2 | 3.7 |
| KK8 | 456.7 | 133.0 | 45.5 | 11.7 | 19.2 | 29.5 | 29.7 | 35.5 |
| KK9 | 230.0 | 341.5 | 26.0 | 29.8 | 40.8 | 82.1 | 14.2 | 19.6 |
| KK10 | 345.6 | 62.8 | 55.0 | 12.6 | 9.8 | 17.0 | 63.5 | 56.6 |
| KK11 | 312.5 | 39.7 | 45.8 | 5.0 | 16.0 | 23.2 | 266.8 | 82.9 |
| KK12 | 385.7 | 194.3 | 38.2 | 22.4 | 25.2 | 49.5 | 26.4 | 43.3 |
| KK13 | 419.7 | 73.3 | 49.4 | 13.4 | 12.2 | 19.8 | 44.8 | 46.3 |
| KK14 | 304.8 | 258.3 | 31.0 | 28.7 | 33.9 | 61.4 | 20.9 | 28.8 |
| KK16 | 346.1 | 59.8 | 51.3 | 6.4 | 9.6 | 16.3 | 184.3 | 73.9 |
| KK17 | 276.1 | 44.1 | 42.9 | 1.8 | 2.8 | 6.1 | 287.5 | 96.1 |
| KK18 | 218.3 | 71.1 | 31.9 | 8.8 | 10.2 | 17.4 | 233.1 | 63.3 |
| KK19 | 280.5 | 43.3 | 46.2 | 1.9 | 6.0 | 8.8 | 295.6 | 80.6 |
| KK20 | 287.6 | 89.4 | 47.9 | -1.0 | 10.2 | 14.0 | 293.2 | 81.0 |
| KK21 | 337.4 | 16.4 | 41.4 | 1.0 | 8.3 | 11.0 | 492.3 | 185.1 |
| KK22 | 341.5 | 65.7 | 47.8 | 6.2 | 8.7 | 10.1 | 547.1 | 177.6 |
| KK23 | 334.3 | 68.6 | 49.5 | 4.2 | 13.0 | 19.2 | 122.2 | 67.7 |
| KK24 | 376.9 | 108.3 | 47.3 | 9.9 | 20.2 | 32.8 | 122.3 | 52.6 |
| KK25 | 51.7 | 400.1 | 20.4 | 47.0 | 51.5 | 98.3 | 36.0 | 14.3 |
| KK26 | 69.8 | 383.9 | 20.6 | 42.8 | 50.5 | 98.3 | 55.0 | 18.7 |
| KK27 | 394.5 | 133.8 | 41.4 | 14.5 | 18.1 | 30.8 | 119.3 | 52.3 |
| KK28 | 257.3 | 87.3 | 43.0 | 7.2 | 13.5 | 20.1 | 254.7 | 72.5 |
| KK29 | 2.1 | 527.4 | 4.7 | 34.9 | 47.8 | 111.7 | -0.5 | 3.8 |
| KK30 | 289.8 | 51.3 | 37.9 | 16.4 | 9.3 | 10.6 | 447.8 | 192.5 |
| KK31 | 254.3 | 19.0 | 41.4 | -0.1 | 4.1 | 1.6 | 399.1 | 162.7 |
| KK32 | 282.9 | 58.6 | 44.9 | 8.3 | 4.0 | -1.9 | 375.3 | 106.7 |
| KK33 | 253.2 | 47.4 | 39.1 | 2.2 | 7.8 | 6.0 | 312.2 | 86.5 |
| KK34 | 61.6 | 295.0 | 14.1 | 35.4 | 29.9 | 68.7 | 0.9 | 6.4 |
| KK35 | 200.9 | 201.5 | 25.8 | 19.1 | 28.5 | 56.4 | 12.0 | 25.1 |
| KK36 | 339.0 | 43.2 | 54.4 | 2.7 | 7.8 | 8.1 | 248.8 | 92.8 |
| KK37 | 466.6 | 99.9 | 47.1 | 11.1 | 15.7 | 23.9 | 35.3 | 39.1 |
| KK50 | 249.5 | 23.6 | 39.3 | 0.7 | 2.3 | 2.1 | 422.3 | 148.0 |
| KK51 | 263.2 | 76.8 | 38.8 | 15.1 | 15.3 | 28.7 | 99.5 | 85.5 |
| KK52 | 247.0 | 32.4 | 39.9 | -2.7 | 2.2 | 0.1 | 280.3 | 158.9 |
| KK53 | 280.3 | 22.6 | 43.9 | -0.3 | 3.8 | 0.9 | 255.0 | 131.3 |
| KK54 | 336.1 | 34.4 | 48.5 | 4.5 | 12.2 | 13.8 | 136.0 | 81.0 |
| KK55 | 315.1 | 23.7 | 41.6 | 7.5 | 7.3 | 8.8 | 139.5 | 82.9 |
| KK56 | 5.9 | 509.5 | 6.7 | 39.8 | 45.7 | 99.7 | 1.0 | 4.8 |
| KK57 | 0.8 | 509.5 | 7.6 | 57.5 | 64.2 | 129.7 | 2.1 | 4.5 |

| | | | | | | | | |
|---|---|---|---|---|---|---|---|---|
| KK58 | 243.4 | 37.7 | 37.8 | 1.7 | 1.0 | -8.2 | 407.0 | 174.0 |
| KK59 | 470.4 | 104.3 | 50.6 | 6.7 | 11.0 | 24.6 | 141.5 | 46.0 |
| KK60 | 341.4 | 182.0 | 41.4 | 19.6 | 26.9 | 36.6 | 71.1 | 32.9 |
| KK62 | 445.0 | 127.1 | 48.0 | 10.7 | 21.1 | 36.8 | 26.7 | 34.7 |
| KK63 | 354.1 | 81.8 | 41.9 | 9.9 | 18.5 | 25.3 | 219.1 | 67.0 |
| KK64 | 392.8 | 126.5 | 44.9 | 11.2 | 19.5 | 38.2 | 25.4 | 38.9 |
| KK65 | 276.8 | 57.4 | 43.8 | -1.5 | 7.6 | 8.4 | 287.3 | 75.8 |
| KK66 | 446.2 | 120.1 | 45.9 | 13.3 | 18.2 | 27.4 | 32.0 | 38.2 |
| KK67 | 1.3 | 513.6 | 6.7 | 53.6 | 62.5 | 124.5 | -3.8 | 2.3 |
| KK68 | 292.0 | 41.9 | 45.3 | 2.2 | 5.6 | 11.0 | 379.4 | 112.6 |
| KK69 | 368.7 | 124.8 | 48.2 | 12.5 | 20.6 | 30.6 | 153.0 | 58.0 |
| KK70 | 383.6 | 120.2 | 41.8 | 12.1 | 17.6 | 32.1 | 119.9 | 51.7 |
| KK71 | 326.6 | 65.2 | 43.5 | 7.9 | 14.8 | 16.0 | 298.7 | 84.7 |
| KK72 | 383.7 | 90.9 | 52.5 | 2.9 | 8.6 | 7.3 | 49.4 | 47.7 |
| KK73 | 377.3 | 100.4 | 45.5 | 10.3 | 10.4 | 12.5 | 68.1 | 52.8 |
| KK75 | 258.7 | 45.4 | 34.4 | 4.1 | 7.6 | 6.7 | 310.3 | 84.2 |
| KK76 | 242.8 | 21.9 | 34.8 | 8.3 | 9.3 | 12.2 | 139.9 | 63.4 |
| KK77 | 347.2 | 251.1 | 36.8 | 24.6 | 29.1 | 53.7 | 15.8 | 28.1 |
| KK78 | 230.6 | 35.6 | 41.8 | -2.0 | 0.4 | -2.3 | 379.1 | 173.3 |
| KK79 | 299.5 | 22.9 | 50.3 | 0.4 | 3.9 | 2.1 | 410.9 | 96.5 |
| KK80 | 324.3 | 203.0 | 39.1 | 19.1 | 27.0 | 45.2 | 59.5 | 33.6 |
| KK81 | 250.7 | -7.9 | 46.8 | -2.9 | 3.4 | -2.1 | 426.0 | 110.1 |
| KK82 | 373.0 | 105.6 | 49.8 | 8.2 | 15.5 | 24.3 | 48.7 | 52.5 |
| KK83 | 426.5 | 79.7 | 43.3 | 7.2 | 19.6 | 34.7 | 29.6 | 38.2 |
| KK84 | 397.5 | 60.0 | 42.6 | 4.5 | 10.4 | 7.7 | 36.1 | 56.1 |
| KK85 | 446.7 | 122.0 | 46.2 | 14.2 | 16.8 | 23.8 | 31.8 | 36.9 |
| KK86 | 132.6 | 301.3 | 20.8 | 33.3 | 39.3 | 74.6 | 31.1 | 19.0 |
| KK87 | 271.3 | 88.0 | 42.2 | 13.8 | 15.2 | 18.2 | 229.2 | 75.0 |
| KK88 | 378.8 | 88.8 | 48.1 | 10.5 | 12.1 | 15.3 | 63.2 | 61.0 |
| KK89 | 373.7 | 68.9 | 42.9 | 7.3 | 9.7 | 17.3 | 39.0 | 44.5 |
| KK90 | 438.0 | 135.7 | 45.7 | 6.8 | 15.9 | 19.8 | 30.6 | 37.5 |
| KK91 | 445.1 | 119.2 | 47.6 | 11.0 | 13.1 | 18.9 | 27.0 | 37.3 |
| KK92 | 390.1 | 88.2 | 43.1 | 7.7 | 14.7 | 19.2 | 155.6 | 85.9 |
| KK93 | 452.9 | 116.7 | 47.0 | 6.5 | 14.8 | 25.5 | 32.1 | 39.2 |
| KK94 | 178.3 | 208.5 | 20.5 | 24.2 | 30.5 | 63.4 | 8.7 | 22.0 |
| KK95 | 202.9 | 190.2 | 25.7 | 23.8 | 34.1 | 55.7 | 8.7 | 25.3 |
| KK96 | 188.2 | 213.3 | 25.6 | 23.3 | 26.3 | 53.8 | 16.2 | 25.5 |
| KK97 | 473.7 | 89.8 | 49.5 | 6.2 | 10.7 | 12.4 | 79.6 | 48.6 |
| KK98 | 175.4 | 197.8 | 22.3 | 32.1 | 31.2 | 64.3 | 7.6 | 19.7 |
| KK99 | 429.1 | 103.2 | 49.3 | 5.9 | 8.0 | 3.2 | 90.8 | 58.7 |
| KK100 | 381.7 | 124.1 | 41.0 | 14.8 | 15.3 | 22.9 | 116.3 | 51.5 |
| KK101 | 463.8 | 119.4 | 46.8 | 12.5 | 13.3 | 21.1 | 72.9 | 48.4 |
| KK102 | 459.8 | 79.1 | 48.8 | 4.5 | 17.7 | 20.3 | 79.4 | 49.1 |
| KK103 | 458.4 | 149.9 | 46.7 | 5.9 | 14.4 | 26.7 | 31.7 | 37.0 |

| | | | | | | | | |
|---|---|---|---|---|---|---|---|---|
| KK104 | 316.4 | 67.0 | 41.9 | 6.8 | 12.8 | 10.2 | 125.0 | 85.8 |
| KK105 | 239.6 | 38.7 | 50.1 | 2.3 | -1.2 | 0.6 | 391.0 | 105.7 |
| KK106 | 429.5 | 84.7 | 49.1 | 7.0 | 10.6 | 17.6 | 146.4 | 67.5 |
| KK107 | 459.5 | 99.4 | 43.3 | 10.1 | 15.9 | 30.7 | 35.2 | 37.8 |
| KK108 | 466.3 | 107.8 | 47.8 | 8.5 | 16.7 | 17.1 | 96.1 | 54.7 |
| KK109A | 435.0 | 78.3 | 48.9 | 8.8 | 12.6 | 28.3 | 145.9 | 65.6 |
| KK109B | 414.0 | 130.4 | 43.0 | 2.5 | 12.4 | 16.8 | 146.6 | 66.2 |
| KK110 | 417.9 | 84.2 | 48.9 | 6.9 | 15.0 | 22.7 | 145.2 | 67.1 |
| KK111 | 465.7 | 99.6 | 48.8 | 10.9 | 13.6 | 26.4 | 98.2 | 54.3 |
| KK112 | 461.0 | 90.5 | 49.3 | 12.4 | 12.5 | 18.3 | 93.9 | 53.9 |
| KK113 | 444.4 | 68.6 | 46.9 | 9.9 | 12.2 | 26.3 | 152.4 | 68.3 |
| KK114 | 442.1 | 110.1 | 49.6 | 7.2 | 9.2 | 12.9 | 147.7 | 66.2 |
| KK115 | 418.4 | 71.9 | 43.6 | 7.2 | 11.3 | 15.5 | 149.5 | 68.7 |
| KK116 | 299.8 | 65.9 | 43.9 | 22.8 | 4.0 | 2.6 | 180.4 | 107.6 |
| KK117 | 467.7 | 109.3 | 45.5 | 12.6 | 17.9 | 31.6 | 37.5 | 38.2 |
| KK118 | 446.8 | 86.9 | 49.8 | 11.7 | 8.1 | 17.4 | 94.2 | 53.4 |
| KK119 | 444.4 | 93.6 | 51.8 | 10.9 | 12.8 | 14.8 | 156.9 | 70.5 |
| KK120 | 420.6 | 69.1 | 47.1 | 4.5 | 10.5 | 15.8 | 93.8 | 61.0 |
| KK121 | 123.2 | 292.1 | 23.8 | 39.9 | 42.0 | 82.7 | 39.7 | 22.8 |
| KK122 | 502.8 | 98.7 | 50.3 | 9.6 | 14.6 | 21.8 | 96.6 | 56.9 |
| KK123 | 434.9 | 57.9 | 49.2 | 3.2 | 13.7 | 17.9 | 139.9 | 64.3 |
| KK124 | 464.1 | 87.0 | 49.6 | 5.5 | 15.0 | 24.4 | 88.3 | 53.9 |
| KK125 | 454.8 | 69.9 | 47.5 | 3.0 | 12.3 | 11.9 | 88.7 | 53.8 |
| KK127 | 472.9 | 98.8 | 46.3 | 12.5 | 18.4 | 32.8 | 31.5 | 38.0 |
| KK128 | 463.1 | 93.3 | 46.3 | 12.9 | 12.7 | 14.5 | 115.4 | 59.7 |
| KK129 | 477.3 | 89.8 | 53.4 | 8.2 | 15.0 | 17.6 | 108.7 | 60.4 |
| KK130 | 436.2 | 77.6 | 47.9 | 11.3 | 11.6 | 16.0 | 135.5 | 64.8 |
| KK131 | 414.5 | 129.2 | 47.0 | 38.9 | 16.5 | 30.5 | 106.2 | 51.7 |
| KK132 | 392.5 | 103.9 | 45.3 | 11.4 | 16.8 | 24.7 | 105.0 | 51.7 |
| KK133 | 419.5 | 122.0 | 44.6 | 11.5 | 16.3 | 27.3 | 103.4 | 51.3 |
| KK134 | 413.5 | 161.7 | 42.6 | 12.1 | 15.8 | 23.6 | 109.4 | 51.0 |
| KK135 | 405.8 | 111.9 | 44.3 | 8.6 | 18.6 | 30.5 | 103.9 | 47.8 |
| KK136 | 204.7 | 204.5 | 38.2 | 22.4 | 36.3 | 52.5 | 5.6 | 4.7 |
| KK137 | 393.5 | 110.6 | 40.1 | 12.3 | 18.4 | 24.9 | 114.8 | 49.7 |
| KK138 | 386.1 | 82.4 | 47.3 | 14.4 | 19.3 | 23.8 | 160.2 | 62.9 |
| KK139 | 410.1 | 95.6 | 43.4 | 30.1 | 16.9 | 28.2 | 115.3 | 43.3 |
| KK140 | 272.6 | 27.3 | 49.0 | 2.3 | 2.7 | 8.8 | 408.3 | 123.0 |
| KK141 | 274.9 | 48.8 | 42.0 | 2.4 | 3.7 | 6.7 | 407.0 | 118.0 |
| KK142 | 313.2 | 34.3 | 45.2 | 4.1 | 7.4 | 5.0 | 377.5 | 112.8 |
| KK143 | 275.0 | 35.5 | 46.8 | 3.6 | 6.3 | 0.4 | 401.4 | 117.9 |
| KK144 | 437.6 | 129.2 | 41.8 | 8.5 | 11.1 | 22.6 | 29.9 | 39.2 |
| KK145 | 361.3 | 63.9 | 46.6 | 7.7 | 20.2 | 36.7 | 84.9 | 63.8 |
| KK147 | 389.2 | 81.1 | 41.3 | 33.8 | 10.4 | 16.5 | 122.0 | 47.6 |
| KK148 | 400.8 | 71.8 | 45.0 | 39.9 | 12.0 | 18.1 | 177.6 | 73.6 |

| | | | | | | | | |
|---|---|---|---|---|---|---|---|---|
| KK149 | 450.3 | 60.3 | 49.1 | 8.9 | 15.6 | 17.7 | 157.5 | 68.7 |
| KK150 | 416.5 | 74.8 | 44.1 | 7.1 | 7.7 | 14.7 | 174.2 | 73.8 |
| KK151 | 291.6 | 51.4 | 35.5 | 3.2 | 9.5 | 17.5 | 336.1 | 129.4 |
| KK152 | 384.6 | 72.2 | 47.7 | 9.1 | 8.4 | 12.1 | 291.5 | 105.0 |
| KK153 | 236.0 | 116.1 | 40.0 | 16.7 | 20.9 | 29.3 | 240.3 | 67.6 |
| KK154 | 496.8 | 92.3 | 54.4 | 6.9 | 15.9 | 18.5 | 25.5 | 40.4 |
| KK155 | 361.1 | 105.4 | 45.0 | 5.8 | 20.3 | 23.5 | 76.3 | 61.5 |
| KK156 | 475.3 | 113.7 | 48.9 | 12.9 | 8.6 | 14.7 | 23.1 | 39.9 |
| KK157 | 467.0 | 150.4 | 41.4 | 19.3 | 28.4 | 44.9 | 20.6 | 29.4 |
| KK158 | 312.7 | 72.9 | 45.5 | 5.7 | 7.1 | -2.2 | 228.8 | 83.6 |
| KK159 | 409.6 | 55.4 | 47.7 | 9.6 | 13.4 | 21.0 | 61.8 | 46.9 |
| KK160 | 373.5 | 58.9 | 47.9 | 8.0 | 11.5 | 22.0 | 47.4 | 56.4 |
| KK161 | 320.0 | 50.4 | 47.1 | 16.2 | 9.9 | 10.3 | 325.0 | 73.1 |
| KK162 | 205.0 | 258.4 | 29.7 | 37.4 | 36.4 | 75.0 | 48.6 | 24.4 |
| K2 | 7.7 | 463.3 | 5.1 | 51.8 | 44.3 | 101.1 | 0.1 | 5.8 |
| IC9 | 3.2 | 536.6 | 4.6 | 61.5 | 62.7 | 132.0 | 1.0 | 6.0 |
| IC10 | 364.4 | 91.9 | 43.6 | 4.4 | 9.7 | 16.3 | 280.8 | 110.1 |
| SNA24 | 345.5 | 73.4 | 45.0 | 6.4 | 9.1 | 12.8 | 388.3 | 150.8 |
| SNA26 | 388.0 | 65.5 | 48.2 | 10.1 | 8.2 | 10.9 | 316.3 | 120.3 |
| 84 | 343.0 | 46.1 | 44.7 | 6.7 | 13.6 | 21.1 | 388.3 | 152.0 |
| 84-05 | 479.6 | 77.4 | 40.5 | 18.8 | 14.8 | 25.1 | 124.3 | 63.3 |
| 84-19 | 378.6 | 89.8 | 49.2 | 18.9 | 11.8 | 6.5 | 302.4 | 103.0 |
| KRA118 | 477.4 | 102.5 | 49.5 | 5.1 | 9.9 | 21.6 | 144.9 | 68.2 |

| Sample | ppm Cu | Zn | Pb | Th | Rb | Sr | Y | Zr | Nb |
|---|---|---|---|---|---|---|---|---|---|
| KK1 | 159.4 | 108.6 | 0.0 | -0.6 | 0.6 | 151.0 | 28.2 | 86.5 | 7.5 |
| KK2 | 146.6 | 94.6 | -1.3 | -2.3 | 2.4 | 151.4 | 25.4 | 77.9 | 7.5 |
| KK3 | 8.8 | 111.8 | 6.1 | 8.1 | 68.6 | 93.9 | 98.5 | 591.3 | 50.3 |
| KK4 | 197.8 | 87.7 | 1.5 | 0.1 | 0.1 | 107.8 | 25.6 | 72.2 | 6.1 |
| KK6 | 4.6 | 199.1 | 4.7 | 8.3 | 67.1 | 117.6 | 86.3 | 656.0 | 62.0 |
| KK7 | 5.3 | 121.9 | 4.5 | 7.8 | 65.9 | 114.3 | 87.1 | 629.3 | 58.9 |
| KK8 | 128.2 | 144.4 | 0.9 | -1.0 | 11.2 | 150.5 | 46.6 | 190.0 | 17.7 |
| KK9 | 63.0 | 132.3 | 1.8 | 3.8 | 36.2 | 122.6 | 66.8 | 336.9 | 30.1 |
| KK10 | 161.5 | 110.2 | 0.7 | -0.7 | 5.7 | 149.0 | 32.4 | 106.7 | 11.3 |
| KK11 | 32.6 | 90.3 | 0.8 | -0.1 | 5.0 | 182.1 | 28.2 | 113.9 | 12.4 |
| KK12 | 181.4 | 141.8 | 3.2 | 2.5 | 19.0 | 142.5 | 51.8 | 231.7 | 21.0 |
| KK13 | 203.6 | 124.6 | 0.0 | -2.3 | 3.2 | 148.7 | 34.5 | 108.9 | 9.3 |
| KK14 | 79.0 | 134.0 | 1.9 | 2.5 | 27.6 | 128.6 | 60.8 | 292.9 | 26.3 |
| KK16 | 142.4 | 92.2 | 0.1 | -1.2 | 2.9 | 152.2 | 24.8 | 87.4 | 7.9 |
| KK17 | 128.0 | 74.4 | 0.4 | -0.4 | 2.3 | 138.3 | 19.3 | 57.9 | 4.7 |
| KK18 | 100.0 | 68.7 | -0.1 | -1.0 | 5.4 | 134.4 | 24.9 | 107.3 | 8.0 |
| KK19 | 105.0 | 82.8 | 0.9 | -0.4 | 4.2 | 124.0 | 26.5 | 96.6 | 7.4 |
| KK20 | 117.1 | 85.9 | 0.6 | -0.1 | 5.6 | 124.6 | 28.5 | 114.7 | 8.9 |
| KK21 | 109.9 | 84.2 | -0.1 | -0.8 | 2.3 | 165.7 | 22.0 | 79.5 | 7.2 |
| KK22 | 113.1 | 98.3 | 0.7 | 0.0 | 5.0 | 179.0 | 23.0 | 85.5 | 8.3 |
| KK23 | 126.3 | 87.2 | 1.6 | -0.7 | 1.7 | 168.1 | 24.4 | 88.8 | 9.2 |
| KK24 | 111.0 | 125.3 | 0.2 | -1.0 | 7.5 | 161.0 | 35.5 | 149.7 | 14.4 |
| KK25 | 21.7 | 126.1 | 3.1 | 5.1 | 47.9 | 129.7 | 80.1 | 612.3 | 44.2 |
| KK26 | 30.2 | 127.3 | 3.2 | 3.8 | 45.1 | 128.2 | 75.8 | 572.5 | 41.1 |
| KK27 | 110.4 | 121.7 | -1.1 | -0.2 | 8.7 | 159.7 | 36.5 | 150.1 | 13.7 |
| KK28 | 117.5 | 82.8 | 1.5 | -0.3 | 8.5 | 131.5 | 29.8 | 138.7 | 10.1 |
| KK29 | 3.5 | 88.7 | 5.7 | 8.4 | 76.2 | 91.4 | 65.9 | 486.9 | 48.1 |
| KK30 | 115.9 | 96.0 | 0.2 | -0.3 | 2.0 | 215.0 | 25.0 | 111.5 | 11.2 |
| KK31 | 109.7 | 68.4 | -1.0 | -2.6 | 0.3 | 106.2 | 17.5 | 37.8 | 3.3 |
| KK32 | 136.6 | 81.0 | -0.7 | 0.0 | 1.8 | 118.0 | 21.1 | 61.5 | 5.4 |
| KK33 | 114.0 | 85.5 | 1.2 | 0.0 | 3.8 | 137.8 | 25.5 | 96.0 | 8.4 |
| KK34 | 37.3 | 78.3 | 3.4 | 4.5 | 27.6 | 170.6 | 44.0 | 365.4 | 18.6 |
| KK35 | 101.7 | 103.0 | 2.0 | 1.8 | 15.7 | 165.6 | 44.6 | 301.7 | 18.9 |
| KK36 | 119.9 | 85.9 | -2.0 | -1.0 | 1.4 | 123.2 | 23.6 | 68.0 | 4.9 |
| KK37 | 156.7 | 131.1 | 1.2 | -1.2 | 8.2 | 151.2 | 37.3 | 142.4 | 12.3 |
| KK50 | 124.1 | 68.7 | 1.0 | -0.6 | -0.1 | 85.3 | 18.3 | 33.0 | 3.3 |
| KK51 | 149.3 | 103.9 | -0.3 | -2.3 | 4.5 | 146.4 | 37.6 | 167.7 | 14.6 |
| KK52 | 116.2 | 70.1 | -0.9 | -0.9 | 0.3 | 92.3 | 20.8 | 49.1 | 4.7 |
| KK53 | 125.3 | 76.0 | -0.1 | -1.4 | 0.2 | 86.1 | 20.0 | 38.6 | 3.6 |
| KK54 | 100.3 | 87.7 | 0.4 | -0.5 | 2.1 | 155.4 | 25.6 | 87.1 | 7.7 |
| KK55 | 128.6 | 83.6 | 0.9 | -1.4 | 2.5 | 157.1 | 23.7 | 81.7 | 6.7 |
| KK56 | 10.5 | 73.1 | 6.0 | 9.0 | 71.9 | 89.9 | 71.8 | 471.5 | 34.6 |
| KK57 | 10.2 | 110.1 | 5.6 | 10.1 | 69.1 | 91.6 | 99.4 | 590.3 | 50.0 |

| | | | | | | | | | |
|---|---|---|---|---|---|---|---|---|---|
| KK58 | 99.9 | 64.6 | -0.9 | -0.7 | 0.9 | 105.3 | 15.8 | 34.2 | 2.5 |
| KK59 | 95.7 | 144.5 | 1.4 | -0.6 | 4.4 | 166.9 | 29.9 | 131.6 | 12.9 |
| KK60 | 69.4 | 139.0 | 0.3 | -1.1 | 13.3 | 167.4 | 44.5 | 202.7 | 18.7 |
| KK62 | 93.1 | 129.1 | 3.6 | -1.0 | 7.8 | 156.2 | 38.2 | 145.4 | 12.1 |
| KK63 | 135.0 | 108.1 | 1.8 | -0.1 | 3.6 | 186.2 | 33.4 | 145.8 | 13.4 |
| KK64 | 189.9 | 112.3 | 1.7 | -0.9 | 7.1 | 189.0 | 34.7 | 140.4 | 15.3 |
| KK65 | 128.0 | 75.5 | 2.8 | -0.5 | 2.5 | 127.8 | 23.4 | 71.7 | 5.8 |
| KK66 | 173.4 | 127.5 | 1.1 | -1.2 | 7.7 | 151.5 | 38.7 | 141.0 | 12.7 |
| KK67 | 8.0 | 110.3 | 7.2 | 8.9 | 69.8 | 91.4 | 97.6 | 579.4 | 49.9 |
| KK68 | 128.4 | 79.2 | 2.5 | -1.7 | 1.2 | 127.9 | 22.0 | 65.0 | 5.6 |
| KK69 | 114.9 | 125.1 | 3.3 | -0.1 | 7.6 | 157.1 | 35.5 | 145.3 | 14.1 |
| KK70 | 101.8 | 117.9 | 0.8 | -0.2 | 8.2 | 157.5 | 35.3 | 140.0 | 13.5 |
| KK71 | 136.2 | 92.1 | 1.1 | -1.7 | 2.8 | 181.8 | 27.1 | 106.8 | 11.5 |
| KK72 | 138.5 | 101.5 | 2.4 | -1.9 | 2.7 | 152.8 | 27.7 | 78.4 | 6.8 |
| KK73 | 150.9 | 99.4 | 1.7 | 0.7 | 5.0 | 187.2 | 29.9 | 108.0 | 11.3 |
| KK75 | 92.9 | 73.0 | 2.4 | -1.7 | 1.4 | 197.1 | 22.5 | 84.8 | 9.3 |
| KK76 | 102.7 | 67.3 | 2.3 | -1.5 | 1.3 | 139.8 | 19.2 | 54.3 | 5.3 |
| KK77 | 92.5 | 139.9 | 3.9 | 2.3 | 24.4 | 135.1 | 56.2 | 258.4 | 24.0 |
| KK78 | 105.1 | 64.3 | 2.1 | -1.9 | 0.2 | 105.1 | 17.4 | 34.0 | 2.9 |
| KK79 | 114.1 | 71.9 | 2.5 | -0.8 | 0.4 | 100.8 | 20.9 | 42.1 | 2.8 |
| KK80 | 71.3 | 126.7 | 3.0 | 0.4 | 15.5 | 197.5 | 42.5 | 176.0 | 20.6 |
| KK81 | 113.9 | 68.0 | 1.7 | 0.2 | 0.1 | 92.0 | 17.7 | 34.2 | 2.4 |
| KK82 | 139.8 | 102.7 | 2.2 | -0.6 | 3.8 | 171.2 | 28.0 | 101.4 | 10.1 |
| KK83 | 164.0 | 126.7 | 1.1 | -0.1 | 7.8 | 153.1 | 38.6 | 141.7 | 12.3 |
| KK84 | 206.8 | 117.4 | 2.3 | -1.0 | 3.5 | 142.9 | 30.8 | 96.4 | 8.6 |
| KK85 | 154.1 | 128.1 | 1.5 | 0.3 | 8.2 | 156.6 | 38.5 | 140.2 | 12.1 |
| KK86 | 63.7 | 106.9 | 4.5 | 3.5 | 29.8 | 153.5 | 54.9 | 362.7 | 25.2 |
| KK87 | 105.9 | 93.7 | 2.7 | -0.4 | 6.9 | 126.8 | 31.1 | 133.0 | 10.4 |
| KK88 | 156.5 | 109.2 | 2.8 | -0.6 | 6.1 | 148.1 | 33.5 | 132.4 | 12.6 |
| KK89 | 161.3 | 106.0 | 2.6 | -0.2 | 5.0 | 150.3 | 31.5 | 107.3 | 9.5 |
| KK90 | 149.5 | 123.5 | 0.8 | 0.4 | 7.7 | 157.2 | 36.3 | 135.3 | 10.9 |
| KK91 | 154.9 | 132.3 | 1.2 | 0.5 | 7.8 | 151.8 | 38.6 | 141.5 | 12.1 |
| KK92 | 160.7 | 111.6 | 2.2 | -1.3 | 5.4 | 166.4 | 30.8 | 105.6 | 9.6 |
| KK93 | 159.7 | 129.4 | 2.6 | -0.5 | 7.9 | 151.1 | 39.0 | 140.4 | 12.1 |
| KK94 | 94.6 | 101.8 | 4.2 | 1.8 | 17.1 | 169.2 | 45.7 | 320.4 | 19.8 |
| KK95 | 98.7 | 105.1 | 2.9 | -0.1 | 14.7 | 163.9 | 44.3 | 295.3 | 18.9 |
| KK96 | 97.1 | 102.9 | 3.6 | 1.2 | 16.2 | 167.9 | 45.3 | 312.2 | 20.1 |
| KK97 | 147.9 | 132.4 | 2.2 | -0.7 | 6.0 | 151.3 | 35.1 | 117.0 | 10.6 |
| KK98 | 81.4 | 99.7 | 2.5 | 1.1 | 17.5 | 172.1 | 46.9 | 328.1 | 20.6 |
| KK99 | 156.4 | 117.9 | 3.3 | -2.0 | 4.9 | 141.4 | 30.5 | 95.8 | 7.9 |
| KK100 | 104.7 | 119.6 | 2.5 | 0.2 | 8.5 | 161.3 | 35.1 | 142.0 | 13.6 |
| KK101 | 151.5 | 130.2 | 1.0 | -1.3 | 6.4 | 153.2 | 35.8 | 119.1 | 11.0 |
| KK102 | 148.9 | 128.8 | -0.4 | -2.0 | 5.9 | 152.9 | 35.7 | 118.9 | 11.3 |
| KK103 | 161.3 | 132.2 | 1.8 | -1.8 | 7.9 | 155.5 | 38.1 | 145.5 | 12.6 |

| | | | | | | | | | |
|---|---|---|---|---|---|---|---|---|---|
| KK104 | 134.7 | 85.5 | 2.7 | -1.8 | 2.0 | 159.5 | 25.3 | 84.4 | 7.5 |
| KK105 | 136.8 | 80.2 | 1.7 | -1.9 | 0.8 | 111.1 | 20.3 | 54.4 | 4.5 |
| KK106 | 150.4 | 120.3 | 2.6 | -0.5 | 4.9 | 152.3 | 32.1 | 104.1 | 9.1 |
| KK107 | 154.0 | 130.1 | 2.2 | -1.0 | 7.5 | 155.5 | 37.8 | 140.5 | 12.0 |
| KK108 | 131.8 | 127.8 | 2.2 | -1.1 | 5.7 | 150.4 | 34.2 | 114.7 | 10.2 |
| KK109A | 142.2 | 119.5 | 1.8 | -1.9 | 4.8 | 149.8 | 31.5 | 105.3 | 9.5 |
| KK109B | 144.7 | 115.4 | 2.6 | -1.3 | 5.6 | 152.5 | 32.1 | 104.5 | 9.5 |
| KK110 | 145.0 | 117.5 | 2.2 | -1.1 | 5.0 | 151.4 | 32.3 | 105.4 | 9.0 |
| KK111 | 151.6 | 130.0 | 2.2 | -0.5 | 6.1 | 138.3 | 33.1 | 112.1 | 9.7 |
| KK112 | 155.8 | 127.8 | 1.7 | -1.0 | 5.7 | 141.9 | 32.9 | 106.6 | 9.8 |
| KK113 | 154.3 | 120.8 | 0.6 | -3.4 | 4.0 | 147.7 | 31.8 | 103.3 | 9.3 |
| KK114 | 156.9 | 121.6 | 1.7 | -0.9 | 5.2 | 147.7 | 32.0 | 103.1 | 9.2 |
| KK115 | 151.4 | 115.2 | 1.7 | -0.6 | 5.4 | 152.8 | 31.1 | 102.7 | 9.2 |
| KK116 | 157.1 | 84.2 | 1.8 | -1.3 | 0.7 | 105.1 | 22.7 | 59.0 | 4.4 |
| KK117 | 150.1 | 134.4 | 2.0 | -0.7 | 7.5 | 153.0 | 38.5 | 141.6 | 12.7 |
| KK118 | 144.0 | 131.0 | 1.0 | -1.3 | 5.2 | 140.3 | 32.6 | 105.6 | 9.5 |
| KK119 | 151.7 | 126.5 | 1.9 | -1.1 | 4.6 | 147.3 | 32.0 | 104.1 | 9.6 |
| KK120 | 161.0 | 118.4 | 1.3 | -1.0 | 4.9 | 140.8 | 30.9 | 95.0 | 8.5 |
| KK121 | 70.6 | 110.1 | 3.9 | 3.3 | 24.6 | 151.7 | 57.1 | 385.0 | 27.3 |
| KK122 | 143.4 | 144.2 | 1.9 | -0.8 | 6.6 | 140.0 | 36.5 | 129.2 | 11.7 |
| KK123 | 147.6 | 119.3 | 1.2 | -1.5 | 5.0 | 148.1 | 31.6 | 103.7 | 9.2 |
| KK124 | 152.1 | 126.8 | 2.3 | -1.2 | 5.8 | 147.6 | 33.7 | 109.5 | 10.7 |
| KK125 | 157.2 | 125.5 | 1.2 | -0.4 | 5.3 | 146.2 | 33.5 | 108.2 | 10.2 |
| KK127 | 161.7 | 133.4 | 2.4 | -0.2 | 8.0 | 152.1 | 38.8 | 143.8 | 13.0 |
| KK128 | 136.5 | 123.2 | 0.4 | -3.1 | 5.3 | 139.2 | 32.1 | 101.3 | 8.9 |
| KK129 | 158.2 | 130.9 | 0.9 | -2.1 | 5.4 | 142.0 | 33.4 | 106.3 | 9.5 |
| KK130 | 154.3 | 121.0 | 1.6 | -2.2 | 5.6 | 150.1 | 32.1 | 104.7 | 9.5 |
| KK131 | 114.8 | 128.4 | 2.3 | -0.2 | 8.7 | 155.7 | 36.9 | 148.1 | 14.9 |
| KK132 | 116.4 | 124.6 | 1.8 | -0.9 | 8.3 | 154.5 | 35.4 | 143.9 | 13.5 |
| KK133 | 115.6 | 126.0 | 1.0 | 0.0 | 8.7 | 158.3 | 36.4 | 147.7 | 14.6 |
| KK134 | 118.2 | 126.5 | 2.5 | -1.5 | 7.9 | 157.2 | 36.6 | 146.2 | 14.4 |
| KK135 | 102.5 | 124.5 | 1.5 | -1.9 | 7.6 | 156.7 | 36.5 | 149.7 | 14.0 |
| KK136 | 26.6 | 163.3 | 2.5 | -1.7 | 13.9 | 190.9 | 56.4 | 267.5 | 28.5 |
| KK137 | 119.2 | 120.1 | 3.0 | -0.3 | 8.4 | 158.6 | 36.1 | 144.8 | 14.7 |
| KK138 | 115.9 | 120.2 | 1.3 | -2.1 | 7.2 | 150.3 | 34.3 | 133.3 | 13.0 |
| KK139 | 116.9 | 110.3 | 2.7 | -1.4 | 5.9 | 151.3 | 31.6 | 118.8 | 11.5 |
| KK140 | 131.2 | 73.4 | 1.7 | -1.2 | 0.7 | 117.3 | 19.0 | 44.6 | 4.2 |
| KK141 | 124.6 | 73.7 | 0.1 | -1.4 | 0.4 | 113.8 | 19.3 | 47.6 | 3.9 |
| KK142 | 123.1 | 86.1 | 1.2 | -1.8 | 1.6 | 135.9 | 24.4 | 74.3 | 6.9 |
| KK143 | 131.2 | 73.8 | 1.1 | -2.3 | 0.9 | 117.2 | 19.5 | 46.1 | 4.4 |
| KK144 | 173.0 | 127.1 | 2.4 | -1.0 | 7.6 | 151.9 | 38.8 | 139.7 | 12.3 |
| KK145 | 139.8 | 108.1 | 3.0 | 0.6 | 3.4 | 165.0 | 33.1 | 132.8 | 13.2 |
| KK147 | 124.5 | 107.7 | 1.5 | -1.3 | 4.9 | 142.2 | 29.9 | 108.7 | 11.7 |
| KK148 | 134.9 | 114.9 | 1.2 | -1.4 | 5.1 | 158.2 | 31.5 | 103.7 | 9.2 |

| | | | | | | | | | |
|---|---|---|---|---|---|---|---|---|---|
| KK149 | 142.2 | 122.2 | 2.2 | 0.3 | 5.2 | 144.3 | 32.0 | 103.8 | 10.0 |
| KK150 | 144.5 | 117.3 | 0.9 | -1.4 | 5.6 | 157.2 | 31.3 | 102.2 | 9.6 |
| KK151 | 142.6 | 101.2 | 1.9 | -0.6 | 1.6 | 207.7 | 28.1 | 115.3 | 12.0 |
| KK152 | 132.0 | 104.4 | 1.3 | -1.2 | 3.7 | 157.5 | 27.3 | 92.4 | 9.2 |
| KK153 | 78.7 | 86.8 | 3.0 | 1.2 | 10.5 | 128.6 | 32.7 | 160.9 | 11.9 |
| KK154 | 174.2 | 133.3 | 2.5 | -0.6 | 5.4 | 141.2 | 35.2 | 109.8 | 9.2 |
| KK155 | 108.8 | 106.2 | 1.5 | -1.2 | 5.2 | 165.7 | 33.0 | 139.1 | 13.7 |
| KK156 | 159.8 | 129.0 | 0.2 | -2.0 | 5.6 | 139.4 | 34.4 | 106.5 | 9.6 |
| KK157 | 99.0 | 144.5 | 3.2 | -1.5 | 12.6 | 172.1 | 45.6 | 202.3 | 19.5 |
| KK158 | 136.9 | 82.2 | 1.3 | -1.1 | 1.8 | 125.5 | 24.2 | 66.3 | 4.8 |
| KK159 | 89.6 | 109.1 | 0.5 | -1.1 | 4.1 | 166.3 | 29.4 | 109.0 | 10.5 |
| KK160 | 175.9 | 114.0 | 1.0 | -0.5 | 3.5 | 165.4 | 31.0 | 108.4 | 9.6 |
| KK161 | 129.1 | 91.0 | 0.9 | -1.3 | 1.9 | 154.4 | 24.2 | 79.2 | 7.7 |
| KK162 | 65.8 | 133.0 | 4.5 | 4.2 | 27.2 | 163.0 | 62.7 | 343.1 | 30.1 |
| K2 | 4.3 | 60.3 | 9.2 | 8.9 | 74.2 | 78.8 | 68.8 | 444.0 | 34.5 |
| IC9 | 5.0 | 134.7 | 13.9 | 16.9 | 61.9 | 94.5 | 97.2 | 550.0 | 54.1 |
| IC10 | 135.7 | 103.1 | 9.1 | 7.3 | 3.7 | 158.8 | 27.0 | 90.7 | 9.3 |
| SNA24 | 132.3 | 95.6 | 0.5 | -0.7 | 2.7 | 153.9 | 23.2 | 78.8 | 8.1 |
| SNA26 | 134.1 | 108.0 | 1.9 | -0.6 | 4.5 | 158.9 | 27.1 | 93.9 | 8.6 |
| 84 | 134.8 | 97.4 | 0.7 | -2.0 | 3.3 | 159.8 | 23.9 | 81.8 | 8.2 |
| 84-05 | 141.4 | 131.2 | 1.9 | -0.5 | 5.5 | 148.2 | 35.4 | 118.5 | 12.6 |
| 84-19 | 133.2 | 101.7 | 1.4 | -1.4 | 3.8 | 158.1 | 25.7 | 89.7 | 8.6 |
| KRA118 | 132.0 | 131.0 | -1.2 | -2.4 | 6.1 | 152.0 | 34.5 | 118.2 | 11.3 |

# APPENDIX V:

# REE concentrations

| Idents. | ppm La | Ce | Pr | Nd | Sm | Eu | Gd | Dy | Ho | Er | Tb | Lu |
|---|---|---|---|---|---|---|---|---|---|---|---|---|
| KKC0 | 7.9 | 18.88 | 2.97 | 13.2 | 3.41 | 1.16 | 4.43 | 5.34 | 1.03 | 3.17 | 3.02 | 0.46 |
| KKC1 | 6.3 | 15.42 | 2.11 | 11.1 | 2.86 | 1.06 | 3.63 | 4.03 | 0.77 | 2.27 | 2.1 | 0.32 |
| KKC3 | 36.24 | 90.75 | 11.02 | 46.9 | 11.05 | 2.74 | 12.63 | 14.37 | 2.78 | 8.44 | 8.44 | 1.3 |
| KKC6 | 33.95 | 82.67 | 10.3 | 43.8 | 10.07 | 2.52 | 11.32 | 13.14 | 2.54 | 7.49 | 7.62 | 1.18 |
| KKC8 | 9.3 | 22.02 | 2.92 | 14.4 | 3.67 | 1.18 | 4.62 | 5.42 | 1.05 | 3.21 | 3.08 | 0.47 |
| KKC0 | 8.29 | 21.44 | 3.08 | 15.5 | 4.07 | 1.51 | 5.01 | 5.18 | 0.96 | 2.73 | 2.4 | 0.36 |
| KKC2 | 4.47 | 11.44 | 1.69 | 8.9 | 2.44 | 0.94 | 3.47 | 4.13 | 0.82 | 2.45 | 2.32 | 0.36 |
| KKC4 | 26.95 | 62.06 | 7.06 | 28.9 | 6.21 | 1.79 | 6.92 | 7.66 | 1.46 | 4.47 | 4.46 | 0.7 |
| KKC5 | 22.67 | 51.43 | 6.33 | 27.5 | 6.26 | 1.91 | 7.26 | 8.09 | 1.56 | 4.68 | 4.58 | 0.71 |
| KKC7 | 11.67 | 28.89 | 3.96 | 18.8 | 4.89 | 1.68 | 6.29 | 7.33 | 1.41 | 4.27 | 4.06 | 0.62 |
| KKC0 | 2.44 | 6.29 | 0.98 | 5.3 | 1.38 | 0.65 | 2.49 | 3.36 | 0.67 | 2.09 | 2.04 | 0.32 |
| KKC1 | 12.29 | 29.89 | 4.12 | 19.2 | 4.89 | 1.65 | 6.17 | 6.79 | 1.31 | 3.84 | 3.63 | 0.56 |
| KKC2 | 3.98 | 8.73 | 1.32 | 6.9 | 2 | 0.78 | 2.96 | 3.78 | 0.75 | 2.28 | 2.2 | 0.33 |
| KKC5 | 6.18 | 15.08 | 2.23 | 10.8 | 2.96 | 1.09 | 3.91 | 4.34 | 0.84 | 2.45 | 2.26 | 0.35 |
| KKC6 | 40.48 | 86.51 | 9.95 | 40.2 | 9.06 | 1.76 | 10.38 | 11.98 | 2.34 | 7.23 | 7.52 | 1.18 |
| KKC8 | 2.38 | 6.2 | 0.99 | 5.3 | 1.54 | 0.64 | 2.29 | 2.93 | 0.59 | 1.78 | 1.72 | 0.27 |
| KKC9 | 8.09 | 20.85 | 3.08 | 15.6 | 4.19 | 1.55 | 5.25 | 5.9 | 1.11 | 3.27 | 3.09 | 0.47 |
| KKC0 | 17.28 | 41.08 | 5.47 | 25.5 | 6.4 | 2.12 | 7.81 | 8.53 | 1.62 | 4.78 | 4.51 | 0.69 |
| KKC2 | 11.28 | 27.75 | 3.8 | 18.2 | 4.84 | 1.69 | 6.32 | 7.23 | 1.39 | 4.2 | 4.04 | 0.62 |
| KKC7 | 48.38 | 111.56 | 13.4 | 56.3 | 13.15 | 2.63 | 14.95 | 17.43 | 3.39 | 10.34 | 10.47 | 1.59 |
| KKC8 | 5.08 | 12.48 | 1.85 | 9.5 | 2.62 | 0.99 | 3.57 | 4.15 | 0.81 | 2.41 | 2.29 | 0.35 |
| KKC9 | 2.58 | 6.58 | 1.08 | 6 | 1.79 | 0.73 | 2.73 | 3.56 | 0.72 | 2.21 | 2.15 | 0.34 |
| KKD1 | 2.38 | 5.75 | 0.93 | 5.2 | 1.51 | 0.62 | 2.34 | 3.02 | 0.61 | 1.88 | 1.85 | 0.29 |
| KKD5 | 11.18 | 27.97 | 3.8 | 18.2 | 4.77 | 1.64 | 6.22 | 7.13 | 1.37 | 4.13 | 3.94 | 0.6 |
| KKD6 | 30.09 | 67.11 | 8.12 | 34.3 | 7.82 | 2.13 | 9.01 | 9.94 | 1.9 | 5.72 | 5.66 | 0.87 |
| KKD2 | 8.57 | 21.26 | 3.01 | 14.4 | 3.8 | 1.38 | 5.04 | 5.61 | 1.09 | 3.24 | 3.09 | 0.48 |
| KKD4 | 24.48 | 55.55 | 6.76 | 28.9 | 6.61 | 1.98 | 7.62 | 8.3 | 1.59 | 4.77 | 4.7 | 0.72 |
| KKD1 | 9.88 | 24.09 | 3.38 | 16.8 | 4.43 | 1.59 | 5.81 | 6.75 | 1.31 | 3.93 | 3.76 | 0.58 |
| KKD5 | 3.6 | 9.3 | 1.4 | 7.4 | 2.12 | 0.81 | 2.94 | 3.56 | 0.7 | 2.12 | 2.01 | 0.31 |
| KKD7 | 11.38 | 27.53 | 3.84 | 18.4 | 4.8 | 1.66 | 6.23 | 7.2 | 1.39 | 4.17 | 3.97 | 0.61 |
| KKD3 | 8.68 | 21.38 | 3.05 | 14.8 | 3.96 | 1.43 | 5.21 | 6 | 1.16 | 3.49 | 3.35 | 0.51 |
| KKD5 | 8.58 | 21.04 | 2.94 | 14.7 | 3.87 | 1.41 | 5.13 | 5.98 | 1.16 | 3.48 | 3.34 | 0.92 |
| KKD6 | 4.08 | 10.1 | 1.51 | 7.7 | 2.22 | 0.86 | 3.28 | 4.04 | 0.8 | 2.47 | 2.41 | 0.38 |
| KKD9 | 9.18 | 23.04 | 3.29 | 16.1 | 4.19 | 1.5 | 5.39 | 5.88 | 1.11 | 3.3 | 3.08 | 0.47 |
| KKD4 | 3.54 | 9.26 | 1.39 | 7.7 | 2.07 | 0.81 | 2.95 | 3.66 | 0.72 | 2.16 | 2.05 | 0.32 |
| KKD2 | 5.97 | 13.81 | 2.08 | 10.8 | 2.89 | 1.09 | 3.86 | 4.42 | 0.85 | 2.55 | 2.36 | 0.37 |
| KKD2 | 7.27 | 18.54 | 2.7 | 13.4 | 3.56 | 1.31 | 4.6 | 5.12 | 1 | 2.98 | 2.77 | 0.43 |
| KKD8 | 4.46 | 11.62 | 1.79 | 9.3 | 2.59 | 0.99 | 3.66 | 4.43 | 0.87 | 2.62 | 2.49 | 0.38 |
| KKD9 | 8.88 | 22 | 3.07 | 15 | 3.87 | 1.39 | 4.92 | 5.54 | 1.06 | 3.16 | 2.98 | 0.46 |
| KKD0 | 7.38 | 18.84 | 2.76 | 13.7 | 3.69 | 1.35 | 4.82 | 5.46 | 1.04 | 3.1 | 2.91 | 0.44 |
| KKD1 | 5.88 | 15.26 | 2.24 | 11.5 | 3.08 | 1.16 | 4.05 | 4.51 | 0.87 | 2.54 | 2.36 | 0.33 |
| KKD2 | 27.6 | 64.4 | 8.43 | 37.8 | 9.17 | 2.97 | 10.67 | 11.91 | 2.26 | 6.81 | 6.5 | 0.98 |
| KK | 42.7 | 90.74 | 10.53 | 43.1 | 9.39 | 1.85 | 10.26 | 11.94 | 2.31 | 7.14 | 7.21 | 1.1 |
| KKC9 | 55.99 | 123.95 | 14.92 | 61.8 | 14.02 | 2.79 | 15.51 | 17.78 | 3.41 | 10.31 | 10.31 | 1.57 |
| KKD24 | 7.28 | 16.36 | 2.38 | 12 | 3.14 | 1.17 | 4.01 | 4.54 | 0.87 | 2.57 | 2.41 | 0.37 |
| 84-05 | 10.15 | 24.1 | 3.38 | 16.9 | 4.42 | 1.58 | 5.81 | 6.72 | 1.3 | 3.88 | 3.69 | 0.58 |
| 84-19 | 7.08 | 17.6 | 2.91 | 12.4 | 3.22 | 1.22 | 4.29 | 4.83 | 0.93 | 2.77 | 2.6 | 0.4 |
| KKA10 | 9.49 | 23.39 | 3.26 | 15.8 | 4.23 | 1.51 | 5.55 | 6.29 | 1.21 | 3.63 | 3.48 | 0.54 |

# Appendix VI
# Analytical methods

## (a) X-Ray fluorescence Spectrometry (XRF)

Samples were analysed for 10 major and 17 trace elements using Philips PW1450 and PW1480 automatic XRF spectrometers. Major elements were analysed on glass discs prepared by fusion using a borate flux (Johnson Matthey Spectroflux 105®). Rock powders were in general not ignited prior to fusion, as most samples are very fresh and gave good totals. Exceptions to this were some of the hyaloclastites, which gave slightly low totals. LOI values were determined by ignition for these samples and reported in Appendix IV. Trace elements were analysed on pressed powder pellets with matrix corrections calculated from sample major element compositions.

Details of rock crushing procedure, and preparation of fused glass discs and pressed powder pellets are given by Thirlwall (1979), Fitton *et al.* (1984) and Fitton & Dunlop (1985). Samples were analysed along with USGS and CRPG international standards and standard concentrations as reported by Abbey (1980) were used to calibrate each element. All sample counts were ratioed to monitor counts in order to correct for instrument drift. Six additional separate glass discs and pressed powders of basaltic sample KK18 were analysed. The mean and standard deviation of the results are reported in Table VI.1, together with RMSD estimates for the accuracy of the XRF calibration

## (b) Electron probe microanalysis

Mineral analyses were carried out using the Cambridge Instruments Microscan 5 electron probe in the Grant Institute, University of Edinburgh. A focussed 1-2 μm beam was used with a sample penetration depth of about 3 μm. Standards were used for Si, Al, Mg, Fe, Ti, Mn, K, Na, Ca, Cr and Ba, and corrections were made for dead-time, atomic number, atomic absorption and fluorescence, after the method of Sweatman & Long (1969). Further procedural details are given by Thirlwall (1979) and details of detection limits and precision are outlined by Russell (1985).

## (c) Inductively coupled plasma (ICP) spectrometry

Forty eight samples were chosen for REE analysis using the Philips PV8210 1.5-m ICP spectrometry at Royal Holloway & Bedford New College, University of London, Egham, Surrey. The ICP method involves the chromatographic separation of REE from rock powders using cation exchange columns. The analyte solution is

| | Mean wt% (n=7) | 2s | RMSD |
|---|---|---|---|
| $SiO_2$ | 50.48 | 0.24 | 0.21 |
| $Al_2O_3$ | 18.05 | 0.14 | 0.13 |
| $Fe_2O_3$ | 9.33 | 0.16 | 0.04 |
| MgO | 5.95 | 0.12 | 0.03 |
| CaO | 12.83 | 0.02 | 0.03 |
| $Na_2O$ | 2.10 | 0.09 | 0.04 |
| $K_2O$ | 0.28 | 0.01 | 0.01 |
| $TiO_2$ | 0.90 | 0.01 | 0.01 |
| MnO | 0.16 | 0.004 | 0.005 |
| $P_2O_5$ | 0.10 | 0.01 | 0.01 |
| | ppm | | |
| Ni | 63.6 | 0.7 | 4.3 |
| Cr | 232.7 | 5.3 | 11.0 |
| V | 219.0 | 1.9 | 11.5 |
| Sc | 35.1 | 5.2 | 2.4 |
| Cu | 98.9 | 1.7 | 5.3 |
| Zn | 68.8 | 1.0 | 5.0 |
| Sr | 135.0 | 0.9 | 9.6 |
| Rb | 5.6 | 0.8 | 3.5 |
| Zr | 107.8 | 0.9 | 14.8 |
| Nb | 7.9 | 0.3 | 2.4 |
| Ba | 65.6 | 24.2 | 39.0 |
| Pb | 0.3* | 1.2 | 4.0 |
| Th | -0.7* | 1.5 | 2.8 |
| La | 3.0 | 6.2 | 5.6 |
| Ce | 11.6 | 11.5 | 13.5 |
| Nd | 16.2 | 5.5 | 3.6 |
| Y | 25.0 | 0.6 | 3.4 |

* = Below detection limit.

**Table VI.1** Reproducibility results (2σ) for the sample KK18 (basalt) and typical accuracy for the XRF results (root mean squared deviation (RMSD)). RMSD values for the trace-element concentrations are taken from Fitton *et al.* (1984).

injected into a high temperature (6000-10000K) flame such that spectral lines are excited by ionic as well as atomic species. Details of selected spectral lines and operating parameters used in the analysis are reported by Walsh *et al.* (1981).

## Dissolution procedure

Dissolution of rock powders was performed by weighing 0.500±0.01 g of sample into a platinum crucible. 15 ml of a 2:1 HF-$HClO_4$ mix was added to each sample, and the samples were evaporated to dryness in a sand bath. The samples were cooled and 5 ml of conc. HCl was poured into each crucible, the samples warmed gently to achieve dissolution of the residues, then the crucibles were half-filled with distilled water and heated for 15 minutes on the edge of the sandbath. The solutions were filtered when hot, using number 42 filter paper. The residues were added to the filter-papers by scraping the crucibles with a "rubber policeman" and washing thoroughly: the filtrate was collected in 100 ml beakers. After filtration (overnight) the filter papers were folded up and placed in silver crucibles (cleaned in hot water, conc. HCl, water, and finally in distilled water). The crucibles were loaded into a furnace and the temperature was set to 250°C. After warming up, the furnace was left at 250°C for 30 min. The temperature was then increased to 400°C for another 30 min, and finally raised to 800°C for 30 min. The samples were removed from the furnace and 5 pellets of NaOH were added to each of the crucibles. The crucibles were returned to the furnace for a further 30 min at 800°C, and then removed, swirled holding each crucible with tongs until the NaOH was solid. When the crucibles were cool, then 5 ml distilled water was added to each crucible, followed by 3 ml conc. HCl (fizz!). The crucibles were stirred with "rubber policemen" to remove any final patches of NaOH. Each crucible's contents was added to its respective filtrate from the filtration stage, washing the crucibles carefully. Each solution was made up to 100 ml with distilled water. The solutions are ready for use on the columns, in the procedure described below.

## REE separation

Chromatographic separation was performed using glass columns of 20 mm internal diameter and 250 mm in length, with a glass sinter disc and PTFE burette tap at the base (Walsh *et al.*, 1981). Columns were loaded to a settled height of 12 cm with Dowex® AG50W-X8, 200-400 mesh cation exchange resin and washed with 200 ml of distilled water prior to sample loading. Samples were loaded on the columns, and once passed through the resin they were washed with 500 ml of 1.7M HCl, collecting and disposing of the eluate. A further 600 ml of 4M HCl was then

added to elute the REEs, collecting the solutions in 800 ml beakers. These solutions, containing the REEs, were evaporated till only about 15 ml of the solution remained, transferred to 50 ml beakers (carefully washing with distilled water) and eventually evaporated to dryness. The beakers were covered with "clingfilm" when cool and stored until they were ready to run on the ICP spectrometer, when they were redissolved in 5 ml of 10% $HNO_3$.

**Standards and blanks**

Ion exchange separations were carried out in groups of 8; each group contained one blank, one standard (internal RHBNC standard) and six samples. The blank and standard were processed in exactly the same way as for the samples. The mean value of the blank is shown in Table VI.2. The blank concentrations were negligible. Analytical precision using the ICP technique for determining REE concentrations has been calculated by Walsh *et al.* (1981) and is shown in Table VI.2. The standards used are KC10,11,13 and mean analyses measured in the present study are shown in Table VI.2, together with accepted values (J.N. Walsh, pers. comm. 1989). It should be noted that the values of La and Ce show poor agreement between accepted and measured values for sample KC13.

The elements La, Ce, Nd were determined by both XRF and ICP spectrometry. In Fig. VI.1 $La_{XRF}$ is plotted against $La_{ICP}$. This shows that there is poor agreement between the two techniques for samples containing low concentrations of these elements, whereas at higher concentrations the agreement is much better, although XRF values are generally higher than those determined by ICP. The errors in the ICP determinations of the REEs only becomes significant for the most primitive samples (e.g. KK50 or KK81) (see Table VI.2). This is apparent from the REE variation diagram for selected samples with less than 8 wt% MgO (see Fig. 5.12).

A synthetic standard containing all the REE and Y was analysed after every tenth sample to check for instrument drift. Although concentrations tended to be 1-2% higher than their true values, this error was considerably less than the estimates of analytical precision.

In addition, a set of interference standards: Nd (10 ppm), Ce (20 ppm), Zr (50 ppm), Sr (50 ppm), Ba (100 ppm), Ca (100 ppm) and Fe (100 ppm) were analysed between sample analyses in order to determine the interferences from these elements on the REE, Pr. Er and Gd analyses have been corrected for interference effects from Ca and Fe.

a)

| Precision estimate | | | Blank | |
|---|---|---|---|---|
| | Mean (ppm) | 2σ (ppm) | | Mean (ppm) |
| La | 5.83 | 0.75 | La | 0.18 |
| Ce | 12.30 | 0.86 | Ce | 0.41 |
| Pr | 1.89 | 0.16 | Pr | 0.09 |
| Nd | 9.64 | 0.67 | Nd | 0.26 |
| Sm | 2.48 | 0.11 | Sm | 0.06 |
| Eu | 0.90 | 0.02 | Eu | 0.01 |
| Gd | 2.59 | 0.14 | Gd | 0.07 |
| Dy | 2.96 | 0.05 | Dy | 0.05 |
| Ho | | | Ho | 0.02 |
| Er | 1.75 | 0.08 | Er | 0.05 |
| Yb | 1.79 | 0.04 | Yb | 0.02 |
| Lu | 0.28 | 0.01 | Lu | 0.005 |

b)

| Standards | | | | | | |
|---|---|---|---|---|---|---|
| | KC10m | a | KC11m | a | KC13m | a |
| La | 4.54 | 4.3 | 24.10 | 23.0 | 61.59 | 59 |
| Ce | 10.57 | 9.2 | 52.64 | 49.0 | 131.18 | 120 |
| Pr | 1.45 | 1.6 | 6.30 | 5.9 | 15.25 | 13 |
| Nd | 7.00 | 6.8 | 26.90 | 26.5 | 58.80 | 58 |
| Sm | 1.69 | 1.7 | 5.16 | 5.2 | 14.07 | 14 |
| Eu | 0.74 | 0.75 | 1.45 | 1.4 | 0.58 | 0.57 |
| Gd | 2.10 | 1.9 | 5.28 | 5.0 | 16.43 | 15 |
| Dy | 2.25 | 2.0 | 5.00 | 4.5 | 21.53 | 18 |
| Ho | 0.43 | 0.43 | 0.93 | 1.0 | 4.16 | 4 |
| Er | 1.27 | 1.25 | 2.67 | 2.7 | 12.76 | 11.8 |
| Yb | 1.14 | 1.1 | 2.34 | 2.2 | 12.61 | 11.2 |
| Lu | 0.17 | 0.16 | 0.35 | 0.3 | 1.76 | 1.5 |

m = measured concentration; a = accepted concentration

Table VI.2(a) Precision estimates for the REE concentrations determined by ICP, based on 15 replicate analyses from Walsh *et al.* (1981), and average REE concentrations for 8 blank runs during the ICP determinations.
(b) Accepted and measured REE concentrations for standards KC10, KC11 and KC13. Accepted values obtained from J.N.Walsh pers. comm. 1989.

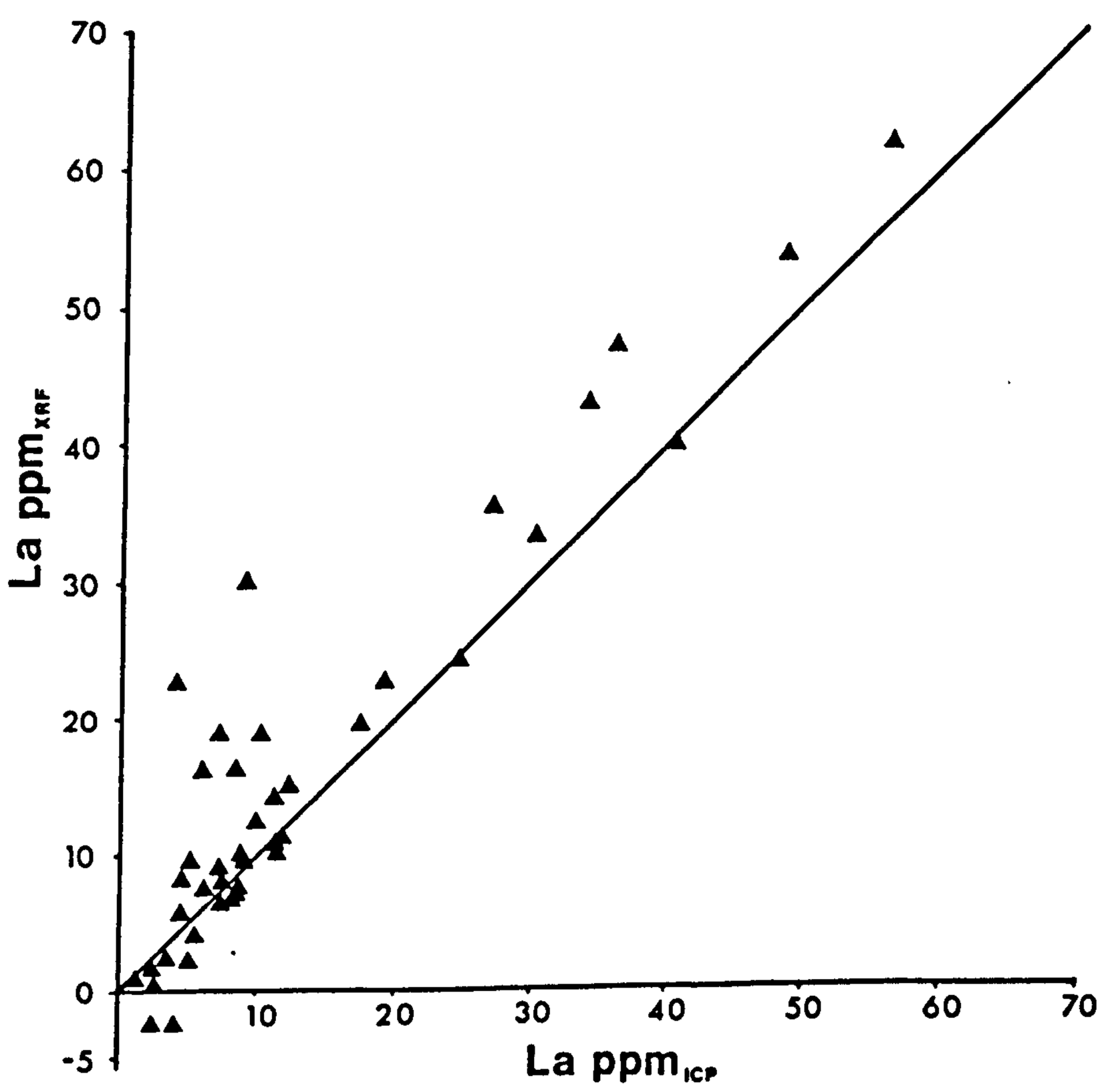


**Fig. VI.1** La (ppm) XRF vs La (ppm) ICP for selected samples from Krafla.

### (d) Sr- and Nd-isotopic analysis

Sr- and Nd-isotopic analyses were performed at the Scottish Universities Research and Reactor Centre at East Kilbride. Both Sr and Nd isotopic analysis were carried out using a VG Isomass 54E mass spectrometer. All chemical separations were carried out in clean laboratories. All teflonware was thoroughly cleaned in $HNO_3$, HCl and distilled water prior to use. Only one sample was spiked to determine the Rb concentration (KK50).

### Sample dissolution

Samples were accurately weighed (around 100 mg) into clean screw-top PFA teflon beakers. Samples were then dissolved in 10 ml 40% HF, with 1 ml 14M $HNO_3$ added to prevent the precipitation of insoluble fluorides. Samples were then left on a hotplate for 48 hours at 150°C before evaporation to dryness. Following this step, approximately 5 ml of 14M $HNO_3$ were added to each beaker and samples were again left overnight on the hotplate. After evaporation to dryness the residue was dissolved in 5 ml 6M HCl, left overnight on a hotplate and dried down. Subsequently the samples were dissolved in 2 ml of 2.5M HCl and centrifuged. The samples were then ready for Sr separation by ion exchange methods.

### Ion exchange procedure.

Sr and REE (and Rb for KK50) were separated using cation ion exchange chromatography in columns loaded with Bio Rad® AG50W X8 200-400 mesh cation resin. Columns were cleaned before use in 6M HCl, distilled water and 2.5 M HCl and were pretreated using 2.5M HCl. The washing and elution of Rb and Sr was carried out in 2.5M HCl, and following this the solutions were evaporated to dryness. A REE fraction containing both Sm and Nd was obtained by further elution in 3M $HNO_3$. This fraction was also evaporated to dryness. Nd was separated from the other REEs using PTFE teflon-filled columns. Columns were pretreated and samples loaded using 0.31M HCl. Washing was carried out using 0.155M HCl, 0.31M HCl and 0.62M HCl. The aliquots of Nd were collected in 0.31M HCl.

### Mass spectrometry

Sr was analysed using outgassed single Ta filament assemblies. The Sr fraction was dissolved in ~1 µl of 1M $H_3PO_4$ and loaded onto the Ta filament. A current was then passed through the filament until the solution dried; the $H_3PO_4$ fumed off and the filament glowed a dull red. Sr beams were managed to give a beam intensity of 0.15V on the $^{86}Sr$ peak. All isotopic data were corrected for machine

fractionation using a value of $^{88}Sr/^{86}Sr$ of 8.37521. Rb interference on the $^{87}Sr$ peak was checked by monitoring the $^{85}Rb$. The average value of $^{87}Sr/^{86}Sr$ for the standard NBS987 during the course of the study was 0.71028±1 (2σ). All samples' $^{87}Sr/^{86}Sr$ values were converted to a value of 0.71022.

Nd samples were all analysed as metal species using standard triple filament assemblages with Ta side filaments and a Re centre filament. The filaments, prior to sample deposition, were outgassed at 4.25A for 15 min in a vacuum better than $10^{-5}$ torr. Nd samples were dissolved in ~1 µl of 0.01M $H_3PO_4$ and loaded onto one of the side filaments. A current of ~0.5A was passed through the filament until the sample was dry. Nd beams were managed to give a signal of 0.4V on the $^{144}Nd$ peak. The $^{143}Nd/^{144}Nd$ ratio was corrected for machine fractionation using $^{146}Nd/^{144}Nd = 0.7219$. The JM Nd standard gave a value of $^{143}Nd/^{144}Nd = 0.511323±9$ during the course of this study.

**(e) Oxygen isotopic analysis**

Oxygen isotope determinations were undertaken at the S.U.R.R.C. (East Kilbride) following the technique of Borthwick & Harmon (1982). Some additional details are included in Chapter 7.

**(f) U-series disequilibrium analysis/Isotope dilution**

**I. Chemical separation method for isotope dilution determination of Th and U concentrations.**

The method essentially follows that described by Condomines *et al.* (1982), with a few modifications appropriate for the analysis of tholeiites.

(i) Samples of powder (>200 mesh) are weighed out (to 0.01 mg) into small teflon beakers (100-200 mg of sample) and a spike enriched in $^{230}Th+^{235}U$ (quantity added to get an estimated 1:1 concentration ratio of Th and U in the mixture; $K_2O$ concentrations are used as a guide to the concentrations of Th in the samples).

(ii) A mixture of concentrated acids was added to the powder and spike (1ml $HClO_4$, 2ml $HNO_3$, 2ml HF). The acids were analytical grade. In the case of the lower $K_2O$ wt% basalts (shown later to be <0.6 ppm Th) the analytical grade acids are doubly-distilled as well, to reduce the Th concentration in the blank. The powder is wetted, lids to containers secured and the samples (in groups of 4) are left overnight to react. The lids are removed the following morning and washed into the containers with distilled water (temperature increased). In the evening the temperature is increased once again to evaporate the final acid (mostly perchloric).

(iv) When the containers are dry (and cool), add 2 ml conc. HCl and evaporate, increasing the temperature as in (iii) to remove the remaining perchloric acid. Set up anion exchange columns (15 cm AG1X8 200-400 mesh resin) using 1M $HNO_3$. Add water to the columns (+stops) and leave until the columns are required.

(v) Before adding samples to the columns, add 2 ml 7M $HNO_3$ to each of the dried residues and leave to dissolve on top of the heater.

(vi) Take off the stops on the columns and let the water flow through. Add 4 ml 7M $HNO_3$ to the columns and let it go through. Put samples into centrifuge tubes and centrifuge for 10 min. Add 7 ml of 7M $HNO_3$ to the sample container. Add sample from the centrifuge tube to the columns (with a pipette). Wash the columns with 7 ml of 7M $HNO_3$ (from the sample containers). Elute the samples with 5 ml water. Evaporate the samples. Wash the columns with 5 ml 6M HCl, then fill the columns with water (and let drain through), followed by 1M $HNO_3$ and finally half-full with water.

(vii) After evaporation, add 0.3 ml 7M $HNO_3$ to each sample and heat gently to dissolve. Set up "little columns" (few cm resin), add 1 ml 7M $HNO_3$ to columns. Then add samples to the columns. Put 1.5 ml 7M $HNO_3$ into the sample beakers for a wash (add to columns when sample has passed through). Add another similar wash directly to the columns with a pipette. After 2nd wash, elute (collecting in same beakers as the samples started in) with 2 ml water, followed by 2 ml 6M HCl. Finally evaporate as before.

(viii) When dry the samples are ready for electrodeposition on Rh filaments (triple filaments; sample on central one). The sample (Th, U mostly) is dissolved in a few µl of 6M HCl, taken up in a catheter and dropped onto the central filament at 1.8 A current (filament evaporated at 1.2 A before this).

(ix) The filament is loaded into the mass spectrometer (Thomson THN206) and the ratios of $^{230}Th/^{232}Th$ and $^{235}U/^{238}U$ are determined using either metal or oxide species depending upon the sample (3 sets of repeat analyses, until the errors are less than 1%.). The Th and U concentrations of the sample may be calculated since the spike's Th and U concentrations and isotope ratios are known and the sample contains a negligible concentration $^{230}Th$ (using a computer program for the isotope dilution technique, written by M.Condomines).

## II Method for determining ($^{230}Th/^{232}Th$) activity ratios by α-spectrometry

(i) Weigh out sample (between 2.5-10 g) into teflon container(s) (if over 5 g then put equal quantities into 2 beakers). Add 20 ml conc. $HNO_3$, then 20 ml conc. HF to each

container (5 ml of each acid for each 1 g powder). Put on heater (lids closed) for 24 hours at a low heat. Then take off lids (rinse lids with water back into sample container) and evaporate until dry.

(ii) When dry add ~10 ml conc. $HNO_3$ to each residue. Leave to evaporate again. Repeat.

(iii) Add 15 ml 6M HCl and put lids back on; leave for 4+ hours on heater.

(iv) Take off the heat. Add 1 ml lanthanum nitrate solution and $NH_4OH$ until the pH = 8-9 (Merck indicator stick). Pour into centrifuge tubes and centrifuge for 5 min (4000 $s^{-1}$). Retain the precipitate and pour away the supernatant (unless analysing for U isotope ratios). Add water, stir and re-centrifuge. Add 10ml HF (50% diluted) and stir; Th stays in ppt of $LaF_3$, dispose of supernatant. Dissolve precipitate in 5 ml conc. $HNO_3$ (+ a squirt of water) and add 2-3 ml conc. HF, then centrifuge. Keep precipitate. Repeat dissolution in conc. $HNO_3$ etc.

(v) Add 15 ml conc. $HNO_3$ then put on heater to evaporate (overnight). Next morning add 10 ml 7M $HNO_3$, re-evaporate and add another 10 ml 7M $HNO_3$.

(vi) Then add 10 ml saturated solution of $Al(NO_3)_3$ and dissolve by stirring and heating with the lids on (about 2 hours). Cool.

(vii) Set up separating funnels with stoppers in. Add samples in $Al(NO_3)_3$ to the funnels. Then add 10 ml mesityl oxide to each sample. Shake by hand for 1 min. Let the solution settle and decant the lower layer ($Al(NO_3)_3$) (Th stays in organic layer). Add 10 ml more $Al(NO_3)_3$, shake by machine. Decant again. Add 10 ml water, shake. Decant water layer (lower layer) into a teflon beaker for each sample (Th in water now). Make solutions up to pH2 with $NH_4OH$.

(viii) Pour the solutions (pH2) back into separating funnels (wash with water beforehand) and add 10 ml of a solution of TTA in benzene. Shake for 5 min by machine. Decant lower layer (water) and Th stays in organic layer. Add 10 ml pH2.5 $HNO_3$ to separating funnels. Shake for 5 min by machine. Decant and dispose of aqueous layer. Add 10 ml 2M $HNO_3$; shake for 7 min. Decant lower layer and retain this layer (it now has most of the Th in it). Evaporate.

(ix) After evaporation re-dissolve in conc. $HNO_3$ (few drops) and evaporate. Repeat once again and take dry residue and dissolve in 0.4 ml 7M $HNO_3$; heat for short time to dissolve residue. Prepare small columns (as above). Add 1 ml 7M $HNO_3$ to the columns, then 0.4 ml 7M $HNO_3$ with the sample. Wash the columns with 2 ml 7M $HNO_3$. Put sample beakers back under columns and elute with 2 ml water and 2 ml 8M HCl. Evaporate (overnight). Leave stops on the columns overnight.

(x) Redissolve residue in 0.4 ml 8M HCl, heat a little, then put straight on the column, putting sample beaker immediately underneath the column to collect the sample. Add 1.5 ml 8M HCl for a wash (directly) and collect wash. Evaporate once again.
(xi) Dissolve the residue in 0.4 ml (50% diluted) $H_2SO_4$ (heat a little to dissolve). Add 3 ml water. Change the pH to 2 (with $NH_4OH$). Stir the solution with the wire of electroplating apparatus. Assemble the electroplating cell (wash, dry first), using teflon tape as a seal. Take the plastic covers off the electroplating discs, wash with alcohol, and place at bottom of electroplating apparatus. Wash the cell out with water, checking that the seal functions. Pour the sample solution into the cell and add 4 ml 1M $(NH4)_2SO_4$ (pH2) as a wash. Attach the power connections and set the current to 1.2A. Electroplate for 75 min. To finish, add 1 ml conc. $NH_4OH$, leave for 1 min with the power on. Remove the cathode, pour sample solutions into the beakers and rinse 2 or 3 times with 0.1M $NH_4OH$. Undo the electroplating cell and remove the disc with tweezers. Wash the disc with ethanol (pH8) and dry on the heater.
(xii) The dry discs are placed inside the counters on an α-spectrometer, Intertechnique SA 40B, with Ortec Si detectors. The spectrum examined includes $^{232}Th$ (4.00 MeV), $^{230}Th$ (4.68 MeV), $^{228}Th$ (5.42 MeV). Counting times ranged from 10 days (KK56 and KK26) to 2 months (basalts). Analytical precision is a function of the number of α-counts recorded:

Relative error $(\Delta R/R) = \pm\alpha.(1/N_1 + 1/N_2)$, where for $1\sigma$, $\alpha = 1$.
i.e. 5000 counts for each isotope gives ±2% precision.

# APPENDIX VII

# AFC FORTRAN PROGRAM

This is a program to calculate $\delta^{18}O$, ($^{230}Th/^{232}Th$) and Th values during assimilation coupled to fractional crystallisation (single-stage model). This program uses the equations of DePaolo (1981) and Taylor & Sheppard (1986).

The program calculates separate AFC models for different values of $C_a$ (K), $C_o$ (J) and r (I) over a range of f (L) values from 1 to 0.05. The resultant output is screened to eliminate values of $\delta^{18}O$ and ($^{230}Th/^{232}Th$) when f=0.1, outside the limits given in the program (i.e. OXMAX, OXMIN, RATMAX, RATMIN). Solutions outside this range are labelled in the output file by the number -50. These unacceptable results may be eliminated from the output by a bulk edit of the output file (OUT1). *Comments have been added in italics.*

```
      PROGRAM AFC
      DIMENSION A(12,4,8,20)
      DIMENSION B(12,4,8,20)
      DIMENSION C(12,4,8,20)
      REAL SNAKE

*     Defines zero matrix initially.

      DO 2 I=1,12
      DO 4 J=1,4
      DO 6 K=1,8
      DO 8 L=1,20
      A(I,J,K,L)=0
      B(I,J,K,L)=0
      C(I,J,K,L)=0
    8 CONTINUE
    6 CONTINUE
    4 CONTINUE
    2 CONTINUE

*     OX is the δ18O value of the assimilant.
*     U is the (230Th/232Th) value of the initial primary magma.

      OX=-4
      U=1.25
      RATMIN=0.95
      RATMAX=1.00

*     CONMAX and CONMIN may be used to screen the output for realistic
*     Th concs. In this instance they are not being used.
*     DEL is the δ18O fractionation factor between melt and crystals.
*     T is the (230Th/232Th) value of the assimilant.

      CONMAX=9
      CONMIN=7
      DEL=0
      T=0.93
      OXMAX=2.5
      OXMIN=1.0
```

*Main loop of the program to calculate the values of $\delta^{18}O$, ($^{230}Th/^{232}Th$) and Th, for different values of r (RA), $C_a$ (K) and $C_o$ (AA).*

```
      DO 10 I=1,11
      RA=0.01*I+0.54
      DO 20 J=1,4
      AA=0.10*J+0.05
      DO 30 K=1,8
      DO 40 L=1,20
      KK=K
      SNAKE=L
```

*SNAKE is equal to 20.f; included to get round real/integer problem.*
*ZEFA is equal to f.*
*CON is the resultant Th conc., RAT is the resultant ($^{230}Th/^{232}Th$) value and DOX is the resultant value of $\delta^{18}O$. BEN is a handy variable that has no particular physical significance.*

```
      ZEFA=SNAKE/20
      BEN=(RA/(RA-1))*KK*(1-(1/ZEFA))
      CON=(AA/ZEFA)+BEN
      RAT=((BEN*T)+(U*AA/ZEFA))/(BEN+(AA/ZEFA))
      DOX=OX*(1-ZEFA**(RA/(1-RA)))+5.5
      A(I,J,K,L)=CON
      B(I,J,K,L)=RAT
      C(I,J,K,L)=DOX
40    CONTINUE
30    CONTINUE
20    CONTINUE
10    CONTINUE
```

*Screening loop.*

```
      DO 50 I=1,11
      DO 60 J=1,4
      DO 70 K=1,8
      DO 80 L=1,20
      IF ((B(I,J,K,2) .GT. RATMAX) .OR. (B(I,J,K,2) .LT. RATMIN))
      GOTO 77
      IF ((C(I,J,K,2) .GT. OXMAX) .OR. (C(I,J,K,2) .LT. OXMIN))
      GOTO 77
      GOTO 80
77    C(I,J,K,L)=-50
80    CONTINUE
70    CONTINUE
60    CONTINUE
50    CONTINUE
```

```
*Sends the output to a character file OUT1.
*Data output as shown below: I,J,K,L followed by DOX, RAT and CON.

      OPEN(7,FILE='OUT1',FILETYPE='C')
      DO 90 I=1,11
      DO 100 J=1,4
      DO 110 K=1,8
      DO 120 L=1,20
      WRITE(7,200) I,J,K,L, C(I,J,K,L),B(I,J,K,L),A(I,J,K,L)
  120 CONTINUE
  110 CONTINUE
  100 CONTINUE
   90 CONTINUE
  200 FORMAT(4I4,3F8.4)
      STOP
      END
```